UNIVERSITÀ
DEGLI STUDI
DI PADOVA

Head Office: Università degli Studi di Padova

Department of Chemical Science (Disc)

Ph.D. COURSE IN: Molecular Science
CURRICULUM: Chemical Science
SERIES XXXVI

MOLECULAR GOLD NANOCLUSTERS CAPPED BY N-HETEROCYCLIC CARBENE LIGANDS

Coordinator: Prof. Stefano Corni
Supervisor: Prof. Andrea Biffis

Ph.D. student: Matteo Bevilacqua

ABSTRACT

Gold nanoparticles (AuNPs) and gold complexes are among the most studied chemical entities for their luminescence behavior and catalytic applications. However, other gold species started to attract worldwide scientific interest in the course of the last years: molecular gold nanoclusters (AuNCs). These are generally composed by several gold atoms forming a metallic core, in which part of the gold atoms are formally zerovalent. Despite their particle-like structure, AuNCs show molecular proprieties, such as a discrete orbital structure and a precise stoichiometric formula. So far, AuNCs stabilization has been mainly reached exploiting thiolate, alkynyl and phosphine ligands, which form a layer saturating and protecting the cluster core. However, the steric and electronic properties of such ligands cannot be independently varied. For this reason, N-heterocyclic carbenes (NHCs) are currently studied as alternative ligands to achieve core protection, also considering the better stabilization obtained with these.

Hitherto, AuNCs synthesis has been performed through gold complex reduction using $NaBH_4$, although the reduction mechanism is still unknown and consequently this synthesis is complicate to control. Exploited this methodology, in this PhD thesis the role of different NHCs has been investigated, showing as such ligands generally provide superatomic (SA) clusters, characterized by $[Au_{11}]^{3+}$ or $[Au_{13}]^{5+}$ metallic cores, presenting therefore a complete SA electronic configuration providing further stabilization of the cluster. The role of reducing agent and solvent has been also evaluated, underlining as it is possible to tune the reduction pathways, changing therefore the reduction products. For instance, it is possible to obtain CH_3 anionic ligands bind on clusters core when the reduction promoted by $NaBH_4$ is performed in presence of CH_2Cl_2, used as solvent. Using instead hydrazine as reducing agent $[Au_6(C)]^{2+}$ clusters can be obtained. Notwithstanding the interesting products derived

from these syntheses, these reductions are generally not selective, limiting therefore their use.

Considering these limitations, in this thesis we have developed another method to isolate such molecular species, called stepwise approach, in which the obtained AuNCs are stabilized by triphenylphosphine (PPh_3) and di-NHCs. With this latter method a reaction between a pre-formed PPh_3-stabilized $[Au_{11}(PPh_3)_8Cl_2]^+$ cluster and [(di-NHC)Au_2Cl_2] gold(I) complexes occurs. Depending on starting complex and reaction conditions, a metathesis cluster $[Au_{11}$(di-NHC)$(PPh_3)_6Cl_2]^+$ is produced first, followed by formation of $[Au_{13}$(di-NHC$)_2(PPh_3)_4Cl_4]^+$ via a subsequent metal complex addition. In some cases, a further metathesis takes place, providing $[Au_{13}$(di-NHC$)_3(PPh_3)_3Cl_3]^{2+}$.

We have tested these clusters as anticancer pro-drugs, demonstrating as these can accumulate in cancer cells thanks to enhanced permeation and retention (EPR) effect, affording high anticancer efficiency too. Likely the antitumor activity derived from AuNCs degradation in biological environment, providing gold complexes acting like anticancer drugs.

Finally, thanks to a collaboration with Prof. Dominik Munz at Saarland University (Germany), we have extended our studies towards the synthesis of an unsaturated and cubic palladium cluster and started also a study regarding the stabilization of gold nanowires using NHC ligands.

TABLE OF CONTENTS

1.0 INTRODUCTION

1.1 HYSTORY OF GOLD BETWEEN METALLIC COMPLEXES AND NANOMATERIALS

Elemental gold is one of the most characteristic metals in the periodic table thanks to its unique yellow color, low reactivity, high malleability and high electronic conductivity, properties making it useful to fabricate different artefacts, from jewelries[1] to microchips.[2] Since these features, it is not surprising how this metal has attracted great interest also in its molecular forms.[3] Au(I) and Au(III) complexes generally do not react easily with oxygen or water, maintaining the “nobility” of elemental gold also as molecular complex. Due to this, gold complexes are exploited for several catalytic[4], optical[5] and medical applications.[6] However, elemental and molecular states of gold represent only two extremes of its chemistry. Indeed, when gold centers interact to each other forming nano-aggregates of hundreds or thousands of atoms, it is possible to obtain gold nanomaterials, such as gold nanoparticles (AuNPs)[7,8], species presenting properties that deeply differ from the other two forms mentioned before.[9] To clarify this, it is interesting to briefly explain the different mechanisms involved in the color appearance of these gold species. The color of elemental gold is attributed to electronic transitions between the d band, formed by overlap of d orbitals, and the sp band containing the Fermi level of the bulky system. Through the absorption of blue radiation, this electronic transition can be achieved, providing its characteristic yellow color, as highlighted in **Figure 1.1 a**[10] When instead single Au(I) complexes are taken in account, the system is classically described with the molecular orbital theory, as showed in **Figure 1.1 b**. The color of metallic complexes depends on HOMO-LUMO gap, but the d^{10} configuration associated to Au(I) complexes does not allow electronic transition between t_{2g} and e_g orbitals, affording consequently

colorless species, usually with the appearance of white powder, as reported in **Figure 1.1 b**.

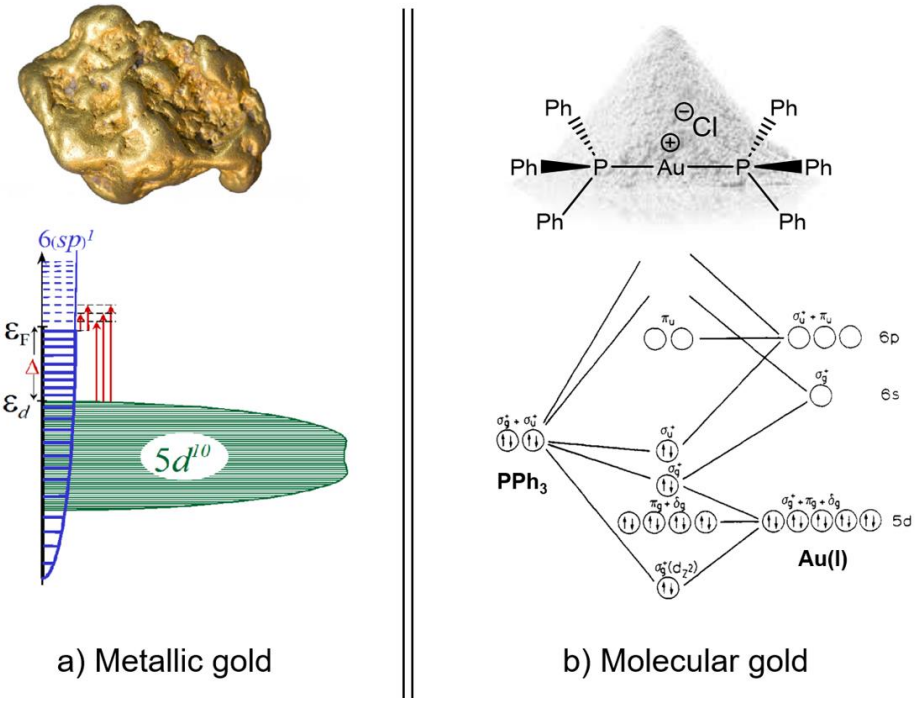

Figure 1.1: a) metallic gold (above) and simplified scheme of electronic transitions between d bands providing its color; b) an example of Au(I) complex in its solid form as white powder (above) and simplified orbital structure derived from the molecular orbital theory.[11,12]

These two theories explain the colors of bulky and molecular gold, but without clarifying AuNPs color, since this depends on their sizes and shapes, thus in contrast with previous studied cases. Gold nanoparticles, generally with sizes between 5 and 200 nm, support localized surface plasmon resonances (LSPRs) which are coherently localized oscillations of free conduction bands in the AuNP surface, as schemed in **Figure 1.2 a**.[13] The electrons in these bands are highly polarizable and the resonance between electronic plasmon and an incident light can be achieved, giving rise to a net charge difference at the nanoparticle boundaries thanks to electron oscillation. Thanks to LSPRs, incident light can be absorbed, providing characteristic AuNPs colors, affected by surface properties, such as particle shape or size. For instance, as reported in **Figure 1.2**; the variation of length of gold nanorods (**Figure**

1.2 d-h) provides different absorption spectra (**Figure 1.2 c**). Consequently, varying the shape of these nano-systems their optical properties can be tuned.[14]

From this comparison, it appears clear how the “confined surface” related to AuNPs gives rise to their peculiar properties. AuNPs not only are very tunable materials but they present generally low toxicity[15], high conductivity[16] and higher reactivity than elemental and molecular gold. Their exposed surface is the key to get this reactivity, exploited for instance to catalyze challenging reactions, such as catalytic oxidation of alcohol[17], but this favors aggregation processes too, aiming to decrease particle surface energy. To prevent this, different ligands can be used to stabilize AuNPs, such as thiolates (SRs)[18], polymers[19] and others[20], forming a protecting layer surrounding the particles. Furthermore, these ligands represent another useful tools in nano-chemistry, since varying ligand properties also AuNPs properties can be tuned, for instance varying their affinity to substrates in catalytic applications or changing their solubility.[21]

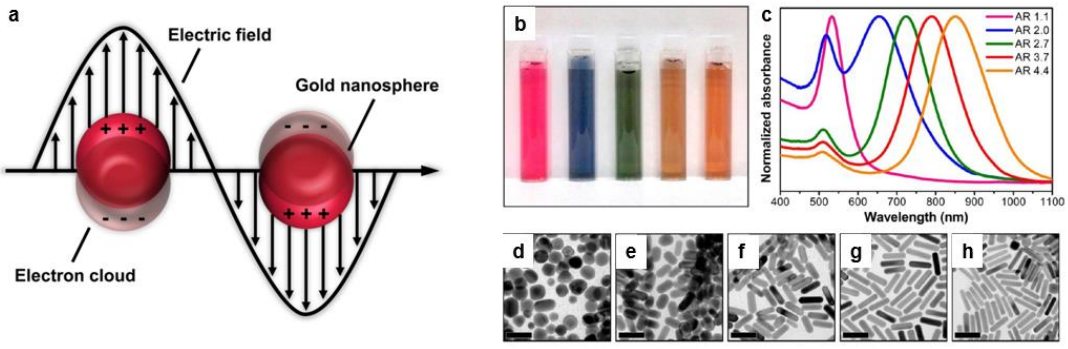

Figure 1.2: a) Schematic representation of the localized surface plasmon resonance on spherical AuNP; b) different colors derived from variation of nanorod shapes; c) UV-Vis spectra of gold nanorods with different length. d-h) TEM of gold nanorods with different sizes. Scale bars = 50 nm.[14]

Despite these advantages, AuNPs present some important drawbacks. One of the most critical is that AuNPs cannot be obtained as mono-dispersed samples, since their synthesis always provides a distribution of nanoparticles with different sizes. The

size distribution can be determined by TEM analysis[7], as reported in **Figure 1.3**[22], and partially controlled during the synthesis, but it is not possible to get AuNPs like truly molecular species, complicating their interpretation at molecular level.

For instance, single crystal X-ray diffractometry (SCXRD) allows to shed light on the molecular structure of metallic complexes or organic molecules, but it is not available for AuNPs, since it is not possible to crystalize these species. For this reason, AuNPs structure remains elusive, not allowing therefore structure-properties correlations, fundamental to fully understand their chemical and physical features. AuNPs are classically analyzed by surface characterization techniques that allow to study their shape and composition, such as XPS[23,24], small angle X-ray scattering[25], AFM[26] and others. Molecular characterization can be used to understand these nano-systems too but without provides real molecular information. For instance, the interactions between a gold surface and ligands can be studied using IR[27] or Raman[28] spectroscopy, to confirm the presence of ligands on the particle surface, but these analyses can be hardly correlated with AuNPs structures.

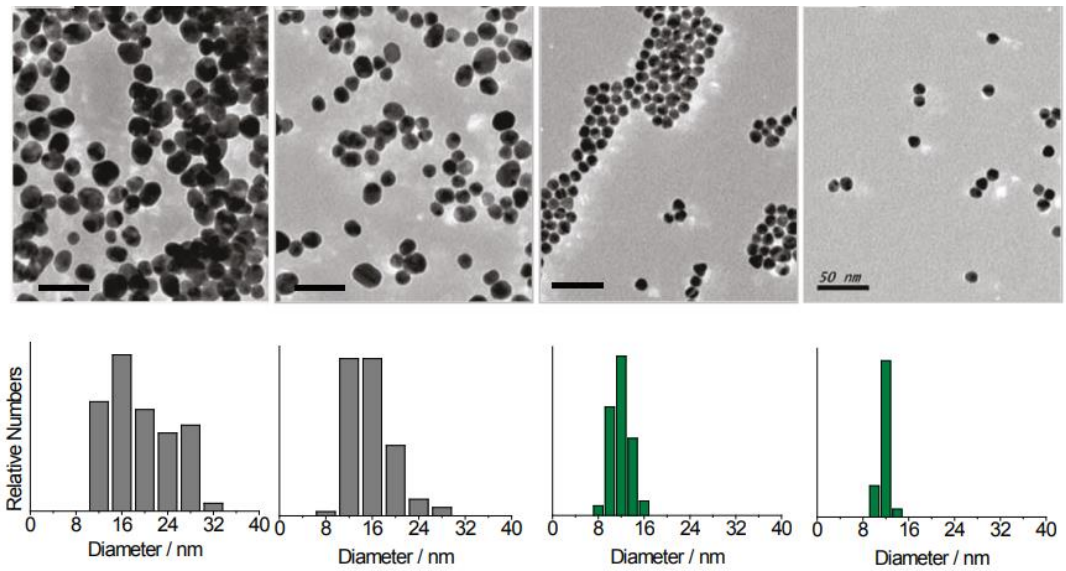

Figure 1.3: The size distributions of different AuNPs calculated by TEM analysis.[22]

Due to these limitations, the border between molecular and nanomaterial chemistry is still not totally clarified nowadays, affecting therefore the control of AuNPs growth at atomic level, which is aimed at perfectly tuning their properties. This “missed ring” in the story of gold chemistry is represented by organized agglomeration of gold atoms, yielding mono-dispersed species still presenting nano-sizes but characterized by a precise stoichiometric formula, and consequently differing from AuNPs which do not present this “molecularity”. These species are called molecular gold nanoclusters (AuNCs).[29]

1.2 MOLECULAR GOLD NANOCLUSTERS: PECULIAR PROPERTIES BETWEEN COMPLEXES AND PARTICLES

As mentioned in the previous paragraph, AuNCs can be defined as agglomeration of gold atoms, generally in different oxidation states; the gold atoms form a precise nano-sized metallic core, stabilized by ligands and characterized by an unambiguous stoichiometric formula.[29–37] Starting from this definition, it is possible to notice that AuNCs present the structure of a single AuNP[38], as reported in **Figure 1.4**, based on a metallic core and ligands stabilizing the surface, but at variance with AuNPs they are molecular species, characterized by a precise molecular formula and well-defined structure, often discrete determined by single crystal X-ray diffraction (SCXRD), such as common organic or inorganic molecules.[39]

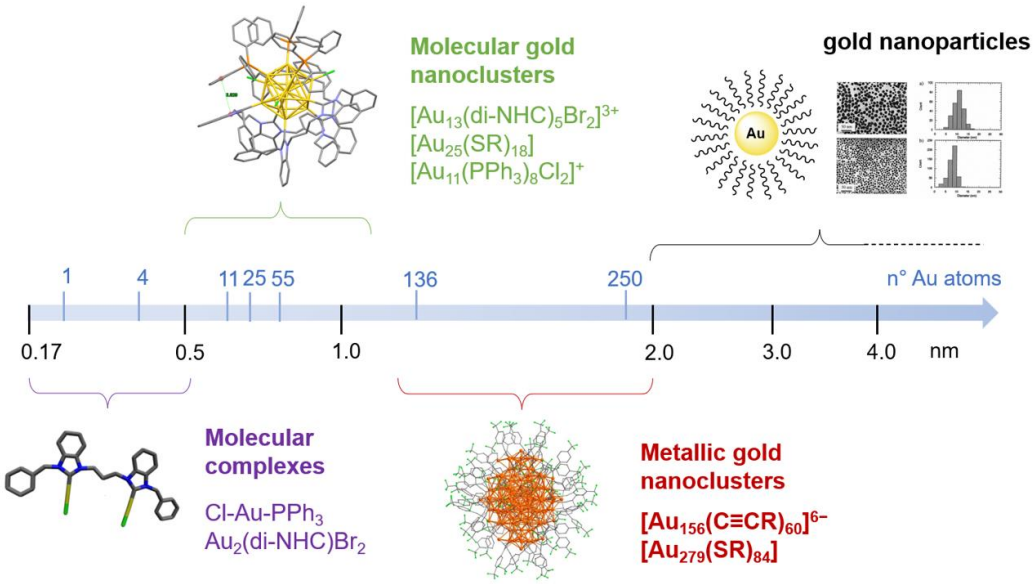

Figure 1.4: Schematic representation of the "gold-line" from molecular gold complexes to AuNPs increasing sizes and number of gold atoms.

Thanks to these “molecularity” it is possible to study these species with common solution techniques, such as NMR spectroscopy[40], high resolution mass spectrometry (HRMS)[41] and cyclic voltammetry (CV).[42] In particular, the latter has been useful to shed light on the boundary between the molecular and metallic

behavior of AuNCs increasing the number of gold atoms. Ramakrishna et al. proved that increasing the AuNCs size, the transition from molecular behavior, characterized by discrete orbital energies, to metallic behavior, characterized by orbital bands, can be observed.[42] Indeed, increasing the number of metallic centers gives rise to a corresponding increase in the number of orbitals in the system, modifying their energies as well. Due to this, the orbital energy levels become more and more close to each other, forming small-conductive bands, like in the AuNPs case. This is clearly observed in the cyclic voltammograms, reported in **Figure 1.5**, of [Au_{25}], [Au_{38}], [Au_{67}], [Au_{102}], [Au_{144}] and [Au_{333}] thiolate-protected clusters. Their HOMO-LUMO band gaps, measured through the energy difference in reduction and oxidation peaks in the voltammograms, decrease by increasing the number of gold atoms in the core. For instance, [Au_{333}] shows an undefined orbital structure due to its size, shown by the disappearance of discrete peaks in the CV, suggesting the formation of conductive bands.

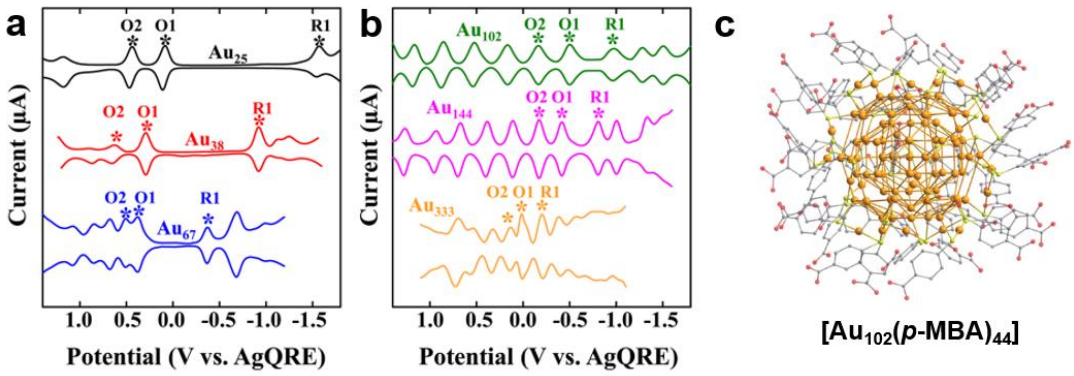

Figure 1.5: cyclic voltammetry analyses of a) small and b) big AuNCs capped by SRs.[42] c) X-ray structure of [Au_{102}] cluster.[43]

Small clusters, counting between Au_3 and Au_{200} atoms, are described as "semiconductor" clusters, characterized by discrete orbital energies. Instead, big clusters with more than 200 gold atoms in the core are defined as metallic clusters (>Au_{200}), since they show metallic behavior, simulating common AuNPs. Thanks to

these features, AuNCs truly represent the border between molecular and metallic behavior of gold, presenting advantages derived from both states. Another important information related with AuNCs is their X-ray structures, since AuNCs can be synthesized as mono-dispersed samples with high purity, affording single crystals indispensable for SCXRD. Thanks to this analysis, the structure-property relationships can be fully clarified, providing information on core-ligands interaction. Exploiting SCXRD, coordination modes of thiolate (SRs), alkynyl, phosphine (PR_3) and N-heterocyclic carbene (NHCs) ligands bound to gold cores can be revealed, showing interesting ligand-core arrangements related to the ligand used. Finally, HRMS is one of the most used techniques in cluster chemistry since it clarifies cluster stoichiometric formulas, providing therefore the first information to define AuNCs as molecular species.

Differing from AuNPs, the cluster molecularity is also related with the rule “each atom count”.[44] When AuNPs are synthesized, a narrow size distribution can be obtained in the sample but it is impossible to isolate a truly mono-dispersed sample with all NPs bearing exactly the same stoichiometry and geometrical features (e.g. size, structural arrangement of metal core and ligand sphere etc.). For this reason, AuNPs are defined as nanomaterials and not molecular compounds. The size distribution not only defines the kind of AuNPs but also their chemical and physical properties. For instance, if two samples of AuNPs are composed by $[Au_{210\text{-}300}]$ and $[Au_{180\text{-}310}]$ particles respectively with narrow size distributions, their properties will be similar since the average size of the NPs are quite similar as well. Instead, the atomic precision of AuNCs makes each gold atom essential to define the cluster properties, since even a variation by a single atom deeply changes their behavior. For instance, $[Au_{10}]^{4+}$ and $[Au_{11}]^{3+}$ cluster cores present totally different properties despite differing by a single Au atom.

To understand this rule, it is essential to define “super atomic” clusters or “super-atom” (SA), species presenting precise combination of atoms forming M_n cores more stable than others.[45] One of the first evidences of these SA clusters has been found in 1984 by Knight et al.[46], when recording the mass spectrum of sodium gas they detected sodium clusters. Na_n clusters presenting n equal to 2, 8, 20, 40 show more intense peaks than other combinations, revealing therefore particular stability in gas phase during the analysis. These n values afford SA clusters and for this reason they are called “magic numbers”. Later on, the same group proposed an explanation of this behavior, calculating the orbital structures of these “magic” clusters assuming a “jellium model”, thus describing each Na^+ as a perfect sphere with uniform distribution of positive charge density. This study shows that the shape of these orbitals recalls the shape of common s, p, d, f orbitals, called in this system “super-orbital” S, P, D, F, and so on. Furthermore, it is possible to complete an electronic shell in the electronic configuration of the SA clusters, providing a rationale for the enhanced stability of these clusters. When n numbers are 2, 8, 20, 40, or other magic numbers, the valence electrons are placed in $1S^2$, $1S^2\ 1P^6$, $1S^2\ 1P^6\ 1D^{10}\ 2S^2$, $1S^2\ 1P^6\ 1D^{10}\ 2S^2\ 1F^{14}\ 2P^6$ closed shell configurations respectively, affording SA clusters.

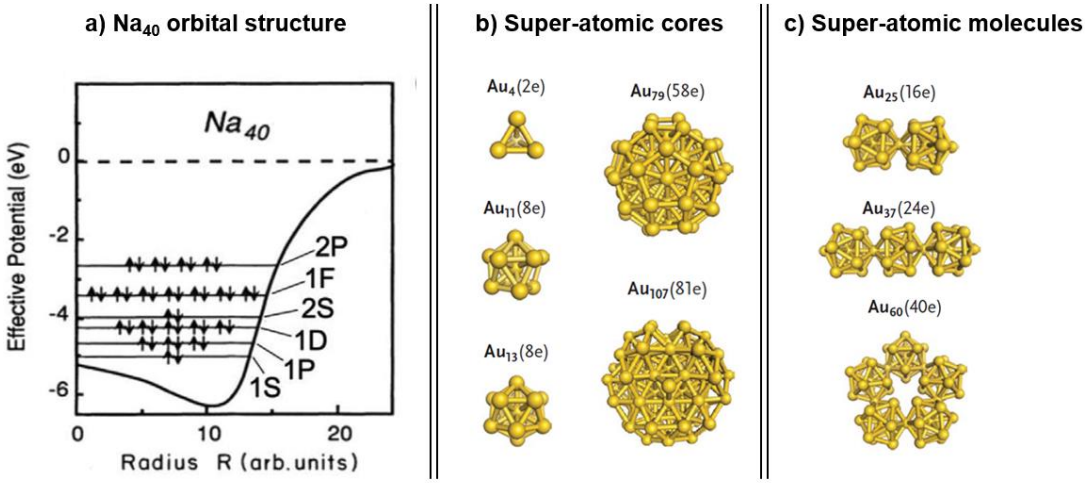

Figure 1.6: a) orbital levels of Na_{40} cluster, b) characteristic SA cores of AuNCs, c) common SA molecules derived from fusion of SA cores.[37,45]

Despite the success of this theory in describing Na clusters, it can be applied only to simple metal centers, such as Na, K, Al, and generally it ignores the geometry of the cluster core, assuming it like a spherical continuum.[45] Fortunately, there are some useful exceptions, since this model can be applied also with coinage metals Au, Ag and Cu, characterized by a single valence electron.[37] This means that metallic cores $[Au_{11}]^{3+}$, $[Au_{13}]^{5+}$, $[Au_{25}]^{9+}$ are SA clusters and in fact these are among the gold clusters cores most frequently reported in the literature, thanks to the stability provided by their super-orbital structures. The jellium model can be also applied to clusters that do not present a spherical symmetry, once opportunely approximated. For instance, $[Au_{25}]^{9+}$ clusters, presenting a rod shape, can be described as sum of two icosahedral $[Au_{13}]^{5+}$ cores sharing an edge, in which one loses an Au(I) cation forming $[Au_{12}]^{4+}$, maintaining therefore the SA feature. [37] In this case, the electronic configuration can be described as 8+8 valence electrons, affording a SA molecule composed by two SA atoms. Thanks to the SA theory, it is easy to understand the reason why AuNCs not presenting SA configuration are generally more reactive. For instance, this theory explains the reactivity of $[Au_{10}]^{4+}$ cluster reported by Crudden et al., bearing 6 valence electrons and not presenting SA stabilization.[47] This cluster tends to rearrange, forming an $[Au_{25}]^{9+}$ cluster presenting instead SA number ensuring enhanced stability due to the gold arrangement. The same reactivity has been not reported for other clusters bearing similar ligands but characterized by $[Au_{11}]^{3+}$ SA cores.[48,49] These Au_{11} clusters are too stable once formed, since stabilized by their closed electronic shell.

From these examples it appears clear that the “each atom counts” rule can be explained by SA theory, since a simple variation by one gold atom directly affects the cluster orbital structure, with consequent variations in stability and chemical behavior.

Finally, this theory explains the stability of clusters presenting distorted cores, too. For instance, the variation of oxidation state of $[PdAu_{24}(SR)_{18}]^{-2}$ to get $[PdAu_{24}(SR)_{18}]^{0}$, provides the distortion of core geometry, with a consequent variation of orbital

structure.[31] The $6e^-$ cluster $[PdAu_{24}(SR)_{18}]^0$ present an oblate structure, which can be interpreted as a distortion of the jellium model, as reported in **Figure 1.7**, allowing a split of P-type super-orbitals, similar to the Jahn-Teller effect described in the chemistry of metallic complexes. This concept is valid also for smaller $[Au_7]^+$ and $[Au_8]^{2+}$ clusters, presenting always six valence electrons and oblate shapes derived by a compression on their z axis. This distortion provides a new orbital rearrangement, in which only P_x, P_y are degenerate at lower energy, explaining the stability of these clusters.[37]

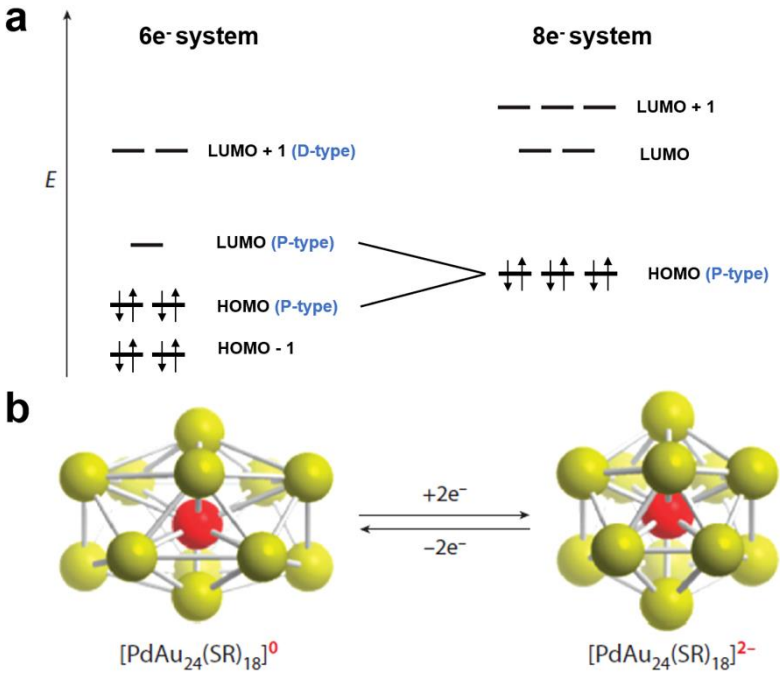

Figure 1.7: distortion of orbital structure related to the change of oxidation state and the consequent variation of core shape of $[PdAu_{24}(SR)_{18}]$ clusters.[31]

The SA theory is an efficient tool to understand the reactivity and the stability of AuNCs. Using the jellium model it is possible to justify the structures of most AuNCs reported in literature.

1.3 SYNTHETIC METHODS TO ISOLATE MOLECULAR GOLD NANOCLUSTERS

Despite the interesting properties related to AuNCs, it is still challenging to control their synthesis. In the literature, different methods are reported to isolate such clusters, generally related to the employed ligand. Indeed, the nature of the ligands represents one of the main parameters influencing cluster chemistry, since upon ligand variation several AuNCs can be isolated, despite not always like mono-dispersed samples. For this reason, a precise atomic control on cluster synthesis is desirable, aiming at getting only one kind of cluster as single product, avoiding therefore complicated separation methods. In the following, the main synthetic methods to get AuNCs are summarized, with some hints regarding the separation methodologies too.

1.3.1 DIRECT REDUCTION AND SIZE ETCHING

The synthesis of AuNCs is dominated by this approach, in which Au(I) or Au(III) complexes are reduced with $NaBH_4$.[50,51] Despite this method being the most used in literature, it is generally difficult to control, since it depends on a series of parameters not fully rationalized. For instance, starting from the same complex but changing the rate of stirring, the rate of addition of $NaBH_4$ or the kind of atmosphere in the reaction apparatus, different clusters can be obtained.[51] This method works well with all ligands exploited so far to cap AuNCs and, despite the difficulties to rationalize it, allows to obtain clusters with different nuclearities too. The isolation of AuNCs presenting different gold cores but same ligand shell is important to compare similar clusters and to shed light on their different properties, such as the appearance of metallic behavior upon increasing the core size explained before.

The direct reduction approach has been partially rationalized in the case of SR-stabilized cluster, due to the studies conducted in the past decades on AuNPs capped

by the same ligands.[52] The reduction to get SR-protected AuNCs starts from $HAuCl_4$ or $HAuBr_4$ precursors and protonated thiolate ligands in solution. In these syntheses, the Au(III):SR molecular ratio needs to be carefully chosen, since it leads the first step in this reduction. Indeed, the mechanism of formation of these AuNCs involves firstly a reduction of Au(III) to Au(I) with concomitant oxidation of HSR in solution, affording a first polymeric species $[Au(SR)]_n$, in which gold presents oxidation state +1. Subsequently, $NaBH_4$ is added, leading to a second reduction step and affording the desired mixture of clusters as poly-dispersed sample. The control of these two steps of reaction, reported in **Figure 1.8**, is the key to perform AuNCs synthesis with atomic precision, therefore controlling the reduction pathway aiming at getting one single clusters.

One of the first to perform this uncontrolled reduction has been Whetten's group in 1998.[53] Using glutathione (GSH) as thiol, they reported the synthesis and separation of the first $[Au_{25}(GS)_{18}]$ cluster. It is important to highlight that in this experiment the reduction provides a mixture of AuNCs, without the atomic control cited above. To isolate $[Au_{25}(GS)_{18}]$ cluster, electrophoresis (PAGE) needs to be performed, despite the low purity of the final sample. Other methods of separation, such as HPLC[54], solvent extraction[55] or size-selective precipitation[56], are currently used to isolate $[Au_{25}(SR)_{18}]$ clusters capped by other SRs, suggesting the stability of this stoichiometric rearrangement.

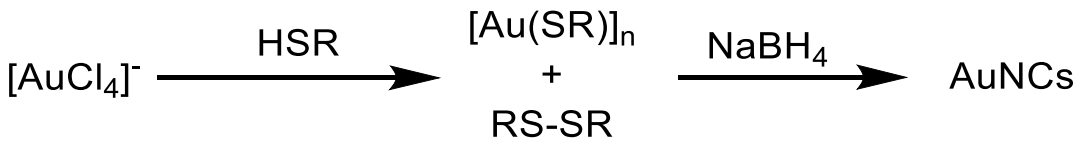

Figure 1.8: Schematic representation of direct reduction synthesis of SR-capped AuNCs.

Later, a more precise PAGE separation of the mixture obtained from Whetten's method has been performed by Tsukuda's and Negishi's groups.[57,58] In their work, they reported clearer HRMS spectra of the different fractions derived from PAGE separation, demonstrating that it is possible to isolate AuNCs with high purity using modern separation techniques. However, the separation of these mixtures is complicated to perform, since it involves a series of PAGE or HPLC apparatuses combined in series. Consequently, continuing efforts targeted the achievement of atomic control on these syntheses, rather than troublesome cluster purification from mixtures. Jin et al. achieved this purpose in 2008, reporting for the first time the focused synthesis of a $[Au_{25}(GS)_{18}]$ cluster.[59] By operating under kinetic control by optimizing temperature and stirring rate, they were able to control the size of the intermediate $[Au(SR)]_n$ oligomers and their subsequent evolution into the desired $[Au_{25}]$ in the second reduction step led by $NaBH_4$. This kinetic control was also applied in the synthesis of other AuNCs, such as $[Au_{25}]$ [60] and $[Au_{20}]$ [61] capped by 2-phenylethanethiolate. However, it is not trivial perform this kinetic control to get all SR-stabilized AuNCs reported in literature.

To overcome this limitation, chemical etching can be used to promote a size focusing process on poly-dispersed samples of AuNCs.

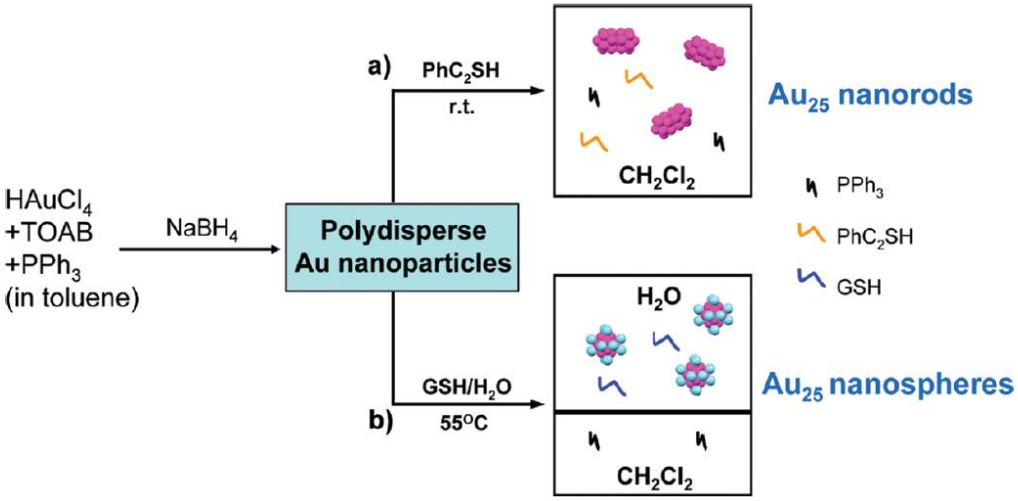

Figure 1.9: Schematic representation of synthesis of SR-capped AuNCs through etching process led by SRs ligands.[62]

During 2009, it has been proved that starting from a mixture of PPh_3-capped small AuNPs and adding GSH or 2-phenylethanethiol, $[Au_{25}(SR)_{18}]$ with rod or sphere shapes, respectively, can be isolated, as reported in **Figure 1.9**.[62] Tsukuda et al. proved that formation of $[Au_{38}]$ and $[Au_{144}]$ clusters[63] can be also obtained by adding, during the second reduction step, several alkyl thiols as etching agents, strongly decreasing the number of AuNCs in solution.

There are several examples of clusters obtained through the direct reduction approach upon kinetic control or through etching processes[64–66], but despite these optimized methodologies are useful to get the desired atomic precision, it is not generally possible to completely focus the final mixture, making the separations methods still fundamental in the isolation of SR-capped AuNCs with high purity.

Regarding other kinds of ligand, such as alkynyl, PR_3 or NHCs, the direct reduction approach seems to be more efficient to get directly mono-dispersed AuNCs. At variance with SR-stabilized clusters, Au(I) complexes with the target ligands are used as precursor, such as $[Au(C{\equiv}CR)]_n$ or [X-Au-L] (L: PR_3 or NHC, X: anionic ligand), and their reduction provides mono-dispersed cluster samples, therefore avoiding the

complicated separation methods cited above. Despite these important advantages, there are limited information in literature regarding the mechanism of reduction of these Au precursors, affecting the atomic control of these reactions. These syntheses are reported **in Figure 1.10.**

Depending on the studied case, it is possible to add during the reduction free ligands or dopants too, therefore changing the final product by modifying the reaction stoichiometry or starting mixture composition. For instance, complexes with formula $[Au(C{\equiv}CR)]_n$ can be directly used as precursors to get alkynyl-capped clusters.[67,68] However, it is possible to exploit alkynes and $[Cl\text{-}Au\text{-}SMe_2]$ as precursors too. In this case, $NaBH_4$ is still used as reducing agent but also acts as base to deprotonate the alkyne, affording active ligands to cap the gold core and making the synthesis more tunable than in the previous case.[69–71] In the literature, pure alkynyl-capped gold clusters obtained with the direct reduction approach are still rare, since generally these are synthesized in combination with other ligands, such as phosphines or NHCs[36]; this topic will be discussed in **Paragraph 1.4.2**.

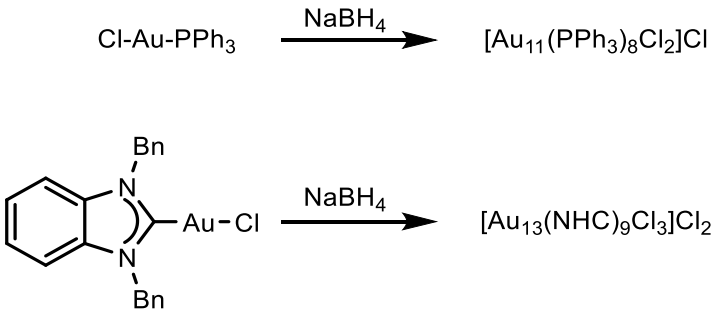

Figure 1.10: Schematic synthesis of PR_3 and NHC-stabilized AuNCs.

Regarding AuNCs capped by PR_3, starting from the synthesis of $[Au_{11}(PPh_3)(SCN)_3]$ in 1969[72] plenty of AuNCs have been synthesized using direct reduction.[50] The control of these reactions is mainly achieved exploiting different conditions and/or PR_3 used. It is known that using $[X\text{-}Au\text{-}PR_3]$ as starting complex, where X is a coordinating anion (Cl^-, CN^-, SCN^-, …), clusters with formula $[Au_{11}(PR_3)_7X_3]$ or $[Au_{11}(PR_3)_8X_2]^+$ can

be isolated.[72] Instead, when X is a noncoordinating anion (NO_3^-, PF_6^-…), the reduction provides $[Au_9(PR_3)_9]^{3+}$ clusters.[73] Also the variation of reducing agent, that it will be discussed with more details in **Paragraph 4.0**, can be used to tune the reaction outcome, affording generally monodispersed products.[74–77] As in the case of SR-stabilized AuNCs, the synthesis of PR_3-stabilized-clusters is affected by the chemical environment too, which may affect the features of the resulting cluster core and/or of the ligand shell. For instance, starting from [Cl-Au-PPh_3] and performing the reduction in EtOH/DCM using 0.25 eq. of $NaBH_4$ allows the isolation of $[Au_{11}(PPh_3)_8Cl_2]^+$ as single product. If the same reaction is performed in THF and using 5 eq. of $NaBH_4$ the final product will be $[Au_{11}(PPh_3)_7Cl_3]$.[78] Another methodology to get PPh_3-capped clusters as monodispersed samples, such as $[Au_{20}(PPh_3)_8]^{2+}$ or $[Au_{101}(PPh_3)_{21}Cl_5]$ clusters, is to use biphasic reduction, in which $NaBH_4$ is dissolved in a polar solvent immiscible with the one in which the gold precursor is dissolved, so that the reduction takes place at the liquid-liquid interface.[79–81]. Furthermore, also the ligand properties are tools to control AuNCs synthesis. For instance, di-phosphine (di-PR_3) or poly-phosphine ligands are good alternatives to mono-PR_3, since their chelating properties help to isolate cluster not easily stabilized with mono-dentate PR_3, such as $[Au_{22}]^0$, $[Au_{13}]^{5+}$ or $[Au_7]^{4+}$ clusters.[82–85] In particular, it is interesting the work reported by Bertino et al., in which increasing the length of the alkyl chains between PR_2 units in di-PR_2 ligands, a decrease of the core size can be achieved, but leading also to a partial decrease of the mono-dispersity of the sample.[86]

Despite the direct reduction synthesis of PR_3-capped AuNCs apparently does not involve an etching process, some mechanistic investigations suggest that PR_3 can act not only as ligands but as etching agent too.[87,88] Indeed, fast reduction generally provides formation of poly-dispersed mixtures of clusters. However, the resulting cluster mixture may undergo a subsequent etching process provided by free PR_3 in solution, in which extraction of $[Au(PR_3)]^+$ or $[Au(PR_3)_2]^+$ from the cluster cores can be

observed, affording the final mono-dispersed samples. Thanks to these studies, it is evident that an etching process helps the size-focusing of PR_3-capped clusters during or after the reduction. As well as in the case of SR-stabilized AuNCs, also with PR_3 clusters external etching agents can be used, such as HCl[82], NH_3[89] or SRs[62] to produce the size focusing.

Mono- and di-NHC capped AuNCs have been synthetized with direct reduction too. These reactions will be discussed in detail in **Paragraph 2.0**, but these are similarities with the synthesis of PR_3-capped clusters, since NHCs and PR_3 ligands show similar properties.

Generally, their synthesis starts from Au(I) complexes with formula [(NHC)-Au-X] or [(di-NHC)Au_2X_2], in which X are halides. When these complexes are reduced with $NaBH_4$, mono-dispersed sample of AuNCs can be isolated. So far, it is possible to tune the reaction product only changing the starting NHC or the anionic ligand, forming $[Au_{10}]^{4+}$, $[Au_{11}]^{3+}$, $[Au_{13}]^{5+}$, $[Au_{24}]^{8+}$ and $[Au_{25}]^{9+}$ clusters.[49,90–100] In some cases, a mixture of AuNCs is obtained, but also here an etching process can be used to focus the mixture after the reduction, providing the desired mono-dispersed product.[90,92]

It is important to underline that the direct reduction approach is useful also to get alloy clusters, species presenting heterometallic centers in the cores, like Cu, Ag, Pt or Pd.[101] The co-reduction of gold precursor in the presence of heterometallic complexes provides directly doped AuNCs.[36] However, the synthesis of alloy-clusters through direct reduction remains still empirical, since it is not simple to study the AuNCs mechanism of growth when other metal centers are involved in the process.

1.3.2 CLUSTER REACTION WITH METALLIC COMPLEXES OR FREE LIGANDS

Another synthetic method to get AuNCs is to exploit their reactivity towards ligands and/or metallic complexes. These reactions change in relation to the kind of cluster used as starting reagent. In the case of SRs-stabilized AuNCs, we have already explained how etching processes focus poly-dispersed mixtures of clusters, providing a mono-dispersed product. In the direct reduction approach, the thiolates employed in the etching step are also used in the starting mixture as capping ligands. Instead, when the etching agent differs from the starting thiolate, the process is called “ligand exchange” since the final product is (co)stabilized by the “etching” ligand.[102] This exchange can be used when a single cluster is exploited as starting reagent too. In this latter case the first reduction provides a metastable cluster, enough stable to be isolated and characterized, but still enough reactive to undergo further reactions. Despite several SR-capped clusters show this reactivity[102], one of the most interesting examples has been reported by Zheng et al.[103], in which a $[Au_{38}(SC_2H_4Ph)_{24}]$ rod cluster undergoes ligand exchange reaction upon 4-*tert*-butylbenzenethiol (SPh-*t*Bu) addition, affording tetrahedral $[Au_{36}(SPh\text{-}tBu)_{24}]$. This group studied the reaction mechanism, reported in **Figure 1.11**, using both mass spectrometry and UV-Vis spectroscopy, identifying several steps of evolution.

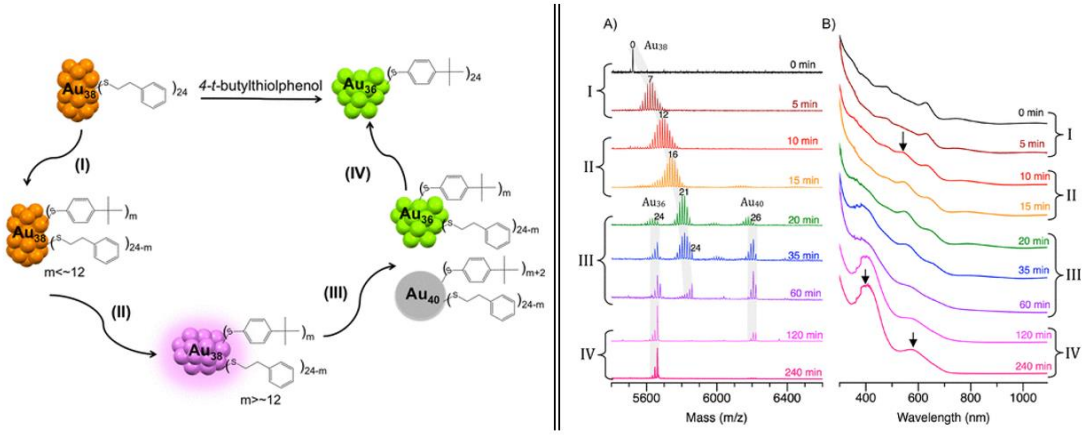

Figure 1.11: Left) mechanism proposed by Zheng et al. for the ligand exchange reaction promotes by thiolate ligands. Right) Mass and UV-Vis spectra of the reaction steps involved in this reaction.[103]

In this mechanism a "disproportionation" step is proposed, in which $[Au_{38}(SC_2H_4Ph)_{24}]$ cluster forms $[Au_{40}(SPh\text{-}tBu)_{m+2}(SC_2H_4Ph)_{24-m}]$ and $[Au_{36}(SPh\text{-}tBu)_{24}]$. The Au_{36} cluster represents the final product and Au_{40} likely undergoes an additional size focusing process, losing two [Au(SR)] fragments.

A similar reaction has been reported by Teranishi et al., in which a $[Au_{11}(PPh_3)_8Cl_2]^+$ cluster reacts with GSH forming a $[Au_{25}(GS)_{18}]$, cluster completely capped by thiolate ligands.[104] Notably, PR_3-stabilized clusters are often building blocks used in this kind of reactions. Mingos et al. reported a series of clusters obtained through complex addition and ligand exchange reactions from $[Au_{11}(PR_3)_{10}]^{3+}$ clusters.[77] Using 4 eq. of $[Cl\text{-}M\text{-}PR_3]$ complexes, where M is Au, Cu or Ag, $[Au_9M_4(PR_3)_8Cl_4]^+$ can be isolated, therefore forming new SA and doped AuNCs. This "complex addition" has been also used by Wang's group[106], in which the conversion $[Au_9(R/S\text{-}BINAP')_4]^{3+}$→$[Au_{10}(R/S\text{-}BINAP')_4(C{\equiv}CR)]^{3+}$ (BINAP': 2,2′-bis(diphenylphosphino)-1,1′-binaphthyl) can be achieved exploiting an excess of $[Au(C{\equiv}CR)]_n$ complex. Furthermore this process can be also inverted, using free BINAP ligand, providing again $[Au_9]^{3+}$ core. Another classic cluster to get this reactivity is $[Au_9(PPh_3)_8]^+$ since the metallic core presents an unsaturated Au center, making this AuNC particularly reactive.[107,108] For instance, this

can form $[Au_6(dddp)_4]^{2+}$ using 1,3-bis(diphenylphosphino)propane (dddp) ligand etching.[109] Moreover, $[Au_6(dddp)_4]^{2+}$ can undergo other reactions, forming $[Au_8(dddp)_4Cl_2]^{2+}$ upon reaction with [Cl-Au-PPh_3] [110] or $[Au_7(dddp)_4]^{3+}$ upon reaction with $AgBF_4$.[84] This series of reactions is displayed in **Figure 1.12**.

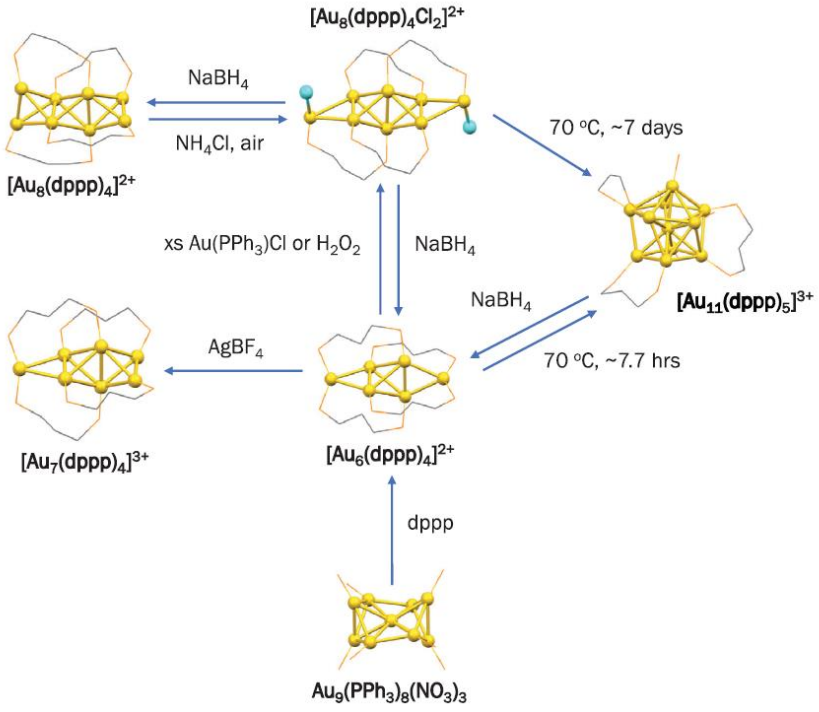

Figure 1.12: series of AuNCs achieved through metal complex addition, ligand exchange or cluster to cluster evolution.[50]

Starting from another phosphine-stabilized $[Au_{13}(dppe)_5Cl_2]^{3+}$, where dppe is 1,3-bis(diphenylphosphino)ethane, Konishi's group has been able to produce the same cluster core but stabilized by phenylacetylenyl, exchanging therefore the starting chloride ligands on the core with alkynyl ligands.[111]

Finally, one of the most characteristic examples of this reactivity is the $[HAu_9(PPh_3)_8]^{2+}$ cluster. This hydride-stabilized cluster can indeed form SA $[Au_{13}]^{5+}$ clusters reacting with a [Cl-Au-THT] (THT: tetrahydrothiophene) complex. Similar reactions can be obtained when $[HPdAu_8(PPh_3)_8]^{2+}$ or $[HPtAu_8(PPh_3)_8]^{2+}$ react with $[Au(SR)]_n$ or $[Au(C{\equiv}CR)]_n$ oligomers, leading the formation of $[MAu_{24}]$ clusters.[112]

Furthermore, $[HMAu_8(PPh_3)_8]^{2+}$ can undergo a fusion reaction with $[M'Au_{24}(SR)_{18}]^-$ clusters, forming a $[MM'Au_{36}(SR)_{24}]$ cluster, *i.e.* completely losing its phosphine ligands in the final product.[113]

More recently, this reaction has been used also by Crudden et al. to synthesize the first NHC-stabilized gold clusters.[114] In this work, $[Au_{11}(PPh_3)_8Cl_2]^+$ undergoes a ligand exchange reaction in the presence of free NHCs, formed *in situ*, affording a series of $[Au_{11}(PPh_3)_{8-n}(NHC)_nCl_2]^+$ clusters as poly-dispersed mixture. Despite the novelty of this discovery, this process is selective only with one of the employed NHCs, making ligand exchange difficult to control in case of free NHCs.

1.3.3 CLUSTER TO CLUSTER EVOLUTION

The "cluster to cluster" reactivity represents another interesting tool to get new AuNCs, despite it is one of the less used synthetic approaches. To exploit this, a starting meta-stable cluster needs to be isolated, which should be stable enough to be purified but still reactive to provide subsequent evolution, without using an external chemical trigger. Since this necessary balance between stability and reactivity, it is not surprising that this synthetic approach is not popular in cluster chemistry. Nevertheless, some interesting clusters have been obtained with it.

Maran's group demonstrated that $[Au_{38}(SR)_{24}]$ clusters can be obtained by fusion of $[Au_{25}(SR)_{18}]$ clusters. Despite the obtained cluster was previously known in literature, it is interesting to notice that after several days at 65°C the formation of $[Au_{38}(SR)_{24}]$ is complete, proving that there is still interesting chemistry to be disclosed with well-known clusters, too.[115]

Recently a cluster evolution $[Au_{10}(NHC)_6X_3]^+ \rightarrow [Au_{25}(NHC)_{10}X_7]^{2+}$, where X are Cl or Br, has been observed by Crudden et al.[116], as reported in **Figure 1.13**.The starting $[Au_{10}]^{4+}$ bears 6 valence electrons, therefore it does not present SA feature. Consequently, $[Au_{10}]^{4+}$ is thermodynamically unfavored compared with the more

stable $[Au_{25}]^{9+}$ core, presenting instead SA behavior.[91] This reaction is guided by the halides placed on the $[Au_{10}]^{4+}$ core. These favor the formation of halogen-bridged units, essential to stabilize rod-shape $[Au_{25}]^{9+}$ super-molecules. Indeed, in this case two $[Au_{13}]$ icosahedral cores are bridged together through these halides, forming bonds between $[Au_{13}]$ cores and stabilizing the rod structure. If chlorides are present in the starting complex, the reduction allows the isolation of $[Au_{10}]^{4+}$ core but not its evolution into $[Au_{25}]^{9+}$, since chlorides are too small to form bridged bonds. At the contrary, if iodides are present in the starting complex the reduction provides directly $[Au_{25}]^{9+}$, since the sizes of these anions favor the formation of bridged bonds.

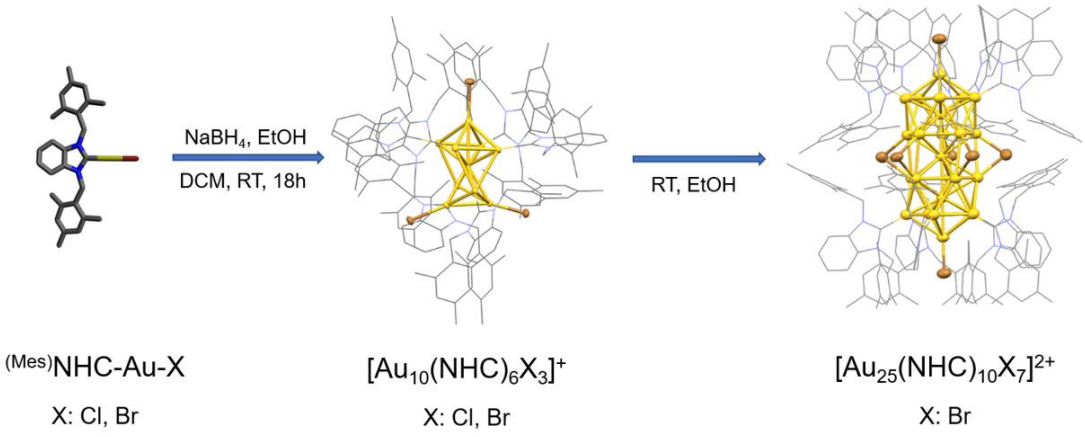

Figure 1.13: Synthesis of $[Au_{10}]^{4+}$ clusters and their evolution into $[Au_{25}]^{9+}$ reported by Crudden et al.[116]

A similar behavior is reported also with $[Au_6(dppp)_4]^{2+}$ and $[Au_8(dppp)_4Cl_2]^{2+}$ clusters. When these are warmed at 70°C in solution of EtOH for several days, it is possible to get the corresponding $[Au_{11}(dppp)_4Cl_2]^{+}$ clusters, more stable than the previous ones given their SA structure.[117]

Finally, in the case of alkynyl-stabilized AuNCs, only one example of this reactivity has been reported. $[Au_{28}(C{\equiv}CR)_{12}(THT)_8]^{3+}$ forms spontaneously $[Au_{23}(C{\equiv}CR)_9(THT)_6]^{2+}$ when dissolved in MeOH.[118] DFT calculations justify this evolution with the SA feature

of $[Au_{23}]^{11+}$ cluster, since this cluster shows a splitting of 1D super-orbitals, derived from the distortion of the core, which results in a closed shell electronic configuration.

1.4 LIGAND DESIGN TO TUNE CLUSTER PROPERTIES

In AuNCs chemistry, ligands are powerful tools to control the formation of AuNCs, since these are not stable without the protection of the coordination sphere, making ligands fundamental to isolate these unstable molecular species.[119] It is possible to study the cluster structures thanks to SCXRD, therefore understanding how such ligands interact with the core and how these tune AuNCs properties. Furthermore, the study on cluster coordination sphere affords important clues regarding ligand-surface interactions present in nanoparticle systems too, making AuNCs essential to better understand AuNPs chemistry.

Depending on ligand coordination modes, it is possible to get a great variability of cluster cores and coordination spheres. For instance, exploiting PR_3 and NHCs as capping agents, only on-top coordination with cluster core can be achieved. These ligands indeed present a single electronic doublet, forming consequently only σ-coordination bonds, perpendicular with cluster core, which limits the number of clusters synthesizable with these ligands.[34] On the contrary, SRs, alkynyls, halogens and hydrides are species forming bridged bonds too, affording consequently a broader series of structures. The different coordination modes related to ligands on cluster surface are reported in **Figure 1.14**.

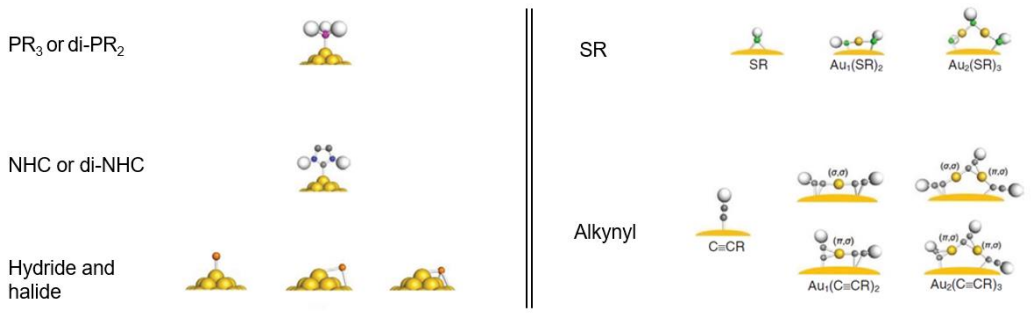

Figure 1.14: Ligand coordination modes in cluster chemistry. Color code: yellow (Au), magenta (P), blue (N), grey (C), green (S), orange (halogens and hydrides).[37]

Furthermore, different ligand types can be used together, forming mixed coordination spheres generally obtained directly from the synthesis. For instance, in the reduction of [Cl-Au-PPh_3], both Cl^- and PPh_3 cap the formed metallic core, affording $[Au_{11}(PPh_3)_8Cl_2]^+$ as unique product. Only by first removing chloride from the Au(I) precursor, reducing therefore $[Au(PPh_3)](NO_3)$, it is possible to get $[Au_9(PPh_3)_8]^+$.[50] In some cases, the reduction performed by $NaBH_4$ provides hydrides acting as reducing agents and capping ligands.[32] A remarkable example of this, it is the synthesis of $[Au_{24}(NHC)_{14}Cl_2H_3]^{3+}$ performed by Crudden et al., in which two icosahedron-based $[Au_{12}]$ cores joined together through a triangular face, with hydrides bridging these units, as proved by SCXRD and DFT calculation. Furthermore, exploiting $NaBD_4$ for the reduction, $[Au_{24}(NHC)_{14}Cl_2D_3]^{3+}$ can be isolated, proving how these hydrides derived from the reducing agent.[96]

Ligands and their different properties directly affect AuNCs synthesis, making them active protagonists in the assembling of gold cores. In this paragraph, the most studied ligands exploited to cap AuNCs will be discussed, focusing on the different interactions and coordination modes of these, with some hints regarding the correlation ligand-reactivity.

1.4.1 THIOLATES: ORGANOMETALLIC STAPLES PROTECTING CLUSTER CORES

The most common ligands exploited in cluster chemistry are thiolates.[33,35,102] Forming complicate motif of $[Au(SR)]_n$ units, these ligands can indeed stabilize cluster cores, allowing formation of several cluster geometries. In their electronic structure, SRs present three lone pairs favoring the formation of these organometallic staples. One of most common staple is [(SR)-Au-(SR)-Au-(SR)], in which two terminal thiolates bind the core and the central SR binds Au(SR) units, closing this chelating staple. Furthermore, also simpler motifs have been reported, like on-top coordination, where a single SR interacts directly with the gold core[120], or $[Au(SR)_2]$, a chelating staple similar to $[Au_2(SR)_3]$ but without the central SR. These different coordination modes guarantee stability also to unstable clusters, generally not isolable exploiting PR_3 or NHCs as single capping agents.[121]

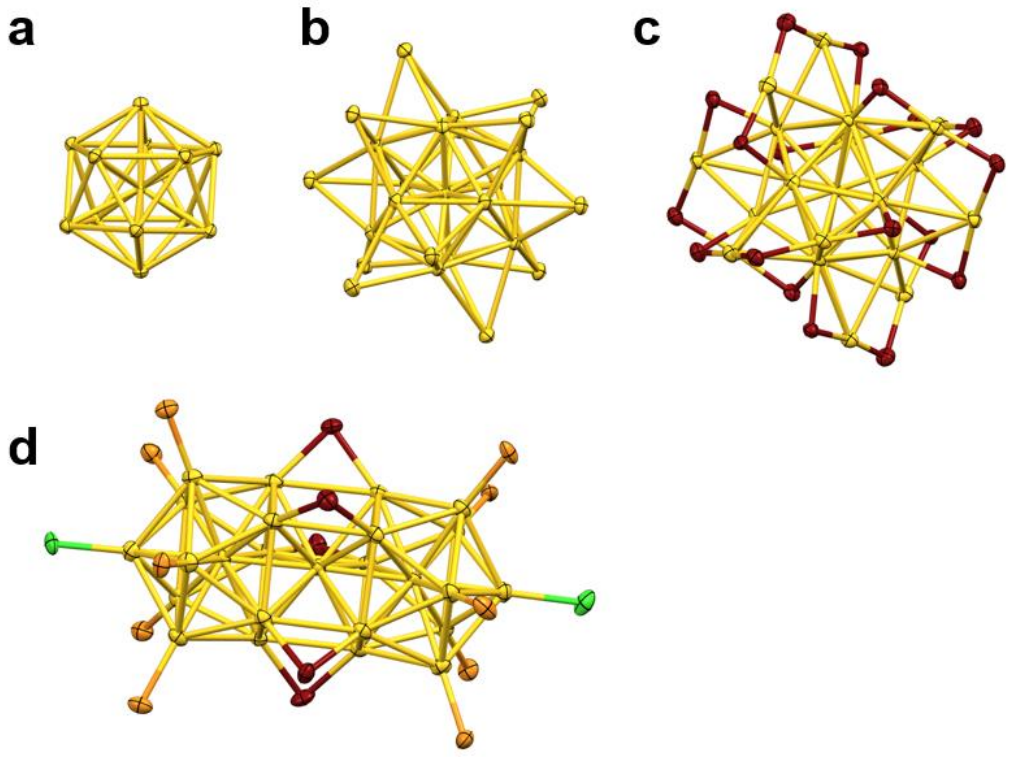

Figure 1.15: X-ray structure of $[Au_{25}(SG)_{18}]$, in which a) is $[Au_{13}]$ icosahedral core, b) is the metallic core surrounded by 12 Au, c) is the $[Au_{25}(SG)_{18}]$ complete structure, including $[Au_2(SG)_3]$ motifs and d) is the X-ray structure of $[Au_{25}(SG)_{10}(PPh_3)_{10}Cl_2]$. Color code: green (Cl), orange (P), red (S), yellow (Au).

The first evidence of these staples arrived in 2008, when Jin et al. reported the X-ray structure of $[Au_{25}(GS)_{18}]$, reported in **Figure 1.15 c**.[122] $[Au_{25}(GS)_{18}]$ structure can be disassembled in the central core, formally considered $[Au_{13}]^{6+}$ and presenting 7 valence electrons, stabilized by 6 $[Au_2(GS)_3]^-$ units guaranteeing the neutrality of the final structure. Since its electronic count does not fit with the "magic-number rule", this SR-capped cluster is not SA but despite this the net of organometallic motifs stabilizes the core, proving that $[Au_2(SR)_3]$ staples are able to protect unstable species. Furthermore, $[Au_{25}(GS)_{18}]$ structure is completely different to $[Au_{25}(PPh_3)_{10}(GS)_5Cl_2]$, reported in **Figure 1.15 d**, in which SRs bind two $[Au_{13}]$ icosahedral units, forming bridged bonds and stabilizing its rod shape.[123]

Considering the different way that these ligands can use to cap AuNCs, it is clear that SRs are very tunable ligands, since they can adapt themselves in relation to AuNC geometry. In fact, SRs are essential to isolate "metallic" clusters, *i.e.* AuNCs large enough to mimic AuNPs behavior.[121]

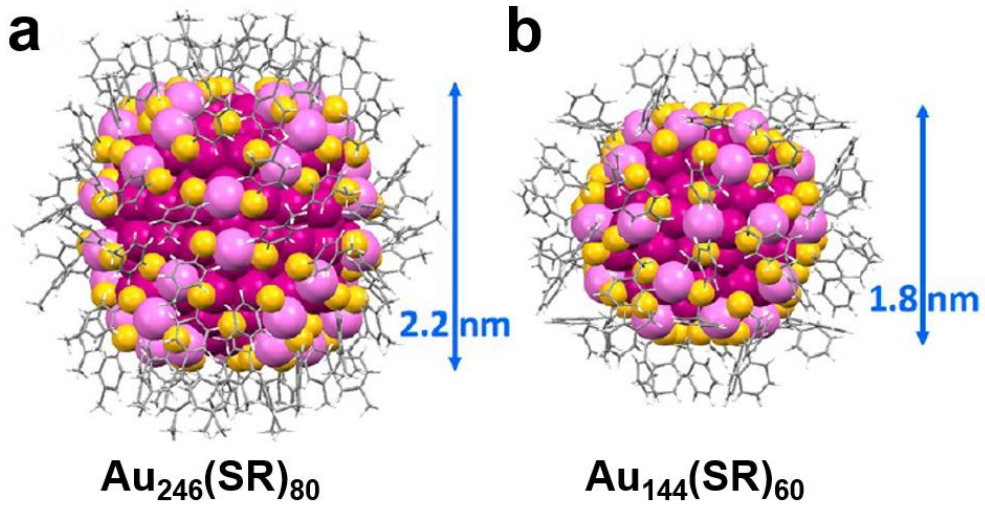

Figure 1.16: X-ray structures of a) $[Au_{246}(SR)_{80}]$ and b) $[Au_{144}(SR)_{60}]$. Color code: magenta/pink (Au), yellow (S), grey (C).[121]

Indeed, staples of $[Au_2(SR)_3]$ have been found also in $[Au_{102}]$, $[Au_{144}]$ and $[Au_{246}]$ clusters[124–126], reported in **Figure 1.16**, demonstrating how SRs present the same coordination modes also in quasi-nanoparticle structures[124], highlighting once more how cluster chemistry can shed light on AuNPs structure too.

From these examples, it appears clear that X-ray diffractometry represents the most direct analysis to understand these gold species. For instance, $[Au_{25}(PPh_3)_{10}(GS)_5Cl_2]$ and $[Au_{25}(GS)_{18}]$ apparently present the same gold cores, since the similarities in their stochiometric formulas detected by HRMS. Only using SCXRD their real core geometries are revealed, showing that they are completely different and demonstrating that the use of mixed coordination spheres can afford unexpected results. Other remarkable examples of this behavior are the syntheses of PR_3-capped clusters. The bigger cluster completely stabilized by PR_3 is $[Au_{22}]$ [83,85], despite using halogens as co-capping agent it is possible to get $[Au_{110}]^{5+}$, considerably expanding therefore the obtainable cluster size.[81]

The organometallic motifs related to SR-stabilized AuNCs present other important advantages. Considering always $[Au_{25}(SR)_{18}]$, its staples allow to get reversable redox processes on cluster core. Both chemical and electrochemical redox processes can be exploited to oxidize it, affording $[Au_{25}(SR)_{18}]^{+1}$ and $[Au_{25}(SR)_{18}]^{+2}$, or reduce it, providing $[Au_{25}(SR)_{18}]^{-1}$ and $[Au_{25}(SR)_{18}]^{-2}$.[127] As showed in **Paragraph 5.3**, If mono-electronic oxidation is performed on similar $[Au_{13}]^{5+}$ clusters capped by PR_3 and NHC, the obtained $7e^-$ cluster is not enough stable to survive, affording its degradation. The metal-organic framework in SR-capped clusters stabilizes their oxidized or reduced forms, despite the absence of SA features in the resulting products.

These examples highlight how the SR coordination sphere is perfect to ensure stability on the core; however, it presents some important drawbacks too. First, this complicated metal-organic framework is one of the reasons why these clusters are generally obtained as poly-dispersed sample. During the reduction, SRs cap unstable

clusters too, thanks to their different coordination modes, which stops therefore the thermodynamic SA focusing useful to get mono-dispersed samples. This is indeed an advantage for the isolation of meta-stable AuNCs but it also strongly complicates their synthesis since it is difficult to obtain mono-dispersed clusters. Furthermore, when SR-capped clusters are used for catalytical purposes, their activity cannot directly involve the gold core, since this is completely saturated by [Au(SR)] staples, preventing core-substrate interactions.[128] Finally, the structure of SRs presents also an important limitation, since electronic and steric properties of theses ligands can not be independently varied. Indeed, the R group can be modified, but variations of its electronic properties affect its steric features too. For instance, when R is varied from a linear alkyl chain to a phenyl group, both electronic and steric properties change, complicating the ligand design.

1.4.2 ALKYNYL LIGANDS: NEW ORGANOMETALLIC FRAMEWORKS TO INCREASE CLUSTER SIZE

Alkynyl-stabilized AuNCs show structure similar to SR-protected clusters since these ligands form $[Au_x(C{\equiv}CR)_y]_z$ staples, therefore mimic $[Au_2(SR)_3]$ staples described before.[129] $[Au_x(C{\equiv}CR)_y]_z$ frameworks are more complicated, since they do not coordinate the core only through σ-coordination but using also π-interactions derived from the alkynyl triple bond. For instance, the structure of $[Au_{22}(C{\equiv}CR)_{18}]$ reported by Tsukuda et al., can be viewed as bitetrahedral $[Au_7]^{3+}$ core surrounded by one $[Au_6(C{\equiv}CR)_6]$ ring and bridged by three bidentate $[Au_3(C{\equiv}CR)_4]^-$ staples. Thus, $[Au_{22}(C{\equiv}CR)_{18}]$ can be disassembled as $[Au_7][Au_6(C{\equiv}CR)_6][Au_3(C{\equiv}CR)_4]_3$, as displayed in **Figure 1.17**.[68]

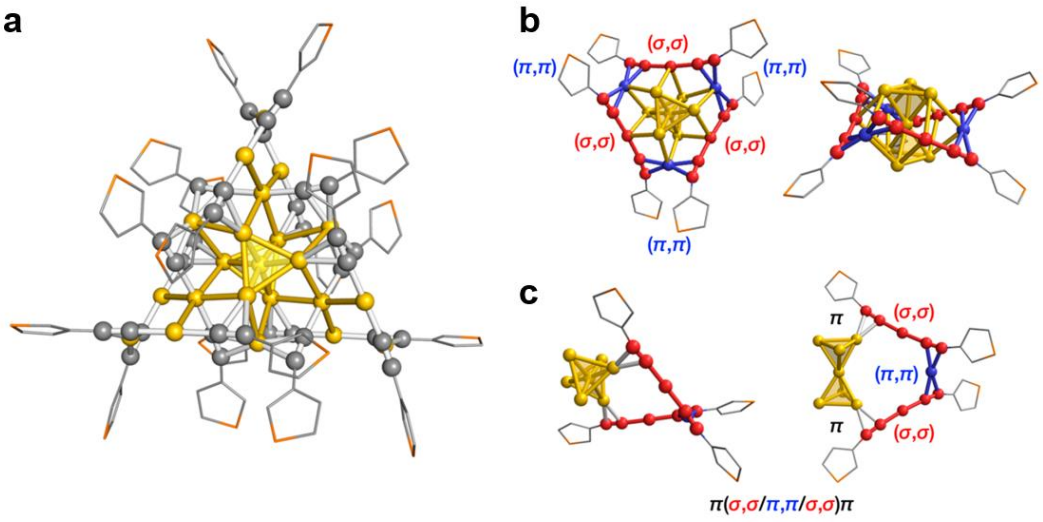

Figure 1.17: a) X-ray structure of $[Au_{22}(C{\equiv}CR)_{18}]$. Schematic illustration of b) $[Au_6(C{\equiv}CR)_6]$ ring and (c) $[Au_3(C{\equiv}CR)_4]^-$ oligomers. Red and blue moieties represent linear R−C≡C−Au−C≡C−R units and π−Au−π bonds, respectively.[68]

Despite these ligands presenting similar advantages of SRs, there are only a small library of homometallic gold clusters completely stabilized by alkynyls.[36] Indeed, alkynyls are usually exploited with other ligands, such as PR_3 or NHCs, forming mixed coordination sphere generally providing clusters with higher nuclearity. Proof of this

are NHC-capped AuNCs, since they are generally small and SA clusters, such as $[Au_{13}]^{5+}$ or $[Au_{11}]^{3+}$, but when the stabilization involves alkynyls too, the cluster-sizes increases. Zheng et al. reported the synthesis of $[Au_{16}(\text{di-NHC})_5(C{\equiv}CR)_3Br_2]^{3+}$, a new SA cluster presenting novel coordination staples. In its structure, reported in **Figure 1.18**, three staples [(di-NHC)Au(C≡CR)] bind classical $[Au_{13}]^{5+}$ core, chelating it. Furthermore, modifying the stochiometric ratio $[(\text{di-NHC})Au_2Br_2]$:[Au(C≡CR)] during the reduction, $[Au_{17}(\text{di-NHC})_4(C{\equiv}CR)_4Br_4]^{+}$ cluster can be isolated, in which an additional [(di-NHC)Au(C≡CR)] motif anchors the core.[130] In this staple, di-NHCs present one NHC unit binding on core, whereas the other NHC binds an external Au(I) center, binding in turn an alkynyl ligand. This latter presents a π-bond with the core, completing the chelating staple. The core is saturated by remaining di-NHC and Br^- ligands, directly binding the metallic kernel with on-top coordination.

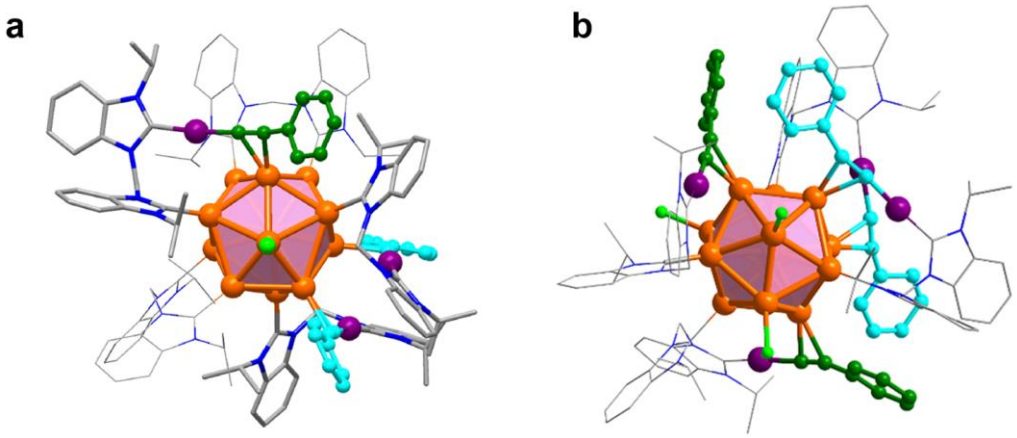

Figure 1.18: X-ray structures of a) $[Au_{16}(NHC)_5(C{\equiv}CR)_3Br_2]^{3+}$and b) $[Au_{17}(NHC)_4(C{\equiv}CR)_4Br_4]^{+}$. [(di-NHC)Au(C≡CR)] staples are highlighted in green and in turquoise. Color legends: orange (Au in the core), violet (Au belonging to staples), light green,(Br), blue (N) and gray(C).[130]

Another example has been reported by Tsukuda et al., in which $[Au_{23}(NHC)_6(C{\equiv}CR)_9]^{2+}$ cluster, presenting an uncommon $[Au_{17}]^{5+}$ core with 12 valence electrons, is stabilized by three $[Au_2(C{\equiv}CR)_3]^-$ samples and six NHCs.[131] This structure recalls the $[Au_{23}(PPh_3)_6(C{\equiv}CR)_9]^{2+}$ structure, in which NHCs are substituted by PPh_3.[132] Finally, another important NHC/alkynyl-capped AuNCs is

$[Au_{44}(NHC)_9(C{\equiv}CR)_6Br_8]$, the bigger cluster capped by NHCs reported so far, demonstrating again that these variegated coordination spheres can provide unexpected results.[133] In this latter case there are not NHC/alkynyl staples, since NHCs present simple on-top coordination, instead alkynyls show classical $[Au_3(C{\equiv}CR)_2]^-$ staples chelating the metallic $[Au_{29}]$ kernel. Since their similarities with NHCs, PR_3 or di-PR_2 ligands can provide higher cluster nuclearity when mixed with alkynyls. Some examples are $[Au_{19}(di\text{-}PR_2)_4(C{\equiv}CR)Cl_4]$, $[Au_{24}(C{\equiv}CR)_{14}(PPh_3)_4]^{2+}$ and $[Au_{40}(C{\equiv}CR)_{20}(di\text{-}PR_2)_4]^{4+}$ clusters.[134–136] Furthermore, also simple σ-coordination can be observed for alkynyl ligands. One example are the two alkynyls in $[Au_{11}(BINAP)_4(C{\equiv}CR)_2]^+$ structure, presenting simple σ-bonds with 2 gold atoms, demonstrating again that these ligands adapt their coordination as well as SRs.[134]

Finally, it is important to point out that also alkynyls can not vary independently their steric and electronic properties, since both depend on R groups, representing therefore an important limit of these ligands.

1.4.3. PR_3: PROTECTED BUT REACTIVE CLUSTERS

Phosphines are the oldest ligands used to cap molecular clusters. The first X-ray structure of AuNCs has been reported in 1969, regarding $[Au_{11}(PPh_3)_7(SCN)_3]$ cluster[72,137], in which for the first time the stabilization of a molecular cluster has been observed, shedding light on core-PR_3 coordination. These ligands deeply differ from alkynyls or thiolates, since they form simple σ-bonds with the gold core, achieving only on-top coordination mode. Indeed, the lone pair of PR_3 can bind one single atom in the core, without formation of organometallic frameworks protecting it, which obviously limits the synthesis of PR_3-capped clusters. For instance, the biggest clusters completely stabilized by di-PR_2 are $[Au_{22}]$ clusters[83,85], but $[Au_{55}]^{6+}$ or $[Au_{101}]^{5+}$ clusters can be obtained when halogens are involved in the protection layer, expanding the core size.[81,138]

The properties of PR_3 can be tuned changing R groups, with important advantages compared to thiolates and alkynyls. Indeed, it is possible to change independently the three R groups in PR_3, allowing a more flexible variation of electronic and steric properties. For instance, Wang et al. reported that varying the length of alkyl bridge in $Ph_2P\text{-}(CH_2)_n\text{-}PPh_2$ different clusters can be isolated, depending on the flexibility of the bridge unit.[86]

Despite PR_3 ligands presenting a lot of advantages compared with ligands reported in previous paragraphs, their corresponding AuNCs are not very stable and generally present higher reactivity. As explained before, SR or alkynyl staples are perfect to protect the core, but they also limit its reactivity. Instead, simpler PR_3 coordination provides reactive clusters due to decreased protection, in which the cluster core/ligand layer can be easier modified. Furthermore, phosphines allow the formation of coordinatively unsaturated cluster too, since PR_3 are generally bulkier ligands than SRs or alkynyls, more efficiently protecting unsaturated centers.

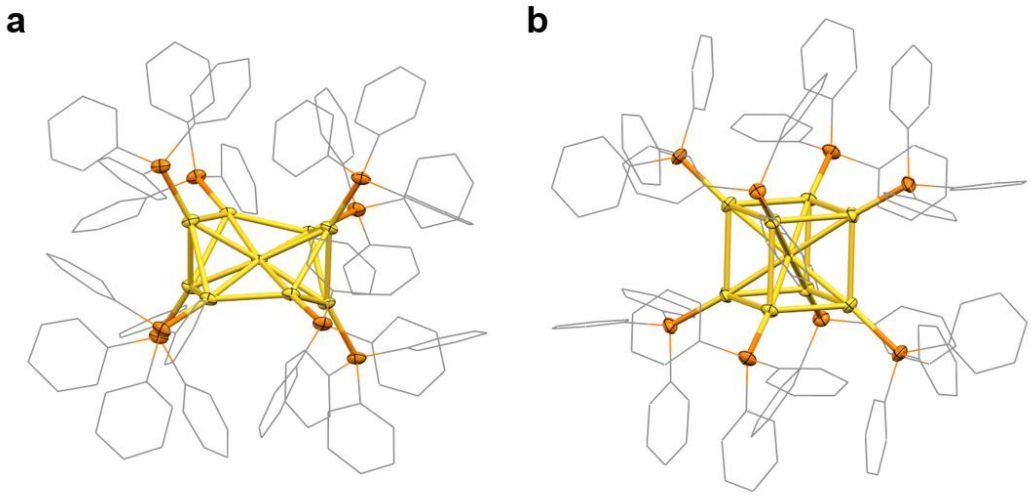

Figure 1.19: structural isomers of $[Au_9(PPh_3)_8]^+$, presenting a) boat-shape and b) cubic geometry. Color code: orange (P), grey (C) and yellow (Au).[139,140]

For instance, it is possible to isolate $[MAu_8(PPh_3)_8]^{4+}$ clusters, in which the central Au, Pd or Pt are unsaturated centers.[113,137,141] The synthesis of unsaturated AuNCs generally is not achievable with SR-capped AuNCs, due to their chelating metal-organic frameworks disfavoring the formation of unsaturated cores. The $[Au_9(PPh_3)_8]^{4+}$ structure, reported in **Figure 1.19 a**, can be viewed as a centered icosahedron in which a rectangle of four gold atoms is removed, producing the centrally unsaturated cluster and providing its "boat" shape.[139] This unsaturation allows the reactivity with $NaBH_4$, with formation of $[HMAu_8(PPh_3)_8]^{3+}$ [141,142], more reactive than the previous one. This latter can further react with PR_3, SR or alkynyl gold(I) complexes, affording SA clusters.[109,113] Furthermore, it is possible to get also the structural isomer of $[Au_9(PPh_3)_8]^+$, as reported in **Figure 1.19 b**. The cluster isolated by Zheng et al., despite having the same formula reported above, presents a cubic quasi-body centered structure.[143,144]

It is important to highlight that $[HMAu_8(PPh_3)_8]^{3+}$ reactivity is particularly favored due to its non-SA cores, but also SA clusters show similar reactions. As it will be more thoroughly discussed in the following **Paragraph 5.0,** Biffis et al. have exploited

$[Au_{11}(PPh_3)_8Cl_2]^+$ cluster to develop a stepwise process, in which the starting cluster reacts with $[(di\text{-}NHC)Au_2Cl_2]$ complexes, undergoing a first ligand metathesis and obtaining $[Au_{11}(di\text{-}NHC)(PPh_3)_6Cl_2]^+$. This cluster undergoes a following complex addition reaction, forming $[Au_{13}(di\text{-}NHC)_2(PPh_3)_4Cl_4]^+$ and $[Au_{13}(di\text{-}NHC)_3(PPh_3)_3Cl_3]^{2+}$ clusters.[145] The X-ray structures of $[Au_{11}(PPh_3)_8Cl_2]^+$ and $[Au_{13}(PPh_3)_3(di\text{-}NHC)_3Cl_3]^{2+}$ are reported in **Figure 1.20**.

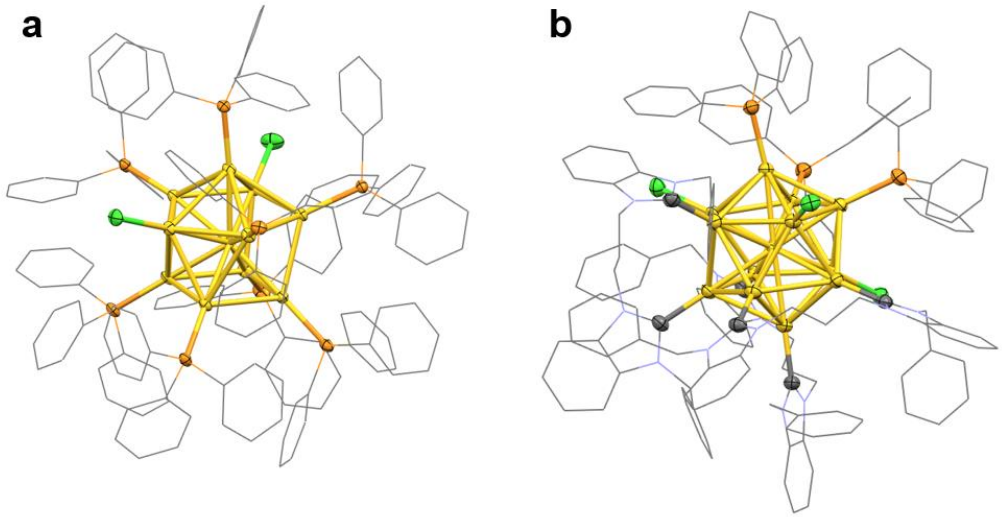

Figure 1.20: X-ray structures of a) $[Au_{11}(PPh_3)_8Cl_2]^+$ and b) $[Au_{13}(di\text{-}NHC)_3(PPh_3)_3Cl_3]^{2+}$. Color code: green (Cl), orange (P), red (S), yellow (Au).

PR_3 ligands are useful tool to get reactive clusters but generally they cannot provide clusters stable for long time. PR_3-capped AuNCs present indeed good stabilization in the solid state, but in solution they tend to form AuNPs or Au complexes with time. It is possible to exploit di-PR_2 ligands to ensure higher stability, thanks to their chelating properties, without compromising the cluster reactivity, as explained in **Paragraph 1.3.2**. However, the stability reached using SRs or alkynyls remains the best so far.

The ligands that we listed above present different advantages related with their properties. When SRs and alkynyls are used to cap AuNCs, the metallic core is perfectly protected but the organometallic framework compromises its reactivity. At

the contrary, when PR_3 are exploited, reactive AuNCs can be isolated but losing stability. Moreover, several ligands cited so far cannot variate independently their electronic and steric properties, since it is not possible to change R groups to tune the steric properties without modifying electronic properties. This represents the most important limitation of SRs, alkynyls and PR_3 ligands.

From this drawback, in the last four years NHCs have attracted increasing interest in cluster chemistry, due to their tunable properties.

1.4.4 FROM PR_3 TO NHC: SUPER-STABLE CLUSTERS

In the last four years, NHCs have been revealed a remarkable alternative to ligands cited in previous sections. Indeed, NHCs present a high affinity with gold, forming generally stronger Au-NHC bonds compared with Au-PR_3 or Au-SR bonds.[146,147]

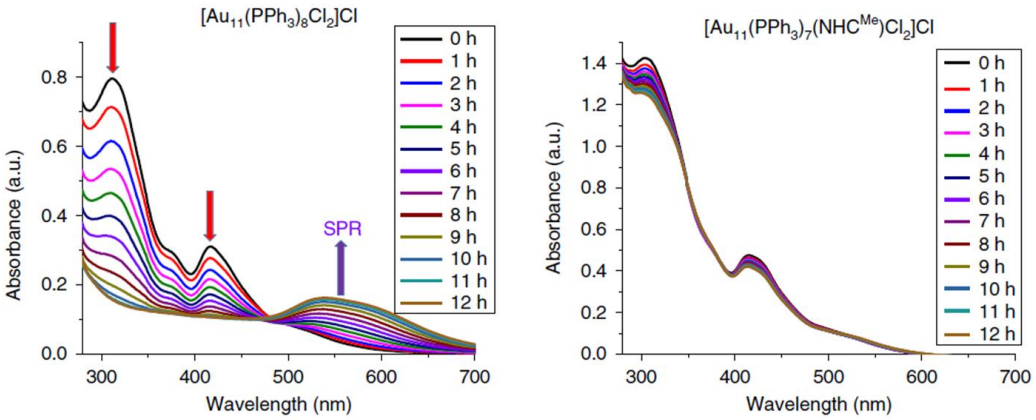

Figure 1.21: UV-Vis spectra of clusters $[Au_{11}(PPh_3)_8Cl_2]^+$ and $[Au_{11}(NHC)(PPh_3)_7Cl_2]^+$ in pentanol at 70°C over 12 h. $[Au_{11}(PPh_3)_8Cl_2]^+$ decomposes to nanoparticles, evident by the loss of molecular signals at 405 and 310 nm and growth of the signal at 550 nm, while $[Au_{11}(NHC)(PPh_3)_7Cl_2]^+$ is stable in the same conditions.[114]

The first NHC-stabilized AuNC has been reported by Crudden et al. in 2019, isolated from ligand exchange reaction performed between $[Au_{11}(PPh_3)_8Cl_2]^+$ and free NHCs in solution. This paper reports that $[Au_{11}(PPh_3)_8Cl_2]^+$ cluster, capped by PR_3, shows a lower stability in solution than corresponding $[Au_{11}(NHC)(PPh_3)_6Cl_2]^+$, in which one PPh_3 is substituted by NHC. UV-Vis spectroscopy have been used to study their stability, showing that first cluster degrades after 12 h at 70°C in pentanol, the second one instead survives in same conditions, proving as NHC can outperform PR_3 ligands to ensure stability of AuNCs. The UV-Vis spectra mentioned before are reported in **Figure 1.21**.[114]

The important thermal stabilization derived from strong core-NHC bonds is not the only advantage represented by NHCs, since these can variate independently their

steric and electronic properties, thus completely differing from most previously studied ligands.[148] The structure of NHCs, reported in **Figure 1.22**, usually presents an imidazolium or benzimidazolium ring in which the carbene lone pair is placed on the $sp^2(\sigma)$ C2 orbital, between nitrogen atoms, and where two R groups, called “wingtips”, are bound to nitrogen atoms, sp^2 hybridized as well. This definition is valid for acyclic NHCs too, presenting instead $(R_2N)_2C$: structures and higher reactivity than cyclic NHC.

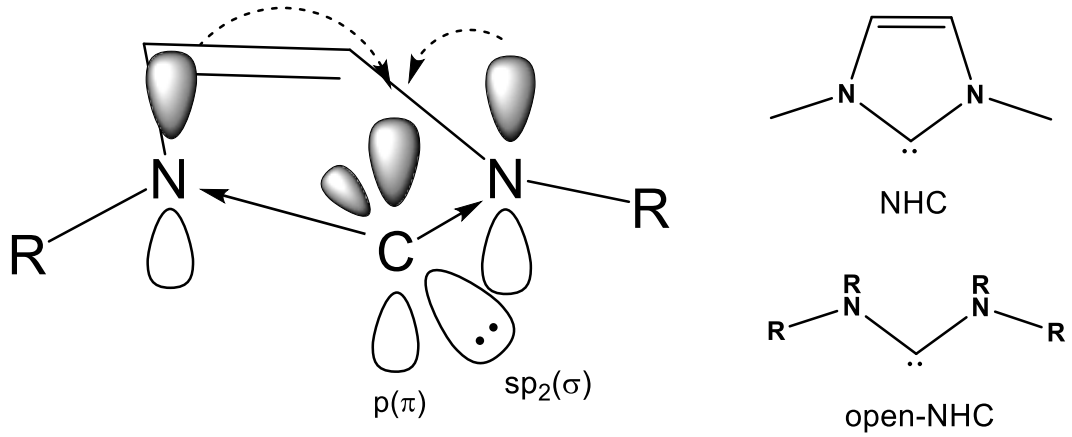

Figure 1.22: schematic structure of NHC ligands, in which the inductive (continue arrow) and mesomeric (dash arrow) effects are highlighted.

The stability of NHCs results from two distinct effects related to nitrogen present in these ligands: the inductive effect, due to the higher electronegativity of nitrogen, affecting σ(C-N) bonds, and the mesomeric effect, affecting instead π-orbitals involving the same three atoms.[149,150] The nitrogen lone pairs are partially donated to carbene p(π) orbital, favoring its singlet state. The triplet state is generally unfavored in these ligands, since the mesomeric effect decreases $sp^2(\sigma)$ orbital energy, guaranteeing therefore the singlet state. Furthermore, the NHC electronic doublet is stabilized by the inductive effect too, decreasing $sp^2(\sigma)$ orbital energy as well.[151] The combination of such electronic interactions makes NHCs useful as strong σ-donor ligands toward soft metal centers.[152] In fact, NHCs generally do not show significant π metal-ligand backdonation, since the mesomeric effect makes p(π) orbitals

unwilling to accept electronic density arising from complex d(π) orbitals. Consequently, such ligands mainly donate their lone pair through interactions with empty σ-symmetry orbitals of metals.

Generally, NHCs present cyclic structures, since further stabilization of about 6 KJ mol^{-1} can be achieved in this form, compared with corresponding "open" NHCs. Additional stabilization occurs when an unsaturation is present in the ring backbone, affording aromatic behavior and decreasing energy by 20 KJ mol^{-1} more.[153]

However, electronic features are not sufficient to ensure stability on free NHCs in solution. NHCs tend to dimerize by coupling reactions, forming double bonds when NHCs share their lone pairs, affording consequently chromophore molecules as products.[154] The dimerization can be disfavored tailoring the steric hindrance of R groups, with the possibility to isolate the free carbene ligand from solution. For example, adamantyl groups have been exploited by Arduengo et al. to isolate the first stable NHC in solid state, demonstrating that also wingtips need to be carefully chosen to improve NHC stability.[155]

In the isolation of free NHCs, imidazolium salts can be exploited as ligand precursors. To get these salts, electrophilic attack on imidazole can be used, providing the desired salt due to functionalization of nitrogen atoms. Changing stoichiometry and electrophile, symmetric and non-symmetric imidazolium salts can be isolated.[156] When good electrophiles are not available, cyclization reaction between primary ammine, formaldehyde and glyoxal can be exploited.[157] These methods are reported in **Figure 1.23 a**.

Using a strong base in the presence of imidazolium salt, the proto-carbene position can be deprotonated, forming free carbene in solution, as reported in **Figure 1.23 b**. Despite NHCs are useful also in their free form (*e.i.* in catalytic applications[158]), they are reactive species, since the high pK_a values of their corresponding acid forms,

make them strong bases. At the same time, they can act like nucleophiles too, through their available lone pair.[159] For this reason, they are still mainly used as ligands in organometallic chemistry.

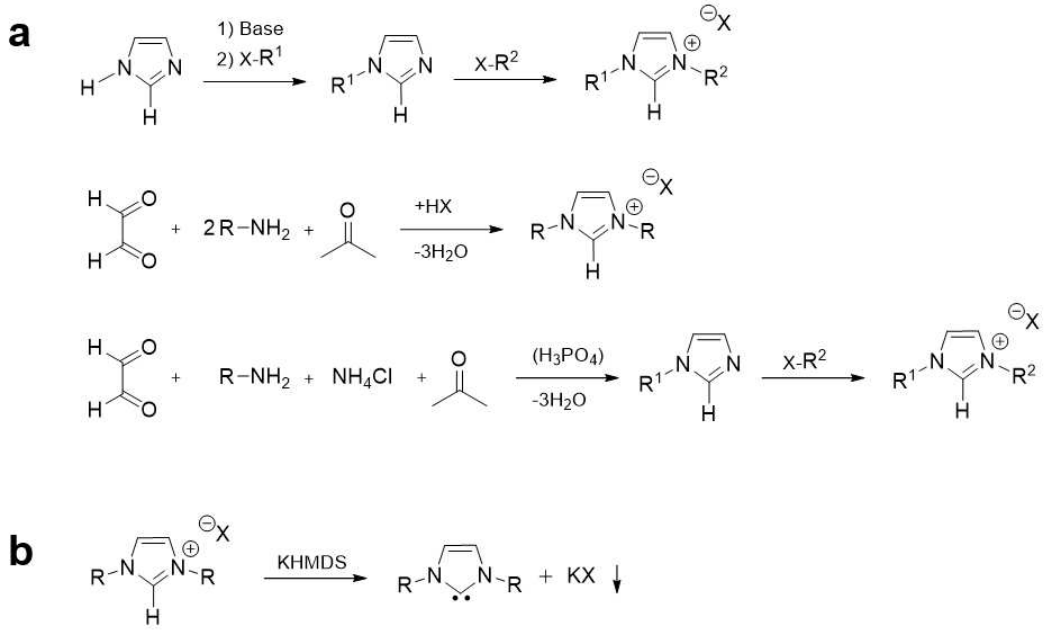

Figure 1.23: different synthetic methods to get a) symmetrical and asymmetrical imidazolium salts. b) formation of free NHC using a strong base to deprotonate the corresponding imidazolium salt.[157]

To synthesize NHC-Au(I) complexes, free NHCs can be formed in solution through deprotonation of the corresponding imidazolium salt. Later, Au(I) complex presenting releasable ligands, such as dimethylsulfide (SMe_2), are added, providing a ligand exchange reaction and affording NHC-Au(I) complex as final product. This "free-NHC" approach is reported in **Figure 1.24 a**.[160]

However, NHCs are reactive molecules, thus this method is not always available to get Au(I) complexes. Aiming to avoid the "free-NHC" route, in the last years other synthetic approaches have been developed to synthetize such complexes. One example is deprotonation of imidazolium salt upon addition of Ag_2O, as reported in **Figure 1.24 b**, affording linear $[Ag(NHC)_2]^+$ complexes. These latter can undergo metathesis reaction in presence of Au(I) complex, affording NHC-Au(I) complex as

metathesis product.[161] Similar reactions can be achieved also using Cu_2O as base, with the intermediacy of $[Cu(NHC)_2]^+$ complexes.[162]

More recently, the "weak base" method has been reported, in which weak bases favor deprotonation of imidazolium salt.[163,164] Indeed, imidazolium salt firstly reacts with [Cl-Au-SMe_2], leading to the formation of [(NHC)H]$AuCl_2$, since chloride ligands interact to the gold(I) center better than SMe_2. The proximity effect presented in the imidazolium salt with aurate counteranion facilitates the deprotonation, affording a deprotonation-metalation mechanism. In this mechanism, deprotonation of salt and NHC coordination simultaneously take place, due to proximity between gold and C-H bond involved in the process. This reaction is reported in **Figure 1.24 c.**

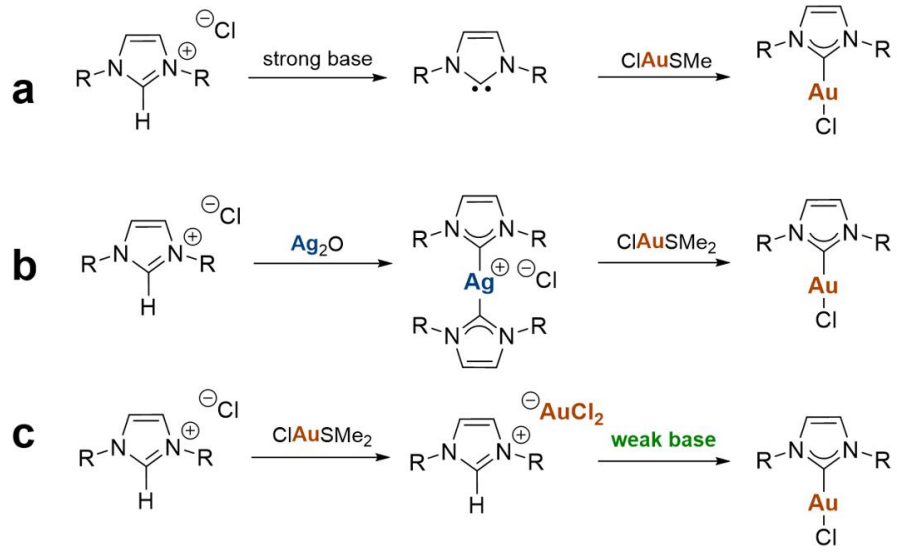

Figure 1.24: most common methods to prepare [NHC-Au-Cl] neutral complexes. a) strong base route, b) metathesis route and c) weak base route.[165]

As explained before, NHCs can effectively modulate their steric hindrance properties without compromising their electronic features. However, it is not clear how the modulation of these properties affects AuNCs synthesis, despite some important clues have been acquired in last years, in particular regarding the role of wingtip

groups. These dominate NHC hindrance properties, playing important role in the stabilization of NHC complexes too. For instance, when Au(I) complexes are used as catalysts, using bulky group, such as 2,6-di-isopropylphenyl (Dip), the catalyst is more stabilized, since its metallic center is protected.[166] As well as in metal complexes, wingtips present also an important role in AuNCs and AuNPs stabilization, directing the reduction of gold complexes forming these nano-aggregates.

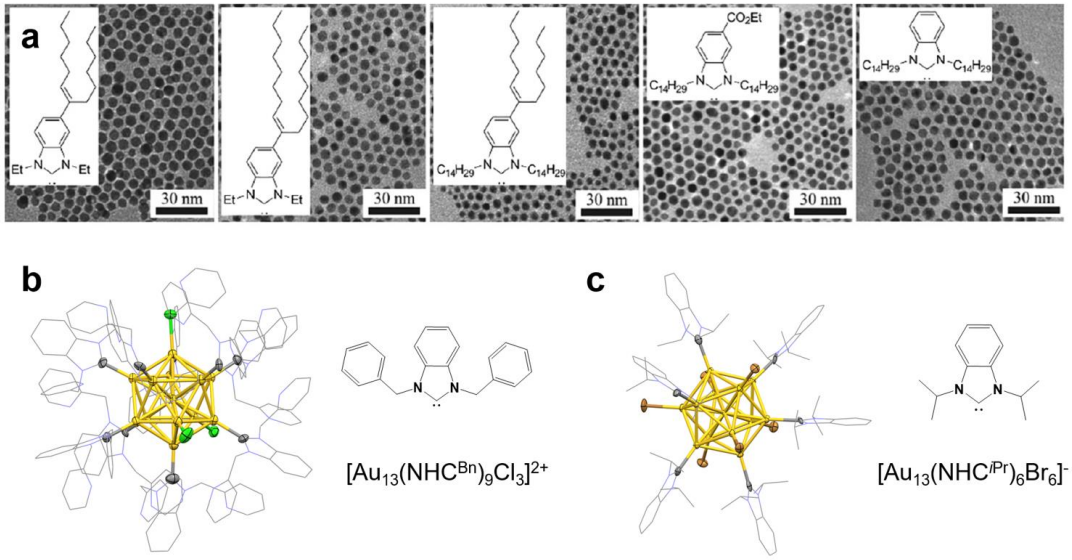

Figure 1.25: a) NHC-capped AuNPs presenting long chains in NHC backbones or as wingtip groups. b) $[Au_{13}(NHC)_9Cl_3]^{2+}$ and c) $[Au_{13}(NHC)_6Br_6]^{-}$ clusters stabilized by NHCs presenting benzylic or isopropyl wingtips groups. Color code: green (Cl), orange (P), brown (Br), yellow (Au), grey (C).[34,90,92]

With NHC Au(I) complexes presenting long chains as wingtips, $NaBH_4$ reduction affords AuNPs, since long chains favor Van der Waals interactions with the particle surface, stabilizing it.[167] Furthermore, these chains can be placed in the ring backbone too, favoring the formation of amphiphilic organic layer on the particle surface, derived from ligand stacking, and preventing AuNPs aggregation.[168] TEM analyses of NHC-stabilized AuNPs are reported in **Figure 1.25 a**. When shorter wingtips are instead employed, the formation of stable AuNPs is disfavored, since these do not provide Van der Waals interactions or amphiphilic ligand layer, fundamental in AuNPs stabilization. Indeed, their lower steric hindrance leads the

reduction pathway towards AuNCs formation, since these NHCs can easily bind the cluster kernel, without compromising its stability. Two examples of NHC-capped AuNCs are reported in **Figure 1.25 b** and **Figure 1.25 c**.

The variability of wingtips is useful also to get di-NHC ligands, in which one of R groups is a bridge unit connecting two NHC scaffolds.[169] As well as in di-PR_2 ligands, di-NHC are useful in cluster chemistry since these chelate the metallic core, providing it with further stability.[94,98,130]

There are three methods to synthesize NHC-stabilized AuNCs reported so far: 1) direct reduction, that remains the main method to produce these AuNCs[90], 2) ligand exchange reaction with free NHC, mainly exploiting pre-formed PR_3-stabilized cluster[170] and 3) stepwise process developed in the course of this PhD project, that will be discussed in detail within **Paragraph 5.0**.[145] Upon changing the nature of the NHC ligand, several AuNCs can be isolated using all methods cited above, forming in some case not SA clusters too.

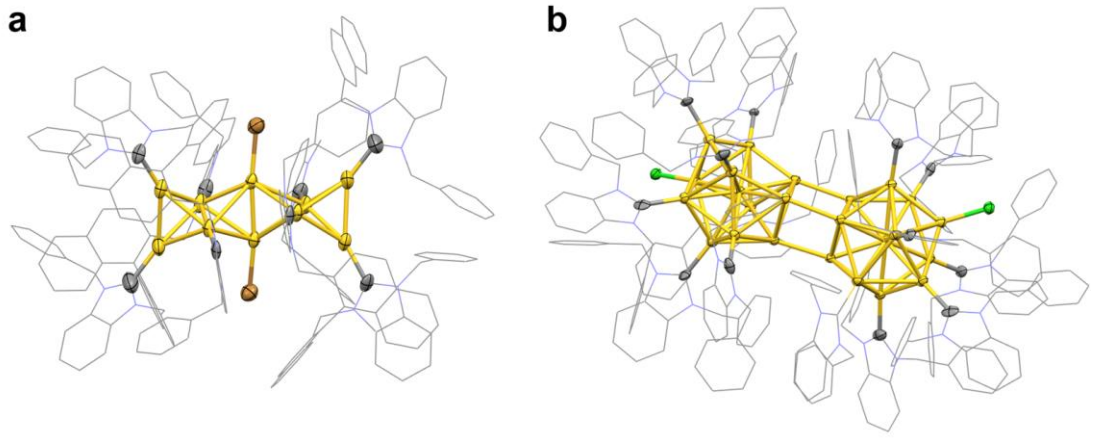

Figure 1.26: X-ray structures of a) $[Au_{10}(di\text{-}NHC)_4Br_2]^{2+}$ and b) $[Au_{24}(NHC)_{14}Cl_2H_3]^{3+}$ clusters. Color code: green (Cl), brown (Br), grey (C), yellow (Au).[94,96]

For instance, Crudden et al. have tailored the synthesis of a not SA $[Au_{10}]^{4+}$ cluster stabilizing it with rigid di-NHCs, reported in **Figure 1.26 a**, in which two NHCs units

are bridged by a binaphthyl group, inspired by a similar di-PR_2-capped AuNC.[94] The same group has exploited a 2,4,6-trimethylbenzyl wingtip substituent to promote the formation of another $[Au_{10}]^{4+}$ cluster. The bulky groups protect the cluster core favoring also its evolution into $[Au_{25}]^{7+}$ cluster, more stable thanks to its SA feature.[116] Also changing the anion in the starting complexes can lead the synthesis of novel SA clusters, isolating for instance $[Au_{24}]^{8+}$ hydride/NHC-capped cluster, reported in **Figure 1.26 b**.[96] NHCs can lead the formation of unsaturated clusters too, such as $[PdAu_9(NHC)_7Br_2]^+$ reported in **Figure 1.29 c** (next paragraph), presenting indeed an unsaturated Pd center. From these examples, it is clear that NHC-capped AuNCs present huge variability in geometry, composition and reactivity.

It is interesting to highlight that NHC coordination modes in AuNPs and clusters vary considerably. Studies conducted on NHC-capped AuNPs and gold surfaces show that NHCs can bind on the AuNPs surface presenting on-top coordination, in which the planar heterocycle is placed perpendicularly to the particle surface, or lying-coordination, in which the heterocyclic ring is quasi-parallel to the gold surface and binds an adatom.[171] These studies shed light on alternative coordination modes of NHCs in nanoparticle systems, not excluding that these could be present in undiscovered AuNCs too, presenting size comparable with AuNPs. So far, only small clusters have been stabilized by NHCs, showing in almost all studied cases exclusively on-top coordination mode. The sizes of NHC-capped AuNCs are still too small to allow lying-coordination, considering that it requires ample spaces on cluster core. However, these studies demonstrate how NHCs can use both ways to interact with gold surfaces, adapting to the nano-system, enforcing therefore efforts to get new kinds of NHC-stabilized AuNCs. Other kinds of interactions for instance can be observed when NHCs are mixed with alkynyls, forming [(di-NHC)-Au-(C≡CR)] staples, as explain before.

Despite these ligands are used from 2019 to cap AuNCs, NHC electronic properties have not been extensively varied, making benzimidazole-2-ylidene the unique scaffold exploited so far. These properties can be varied changing the backbone of imidazolium ring; for instance, using the simple imidazole-2-ylidene scaffold, the NHC lone pair is more prone to be shared with gold forming Au-C bonds, since the heterocyclic backbone is less electron-withdrawing (and also less π-accepting) than in the benzimidazole case. Conversely, when caffeine is used as an NHC-scaffold, the CO and NR groups present in the backbone provide electron withdrawing effects, which significantly change the NHC electronic properties and render it less electron-donating. Also changing position of lone pair in the imidazole ring or exploiting others heterocycles affect the electronic properties, as showed in **Figure 1.27.**[172] For instance, on going from non-aromatic to aromatic "classical" NHCs, higher HOMO-LUMO gaps can be obtained, whereas cyclic alkyl amino carbene (CAAC) ligands present lower HOMO-LUMO energy gaps.

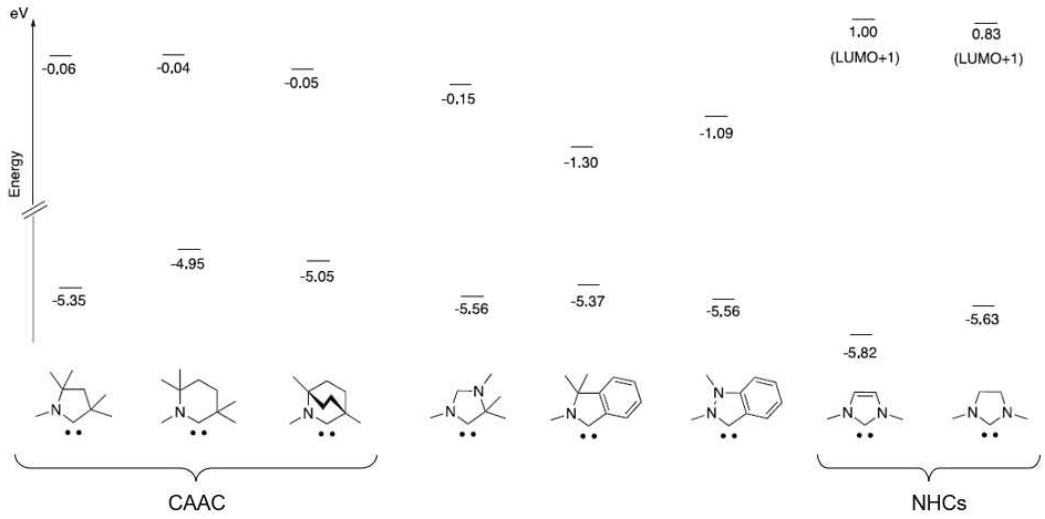

Figure 1.27: Different kinds of NHCs ligands and corresponding HOMO-LUMO energy gaps.[172]

Despite NHCs presenting advantages in cluster stabilization, it is important to point out their drawbacks too. Indeed, the single NHC lone pair affords only on-top

coordination on cluster core, similarly to PR_3. However, this drawback is overcome when NHC/alkynyls ligands shells are exploited. Use of this mixed coordination spheres may be the key to isolate larger NHC-stabilized AuNCs, possibly reaching the first “metallic” AuNCs capped by NHCs, but further experiments need to be performed in this direction. In any case, upon considering the diversity of NHCs properties and their strong Au-C bonds, these ligands are the best option to isolate stable AuNCs.

1.5 ALLOY GOLD NANOCLUSTERS: TUNING THE PROPERTIES WITH METAL DOPING

In this thesis, AuNCs have been analyzed so far considering core sizes and geometries, both related with the ligands used. However, AuNCs can be modified also changing their composition, by introducing heterometallic centers. So far, AuNCs have been mainly doped with Ag(I), Cu(I), Pd(0), Pt(0), Cd(II) and Hg(II), usually taking advantage of SRs as capping agents.[173] Doped clusters can be obtained with the methods already cited before. Exploiting direct reduction, doped-AuNCs can be isolated by co-reducing Au(I)/Au(III) complexes with heterometallic precursors. Neghishi's and Murray's groups have synthesized several $[Au_{25-x}Ag_x(SR)_{18}]$ with this method.[174,175] Metal exchange reactions can be also exploited, in which AuNCs reacts with heterometallic NPs, complexes or clusters to form the desired alloy clusters. $[Au_{25-x}Ag_x(SR)_{18}]$, $[Au_{25-x}Cu_x(SR)_{18}]$ and $[MAu_{24}(SR)_{18}]$ where M are Pd(0), Pt(0), Cd(II) and Hg(II), have been synthetized with these exchange reactions.[176]

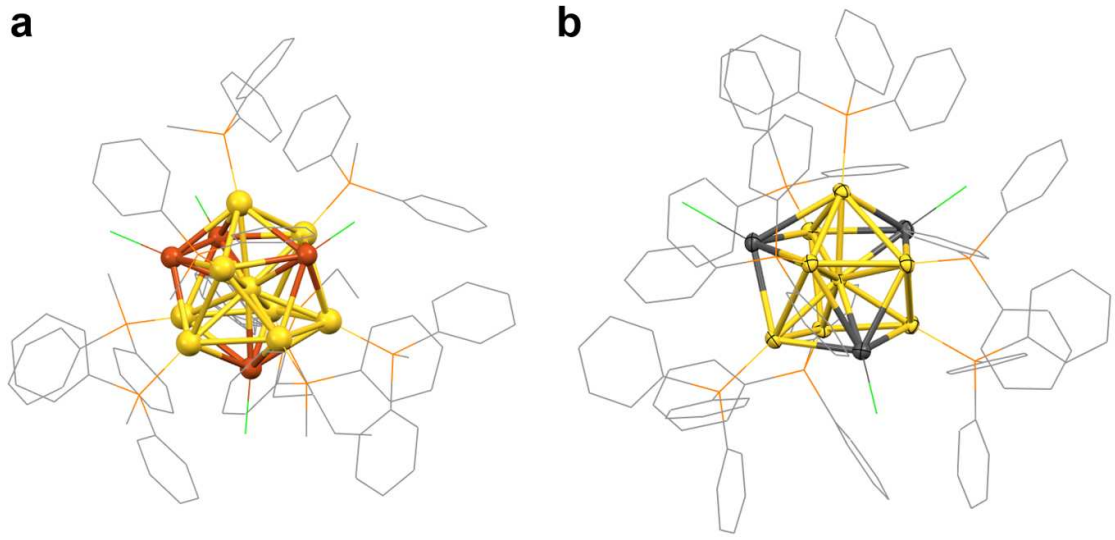

Figure 1.28: X-ray structures of a) $[Cu_4Au_9(PR_3)_8Cl_4]^+$ and b) $[Ag_3Au_8(PR_3)_7Cl_3]$ clusters. Color code: yellow (Au), red (Cu), grey (Ag), orange (P), green (Cl) and grey (C).[105]

The use of different synthetic methods and ligands allows the isolation of several clusters, but it needs to be remarked that the dopant significantly affects the reaction

products. For instance, Zhu et al. proved that co-reducing $PdCl_2$ and $HAuBr_4$, in presence of PPh_3, $[Pd_2Au_{23}(PPh_3)_{10}Br_7]^{3+}$ can be isolated. Instead, well-known $[Au_{11}(PPh_3)_8Br_2]^+$ is obtained when Pd complex is not present in starting mixture, demonstrating that the Pd reagent modifies the reduction pathway.[177]

There are some general behaviors observed with the metals used in the doping process. When metals of groups 11 and 12 dope SR-capped AuNCs, heterometallic centers substitute "surface" positions in gold core, generally without getting involved in $[Au_2(SR)_3]$ staples.[178,179] This is valid for PR_3-capped AuNCs too: Mingos's and Li's groups reported similar findings also for $[M_4Au_9(PR_3)_8Cl_4]^+$ (M: Cu and Ag) and $[Ag_3Au_8(PR_3)_7Cl_3]$ clusters, both reported in **Figure 1.28**, in which Cu and Ag centers are placed in external and not in the central position of icosahedral cores.[180,105,181] When instead Pd or Pt are involved, these generally substitute the central Au in the metallic kernel. For instance, in both $[MAu_{25}(SR)_{18}]$.and $[M_2Au_{36}(SR)_{24}]$ (M: Pd or Pt) the heterometals are found in the center of mono- o bis-icosahedral cores, respectively.[182–184] The $[PdAu_{25}(SR)_{18}]$ structure is reported in **Figure 1.29 a**. Similarly, this displacement is reported for $[PdAu_8(PPh_3)_8]^+$ and $[PdAu_9(NHC)_7Br_2]^+$ too, despite their unsaturated "boat-shaped" cores. These clusters are reported in **Figure 1.29 b** and **Figure 1.29 c**, respectively. These examples highlight how group 10 metals prefer this arrangement whatever are the ligands involved in cluster stabilization.[185,186]

Several experimental and theoretical investigations allow to understand the doping effect on AuNCs, confirming that metal substitution modifies cluster electronic properties, changing therefore their magnetic, optical and electrochemical features, as well as affecting cluster stability and reactivity. For instance, it is known that $[Au_{25}(SR)_{18}]^0$ clusters are paramagnetic due to the presence of an unpaired electron in their electronic configuration, which is detectable with EPR spectroscopy. The reduced form $[Au_{25}(SR)_{18}]^{1-}$ presents instead diamagnetic properties, since its 8

valence electrons provide complete super-orbital configuration, as highlighted by NMR analysis.[187]

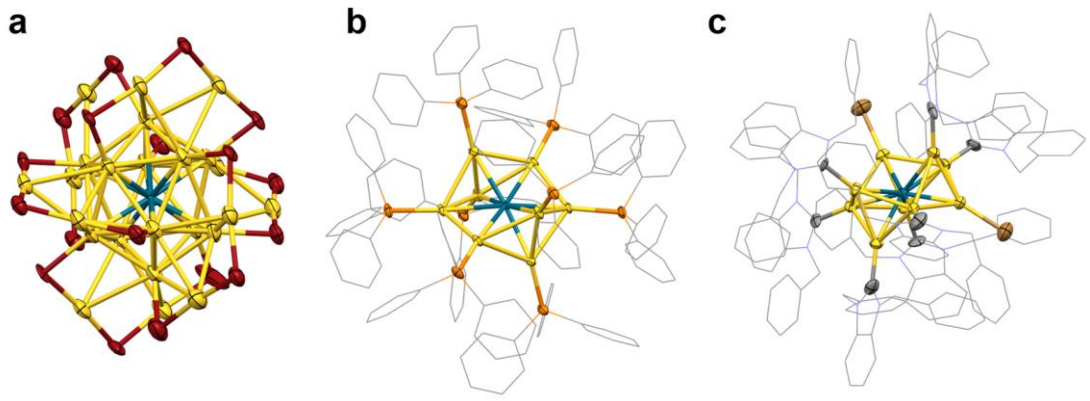

Figure 1.29: X-ray structures of a) $[PdAu_{24}(SR)_{18}]$, b) $[PdAu_8(PPh_3)_8]^+$ and c) $[PdAu_9(NHC)_7Br_2]^+$ clusters. Color code: red (S), orange (P), brown (Br), grey (C), blue (Pd), yellow (Au).

The presence of Pd and Pt changes this behavior, due to the variation of electron count derived from heteroatomic doping. Indeed, $[MAu_{24}(SR)_{18}]^0$ clusters present diamagnetic behavior[188] whereas the reduced form $[MAu_{24}(SR)_{18}]^{1-}$ is a paramagnetic species, counting indeed 7 electrons.[189]

The doping does not affect only electronic count, since HOMO-LUMO energy gaps (E^a) change too.[190] In all these cases the SA theory helps in the interpretation of the doping effect. The total jellium model is now described like two interconnected systems, the host and dopant atoms, providing different and uniform positively charged backgrounds. According to this theory, dopants are placed in the center of jellium system, approximately in the central position of $[Au_{13}]$ core. If dopants present higher valence (Pd, Pt), the cluster negative orbital energies are stabilized by the higher positive charge derived from the core. On the contrary, when lower-valence dopants (Ag, Cu) are placed in the same position, the lower potential in the system provides an increase of orbital energies, destabilizing the cluster structure.[37] These concepts are represented in **Figure 1.30**.

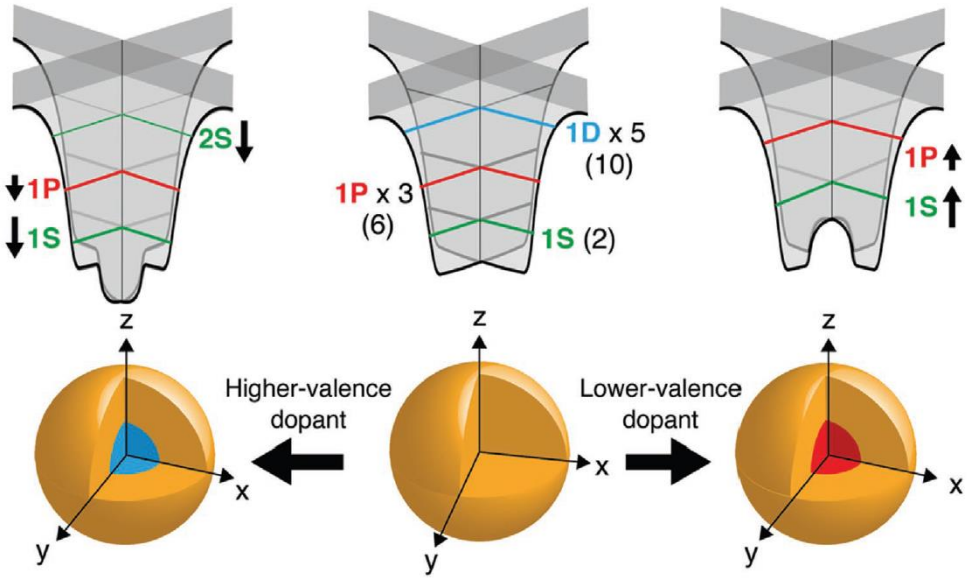

Figure 1.30: Schematic representation of jellium potentials upon doping of higher and lower valence elements. In parentheses the number of valence electrons that can be placed for each SA orbital.[37]

Both UV-Vis absorption spectroscopy and electrochemical analysis confirm the variation of E^a in doped AuNCs, showing shifted peaks in the spectra compared to homometallic counterparts. Due to this, alloy clusters affect photoluminescence properties too. For instance, the photoluminescence properties of SR-capped AuNCs can be improved adding Ag(I) centers. These directly affect E^a, decreasing it and affecting consequently the population of first excited state, making HOMO-LUMO transitions more favorable.

Finally, SCXRD analysis of doped clusters confirms this theory. Pd and Pt are placed centrally in cluster-core, whereas Ag and Cu dope the core “surface”, since the central position does not guarantee cluster stability. Generally, improvements in cluster stability are detected when Pd or Pt are used as dopants, confirming the calculation performed on these systems and increasing their possible application in catalysis.[191] Conversely, Pd/Pt doped AuNCs are generally less surface-reactive than their homometallic counterpart, since they possess higher stability, whereas Ag and Cu doped AuNCs are more reactive species.[192]

1.6 APPLICATION OF MOLECULAR GOLD CLUSTERS

1.6.1 CATALYTIC APPLICATIONS

Gold complexes and nanoparticles are commonly used as catalysts, since these species promote kinetically unfavored reactions, making industrial application of these fundamental to synthetize several chemicals.[193] In particular AuNPs surfaces guarantee the presence of catalytic centers, on which reactions take place exploiting substrate-surface interactions. Despite this advantage, their poly-disperse nature makes the correlation structure-properties difficult to achieve, complicating the corresponding catalytic studies. On the contrary, AuNCs are molecular species, thus presenting perfectly tunable features related to metal core and ligand shell, which jointly define potential catalytic centers present on them. These properties make AuNCs a class of very promising catalysts, due to their particle-like shape and the atomic control achievable in their synthesis. In the following, a brief description of catalytic applications of AuNCs in homogeneous and heterogeneous catalysis is reported.

1.6.1.1 HOMOGENEOUS CATALYSIS

The principles valid for metal complex catalysts can be exploited to describe cluster catalysts, too.[194] For instance, cluster catalysts generally need to be stable enough to promote the catalytic cycle, avoiding undesirable deactivation routes promoted by catalyst degradation. The catalytic performance of AuNCs is deeply connected with the ligands employed, since they guarantee stability to the core, providing also partial unsaturation centers on it and favoring therefore its catalytic activity. Consequently, ligand engineering is essential to isolate active clusters. As well as in gold complexes, bulky groups can be exploited to protect unsaturated centers, granting at the same time interaction with substrates. However, despite this concept is easily applicable in complex catalysis, it is not simple to isolate AuNCs stabilized by bulky ligands, since the size of the cluster core limits the degree of steric bulkiness of ligands used to stabilize it. Recently, new stibine-protected AuNCs have been isolated by Leong's and Das's groups, respectively with formula $[Au_{13}(SbR_3)_8X_4]^+$ (X: Cl, Br), in which stibines present on-top coordination mode, similar to PR_3-capped AuNCs but also weaker bonds with the gold core.[195,196] This feature makes it possible to completely substitute SbR_3 with PR_3 or to further react these clusters with thiolates, forming new $[Au_{18}(SR)_8(SbR_3)_4Br_4]$ or $[Au_{25}(SR)_{18}]$ clusters, depending on the SR used. Stibines could be interesting ligands for catalytic application, since it is possible to get stabilized AuNCs without compromising the formation of free coordination centers. However, no applications of these clusters have been reported so far in this field. On the contrary, the structure of $[Au_{23}(PR_3)(dpa)_2Cl]^+$ (dpa= dipyridylamido) is the key for its high activity toward oxidation of benzylic alcohol, since this cluster presents 8 unsaturated centers in the core.[197] This catalyst present higher conversion than AuCl homogeneous catalysis exploited by Shi et al. for the same reaction, even if this latter presents an higher catalyst load.[198] However, it is not simple to compare such homogeneous catalysis with Au(I) complexes, since these latter generally do not

promote such reaction, catalyzed instead by supported AuNPs. Another interesting work regarding homogeneous catalysis promoted by clusters has been reported by Li et al., in which the hydrogenation of nitrophenol is catalyzed by $[Au_{25}(SR)_{18}]$ species.[199] In these library of AuNCs, R groups are alkyl chains presenting different lengths, which makes correlations length-activity possible. Indeed, shorter chains provide better activity in term of conversion, thus demonstrating that catalytic activity is promoted since shorter ligands guarantee better interactions core-substrate than longer ones.

Since SR-capped clusters are among the most studied AuNCs, they are also the most applied catalysts in literature, but generally not like homogeneous catalysis. In fact, despite the stabilization provides by their metal-organic framework of “staples”, using these as homogeneous catalysis is not the best options, since $[Au_n(SR)_m]$ staples disfavor interaction with substrates, affecting their application in this field. Thus, SR-capped AuNCs are generally deposited on surfaces and exploited as heterogenous catalysts.

Since the difficult interactions kernel-substrate with SR-capped AuNCs, the use of other ligands should be preferred to get active catalyst, like the stibines cited above or PR_3 ligands. However, these ligands could not ensure enough stability to perform the catalytic cycle. At the same time, NHCs impart higher stability to cluster core, but generally NHC-capped clusters do not present unsaturated metallic centers, therefore complicating their application in this field.

Despite generally SR-capped AuNCs are not applied in homogeneous catalysis, their stability in different oxidation states provides several applications of these as electrocatalysts or initiators of redox process in homogeneous systems. It is demonstrated that neutral $[Au_{25}(SR)_{18}]^0$ clusters react with electro-donating molecules (EDM), affording $[Au_{25}(SR)_{18}]^-[EDM]^+$ salts, according to the reduction potential of the species involved.[200] This reactivity is used to initiate chain electron transfer process,

in which $[Au_{25}(SR)_{18}]^-[TOA]^+$ (TOA: tetraoctylammonium) can donate electrons to *o*-nitrobenzonitrile, forming active species reacting with $NaBH_4$ and affording *o*-aminobenzamide as final product. In this cycle, cluster oxidation is confirmed by NMR and EPR analyses. Due to their electrochemical features, they can participate to catalytic cycle too, jumping between different oxidation states without lose their stability. For instance, SR-capped AuNCs electrocatalyze nitrophenol reduction, showing generally higher conversion than AuNPs promoting the same reaction. Furthermore, also in electrochemical process, ligands and core structure affect AuNCs catalytic activity, in agreement with the discussion above on structure-properties relationships.[201–203]

1.6.1.2 HETEROGENEOUS CATALYSIS

As mentioned in the previous paragraph, AuNCs present catalytic activity towards different reactions. However, despite some exceptions, AuNCs are not exceedingly stable molecules, which make their use as homogeneous catalysts difficult. To improve their stability, it is possible to deposit AuNCs on surfaces, such as carbon sheets, metal organic frameworks (MOFs), polymers and others.[204–206] The deposition affords robustness to AuNCs since aggregation processes are disfavored when these are anchored on surfaces. Furthermore, the catalytic activity can be tested with or without ligands on metallic core. Using chemical, electrochemical or thermal treatments, the ligand shell can be partially or completely removed, changing therefore the AuNCs properties too. In heterogeneous catalysis the kind of surface employed for cluster heterogenization is another parameter to tailor, providing different kinds of cluster-surface interaction and consequently another tool to improve the catalytic system. However, AuNCs deposition should be carefully analyzed since cluster molecular properties can be affected by deposition process. For instance, thermal treatment of deposited AuNCs could enforce aggregation process if AuNCs are not well dispersed on the surface. For these reasons, cluster heterogeneous catalysts need to be studied in detail, without taking for granted that the molecular features of AuNCs are maintained after the deposition. Moreover, understanding the fate of the deposited catalyst before and after the catalytic cycle is not trivial, since it is not possible to perform molecular analysis on these systems. Other material chemistry techniques can be employed, such as XPS or TEM, affording important information regarding cluster composition or sizes.

The principles discussed before for homogenous catalysis are valid in heterogeneous catalysis too. For instance, when ligands are removed from cluster core, unsaturated AuNCs are more catalytically active compared to coordinated ones, allowing easier interactions core-substrate.[207] However, if ligand removal leads to aggregation

process, in which small poly-dispersed AuNPs can be formed, a decreased catalytic activity is generally detected, since the smaller active surface present in size-increased gold system.[208] This drawback can be avoided by controlling the unsaturation grade of deposited AuNCs, thus removing only partially the ligand shell on the core surface.[209] These concepts are valid for several reaction catalyzed by AuNCs, such as hydrogenation, oxidation and C-C coupling reactions.[206]

Focusing on NHC-capped AuNCs, Zheng's group is the leader in heterogeneous catalysis promoted by these clusters supported on active carbon, showing how these systems are active towards reduction reactions. For instance, they synthetized Pd-doped NHC-capped clusters useful to promote catalysis since their metal core is unsaturated.[186] This cluster catalyzes the regioselective hydrogenation of alkynes, in which the Pd center actives molecular H_2, promoting the desired hydrogenation. Another NHC-capped cluster applied in catalysis is $[Au_{44}(NHC)_9(C{\equiv}CR)_6Br_8]$, capable to promote hydration of alkynes. The cluster stability is provided by NHC ligands, whereas Au(I) centers present in $[Au_3(C{\equiv}CR)_2]$ staples are the catalytic centers. Therefore, the metallic kernel does not participate directly to catalysis but acts as a scaffold on which reaction takes place.[133] Similar examples are $[Au_{16}(NHC)_5(C{\equiv}CR)_3Br_2]^{3+}$ and $[Au_{17}(NHC)_4(C{\equiv}CR)_4Br_4]^{+}$, characterized by three and four staples [(di-NHC)Au(C≡CR)], respectively, which promote the hydroamination of alkynes. Also in these cases the kernel represents only the catalyst scaffold, which is stabilized by the presence of the NHC ligands, whereas the organometallic framework is the catalytic center.[130] This is confirmed by the crystallization of $[Au_{16}(NHC)_5(C{\equiv}CR)_2(4\text{-}MePhC{\equiv}C)Br_2]^{3+}$ after the hydroamination catalyzed by Au_{16} cluster in homogeneous condition, using 4-ethynyltoluene as substrate. The variation of ligand staples, together with DFT calculation, confirm the supposed mechanism, reported in **Figure 1.31**.

Similar mechanisms have been proposed also in the semi-hydrogenation of alkynes promoted by SR-capped AuNCs, affording alkenes as products. This reaction has been studied comparing two clusters as heterogeneous catalysts supported on TiO_2, $[Au_{25}(SR)_{18}]$ and $[Au_{25}(PR_3)_{10}(C{\equiv}CR)_5Cl_2]$, and also in this case $[Au_2(SR)_3]$ and $[Au_2(C{\equiv}CR)_3]$ staples promote the catalysis.[210]

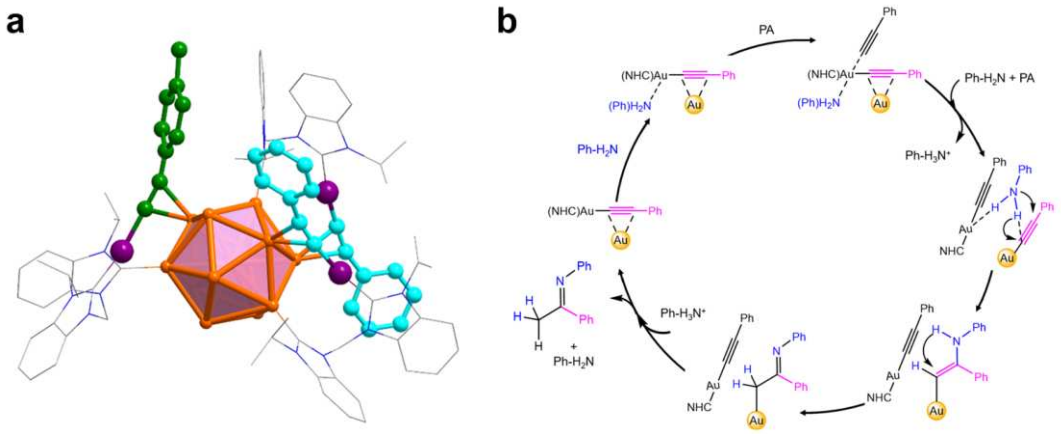

Figure 1.31: a) Total structure of the Au_{16} cluster after catalytic hydroamination of 4-ethynyltoluene determined by single crystal X-ray diffraction. The phenyl alkyne (PA) ligand on the isolated organometallic motif is replaced by 4-ethynyltoluene (highlighted in green). b) Mechanistic scheme showing the reaction steps taking place on the surface-isolated NHC-Au-PA organometallic motif together with the core. The metallic Au atoms are highlighted as yellow spheres.[130]

Other reductions catalyzed by supported AuNCs involve carbonyl compounds, which can be hydrogenated with reagents such as H_2 or $NaBH_4$. In these cases, also the metallic core participates in the catalytic process, since its ability to weakly bind carbonyl substrates upon C=O coordination enables a more efficient interaction with hydrides placed on staples.[211,212] Furthermore, SR-capped AuNCs have been studied as heterogeneous catalysts towards carbon-carbon coupling, pointing out also in this case that the metal-organic staples framework is indeed the catalytically active site of the AuNCs.[213,214]

Catalytic processes afforded by supported AuNCs involve oxidation reactions too. A classic process to study in this field is CO oxidation with O_2 to yield CO_2, which is a

reaction typically catalyzed by AuNPs and in which product and substrate are simple molecules, making the process easier to study.[215] In these systems, the support is deeply involved in tuning the catalytic behavior. For instance, AuNPs/TiO_2 catalyst is reported to be one of the most useful catalysts towards CO oxidation, whereas $[Au_{25}(SR)_{18}]/TiO_2$ presents no catalytic activity. On the other hand, $[Au_{25}(SR)_{18}]/CeO_2$ is active, showing the important role of the surface. Characterization on this latter heterogeneous system reveals that SRs ligands remain coordinated on cluster core after the deposition. Furthermore, a pretreatment at 150°C under O_2 actives the catalyst, forming oxygen active species on the CeO_2 surface. These species can not be detected when TiO_2 is used as support, explaining therefore its low activity.[216]

Ligand removal not always provides catalyst activation in oxidation reactions since it depends on the studied system. For instance, when $[Au_{38}(SR)_{18}]/CeO_2$ presents complete coordination sphere after thermal treatment, it is not active towards CO oxidation. Only by partially removing the metal-organic staples the catalyst can be activated. Thus, cluster unsaturation needs to be carefully controlled, since when ligands are completely removed from $[Au_{38}(SR)_{18}]$, its activity drops, because aggregation processes are favored.[217] A similar behavior can be found also in heterogeneous catalysis of oxidation of benzyl alcohol[209], cyclohexane[218] and styrene[219] promoted by AuNCs. Each catalyst needs to be studied to tune its catalytic properties, for instance by changing deposition method, calcination process or kind of ligand, aiming at improving catalytic performance.

1.6.2 BIOLOGICAL APPLICATIONS

As outlined above, molecular clusters present particle-like structure characterized by precise gold core and ligand shell, making them truly molecular species. Despite this definition being currently in use to describe AuNCs in literature, this acronym also describes poly-dispersed AuNPs presenting sizes between 1-5 nm. These kinds of clusters do not present “molecularity”, since they are poly-dispersed samples, not presenting therefore defined stoichiometric formulas and differing from all clusters discussed so far in this thesis. However, they exhibit low toxicity, as well as larger AuNPs, which makes these species useful for biological applications.[220] These small gold particles are generally capped by biological molecules, such as DNA, proteins, polysaccharides and polypeptides, providing perfect ligand shells to interact with the biological environment.[221] Their synthesis starts from Au(III) salts dissolved in aqueous environment in presence of bio-ligands. These interact in solution forming Au-intermediates, whose nature changes with the ligand type, and subsequent chemical or thermal treatment provides Au(III) reduction, forming the desired bio-compatible AuNCs. The bio-organic layer protects AuNCs, making them able to penetrate and survive in biological environment, with possible applications in drug delivery, therapy and imaging.[222,223] This latter application is the most studied with these small particles, since these show interesting near-infrared (NIR) photoemission, useful for *in vivo* bioimaging.[224] Biological tissues are transparent to NIR radiation and its emission does not compromise excessively bio-environments, resulting a perfect tool for imaging applications. However, these photoluminescent systems present important drawbacks. First, there is no unified theory explaining the mechanism of AuNCs photoluminescence. As explain before, AuNCs optical properties can be finely tailored in molecular systems since they depend on several parameters, such as the presence of dopants or the kind of employed ligands/staples. However, this high number of variables complicates the studies on their emission

features, making it rather complicated to find a unified theory explaining them. In addition, in biological applications poly-dispersed AuNCs are used, not presenting therefore molecular properties, which further complicates the emergence of structure-properties correlations. Furthermore, AuNCs generally present photoemission characterized by low luminescence quantum yields (QYs), reaching values between 1-10%, despite some remarkable exceptions.[225] To achieve real applications of these clusters in bioimaging, QYs need to be improved, for instance adding Ag as dopant, as explained in **Paragraph 1.5**.[226] Also preventing structural vibrations using rigid ligands is an option to promote higher QYs, since radioactive relaxation pathways are favored in the presence of a rigid ligand shell.

The huge diversity of ligands applicable in AuNCs chemistry allows formation of coordination spheres presenting ancillary groups able to interact with biological receptors. This clusters are used as bio-markers[227], affording guided accumulation of clusters in body and making it possible to use them as biological probes, drug-delivery systems and radio- or phototherapy for cancer treatment.[220]

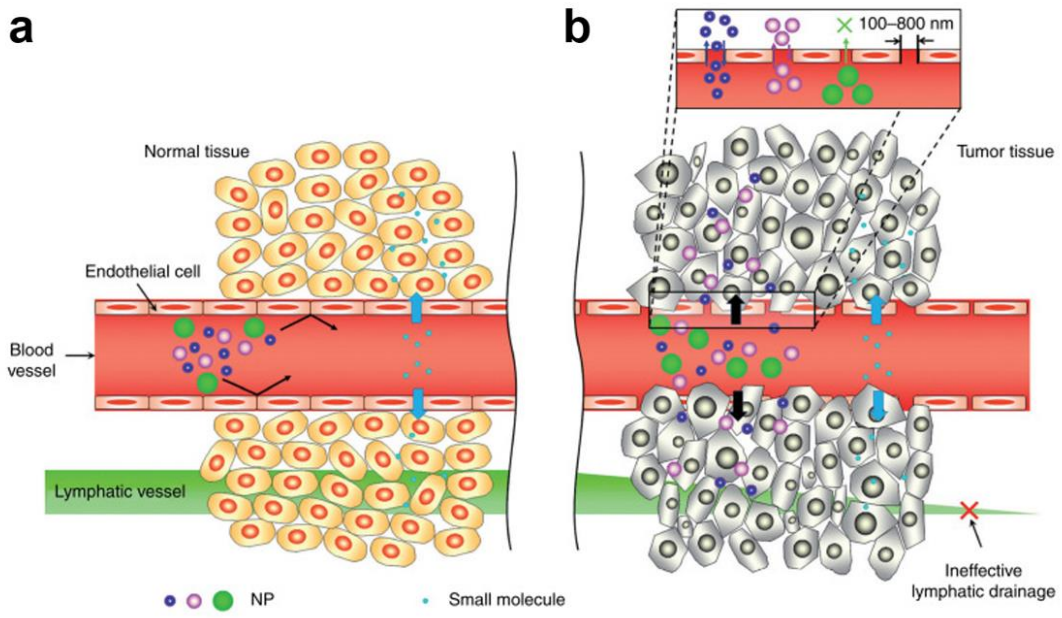

Figure 1.32: Different uptake of small NPs and molecules based on their size across a) normal and b) cancerous tissue.[228]

The latter application is one of the most promising, in which AuNCs can act like a photosensitizer. In this process, excited AuNCs can transfer energy or electrons to the biological environment, forming for example reactive oxygen species (ROS), leading the apoptosis of cancer tissue.[229] Finally, AuNCs present high “Enhanced Permeability and Retention” (EPR) effect due to their size. AuNCs are indeed able to cross channels among endothelial cells present in tumor issue, increasing therefore their selectivity towards cancer cells, as represented in **Figure 1.32**. This high selectivity towards cancer tissue is useful also to create new drug-delivery systems, in which AuNCs is used as drug-scaffold with ligands suitably engineered to deliver drug molecules to cancer cells.

Despite such small AuNPs are useful in biological applications, it is important to underline that these are generally poly-dispersed, therefore without the desire atomically control cited before. This molecularity indeed is one of the keys to further improve the bio-properties of such compounds, aiming at perfectly tuning the cluster proprieties. However, in literature this approach is limited and only few applications of atomically precise AuNCs are reported.[230] For instance, Luo et al. designed Au_{25} NCs with the ability to target PSMA receptor positive cancer cells (PC3pip), affording an enhanced tumor-suppressing using X-ray irradiation for the cancer phototherapy treatment.[231] Another mono-dispersed AuNC used in biology is Au_{102} capped by *para*-mercaptobenzoic acid (*p*-MBA), ligand that guarantee aqueous solubility to the gold species in biological tissues. This cluster targets cysteine sites of capsid proteins in virus, without compromising their infectivity and allowing their individuation in the infected cells thanks to cluster luminescence proprieties.[232]

1.7 BIBLIOGRAPHY

[1] R. Batchelor, D. Gulley, *Resour. Policy* **1995**, *21*, 37–42.
[2] Y. S. Kim, H. S. Jung, T. Matsuura, H. Y. Lee, T. Kawai, M. B. Gu, *Biosens. Bioelectron.* **2007**, *22*, 2525–2531.
[3] R. P. Herrera, M. C. Gimeno, *Chem. Rev.* **2021**, *121*, 8311–8363.
[4] S. Witzel, A. S. K. Hashmi, J. Xie, *Chem. Rev.* **2021**, *121*, 8868–8925.
[5] T. P. Seifert, V. R. Naina, T. J. Feuerstein, N. D. Knöfel, P. W. Roesky, *Nanoscale* **2020**, *12*, 20065–20088.
[6] S. Yue, M. Luo, H. Liu, S. Wei, *Front. Chem.* **2020**, *8*, 543.
[7] T. Xiao, J. Huang, D. Wang, T. Meng, X. Yang, *Talanta* **2020**, *206*, 120210.
[8] R. Herizchi, E. Abbasi, M. Milani, A. Akbarzadeh, *Artif. Cells Nanomedicine Biotechnol.* **2016**, *44*, 596–602.
[9] X. Hong, C. Tan, J. Chen, Z. Xu, H. Zhang, *Nano Res.* **2015**, *8*, 40–55.
[10] K. E. Saeger, J. Rodies, *Gold Bull.* **1977**, *10*, 10–14.
[11] J. T. Khoury, **1999**, DOI 10.13140/RG.2.1.1837.4086/1.
[12] G. M. Bancroft, T. Chan, R. J. Puddephatt, J. S. Tse, *Inorg. Chem.* **1982**, *21*, 2946–2949.
[13] N. S. Abadeer, C. J. Murphy, *J. Phys. Chem. C* **2016**, *120*, 4691–4716.
[14] N. S. Abadeer, M. R. Brennan, W. L. Wilson, C. J. Murphy, *ACS Nano* **2014**, *8*, 8392–8406.
[15] N. Li, P. Zhao, D. Astruc, *Angew. Chem. Int. Ed.* **2014**, *53*, 1756–1789.
[16] P. Yotprayoonsak, N. Anusak, J. Virtanen, V. Kangas, V. Promarak, *Microelectron. Eng.* **2022**, *255*, 111718.
[17] N. Heidary, N. Kornienko, *Chem. Commun.* **2019**, *55*, 11996–11999.
[18] S. Engel, E.-C. Fritz, B. J. Ravoo, *Chem. Soc. Rev.* **2017**, *46*, 2057–2075.
[19] A. J. Nathanael, T. H. Oh, *Polymers* **2020**, *12*, 3061.
[20] A. M. Smith, K. A. Johnston, S. E. Crawford, L. E. Marbella, J. E. Millstone, *The Analyst* **2017**, *142*, 11–29.
[21] A. Gupta, W. Ndugire, C.-M. Hirschbiegel, L. Grigely, V. M. Rotello, *Acc. Chem. Res.* **2023**, *56*, 2151–2169.
[22] C. Li, D. Li, G. Wan, J. Xu, W. Hou, *Nanoscale Res. Lett.* **2011**, *6*, 440.
[23] C. Battocchio, F. Porcaro, S. Mukherjee, E. Magnano, S. Nappini, I. Fratoddi, M. Quintiliani, M. V. Russo, G. Polzonetti, *J. Phys. Chem. C* **2014**, *118*, 8159–8168.
[24] N. L. Dominique, R. Chen, A. V. B. Santos, S. L. Strausser, T. Rauch, C. Q. Kotseos, W. C. Boggess, L. Jensen, D. M. Jenkins, J. P. Camden, *Inorg. Chem. Front.* **2022**, *9*, 6279–6287.
[25] M. Azubel, J. Koivisto, S. Malola, D. Bushnell, G. L. Hura, A. L. Koh, H. Tsunoyama, T. Tsukuda, M. Pettersson, H. Häkkinen, R. D. Kornberg, *Science* **2014**, *345*, 909–912.
[26] A. Leifert, Y. Pan-Bartnek, U. Simon, W. Jahnen-Dechent, *Nanoscale* **2013**, *5*, 6224.
[27] F. Annesi, A. Pane, L. Pezzi, P. Pagliusi, M. A. Losso, B. Stamile, A. Qualtieri, G. Desiderio, M. Contardi, A. Athanassiou, G. Perotto, L. De Sio, *Colloids Surf. Physicochem. Eng. Asp.* **2021**, *625*, 126950.
[28] W. Ahmed, İ. M. Öztürk, R. M. F. Iftikhar, A. Bek, *Mater. Chem. Phys.* **2022**, *278*, 125589.
[29] J. Nishigaki, K. Koyasu, T. Tsukuda, *Chem. Rec.* **2014**, *14*, 897–909.
[30] R. H. Adnan, J. M. L. Madridejos, A. S. Alotabi, G. F. Metha, G. G. Andersson, *Adv. Sci.* **2022**, *9*, 2105692.
[31] K. L. D. M. Weerawardene, H. Häkkinen, C. M. Aikens, *Annu. Rev. Phys. Chem.* **2018**, *69*, 205–229.
[32] C. Sun, B. K. Teo, C. Deng, J. Lin, G.-G. Luo, C.-H. Tung, D. Sun, *Coord. Chem. Rev.* **2021**, *427*, 213576.
[33] H. Hirai, S. Ito, S. Takano, K. Koyasu, T. Tsukuda, *Chem. Sci.* **2020**, *11*, 12233–12248.
[34] H. Shen, G. Tian, Z. Xu, L. Wang, Q. Wu, Y. Zhang, B. K. Teo, N. Zheng, *Coord. Chem. Rev.* **2022**, *458*, 214425.
[35] W. Kurashige, Y. Niihori, S. Sharma, Y. Negishi, *Coord. Chem. Rev.* **2016**, *320–321*, 238–250.
[36] M.-M. Zhang, X.-Y. Dong, Y.-J. Wang, S.-Q. Zang, T. C. W. Mak, *Coord. Chem. Rev.* **2022**, *453*, 214315.
[37] T. Omoda, S. Takano, T. Tsukuda, *Small* **2021**, *17*, 2001439.
[38] S. Kenzler, A. Schnepf, *Chem. Sci.* **2021**, *12*, 3116–3129.
[39] J. W. Fagan, K. L. D. M. Weerawardene, A. Cirri, C. M. Aikens, C. J. Johnson, *J. Chem. Phys.* **2021**, *155*, 014301.
[40] M. Agrachev, M. Ruzzi, A. Venzo, F. Maran, *Acc. Chem. Res.* **2019**, *52*, 44–52.
[41] Y. Negishi, N. K. Chaki, Y. Shichibu, R. L. Whetten, T. Tsukuda, *J. Am. Chem. Soc.* **2007**, *129*, 11322–11323.
[42] K. Kwak, V. D. Thanthirige, K. Pyo, D. Lee, G. Ramakrishna, *J. Phys. Chem. Lett.* **2017**, *8*, 4898–4905.
[43] J. Koivisto, X. Chen, S. Donnini, T. Lahtinen, H. Häkkinen, G. Groenhof, M. Pettersson, *J. Phys. Chem. C* **2016**, *120*, 10041–10050.

[44] Y. Zheng, L. Lai, W. Liu, H. Jiang, X. Wang, *Adv. Colloid Interface Sci.* **2017**, *242*, 1–16.
[45] P. Jena, Q. Sun, *Chem. Rev.* **2018**, *118*, 5755–5870.
[46] W. D. Knight, K. Clemenger, W. A. De Heer, W. A. Saunders, M. Y. Chou, M. L. Cohen, *Phys. Rev. Lett.* **1984**, *52*, 2141–2143.
[47] P. A. Lummis, K. M. Osten, T. I. Levchenko, M. Sabooni Asre Hazer, S. Malola, B. Owens-Baird, A. J. Veinot, E. L. Albright, G. Schatte, S. Takano, K. Kovnir, K. G. Stamplecoskie, T. Tsukuda, H. Häkkinen, M. Nambo, C. M. Crudden, *JACS Au* **2022**, jacsau.2c00004.
[48] A. I. Sullivan, J. F. DeJesus, S. Malola, S. Takano, T. Tsukuda, H. Häkkinen, C. M. Crudden, *Chem. Mater.* **2023**, *35*, 2790–2796.
[49] P. Luo, S. Bai, X. Wang, J. Zhao, Z. Yan, Y. Han, S. Zang, T. C. W. Mak, *Adv. Opt. Mater.* **2021**, *9*, 2001936.
[50] R. H. Adnan, J. M. L. Madridejos, A. S. Alotabi, G. F. Metha, G. G. Andersson, *Adv. Sci.* **2022**, *9*, 2105692.
[51] Y. Du, H. Sheng, D. Astruc, M. Zhu, *Chem. Rev.* **2020**, *120*, 526–622.
[52] P. Slepička, N. Slepičková Kasálková, J. Siegel, Z. Kolská, V. Švorčík, *Materials* **2019**, *13*, 1.
[53] T. G. Schaaff, G. Knight, M. N. Shafigullin, R. F. Borkman, R. L. Whetten, *J. Phys. Chem. B* **1998**, *102*, 10643–10646.
[54] V. L. Jimenez, D. G. Georganopoulou, R. J. White, A. S. Harper, A. J. Mills, D. Lee, R. W. Murray, *Langmuir* **2004**, *20*, 6864–6870.
[55] R. L. Donkers, D. Lee, R. W. Murray, *Langmuir* **2004**, *20*, 1945–1952.
[56] M. M. Alvarez, J. T. Khoury, T. G. Schaaff, M. Shafigullin, I. Vezmar, R. L. Whetten, *Chem. Phys. Lett.* **1997**, *266*, 91–98.
[57] Y. Negishi, Y. Takasugi, S. Sato, H. Yao, K. Kimura, T. Tsukuda, *J. Am. Chem. Soc.* **2004**, *126*, 6518–6519.
[58] Y. Negishi, K. Nobusada, T. Tsukuda, *J. Am. Chem. Soc.* **2005**, *127*, 5261–5270.
[59] M. Zhu, E. Lanni, N. Garg, M. E. Bier, R. Jin, *J. Am. Chem. Soc.* **2008**, *130*, 1138–1139.
[60] Z. Wu, J. Suhan, R. Jin, *J Mater Chem* **2009**, *19*, 622–626.
[61] M. Zhu, H. Qian, R. Jin, *J. Am. Chem. Soc.* **2009**, *131*, 7220–7221.
[62] H. Qian, M. Zhu, E. Lanni, Y. Zhu, M. E. Bier, R. Jin, *J. Phys. Chem. C* **2009**, *113*, 17599–17603.
[63] N. K. Chaki, Y. Negishi, H. Tsunoyama, Y. Shichibu, T. Tsukuda, *J. Am. Chem. Soc.* **2008**, *130*, 8608–8610.
[64] A. Das, T. Li, K. Nobusada, C. Zeng, N. L. Rosi, R. Jin, *J. Am. Chem. Soc.* **2013**, *135*, 18264–18267.
[65] D. Crasto, S. Malola, G. Brosofsky, A. Dass, H. Häkkinen, *J. Am. Chem. Soc.* **2014**, *136*, 5000–5005.
[66] C. Zeng, Y. Chen, G. Li, R. Jin, *Chem. Mater.* **2014**, *26*, 2635–2641.
[67] X.-K. Wan, Z.-J. Guan, Q.-M. Wang, *Angew. Chem. Int. Ed.* **2017**, *56*, 11494–11497.
[68] S. Ito, S. Takano, T. Tsukuda, *J. Phys. Chem. Lett.* **2019**, *10*, 6892–6896.
[69] T.-T. Jia, G. Yang, S.-J. Mo, Z.-Y. Wang, B.-J. Li, W. Ma, Y.-X. Guo, X. Chen, X. Zhao, J.-Q. Liu, S.-Q. Zang, *ACS Nano* **2019**, *13*, 8320–8328.
[70] Z. Lei, X.-K. Wan, S.-F. Yuan, Z.-J. Guan, Q.-M. Wang, *Acc. Chem. Res.* **2018**, *51*, 2465–2474.
[71] Z. Lei, J. Li, X. Wan, W. Zhang, Q. Wang, *Angew. Chem. Int. Ed.* **2018**, *57*, 8639–8643.
[72] M. McPartlin, R. Mason, L. Malatesta, *J Chem Soc D* **1969**, *0*, 334–334.
[73] F. Cariati, L. Naldini, *J. Chem. Soc. Dalton Trans.* **1972**, 2286.
[74] A. Olivares, J. Laskin, G. E. Johnson, *J. Phys. Chem. A* **2014**, *118*, 8464–8470.
[75] S. Kenzler, C. Schrenk, A. R. Frojd, H. Häkkinen, A. Z. Clayborne, A. Schnepf, *Chem. Commun.* **2018**, *54*, 248–251.
[76] F. Fetzer, C. Schrenk, N. Pollard, A. Adeagbo, A. Z. Clayborne, A. Schnepf, *Chem. Commun.* **2021**, *57*, 3551–3554.
[77] D. Michael, P. Mingos, *Polyhedron* **1984**, *3*, 1289–1297.
[78] L. C. McKenzie, T. O. Zaikova, J. E. Hutchison, *J. Am. Chem. Soc.* **2014**, *136*, 13426–13435.
[79] Z. Wu, R. Jin, *Chem. - Eur. J.* **2013**, *19*, 12259–12263.
[80] H.-F. Zhang, M. Stender, R. Zhang, C. Wang, J. Li, L.-S. Wang, *J. Phys. Chem. B* **2004**, *108*, 12259–12263.
[81] W. W. Weare, S. M. Reed, M. G. Warner, J. E. Hutchison, *J. Am. Chem. Soc.* **2000**, *122*, 12890–12891.
[82] Y. Shichibu, K. Konishi, *Small* **2010**, *6*, 1216–1220.
[83] J. Chen, Q.-F. Zhang, T. A. Bonaccorso, P. G. Williard, L.-S. Wang, *J. Am. Chem. Soc.* **2014**, *136*, 92–95.
[84] Y. Shichibu, M. Zhang, Y. Kamei, K. Konishi, *J. Am. Chem. Soc.* **2014**, *136*, 12892–12895.
[85] Q.-F. Zhang, P. G. Williard, L.-S. Wang, *Small* **2016**, *12*, 2518–2525.
[86] M. F. Bertino, Z.-M. Sun, R. Zhang, L.-S. Wang, *J. Phys. Chem. B* **2006**, *110*, 21416–21418.
[87] J. M. Pettibone, J. W. Hudgens, *ACS Nano* **2011**, *5*, 2989–3002.
[88] J. W. Hudgens, J. M. Pettibone, T. P. Senftle, R. N. Bratton, *Inorg. Chem.* **2011**, *50*, 10178–10189.
[89] T. Huang, L. Huang, W. He, X. Song, Z. Sun, Y. Jiang, G. Pan, S. Wei, *J. Phys. Chem. C* **2018**, *122*, 6405–6411.

[90] M. R. Narouz, S. Takano, P. A. Lummis, T. I. Levchenko, A. Nazemi, S. Kaappa, S. Malola, G. Yousefalizadeh, L. A. Calhoun, K. G. Stamplecoskie, H. Häkkinen, T. Tsukuda, C. M. Crudden, *J. Am. Chem. Soc.* **2019**, *141*, 14997–15002.
[91] H. Shen, G. Deng, S. Kaappa, S. Malola, B. K. Teo, H. Hakkinen, N. Zheng, T. Tan, Y. Han, S. Lin, *Highly Robust but Surface-Active: N-Heterocyclic Carbene-Stabilized Au25 Nanocluster as a Homogeneous Catalyst*, **2019**.
[92] H. Shen, S. Xiang, Z. Xu, C. Liu, X. Li, C. Sun, S. Lin, B. K. Teo, N. Zheng, *Nano Res.* **2020**, *13*, 1908–1911.
[93] H. Yi, K. M. Osten, T. I. Levchenko, A. J. Veinot, Y. Aramaki, T. Ooi, M. Nambo, C. M. Crudden, *Chem. Sci.* **2021**, *12*, 10436–10440.
[94] R. W. Y. Man, H. Yi, S. Malola, S. Takano, T. Tsukuda, H. Häkkinen, M. Nambo, C. M. Crudden, *J. Am. Chem. Soc.* **2022**, *144*, 2056–2061.
[95] H. Shen, X. Tang, Q. Wu, Y. Zhang, C. Ma, Z. Xu, B. K. Teo, N. Zheng, *ACS Nanosci. Au* **2022**, acsnanoscienceau.2c00026.
[96] V. K. Kulkarni, B. N. Khiarak, S. Takano, S. Malola, E. L. Albright, T. I. Levchenko, M. D. Aloisio, C.-T. Dinh, T. Tsukuda, H. Häkkinen, C. M. Crudden, *J. Am. Chem. Soc.* **2022**, *144*, 9000–9006.
[97] P. A. Lummis, K. M. Osten, T. I. Levchenko, M. Sabooni Asre Hazer, S. Malola, B. Owens-Baird, A. J. Veinot, E. L. Albright, G. Schatte, S. Takano, K. Kovnir, K. G. Stamplecoskie, T. Tsukuda, H. Häkkinen, M. Nambo, C. M. Crudden, *JACS Au* **2022**, *2*, 875–885.
[98] X. Wang, R. Liu, L. Tian, J. Bao, C. Zhao, F. Niu, D. Cheng, Z. Lu, K. Hu, *J. Phys. Chem. C* **2022**, *126*, 18374–18382.
[99] J. Sun, X. Tang, J. Tang, Y. Zhang, Z. Li, Chaolumen, S. Guo, H. Shen, *Inorg. Chem.* **2023**, *62*, 5088–5094.
[100] P. Luo, X. Zhai, S. Bai, Y. Si, X. Dong, Y. Han, S. Zang, *Angew. Chem.* **2023**, *135*, e202219017.
[101] X. Kang, Y. Li, M. Zhu, R. Jin, *Chem. Soc. Rev.* **2020**, *49*, 6443–6514.
[102] Y. Wang, T. Bürgi, *Nanoscale Adv.* **2021**, *3*, 2710–2727.
[103] C. Zeng, C. Liu, Y. Pei, R. Jin, *ACS Nano* **2013**, *7*, 6138–6145.
[104] Y. Shichibu, Y. Negishi, T. Tsukuda, T. Teranishi, *J. Am. Chem. Soc.* **2005**, *127*, 13464–13465.
[105] R. C. B. Copley, D. M. P. Mingos, *J. Chem. Soc. Dalton Trans.* **1996**, 491.
[106] J.-Q. Wang, Z.-J. Guan, W.-D. Liu, Y. Yang, Q.-M. Wang, *J. Am. Chem. Soc.* **2019**, *141*, 2384–2390.
[107] F. Demartin, M. Manassero, L. Naldini, R. Ruggeri, M. Sansoni, *J Chem Soc Chem Commun* **1981**, 222–223.
[108] J. W. A. Van Der Velden, J. J. Bour, W. P. Bosman, J. H. Noordik, *J. Chem. Soc. Chem. Commun.* **1981**, 1218.
[109] J. W. A. Van Der Velden, J. J. Bour, J. J. Steggerda, P. T. Beurskens, M. Roseboom, J. H. Noordik, *Inorg. Chem.* **1982**, *21*, 4321–4324.
[110] Y. Kamei, Y. Shichibu, K. Konishi, *Angew. Chem.* **2011**, *123*, 7580–7583.
[111] M. Sugiuchi, Y. Shichibu, T. Nakanishi, Y. Hasegawa, K. Konishi, *Chem. Commun.* **2015**, *51*, 13519–13522.
[112] S. Takano, S. Ito, T. Tsukuda, *J. Am. Chem. Soc.* **2019**, *141*, 15994–16002.
[113] E. Ito, S. Takano, T. Nakamura, T. Tsukuda, *Angew. Chem. Int. Ed.* **2021**, *60*, 645–649.
[114] M. R. Narouz, K. M. Osten, P. J. Unsworth, R. W. Y. Man, K. Salorinne, S. Takano, R. Tomihara, S. Kaappa, S. Malola, C.-T. Dinh, J. D. Padmos, K. Ayoo, P. J. Garrett, M. Nambo, J. H. Horton, E. H. Sargent, H. Häkkinen, T. Tsukuda, C. M. Crudden, *Nat. Chem.* **2019**, *11*, 419–425.
[115] T. Dainese, S. Antonello, S. Bogialli, W. Fei, A. Venzo, F. Maran, *ACS Nano* **2018**, *12*, 7057–7066.
[116] P. A. Lummis, K. M. Osten, T. I. Levchenko, M. Sabooni Asre Hazer, S. Malola, B. Owens-Baird, A. J. Veinot, E. L. Albright, G. Schatte, S. Takano, K. Kovnir, K. G. Stamplecoskie, T. Tsukuda, H. Häkkinen, M. Nambo, C. M. Crudden, *JACS Au* **2022**, *2*, 875–885.
[117] X. Ren, J. Fu, X. Lin, X. Fu, J. Yan, R. Wu, C. Liu, J. Huang, *Dalton Trans.* **2018**, *47*, 7487–7491.
[118] J. Wang, Z. Wang, S. Li, S. Zang, T. C. W. Mak, *Angew. Chem. Int. Ed.* **2021**, *60*, 5959–5964.
[119] M. Wang, Y. Chen, C. Tang, *Chem. – Asian J.* **2023**, e202300463.
[120] C. Zeng, H. Qian, T. Li, G. Li, N. L. Rosi, B. Yoon, R. N. Barnett, R. L. Whetten, U. Landman, R. Jin, *Angew. Chem. Int. Ed.* **2012**, *51*, 13114–13118.
[121] Y. Li, R. Jin, *J. Am. Chem. Soc.* **2020**, *142*, 13627–13644.
[122] M. Zhu, C. M. Aikens, F. J. Hollander, G. C. Schatz, R. Jin, *J. Am. Chem. Soc.* **2008**, *130*, 5883–5885.
[123] Y. Shichibu, Y. Negishi, T. Watanabe, N. K. Chaki, H. Kawaguchi, T. Tsukuda, *J. Phys. Chem. C* **2007**, *111*, 7845–7847.
[124] P. D. Jadzinsky, G. Calero, C. J. Ackerson, D. A. Bushnell, R. D. Kornberg, *Science* **2007**, *318*, 430–433.
[125] N. Yan, N. Xia, L. Liao, M. Zhu, F. Jin, R. Jin, Z. Wu, *Sci. Adv.* **2018**, *4*, eaat7259.
[126] C. Zeng, Y. Chen, K. Kirschbaum, K. J. Lambright, R. Jin, *Science* **2016**, *354*, 1580–1584.
[127] S. Antonello, N. V. Perera, M. Ruzzi, J. A. Gascón, F. Maran, *J. Am. Chem. Soc.* **2013**, *135*, 15585–15594.

[128] M. F. Matus, H. Häkkinen, *Nat. Rev. Mater.* **2023**, *8*, 372–389.
[129] X. Han, X. Luan, H. Su, J. Li, S. Yuan, Z. Lei, Y. Pei, Q. Wang, *Angew. Chem. Int. Ed.* **2020**, *59*, 2309–2312.
[130] H. Shen, Q. Wu, S. Malola, Y.-Z. Han, Z. Xu, R. Qin, X. Tang, Y.-B. Chen, B. K. Teo, H. Häkkinen, N. Zheng, *J. Am. Chem. Soc.* **2022**, *144*, 10844–10853.
[131] K. Hirano, S. Takano, T. Tsukuda, *J. Phys. Chem. C* **2021**, *125*, 9930–9936.
[132] X.-K. Wan, S.-F. Yuan, Q. Tang, D. Jiang, Q.-M. Wang, *Angew. Chem. Int. Ed.* **2015**, *54*, 5977–5980.
[133] H. Shen, Z. Xu, M. S. A. Hazer, Q. Wu, J. Peng, R. Qin, S. Malola, B. K. Teo, H. Häkkinen, N. Zheng, *Angew. Chem. Int. Ed.* **2021**, *60*, 3752–3758.
[134] W.-D. Si, Y.-Z. Li, S.-S. Zhang, S. Wang, L. Feng, Z.-Y. Gao, C.-H. Tung, D. Sun, *ACS Nano* **2021**, *15*, 16019–16029.
[135] X.-K. Wan, W. W. Xu, S.-F. Yuan, Y. Gao, X.-C. Zeng, Q.-M. Wang, *Angew. Chem. Int. Ed.* **2015**, *54*, 9683–9686.
[136] T. Wang, W.-H. Zhang, S.-F. Yuan, Z.-J. Guan, Q.-M. Wang, *Chem. Commun.* **2018**, *54*, 10367–10370.
[137] J. W. A. Van Der Velden, J. J. Bour, W. P. Bosman, J. H. Noordik, *Inorg. Chem.* **1983**, *22*, 1913–1918.
[138] G. Schmid, R. Pfeil, R. Boese, F. Bandermann, S. Meyer, Gijs. H. M. Calis, J. W. A. Van Der Velden, *Chem. Ber.* **1981**, *114*, 3634–3642.
[139] F. Wen, U. Englert, B. Gutrath, U. Simon, *Eur. J. Inorg. Chem.* **2008**, *2008*, 106–111.
[140] G. Xu, L. Wu, X. Chang, T. W. H. Ang, W. Wong, J. Huang, C. Che, *Angew. Chem. Int. Ed.* **2019**, *58*, 16297–16306.
[141] S. Takano, H. Hirai, S. Muramatsu, T. Tsukuda, *J. Am. Chem. Soc.* **2018**, *140*, 12314–12317.
[142] S. Takano, H. Hirai, S. Muramatsu, T. Tsukuda, *J. Am. Chem. Soc.* **2018**, *140*, 8380–8383.
[143] J. J. Bour, R. P. F. Kanters, P. P. J. Schlebos, J. J. Steggerda, *Recl. Trav. Chim. Pays-Bas* **2010**, *107*, 211–215.
[144] H. Shen, E. Selenius, P. Ruan, X. Li, P. Yuan, O. Lopez-Estrada, S. Malola, S. Lin, B. K. Teo, H. Häkkinen, N. Zheng, *Chem. – Eur. J.* **2020**, *26*, 8465–8470.
[145] M. Bevilacqua, M. Roverso, S. Bogialli, C. Graiff, A. Biffis, *Inorg. Chem.* **2023**, *62*, 1383–1393.
[146] H. V. Huynh, *Chem. Rev.* **2018**, *118*, 9457–9492.
[147] D. J. Nelson, S. P. Nolan, *Chem. Soc. Rev.* **2013**, *42*, 6723.
[148] M. N. Hopkinson, C. Richter, M. Schedler, F. Glorius, *Nature* **2014**, *510*, 485–496.
[149] R. Hoffmann, G. D. Zeiss, G. W. Van Dine, *J. Am. Chem. Soc.* **1968**, *90*, 1485–1499.
[150] N. C. Baird, K. F. Taylor, *J. Am. Chem. Soc.* **1978**, *100*, 1333–1338.
[151] D. Feller, W. Thatcher Borden, E. R. Davidson, *Chem. Phys. Lett.* **1980**, *71*, 22–26.
[152] E. Peris, *Chem. Rev.* **2018**, *118*, 9988–10031.
[153] D. Bourissou, O. Guerret, F. P. Gabbaï, G. Bertrand, *Chem. Rev.* **2000**, *100*, 39–92.
[154] J. Messelberger, M. Kumar, S. J. Goodner, D. Munz, *Org. Chem. Front.* **2021**, *8*, 6663–6669.
[155] A. J. Arduengo, R. L. Harlow, M. Kline, *J. Am. Chem. Soc.* **1991**, *113*, 361–363.
[156] L. Benhamou, E. Chardon, G. Lavigne, S. Bellemin-Laponnaz, V. César, *Chem. Rev.* **2011**, *111*, 2705–2733.
[157] F. E. Hahn, M. C. Jahnke, *Angew. Chem. Int. Ed.* **2008**, *47*, 3122–3172.
[158] M. H. Wang, K. A. Scheidt, *Angew. Chem. Int. Ed.* **2016**, *55*, 14912–14922.
[159] Y. Chu, H. Deng, J.-P. Cheng, *J. Org. Chem.* **2007**, *72*, 7790–7793.
[160] P. De Frémont, N. M. Scott, E. D. Stevens, S. P. Nolan, *Organometallics* **2005**, *24*, 2411–2418.
[161] H. M. J. Wang, I. J. B. Lin, *Organometallics* **1998**, *17*, 972–975.
[162] M. R. L. Furst, C. S. J. Cazin, *Chem. Commun.* **2010**, *46*, 6924.
[163] A. Collado, A. Gómez-Suárez, A. R. Martin, A. M. Z. Slawin, S. P. Nolan, *Chem. Commun.* **2013**, *49*, 5541.
[164] T. Scattolin, N. V. Tzouras, L. Falivene, L. Cavallo, S. P. Nolan, *Dalton Trans.* **2020**, *49*, 9694–9700.
[165] T. Scattolin, G. Tonon, E. Botter, S. G. Guillet, N. V. Tzouras, S. P. Nolan, *Chem. – Eur. J.* **2023**, e202301961.
[166] P. Teixeira, S. Bastin, V. César, *Isr. J. Chem.* **2022**, e202200051.
[167] X. Ling, S. Roland, M.-P. Pileni, *Chem. Mater.* **2015**, *27*, 414–423.
[168] M. R. Narouz, C.-H. Li, A. Nazemi, C. M. Crudden, *Langmuir* **2017**, *33*, 14211–14219.
[169] S. Ibáñez, M. Poyatos, E. Peris, *Acc. Chem. Res.* **2020**, *53*, 1401–1413.
[170] M. R. Narouz, K. M. Osten, P. J. Unsworth, R. W. Y. Man, K. Salorinne, S. Takano, R. Tomihara, S. Kaappa, S. Malola, C.-T. Dinh, J. D. Padmos, K. Ayoo, P. J. Garrett, M. Nambo, J. H. Horton, E. H. Sargent, H. Häkkinen, T. Tsukuda, C. M. Crudden, *Nat. Chem.* **2019**, *11*, 419–425.
[171] C. A. Smith, M. R. Narouz, P. A. Lummis, I. Singh, A. Nazemi, C.-H. Li, C. M. Crudden, *Chem. Rev.* **2019**, *119*, 4986–5056.
[172] R. Jazzar, M. Soleilhavoup, G. Bertrand, *Chem. Rev.* **2020**, *120*, 4141–4168.
[173] X. Kang, Y. Li, M. Zhu, R. Jin, *Chem. Soc. Rev.* **2020**, *49*, 6443–6514.
[174] J.-P. Choi, C. A. Fields-Zinna, R. L. Stiles, R. Balasubramanian, A. D. Douglas, M. C. Crowe, R. W. Murray, *J. Phys. Chem. C* **2010**, *114*, 15890–15896.

[175] Y. Negishi, T. Iwai, M. Ide, *Chem. Commun.* **2010**, *46*, 4713.
[176] S. Wang, Y. Song, S. Jin, X. Liu, J. Zhang, Y. Pei, X. Meng, M. Chen, P. Li, M. Zhu, *J. Am. Chem. Soc.* **2015**, *137*, 4018–4021.
[177] X. Kang, J. Xiang, Y. Lv, W. Du, H. Yu, S. Wang, M. Zhu, *Chem. Mater.* **2017**, *29*, 6856–6862.
[178] C. Kumara, C. M. Aikens, A. Dass, *J. Phys. Chem. Lett.* **2014**, *5*, 461–466.
[179] W. Fei, S. Antonello, T. Dainese, A. Dolmella, M. Lahtinen, K. Rissanen, A. Venzo, F. Maran, *J. Am. Chem. Soc.* **2019**, *141*, 16033–16045.
[180] M. Zhou, J. Zhong, S. Wang, Q. Guo, M. Zhu, Y. Pei, A. Xia, *J. Phys. Chem. C* **2015**, *119*, 18790–18797.
[181] Z. Qin, D. Zhao, L. Zhao, Q. Xiao, T. Wu, J. Zhang, C. Wan, G. Li, *Nanoscale Adv.* **2019**, *1*, 2529–2536.
[182] Y. Negishi, K. Igarashi, K. Munakata, W. Ohgake, K. Nobusada, *Chem Commun* **2012**, *48*, 660–662.
[183] X. Liu, E. Wang, M. Zhou, Y. Wan, Y. Zhang, H. Liu, Y. Zhao, J. Li, Y. Gao, Y. Zhu, *Angew. Chem. Int. Ed.* **2022**, *61*, e202207685.
[184] K. Kwak, Q. Tang, M. Kim, D. Jiang, D. Lee, *J. Am. Chem. Soc.* **2015**, *137*, 10833–10840.
[185] Y. Fujiki, T. Matsuyama, S. Kikkawa, J. Hirayama, H. Takaya, N. Nakatani, N. Yasuda, K. Nitta, Y. Negishi, S. Yamazoe, *Commun. Chem.* **2023**, *6*, 129.
[186] H. Shen, Q. Wu, M. S. Asre Hazer, X. Tang, Y.-Z. Han, R. Qin, C. Ma, S. Malola, B. K. Teo, H. Häkkinen, N. Zheng, *Chem* **2022**, *8*, 2380–2392.
[187] M. Zhu, C. M. Aikens, M. P. Hendrich, R. Gupta, H. Qian, G. C. Schatz, R. Jin, *J. Am. Chem. Soc.* **2009**, *131*, 2490–2492.
[188] S. Tian, L. Liao, J. Yuan, C. Yao, J. Chen, J. Yang, Z. Wu, *Chem. Commun.* **2016**, *52*, 9873–9876.
[189] M. Suyama, S. Takano, T. Nakamura, T. Tsukuda, *J. Am. Chem. Soc.* **2019**, *141*, 14048–14051.
[190] Y. Li, T.-Y. Luo, M. Zhou, Y. Song, N. L. Rosi, R. Jin, *J. Am. Chem. Soc.* **2018**, *140*, 14235–14243.
[191] Y. Negishi, W. Kurashige, Y. Niihori, T. Iwasa, K. Nobusada, *Phys. Chem. Chem. Phys.* **2010**, *12*, 6219.
[192] Y. Niihori, M. Eguro, A. Kato, S. Sharma, B. Kumar, W. Kurashige, K. Nobusada, Y. Negishi, *J. Phys. Chem. C* **2016**, *120*, 14301–14309.
[193] C. M. Hendrich, K. Sekine, T. Koshikawa, K. Tanaka, A. S. K. Hashmi, *Chem. Rev.* **2021**, *121*, 9113–9163.
[194] M. Wang, Y. Chen, C. Tang, *Chem. – Asian J.* **2023**, *18*, e202300463.
[195] Y.-Z. Li, R. Ganguly, K. Y. Hong, Y. Li, M. E. Tessensohn, R. Webster, W. K. Leong, *Chem. Sci.* **2018**, *9*, 8723–8730.
[196] J. B. Patty, S. Havenridge, D. Tietje-Mckinney, M. A. Siegler, K. K. Singh, R. Hajy Hosseini, M. Ghabin, C. M. Aikens, A. Das, *J. Am. Chem. Soc.* **2022**, *144*, 478–484.
[197] S. Yuan, Z. Lei, Z. Guan, Q. Wang, *Angew. Chem. Int. Ed.* **2021**, *60*, 5225–5229.
[198] H. Li, B. Guan, W. Wang, D. Xing, Z. Fang, X. Wan, L. Yang, Z. Shi, *Tetrahedron* **2007**, *63*, 8430–8434.
[199] J. Li, R. R. Nasaruddin, Y. Feng, J. Yang, N. Yan, J. Xie, *Chem. - Eur. J.* **2016**, *22*, 14816–14820.
[200] F. Fu, A. Dedieu, W. Wang, T. Chen, Y. Song, E. Fouquet, J.-R. Hamon, M. Zhu, D. Astruc, *Chem. Commun.* **2019**, *55*, 10277–10280.
[201] A. Shivhare, S. J. Ambrose, H. Zhang, R. W. Purves, R. W. J. Scott, *Chem Commun* **2013**, *49*, 276–278.
[202] S. Zhao, A. Das, H. Zhang, R. Jin, Y. Song, R. Jin, *Prog. Nat. Sci. Mater. Int.* **2016**, *26*, 483–486.
[203] H. Yamamoto, H. Yano, H. Kouchi, Y. Obora, R. Arakawa, H. Kawasaki, *Nanoscale* **2012**, *4*, 4148.
[204] Y.-M. Li, J. Hu, M. Zhu, *Coord. Chem. Rev.* **2023**, *495*, 215364.
[205] B. Casteleiro, J. M. G. Martinho, J. P. S. Farinha, *Nanoscale* **2021**, *13*, 17199–17217.
[206] J. Zhao, R. Jin, *Nano Today* **2018**, *18*, 86–102.
[207] M. Haruta, T. Kobayashi, H. Sano, N. Yamada, *Chem. Lett.* **1987**, *16*, 405–408.
[208] X. Nie, C. Zeng, X. Ma, H. Qian, Q. Ge, H. Xu, R. Jin, *Nanoscale* **2013**, *5*, 5912.
[209] T. Yoskamtorn, S. Yamazoe, R. Takahata, J. Nishigaki, A. Thivasasith, J. Limtrakul, T. Tsukuda, *ACS Catal.* **2014**, *4*, 3696–3700.
[210] G. Li, R. Jin, *J Am Chem Soc* **2014**, 8.
[211] Y. Zhu, H. Qian, R. Jin, *J. Mater. Chem.* **2011**, *21*, 6793.
[212] Y. Zhu, H. Qian, B. A. Drake, R. Jin, *Angew. Chem. Int. Ed.* **2010**, *49*, 1295–1298.
[213] G. Li, D. Jiang, C. Liu, C. Yu, R. Jin, *J. Catal.* **2013**, *306*, 177–183.
[214] G. Li, C. Liu, Y. Lei, R. Jin, *Chem. Commun.* **2012**, *48*, 12005.
[215] H.-J. Freund, G. Meijer, M. Scheffler, R. Schlögl, M. Wolf, *Angew. Chem. Int. Ed.* **2011**, *50*, 10064–10094.
[216] X. Nie, H. Qian, Q. Ge, H. Xu, R. Jin, *ACS Nano* **2012**, *6*, 6014–6022.
[217] B. Yoon, H. Häkkinen, U. Landman, A. S. Wörz, J.-M. Antonietti, S. Abbet, K. Judai, U. Heiz, *Science* **2005**, *307*, 403–407.

[218] Y. Liu, H. Tsunoyama, T. Akita, S. Xie, T. Tsukuda, *ACS Catal.* **2011**, *1*, 2–6.
[219] Y. Zhu, H. Qian, R. Jin, *Chem. – Eur. J.* **2010**, *16*, 11455–11462.
[220] S. M. van de Looij, E. R. Hebels, M. Viola, M. Hembury, S. Oliveira, T. Vermonden, *Bioconjug. Chem.* **2022**, *33*, 4–23.
[221] D. Hao, X. Zhang, R. Su, Y. Wang, W. Qi, *J. Mater. Chem. B* **2023**, *11*, 5051–5070.
[222] A. S. Krishna Kumar, W.-L. Tseng, *Anal. Methods* **2020**, *12*, 1809–1826.
[223] S. Kundu, M. Ghosh, N. Sarkar, *Langmuir* **2021**, *37*, 9281–9301.
[224] S. Ni, Y. Liu, S. Tong, S. Li, X. Song, *J. Anal. Test.* **2023**, *7*, 260–271.
[225] Y. Li, T. Zhai, J. Chen, J. Shi, L. Wang, J. Shen, X. Liu, *Chem. – Eur. J.* **2022**, *28*, e202103736.
[226] M. Ganguly, J. Jana, A. Pal, T. Pal, *RSC Adv.* **2016**, *6*, 17683–17703.
[227] L. Han, C. Ding, Y. Guo, Y. Wang, Y. Ding, *Anal. Bioanal. Chem.* **2020**, *412*, 3695–3702.
[228] N. Alasvand, A. M. Urbanska, M. Rahmati, M. Saeidifar, P. S. Gungor-Ozkerim, F. Sefat, J. Rajadas, M. Mozafari, in *Multifunct. Syst. Comb. Deliv. Biosensing Diagn.*, Elsevier, **2017**, pp. 245–259.
[229] H. Santhakumar, R. V. Nair, D. M. Govindachar, G. Periyasamy, R. S. Jayasree, *ACS Sustain. Chem. Eng.* **2023**, *11*, 2102–2114.
[230] M. F. Matus, H. Häkkinen, *Small* **2021**, *17*, 2005499.
[231] D. Luo, X. Wang, S. Zeng, G. Ramamurthy, C. Burda, J. P. Basilion, *Small* **2019**, *15*, 1900968.
[232] V. Marjomäki, T. Lahtinen, M. Martikainen, J. Koivisto, S. Malola, K. Salorinne, M. Pettersson, H. Häkkinen, *Proc. Natl. Acad. Sci.* **2014**, *111*, 1277–1281.

2.0 RESULTS AND DISCUSSION: DIRECT REDUCTION OF di-NHC GOLD(I) COMPLEXES WITH $NaBH_4$

2.1 INTRODUCTION: SYNTHESIS OF NHC-PROTECTED AuNCs

The first NHC-capped AuNC has been reported by Sadighi et al., in which a triangular $[Au_3]^+$ core is saturated by three NHCs.[1] This cluster is SA, since it exhibits 2 valence electrons, but due to its planar structure bulky ligands are used to further stabilize it. $[Au_3(NHC)_3]^+$ is synthetized through reduction of the corresponding $[(\mu_3\text{-}CO_3)Au_3(NHC)_3]^+$ complex promoted by CO. As reported in **Figure 2.1 a**, the reducing agent extracts one coordinated oxygen, affording the desired cluster and CO_2 as by-product.

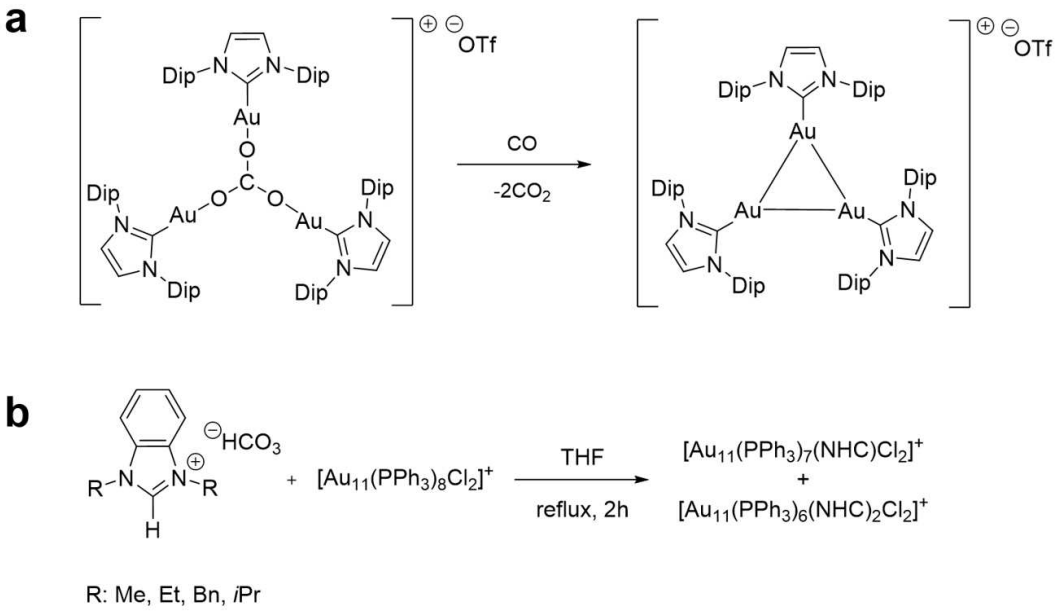

Figure 2.1:a) $[Au_3(NHC)_3]^+$ synthesis and b) ligand exchange on PPh_3-capped clusters using free NHCs.[1,2]

However, this synthesis is limited by the need for isolation of the corresponding $[(\mu_3\text{-}CO_3)Au_3(NHC)_3]^+$ complex, exclusively achievable using sterically hindered NHCs. Moreover, this decarboxylation reaction affords exclusively $[Au_3]^+$ clusters, without

providing AuNCs with higher nuclearities. This triangular core can be capped by bulky CAAC or PR_3 ligands too, when corresponding pyramidal $[(\mu_3\text{-}O)Au_3L_3]^+$ complexes are reduced by CO.[3]

More recently, a second type of NHC-protected AuNC has been reported by Crudden's group, in which ligand exchange reaction between $[Au_{11}(PPh_3)_8Cl_2]^+$ and free NHCs takes place, allowing the isolation of multiple clusters with general stoichiometries $[Au_{11}(PPh_3)_{8\text{-}n}(NHC)_nCl_2]^+$.[4] This reaction, reported in **Figure 2.1 b**, proves how NHCs are able to cap clusters presenting higher nuclearity than $[Au_3]^+$, expanding therefore the use of such ligands in cluster chemistry. However, this reaction presents low selectivity, since only NHC^{iPr} focuses the exchange towards one single product, presenting formula $[Au_{11}(PPh_3)_7(NHC^{iPr})Cl_2]^+$.

Given this drawback, AuNC synthesis is nowadays mainly performed using the "direct reduction approach", in which [(NHC)AuX] or $[(\text{di-NHC})Au_2X_2]$ (X: Cl, Br or I) complexes are reduced with $NaBH_4$, affording generally SA mono-dispersed $[Au_{13}]^{5+}$ clusters as products and overcoming the low selectivity reported before.[5–17] Moreover, if poly-dispersed clusters are obtained, it is still possible to use etching agents to focus the cluster mixture, promoting the formation of the most stable clusters.

As showed in **Figure 2.2**, the variation of wingtip groups modifies the reduction pathway, allowing the isolation of other SA cores, like $[Au_{25}]^{9+}$and $[Au_{24}]^{8+}$. In addition, isolation of $[Au_{11}]^{3+}$ clusters can be reached using di-NHCs, due to their chelating proprieties.[17] With these bidentate ligands, several bridges units between NHC scaffolds can be exploited to cap AuNCs, providing an additional tool to tailor the properties of the product.

Whereas NHCs provide generally SA clusters, these ligands can also cap clusters not presenting SA behavior, obtained when rigid or bulky NHCs force their stabilization.

Indeed, a rigid di-NHC^{BINAP} leads to the isolation of $[Au_{10}]^{4+}$ cluster, and a similar product is obtained when sterically hindered 2,4,6-trimethylbenzyl wingtips are used in mono-NHC.[10,15] These clusters are reported in **Figure 2.4**.

From these examples we can understand that these syntheses are influenced by the steric proprieties of the NHC ligand, which can be tuned through a proper choice of the wingtip substituents.

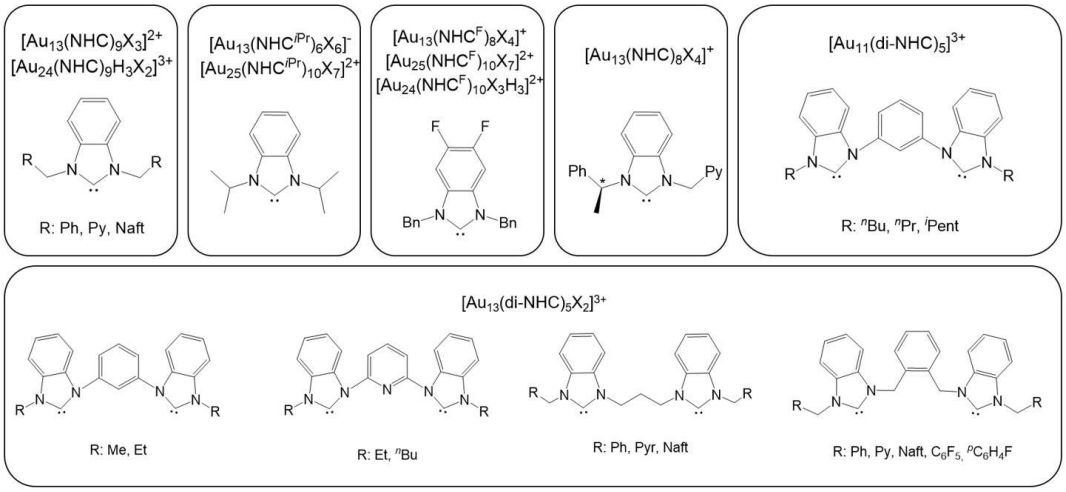

Figure 2.2: NHCs and corresponding super-atomic AuNCs synthesized so far. X are chlorides, bromides or iodides.

However, also the variation of starting reagents represents an approach to tailor these reductions. One example is the reduction of [(NHC^{iPr})AuBr], in which the reaction is focused towards the $[Au_{25}]^{9+}$ core using an additional Au(I) complex as co-reagent, correcting therefore the reduction stoichiometry. Indeed, simple direct reduction of [(NHC^{iPr})AuBr] provides classic $[Au_{13}(NHC^{iPr})_6Br_6]^-$ as product.[14] When instead $[ClAu(SMe_2)]$ is co-reduced with the NHC complex, $[Au_{25}(NHC^{iPr})_{10}Br_7]^{2+}$ cluster can be isolated.[8] These reactions are reported in **Figure 2.3**.

Another alternative is to exploit heterometallic complexes as regents, aiming at getting novel and doped clusters. For instance, $[PdAu_9(NHC^{Bn})_7X_2]^+$ is obtained when $Pd(dba)_2$ (dba: dibenzylideneacetone) is co-reduced with [(NHC^{Bn})AuX] upon $NaBH_4$

addition. Despite its unsaturated metallic core and its 6 valence electrons, this cluster shows high stability, thanks to Pd placed in the core.[11] Furthermore, a higher concentration of $NaBH_4$ varies the reduction profile, affording instead $[PdAu_{12}(NHC^{Bn})_7X_3]^+$, which presents 8 valence electron and mimic the geometry of $[Au_{13}]^{5+}$ core. These clusters are reported in **Figure 2.4**.

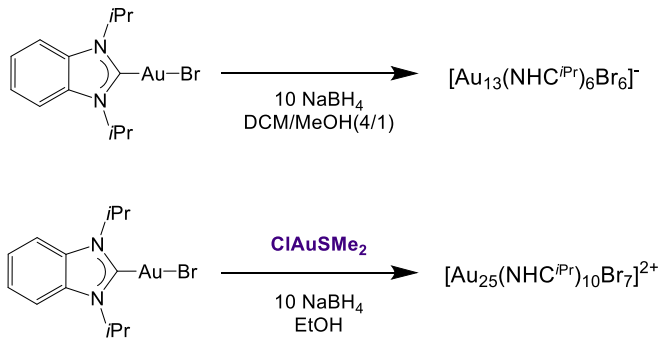

Figure 2.3: synthesis of $[Au_{13}]^{5+}$ (above) and $[Au_{25}]^{9+}$ (below) clusters reported by Zheng et al.[8,14]

Finally, the reduction pathway can be varied using cationic NHC complexes too. The first NHC/hydride-capped AuNC has been obtained through reduction of a $[(NHC)Au(py)]^+$ (py: pyridine) complex, isolating $[Au_{24}(NHC^{Bn})_9H_3Cl_2]^{3+}$ cluster.[9] This cluster is interesting since it presents 8+8 valence electrons, thus presenting a magic number despite its peculiar metallic core, formed by two Au_{12} distorted body centered icosahedra sharing one triangular face and bridged by three hydrides. Furthermore, chloride anions derive from DCM traces purposely added to the reaction mixture, which undergo chloride extraction promoted by borohydride anion, species favoring the reduction of DCM and gold complex at the same time.

From the examples reported so far, it is logical to hypothesize that these reductions of NHC-Au(I) complexes are generally guided by thermodynamic parameters, since apparently only the variation of starting reagents tunes the reduction products. For instance, it is possible to increase the reduction yields using di-NHCs due to their chelating effects. Furthermore, in literature kinetic parameters are randomly varied,

without ever clarifying how these affect the reaction profile. For instance, the product selectivity is not affected by the temperature of the system, highlighting how such reductions are not under kinetic control.[12,14] A single example of kinetic control is reported by Zheng et al., in which, slowing down the speed of addition of reductant and decreasing the amount of $NaBH_4$, $[Au_{24}(NHC^F)_9H_3Br_2]^{3+}$ can be exclusively formed, thus without $[Au_{25}(NHC^F)_{10}Br_7]^{2+}$ as co-product.[5]

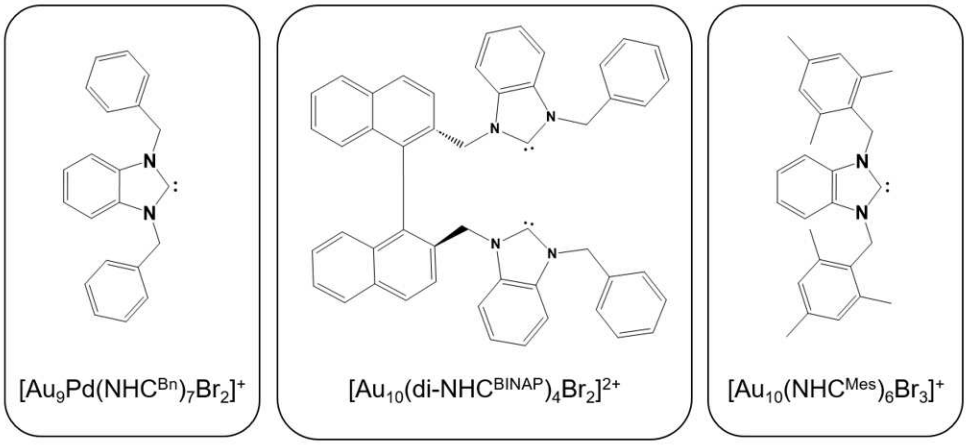

Figure 2.4: NHCs and corresponding NHC-capped AuNCs not characterized by SA behavior.

However, this remains an exception, since the corresponding $[Au_{13}]^{5+}$ core can be prepared only varying the starting species. Indeed, $[Au_{13}(NHC^F)_8Br_4]^+$ cluster can be isolated exclusively when anionic $[Au(dpa)_2]^-$ (dpa: 2, 2'-bipyridylamine) complex is reduced by $NaBH_4$ in presence of $[(NHC^F)H]Br$ imidazolium salts, demonstrating again how thermodynamic parameters govern the reduction pathway.[13] These three syntheses are reported in **Figure 2.5**.

Aiming at shedding light on the reduction mechanism, Hein et al. have attempted the analysis of intermediates in $[(NHC^{Bn})AuX]$ (X: Cl and py) reductions.[18] Coupling HRMS and HPLC techniques, they found $[Au_3(NHC^{Bn})_3]^+$ as small cluster intermediate. Interestingly, they detected also another intermediate, with formula $[Au_{14}(NHC^{Bn})_9Cl_3]^{2+}$, that formally loses one Au(0) center affording $[Au_{13}(NHC^{Bn})_9Cl_3]^{2+}$

as final product. Despite these interesting intermediates, a growth mechanism is not proposed in this paper, since it is not possible to clarify the aggregation steps affording $[Au_3]^+$ and $[Au_{14}]^{5+}$ cores.

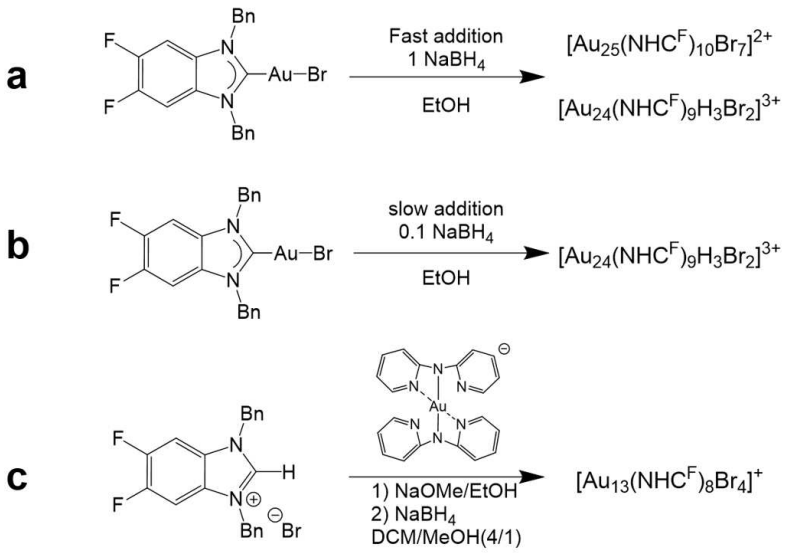

Figure 2.5: a) uncontrolled and b) kinetically controlled synthesis of $[Au_{24}]^{8+}$ clusters reported by Zheng et al. c) Isolation of $[Au_{13}]^{5+}$ cluster from reduction of a gold precursor in presence of $[(NHC^F)H]Br$ imidazolium salt.[5,13]

The absence of mechanistic information strictly affects the use of the direct reduction approach, complicating its control. Moreover, these reductions generally provide AuNCs presenting SA and saturated cores. The SA behavior is useful to stabilize clusters, but generally it prevents their reactivity, making ligand exchange or similar reactions complicated to perform. Finally, NHC scaffolds and reducing agents have been never varied in these reductions, exclusively involving benzimidazol-2-ylidenes and $NaBH_4$, respectively. So far, only one example of variation of the latter has been reported by Crudden et al., in which a $[Au_{11}(NHC^{Bn})_8X_2]^+$ cluster has been obtained when the corresponding Au(I) complex is reduced by potassium graphite (KC_8). Similar reduction but using $NaBH_4$ provides instead classical $[Au_{13}]^{5+}$, showing how the reducing agent directly affects the reduction product.[19]

Since the limited studies conducted on these two aspects, the variation of both NHCs scaffold and reducing agent will be taken in account in this elaborate. di-NHCs will be particularly studied, given the expertise of our groups on these ligands. Moreover, their chelating properties are useful to impart higher stability to cluster cores.

2.2 DIRECT REDUCTIONS TESTS OF DI-NHC GOLD(I) COMPLEXES

Following the intentions described above, a library of previously reported neutral dinuclear complexes, with general formula [(di-NHC)Au_2Br_2], and one dicationic complex, with stoichiometry [(di-NHC)$_2Au_2$]$(PF_6)_2$, have been synthetized. After that, the gold complexes are reduced as follow: gold complexes are dissolved in DCM:MeOH (4:1 v:v) and subsequently their reduction with tenfold excess of $NaBH_4$ pre-dissolved in EtOH is performed. After 9 h at room temperature, the solutions are divided in two equal portions. In one, 100 eq. of HBr (48%) are added and left under stirring at room temperature for 16 h. In the second, acid etching is not performed and the mixture is left under stirring at room temperature for another 16 h. We chose to add acid only in half of the solution in order to understand its role in these syntheses, which has not been much clarified in literature. These reaction conditions have been generally employed in the literature to get NHC-capped clusters, therefore we decided to use the same as well. High resolution mass spectrometry (HRMS) analysis has been used to detect AuNCs formation and their stoichiometric formulas.

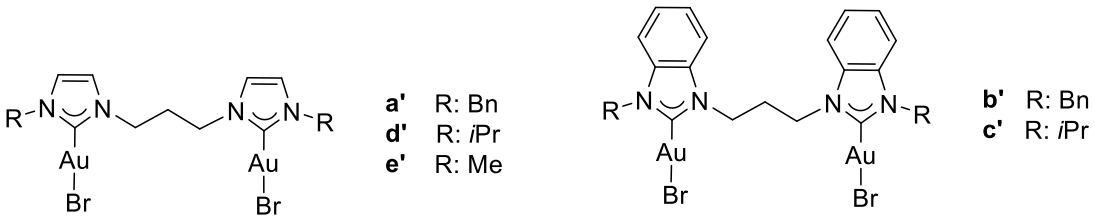

Figure 2.6: first generation of di-NHC Au(I) complexes used in this study.

We decided to test firstly complexes presenting small and/or flexible wingtip groups (benzyl, isopropyl and methyl groups) and different imidazole-2-ylidene scaffolds, reported here in **Figure 2.6**. NHCs presenting these wingtips should favor AuNCs formation, since their small sizes match well with the dimensions of gold core. 1,3-propylene bridge between the carbene units has been used, since in our experience it ideally matches the length and flexibility to bridge two mutually interacting gold

centers.[20] Furthermore, this has been already exploited in literature for the same purpose.[7,14]

In these tests, the synthesis provides AuNCs formation with complexes **a'**, **b'**, previously reported by Zheng at al. and here used only as reaction benchmark[14], and **c'**. In **Figure 2.7** these reductions are reported, showing that, basing on the ligand used, mixtures or single clusters are obtained post-reduction. The products/product mixtures derived from reductions are named **1a'**, **1b'** and **1c'**, in relation with their corresponding Au(I) complexes. Conversely, **d'** and **e**' complexes do not provide clusters upon reduction.

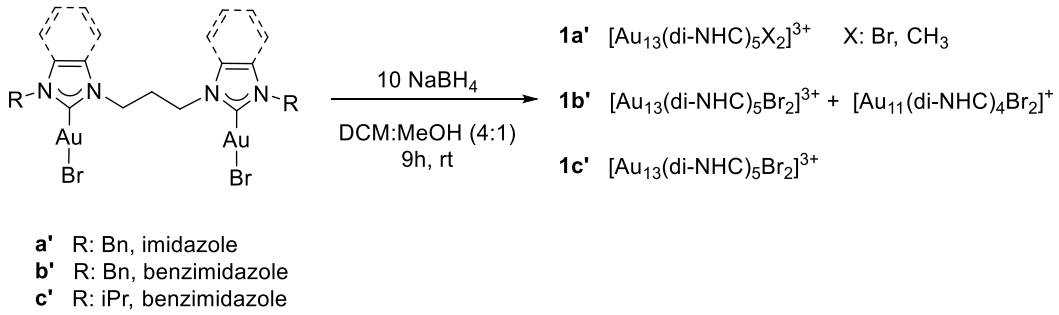

Figure 2.7: Synthesis of **1a'**, **1b'** and **1c'** cluster mixtures exploiting direct reduction approach.

From reduction of **a'**, **b'** and **c'** complexes, the obtained clusters present classical SA structures, in which $[Au_{13}]^{5+}$ or $[Au_{11}]^{3+}$ cores are capped by di-NHCs and anionic ligands, saturating the cluster coordination spheres.

In case of **a'** reduction, the crude mixture analyzed by HRMS presents three clusters, centered at 1500.81, 1479.17 and 1457.54 m/z, with formula $[Au_{13}(di\text{-}NHC^a)_5Br_2]^{3+}$, $[Au_{13}(di\text{-}NHC^a)_5Br(CH_3)]^{3+}$ and $[Au_{13}(di\text{-}NHC^a)_5(CH_3)_2]^{3+}$ respectively. These clusters, called hereafter **$[Br_2]$**, **$[Br(CH_3)]$** and **$[(CH_3)_2]$**, differ from the anionic ligands bonded on the cluster core. The presence of CH_3^- anionic ligands in **1a'** mixture will be discussed in detail in next sections of this thesis.

Also in **b'** reduction a product mixture is obtained, affording two products with formula $[Au_{11}(di\text{-}NHC^{b})_4Br]^{2+}$ and $[Au_{13}(di\text{-}NHC^{b})_5Br_2]^{3+}$, detected in mass spectrum at 2036.24 m/z and 1667.94 m/z, respectively. Here the HBr etching is useful to focus the reaction towards $[Au_{13}(di\text{-}NHC^{b})_5Br_2]^{3+}$, more stable than the $[Au_{11}]^{3+}$ counterpart.

However, the etching process does not invariably provide the desired size focusing. If HBr is used to etch **1a'** mixture, only disappearance of $[Au_{13}(di\text{-}NHC^{a})_5(CH_3)_2]^{3+}$cluster can be observed in mass spectrum, whereas $[Au_{13}(di\text{-}NHC^{a})_5Br(CH_3)]^{3+}$ survives to the addition. In **Figure 2.8** the mass spectra of **1a'** before and after acid addition are reported.

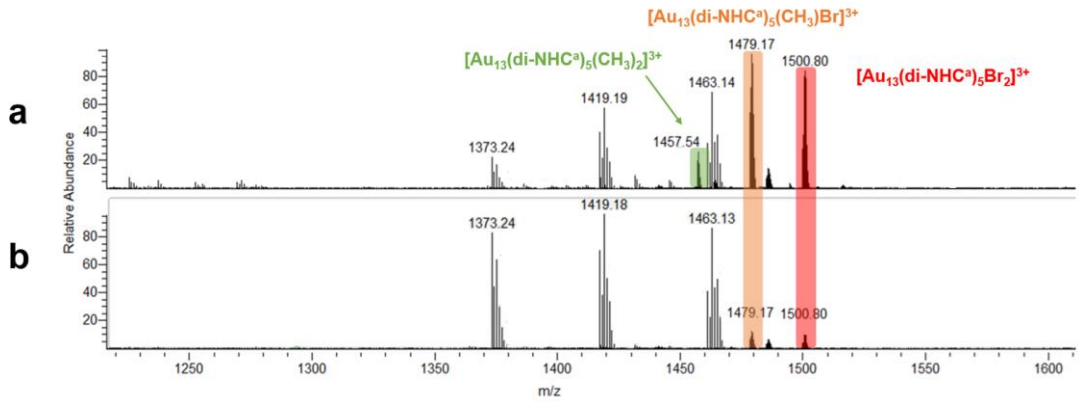

Figure 2.8: mass spectra of **1a'** a) before and b) after acid etching. Color code: $[Au_{13}(di\text{-}NHC^{a})_5Br_2]^{3+}$ (red), $[Au_{13}(di\text{-}NHC^{a})_5Br(CH_3)]^{3+}$ (orange) and $[Au_{13}(di\text{-}NHC^{a})_5(CH_3)_2]^{3+}$ (green).

The reduction of **c'** affords instead $[Au_{13}(di\text{-}NHC^{c})_5Br_2]^{3+}$ as unique cluster product, detected at 1507.51 m/z in mass spectrum. Despite the higher selectivity of this reduction, it has not been possible to isolate **1c'**, since using common purification procedures, such as chromatography column or solvent extraction, the cluster does not reach the desired purity. Furthermore, the use of acid etching does not improve the reaction yield and neither the formation of other AuNCs. However, the detection of **1c'** allows some considerations regarding the stability provided by NHC scaffolds used in these experiments, by comparing the reductions of tested complexes. Indeed,

the complex **d'**, presenting imidazole-2-ylidene scaffolds, does not favor AuNCs growth with its reduction. At the contrary, complex **c'**, presenting instead benzimidazole-2-ylidene scaffold, forms $[Au_{13}(di\text{-}NHC^{c})_5Br_2]^{3+}$ as single cluster product.

From these data we can assume that the low oxidation state of the gold kernel is better stabilized through core→ligand back-donation. This back-donation is more significant with benzimidazol-2-ylidenes than with imidazol-2-ylidenes, since its lower-energy LUMO.

Another confirmation of this behavior comes from AuNCs yields in the synthesis of **1b'** and **1a'**. In the previously reported case, $[Au_{13}(di\text{-}NHC^{b})_5Br_2]Br_3$ cluster from **b'** reduction can be isolated with 78% yield after acid etching. When instead **a'** is reduced, the yield is only 7%. The latter has been calculated based on $[Au_{13}(di\text{-}NHC)_5Br_2]Br_3$ molecular weight due to the poly-dispersed nature of **1a'**. This much lower yield means that the electronic back-donation is not optimal in **1a**' clusters, providing therefore a lower amount of AuNCs post-reduction. Despite the low yield, it is important to highlight that **1a'** clusters represent the first AuNCs capped by imidazole-2-ylidene units and methyl ligands reported so far.

Finally, **e'** complex has been exploited as staring complex too, but without isolation of novel clusters after its reduction. This complex is only slightly soluble in DCM:MeOH mixture, hence this reaction has been attempted also in CH_3CN:EtOH, in which the complex is more soluble. Also in this latter case, no AuNCs signals can be observed in mass spectrum. Likely, the Me groups do not guarantee good protection of the gold core, negatively affecting therefore cluster stability. Furthermore, the NHC ligands in complex **e'** do not present the benzimidazole-2-ylidene scaffold, apparently the best to isolate such AuNCs.

From this first set of experiments, it appears clearly that NHCs need to be tailored to cap AuNCs, varying wingtip proprieties and exploiting benzimidazole rather than imidazole units. R groups need to be small and flexible to favor ligand arrangement on cluster core, providing weak interactions among ligands or with the core to further stabilize the cluster structure.

It is interesting that benzylic-type groups seem to help in cluster stabilization. As showed in **Figure 2.2** and **Figure 2.4**, in literature these groups are the ones mainly exploited to synthetize NHC-capped AuNCs. Furthermore, modifying their proprieties it is possible to vary the cluster proprieties too; for instance, they allow to isolate chiral clusters when benzylic wingtips bearing stereocenters in the benzylic position.[6,15] In case of di-NHCs, also their helicoidal disposition on gold cores provides chirality to the cluster, making possible the isolation of two enantiomers using a chiral column.[16] However, it is still not completely clarified the reasons whereby such benzylic groups favor formation of AuNCs. They can form π-π, CH-π or CH···Au interactions stabilizing the coordination sphere[12,17]; however, these interactions are not always present in the crystallographically characterized cluster coordination spheres reported so far.

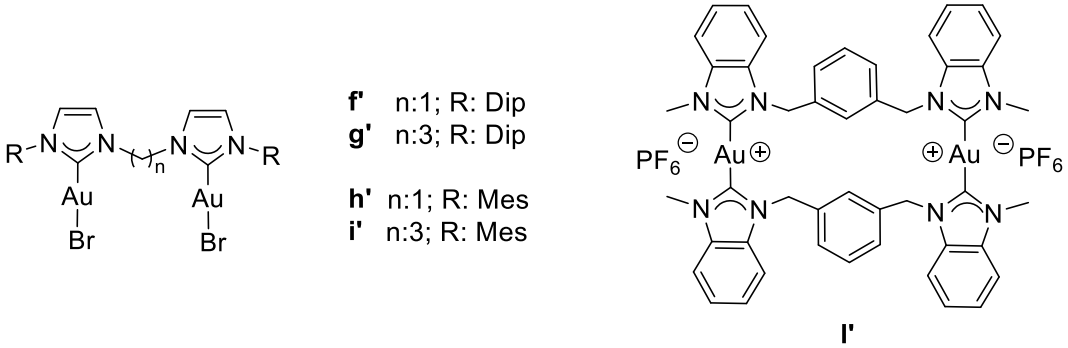

Figure 2.9: second generation of di-NHC Au(I) complexes used in this study.

After the studies conducted on these complexes, we decided to produce another library of literature reported complexes, differing from previous ones by bulky groups as wingtips and methylene bridges between two imidazole-2-ylidene units, aiming to

confirm that only small and flexible wingtips can stabilize clusters, together with benzimidazole scaffold. One $[Au_2(di\text{-}NHC^{I})_2]^{2+}$ cationic complex has been tested upon direct reduction. These complexes are reported in **Figure 2.9**.

Four of the complexes reported above are characterized by two bulky wingtip groups mesityl (Mes) and 2,6-di-isopropylphenyl (Dip), and different bridge lengths. Exploiting these complexes, no cluster formation can be detected with HRMS after the reduction procedure. The reason is probably related to the short bridge length (complexes **h'** and **f'**) and with the presence of bulky wingtip groups, not allowing formation of a proper ligand shell due to the limited space on cluster core. These data confirm the considerations presented before.

Consequently, the di-cationic complex **l'** has been tested but in this case no reduction whatsoever is observed under the standard employed reaction conditions. Likely, the metallacyclic structure of this complex stabilizes the gold(I) centers, preventing their reduction. Furthermore, complex **l'** does not present halide counter anions, fundamental to saturate coordination sphere of formed cluster. However, also by adding external bromide source, as LiBr, we can not detect AuNCs formation. It is important to remark that in all performed direct reductions the main reaction by-product is invariably the corresponding $[Au_2(di\text{-}NHC)_2]^{2+}$ complex, detected both with mass spectrometry and NMR spectroscopy. This is a further evidence that such metallacyclic, dicationic complexes are stable and do not provide cluster through their reduction. Similar by-products have been found also in the synthesis of mono-NHC-protected AuNCs, presenting instead formula $[Au(NHC)_2]^{+}$.[5]

Since clusters **1b'** have been already reported and purification of **1c'** is problematic, we decided to focus our efforts to isolate **$[(CH_3)_2]$** cluster in **1a'** mixture, intrigued by the formation of CH_3 anions bind on $[Au_{13}]^{5+}$ core. This discussion is reported in **Paragraph 2.3**.

2.3 THE FIRST CH_3-CAPPED GOLD CLUSTER ISOLATED UPON STOICHIOMETRIC CONTROL

In this section the reduction of **a'** complex will be reconsidered and the peculiar AuNCs derived from it will be investigated. As illustrated above, **a'** reduction provides three clusters, presenting $[Au_{13}(di\text{-}NHC^a)_5Br_2]^{3+}$, $[Au_{13}(di\text{-}NHC^a)_5Br(CH_3)]^{3+}$ and $[Au_{13}(di\text{-}NHC^a)_5(CH_3)_2]^{3+}$stoichiometry, renamed here as **$[Br_2]$**, **$[(CH_3)Br]$** and **$[(CH_3)_2]$,** respectively. The first cluster (1500.81 m/z) presents two bromide anions coordinated to the metallic core, in agreement with most common SA clusters presenting the same stoichiometry.[6,7,12–14,16,17] The other two AuNCs (1479.18 and 1457.68 m/z), are stabilized by one and two CH_3^- anions, respectively, substituting the bromide anions in **$[Br_2]$**. This result is truly interesting, since whereas it is known that AuNCs can be protected by hydrides, in particular when phosphine ligands are involved in the cluster stabilization[21], a cluster exhibiting a methyl groups bonded to the core is unprecedented in cluster chemistry. In the following, we will provide experimental evidence that allows us to claim that **$[(CH_3)Br]$** and **$[(CH_3)_2]$** are indeed the first reported gold species with coordinated methyl anions.

The first problem to be tackled was the separation and purification of these AuNCs. Whereas all three AuNCs appeared reasonably stable, they presented similar chemical and physical proprieties, making common separation methods useless for this purpose. Preferential formation of **$[Br_2]$** could be achieved using only one mole of $NaBH_4$, 3 h reaction time and LiBr as bromide source, together with **$[(CH_3)Br]$** as minor co-product which proved impossible to convert to **$[Br_2]$** even by reaction with excess HBr, which suggests a strong Au_{13}-CH_3 interaction. Furthermore, **$[Br_2]$** proved to slowly degrade with time in CD_3CN solution, providing after a few days at 4°C the starting gold complex as degradation product. These results suggest that CH_3^- anions provide higher stabilization towards cluster core rather than bromide ligands. Despite this peculiar behavior, the main question in this synthesis is where the methyl group

comes from, since no obvious methyl source has been employed in the reaction. Considering the performed experiment, it is possible that $NaBH_4$ reduces gold complexes and DCM used as solvent. Reductions of halogenated solvents are known[22,23] and these are performed using strong bases, forming carbene molecules as product. For instance, starting from $CHCl_3$ it is possible to form Cl_2C: carbene exploited solvent deprotonation. The strong base deprotonates chloroform, affording CCl_3^- anion and this latter forms Cl_2C: losing a chloride anion.[23,24] According to this chemistry, we can suppose the mechanism of formation of methyl-capped clusters reported in **Figure 2.10.**

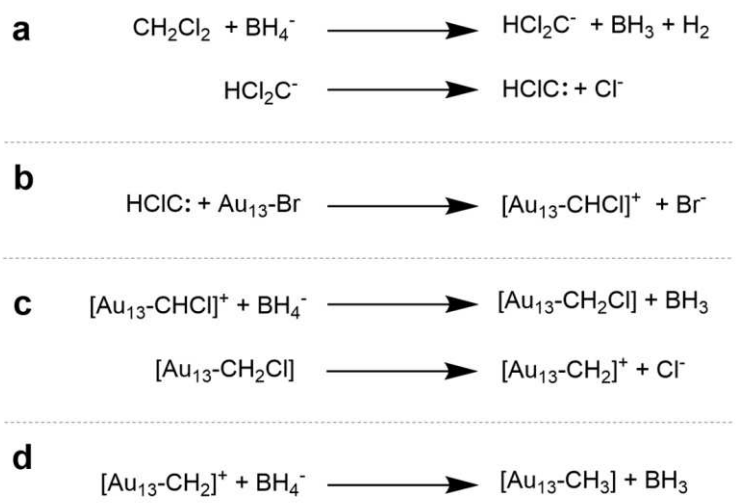

Figure 2.10: hypothetic mechanism of formation of coordinated methyl anion on $[Au_{13}]^{5+}$ core.

We suppose that first the formation of **$[Br_2]$** cluster takes place, since bromide anions are closer to gold centers during the reduction of **a'**. The formation of **$[Br_2]$** provides a scaffold where the reduction of DCM can take place. The initial steps (**Figure 2.10 a**) are formation of HClC: carbene from DCM, analogous to formation of Cl_2C: from $CHCl_3$. The formed carbene substitutes a bromide anion on the cluster core, sharing its lone pair and capping it (**Figure 2.10 b**). The resulting cluster might undergo a hydride transfer to the carbene carbon by $NaBH_4$, forming a CH_2Cl^- anion bonded to

the core. The latter can lose another Cl^- anion, forming coordinated H_2C: on the gold core. (**Figure 2. 10 c**). Finally, another hydride transfer from $NaBH_4$ provides the final hydride to form the methyl group (**Figure 2. 10 d**).

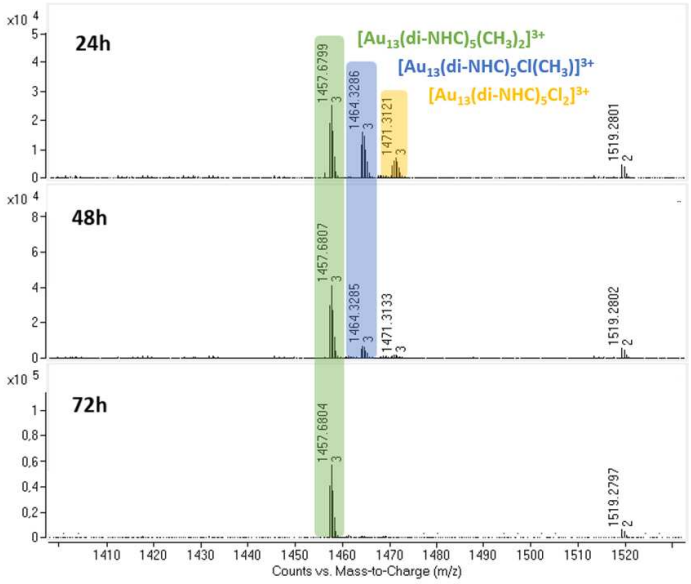

Figure 2.11: HRMS analyses of withdrawals of reaction mixture after (from above) 24 h, 48 h and 72 h related to not-optimized synthesis of **[$(CH_3)_2$]** performed using DCM:EtOH (4:1 v:v) as solvent. **[Cl_2]** is highlighted in yellow, **[$(CH_3)Cl$]** in blue and **[$(CH_3)_2$]** in green.

To confirm this hypothesis, further isolation of **[Br_2]** has been attempted, to understand if the reduction of DCM can be catalyzed by its $[Au_{13}]^{5+}$ core. Unfortunately, several attempts have been performed to isolate again **[Br_2]** cluster, but this cluster is not stable enough and its isolation has been performed only one time. Considering this, we focused our attention on the isolation of **[$(CH_3)_2$]**. We suppose that a weaker Au-X bond, for instance Au-Cl instead of Au-Br, could promote this reactivity, favoring therefore the formation of **[$(CH_3)_2$]** cluster. Furthermore, it is evident that an excess of $NaBH_4$ should favor this mechanism, since it involves both gold complex and DCM reductions. For these reasons, we carried out the synthesis of **a** complex, analogous to **a'** but presenting chloride instead of bromide as anionic ligands. The reduction of **a** has been performed using 72 h reaction time and 30 moles

of $NaBH_4$, divided in three portions of 10 moles each and added every 24 h. As solvent we used DCM:EtOH (4:1 v:v), removing therefore MeOH used in previous synthesis to understand if our hypothesis regarding the reduction of DCM was reasonable.

The reaction has been followed by HRMS, as reported in **Figure 2.11**. After 24 h and 10 moles of $NaBH_4$, it is possible to detect three clusters: **[$(CH_3)_2$]** ([Au_{13}(di-$NHC^a)_5(CH_3)_2]^{3+}$, 1457.68 m/z), **[$(CH_3)Cl$]** ([Au_{13}(di-$NHC^a)_5(CH_3)Cl]^{3+}$, 1464.33 m/z) and **[Cl_2]** ([Au_{13}(di-$NHC^a)_5Cl_2]^{3+}$, 1471.31 m/z). After addition of 20 moles more of $NaBH_4$ and 72 h reaction time, only **[$(CH_3)_2$]** is present and can be isolated, albeit with a reaction yield of only 5% after work-up. In order to improve the yield, we decided to use a molar amount of an external gold complex in order to reproduce in the reaction mixture the same gold:ligand ratio present in the final cluster product. Indeed, the starting complex presents Au:di-NHC molar ratio of 2:1, but in **[$(CH_3)_2$]** the molar ratio is 13:5. Therefore, to balance the amount of gold, 0.6 moles of [$ClAu(SMe_2)$] have been added to the reaction mixture. In this way, a significant increase in the reaction yield is achieved, obtaining a value of 22% after purification. The optimized synthesis of **[$(CH_3)_2$]** is reported in **Figure 2.12**.

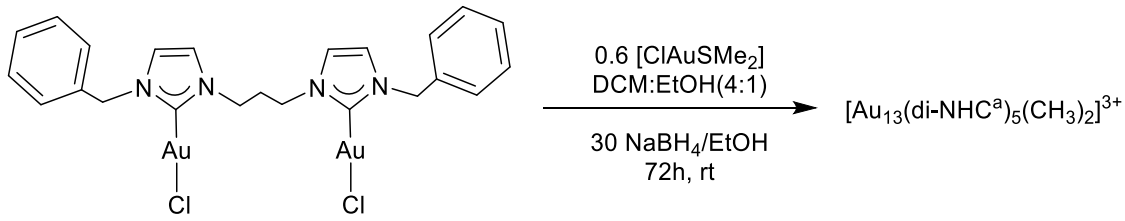

Figure 2.12: optimized synthesis of **[$(CH_3)_2$]** cluster.

After the optimization of the synthesis, we focused our efforts on the rationalization of the Au-CH_3 interaction. First of all, we verified that the imidazole-2-ylidene moieties present in our di-NHC ligand favor the formation of AuNCs capped by methyl ligands. To confirm this, we run our optimized synthesis using Zheng's complex **b** (**Figure 2.13 a**) bearing chlorides instead of bromides as anionic ligands. After addition of 30 total

moles of $NaBH_4$ and 72 h reaction time, it is possible to detect the formation of three stable SA clusters, with formula $[Au_{11}(di\text{-}NHC^b)_5]^{3+}$ (1483.01 m/z), $[Au_{13}(di\text{-}NHC^b)_5Cl(CH_3)]^{3+}$ (1631.33 m/z) and $[Au_{13}(di\text{-}NHC^b)_5Cl_2]^{3+}$ (1637.97 m/z), with cluster $[Au_{13}(di\text{-}NHC^b)_5(CH_3)_2]^{3+}$ (1624.34 m/z) barely present in the mass spectra, reported in **Figure 2.13 b**. This result confirms that imidazol-2-ylidene ligands have a key role in the stabilization of AuNCs exhibiting Au-CH_3 interactions.

Further investigations have been conducted to shed light on origins of the methyl groups. As it has been outlined above, in our hypothesis the methyl groups derive from reduction of DCM catalyzed by $[Au_{13}]^{5+}$ clusters. For this reason, we conducted the same experiments to get **$[(CH_3)_2]$** but without using DCM as co-solvent and using instead a DCE:EtOH (4:1 v:v) (DCE: 1,2-dichloroethane) mixture. This reaction has been monitored with HRMS. In the mass spectra, it is possible to observe the presence of appreciable amount of **$[Cl_2]$** after 1 h from $NaBH_4$ addition, despite mass spectra at 24 h, 48 h and 72 h do not provide similar signals. These data suggest that DCM is indeed the methyl source in this reduction. Furthermore, our starting hypothesis can be confirmed, since the first cluster obtained with this reduction is indeed **$[Cl_2]$**, confirming that Au_{13} core likely acts as catalyst in DCM reduction.

The AuNCs were subsequently characterized using different techniques beside HRMS. The ^1H NMR spectra of **$[Br_2]$** and **$[(CH_3)_2]$** are similar but differ for: 1) the position of the peaks and 2) the absence in the **$[Br_2]$** spectrum of signals attributable to CH_3^-. Both spectra are reported in **Figure 2.14**. In the **$[(CH_3)_2]$** spectrum in CD_3CN it is possible to note a singlet centered at 0.29 ppm, with an integral value equal to 6H, attributable to CH_3^- anions. The same signals and integrals can be found in the spectrum of **$[(CH_3)_2]$** recorded in CD_2Cl_2, reported in **Figure 2.15**. As mentioned before, there are no examples in the literature regarding AuNCs with coordinated CH_3; however it is possible to compare the **$[(CH_3)_2]$** spectrum with complexes presenting $[(di\text{-}NHC)Au_2(CH_3)_2]$ stoichiometry. These present methyl signals centered around

0.32-0.19 ppm in their proton spectra, matching perfectly with the signal attributed to methyl groups observed in **[(CH$_3$)$_2$]** spectra.[25,26]

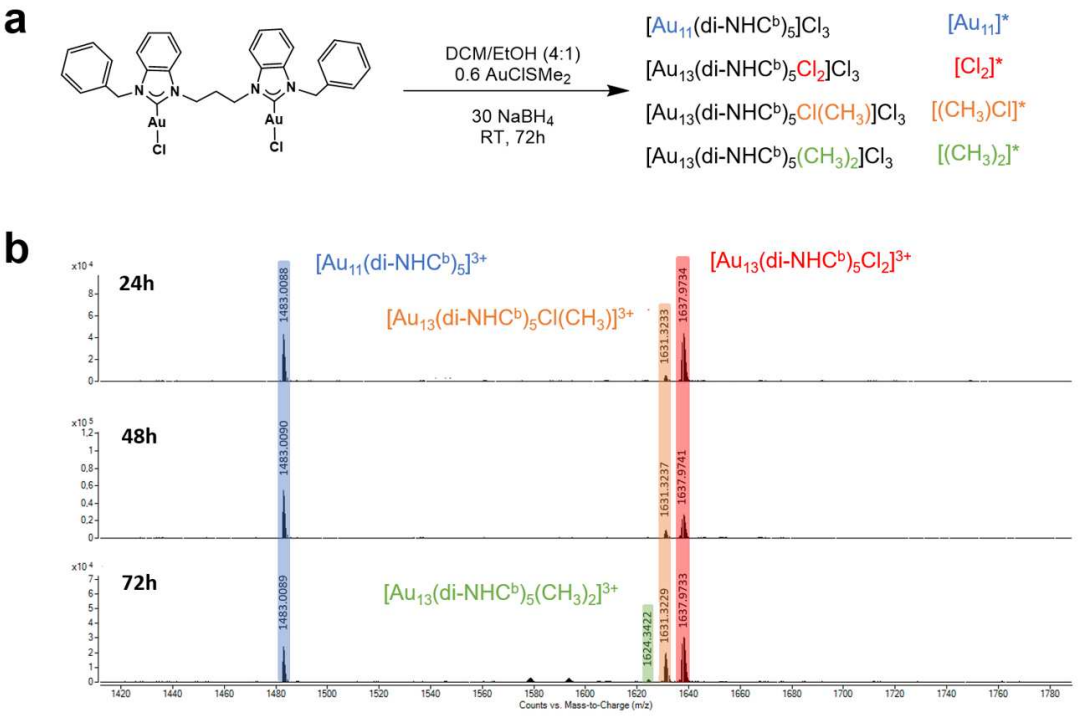

Figure 2.13:a) reduction of **b** complex and b) its mass spectra at 24 h, 48 h and 72 h.

To confirm our mechanism, we performed the same synthesis employed to obtain **[(CH$_3$)$_2$]** but using $NaBD_4$ as reagent, aiming at observing formation of mixed $CD_{3-n}H_n$ groups bonded to cluster cores. The singlet at 0.29 ppm remains present in the ^{1}H NMR spectrum, but with an integral of 4H and shifted at 0.26 ppm, therefore pointing towards formation of CH_2D groups, together with another small peak centered at 0.28 ppm. The HRMS analysis confirms this peculiar result, highlighting a peak centered at 1458.19 m/z for which it is difficult to provide an unambiguous interpretation. The difference in mass between **[(CH$_3$)$_2$]** and this new cluster is 1.5 Da, suggesting indeed a cluster stoichiometry close to $[Au_{13}(di\text{-}NHC)_5(CH_2D)_2]^{3+}$, with a calculated value of 1458.21 m/z, supporting the ^{1}H NMR analysis. Despite this, the isotopic pattern of the experimental signal does not match with the calculated one, which leads to the hypothesis that a mixture of clusters has formed during the reduction, leading to an

overlapping of peaks in the mass spectrum. These data partially confirm our hypothesis, since deuteride placed on final cluster can derive only from $NaBD_4$.

The electrochemical behavior of di-NHC-capped AuNCs in DCM also confirms the promotion of DCM reduction performed by cluster core. Indeed, it is interesting to notice than when $[Au_{13}(di\text{-}NHC^b)_5Br_2]^{3+}$cluster is reduced in DCM during the CV analysis, a strong increase of current density can be detected. This behavior can be described in terms of a catalytic electron transfer from the reduced cluster to DCM present as solvent. This cluster is likely not stable in its reduced form and consequently it loses the newly acquired electron, donating it to the solvent and affording its reduction. Furthermore, this catalysis of DCM reduction can be detected in several clusters capped by PPh_3 and di-NHCs, further discussed in **Paragraph 5.0**. Given the impossibility to isolate **$[Cl_2]$**, to confirm this behavior, in the future we will synthesize $[Au_{13}(di\text{-}NHC^b)_5Cl_2]^{3+}$, $[Au_{13}(di\text{-}NHC^b)_2(PPh_3)_4Cl_4]^+$ and $[Au_{13}(di\text{-}NHC^b)_3(PPh_3)_3Cl_3]^{3+}$ clusters, bearing instead benzimidazol-2-ylidene and/or PPh_3 ligands. We aim to functionalize these with CH_3^- anions, exposing them to continuous reducing voltage in DCM. After this, an HRMS analysis will be performed to probe the solution after the treatment, looking if it is possible to detect CH_3-functionalized AuNCs, which would further confirm our mechanistic hypothesis on the formation of these methyl groups.

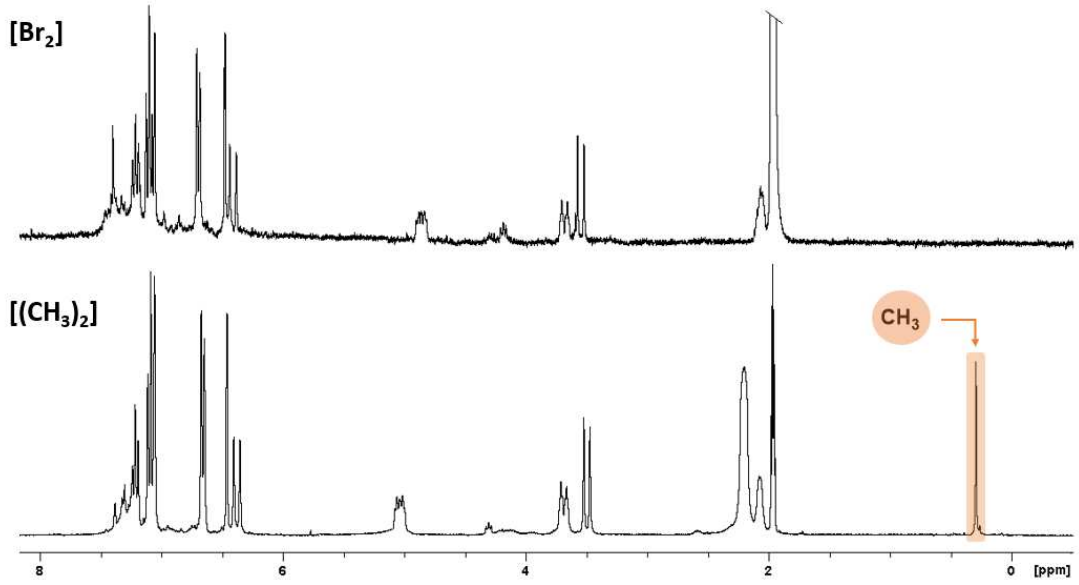

Figure 2.14: ^{1}H NMR spectra of **[Br$_2$]** (above) and **[(CH$_3$)$_2$]** (below) in CD_3CN. The **CH$_3$** peak is highlighted in orange.

We decided to perform a TOCSY NMR experiment on the **[(CH$_3$)$_2$]** sample, to shed light on the other proton signals belonging to di-NHCs. The ^{1}H NMR signals of the 1,3-propylenic bridge (centered at 5.04, 3.69 and 2.07 ppm, respectively) present an anisotropy due to chelate coordination, providing increased rigidity to the system. The methylene groups belonging to the benzylic wingtips undergo a similar fate; indeed, they appear in the spectrum as two doublets centered at 6.66 and 3.50 ppm, therefore presenting a diasterotopic behavior, again due to the rigidity of the ligand. The methyl signal present only diagonal cross peak, as expected from its nature. Finally, HMQC NMR experiment confirms the presence of CH_3 groups, thanks to the cross peak between carbon and hydrogen spectra**.** For the experimental data discussed so far, see the **Experimental Section**.

A particular chemical behavior of the **[(CH$_3$)$_2$]** cluster needs also to be reported, since this allows to confirm what has been discussed so far. Indeed, an inner-external sphere exchange of anionic ligands appears to take place in solid state, proving indirectly the interaction Au-CH_3. To understand this, it is fundamental to remember

that the counter anions of **[(CH₃)₂]** are chlorides, which is confirmed also by the X-ray structure (see below). Thanks to the proximity between the cluster core and chloride anions, after about 20 days in solid state at -16°C, a new cluster is obtained from the total conversion of previous one, with formula $[Au_{13}(di\text{-}NHC^a)_5(CH_3)Cl]^{3+}$, called **[(CH₃)Cl]**. This cluster has been analyzed both with HRMS and ^1H NMR. The mass spectrum confirms the result, detecting the peaks $[Au_{13}(di\text{-}NHC^a)_5(CH_3)Cl]^{3+}$ and $[Au_{13}(di\text{-}NHC^a)_5(CH_3)Cl]Cl^{2+}$ centered respectively at 1464.19 m/z and 2214.28 m/z. In the ^1H NMR spectrum of **[(CH₃)Cl]**, obtained in CD_2Cl_2, almost all signals are split in two new sets of signals, indicating a break of symmetry compared to **[(CH₃)₂]**. Furthermore, the singlet belonging to the CH_3 is centered at 0.66 ppm, with an integral value of 3H, according with stoichiometry detected with HRMS. This signal has been detected in cationic Au(III) complexes bearing methyl ligands, in which CH_3 signal falls at 0.66 ppm, in agreement with **[(CH₃)Cl]** spectrum, since substitution of a methyl group with a chloride ligand renders the cluster core more electron poor.[27]

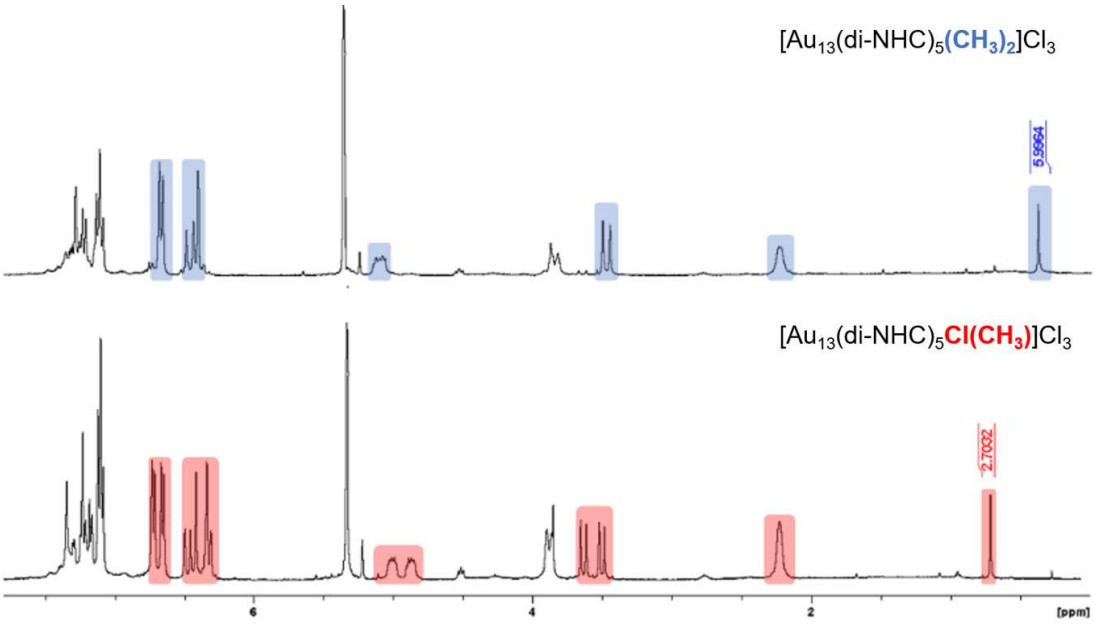

Figure 2.15: ^1H NMR spectra of **[(CH₃)₂]** (above) and **[(CH₃)Cl]** (below) dissolved in CD_2Cl_2. The splitting of signals is highlighted in the two spectra.

In **Figure 2.15** the **[$(CH_3)_2$]** and **[$(CH_3)Cl$]** proton spectra are reported for comparison. To get further confirmation of this behavior, we attempted to carry out the same metathesis reaction in solution, exploiting different deuterated solvent (CD_3OD, CD_2Cl_2 and CD_3CN) and following the evolution of the cluster by ^1H NMR spectroscopy. The experiments have been performed at 40°C, to speed up the exchange. However, despite the presence of excess free chlorides, counter anion of **[$(CH_3)_2$]**, in CD_3OD and CD_3CN solution the exchange does not take place even after eight days of warming. In all three experiments the counter anions of **[$(CH_3)_2$]** cluster remain stable, highlighting that the proximity between Au_{13} core and chloride anions in solid state is fundamental to achieve an extensive metathesis of the anionic ligands.

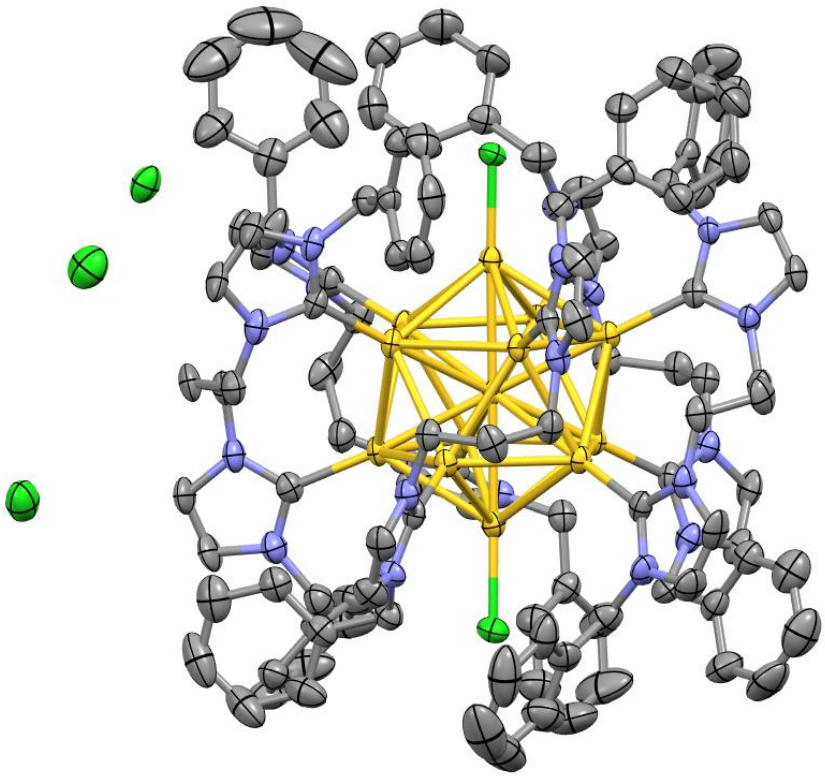

Figure 2.16: X-ray structure of **[Cl_2]** cluster obtained crystalizing **[$(CH_3)_2$]** cluster.

We have been able to obtain crystals from a solution of **[$(CH_3)_2$]** in DCM:acetone and layering *n*-hexane on it. After one week it is possible observe the formation of crystals. The structure is reported in **Figure 2.16**. The crystallized cluster exhibited the

expected icosahedral core with five di-NHCs each bridging two external gold atoms, in agreement with similar AuNCs already reported in literature. However, the apical positions were found to be occupied by chloride anions rather than by the expected methyl anions. Apparently, slow metathesis of the anionic ligands took place in solution, ultimately favoring the crystallization of the least soluble, although minor, species.

Finally, to evaluate the optical proprieties of **[$(CH_3)_2$]**, UV-Vis and emission spectra have been recorded. The analyses have been performed on **[$(CH_3)_2$]** presenting PF_6^- as counter anions. In the UV-Vis spectrum, three weak absorption bands are present, centered respectively at 401 nm, 420 nm and 499 nm, plus another one, more intense, centered at 320 nm. The emission proprieties of this cluster are obtained exciting it with a radiation at 320 nm. The obtained emission spectrum presents one broad band at 722 nm. The emission quantum yield has been evaluated, leading to a value equal to 6.28%, lower than similar cluster reported in literature. These spectra are reported in the **Experimental section.**

In conclusion, we have been able to synthesize the first methyl-substituted, di-NHC protected AuNCs. A reaction yield improvement can be achieved using a stoichiometric amount of [ClAu(SMe_2)] complex as co-reagent, together with the [(di-NHC)Au_2Cl_2] substrate. Using different spectroscopic techniques, we can confirm the presence of CH_3 groups coordinated on the AuNCs. Furthermore, the formation in the solid state of another cluster, **[(CH_3)Cl]**, presenting different mass and NMR spectra, is another proof of the existence of Au-CH_3 interactions. However, the origin of these methyl groups remains elusive and not easy to rationalize, although it seems derived from reduction of DCM promoted by cluster cores in presence of $NaBH_4$. In the future, we are going to perform DFT calculation, to shed light on the thermodynamic state and the orbital structure of **[$(CH_3)_2$]**, **[(CH_3)Cl]**, and **[Cl_2]**, to better understand the gold-methyl bonds present in the firsts two clusters and compare them with the similar

halogen-stabilized cluster. Furthermore, we are going to synthesize a small library of AuNCs, aiming to perform synthesis of CH_3-capped AuNCs from them through electrochemical approach in collaboration with Maran's group at the University of Padova, one of the leaders in the electrochemical studies on AuNCs.[28]

2.4 BIBLIOGRAPHY

[1] T. J. Robilotto, J. Bacsa, T. G. Gray, J. P. Sadighi, *Angew. Chem. Int. Ed.* **2012**, *51*, 12077–12080.

[2] M. R. Narouz, K. M. Osten, P. J. Unsworth, R. W. Y. Man, K. Salorinne, S. Takano, R. Tomihara, S. Kaappa, S. Malola, C.-T. Dinh, J. D. Padmos, K. Ayoo, P. J. Garrett, M. Nambo, J. H. Horton, E. H. Sargent, H. Häkkinen, T. Tsukuda, C. M. Crudden, *Nat. Chem.* **2019**, *11*, 419–425.

[3] L. Jin, D. S. Weinberger, M. Melaimi, C. E. Moore, A. L. Rheingold, G. Bertrand, *Angew. Chem. Int. Ed.* **2014**, *53*, 9059–9063.

[4] M. R. Narouz, K. M. Osten, P. J. Unsworth, R. W. Y. Man, K. Salorinne, S. Takano, R. Tomihara, S. Kaappa, S. Malola, C.-T. Dinh, J. D. Padmos, K. Ayoo, P. J. Garrett, M. Nambo, J. H. Horton, E. H. Sargent, H. Häkkinen, T. Tsukuda, C. M. Crudden, *Nat. Chem.* **2019**, *11*, 419–425.

[5] H. Shen, X. Tang, Q. Wu, Y. Zhang, C. Ma, Z. Xu, B. K. Teo, N. Zheng, *ACS Nanosci. Au* **2022**, *2*, 520–526.

[6] P. Luo, X. Zhai, S. Bai, Y. Si, X. Dong, Y. Han, S. Zang, *Angew. Chem. Int. Ed.* **2023**, *62*, e202219017.

[7] X. Wang, R. Liu, L. Tian, J. Bao, C. Zhao, F. Niu, D. Cheng, Z. Lu, K. Hu, *J. Phys. Chem. C* **2022**, *126*, 18374–18382.

[8] H. Shen, G. Deng, S. Kaappa, T. Tan, Y. Han, S. Malola, S. Lin, B. K. Teo, H. Häkkinen, N. Zheng, *Angew. Chem.* **2019**, *131*, 17895–17899.

[9] V. K. Kulkarni, B. N. Khiarak, S. Takano, S. Malola, E. L. Albright, T. I. Levchenko, M. D. Aloisio, C.-T. Dinh, T. Tsukuda, H. Häkkinen, C. M. Crudden, *J. Am. Chem. Soc.* **2022**, *144*, 9000–9006.

[10] P. A. Lummis, K. M. Osten, T. I. Levchenko, M. Sabooni Asre Hazer, S. Malola, B. Owens-Baird, A. J. Veinot, E. L. Albright, G. Schatte, S. Takano, K. Kovnir, K. G. Stamplecoskie, T. Tsukuda, H. Häkkinen, M. Nambo, C. M. Crudden, *JACS Au* **2022**, *2*, 875–885.

[11] H. Shen, Q. Wu, M. S. Asre Hazer, X. Tang, Y.-Z. Han, R. Qin, C. Ma, S. Malola, B. K. Teo, H. Häkkinen, N. Zheng, *Chem* **2022**, *8*, 2380–2392.

[12] M. R. Narouz, S. Takano, P. A. Lummis, T. I. Levchenko, A. Nazemi, S. Kaappa, S. Malola, G. Yousefalizadeh, L. A. Calhoun, K. G. Stamplecoskie, H. Häkkinen, T. Tsukuda, C. M. Crudden, *J. Am. Chem. Soc.* **2019**, *141*, 14997–15002.

[13] J. Sun, X. Tang, J. Tang, Y. Zhang, Z. Li, Chaolumen, S. Guo, H. Shen, *Inorg. Chem.* **2023**, *62*, 5088–5094.

[14] H. Shen, S. Xiang, Z. Xu, C. Liu, X. Li, C. Sun, S. Lin, B. K. Teo, N. Zheng, *Nano Res.* **2020**, *13*, 1908–1911.

[15] R. W. Y. Man, H. Yi, S. Malola, S. Takano, T. Tsukuda, H. Häkkinen, M. Nambo, C. M. Crudden, *J. Am. Chem. Soc.* **2022**, *144*, 2056–2061.

[16] H. Yi, K. M. Osten, T. I. Levchenko, A. J. Veinot, Y. Aramaki, T. Ooi, M. Nambo, C. M. Crudden, *Chem. Sci.* **2021**, *12*, 10436–10440.

[17] P. Luo, S. Bai, X. Wang, J. Zhao, Z. Yan, Y. Han, S. Zang, T. C. W. Mak, *Adv. Opt. Mater.* **2021**, *9*, 2001936.

[18] J. Liu, Y. Sato, V. K. Kulkarni, A. I. Sullivan, W. Zhang, C. M. Crudden, J. E. Hein, *Chem. Sci.* **2023**, *14*, 10500–10507.

[19] A. I. Sullivan, J. F. DeJesus, S. Malola, S. Takano, T. Tsukuda, H. Häkkinen, C. M. Crudden, *Chem. Mater.* **2023**, *35*, 2790–2796.

[20] M. Baron, C. Tubaro, A. Biffis, M. Basato, C. Graiff, A. Poater, L. Cavallo, N. Armaroli, G. Accorsi, *Inorg. Chem.* **2012**, *51*, 1778–1784.

[21] R. H. Adnan, J. M. L. Madridejos, A. S. Alotabi, G. F. Metha, G. G. Andersson, *Adv. Sci.* **2022**, 2105692.

[22] D. F. Martin, *J. Inorg. Nucl. Chem.* **1975**, *37*, 1941–1944.

[23] A. J. Arduengo, F. Davidson, H. V. R. Dias, J. R. Goerlich, D. Khasnis, W. J. Marshall, T. K. Prakasha, *J. Am. Chem. Soc.* **1997**, *119*, 12742–12749.

[24] Y. Zhang, S. Liu, Z. Zang, Z. Wang, T. Zhu, *Org. Chem. Front.* **2022**, *9*, 6624–6630.

[25] M. V. Baker, P. J. Barnard, S. K. Brayshaw, J. L. Hickey, B. W. Skelton, A. H. White, *Dalton Trans.* **2005**, 37.

[26] E. Tkatchouk, N. P. Mankad, D. Benitez, W. A. Goddard, F. D. Toste, *J. Am. Chem. Soc.* **2011**, *133*, 14293–14300.

[27] F. Rekhroukh, R. Brousses, A. Amgoune, D. Bourissou, *Angew. Chem. Int. Ed.* **2015**, *54*, 1266–1269.

[28] S. Antonello, F. Maran, *Curr. Opin. Electrochem.* **2017**, *2*, 18–25.

3.0 RESULTS AND DISCUSSION: VARIATION OF NHC SCAFFOLDS ON GOLD COMPLEXES TO TAILOR CLUSTER PRODUCTION

3.1 INTRODUCTION: VARIATION OF NHC SCAFFOLDS ON GOLD COMPLEXES

In previous paragraphs we have explained how the variation of NHC steric features allows the isolation of several NHC-capped AuNCs. However, in the literature there are no studies regarding the variation of NHC electronic proprieties. Using imidazole-2-ylidene units, we have been able to isolate clusters capped by CH_3 groups, further stabilizing $[Au_{13}]^{5+}$ cores. Indeed, stabilization through imidazole-2-ylidene scaffolds in this cluster is favored by the presence of methyl groups in the coordination sphere. Furthermore, $[Au_{13}(NHC^{im})_5X_2]^{3+}$, bearing instead bromide or chloride anions, is not stable, confirming the cooperativity between imidazolium and methyl ligands to stabilize the core. Despite this unprecedented result, the other experiments performed in our laboratories highlight how imidazol-2-ylidenes do not necessarily represent the best choice to cap such clusters. We suppose that core→ligands backdonation should stabilize AuNCs, since the electron density centered in the core can be partially delocalized on the coordination sphere, thus stabilizing the core and strengthening the cluster-ligand interaction. Due to this, benzimidazol-2-ylidenes are generally employed in cluster chemistry in preference to imidazole-2-ylidenes. However, plenty of NHC scaffolds have been reported in the literature in the last 20 years, and some of them present markedly higher π-accepting properties while maintaining significant σ-donating ability; these appear ideal electronic proprieties to protect AuNCs. These ligands, which are here termed “abnormal” NHC (aNHC), are characterized by different scaffolds compared to classical NHCs. Whereas we use this definition in a broad sense, in the current literature it generally refers only to mesoionic NHCs.[1,2]

If our hypothesis regarding core→ligand backdonation is correct, we can suppose that, for example, cyclic alkyl amino carbenes (CAACs) could be a good alternative to common NHC ligands.[3] These aNHCs present a lower LUMO level than NHCs, a feature favoring the backdonation cited before. However, CAACs generally are more reactive than common NHCs, due to their smaller HOMO-LUMO energy gap. Due to this, they need to be stabilized by bulky wingtip groups, a feature that does not favor the formation of clusters since the limited space on the cluster surface.

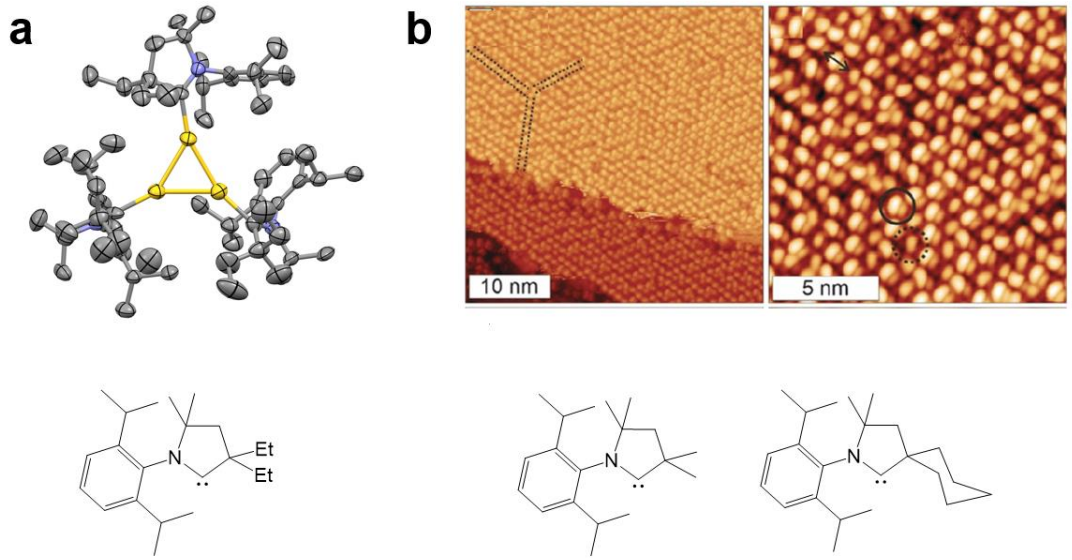

Figure 3.1: a) X-ray structure of $[Au_3(CAAC)_3]^+$ and corresponding ligand used to cap it. b) STM analysis of CAAC-protected Au(111) surfaces and corresponding ligands exploited to protect it.[4,5]

Hitherto, a single example of this stabilization is represented by $[Au_3(CAAC)_3]^+$, reported in **Figure 3.1 a**, in which CAACs completely cap the triangular cluster.[4] However, in this case the steric proprieties of CAACs determine the cluster stability rather than their electronic proprieties. To corroborate this, a simple calculation of oxidation state can be performed, aiming at understanding AuNCs electronic density. We can suppose that the electron density of the core is equally shared in both $[Au_3]^+$ and $[Au_{13}]^{5+}$ kernels, as hypothesized in SA theory too. The first presents a formal positive oxidation state equal to 1/3 (0.33) for each gold atoms, thereby slightly lower

than 5/13 (0.38) presents in $[Au_{13}]^{5+}$ cluster. Since this difference is not high, reasonably also $[Au_{13}]^{5+}$ could be protected by CAAC ligands. However, CAACs coordination is expectedly prevented by their steric hindrance, although CAACs have been used also to cap Au(111) layers and AuNPs, demonstrating that also aNHC can be exploited to functionalize gold surfaces, as reported in **Figure 3.1 b**.[5–7]

Given these drawbacks, it is not simple to tailor aNHCs to cap AuNCs, since their steric hindrance are generally high and does not match with cluster size, complicating the use of such ligands. However, it is possible to functionalize the backbones of common NHCs or use peculiar aNHC not presenting such steric constrictions.

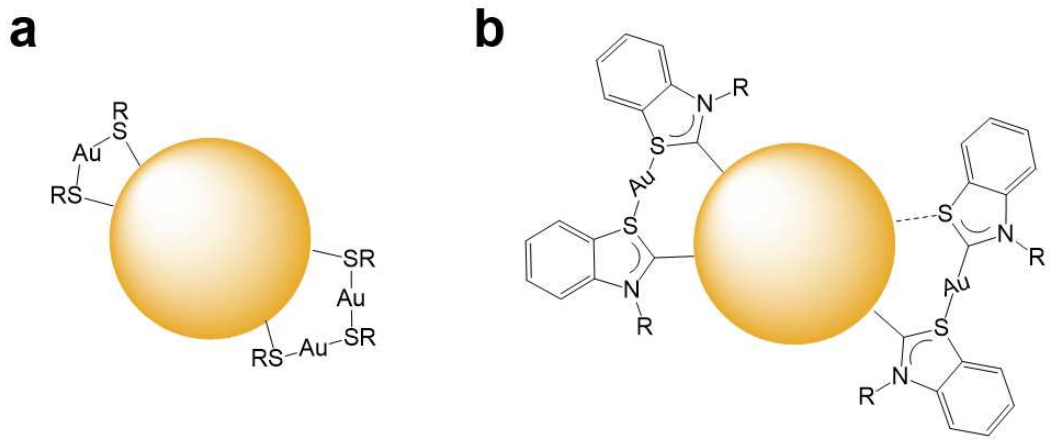

Figure 3.2: schematic a) $[Au_n(SR)_m]$staples and b) possible $Au_n[(S)NHC]_m$ staples anchored on cluster core.

Looking in literature we found another interesting class of aNHC that could be useful to stabilize gold clusters, presenting benzothiazol-2-ylidene units and called here (S)NHC.[8,9] These aNHC exhibit a structure similar to conventional NHCs but in which a sulfur atom substitutes one of the nitrogen atoms. Thus, (S)NHC are similar to NHCs but present instead a free electronic doublet placed on sulfur atom. This lone pair could be useful to achieve new interactions on cluster cores, mimicking the characteristic staples presented in SR or alkynyl-capped AuNCs. Moreover, such

ligands are better π-acceptors than CAACs, considering that their LUMO level is 0.2 eV lower than the value reported for CAACs.[10] Consequently, the advantages of (S)NHCs are related to their electronic proprieties and to their theoretical ability to form this staple.

Finally, also the use of NHCs presenting electron withdrawing groups in the backbone should favor the stabilization of AuNCs. For instance, such ligands can be obtained from theophylline molecules, presenting the ideal scaffold to form NHCs and characterized by carboxylic and amino groups in the backbone.

On the basis of the above, in this paragraph the variation of electronic proprieties of NHCs and the use of (S)NHCs to cap AuNCs will be discussed, always exploiting the reduction of corresponding Au(I) complexes promoted by $NaBH_4$.

3.2 DIRECT REDUCTION ON ABNORMAL NHC GOLD COMPLEXES PROMOTED BY $NaBH_4$

In 2021 we have reported the synthesis of a novel di-NHC gold(I) complex presenting a caffeine scaffold in the structure of the ligand[11], with formula [(di-NHC)Au](BF_4) and here reported in **Figure 3.3**. This complex presents an uncommon bent structure, a property making it unstable and providing its evolution into a bi-metallic complex with formula [(di-NHC)$_2$Au$_2$](BF_4)$_2$, more stable due to linear coordination at gold. The π-acceptor character of the ligand makes this complex a good candidate to synthesize new AuNCs. Furthermore, di-NHCs presenting *o*-xylyl bridges have been already employed in AuNCs synthesis.[12] Despite our starting hypotheses, after the reduction with $NaBH_4$ coupled with a promising change of color, high-resolution mass spectrometry (HRMS) analysis does not highlight any peaks attributable to formation of AuNCs.

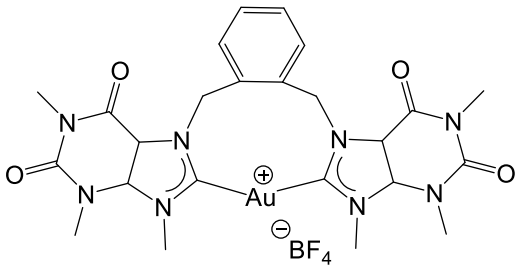

Figure 3.3: caffeine derivative NHC gold (I) complex used in our synthesis.

After this experiment, we decided to focus our work towards di-NHC presenting cyano groups in the ligand-backbone, still to guarantee enhanced π-acceptor proprieties of the ligand, but the synthesis of the corresponding imidazolium salt proved to be challenging. Indeed, it is simple to obtain 1,3-bis(4,5-dicyanoimidazole) propane, reported in **Figure 3.4**, but the electron-withdrawing effect provided by four nitrile groups disfavors further functionalization on free nitrogen atoms, also using strong electrophiles, such as benzyl triflate formed *in situ*. Indeed, only methyl substitution

has been reported in the literature with this kind of substituted imidazoles, which however results in NHC precursors displaying poor solubility.[13]

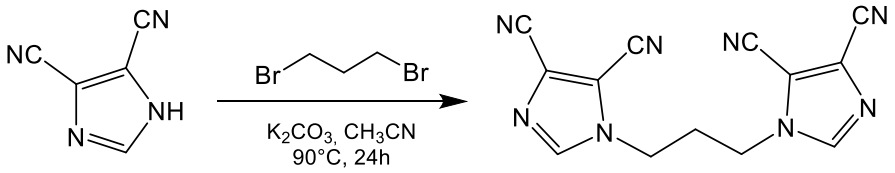

Figure 3.4: synthesis of 1,3-bis(4,5-dicyanoimidazole) propane.

On the basis of the difficulties found in the use of such NHCs, we decided to change our approach, using (S)NHCs.

The synthesis of the gold precursors has been easily achieved by deprotonation *in situ* of the corresponding benzothiazolium salt, provided by K_2CO_3, in the presence of [ClAu(THT)] as gold precursor. As wingtips, we decided to use isopropyl and benzyl groups, since these have been already employed in NHC-stabilized clusters.[14–24] The X-ray structures of these complexes are reported in **Figure 3.5**, presenting respectively **m**, with formula [(S)NHC^{Bn}-Au-Br], and **n**, with formula [(S)NHC^{iPr}-Au-Br].

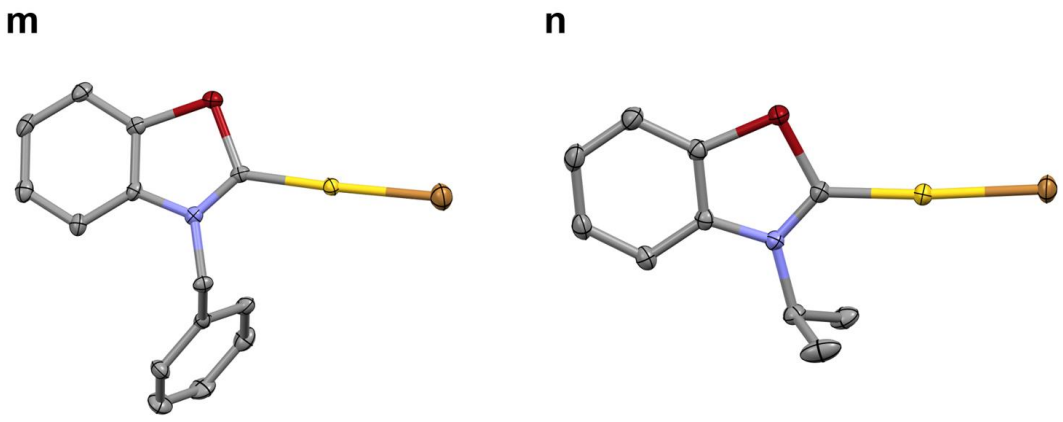

Figure 3.5: X-ray structures of the new (S)NHC-Au(I) complexes **m** and **n** synthesized in this work. Color code: yellow (Au), red (S), brown (Br), purple (N), grey (C).

The ^{1}H and ^{13}C NMR spectroscopies confirm the structures found by single crystal X-ray diffractometry. The proton spectra of these complexes are similar to corresponding spectra of benzothiazolium salts but characterized by the absence of protonic signal in position 2 of the organic rings, confirming the occurred deprotonation. The ^{13}C NMR spectra confirm the carbene nature of such complexes, with carbene signals centered at 205 and 200 ppm for **m** and **n** complexes, respectively. Moreover, also mass spectrometry confirms these data, showing for **m** complex a signal centered at 523.93 m/z, corresponding to sodium positive adduct [**m**-Na]$^{+}$, and for **n** complex a signal centered at 453.95 m/z, corresponding to positive adduct [**n**-H]$^{+}$. The stoichiometric formulas of these are also confirmed by elementary analyses too. The full characterization of such species is reported in **Experimental Section**.

After the synthesis of (S)NHC-Au(I) complexes, their reduction with $NaBH_4$ has been attempted, but no clusters have been detected by HRMS. Also trying some purification methods, such as extractions and chromatographic columns, the HRMS shows only peaks at low m/z ratio, not related with AuNCs. It is not easy to understand why this new class of complexes does not provide clusters after the reduction process, considering that steric proprieties are similar to common NHC and their electronic proprieties should favor cluster stabilization thanks to their lower LUMO level. An explanation could be the absence of the second wingtip group in (S)NHCs, since it has been proved that π-π and CH-π interactions between NHCs bonded to the core increase the rigidity of the ligand shell, helping cluster stabilization.[21,25] Also the formation of supposed staples could be affected by the positive charges related with it. Indeed, [NHC(S)-Au-(S)NHC] staple should present one positive charge, not matchable with classical positive charge of AuNCs. In case of alkynyl or thiolate ligands these staples are negatively charged, favoring the electrostatic interaction with gold cores. Finally, even the starting complexes do not show high stability, since during their purification degradation products are often obtained. For instance, during

crystallization of **n'** complex, bearing iodide anion instead of bromide, it is possible to obtain linear [NHC(S)-Au-(S)NHC][AuI_2]complex, highlighting how (S)NHC neutral complexes tend to form these bimetallic cationic complexes. X-ray structure of the latter is reported in **Figure 3.6**.

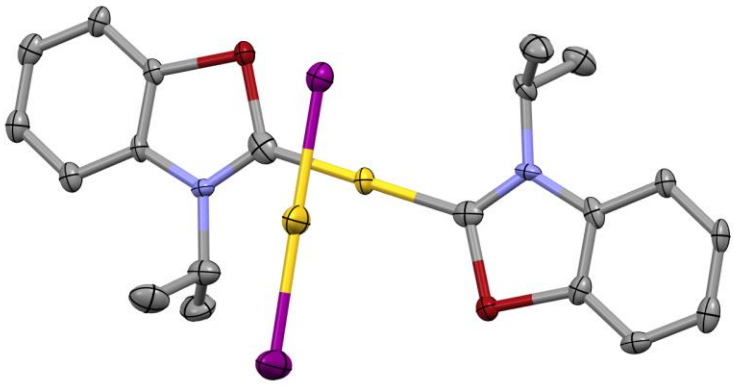

Figure 3.6. X-ray structure of degradation product of **n'** complex. Color code: yellow (Au), red (S), fuchsia (I), purple (N), grey (C).

3.3 BIBLIOGRAPHY

[1] R. H. Crabtree, *Coord. Chem. Rev.* **2013**, *257*, 755–766.
[2] S. C. Sau, P. K. Hota, S. K. Mandal, M. Soleilhavoup, G. Bertrand, *Chem. Soc. Rev.* **2020**, *49*, 1233–1252.
[3] M. Soleilhavoup, G. Bertrand, *Acc. Chem. Res.* **2015**, *48*, 256–266.
[4] L. Jin, D. S. Weinberger, M. Melaimi, C. E. Moore, A. L. Rheingold, G. Bertrand, *Angew. Chem. Int. Ed.* **2014**, *53*, 9059–9063.
[5] A. Bakker, M. Freitag, E. Kolodzeiski, P. Bellotti, A. Timmer, J. Ren, B. Schulze Lammers, D. Moock, H. W. Roesky, H. Mönig, S. Amirjalayer, H. Fuchs, F. Glorius, *Angew. Chem. Int. Ed.* **2020**, *59*, 13643–13646.
[6] M. Ghosh, P. Saha, S. Roy, P. Pillai, A. Dey, S. Khan, *Cyclic(Alkyl)(Amino)Carbene Stabilized Gold Nanoparticles: Efficient Catalyst for Selective Electrochemical Reduction of CO2 to CO*, Chemistry, **2023**.
[7] J. Ren, M. Freitag, Y. Gao, P. Bellotti, M. Das, B. Schulze Lammers, H. Mönig, Y. Zhang, C. G. Daniliuc, S. Du, H. Fuchs, F. Glorius, *Angew. Chem. Int. Ed.* **2022**, *61*, e202115104.
[8] H. G. Raubenheimer, S. Cronje, *J. Organomet. Chem.* **2001**, *617–618*, 170–181.
[9] S. K. Yen, L. L. Koh, F. E. Hahn, H. V. Huynh, T. S. A. Hor, *Organometallics* **2006**, *25*, 5105–5112.
[10] M. Joost, M. Nieger, M. Lutz, A. W. Ehlers, J. C. Slootweg, K. Lammertsma, *Organometallics* **2020**, *39*, 1762–1771.
[11] V. Stoppa, T. Scattolin, M. Bevilacqua, M. Baron, C. Graiff, L. Orian, A. Biffis, I. Menegazzo, M. Roverso, S. Bogialli, F. Visentin, C. Tubaro, *New J. Chem.* **2021**, *45*, 961–971.
[12] H. Yi, K. M. Osten, T. I. Levchenko, A. J. Veinot, Y. Aramaki, T. Ooi, M. Nambo, C. M. Crudden, *Chem. Sci.* **2021**, *12*, 10436–10440.
[13] P. Pinter, A. Biffis, C. Tubaro, M. Tenne, M. Kaliner, T. Strassner, *Dalton Trans.* **2015**, *44*, 9391–9399.
[14] H. Shen, X. Tang, Q. Wu, Y. Zhang, C. Ma, Z. Xu, B. K. Teo, N. Zheng, *ACS Nanosci. Au* **2022**, *2*, 520–526.
[15] P. Luo, X. Zhai, S. Bai, Y. Si, X. Dong, Y. Han, S. Zang, *Angew. Chem. Int. Ed.* **2023**, *62*, e202219017.
[16] X. Wang, R. Liu, L. Tian, J. Bao, C. Zhao, F. Niu, D. Cheng, Z. Lu, K. Hu, *J. Phys. Chem. C* **2022**, *126*, 18374–18382.
[17] H. Shen, G. Deng, S. Kaappa, T. Tan, Y. Han, S. Malola, S. Lin, B. K. Teo, H. Häkkinen, N. Zheng, *Angew. Chem.* **2019**, *131*, 17895–17899.
[18] M. R. Narouz, K. M. Osten, P. J. Unsworth, R. W. Y. Man, K. Salorinne, S. Takano, R. Tomihara, S. Kaappa, S. Malola, C.-T. Dinh, J. D. Padmos, K. Ayoo, P. J. Garrett, M. Nambo, J. H. Horton, E. H. Sargent, H. Häkkinen, T. Tsukuda, C. M. Crudden, *Nat. Chem.* **2019**, *11*, 419–425.
[19] V. K. Kulkarni, B. N. Khiarak, S. Takano, S. Malola, E. L. Albright, T. I. Levchenko, M. D. Aloisio, C.-T. Dinh, T. Tsukuda, H. Häkkinen, C. M. Crudden, *J. Am. Chem. Soc.* **2022**, *144*, 9000–9006.
[20] H. Shen, Q. Wu, M. S. Asre Hazer, X. Tang, Y.-Z. Han, R. Qin, C. Ma, S. Malola, B. K. Teo, H. Häkkinen, N. Zheng, *Chem* **2022**, *8*, 2380–2392.
[21] M. R. Narouz, S. Takano, P. A. Lummis, T. I. Levchenko, A. Nazemi, S. Kaappa, S. Malola, G. Yousefalizadeh, L. A. Calhoun, K. G. Stamplecoskie, H. Häkkinen, T. Tsukuda, C. M. Crudden, *J. Am. Chem. Soc.* **2019**, *141*, 14997–15002.
[22] J. Sun, X. Tang, J. Tang, Y. Zhang, Z. Li, Chaolumen, S. Guo, H. Shen, *Inorg. Chem.* **2023**, *62*, 5088–5094.
[23] H. Shen, S. Xiang, Z. Xu, C. Liu, X. Li, C. Sun, S. Lin, B. K. Teo, N. Zheng, *Nano Res.* **2020**, *13*, 1908–1911.
[24] A. I. Sullivan, J. F. DeJesus, S. Malola, S. Takano, T. Tsukuda, H. Häkkinen, C. M. Crudden, *Chem. Mater.* **2023**, *35*, 2790–2796.
[25] P. Luo, S. Bai, X. Wang, J. Zhao, Z. Yan, Y. Han, S. Zang, T. C. W. Mak, *Adv. Opt. Mater.* **2021**, *9*, 2001936.

4.0 RESULTS AND DISCUSSION: VARIATION OF REDUCING AGENT TO TUNE THE REDUCTION PROFILE

4.1 INTRODUCTION: DIRECT REDUCTION WITHOUT USING SODIUM BOROHYDRIDE TO ISOLATE NOVEL CLUSTER

In previous sections we highlighted how several parameters have been varied aiming at tailoring AuNCs synthesis, despite one of the most interesting has not been investigated in detail: the reducing agent. Indeed, $NaBH_4$ is the most commonly employed reagent in this field, although its oxidation mechanism, concurrent with Au(I) reduction, is not completely clarified. Also in the case of SR-capped clusters the control of such syntheses derives from the first reduction step promoted by SR ligands, affording $[Au(SR)]_n$ oligomers, and not from the second one, promoted instead by $NaBH_4$. Using HRMS and UV-Vis spectroscopy, Xie's group has studied a stoichiometric mechanism of growth of thiolate-capped AuNCs.[1] Considering that formally $NaBH_4$ provides 8 electrons to the reduction, they proposed the stoichiometric rection reported below:

$$32/n\ [Au(SR)]_n + 8\ e^- \rightarrow 7\ [Au(SR)_2]^- + [Au_{25}(SR)_{18}]^-$$

In which 32 moles of [Au(SR)] monomer react with one mole of $NaBH_4$, affording $[Au_{25}(SR)_{18}]^-$ cluster as product and $[Au(SR)_2]^-$ complex as by-product. However, this reaction is conducted in water but no $NaBH_4$ degradation is reported, which is difficult to believe since it is known that this species reacts rather easily with water. Moreover, using a stoichiometric amount of $NaBH_4$ the post reduction mixture presents other AuNCs as co-products, like Au_{38} or Au_{44} clusters, complicating therefore the interpretation of the results. However, when the reduction is followed "electron by

electron", thus adding small aliquots of reducing agent with time, the reaction is more focused, showing exclusively formation of Au_{25} cluster as final product.[2] Furthermore, in the second experiment the presence of $[Au(SR)_2]^-$ as final co-product is confirmed, demonstrating similarities with the synthesis of NHC-capped AuNCs, in which $[Au(NHC)_2]^+$ or $[Au_2(di\text{-}NHC)_2]^{2+}$ are present as co-products. Formation of these complexes represents the main drawback in the reduction pathways to get AuNCs. Au(I) centers prefer to stabilize themselves through formation of linear complexes rather than forming clusters along with their own reduction. Moreover, we have already explained that $[Au(NHC)_2]^+$ and $[Au_2(di\text{-}NHC)_2]^{2+}$ are too stable to undergo a reduction promoted by $NaBH_4$. Once formed, these complexes are stable in reducing environment, decreasing therefore the cluster yield. Inhibiting the accumulation of such species during the reduction is not trivial, since steric proprieties of ligands useful for this purpose affect NHC coordination proprieties too, making impossible the use of bulky ligands. However, it is still possible to change the reduction pathway varying the reducing agents, aiming at disfavoring formation of such by-products, for instance using weaker reducing agents to slow down the reduction.

Despite the fact that a proper choice of the reducing agent should represent one of the most rational ways to control such reductions, in the literature there are only few examples in which the optimization of the reducing agent affords mono-dispersed cluster products. For instance, as explained in **Paragraph 1.6.2**, several biological reducing agents can be employed in aqueous environment, but affording generally poly-dispersed and small AuNPs, thus without the desire molecularity required in this thesis. Some examples have been reported by Xie et al., in which reduction with CO provides mono-dispersed clusters upon controlling the pH of aqueous reaction environment.[3,4]

In the case of PR_3-capped clusters, more examples are reported, for instance using $[Ti(\eta\text{-}C_6H_5CH_3)_2]$ is possible to isolate $[Au_{13}]^{5+}$ clusters, not easily synthesizable with

PR_3.[5–7] More recently, Schnepf's group synthesized the gallium-doped nanocluster $[Au_9Ga(PPh_3)_8Cl_2]^{2+}$ using GaCp (Cp = cyclopentadienyl) as strong reducing agent and gallium source, formed *in situ*, affording oxygen sensitive clusters, a feature that strongly affects their possible applications.[8]

Regarding NHC-protected AuNCs, Crudden et al. have reported the synthesis of $[Au_{11}(NHC^{Bn})_8Br_2]^+$ during 2023, in which KC_8 is used as reducing agent.[9] This reducing agent is stronger than $NaBH_4$ and is commonly used to reduce for instance Pd(II) to Pd(0) complexes.[10] Using KC_8 the reduction does not provide the classic $[Au_{13}]^{5+}$ core but instead the less stable $[Au_{11}]^{3+}$. This latter cluster is oxygen and water sensitive, deeply differing from its Au_{13} counterpart, not sensitive to such species. It is interesting to note that $[Au_{13}]^{5+}$ cluster cannot be synthetized if the reduction is performed using $NaBH_4$ dispersed in THF under nitrogen; this behavior has been not rationalized yet.

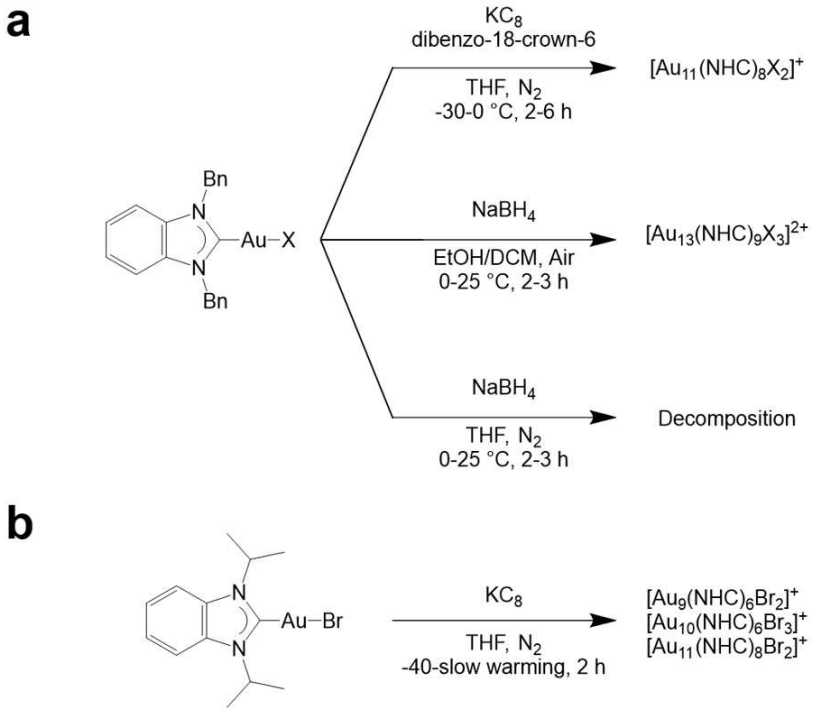

Figure 4.1: Reduction of a) benzyl-NHC Au(I) and b) isopropyl-NHC Au(I) complexes studied by Crudden et al.[9]

Furthermore, also the role of the crown ether is not clarified in Crudden's paper, but likely it is used to cap K^+ ions formed post-reduction from KC_8 oxidation. In addition, this reduction is still strongly affected by wingtips groups, since only benzyl groups provide a monodispersed cluster product. When isopropyl groups are used instead, a mixture of $[Au_9(NHC^{iPr})_6Br_2]^+$, $[Au_{10}(NHC^{iPr})_6Br_3]^+$ and $[Au_{11}(NHC^{iPr})_8Br_2]^+$ is obtained, highlighting the importance of steric parameters in this synthesis. The reactions discussed above are reported in **Figure 4.1**.

Looking into these examples, in which strong reducing agents are used, we decided to test weaker reducing agents, aiming at understanding if such reductants can be exploited to isolate novel clusters, slowing down the reduction rate. In this study, mono-NHC and (S)NHC gold complexes will be taken in account too, since they present more degrees of freedom than di-NHC to cap AuNCs, limited by their chelating proprieties.

We decided to test KH, Na/NaCl (5% w/w) and hydrazine as reducing agents, all presenting lower reducing potentials than $NaBH_4$. The first two reagents are oxygen and air sensitive, therefore these reductions have been performed in glovebox at room temperature. Hydrazine instead is not such sensitive, hence the reductions have been performed in air. These experiments have been in part conducted in the laboratory of Prof. Dominik Munz, at Saarland University.

4.2 Na/NaCl REDUCTIONS

Our work started with the reduction of (S)NHC complexes, reported here in **Figure 4.2**, with Na/NaCl (5% w/w). The syntheses have been performed using THF as solvent, the only solvent that allowed a good dispersion of reducing agent and complexes. The use of solvents such as methanol, ethanol and dichloromethane, usually employed in our work, are not recommended in glovebox, since the possible presence of water and the reactivity that chlorinated solvents have with highly sensitive chemicals, such as alkaline metals. Unfortunately, also using this reducing agent with both (S)NHC complexes, it has not been possible to obtain new clusters. Our hypothesis regarding this failure have been already discussed in **Paragraph 3.2.** We decided to attempt the reduction of di-NHC complexes **b** and **c'** too, also reported in **Figure 4.2** and already studied in our group, to obtain NHC-stabilized AuNCs. In spite of the chelating propriety of these ligands, also in this case the reduction performed with Na/NaCl (5% w/w) has not provided the formation of clusters, as confirmed by the absence of suitable peaks in the HRMS spectrum.

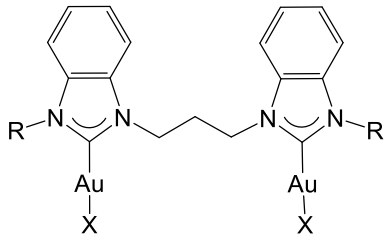

b R: Bn
X: Cl

c' R: *i*Pr
X: Br

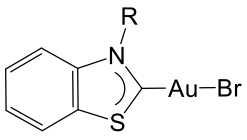

m R: Bn

n R: *i*Pr

Figure 4.2: Au(I) complexes employed in the reduction tests with Na/NaCl.

4.3 KH REDUCTIONS

After the experiments using Na/NaCl as reducing agent, we decided to use KH, similar to $NaBH_4$ due to the presence of hydrides but with a different reducing potential. THF has been used as solvent also in this case. The reduction of [(S)NHC-Au-Br] complexes did not afford AuNCs, but with complex **n**, we were able to obtain small gold nanoparticles stabilized by (S)NHC. After a simple work-up to remove the main impurities, the AuNPs has been analyzed by transmission electron microscopy (TEM), reported in **Figure 4.3**.

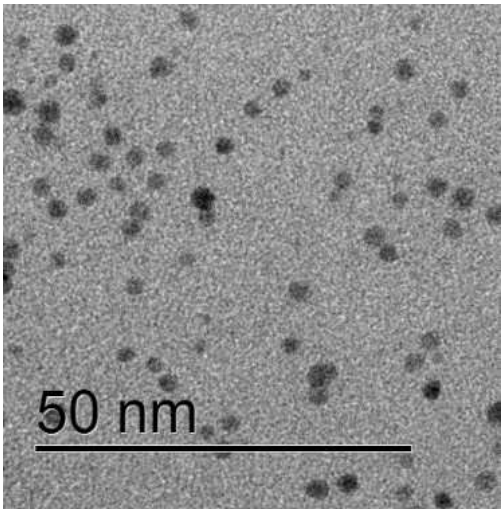

Figure 4.3: TEM imaging of small AuNPs capped by (S)NHC^{iPr} ligands.

The TEM analysis shows small particles with size around 2-3 nm, matching well with similar NHC-stabilized AuNPs reported in literature.[11] In addition, the signals related to (S)NHC are detected in ^{1}H NMR spectrum, meaning that the ligands are anchored on the AuNPs. Despite this result appears interesting, we decided to not focus on the purification and characterization of such system since its poly-dispersed nature.

The reduction of **b** and **c'** with KH has been tested too. Unfortunately, only with **b** complex it is possible to observe in the mass analysis the presence of a new cluster, centered at 1114 m/z in the mass spectrum, but we have not been able to determine

its stoichiometric composition and to purify it yet. Furthermore, classical $[Au_{13}]^{5+}$ clusters have been detected, further complicating the purification of the novel cluster.

4.4 HYDRAZINE REDUCTIONS

Hydrazine monohydrate is one of the best candidates to substitute $NaBH_4$, presenting indeed a lower reducing potential and forming dinitrogen as product of oxidation. Thus, a series of experiments have been made with **a'**, **b'**, **c'** and **o** complexes, reported in **Figure 4.4**, dissolved in DCM:MeOH (4:1 v:v) solution, using 10 equivalents of hydrazine monohydrate as reducing agent and 100 equivalents of KOH to activate it. All the ligands used have been already exploited to cap AuNCs in literature or in our work.

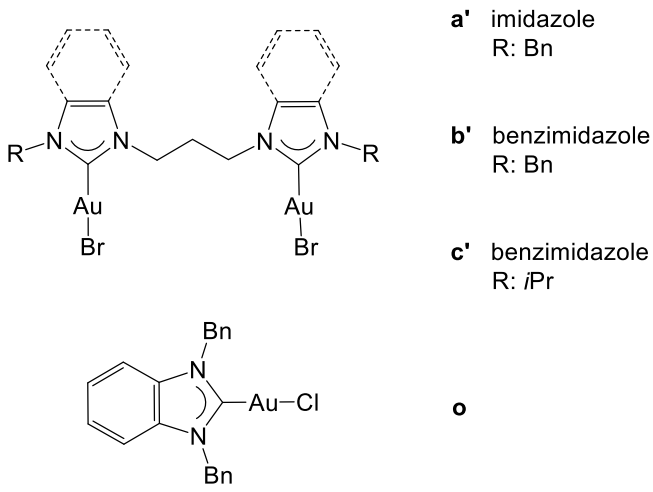

Figure 4.4: Au(I) complexes employed in the reduction tests with hydrazine.

The process has been analyzed with HRMS. With the experiment involving **a'** and **b'**, the results have not been satisfactory. With **a'** only traces of different AuNCs can be detected with HRMS and with **b'** the reduction leads the formation of $[Au_6(C)(di\text{-}NHC^b)_3]^{2+}$ together with classic $[Au_{13}(di\text{-}NHC^b)_5Br_2]^{3+}$ cluster already reported in literature.[12]

The $Au_6(C)$ cluster has been already reported in literature but bearing mono-dentate ligands.[13–17] The six Au(I) atoms interact to each other, forming an octahedral geometry with a carbide ion centered in it, as reported in **Figure 4.5**. This AuNC can

be called “ionic cluster”, since ionic and aurophilic interactions hold up the whole structure. Moreover, formally the gold(I) atoms of the starting complex do not undergo any reduction, since the reducing agent likely reduces DCM used as solvent to form the carbide anion. It is interesting that DCM reduction can be achieved also using hydrazine in presence of Au(I) complexes, with similitudes to the synthesis of CH_3-capped AuNCs reported in **Paragraph 2.3**. Instead of forming CH_3-capped AuNCs, hydrazine oxidation provides C^{4-} anion stabilized through interactions with 6 Au(I) centers, affording the ionic cluster. The synthesis of $[Au_6(C)(NHC)_6]^{2+}$ has been reported firstly by Shionoya et al. in 2018[13]; however, in their synthetic approach it is essential to isolate first an $[(\mu_3\text{-}O)Au_3(NHC)_3]^{+}$ complex as intermediate. This oxo-complex undergoes a subsequent oxygen extraction upon trimethylsilyldiazomethane addition, providing the desire cluster without reduction of Au(I) centers. Furthermore, using chiral NHCs it is possible to observe a distortion of $Au_6(C)$ core, showing a consequent chiral arrangement of Au(I) centers.[14] The first synthesis of $[Au_6(C)(NHC)_6]^{2+}$ is reported in **Figure 4.5**.

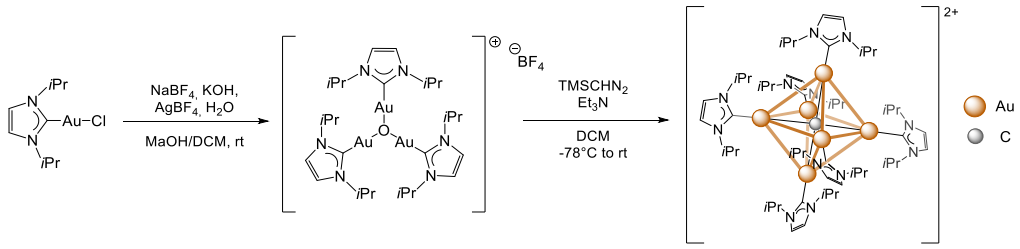

Figure 4.5: synthesis of $[Au_6(C)(NHC)_6]^{2+}$ reported by Shionoya et al.[13]

Returning on experiment involving **b’**, the chromatographic separation of the two clusters has been attempted but without success. One last attempt has been performed, adding an excess of hydrobromic acid to favor an etching process towards $Au_6(C)$ cluster. Unfortunately, etching favors the Au_{13} cluster rather than the ionic cluster, meaning that $Au_6(C)$ does not survive under acid conditions, promoting Au_{13}

formation. This is an interesting feature that could be used to synthesize clusters difficult to obtain with other methods.

With **c'** and **o** complexes the process is more focused, affording exclusively $[Au_6(C)(di\text{-}NHC^c)_3]^{2+}$ and $[Au_6(C)(NHC^o)_6]^{2+}$, respectively. These reactions are reported in **Figure 4.6**.

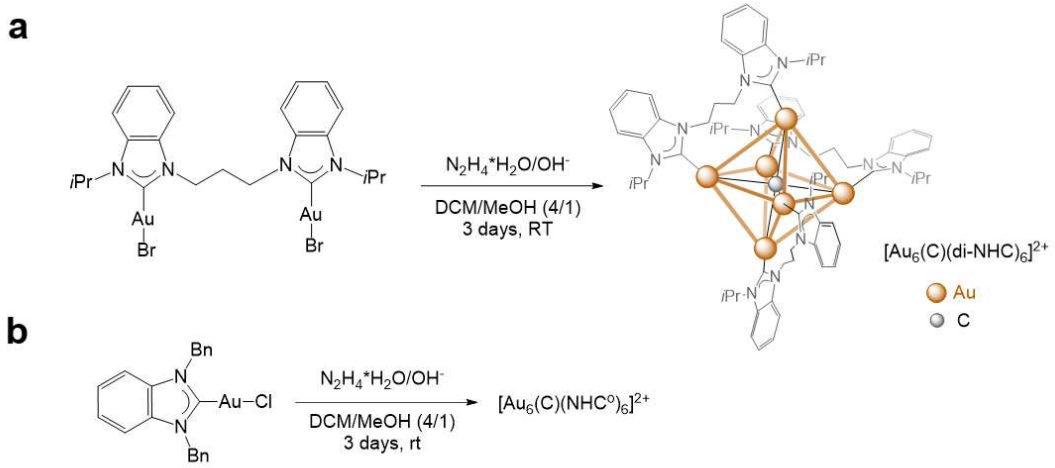

Figure 4.6: Synthesis of $Au_6(C)$ clusters derived from a) **c'** and b) **o** complexes.

It is remarkable that using hydrazine the ionic cluster can be obtained in only one step, unlike Shionoya's method, in which it is necessary to pass through the $[(\mu_3\text{-}O)Au_3(NHC)_3]^+$ intermediate. The strength and the novelty of our method is the synthesis of $Au_6(C)$ bearing di-NHC ligands, *i.e.* clusters that are impossible to obtain using Shionoya's method, considering that the trinuclear intermediate cannot be stabilized by di-NHC ligands. Despite these interesting results, the purification of these ionic clusters is not easily achievable, affecting the study and the isolation of such species. In the literature, the purification of $Au_6(C)$ clusters capped by mono-NHCs is performed by sequential crystallizations, repeated until high purity of final products is achieved. This purification method is favored since the employed synthetic method affords high yields of raw product, according to the literature; comparable

yields are not yet achievable with our method. Indeed, our direct method involving reduction by hydrazine provides rough yields around 2-3% for both detected $Au_6(C)$ clusters. Such low yields are remarkable, in particular considering the chelating proprieties of di-NHC^c, that should increase the cluster stability and consequently its yield. Furthermore, $Au_6(C)$ clusters have been revealed to be unstable in acid conditions, preventing therefore the use of acid etching. Finally, an $[Au_6(C)(NHC^o)_6]^{2+}$ cluster has been already reported by Shionoya et al. during 2022, capped by similar NHCs and isolated through the method reported **Figure 4.5**.[14] Since the similarities with our case, we focused our attention on the test involving **c'**, since the novelty related to it.

The purest cluster has been obtained from a chromatographic column, during which however part of the cluster degrades in column, due to the acid properties of silica. The HRMS are reported in **Figure 4.7**, together with mass spectrum of $[Au_6(C)(NHC^o)_6]^{2+}$. The mass spectra show two main signals, one related to $[Au_6(C)(di\text{-}NHC^c)_3]^{2+}$, or $[Au_6(C)(NHC^o)_6]^{2+}$, and the other related to $[Au_2(di\text{-}NHC^c)_2]^{2+}$, or $[Au(NHC^o)_2]^+$, fragments derived from the mass ionization, as reported in literature.

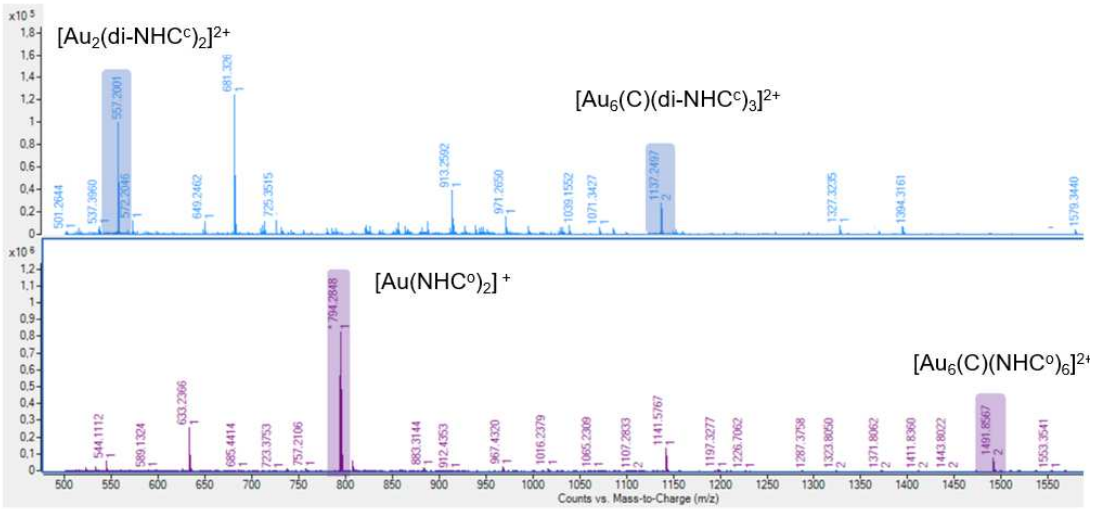

Figure 4.7: HRMS analysis of $[Au_6(C)(di\text{-}NHC^c)_3]^{2+}$(above) and $[Au_6(C)(NHC^o)_6]^{2+}$ (below), in which molecular and fragmentation peaks are highlighted.

The UV-Vis spectrum of $[Au_6(C)(di\text{-}NHC^c)_3]^{2+}$ has been acquired dissolving the cluster in DCM. The spectrum shows two weak bands, centered at 486 nm and 425 nm, and two strong signals at 330 nm and 289 nm, in which this latter presents a shoulder at 284 nm. In the emission spectrum, still obtained dissolving the cluster in DCM, there are one broad band centered at 780 nm, showing a luminescence quantum yield equal to 1.64%. It is interesting that such cluster with di-NHC ligands provides luminescence in solution, in contrast to what is reported in the literature for $[Au_6(C)(NHC)_6]^{2+}$ clusters with mono-NHCs: generally, these ionic clusters are good emitters exclusively in solid state but no luminescence can be observed in solution.[15] Possibly, the di-NHC ligand layer stiffens the cluster structure, preventing vibrational relaxation and consequently favoring its luminescence emission in solution.

In addition, we also tested the redox activity of $[Au_6(C)(di\text{-}NHC^c)_3]^{2+}$ cluster, performing cyclic voltammetry analysis on it with collaboration of Maran's group. We hypothesized that di-NHCs should guarantee enough stability to allow variation of oxidation state without compromising the cluster stability. Despite our hypothesis, the CV analysis did not reveal any oxidation or reduction peaks, meaning that $[Au_6(C)(di\text{-}NHC^c)_3]^{2+}$ does not easily undergo oxidation or reduction processes.

Finally, we attempted ^1H NMR analysis too, despite the low amount of cluster obtained. The signals related to di-NHC ligands are shifted in the spectrum compared to the parent $[(di\text{-}NHC^c)Au_2Br_2]$ complex, but their integral values do not match with the number of protons, indicating impurities in the aromatic area of the spectrum. Furthermore, after the purification it is still possible to detect a small amount of **c'** complex, highlighting a partial degradation of $[Au_6(C)(di\text{-}NHC^c)_3]^{2+}$ post column. Indeed, **c'** complex should be present in first fraction of the column separation due to its neutral charge, but here it is detected in final fractions, confirming therefore the cluster degradation due to the acidity of silica.

Since the low value of QY, the absence of redox activity and the complicated purification, we decided to focus our attention on novel synthetic methods to isolate molecular clusters, avoiding this direct reduction approach.

After the tests involving variation of NHCs scaffold, wingtips groups and reducing agents, we can conclude that the direct reduction does not represent the best approach to isolate such clusters. This seems to work only in specific conditions and generally only small variations on it can be used to tune the reaction products, that generally are SA clusters. We attempted to favor AuNCs formation varying NHC proprieties, affecting only partially the reduction pathways. Moreover, also the change of the reducing agents does not provide satisfactory results in this direction. Since these limitations, we developed a novel method to get AuNCs, in which a preformed PPh_3-capped cluster reacts with [(di-NHC)Au_2Cl_2] complexes, affording novel PPh_3/NHC-capped AuNCs. This process, called stepwise synthesis, will be discussed in the next section.

4.5 BIBLIOGRAPHY

[1] T. Chen, V. Fung, Q. Yao, Z. Luo, D. Jiang, J. Xie, *J. Am. Chem. Soc.* **2018**, *140*, 11370–11377.
[2] T. Chen, Q. Yao, Y. Cao, J. Xie, *Cell Rep. Phys. Sci.* **2020**, *1*, 100206.
[3] Y. Yu, X. Chen, Q. Yao, Y. Yu, N. Yan, J. Xie, *Chem. Mater.* **2013**, *25*, 946–952.
[4] Y. Yu, Z. Luo, Y. Yu, J. Y. Lee, J. Xie, *ACS Nano* **2012**, *6*, 7920–7927.
[5] S. J. Lippard, Ed. , *Progress in Inorganic Chemistry*, John Wiley & Sons, **2009**.
[6] C. E. Briant, B. R. C. Theobald, J. W. White, L. K. Bell, D. M. P. Mingos, A. J. Welch, *J. Chem. Soc. Chem. Commun.* **1981**, 201.
[7] R. C. B. Copley, D. M. P. Mingos, *J Chem Soc Dalton Trans* **1996**, 479–489.
[8] F. Fetzer, C. Schrenk, N. Pollard, A. Adeagbo, A. Z. Clayborne, A. Schnepf, *Chem. Commun.* **2021**, *57*, 3551–3554.
[9] A. I. Sullivan, J. F. DeJesus, S. Malola, S. Takano, T. Tsukuda, H. Häkkinen, C. M. Crudden, *Chem. Mater.* **2023**, *35*, 2790–2796.
[10] N. Marigo, B. Morgenstern, A. Biffis, D. Munz, *Organometallics* **2023**, *42*, 1567–1572.
[11] H. Shen, G. Tian, Z. Xu, L. Wang, Q. Wu, Y. Zhang, B. K. Teo, N. Zheng, *Coord. Chem. Rev.* **2022**, *458*, 214425.
[12] H. Shen, S. Xiang, Z. Xu, C. Liu, X. Li, C. Sun, S. Lin, B. K. Teo, N. Zheng, *Nano Res.* **2020**, *13*, 1908–1911.
[13] H. Ube, Q. Zhang, M. Shionoya, *Organometallics* **2018**, *37*, 2007–2009.
[14] X.-L. Pei, P. Zhao, H. Ube, Z. Lei, K. Nagata, M. Ehara, M. Shionoya, *J. Am. Chem. Soc.* **2022**, *144*, 2156–2163.
[15] L. H. Foianesi-Takeshige, X. Pei, P. Zhao, H. Ube, Z. Lei, M. Ehara, M. Shionoya, *Adv. Opt. Mater.* **2023**, 2301650.
[16] F. P. Gabbaï, A. Schier, J. Riede, H. Schmidbaur, *Chem. Ber.* **1997**, *130*, 111–114.
[17] Z. Lei, K. Nagata, H. Ube, M. Shionoya, *J. Organomet. Chem.* **2020**, *917*, 121271.

5.0 RESULT AND DISCUSSION: STEPWISE SYNTHESIS OF di-NHC/PPh_3-CAPPED SUPER-ATOMIC GOLD CLUSTERS

5.1 INTRODUCTION: A NOVEL METHODOLOGY TO PRODUCE NHC-CAPPED CLUSTERS

In previous paragraphs we have performed several reductions aiming at atomically controlling the synthesis of novel AuNCs. Following this purpose, variation of ligand proprieties and reducing environment have been considered, demonstrating however that the direct reduction of Au(I) complexes is not easily tunable. Considering this limitation, more suitable AuNCs syntheses are required, aiming at better controlling clusters growth, considering their ligands shell too. In particular, the control of the latter is fundamental to get more reactive clusters, a feature that NHC-capped clusters do not usually present since they generally exhibit strong C-Au bonds and coordinatively saturated metallic cores.

Considering instead SR, alkynyl and PR_3 ligands, several examples of reactive AuNCs have been previously reported, in which evolution “cluster to cluster”, ligand exchange and addition of metal complexes represent real alternatives to tailor AuNCs structures. This reactivity is particularly prosperous in PR_3-capped clusters, whose ligands present similarities to NHCs.

Focusing on these latter, Crudden et al. have synthesized AuNCs bearing PPh_3 and mono-NHC ligands starting from a pure PR_3 stabilized cluster, with stoichiometry $[Au_{11}(PPh_3)_8Cl_2]Cl$, exploiting free NHCs in solution.[1] In this synthesis it is possible to variate the coordination sphere of the starting Au_{11} cluster, whereas the variation of metallic kernel cannot be obtained. Different is the case reported by Mingos et al., in which $[ClM(PMePPh_2)]$ complexes (M: Cu, Ag or Au) react with $[Au_{11}(PMePPh_2)_{10}]^{3+}$ clusters to obtain homoleptic $[M_4Au_9(PMePPh_2)_8Cl_4]^+$ clusters.[2] This reaction is reported as follows:

M: Au(I), Ag(I), Cu(I)
X: $C_2B_9H_{12}^-$

Intrigued by this approach, we hypothesized the possibility to exploit similar reactions to get novel AuNCs capped by di-NHCs, using NHC-Au(I) complexes rather than free NHCs in solution. Indeed, the use of preformed gold complexes potentially enables two possible reaction pathways with the cluster, namely ligand metathesis or complex addition reactions, expanding therefore the kinds of AuNCs achievable with this method. Moreover, the use of NHC complexes as starting reagents should enable the isolation of heteroleptic AuNCs, thus clusters bearing both PPh_3 and NHCs ligands, allowing to get stable but still reactive clusters.

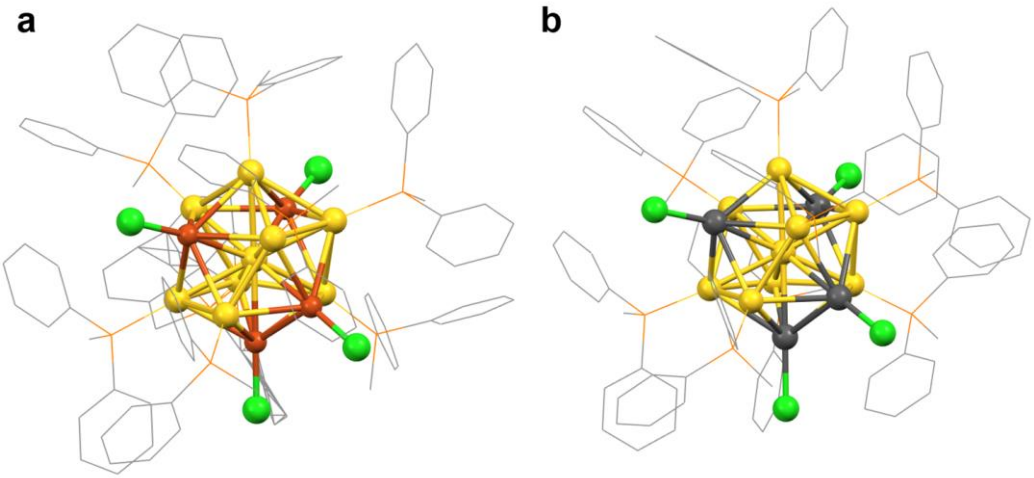

Figure 5.1: X-ray structures of a) $[Cu_4Au_9(PMePh_2)_8Cl_4]^+$ and b) $[Ag_4Au_9(PMePh_2)_8Cl_4]^+$ clusters reported by Mingos's group. CuCl and AgCl fragments are highlighted, together with gold cores. Color code: yellow (Au), red (Cu), dark gray (Ag), green (Cl), orange (P), gray (C).[2]

The similitudes present in NHC and PR_3 ligands reinforce our hypothesis, together with the two SCXRD structures reported by Mingos's group and highlighted in **Figure 5.1**, in which two AgCl and CuCl fragments, derived from starting PR_3 complexes, are close to each other in the corresponding metallic core. This proximity should favor the

use of [(di-NHC)Au_2X_2], in which [(di-NHC)Au_2]$^{2+}$ fragment can be added to the starting [Au_{11}]$^{3+}$ core, affording consequently [Au_{13}]$^{5+}$ clusters, a SA core generally favored with NHC ligands.[3–11] On the basis of these hypotheses, we decided to test the reactivity of [$Au_{11}(PPh_3)_8Cl_2$]$^+$ with our di-NHC complexes.

These experiments have been reported in a paper with title “From Au_{11} to Au_{13}: Tailored Synthesis of Superatomic di-NHC/PPh_3-Stabilized Molecular Gold Nanoclusters”, published in 2023 in Inorganic Chemistry. The results will be further discussed here with additional considerations previously not reported.[12]

5.2 THE STEPWISE APPROACH: HETEROPLETIC LIGAND SHELL PROVIDES STABLE BUT STILL REACTIVE CLUSTERS

In the following, we demonstrate that the "stepwise approach" enables the preparation of a library of heteroleptic $[Au_{11}]^{3+}$ and $[Au_{13}]^{5+}$ clusters protected both by PPh_3 and di-NHCs, starting from $[Au_{11}(PPh_3)_8Cl_2]Cl$ as reagent cluster and reacting it with digold(I) complexes of general formula $[(di\text{-}NHC)Au_2Cl_2]$. Upon changing the stereo-electronic properties of the di-NHC ligand and the reaction conditions, it is possible to control the reaction sequence, that may involve a first metathesis step with formation of $[Au_{11}(di\text{-}NHC)(PPh_3)_6Cl_2]^+$ (type 1 clusters), followed by a thermally induced rearrangement / metal complex addition (see below) to get $[Au_{13}(di\text{-}NHC)_2(PPh_3)_4Cl_4]^+$ (type 2 clusters) and by another metathesis step to obtain $[Au_{13}(di\text{-}NHC)_3(PPh_3)_3Cl_3]^{2+}$ (type 3 clusters). This sequence of reactions is reported in **Figure 5.2**.

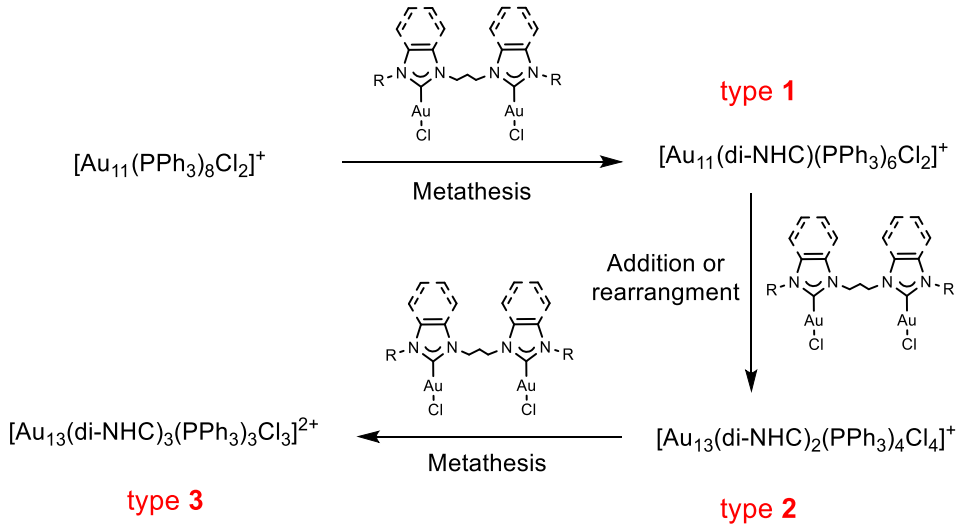

Figure 5.2: Steps involved in stepwise process. From left, above, first metathesis affording type 1 cluster, followed by complex addition or thermal rearrangement affording type 2 cluster. Finally, the last step affords type 3 cluster, thanks to a further metathesis.

The complexes involved in these experiments are reported in **Figure 5.3**. We maintained in all complexes a 1,3-propylene bridge between the carbene units, since it perfectively matches length and flexibility to bridge two mutually interacting gold centers, as observed also before in literature exploiting the direct reduction

approach.[5,9] The digold(I) complexes were then all reacted with the well-known phosphine cluster $[Au_{11}(PPh_3)_8Cl_2]Cl$ in dry dichloromethane under different sets of reaction conditions (see the **Experimental Section** for experimental details). High resolution mass spectrometry (HRMS) has been routinely employed to monitor the reaction progress.

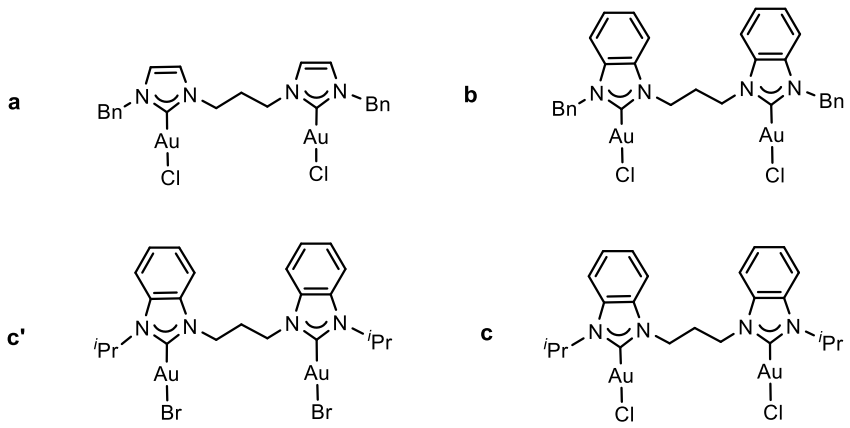

Figure 5.3: di-NHC Au(I) complexes exploited in this work.

The first experiment has been performed at room temperature with a 1:1 molar ratio between $[Au_{11}(PPh_3)_8Cl_2]Cl$ and the **c'** complex. In **Figure 5.4** the corresponding HRMS analyses are reported. A very slow metathesis reaction has been found to take place: after 21 days the appearance of a signal at 4260 m/z corresponding to **1c** cluster, with the formula $[Au_{11}(di\text{-}NHC^c)(PPh_3)_6Br_2]^+$, was recorded, together with the mononuclear complex $[Ph_3P\text{-}Au\text{-}Br]$ as the expected metathesis co-product. After additional 10 days, it became clear that the reaction was not proceeding further; consequently, an overnight warming was used to speed up the process. After 16 hours at 40°C, conversion of the original cluster to **1c** increased and the formation of a new cluster, named **2c**, was identified at 4500-4600 m/z, with general stoichiometric formula $[Au_{13}(di\text{-}NHC^c)_2(PPh_3)_4X_4]^+$ (X: Cl and/or Br). Apparently, the new Au_{13} cluster derives from a metal complex addition which occurs on **1c**. It must be also remarked that after heating at 40°C each cluster species gave rise to multiple signals in the

HRMS mass spectrum due to extensive halide scrambling between chloride and bromide.

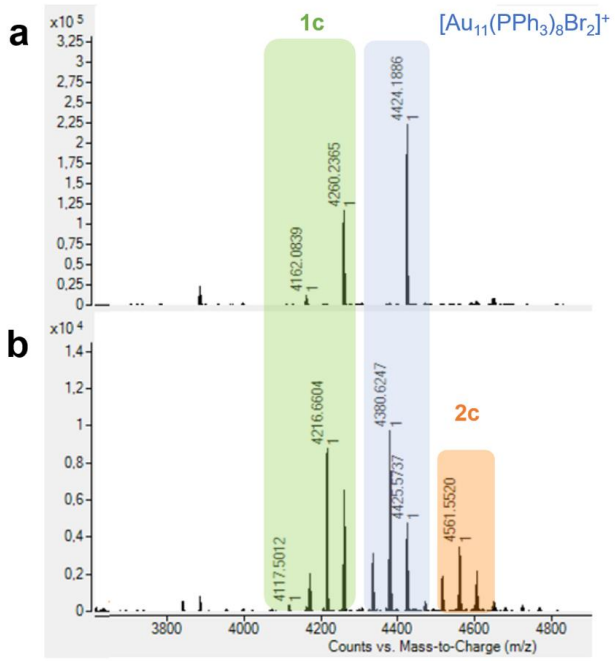

Figure 5.4: HRMS analyses of the reaction of $[Au_{11}(PPh_3)_8Cl_2]Cl$ with complex **c'** after a) 21 days at room temperature and b) after warming at 40 °C. Color code for signal identification: $[Au_{11}(PPh_3)_8Cl_2]^+$ blue, **1c** green, **2c** orange. Multiple signals in b) arise from extensive halide scrambling taking place at 40 °C.

The result of this experiment demonstrates for the first time that a slow metathesis reaction between a phosphine-stabilized AuNC and a di-NHC digold(I) complex is feasible and leads to the first example of a mixed ligand Au_{11} cluster bearing phosphines and a di-NHC ligand (previously, only mixed ligand clusters with mono-NHCs have been prepared).[1] Remarkably, it also shows for the first time that a slight temperature increase can trigger a further reaction, with production of a mixed ligand Au_{13} cluster. The experiment also highlighted some drawbacks of the procedure, namely the very slow rate of the metathesis process at the employed reaction temperature and the extensive scrambling of halide ligands in the clusters, which called for the use of starting materials bearing all the same halide. Consequently, use of complex **c'** as reagent was discontinued in favour of complexes **a**-**c**. In a second set of experiments, we directly exploited an overnight heating of the reaction mixture

to 40°C, to shorten the reaction time. All three complexes **a**, **b** and **c** were evaluated to explore the generality of the synthetic approach and the effect of the different di-NHC ligands on the resulting AuNCs. A molar ratio $[Au_{11}]$:$[(di\text{-}NHC)Au_2Cl_2]$ equal to 1:2 was also employed, to promote the formation of Au_{13} clusters. After 16 hours heating at 40°C, formation of type 1 clusters was detected with all complexes, together with type 2 clusters. Surprisingly, in-depth HRMS analysis highlighted, in the case of complexes **a** and **b**, also the presence of a third type of Au_{13} cluster, namely type 3 clusters **3a** and **3b** (**Figure 5.5**). These latter AuNCs are centered respectively at 2261 m/z and at 2411 m/z, corresponding to $[Au_{13}(di\text{-}NHC)_3(PPh_3)_3Cl_3]^{2+}$ stoichiometry and therefore featuring a third di-NHC ligand bonded to the metallic core. Formation of such type 3 clusters is likely the result of an additional metathesis which takes place between the complexes and the type 2 clusters. It needs to be remarked that after overnight heating the conversion of the reagent cluster $[Au_{11}(PPh_3)_8Cl_2]Cl$ to mixed ligand clusters is in all cases only partial, indicating that the first metathesis process proceeds at a rate comparable to subsequent reactions, at least for what it concerns reactions with complexes **a** and **b**.

Indeed, in the experiments involving **a** and **b**, the reagent cluster is consumed within further 21 and 17 days at room temperature, respectively; within the same time, clusters **1a** and **1b** disappear completely, yielding in both experiments a mixture of Au_{13} clusters of type 2 and 3. In the experiment involving **c**, cluster **1c** persists instead for more than 30 days in solution, only very slowly and partially converting to Au_{13} clusters. In **Figure 5.5** the HRMS analyses at all stages related to the experiment made with **b** are reported.

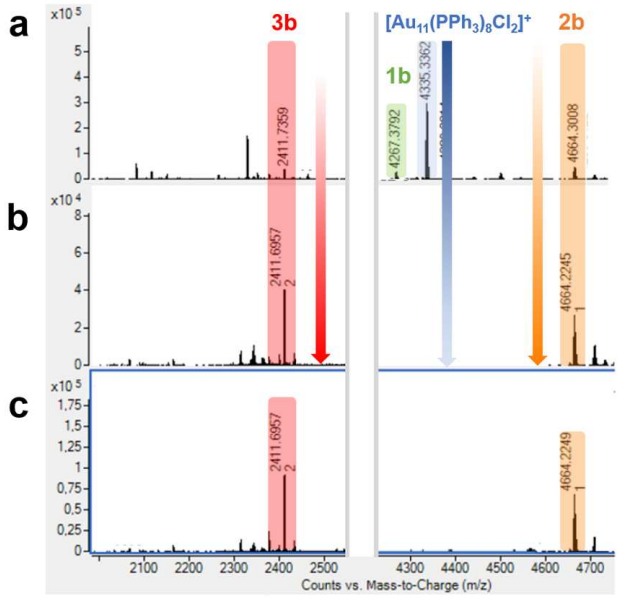

Figure 5.5: HRMS analyses of the reaction of $[Au_{11}(PPh_3)_8Cl_2]Cl$ with 2 equivalents of complex **b**. From above, a) after overnight warming and b) after 17 days at room temperature. In c) the signals of the produced clusters after purification.

The HRMS analyses related with the same experiment made with **a** and **c** are reported in the **Experimental Section**. In the test with complex **a**, the type 3 cluster is produced in minor amount, and it is consequently possible to isolate the type 2 cluster **2a** by recrystallization followed by column chromatography. Repeating the synthesis by doubling the scale of reagents, **3a** cluster can be isolated too. ^{31}P NMR analysis of the clusters apparently confirms the result of mass spectrometry: after the purification, $[Au_{13}(di\text{-}NHC^a)_2(PPh_3)_4Cl_4]^+$ **2a** shows four quartets with equal integration in its ^{31}P spectrum, as reported in **Figure 5.6 a**, instead **3a** shows a single peak centered at 60.03 ppm, suggesting a symmetrical arrangement of PPh_3 ligands. Conversely, in the experiment that involves complex **b**, the type 3 cluster **3b** is present in greater amount compared to type 2 cluster **2b** and is easier to isolate. This cluster has been characterized by ^{31}P NMR as well, and shows a singlet at 60.83 ppm, matching therefore with the signal detected for **3a**. With this information at hand, it is also possible to interpret the ^{31}P NMR spectrum of the original **2b/3b** cluster mixture (**Figure 5.6 b**), and to attribute the signals stemming from the **2b** cluster. ^{31}P NMR

spectra of **2b** is characterized by four quartets with the same integration, similar to what was found with the **2a** cluster. Thus, type 2 clusters appear to feature a lower degree of symmetry in solution, with all phosphine ligands being magnetically inequivalent (see however below), whereas the arrangement of the phosphine ligands is more symmetrical in the case of type 3 clusters.

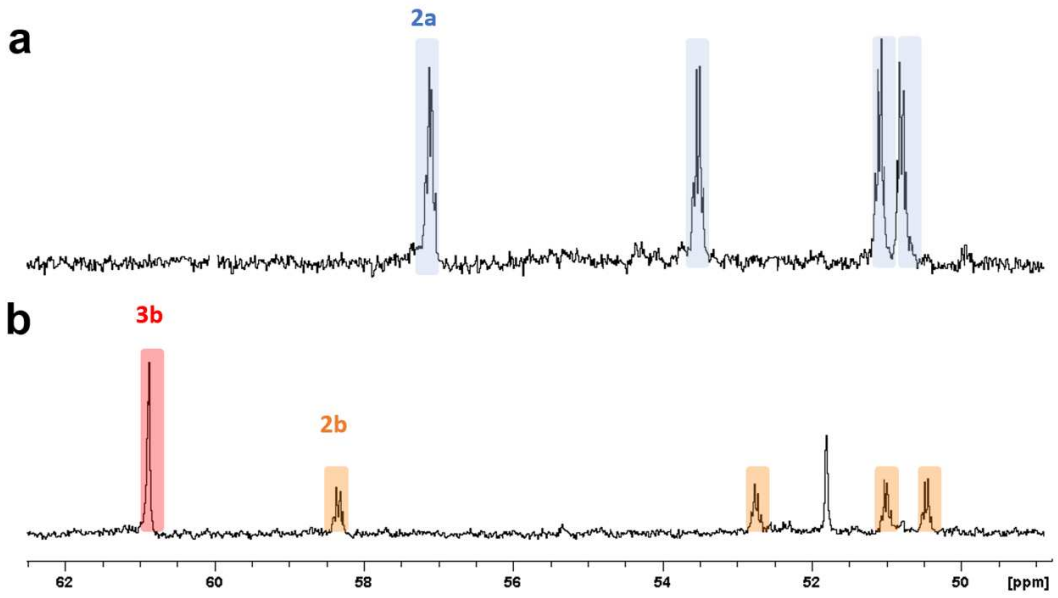

Figure 5.6: ^{31}P NMR spectra of a) cluster **2a** and b) of the crude mixture of clusters **2b** (orange) and **3b** (red) in CD_2Cl_2.

We were able to obtain single crystals of cluster **3b** suitable for X-ray diffraction analysis, layering *n*-hexane on a dichloromethane solution. The molecular structure of **3b** is reported in **Figure 5.7 a**. The cluster core presents the well-known Au_{13} icosahedral structure. The PPh_3 ligands, highlighted in orange in **Figure 5.7**, are all terminally bonded to three gold atoms which define a triangular face of the metallic core. Taking this face as reference **(Figure 5.7 b**), chloride ions are staggered at about 60° from PPh_3 positions and bonded to Au atoms which compose other three triangular faces, sharing one side with the reference face. The remaining six Au atoms bind to three di-NHC ligands, which form a helical system with a C_3 symmetry. This arrangement of the di-NHC ligands renders the cluster structure chiral. The structure

is fully in agreement with the ^{31}P NMR spectrum and HRMS analysis. Interestingly, π-π-interactions are present only between NHC-imidazole rings and PPh_3-phenyl groups, where the average centroids distance is equal to 3.629 Å (**Figure 5.7 c**). The Au-Au distances have a value between 2.888 Å and 3.100 Å. To conclude, the average value of Au-Cl, Au-P and Au-C bonds are, respectively, 2.367 Å, 2.295 Å and 2.049 Å, in agreement with data reported in the literature. The positive charge of the dicationic cluster is neutralized by a chloride and a disordered OH- anion. Several dichloromethane molecules are also present in the crystal packing of the compound.

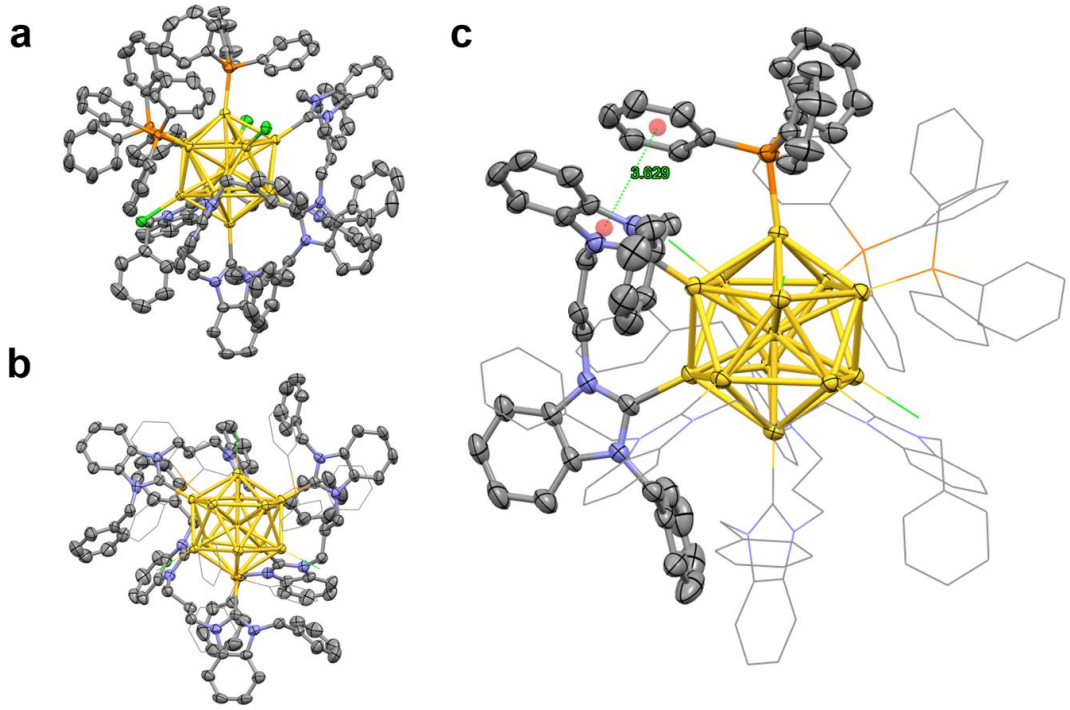

Figure 5.7: X-ray structure of **3b**. a) Full view of the cluster structure, b) full view after removal of the PPh_3 phenyl groups and c) π-π interaction among NHCs and PPh_3 ligands. Color code: yellow (Au), green (Cl), orange (P), purple (N), grey (C).

We tried to further promote the synthesis of the various clusters by prolonging the heating time. If the reaction mixture with complex **c** is kept at 40°C for three days, cluster **1c** is produced as the main product, although it is still possible to record the presence of the reagent cluster and of other clusters around 2000-2300 m/z by HRMS analysis. Even longer heating times increase the complexity of the resulting product

mixture, affording clusters **2c** and **3c** only in small but detectable amounts in HRMS spectra, hence the reaction was stopped after three days and **1c** was purified. In this case, both ^{1}H and ^{31}P NMR can be employed to characterize the AuNC and compare it with the starting $[Au_{11}(PPh_3)_8Cl_2]Cl$. The ^{1}H NMR spectra of **1c** in CD_2Cl_2 (see **Experimental Section**) shows shifted aromatic signals compared with the pure phosphine cluster. Furthermore, it is possible to identify signals from the di-NHC ligand, in particular from the propylene bridge and the isopropyl wingtip substituents, that were very broad and featureless like in the case of the other clusters isolated in this work. In the ^{31}P NMR spectrum instead, the singlet exhibited by $[Au_{11}(PPh_3)_8Cl_2]Cl$ at 52.27 ppm is split into two broad signals, centered at 52.70 ppm (5P) and 51.36 ppm (1P), respectively. Thus, NMR analysis confirms the coordination of one di-NHC ligand to the Au_{11} core, with production of a cluster having $[Au_{11}(\text{di-NHC}^{c})(PPh_3)_6Cl_2]^{+}$ stoichiometry.

Experiments with prolonged heating at 40°C were performed also with complexes **a** and **b**, aiming in particular at accelerating the reaction rate and at selectively producing type 3 clusters; for this reason, a 1:3 $[Au_{11}]$:$[(\text{di-NHC})Au_2Cl_2]$ molar ratio was also employed. However, in the case of the starting complex **a** use of three equivalents of complex caused the formation of a white precipitate in the reaction solution, that was visible already after 24 hours. Using HRMS and ^{1}H NMR, the precipitate was found to contain the dicationic complex $[Au_2(\text{di-NHC}^{a})_2]^{2+}$, which is produced through degradation of **a** and is apparently inert towards reaction (both metathesis and addition) with the clusters. Its low reactivity can be justified with its low solubility in dichloromethane, high positive charge (causing electrostatic repulsion with the positively charged clusters) and high stability, arising from its metallacyclic structure. Using instead **b** as reagent, within 5 days at 40°C, the only cluster present in solution is **3b**, which can be conveniently purified by column chromatography. Furthermore, if the reaction is stopped after three days, both **2b** and **3b** clusters can

be isolated. The ^{31}P NMR spectrum of **3b** prepared in this way presents one singlet at 60.83 ppm, as in the case of the sample prepared through the previously described methodology. Surprisingly, the ^{31}P NMR spectrum referred to **2b** derived from this synthesis is instead different, despite exhibiting exactly the same HRMS peak: whereas previously synthesized **2b** presents four quartets (**Figure 5.6**), the same cluster prepared with the last procedure (*i.e.* upon prolonged heating at 40°C) and hereafter termed **2b'**, presents only one singlet, centered at 27.42 ppm. This suggests that the cluster with stoichiometry $[Au_{13}(di\text{-}NHC^b)_2(PPh_3)_4Cl_4]^+$ can exist in at least two different isomeric forms, and if it is assumed that both isomers share the same icosahedral geometry of the Au_{13} core (which appears plausible), then the two isomeric forms are geometrical isomers featuring different degrees of symmetry. The existence of AuNCs in two isomeric forms is rare but has been reported previously.[13–15]

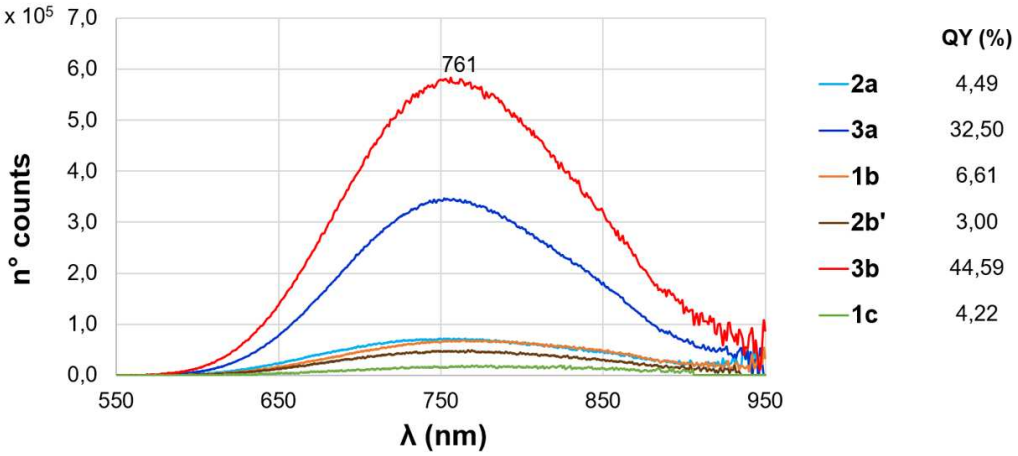

Figure 5.8: overlapped emission spectra of **2a, 3a, 1b, 2b', 3b** and **1c** clusters in CH_2Cl_2. For **2a**, **2b**', **3b** and **1c** λ_{exc}: 350 nm. For **1b** and **3a** λ_{exc}: 330 nm. All reported spectra are normalized upon absorbance value found at 350 nm or 330 nm in the UV-vis spectra. The corresponding quantum yield (QY) values are reported too.

The absorption properties of AuNCs were evaluated with UV-Vis spectroscopy. **2a**, **3a**, **2b'** and **3b** clusters all show a weaker absorption band at around 430 nm and a

much stronger one with a maximum placed around 340-350 nm. Cluster **1b** and **1c** behave instead differently, exhibiting two bands around 420 nm and 320 nm. The luminescence properties of the AuNCs were also studied by exciting the samples at 350 nm or 330 nm. The superimposed emission spectra are reported in **Figure 5.8**, normalized for the cluster absorbance values at the excitation frequency. All AuNCs present a broad emission band centered at 760 nm, yet type 3 clusters show by far the most intense emission, with a 44% quantum yield for **3b** and 33% for **3a**, that ranks among the highest ever reported for a Au_{13} or larger gold cluster.[16,17] This peculiar optical property of **3b** can be rationalized considering its low symmetry degree (*i.e.* only a C_3 axis is present in the structure) and its rather high rigidity due to the presence of three chelating di-NHC ligands, which strongly affect the emission quantum yield of the compound.[18] Assuming that **3a** presents the same ligand arrangement of **3b**, as ^{31}P NMR suggests, its strong emission can be explained in the same way.

Finally, in order to shed more light on the reaction sequence leading to type 2 and type 3 clusters, we decided to monitor the reaction of an isolated sample of cluster **1b** with one equivalent of complex **b** at 40°C. The reaction produced as expected both clusters **2b** and **3b**, in line with the original reaction starting from the parent phosphine cluster reagent. This is a confirmation of the stepwise nature of the process. However, when we performed a control experiment using only the starting **1b** cluster, without addition of complex **b**, we found that the system was still able to evolve producing only **2b** as cluster product, without formation of cluster **3b**. Consequently, we have to conclude that the reaction step leading from type 1 to type 2 clusters must not be necessarily viewed as a complex addition reaction but can take place upon thermal rearrangement of type 1 clusters, albeit this rearrangement might still involve etching of a di-NHC gold(I) complex from a type 1 cluster and its subsequent addition to another type 1 cluster. More work is needed in order to ascertain which is the preferred

mechanistic option in this reaction step. The experiments also confirm that the reaction step leading from type 2 to type 3 clusters is a ligand metathesis process that necessitates the presence of a di-NHC gold(I) complex.

In conclusion, we have reported a new method to synthesize AuNCs stabilized by a mixed ligand sphere composed of PPh_3 and di-NHC ligands. The method is based on the reaction of a preformed, PPh_3-stabilized AuNC with dinuclear di-NHC gold(I) complexes and enables the production and isolation of clusters with different nuclearity and ligand stoichiometry, depending on the di-NHC properties and reaction conditions. A detailed reaction monitoring that has been conducted with HRMS high resolution mass spectrometry allows to hypothesize a reaction sequence involving a first metathesis reaction to produce type 1 clusters, followed by a cluster rearrangement/di-NHC gold complex addition to obtain type 2 clusters and a further metathesis that provides type 3 clusters. Theoretical mechanistic studies are planned to investigate in greater detail all these reaction steps.

Finally, the obtained AuNCs have been characterized with different techniques, including ^{1}H and ^{31}P NMR spectroscopy, UV-Vis and emission spectroscopy and single crystal X-ray diffraction. These studies have provided evidence that at least one of the clusters produced in this work can exist in two isomeric forms (*i.e.* cluster **2b/2b'**). Furthermore, a strong luminescence has been recorded for type 3 clusters, which is in line with the low degree of symmetry and high rigidity exhibited by this cluster. Evidence of such property calls for more detailed studies involving the evaluation of quantum yields and decay times, as well as on the effect of different ligands on the emission properties, which will be conducted in due course.

5.3 FURTHER STUDIES ON STEPWISE PROCESS

After the studies concerning the variation of NHC complexes, we decided to test our stepwise process using another starting cluster, with formula $[Au_9(PPh_3)_8](NO_3)_3$.[19] This AuNC presents a uncoordinated gold center in the metallic core, a feature that makes it more reactive than $[Au_{11}(PPh_3)_8Cl_2]Cl$, used in our previous study. The complexes exploited in these experiments are **b** and **c**, used with different [AuNC]:[(di-NHC)Au_2Cl_2] molar ratios, and the reactions have been followed with HRMS. Despite the variation of reaction conditions, it has not been possible to completely identify the products of these reactions. The fragmentations present in the mass spectra complicate the analysis of the reaction mixtures, therefore making it difficult to characterize the real products. Furthermore, also using an excess of 4 equivalents of Au(I) complexes, it has not been possible to consume all starting $[Au_9]^{3+}$, which complicates the purification of the final products.

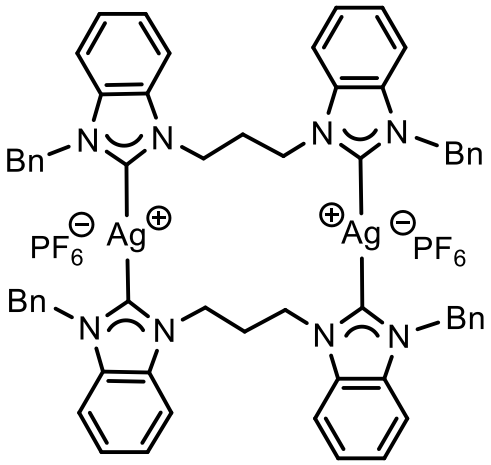

Figure 5.9: di-NHC Ag(I) complex tested in the stepwise process.

Since these difficulties, we decided to return to $[Au_{11}(PPh_3)_8Cl_2]Cl$ as starting cluster but using instead $[Ag_2(di\text{-}NHC^b)_2](PF_6)_2$ complex, reported in **Figure 5.9**, to understand if it would be feasible to get new Ag-doped AuNCs. These experiments took inspiration from similar experiments conducted by Mingos et al., performed with

phosphine ligands instead of di-NHCs.[2] In these tests, [AuNC]:[Ag_2(di-NHC)$_2$(PF_6)$_2$] molar ratios were 1:1; 1:3 and 1:10, aiming to study how the stoichiometry affects the reaction products. In all cases the reactions have been performed in DCM upon continuous warming at 40°C for 72 h. HRMS has been used to follow these reactions.

Using equimolar amounts of silver complex and Au_{11} cluster, several AuNCs are detected in the mass spectra, whereas only one of these have been interpreted. Indeed, it is possible to detect a doped cluster centered at 2061 m/z and 4157 m/z, corresponding to $[Au_9Ag_2(PPh_3)_8Cl]^{2+}$ and $[Au_9Ag_2(PPh_3)_8Cl_2]^{+}$ stoichiometries respectively, in which two Au(I) centers belonging to the starting $[Au_{11}]^{3+}$ cluster are removed to promote the formation of $[Au_9Ag_2]^{3+}$ core and $[Au_2(di\text{-}NHC)_2]^{2+}$ complex as by-product, balancing therefore the reaction stoichiometry.

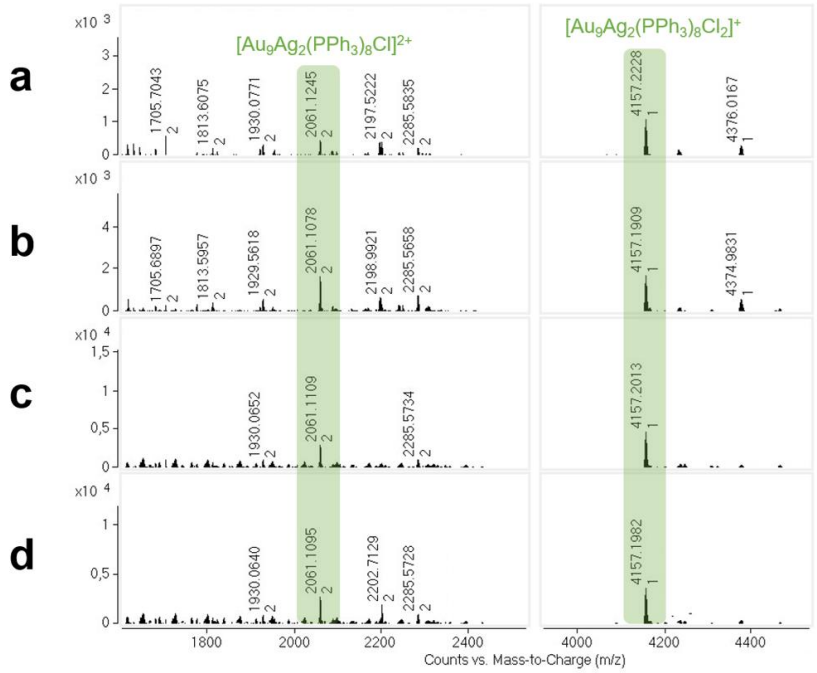

Figure 5.10: reaction with [Au_{11}]:[Ag_2(di-NHC)$_2$(PF_6)$_2$] molar ratio equal to 1:1, monitored at a) 2 h, b) 24 h, c) 48 h and d) 72 h. The peaks highlighted match with $[Au_9Ag_2(PPh_3)_8Cl_2]^{+}$ stoichiometry.

The cluster mixture does not focus itself during the warming, meaning that such clusters are stable in these conditions. The mass spectra related to this test are

reported in **Figure 5.10**. Despite the interesting result, the presence of other unidentified cluster makes the purification of $[Au_9Ag_2(PPh_3)_8Cl_2]^+$ impossible to perform with classical column chromatography.

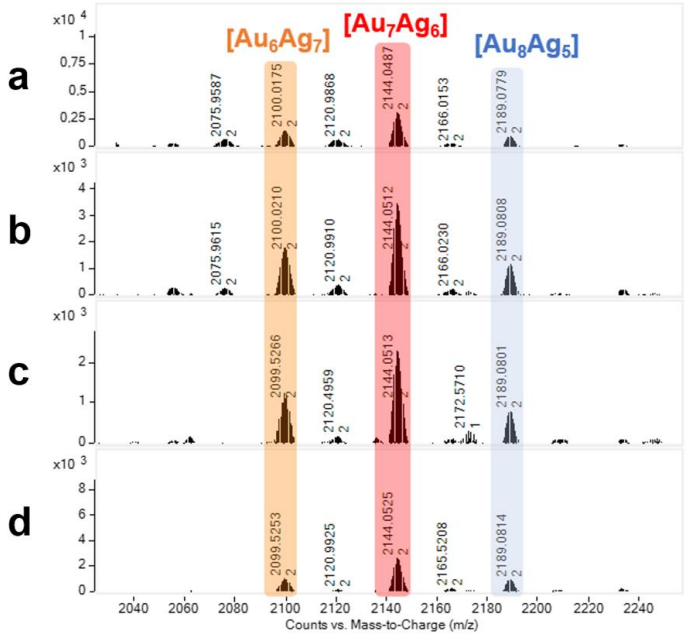

Figure 5.11: reaction with $[Au_{11}]$:$[Ag_2(\text{di-NHC})_2(PF_6)_2]$ molar ratio equal to 1:3, monitored at a) 2 h, b) 24 h, c) 48 h and d) 72 h. The peak highlighted matches with type 3 clusters, respectively with formula, from right, $[Au_8Ag_5(\text{di-NHC}^b)_3(PPh_3)_3Cl_3]^{2+}$ (blue), $[Au_7Ag_6(\text{di-NHC}^b)_3(PPh_3)_3Cl_3]^{2+}$ (red) and $[Au_6Ag_7(\text{di-NHC}^b)_3(PPh_3)_3Cl_3]^{2+}$ (orange) stoichiometries.

Due to this, we decided to increase the concentration of silver complex, using a [AuNC]:$[Ag_2(\text{di-NHC})_2(PF_6)_2]$ molar ratio equal to 1:3 to focus the reaction mixture favoring addition reactions. Indeed, this higher concentration should promote the formation of type 3 clusters, the easiest type of cluster synthesizable with the stepwise process since its higher stability compared to other AuNCs. The HRMS related to this experiment is reported in **Figure 5.11**. In these conditions, the HRMS highlights the presence of a new set of Ag/AuNCs, but unfortunately the process is quite unselective also in this case. Indeed, a mixture of products has been detected, presenting formulas $[Au_{13-n}Ag_n(\text{di-NHC})_3(PPh_3)_3Cl_3]^{2+}$; in which n is 5, 6 or 7. The separation and

purification of this mixture of Ag/AuNCs proved again impossible to perform, since these clusters present similar physical and chemical behavior.

Further increasing the [AuNC]:[Ag_2(di-NHC)$_2$(PF_6)$_2$] ratio, reaching therefore the value 1:10, promotes the metallic exchange, still favoring [$Au_{13-n}Ag_n$(di-NHC)$_3$(PPh_3)$_3Cl_3$]$^{2+}$ cluster but in which n is instead 7, 8 and 9, as showed in **Figure 5.12**. In these clusters Ag atoms overcome the Au centers remaining from the starting cluster, in agreement with similar processes reported in literature.[20] This result demonstrates that Ag doping affords several exchange reactions also in NHC-capped AuNCs, due to the higher reactivity of silver compared to gold.

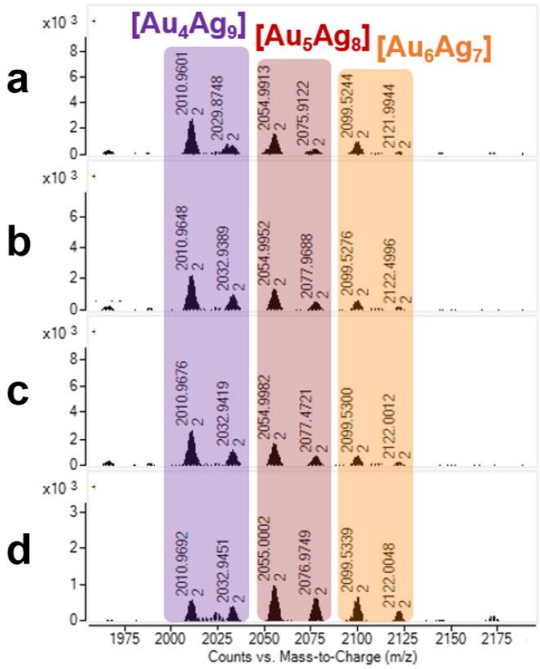

Figure 5.12: reaction with [Au_{11}]:[Ag_2(di-NHC)$_2$(PF_6)$_2$] molar ratio equal to 1:10, monitored at a) 2 h, b) 24 h, c) 48 h and d) 72 h. The peak highlighted matches with type 3 clusters, respectively with formula, from right, [Au_6Ag_7(di-NHC^b)$_3$(PPh_3)$_3Cl_2X$]$^{2+}$ (orange), [Au_5Ag_8(di-NHC^b)$_3$(PPh_3)$_3Cl_2X$]$^{2+}$ (brown) and [Au_4Ag_9(di-NHC^b)$_3$(PPh_3)$_3Cl_2X$]$^{2+}$ (purple) stoichiometries. X: Cl or Br. The bromide anions derive from impurities present during the analysis.

Since the low selectively obtained exploiting Ag complex, we decided to test the reactivity of **1c** cluster, with formula [Au_{11}(di-NHC^c)(PPh_3)$_6Cl_2$]$^+$, with **b** complex, presenting formula [(di-NHC^b)Au_2Cl_2], aiming to get the first cluster capped by two

different types of di-NHCs. Using a **1c**:**b** molar ratio equal to 1:2, in DCM at room temperature, one novel cluster can be detected, presenting formula $[Au_{13}(di\text{-}NHC^{c})_2(di\text{-}NHC^{b})_2(PPh_3)Cl_3]^{2+}$ centered at 2281 m/z, together with $[Au_{13}(di\text{-}NHC^{c})_2(di\text{-}NHC^{b})_2(PPh_3)Cl_2Br]^{2+}$ centered at 2303 m/z, derived from bromide impurities present during the analysis. This new cluster, called **4cb**, presents a weaker signal at 2150 m/z too, derived from a loss of PPh_3 in its own coordination sphere. In this reaction, **1c** is not totally consumed; nevertheless, separation should be easily achievable, given the different charges of **1c** (1+) and **4cb** (2+). When the system is warmed at 40°C for 72 h, the HRMS analysis does not highlight significant variations in the mixture, demonstrating that **4cb** does not degrade in these conditions. The reaction mixtures related to this experiment are reported in **Figure 5.13**.

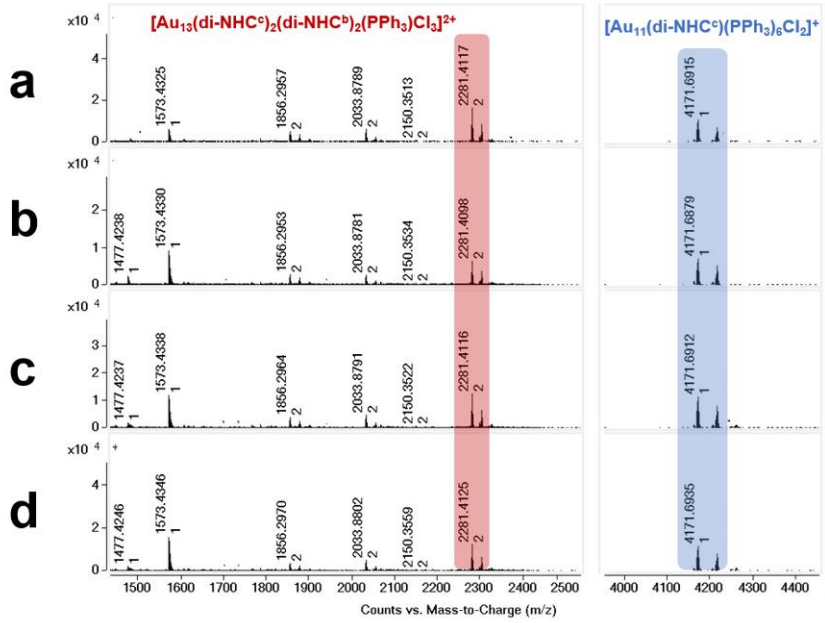

Figure 5.13: Synthesis of **4cb** cluster monitored at a) 0 h, b) 24 h, c) 48 h and d) 72 h at 40°C in DCM. **1c** is highlighted in blue and **4cb** is highlighted in red.

The synthesis of **4cb** is remarkable, since it proves that clusters stabilized by different di-NHCs are synthesizable using stepwise synthesis. These species have been never isolated using direct reduction approach, highlighting again that our method is more tailorable than direct reduction to get novel AuNCs. However, the synthesis of **4cb**

remains only a preliminary result, since we had not time to further investigate in this direction. Nevertheless, this example opens the road to get new libraries of AuNCs using the stepwise approach, characterized by heteroleptic coordination spheres bearing at least two different di-NHCs. Finally, such clusters should be isolable also reacting type 2 clusters, presenting formula $[Au_{13}(di\text{-}NHC)_2(PPh_3)_4Cl_4]^+$, with [(di-NHC)$Au_2Cl_2$] complexes presenting different di-NHC ligand.

5.4 ELECTROCHEMICAL ANALYSIS OF GOLD CLUSTERS CAPPED BY di-NHC AND PPh_3 LIGANDS

As explained in the introduction, the electrochemical analysis of AuNCs provides a series of information useful to further characterize these molecular species, including HOMO-LUMO band gaps and electrochemical stability. In this field, the most studied clusters are SR-capped AuNCs since they present redox active ligands. Moreover, the complicated $[Au_2(SR)_3]$ organometallic staples perfectly protect the cluster core, also when the redox process provides not-SA clusters.[21,22] On the contrary, in literature there is only limited information regarding the electrochemical behavior of AuNCs capped by PR_3, alkynyls or NHCs, limiting therefore the knowledge on these species.[5,23,24] Electrochemical investigations on these latter can be useful in order to understand to which extent ligands and core sizes affect the orbital structure of the clusters, and to compare them with SR-capped AuNCs.

$Au_{11}^{(*)}$	$[Au_{11}(PPh_3)_8Cl_2]^+$	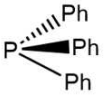
1c	$[Au_{11}(di\text{-}NHC^c)(PPh_3)_6Cl_2]^+$	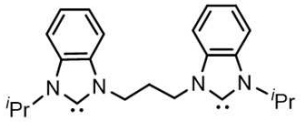
2a	$[Au_{13}(di\text{-}NHC^a)_2(PPh_3)_4Cl_4]^+$	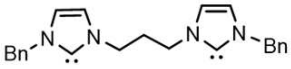
2b' **3b** **$Au_{13}^{(**)}$**	$[Au_{13}(di\text{-}NHC^b)_2(PPh_3)_4Cl_4]^+$ $[Au_{13}(di\text{-}NHC^b)_3(PPh_3)_3Cl_3]^{2+}$ $[Au_{13}(di\text{-}NHC^b)_5Br_2]^{3+}$	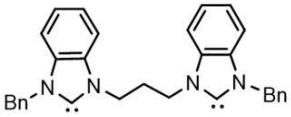

Figure 5.14: clusters tested in electrochemical analyses, corresponding stoichiometric formulas and ligands. **$Au_{11}^{(*)}$** and **$Au_{13}^{(**)}$** clusters have been already reported in literature but have not been electrochemically characterized previously.[1,9]

For these reasons, we decided to study the clusters obtained using our stepwise approach, together with clusters already reported in literature, presenting formulas $[Au_{11}(PPh_3)_8Cl_2]^+$ and $[Au_{13}(di\text{-}NHC^b)_5Br_2]^{3+}$.[1,9] This allows us to compare the electrochemical behavior of similar AuNCs, in particular aiming at understanding the role of the ligands in the redox process. The clusters studied in this section are reported in **Figure 5.14**.

Cyclic Voltammetry (CV) and Differential Potential Voltammetry (DPV) analyses have been performed by Mattia Reato, PhD student in the group of Prof. Maran at the University of Padova. For these experiments, AuNCs are dissolved in CH_3CN or DCM, with a concentration from 0.3 to 0.6 mM. Tetrabutylammonium hexafluorophosphate is used in solution as electrolyte, presenting a concentration of 0.1 M. For more details, read the **Experimental Section**.

In all cases studied, the CV analyses show an irreversible behavior, in which therefore the oxidation state of AuNCs can be varied but at the price of impairing the high stability related to SA counting. Indeed, mono-electronic redox processes provide clusters presenting 7 valence electrons (oxidation) or 9 valence electrons (reduction), both not representing SA clusters.

This loss of stability is not surprising in case of $[Au_{11}(PPh_3)_8Cl_2]^+$ cluster, since Au-PPh_3 bonds are not enough strong to ensure the stability after the variation of electronic counting. At the contrary, this instability was not expected for AuNCs bearing instead di-NHCs. We have already explained that these ligands can improve cluster stability thanks to their chelating proprieties, feature that should also prevent cluster degradation during the redox process. Notwithstanding this, dicarbene ligands do not impart the required stability during the analysis, affording irreversible CV waves. Indeed, even increasing the number of di-NHCs on metallic kernel, *i.e.* studying $[Au_{13}(di\text{-}NHC^b)_5Br_2]^{3+}$, the process is still irreversible.

It is important to highlight that in literature only DPV spectra of NHC-capped AuNCs are reported, an analysis useless to evaluate the reversibility of the such redox process, limiting therefore the information achievable from reported clusters.[5,23,24]

From DPV spectra recorded in CH_3CN, we can analyze the positions of oxidation (or reduction) peaks, correlating these with the electronic proprieties of di-NHCs in the cluster coordination sphere. DPV is used here instead of CV since in the former the variation of peaks position is more easily observed.

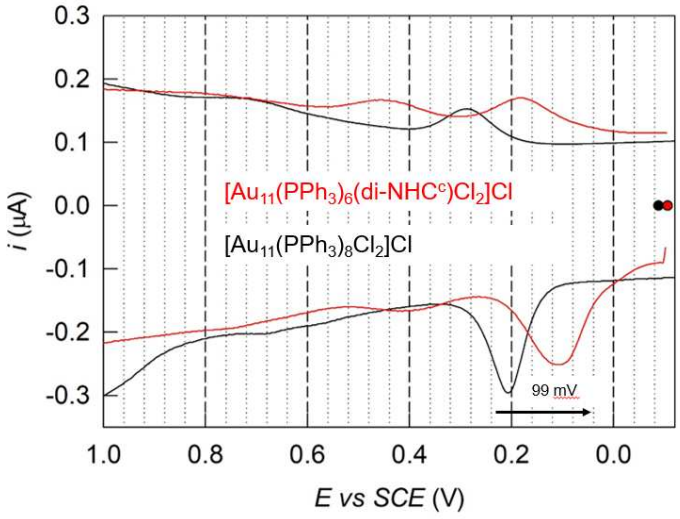

Figure 5.15: detail of DP voltammogram of **1c** (red) and $[Au_{11}(PPh_3)_8Cl_2]^+$ (black) clusters dissolved in CH_3CN. The arrow highlights the shift of the first oxidation peak.

First of all, it is possible to compare $[Au_{11}(PPh_3)_8Cl_2]^+$ with cluster **1c**, with formula $[Au_{11}(di\text{-}NHC^c)(PPh_3)_6Cl_2]^+$, differing therefore only for one di-NHC ligand. As shown in **Figure 5.15**, the oxidation peak of **1c** is anticipated by 99 mV compared to pure PR_3-capped cluster, meaning that the oxidation of **1c** is favored due to the stronger σ-donor proprieties of the dicarbene ligand.

Similar shift can be detected also in the comparison of the DP voltammograms of **2a** and **2b'** clusters, presenting the same stoichiometric formula $[Au_{13}(di\text{-}NHC)_2(PPh_3)_4Cl_4]^+$ but differing for the kind of di-NHC ligands. Indeed, **2a** bears

imidazole-2-ylidenes, instead **2b'** presents benzimidazole-2-ylidenes as NHC scaffold, a variation that directly affect the electrochemistry of AuNCs.

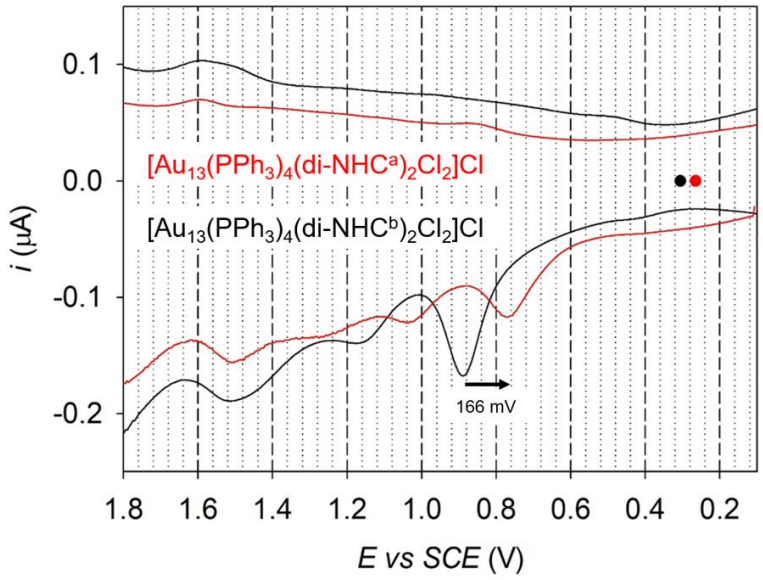

Figure 5.16: details of DP voltammograms of **2a** (red) and **2b'** (black) clusters dissolved in CH_3CN. The arrow highlights the shift of the first oxidation peak.

2a provides more electrons to the $[Au_{13}]^{5+}$ core due to its imidazolium scaffolds, thereby inducing a negative shift of 166 mV in its oxidation peak compared to **2b'**. The latter presents condensed rings in the NHC backbone, affording therefore less electron donation towards the gold core than in the **2a** case and providing consequently an oxidation peak at higher potential. These DP voltammograms are reported in **Figure 5.16**.

Finally, also the comparison between **3b**, with formula $[Au_{13}(di\text{-}NHC^b)_3(PPh_3)_3Cl_3]^{2+}$, and $[Au_{13}(di\text{-}NHC^b)_5Br_2]^{3+}$ can be studied, since these differ for the number of di-NHC^b ligands placed on the icosahedral core. Increasing the number of dicarbene ligands, a negative shift of the oxidation peak around 177 mV can be observed, compared to

3b, due to the higher σ-electron donation deriving from the di-NHCs. These DP voltammograms are reported in **Figure 5.17**.

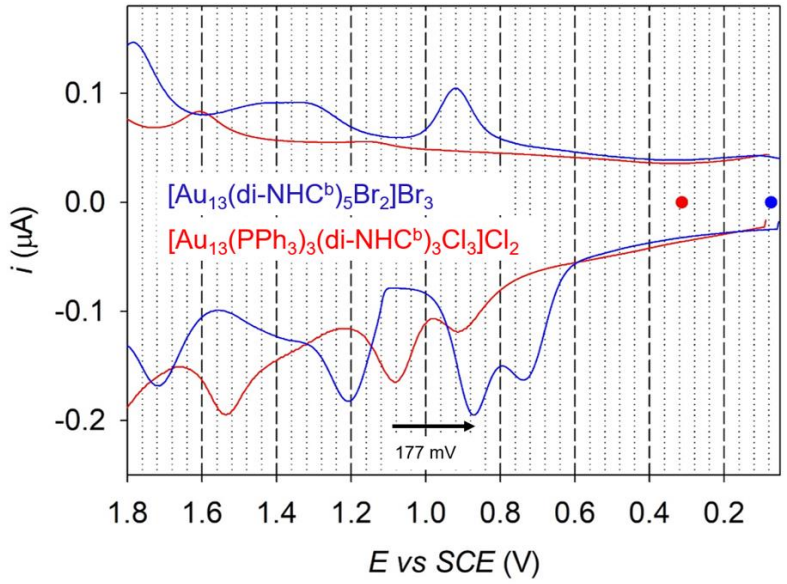

Figure 5.17: detail of DP voltammograms of $[Au_{13}(di\text{-}NHC^b)_5Br_2]^{3+}$ (blue) and **3b** (red) clusters dissolved in CH_3CN. The arrow highlights the shift of the first oxidation peak.

It is possible to compare these results with SR-capped AuNCs, aiming at understanding how much the ligand shell participates in the cluster orbital structure. Murray et al. have studied the electrochemical behavior of a library of $[Au_{38}(SPh\text{-}R)_{24}]$ clusters, in which the electron donating effect provided by R groups on phenyl thiolates is increasing.[25] In **Figure 5.18** it is possible to observe Osteryoung square wave voltammograms in which these variations are better highlighted. Increasing the donating proprieties of ligands, a negative shift of the oxidation peaks is observed, in agreement with our data. Moreover, we can observe that the variations reported by Murray's groups are around 10-15 mV for SRs presenting electron donating groups, thus deeply differing from our cases, in which the variations are around 100-200 mV, meaning that di-NHCs are more involved in cluster orbital structure than thiolate ligands.

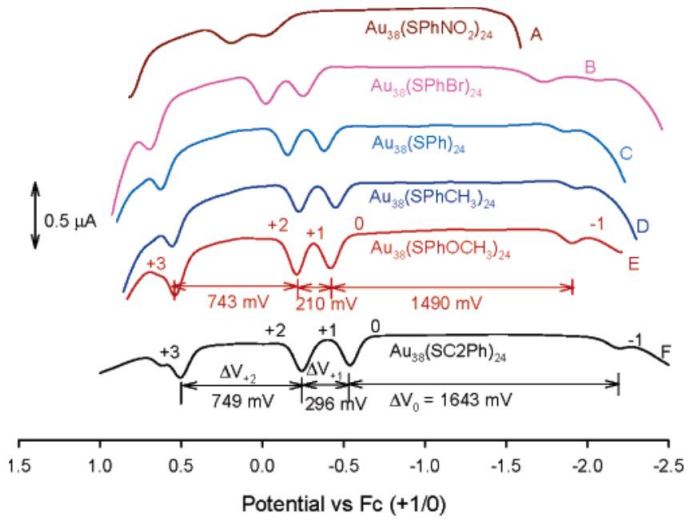

Figure 5.18: Osteryoung square wave voltammograms (positive-going scan only) of A) $Au_{38}(SPhNO_2)_{24}$, B) $Au_{38}(SPhBr)_{24}$, C) $Au_{38}(SPh)_{24}$, D) $Au_{38}(SPhCH_3)_{24}$, E) $Au_{38}(SPhOCH_3)_{24}$, and F) $Au_{38}(SC_2Ph)_{24}$ at 11 °C in 0.1 M Bu_4NClO_4/CH_2Cl_2.[25]

Finally, our data are in agreement with the shift found by Tsukuda et al. comparing $[Au_{23}(PPh_3)_6(C{\equiv}CPh)_9]^{2+}$ and $[Au_{23}(NHC)_6(C{\equiv}CPh)_9]^{2+}$ clusters, in which the second one presents NHCs instead of PPh_3.[24] Also in this case a negative shift of the oxidation peak of NHC-capped cluster is detected, due to the higher sigma donation deriving from NHCs ligands, in agreement with the electrochemical behavior of our clusters.

Another important data obtainable from these analyses is the electrochemical HOMO-LUMO band gaps (E_e) calculated from the difference of oxidation and reduction peaks in DPV spectra. This can be compared with the optical HOMO-LUMO band gaps (E_o) derived from the UV-Vis spectra, calculated from the tangent of absorption profile of the band at lower energy in the spectra, converted in electron Volt (eV). For this comparison, we used DCM as solvent for both DPV and UV-Vis analyses, to get comparable data.

The data are reported in **Table 5.1**, in which it is possible to observe that E_e are quite in agreement with E_o, meaning that HOMO and LUMO orbitals are directly involved in

the cluster electrochemical process. It is possible to notice that E_o are slightly lower than E_e. This difference is due to the additional potential required in electrochemical analysis to charge the orbitals involved in the process. The optical band gap related to **1c** does not match very well with its electrochemical counterpart. The latter derives in this case from a DP voltammogram recorded in CH_3CN, since it is not possible to clearly detect redox peaks in DCM (see below). Due to this difference, E_o^{1c} and E_e^{1c} cannot perfectly match since both optical and electrochemical data are affected by the solvent used in the analyses.

Table 5.1: band gaps of **2a**, **2b**', **3b** and **1c** clusters calculated by UV-Vis (E_o) and cyclic voltammetry (E_e) spectra, both recorded in DCM. The value marked with***** has been obtained from electrochemical data in CH_3CN.

Cluster	E_o (eV)	E_e (V)
2a	2.26	2.43
2b'	2.38	2.43
3b	2.41	2.43
1c	2.40	2.00*

E_e related to our nano-systems are quite in agreement with the E_e reported in literature, in which clusters with formula $[Au_{23}(NHC)_6(C{\equiv}CPh)_9]^{2+}$, $[Au_{17}(NHC)_4(C{\equiv}CPh)_4Br_4]^{+}$ and $[Au_{13}(di\text{-}NHC)_5Cl_2]^{3+}$ present respectively 1.6, 2.08 and 2.06 V as electrochemical band gaps recorded in DCM.[5,23,24] The Au_{23} clusters present an $[Au_{17}]^{5+}$ core, differing from other two reported AuNCs, showing instead classical $[Au_{13}]^{5+}$ cores. Due to this, it is not surprising that these latter present E_e similar to our AuNCs, which present $[Au_{13}]^{5+}$ cores as well, or similar $[Au_{11}]^{3+}$.

Finally, an interesting behavior of NHC-capped AuNCs is detected when voltammograms are recorded in DCM instead of CH_3CN. Indeed, it is possible to observe an unexpected increasing of current during the reduction process, reaching

values between 2.5 and 8.0 μA, not correlated with cluster reduction peak but that may be related to the reduction of solvent. As highlighted in **Figure 5.19**, this reduction appears within the range of stability of DCM in the experimental conditions, suggesting that AuNCs added to solution catalyze the solvent reduction. We have already demonstrated that in CH_3CN the same clusters can be reduced without formation of this high current, meaning that reduced clusters are temporarily stable in CH_3CN. In DCM this behavior is different, since the acquired electron is immediately transferred to the solvent, providing its reduction.

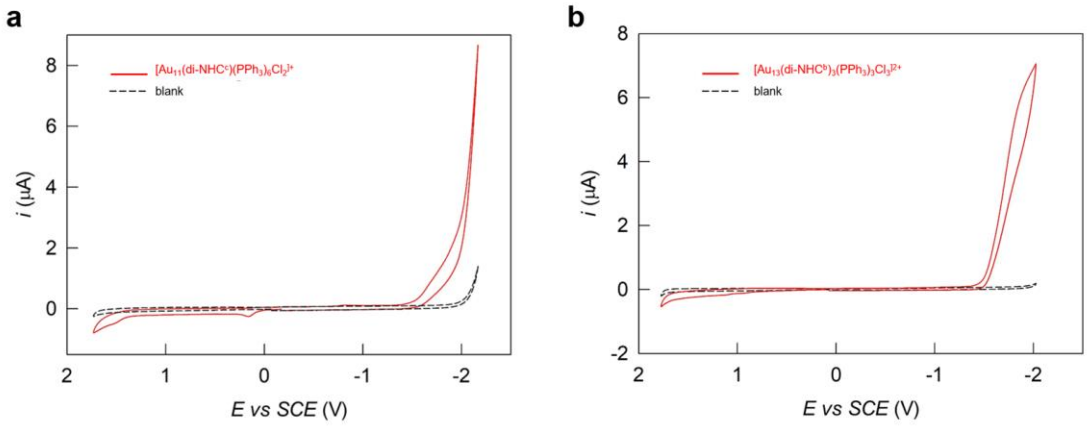

Figure 5.19: Cyclic voltammograms in DCM of a) **1c** and b) **3b** clusters.

All studied clusters show the same electrochemical behavior in DCM, whereas the intensity of generated current change in relation to the used cluster, meaning that core sizes and ligand shells affect their redox activity.

It is interesting that this solvent activation has been never mentioned in literature, albeit cases of "chloride extraction" have been reported during the synthesis of $[Au_{24}]^{8+}$ NHC-capped cluster.[26] Furthermore, the DCM catalysis detected here has been never reported, albeit the same solvent is exploited in literature too.[5,23,24]

DCM reduction is invoked in several sections of this elaborate, spanning from the synthesis of **$[(CH_3)_2]$**, with formula $[Au_{13}(di\text{-}NHC^a)_5(CH_3)_2]^{3+}$, to the formation of

$[Au_6(C)(di\text{-}NHC^c)_3]^{2+}$, presenting a carbide in the cluster core, and finally also through these electrochemical analyses. We believe that it could be feasible to correlate the result of these analyses to the synthesis of **$[(CH_3)_2]$**.

In this latter case, we suppose that the reduction of DCM takes place on the cluster core of $[Au_{13}(di\text{-}NHC^a)_5Cl_2]^{3+}$, formed in solution from reduction of $[(di\text{-}NHC^a)Au_2Cl_2]$ promoted by $NaBH_4$. The same reducing agent promotes DCM reaction too, affording consequently coordinated CH_3^- anions instead of chlorides bonded to the icosahedral core. For more details, the reader is referred to **Paragraph 2.3**. The synthesis of **$[(CH_3)_2]$** works only in presence of DCM, which correlates with the electrochemical behavior of di-NHC/PPh_3-capped clusters, in which the intense reduction peaks are present only when DCM is used as solvent. These observations lead us to infer that AuNCs can transfer electrons to DCM and that this process is involved in the formation of methyl groups that are found on the cluster product, although it is difficult to rationalize the mechanistic steps through which this reduction takes place. To shed more light on this, we are currently planning to test the clusters isolated with our stepwise approach under a continuous reducing potential, aiming at understanding if it is possible to isolate clusters bearing CH_3 groups from this electrochemical reduction. This test will allow us to shed light on the formation mechanism of CH_3-capped AuNCs and gain more understanding on the mechanism of CH_3 formation through DCM electrochemical reduction.

5.5 BIBLIOGRAPHY

[1] M. R. Narouz, K. M. Osten, P. J. Unsworth, R. W. Y. Man, K. Salorinne, S. Takano, R. Tomihara, S. Kaappa, S. Malola, C.-T. Dinh, J. D. Padmos, K. Ayoo, P. J. Garrett, M. Nambo, J. H. Horton, E. H. Sargent, H. Häkkinen, T. Tsukuda, C. M. Crudden, *Nat. Chem.* **2019**, *11*, 419–425.

[2] R. C. B. Copley, D. M. P. Mingos, *J. Chem. Soc. Dalton Trans.* **1996**, 491.

[3] H. Shen, X. Tang, Q. Wu, Y. Zhang, C. Ma, Z. Xu, B. K. Teo, N. Zheng, *ACS Nanosci. Au* **2022**, *2*, 520–526.

[4] P. Luo, X. Zhai, S. Bai, Y. Si, X. Dong, Y. Han, S. Zang, *Angew. Chem. Int. Ed.* **2023**, *62*, e202219017.

[5] X. Wang, R. Liu, L. Tian, J. Bao, C. Zhao, F. Niu, D. Cheng, Z. Lu, K. Hu, *J. Phys. Chem. C* **2022**, *126*, 18374–18382.

[6] H. Shen, Q. Wu, M. S. Asre Hazer, X. Tang, Y.-Z. Han, R. Qin, C. Ma, S. Malola, B. K. Teo, H. Häkkinen, N. Zheng, *Chem* **2022**, *8*, 2380–2392.

[7] M. R. Narouz, S. Takano, P. A. Lummis, T. I. Levchenko, A. Nazemi, S. Kaappa, S. Malola, G. Yousefalizadeh, L. A. Calhoun, K. G. Stamplecoskie, H. Häkkinen, T. Tsukuda, C. M. Crudden, *J. Am. Chem. Soc.* **2019**, *141*, 14997–15002.

[8] J. Sun, X. Tang, J. Tang, Y. Zhang, Z. Li, Chaolumen, S. Guo, H. Shen, *Inorg. Chem.* **2023**, *62*, 5088–5094.

[9] H. Shen, S. Xiang, Z. Xu, C. Liu, X. Li, C. Sun, S. Lin, B. K. Teo, N. Zheng, *Nano Res.* **2020**, *13*, 1908–1911.

[10] H. Yi, K. M. Osten, T. I. Levchenko, A. J. Veinot, Y. Aramaki, T. Ooi, M. Nambo, C. M. Crudden, *Chem. Sci.* **2021**, *12*, 10436–10440.

[11] P. Luo, S. Bai, X. Wang, J. Zhao, Z. Yan, Y. Han, S. Zang, T. C. W. Mak, *Adv. Opt. Mater.* **2021**, *9*, 2001936.

[12] M. Bevilacqua, M. Roverso, S. Bogialli, C. Graiff, A. Biffis, *Inorg. Chem.* **2023**, *62*, 1383–1393.

[13] S. Zhuang, L. Liao, J. Yuan, N. Xia, Y. Zhao, C. Wang, Z. Gan, N. Yan, L. He, J. Li, H. Deng, Z. Guan, J. Yang, Z. Wu, *Angew. Chem. Int. Ed.* **2019**, *58*, 4510–4514.

[14] S. Tian, Y.-Z. Li, M.-B. Li, J. Yuan, J. Yang, Z. Wu, R. Jin, *Nat. Commun.* **2015**, *6*, 8667.

[15] N. Xia, J. Yuan, L. Liao, W. Zhang, J. Li, H. Deng, J. Yang, Z. Wu, *J. Am. Chem. Soc.* **2020**, *142*, 12140–12145.

[16] X. Wang, R. Liu, L. Tian, J. Bao, C. Zhao, F. Niu, D. Cheng, Z. Lu, K. Hu, *J. Phys. Chem. C* **2022**, *126*, 18374–18382.

[17] J. Kong, W. Zhang, Y. Wu, M. Zhou, *Aggregate* **2022**, DOI 10.1002/agt2.207.

[18] M. R. Narouz, S. Takano, P. A. Lummis, T. I. Levchenko, A. Nazemi, S. Kaappa, S. Malola, G. Yousefalizadeh, L. A. Calhoun, K. G. Stamplecoskie, H. Häkkinen, T. Tsukuda, C. M. Crudden, *J. Am. Chem. Soc.* **2019**, *141*, 14997–15002.

[19] T. Matsuyama, S. Kikkawa, Y. Fujiki, M. Tsukada, H. Takaya, N. Yasuda, K. Nitta, N. Nakatani, Y. Negishi, S. Yamazoe, *J. Chem. Phys.* **2021**, *155*, 044307.

[20] X. Kang, Y. Li, M. Zhu, R. Jin, *Chem. Soc. Rev.* **2020**, *49*, 6443–6514.

[21] T. Kawawaki, Y. Negishi, *Dalton Trans.* **2023**, *52*, 15152–15167.

[22] S. Antonello, F. Maran, *Curr. Opin. Electrochem.* **2017**, *2*, 18–25.

[23] H. Shen, Q. Wu, S. Malola, Y.-Z. Han, Z. Xu, R. Qin, X. Tang, Y.-B. Chen, B. K. Teo, H. Häkkinen, N. Zheng, *J. Am. Chem. Soc.* **2022**, *144*, 10844–10853.

[24] K. Hirano, S. Takano, T. Tsukuda, *J. Phys. Chem. C* **2021**, *125*, 9930–9936.

[25] R. Guo, R. W. Murray, *J. Am. Chem. Soc.* **2005**, *127*, 12140–12143.

[26] V. K. Kulkarni, B. N. Khiarak, S. Takano, S. Malola, E. L. Albright, T. I. Levchenko, M. D. Aloisio, C.-T. Dinh, T. Tsukuda, H. Häkkinen, C. M. Crudden, *J. Am. Chem. Soc.* **2022**, *144*, 9000–9006.

6.0 RESULT AND DISCUSSION: APPLICATION OF MOLECULAR GOLD NANOCLUSTERS IN ANTICANCER THERAPY

6.1 INTRODUCTION: MOLECULAR GOLD CLUSTERS IN BIOLOGICAL ENVIRONMENTS

As mentioned in the introduction, AuNPs presenting small sizes (1-5 nm) are extensively used in biology due to their stability and the possibility to provide them biological affinity, when stabilized by biomolecules.[1] In addition, such particles emit NIR radiation (750-1100 nm), affording luminescence proprieties useful for bio-imaging or as probes for the detection of cancer cells.[2] Finally, these are applicable in cancer treatment too, once suitably tailored.[3]

Focusing on cancer therapy, the size of gold nanodrugs needs to be carefully chosen, since particles with sizes larger than 50 nm cannot pass through the outside barrier of the reticuloendothelial system (RES). Furthermore, these particles tend to form larger aggregates (> 100 nm) in circulatory system, which leads to a poor deposition of NPs in tumors.[4] Conversely, AuNPs presenting smaller sizes (< 50 nm) accumulate in cancer cells thanks to the “enhanced permeability and retention” (EPR) effect. The EPR effect aims to enhance the drug accumulation in tumor tissues, generally exploiting interactions between bio-polymeric nanomaterials and anticancer drugs.[5] Moreover, AuNPs presenting sizes smaller than 10 nm do not accumulate in liver and spleen, making therefore such particles bio-releasable after their use.[6]

In spite of the potential utility of small AuNPs, they are poly-dispersed, meaning that it is not possible to precisely control their size and consequent proprieties. To overcome this limitation, the use of molecular gold nanoclusters should be considered, since their molecularity allows easier structure-properties correlations, with tailored features useful in bio-applications. Furthermore, AuNCs and small AuNPs present similar stability and sizes, both fundamental for such applications.

Despite the evident advantages in the use of AuNCs, there are only few examples of their exploitation in biology.

Xie et al. have reported the use of $[Au_{25}(GS)_{18}]$ and $[Au_{25}(BSA)_{18}]$ for the radiotherapy of cancer cells, in which glutathione (GS) and bovine serum albumin (BSA) ligands provide biocompatibility to AuNCs.[7] Exploiting these precise clusters, an EPR effect can be obtained thanks to their sizes (2 nm), favoring cluster accumulation in cancer tissues. When these AuNCs are injected in HeLa cells, a decrease of the cell line viability of 15-30% can be detected after 48 h, confirming therefore their biocompatibility. Aiming to induce cellular apoptosis, X-ray irradiation needs to be used, which provokes an enhanced DNA damage due to the photoelectric effect of the gold centers. Similar applications have been reported for $[Au_{10-12}(GS)_{10-12}]$ and $[Au_{29-43}(GS)_{27-37}]$ too, whereas in these cases the clusters are not mono-dispersed.[8,9]

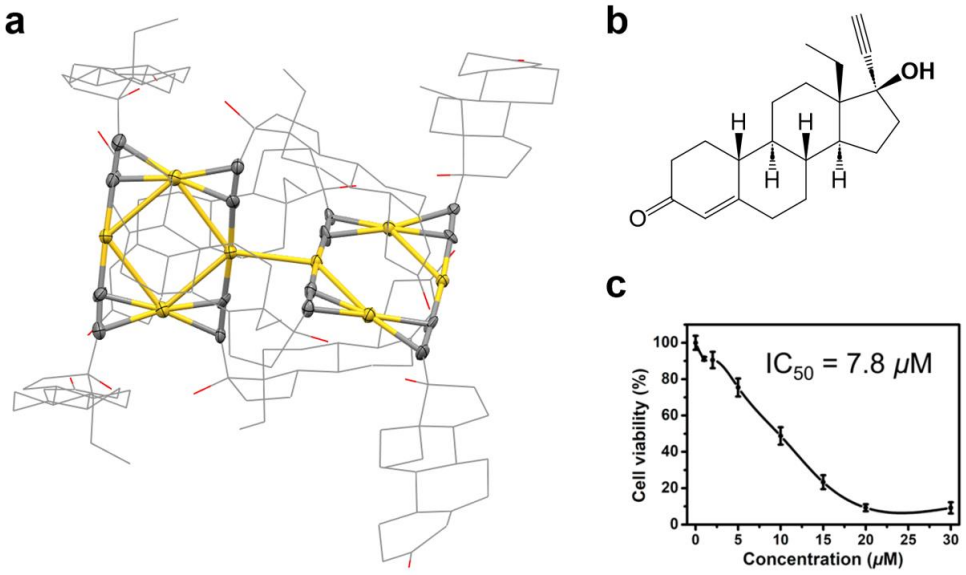

Figure 6.1: a) X-ray structure of Au_8 cluster capped by deprotonated levonorgestrel, in which the C≡C units are highlighted. Color code: yellow (Au), grey (C) and red (O). b) Levonorgestrel molecule. c) Relative cell viability of EC1 cells treated with different concentrations of Au_8NCs and corresponding IC_{50}.[10]

Another cluster useful for radiotherapy in cancer treatment is $[Au_8(C{\equiv}CR^{LEV})_8]$, reported in **Figure 6.1,** in which alkyl ligands are deprotonated levonorgestrel

molecules.[10] When such Au_8 cluster is injected in human esophageal squamous cancer cells (EC1) and treated with X-ray irradiation, the formation of reactive oxygen species (ROS) is promoted, leading to cellular apoptosis. The IC_{50} value found for this cluster, without irradiation, is equal to 7.80 μM, albeit no IC_{50} values are reported for healthy cell lines, thus no information is provided regarding its selectivity against tumor cells.

Another Au_{25} cluster used as mono-dispersed species is $[Au_{25}(MHA)_{18}]$, in which MHA is 6-mercaptohexanoic acid. This cluster has been disclosed as a useful alternative to conventional antibiotic thanks to its ability to kill 90% of tested Gram-positive and Gram-negative bacteria, since it favors accumulation of ROS in microbic systems.[11] An additional work in this field has been reported by Zang et al.[12], in which the antimicrobial activities of $[Au_8(C{\equiv}CR^{LEV})_8]$ and $[Au_{10}(C{\equiv}CR^{LEV})_{10}]$ are compared. They demonstrated that both Au_8 and Au_{10} clusters present antibiotic efficiency but highlighting that Au_8 shows higher activity than Au_{10} counterpart. They assert this improved efficiency to an additional mechanism favored by Au_8, affording the destruction of the bacteria wall and membrane, process not present when Au_{10} is used instead to led the cellular apoptosis. This work highlights that the structure of AuNCs deeply affects their biological applications.

Finally, exploiting ligand exchange reaction, Zhu and co-workers have synthesized $[Au_{18}(GS)_{12}(MPTB)_2]$ cluster from $[Au_{18}(GS)_{14}]$, in which MPTB are (4-carboxybutyl)triphenyl phosphonium bromide. This ligand increases the accumulation of Au_{18} cluster in mitochondrial system, differing in this from $[Au_{18}(GS)_{14}]$ which mainly accumulates in lysosomes. This result shows that upon ligand tailoring a targeted accumulation in cellular systems can be achieved.

To the best of our knowledge, those cited above are the only published examples of mono-dispersed AuNCs used in biological applications. It is particularly interesting that Au_8 and Au_{25} clusters discussed previously do not apparently present direct

anticancer activity, considering that the parent Au(I) complexes can present high antitumor efficiency[13–17], albeit together with low selectivity, since they attack both healthy and cancer cells. Therefore, despite the high accumulation of AuNCs in cancer tissues, their chemotherapeutic efficiency is related with the use of X-ray irradiation, which complicates their application.

To improve the anticancer activity of AuNCs, it should be feasible to combine their high EPR effect with the anticancer efficiency related to gold complexes, favoring *in situ* cluster decomposition to obtain such complexes, and causing consequently cellular apoptosis without using external triggers. Using this method, AuNCs act like pro-drugs, enabling both high accumulation in cancer cells and subsequent release of active drugs with the same molecular system. The Au_8 and Au_{25} clusters cited before are likely too stable to form gold complexes in biological environments, due to their complex ligand staples, and are therefore unsuitable for application as “direct” anticancer drugs. However, this degradation can be induced by tailoring the protecting ligand layer of AuNCs.

Following this hypothesis, we decided to evaluate the anticancer efficiency of our previously synthetized AuNCs, since we have already observed that these can slowly degrade in solution. Indeed, AuNCs capped by di-NHCs and PR_3 do not present complex ligand staples, making it more feasible to obtain gold complexes from these clusters rather than SR- or alkynyl-protected clusters. On the other hand, the chelating proprieties of di-NHCs ensure a partial stability of AuNCs, fundamental to reach the tumor cells before their desired decomposition.

6.2 APPLICATION OF di-NHC/PPh_3 CAPPED CLUSTERS AS SELECTIVE ANTICANCER PRO-DRUGS

The AuNCs exploited in this study have been obtained from the stepwise approach cited before and therefore present different coordination spheres (PPh_3, di-NHC or both) and metallic cores (Au_{11} and Au_{13}), as reported in **Figure 6.2**.[18]

Au_{11}	$[Au_{11}(PPh_3)_8Cl_2]^+$	
1c	$[Au_{11}(di\text{-}NHC^c)(PPh_3)_6Cl_2]^+$	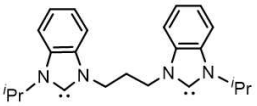
2a	$[Au_{13}(di\text{-}NHC^a)_2(PPh_3)_4Cl_4]^+$	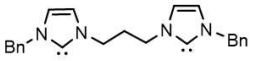
1b **2b'** **3b**	$[Au_{11}(di\text{-}NHC^b)(PPh_3)_6Cl_2]^+$ $[Au_{13}(di\text{-}NHC^b)_2(PPh_3)_4Cl_4]^+$ $[Au_{13}(di\text{-}NHC^b)_3(PPh_3)_3Cl_3]^{2+}$	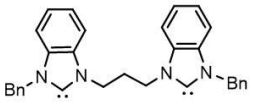

Figure 6.2: library of AuNCs tested as anticancer agents in this study.

We have already underlined that such AuNCs tend to decompose in solution, not affording AuNPs but forming instead $[ClAuPPh_3]$, $[Au_2(di\text{-}NHC)_2]^{2+}$ or $[(di\text{-}NHC)Au_2Cl_2]$ complexes, depending on the cluster. Similar complexes have been already exploited in literature as active chemotherapeutics, although they are generally characterized by a low selectivity against tumor cells.[19] In order to improve this feature using AuNCs as pro-drugs, cluster degradation to form bioactive complexes in the biological system needs to occur slowly, leaving to AuNCs time to accumulate in cancer tissue to subsequently provide the active species. To confirm this behavior, we recorded UV-Vis spectra of **1c**, **2b'** and **3b** clusters in DMSO:H_2O (1:30 v:v) solution at room temperature. Although the employed solvent mixture does not too closely represent a realistic biological environment, the degradation is confirmed for all tested AuNCs, showing a decrease of cluster signals without observable formation of AuNPs

plasmonic bands. This means that the clusters are stable enough in an aqueous environment to be injected in the cellular system, decomposing only after days in these conditions. UV-Vis spectra of **3b** are reported in **Figure 6.3**. The other UV-Vis spectra are reported in the **Experimental Section**. In future, other kinds of solvents will be considered for these UV-Vis analyses, such as blood plasma or similar[20], to further confirm this behavior in more realistic biological environments.

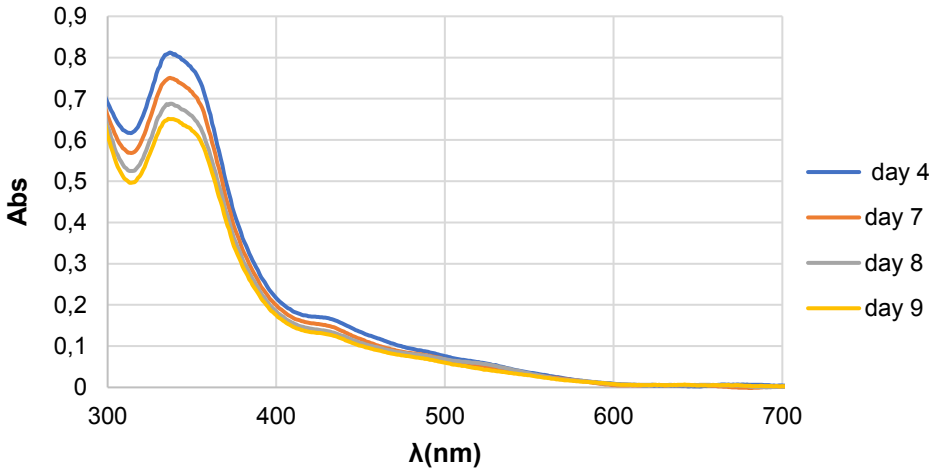

Figure 6.3: monitoring of UV-Vis spectrum of **3b** recorded in H_2O/DMSO (1:30 v:v) solution.

After these tests, we decided to directly use our clusters against different cell lines, to monitor their anticancer efficiency. These experiments have been conducted at the Ca' Foscari University of Venice, in collaboration with Prof. Flavio Rizzolio. The results obtained in this study are reported in **Table 6.1**, in comparison with cis-platin used as benchmark.[21]

Table 6.1: IC_{50} (μM) related to different AuNCs tested in different cancer cellular lines and one healthy cellular line. The name of di-NHCs correspond to **a**: 1,1′-dibenzyl-3,3′-propylenediimidazol-2,2′-diylidene; **b**: 1,1′-dibenzyl-3,3′-propylenedibenzimidazol-2,2′-diylidene; **c**: 1,1′-diisopropyl-3,3′-propylenedibenzimidazol-2,2′-diylidene.

CELL LINES	DRUG	IC_{50} (μM)
HCT	$[Au_{11}(PPh_3)_8Cl_2]Cl$	0,01386
	$[Au_{13}(di\text{-}NHC^a)_2(PPh_3)_4Cl_4]Cl$	0,06755
	$[Au_{11}(di\text{-}NHC^b)(PPh_3)_6Cl_2]Cl$	0,05211
	$[Au_{13}(di\text{-}NHC^b)_2(PPh_3)_4Cl_4]Cl$	0,1026
	$[Au_{13}(di\text{-}NHC^b)_3(PPh_3)_3Cl_3]Cl_2$	0,1023
	$[Au_{11}(di\text{-}NHC^c)(PPh_3)_6Cl_2]Cl$	0,1453
	$Pt(NH_3)_2Cl_2$	1,372
MDA	$[Au_{11}(PPh_3)_8Cl_2]Cl$	1,751
	$[Au_{13}(di\text{-}NHC^a)_2(PPh_3)_4Cl_4]Cl$	0,1585
	$[Au_{11}(di\text{-}NHC^b)(PPh_3)_6Cl_2]Cl$	1,915
	$[Au_{13}(di\text{-}NHC^b)_2(PPh_3)_4Cl_4]Cl$	26,46
	$[Au_{13}(di\text{-}NHC^b)_3(PPh_3)_3Cl_3]Cl_2$	3,533
	$[Au_{11}(di\text{-}NHC^c)(PPh_3)_6Cl_2]Cl$	2,715
	$Pt(NH_3)_2Cl_2$	20,44
OVCAR3	$[Au_{11}(PPh_3)_8Cl_2]Cl$	2,185
	$[Au_{13}(di\text{-}NHC^a)_2(PPh_3)_4Cl_4]Cl$	10,65
	$[Au_{11}(di\text{-}NHC^b)(PPh_3)_6Cl_2]Cl$	3,365
	$[Au_{13}(di\text{-}NHC^b)_2(PPh_3)_4Cl_4]Cl$	~ 12153
	$[Au_{13}(di\text{-}NHC^b)_3(PPh_3)_3Cl_3]Cl_2$	14,85
	$[Au_{11}(di\text{-}NHC^c)(PPh_3)_6Cl_2]Cl$	3,045
	$Pt(NH_3)_2Cl_2$	3,165
MRC5	$[Au_{11}(PPh_3)_8Cl_2]Cl$	~ 169486
	$[Au_{13}(di\text{-}NHC^a)_2(PPh_3)_4Cl_4]Cl$	~ 184480
	$[Au_{11}(di\text{-}NHC^b)(PPh_3)_6Cl_2]Cl$	~ 162165
	$[Au_{13}(di\text{-}NHC^b)_2(PPh_3)_4Cl_4]Cl$	~ 115022
	$[Au_{13}(di\text{-}NHC^b)_3(PPh_3)_3Cl_3]Cl_2$	~ 237304
	$[Au_{11}(di\text{-}NHC^c)(PPh_3)_6Cl_2]Cl$	~ 214301
	$Pt(NH_3)_2Cl_2$	119,9

In these preliminary experiments, AuNCs not only show a good anticancer activity, but they appear selective against cancer cells, too. Indeed, the values of IC_{50} related to cancer lines HCT, MDA and OVACR3 are 10^3-10^5 times lower than MRC5 line, composed by healthy cells. Apart from their high selectivity, it is important to underline their corresponding chemotherapeutic activity too, not observed for SR-capped AuNCs reported in **Paragraph 6.1**.[9] These experiments have been conducted in

vitro, on 2D cellular systems; under these conditions the ligand layers and the different cores do not apparently influence the cancer activity or selectivity, but it is their nano-sizes that provide this high selectivity.

We can compare our data with previously reported $[Au_8(C{\equiv}CR^{LEV})_8]$ cluster, presenting IC_{50} of 7.80 μM.[10] Unfortunately, this is the only molecular cluster whereby IC_{50} has been previously reported, albeit with a cell line (EC1) not employed in our study, which complicates our comparison. Nevertheless, IC_{50} values reported in **Table 6.1** are lower or similar to 7.80 μM provided by the $[Au_8(C{\equiv}CR^{LEV})_8]$ cluster, partially confirming our hypothesis regarding the bioactive role of Au(I) complexes deriving from cluster degradation, given the similar IC_{50} values.

It is important to underline that these are only preliminary results and further studies need to be conducted, such as using 3D cellular systems and organoids, to understand whether ligands and core size can discriminate which of the tested clusters perform best in more realistic conditions.

The mechanism of action of these clusters also needs to be elucidated, which includes the site where AuNCs accumulate in cancer cells. Indeed, it is known that Au(I) complexes tend to be active against thioredoxin reductase inside mitochondria, inhibiting its function and affording ROS accumulation in cancer cells.[19] However, there are currently no evidences that AuNCs present the same mechanism of action or site of deposition. To shed light on this, it is possible to exploit the strong luminescence of type **3** clusters, with formula $[Au_{13}(di\text{-}NHC)_3(PPh_3)_3Cl_3]Cl_2$, which present quantum yields between 30-40%. These emit at 760 nm, with a band width around 300 nm, partially matching with NIR irradiation wavelengths (750-1100 nm) and making it possible to detect AuNCs using bio-imaging techniques. Finally, our hypothesis regarding clusters that slowly decompose liberating biologically active gold(I) complexes needs to be further confirmed experimentally. Prof. Rizzolio and co-workers are currently testing the corresponding $[(di\text{-}NHC)Au_2Cl_2]$ complexes with the

same cell lines, aiming to understand if these are indeed the active species against cancer cells.

6.3 BIBLIOGRAPHY

[1] D. Hao, X. Zhang, R. Su, Y. Wang, W. Qi, *J. Mater. Chem. B* **2023**, *11*, 5051–5070.
[2] S. Ni, Y. Liu, S. Tong, S. Li, X. Song, *J. Anal. Test.* **2023**, *7*, 260–271.
[3] S. M. van de Looij, E. R. Hebels, M. Viola, M. Hembury, S. Oliveira, T. Vermonden, *Bioconjug. Chem.* **2022**, *33*, 4–23.
[4] S. D. Perrault, C. Walkey, T. Jennings, H. C. Fischer, W. C. W. Chan, *Nano Lett.* **2009**, *9*, 1909–1915.
[5] J. Park, Y. Choi, H. Chang, W. Um, J. H. Ryu, I. C. Kwon, *Theranostics* **2019**, *9*, 8073–8090.
[6] J. Lipka, M. Semmler-Behnke, R. A. Sperling, A. Wenk, S. Takenaka, C. Schleh, T. Kissel, W. J. Parak, W. G. Kreyling, *Biomaterials* **2010**, *31*, 6574–6581.
[7] X. Zhang, J. Chen, Z. Luo, D. Wu, X. Shen, S. Song, Y. Sun, P. Liu, J. Zhao, S. Huo, S. Fan, F. Fan, X. Liang, J. Xie, *Adv. Healthc. Mater.* **2014**, *3*, 133–141.
[8] X. Zhang, Z. Luo, J. Chen, X. Shen, S. Song, Y. Sun, S. Fan, F. Fan, D. T. Leong, J. Xie, *Adv. Mater.* **2014**, *26*, 4565–4568.
[9] X.-D. Zhang, Z. Luo, J. Chen, S. Song, X. Yuan, X. Shen, H. Wang, Y. Sun, K. Gao, L. Zhang, S. Fan, D. T. Leong, M. Guo, J. Xie, *Sci. Rep.* **2015**, *5*, 8669.
[10] T.-T. Jia, G. Yang, S.-J. Mo, Z.-Y. Wang, B.-J. Li, W. Ma, Y.-X. Guo, X. Chen, X. Zhao, J.-Q. Liu, S.-Q. Zang, *ACS Nano* **2019**, *13*, 8320–8328.
[11] K. Zheng, M. I. Setyawati, D. T. Leong, J. Xie, *ACS Nano* **2017**, *11*, 6904–6910.
[12] Y. Wang, Y. Hua, Z.-H. Shao, X. Chen, X. Zhao, S.-Q. Zang, *J. Mater. Chem. B* **2022**, *10*, 5028–5034.
[13] N. Mirzadeh, T. S. Reddy, S. K. Bhargava, *Coord. Chem. Rev.* **2019**, *388*, 343–359.
[14] M. Mora, M. C. Gimeno, R. Visbal, *Chem. Soc. Rev.* **2019**, *48*, 447–462.
[15] F. Guarra, A. Pratesi, C. Gabbiani, T. Biver, *J. Inorg. Biochem.* **2021**, *217*, 111355.
[16] M. Fereidoonnezhad, H. Ahmadi Mirsadeghi, S. Abedanzadeh, A. Yazdani, A. Alamdarlou, M. Babaghasabha, Z. Almansaf, Z. Faghih, Z. McConnell, H. R. Shahsavari, M. H. Beyzavi, *New J. Chem.* **2019**, *43*, 13173–13182.
[17] Z. Yang, G. Jiang, Z. Xu, S. Zhao, W. Liu, *Coord. Chem. Rev.* **2020**, *423*, 213492.
[18] M. Bevilacqua, M. Roverso, S. Bogialli, C. Graiff, A. Biffis, *Inorg. Chem.* **2023**, *62*, 1383–1393.
[19] Y. Lu, X. Ma, X. Chang, Z. Liang, L. Lv, M. Shan, Q. Lu, Z. Wen, R. Gust, W. Liu, *Chem. Soc. Rev.* **2022**, *51*, 5518–5556.
[20] S. Keller, Y. C. Ong, Y. Lin, K. Cariou, G. Gasser, *J. Organomet. Chem.* **2020**, *906*, 121059.
[21] S. Dasari, S. Njiki, A. Mbemi, C. G. Yedjou, P. B. Tchounwou, *Int. J. Mol. Sci.* **2022**, *23*, 1532.

7.0: NHC LIGANDS FROM GOLD CLUSTERS TO GOLD NANOWIRES

7.1 INTRODUCTION: GOLD NANOWIRES

During this PhD project, we started a collaboration with Prof Dominik Munz and Prof. Tobias Kraus regarding the stabilization of gold nanowires (AuNWs) using NHC ligands.

As showed in **Figure 7.1 a**, AuNWs are gold nanomaterials presenting diameter around 2 nm and length greater than 1000 nm.[1] They exhibit flexibility, conductivity and transparency proprieties useful in modern technology for producing transparent solar screens or cells.[2,3]

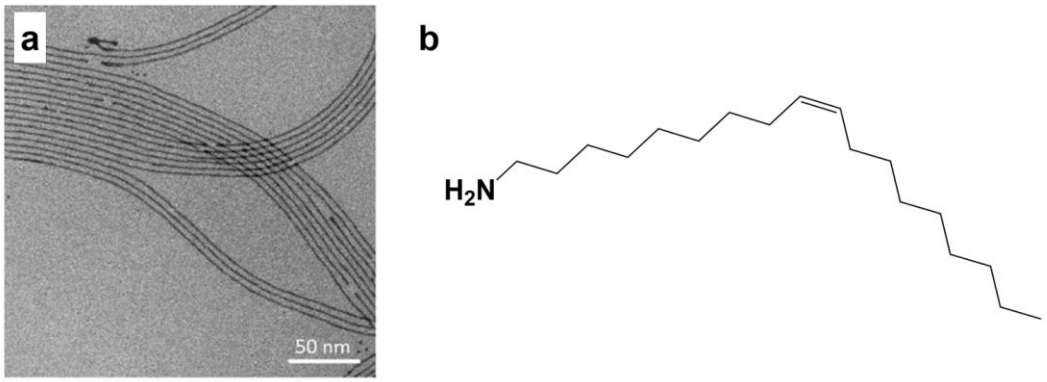

Figure 7.1: a) TEM analysis of AuNWs. b) oleyl amine commonly used as capping agents for AuNWs.[2]

Hitherto, AuNWs stabilization has been mainly achieved using oleyl amine (OLA) as protecting ligand. This amine, reported in **Figure 7.1 b**, prevents degradation of AuNWs thanks to its bent chain, a feature disfavoring the intermolecular packing of OLA chains among wires and consequently preventing aggregation of the resulting colloidal system.

The synthesis of AuNWs is commonly performed through reduction of Au(III) complexes promoted by triisopropylsilane, in the presence of OLA. This latter acts as directing agent, orienting wire growth during the reduction process, as highlighted by time-resolved TEM[4], X-ray absorption spectroscopy (XAS) and small-angle X-ray scattering (SAXS).[5] Moreover, the diameter of ultrathin gold wires can be varied changing the chain length in the starting amine, which allows isolation of AuNWs with diameters from 2.13 nm to 2.65 nm.[6]

The stability of such colloidal system depends on solution composition, since solvent molecules can be adsorbed in the organic layer composed by OLAs, which consequently affects the interactions between wires.[7]

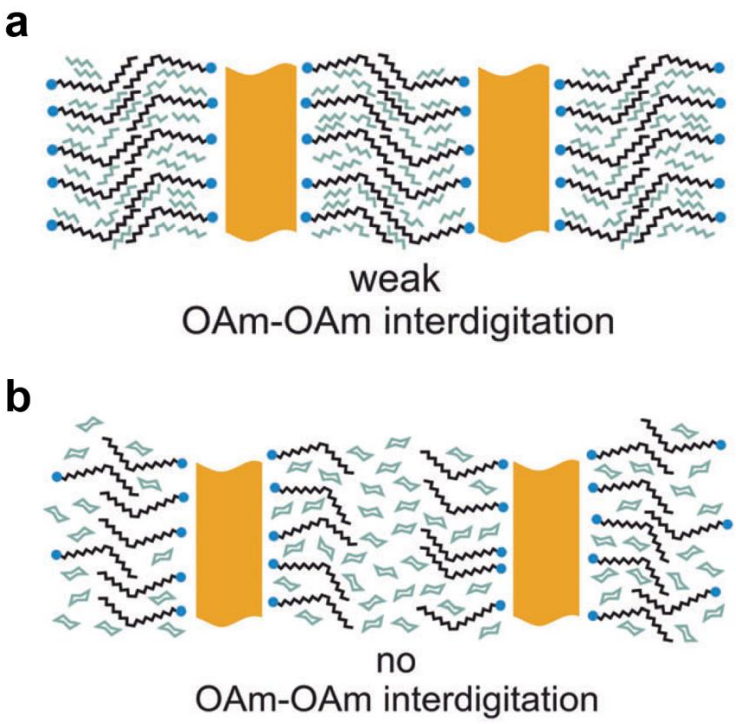

Figure 7.2: illustration of proposed arrangement of solvents in the ligand layer of AuNWs using a) *n*-hexane and b) cyclohexane.[7]

Using linear alkanes, such as *n*-hexane, gold nanowires form hexagonal bundles with diameter of 5.5 nm. Exploiting instead cyclic alkanes, like cyclohexane, formation of this ordered assembly is entirely prevented, thanks to the low flexibility of this solvent

molecule. This “solvent effect” highlights that weak intermolecular interactions dominate the self-assembly of wires, in which linear solvents present appropriate flexibility to intercalate into OLAs layer, unlike cyclic alkanes, characterized instead by lower mobility, a feature that prevents the intercalation cited above. This behavior is represented in **Figure 7.2**.

Despite improvements in AuNWs stabilization can be obtained using linear and nonpolar solvents, these are not stable materials. Due to their length[8] AuNWs naturally tend to rearrange in order to minimize their surface tension, forming consequently gold nanoparticles or nanorods after 3-4 days from their synthesis.[9] Another important drawback derived from OLA used as capping agent is that this ligand forms an insulating organic layer causing high junction resistances at contact interfaces of deposited wires, exhibiting sheet resistances in the megaohm range, unsuitable for most electronic applications. Despite sintering process[10] can enhance AuNWs conductivity, reaching value of 50 Ω sq^{-1}, applications of this colloidal system are far from being at hand.

To solve these limitations, other ligands need to be considered to cap such nanomaterials, presenting conductive proprieties and strong bonds with gold surface. Some efforts in this sense have been reported by Li’s group.[9] They reported H_2S ligand exchange reaction on OLA-protected AuNWs, improving not only the stability of the nano-system but also enhancing its conductivity, reaching values 10^7 times higher than the starting systems and resistance values of 3-5 KΩ sq^{-1}. Similar experiments have been performed by Viau and co-workers[11], in which trioctylphosphine and octylphosphine oxide are used as exchange ligands. Using these ligands an enhanced stability is reported, with formation of AuNWs stable for 7 days, albeit no experiments regarding their conductivity have been conducted.

Despite the remarkable results obtained so far, another possible substitute of OLA is represented by NHCs, never used before to cap AuNWs.[12] These ligands have been

already exploited to cap Au(111) surfaces, forming super-stable self-assembled monolayers (SAM).[13] Moreover, Ravoo and co-workers have obtained patterned SAM of NHC on gold surfaces using microcontact printing.[14] This deposition technique allowed to study the conductivity of decorated and not-decorated surface areas using conductive probe atomic force microscopy (CP-AFM), demonstrating that NHC-protected areas show higher current than undecorated ones. These CP-AFM analyses and corresponding current profiles are reported in **Figure 7.3**.

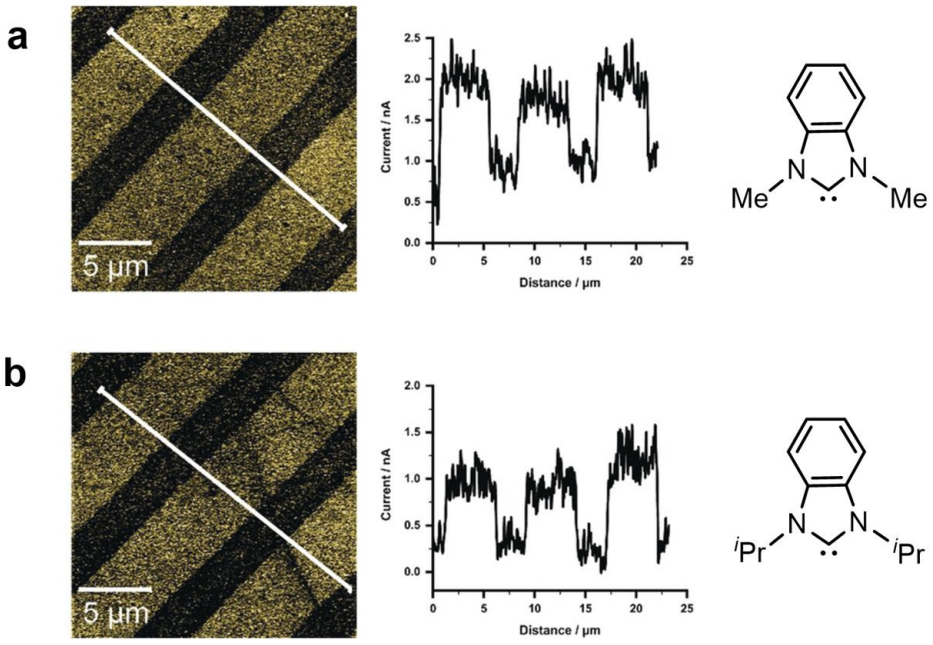

Figure 7.3: CP-AFM images and corresponding current profiles reported for patterned SAM on Au surfaces formed by a) 1,3-bis(methyl)benzimidazol-2-ylidene and b) 1,3-bis(isopropyl)benzimidazol-2-ylidene ligands.[14]

The results cited above inspired us in the use of NHC ligands in the stabilization of AuNWs, considering that NHCs are tunable ligands, in which several variations can be engineered on NHC scaffolds to improve the stability of such system.

Starting from OLA-capped wires, our study involved two different approaches: 1) ligand exchange, using free NHCs to exchange the OLAs on the gold nanowires and

2) addition of (S)NHC gold(I) complexes, to anchor these on AuNWs. As following, we will illustrate the obtained results.

7.2 PRELIMINARY RESULTS ON STABILIZATION OF GOLD NANOWIRES CAPPED BY NHCs

We decided to use firstly the ligand exchange reaction since this represents a versatile process already exploited in literature to cap AuNCs, AuNPs and Au surfaces.[15] In this experiment we exploited the NHC reported in **Figure 7.4**, since its imidazolium salt is commercially available and easy to deprotonate using KHMDS as base. This presents a long chain as wingtips, a group that should guarantee dispersion forces on longitudinal section of gold wires, to further increase their stability. Moreover, based on NMR studies reported in the **Experimental Section**, this NHC is stable at room temperature in benzene for several days, making it perfect for our experiment. Indeed, coupling reactions between NHCs units need to be prevented to avoid formation of NHC=CHN molecules, representing one of the strongest organic reducing agents.[16] Thanks to their delocalized π-orbitals they can be easily oxidized donating electron to AuNWs and compromising their stability.

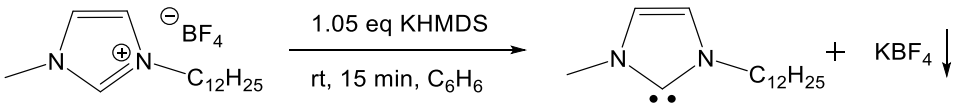

Figure 7.4: synthesis of the NHC exploited in this work.

The synthesis of starting AuNWs has been performed by Yannic Curto, PhD student of Prof. Kraus, as well as analysis on the colloidal systems. Briefly, $HAuCl_4$ complex is reduced in presence of an excess of OLA by triisopropylsilane, using *n*-hexane as solvent. After this, crude AuNWs are purified through precipitation in EtOH, and the final product is dispersed in cyclohexane. Since the stability that such nano-system presents in cyclohexane, we decided to use the same solvent for the exchange as well.

The exchange experiment has been performed using simple Schlenk techniques, in which a cyclohexane solution of free NHC has been added dropwise to the wires dispersion, using [Au]:[NHC] molar ratio equal to 1:10. Interestingly, AuNWs precipitated after the addition, which gave us the clue that the exchange took place.

Aiming to confirm this hypothesis, the supernatant solution of cyclohexane has been analyzed by ^{1}H NMR, highlighting the presence of free oleyl amine, confirming that the exchange worked. After a washing step using EtOH to remove OLA ligand, TEM analysis and UV-Vis spectrum of the precipitate have been recorded. These analyses, reported in **Figure 7.5** in comparison with starting material, confirm that no AuNPs formation took place after the exchange, although it is possible to notice in TEM analysis of NHC-capped wires that these partially decompose after the exchange, showing small aggregates along them. In UV-Vis spectrum, recorded in THF, there are no plasmonic bands related to AuNPs, in line with TEM analysis.

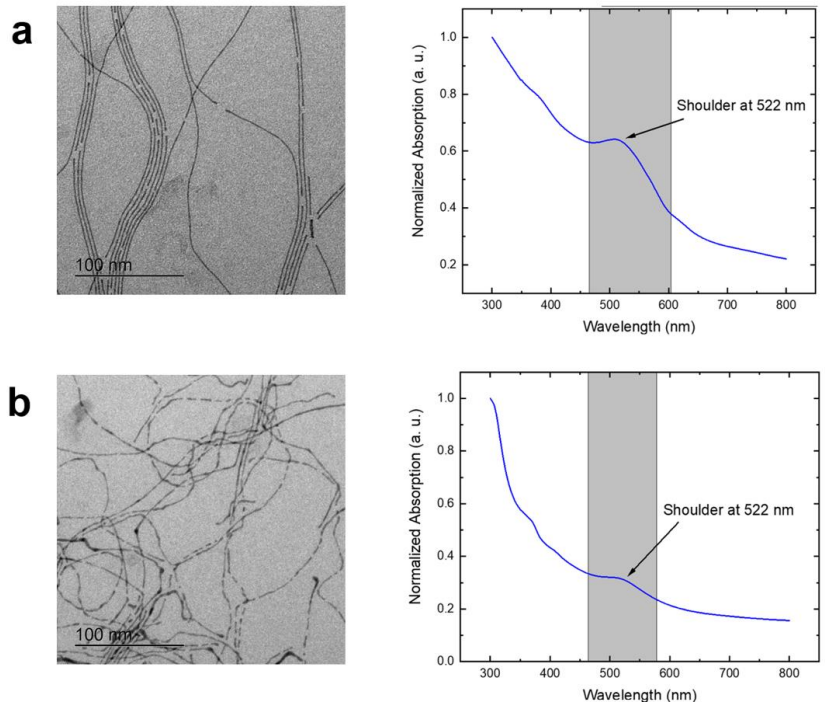

Figure 7.5: TEM and UV-Vis analyses of a) oleyl amine and b) NHC stabilized AuNWs.

To further confirm the presence of NHCs on AuNWs we attempted ^{1}H NMR analysis on the colloidal system, aiming to detect NHC signals in the spectrum. Unfortunately, NHC-stabilized wires are not soluble in most common solvent, thus it has been not yet possible to record ^{1}H NMR spectrum of AuNWs, to confirm the anchoring of NHCs on the gold surface. The precipitation of wires, combined with the difficulties to disperse them in several solvents, suggest that the exchange gave rise to a partial aggregation of AuNWs. Indeed, the used NHC does not present long chains in backbone but only as wingtips, meaning that this group can only interact with the surface, but likely without preventing formation of the bundles cited before. Indeed, in NHC-capped AuNPs[15], the ligands commonly present long chains attached on the NHC backbone to form an amphiphilic layer to protect AuNPs from aggregation, albeit examples of NHCs not presenting such feature are also reported.

Aiming at preventing the aggregation observed with this NHC, we are going to synthetize novel NHCs, reported in **Figure 7.6**, presenting long chains in the ligand backbone, a feature that should disfavor the interactions between wires and increasing consequently their solubility. Enhancing the solubility of the nano-system is fundamental to confirm the presence of NHCs on the wires surface, through ^{1}H and ^{13}C NMR spectroscopic analysis.

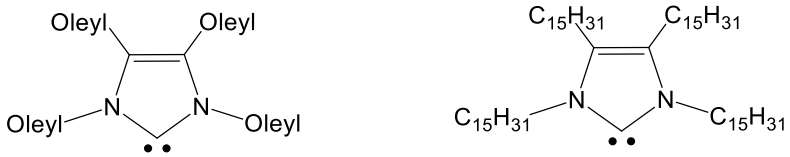

Figure 7.6: novel NHCs that will be exploited to cap AuNWs.

After this first experiment, we decided to use (S)NHC-Au(I) complexes **m** and **n**, already reported in this thesis in **Paragraph 3.2**, aiming at favoring addition reaction on AuNWs surfaces. This approach has been already exploited to cap AuNPs with several NHCs, exploiting $[Au(NHC)_2]Cl$ and [(NHC)AuCl] complexes.[17] Moreover, we

have already explained that reduction of **n** complex provides small AuNPs, suggesting that such ligands may cap AuNWs too.

In this second experiment, we used chloroform as solvent, since both AuNWs and complexes are soluble in it. Unfortunately, this method has not worked properly, affording small AuNPs after the addition. TEM analysis, reported below in **Figure 7.7**, confirms this result, showing formation of large rod- or spheric-shaped aggregates. UV-Vis analysis confirms the result observed with TEM, showing an intense band related to the plasmonic resonance of AuNPs formed after the addition. Moreover, chlorinated solvents are not the best to favor AuNWs stabilization, since the possible traces of HCl can degrade the colloidal system.

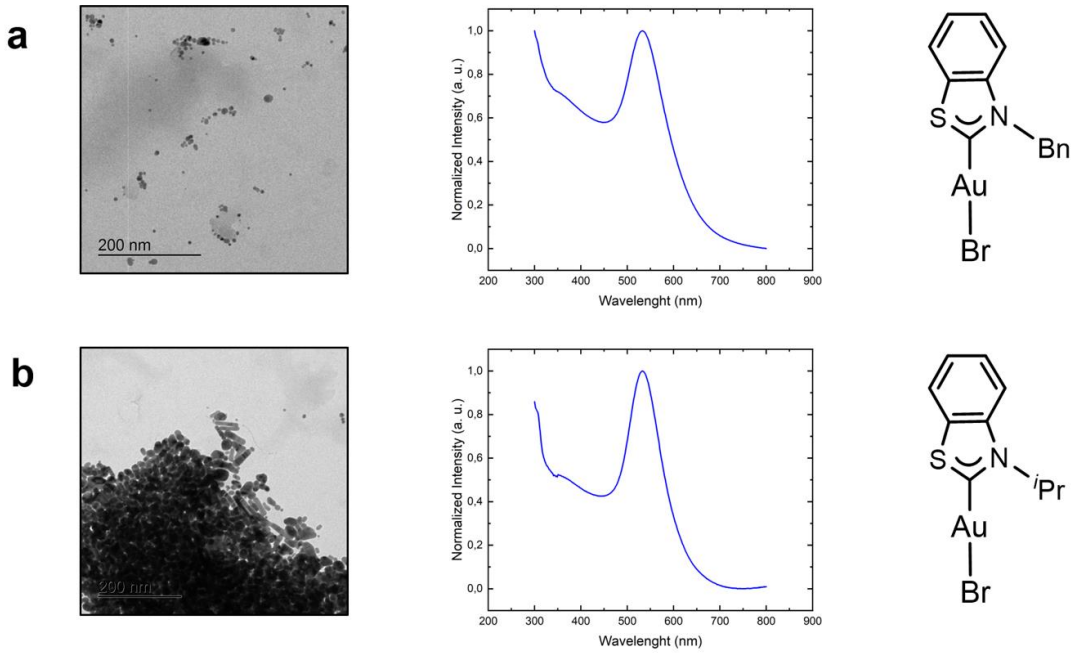

Figure 7.7: TEM and UV-Vis analyses of experiment performed with a) **m** and b) **n** complexes addition to OLA-stabilized AuNWs.

Since this second approach has been revealed not satisfactory, in the future we will focus our efforts on the synthesis of novel NHCs reported in **Figure 7.6**, aiming to get a more soluble sample to better understand the results of ligand exchange.

7.3 BIBLIOGRAPHY

[1] R. Takahata, T. Tsukuda, *Chem. Lett.* **2019**, *48*, 906–915.
[2] B. Reiser, D. Gerstner, L. Gonzalez-Garcia, J. H. M. Maurer, I. Kanelidis, T. Kraus, *Phys. Chem. Chem. Phys.* **2016**, *18*, 27165–27169.
[3] J. H. M. Maurer, L. González-García, I. K. Backes, B. Reiser, S. M. Schlossberg, T. Kraus, *Adv. Mater. Technol.* **2017**, *2*, 1700034.
[4] H. Feng, Y. Yang, Y. You, G. Li, J. Guo, T. Yu, Z. Shen, T. Wu, B. Xing, *Chem. Commun.* **2009**, 1984.
[5] F. Pschunder, J. Puig, L. J. Giovanetti, C. Huck-Iriart, F. G. Requejo, D. Buceta, C. E. Hoppe, J. M. Ramallo-López, *J. Phys. Chem. C* **2018**, *122*, 29051–29061.
[6] C. Morita, H. Tanuma, C. Kawai, Y. Ito, Y. Imura, T. Kawai, *Langmuir* **2013**, *29*, 1669–1675.
[7] B. Reiser, D. Gerstner, L. Gonzalez-Garcia, J. H. M. Maurer, I. Kanelidis, T. Kraus, *Phys. Chem. Chem. Phys.* **2016**, *18*, 27165–27169.
[8] Lord Rayleigh, *Proc. Lond. Math. Soc.* **1878**, *s1-10*, 4–13.
[9] J. Jiang, Y. Zhang, J. Zhou, Y. Jiang, Y. Li, *Adv. Eng. Mater.* **2022**, *24*, 2200509.
[10] J. H. M. Maurer, L. Gonzalez-Garcia, B. Reiser, I. Kanelidis, T. Kraus, *Phys. Status Solidi A* **2016**, *213*, 2336–2340.
[11] E. S. A. Nouh, E. A. Baquero, L.-M. Lacroix, F. Delpech, R. Poteau, G. Viau, *Langmuir* **2017**, *33*, 5456–5463.
[12] C. A. Smith, M. R. Narouz, P. A. Lummis, I. Singh, A. Nazemi, C.-H. Li, C. M. Crudden, *Chem. Rev.* **2019**, *119*, 4986–5056.
[13] C. M. Crudden, J. H. Horton, I. I. Ebralidze, O. V. Zenkina, A. B. McLean, B. Drevniok, Z. She, H.-B. Kraatz, N. J. Mosey, T. Seki, E. C. Keske, J. D. Leake, A. Rousina-Webb, G. Wu, *Nat. Chem.* **2014**, *6*, 409–414.
[14] D. T. Nguyen, M. Freitag, M. Körsgen, S. Lamping, A. Rühling, A. H. Schäfer, M. H. Siekman, H. F. Arlinghaus, W. G. van der Wiel, F. Glorius, B. J. Ravoo, *Angew. Chem. Int. Ed.* **2018**, *57*, 11465–11469.
[15] C. A. Smith, M. R. Narouz, P. A. Lummis, I. Singh, A. Nazemi, C.-H. Li, C. M. Crudden, *Chem. Rev.* **2019**, *119*, 4986–5056.
[16] J. Broggi, T. Terme, P. Vanelle, *Angew. Chem. Int. Ed.* **2014**, *53*, 384–413.
[17] J. F. DeJesus, L. M. Sherman, D. J. Yohannan, J. C. Becca, S. L. Strausser, L. F. P. Karger, L. Jensen, D. M. Jenkins, J. P. Camden, *Angew. Chem.* **2020**, *132*, 7655–7660.

8.0 PHOSPHINIDENE STABILIZED Pd_8 CLUSTER

8.1 INTRODUCTION: METALLIC CLUSTERS SUPPORTED BY PHOSPHINIDENE LIGANDS

The expertise gained during this PhD project in the synthesis of AuNCs allowed to extend investigations towards the synthesis of a novel Pd_8 cluster, stabilized by phosphinidene ligands (PRs), in collaboration with Prof. Dominik Munz of the University of Saarland (Germany).

As underlined so far, cluster chemistry is largely focused on coinage metals[1], with particular attention on AuNCs[2], given their stability against air and water. These features make it easier to manipulate Au clusters than Ag or Cu clusters. Moreover, knowledge related to AuNCs is fundamental to better understand AuNPs, materials used for several applications, spanning from catalysis to bio-imaging.

Notwithstanding the great interest in AuNCs, other metal centers can form molecular nanocluster (MNCs), like for example Al or Ga in the p-block[3]. Furthermore, different s, d or f-blocks metal centers can be combined, which leads to the isolation heterometallic clusters.[4,5] It is also possible to expand the cluster types to include those presenting oxygen[6], sulfur[7] or other species[8] as bridging units between metal centers. For instance, the catalytic center in the Photosystem II of chloroplasts is a cluster with formula Mn_4CaO_5, which favors the photosynthetic process in plants, underlying the important role of clusters in biochemistry, too.[9]

Another interesting class of MNCs is represented by molecular palladium clusters (PdNCs), since their emerging relevance in electronic materials and catalysis, albeit these are commonly used as poly-dispersed species.[10–12] Indeed, several PdNCs have been already reported by Hayton's[13], Crimmin's[14] and Murahashi's[15] groups,

presenting Pd_3, planar Pd_4, Pd_6 and Pd_7 metallic cores, respectively. Also tetrahedral Pd_4 [16–19], a Pd_8 wire [20], as well as Pd_{10} [21], Pd_{13} [22] and Pd_{17} [23] clusters are known.

It is notable that notwithstanding the numerous geometries that have been reported in the literature, only one example of cubic PdNCs has been described[24], with formula $[Pd_9As_6(PPh_3)_8]$ (**Figure 8.1 a**), in which square faces are capped by As centers and the vertexes bind additional PPh_3 ligands, saturating therefore the metallic core. Similar geometries have been reported also with Ni clusters, presenting instead formula $[Ni_8(PPh)_6(CO)_8]$ [25] and $[Ni_8(PPh)_6(PPh_3)_4]$ [26–28] (**Figure 8.1 b** and **Figure 8.1 c**), in which the square faces are capped by phosphinidene ligands (PRs).[29]

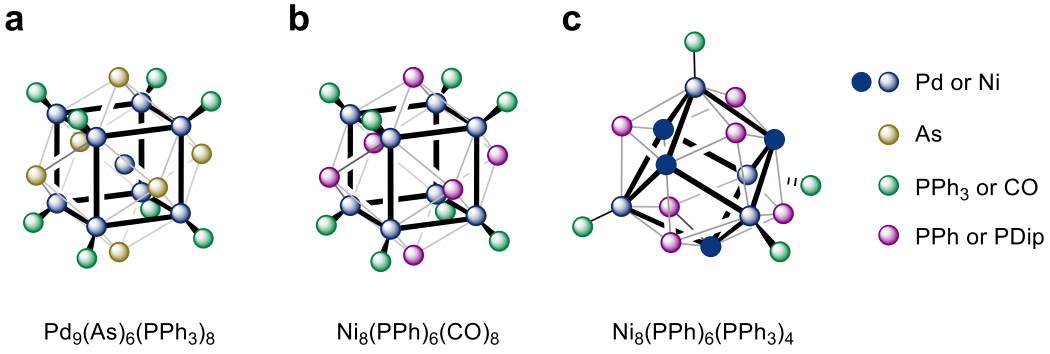

Figure 8.1: Previously reported coordinatively saturated a) palladium b, c) and nickel nanoclusters.

These ligands, reported in **Figure 8.2 a**, are particularly useful to cap such clusters[30], since they present a low-valent phosphorous atom, presenting 6 valence electrons instead of 8, in which free electronic doublets can interact with soft metal centers like in the case of carbene ligands. In addition, PRs can interact simultaneously with several metal centers thanks to their two electronic doublets, as shown in **Figure 8.1**, unlike NHCs, which present instead only one lone pair that form bonds with metallic centers. Using PRs as free ligands is complicated due to their high reactivity, but it is possible to generate these moieties *in situ* from other molecules, like cyclophosphanes $(PR)_n$, allowing the isolation of novel MCs.[31] For instance, Roy and colleagues have synthesized a series of Ni clusters combining a bis(1,5-

cyclooctadiene)nickel(0) complex with cyclophosphanes $(PR)_n$ (R = Me, ^{i}Pr; n = 4, 5) in the presence of trimethyl- or triethylphosphine to saturate the nickel core.[32]

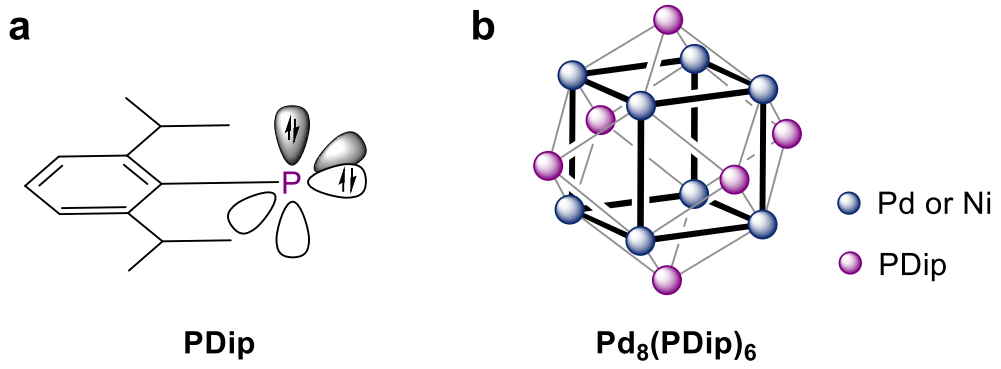

Figure 8.2: a) structure of the phosphinidene ligand used in this work and b) unsaturated palladium cluster **1** capped with it.

Inspired by Roy's paper, we wondered if it was possible to isolate unsaturated PdNCs exploiting only $(PR)_n$ as source of phosphinidenes, thus without using other capping ligands. Hereafter, we will explain the synthesis and derivatization of a cubic Pd_8 metalloid cluster capped by PDip ligands (Dip = 2,6-diisopropylphenyl), reported in **Figure 8.2 b** and called hereafter **1**. At variance with the usual syntheses reported in this thesis, all the operations hereafter reported have been performed in a glovebox, since Pd precursors and cyclophosphanes are strongly air and water sensitive.

8.2 SYNTHESIS AND FUNCTIONALIZATION OF UNSATURATED CUBIC PALLADIUM CLUSTER

Cubic palladium cluster **1** has been obtained through insertion reaction of reactive Pd(0) precursors with a phosphinidene surrogate, namely triphosphirane[30,33–35], in the absence of additional trapping ligands. According to ^{31}P NMR spectroscopy, heating two equiv. of tris(dibenzylideneacetone) palladium, $Pd_2(dba)_3$, with one equivalent of the triphosphirane $(PDip)_3$ [36] in benzene for one day provides a mixture of two phosphorus-containing products. Indeed, the ^{31}P NMR spectrum of the crude mixture presents a first signal at +533 ppm, assigned to cluster **1** according with common signal detected for similar clusters[26], and a second signal falling at -102 ppm, related to a by-product. This latter signal splits into a doublet ($^1J_{P\text{-}H}$ = 231.6 Hz) upon ^{1}H decoupling, indicating a PH moiety not present in the starting $(PDip)_3$, likely deriving from intramolecular CH insertion of the phosphinidene. The synthesis of **1** is reported in **Figure 8.3**. For experimental details see **Experimental section**.

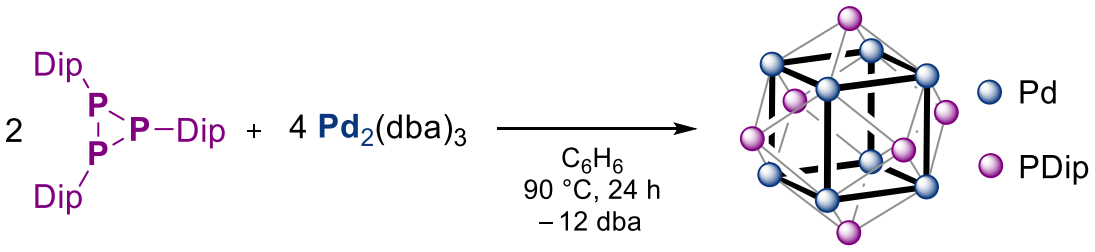

Figure 8.3: Synthesis of cluster **1** by reaction of $Pd_2(dba)_3$ with triphosphirane.

Although the cluster proved to be air sensitive as expected, it is thermally robust with a decomposition point of 291°C. Single-crystals of **1** suitable for X-ray diffraction (SCXRD) have been obtained directly from a benzene solution. The X-ray structure of **1** is reported in **Figure 8.4**.

1 can be identified as a neutral cubic metalloid cluster with formula $[Pd_8(PDip)_6]$, in which a Pd_8 cube is capped by six μ_4-phosphinidene ligands, as showed also for similar structures reported in literature.[26–28] It crystallizes in the space group $R\bar{3}$ comprising a threefold axis of symmetry and an inversion center. The Pd_8 cube shows Pd-Pd bond lengths of 2.6997(6) and 2.6866(6) Å, in agreement with similar values reported for the body-centered Pd_9 cube in **Figure 8.1 a** (2.71 and 2.68 Å). Moreover, Pd-Pd bond lengths in **1** are shorter than the distance (2.75 Å) found in the face-centered cubic structure of bulk palladium metal.[37] The high symmetry of **1** revealed by this analysis perfectly matches with the singlet found in the ^{31}P NMR spectrum, as well as with the signals detected in the ^{1}H NMR spectrum.

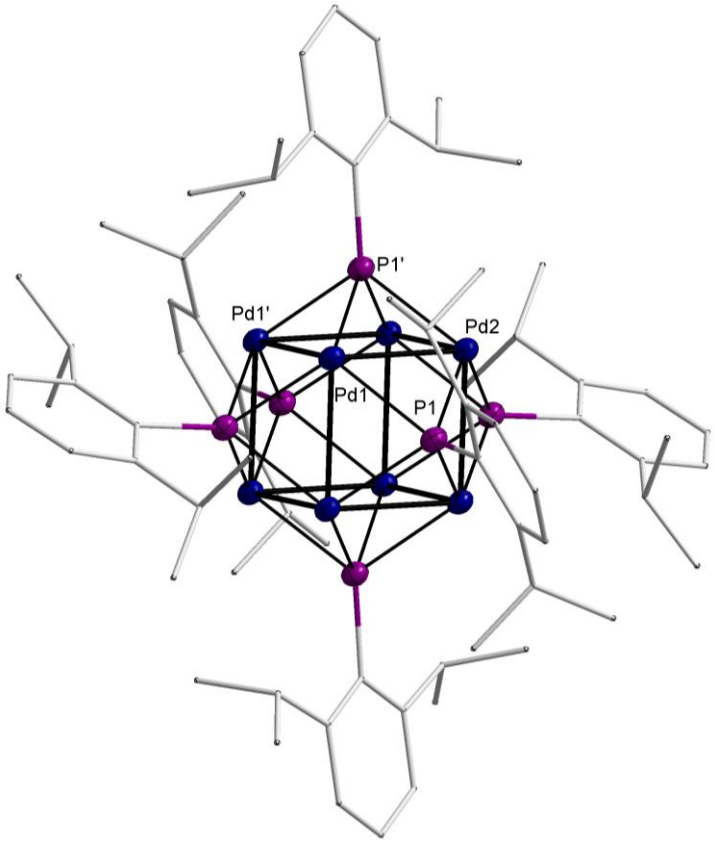

Figure 8.4: X-ray structure of **1** in the solid state. Color code: blue (Pd), purple (P), grey (C).

Finally, also high-resolution mass spectrometry (HRMS) is in accordance with the structure found by SCXRD, matching with the exact mass and isotopic pattern expected for **1**.

The UV-Vis spectrum of cluster **1**, reported in **Figure 8.5**, has been recorded in benzene; it spans a range up to 760 nm, with maxima at 295 nm, 324 nm and 387 nm. The mostly featureless and exceedingly broad spectrum with tailing up to 750 nm is typical for nanoclusters with metal-metal bonding. TD-DFT calculations performed by Prof. Munz and co-workers suggest that the low-energy transitions exhibit metal-to-ligand (Pd→P) charge transfer character, which is consistent with an electron-rich metal cluster and electron-deficient phosphinidene ligands.

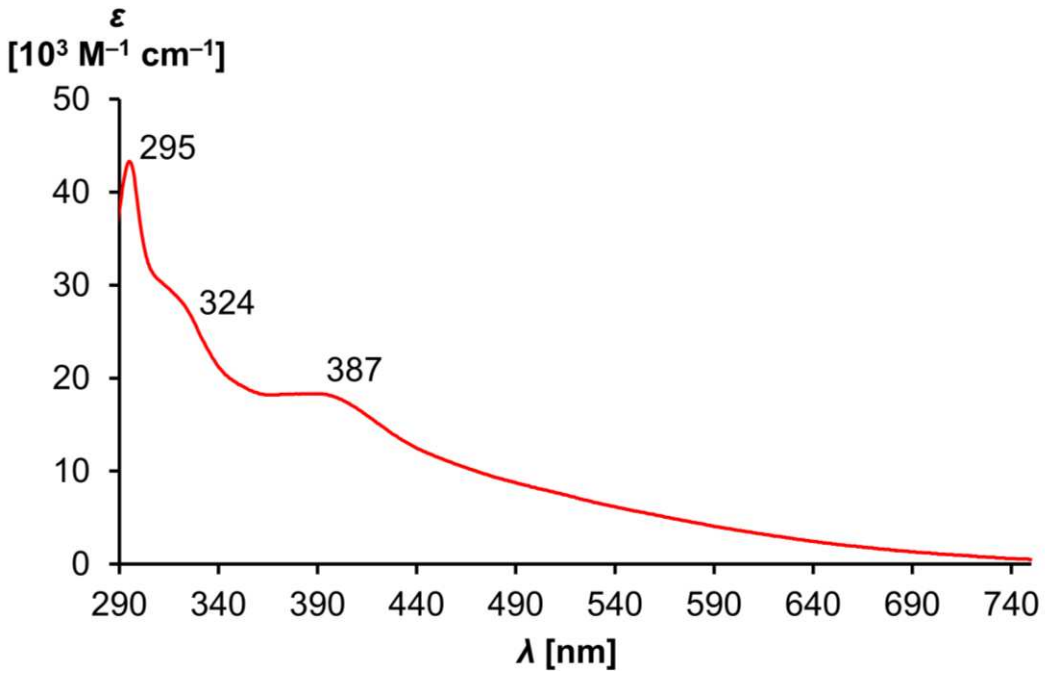

Figure 8 5: UV-Vis spectrum of **1** in benzene.

Surprisingly, the cyclic voltammetry (CV) analysis of **1**, reported in **Figure 8.6**, shows a reversible reduction process at -2.13 V, a behavior not expected considering its unsaturated core. It is not simple to rationalize this reversibility since there are no examples of PdNCs studied through CV analysis in literature. In addition, Pd(0)

presents $4d^{10}$ electronic configuration, thus presenting a complete orbital shell for which the SA theory should be inapplicable.

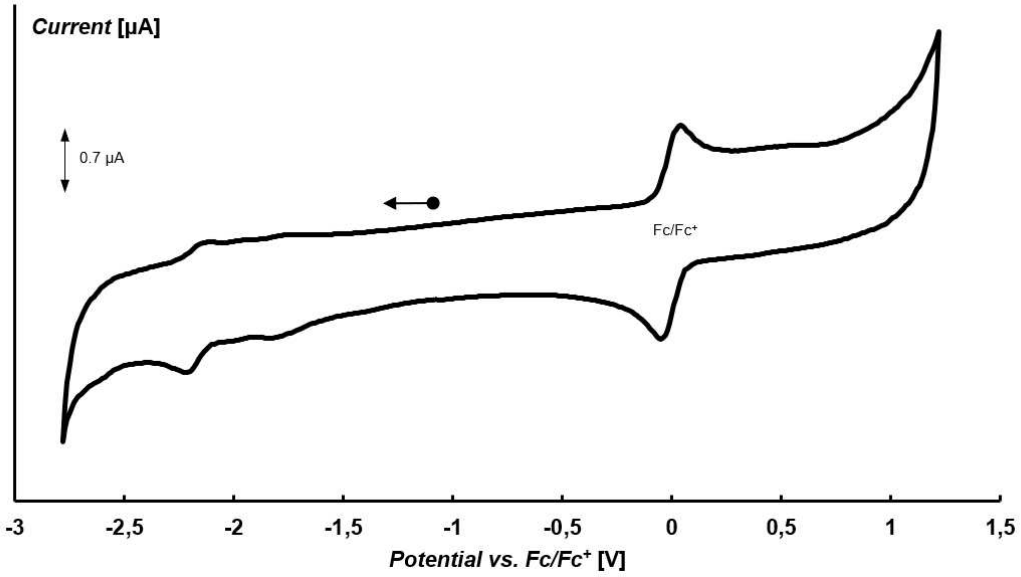

Figure 8.6: Cyclic voltammogram for **1**, measured at 100 mV s^{-1} in 0.2 M NBu_4PF_6 *o*-difluorobenzene solution, in the presence of the internal ferrocene standard (second scan of two is shown). Open-Circuit Potential (OCP; in the absence of ferrocene): -0.05 V).

However, Quantum-chemical calculations, always performed by Munz's group and used to elucidate the electronic structure of **1**, explain the origin of its surprising stability. According to the concept of SA, a filled d^{10} shell provides a *jellium* electron count of zero, which is not consistent with substantial M-M bonding. Thus, Saillard and Halet[38,39] proposed that SA bonding may exist in zerovalent group 10 clusters through level-crossing of 5s with 4d orbitals, allowing to achieve a magical electron number by effectively adopting an electron configuration of $4d^{10-x}\ 5s^{x}$. The calculations corroborate as such Saillard's and Halet's proposition and suggest a superatom with a $1S^2\ 1P^6\ 1D^{10}\ 2S^2\ 1F^{12}$ electron configuration and 32 SA electrons. The unfilled F-shell agrees with computations for hollow cage-clusters, where 32 instead of 34 may become a magic number.[40] Therefore, the reversible reduction process can be explain with the SA stability derived from this mixing of atomic orbitals, in particular

considering the electronegativity of phosphinidene ligands, making them able to accept further electronic density derived from the electrochemical process.

Aiming at better understanding the mechanism of growth of **1**, a more reactive palladium(0) precursor (^{im}CAAC)Pd(py) [41–43], has been exploited, presenting cyclic alkyl amino carbene (CAAC)[44] and pyridine (py) as ligands.

Treating (^{im}CAAC)Pd(py) with $(PDip)_3$ at room temperature in C_6D_6 led to release the free ^{im}CAAC ligand[45] and quantitative conversion to unidentified intermediates. The mixture has been subsequently warmed at 60°C, affording the conversion of the intermediates to provide **1.** When similar reactions are performed in pyridine-d_5 and toluene-d_8, it is possible to observe for both tests the formation of precipitates as single crystals suitable for SCXRD analysis. They have been identified as palladium complexes **2** and **3**, respectively with formulas $[(PDip)_3Pd(py)_2]$ and $[(PDip)_5Pd_2(py)_2]$. In both structures, reported in **Figure 8.7**, insertion of Pd centers in $(PDip)_3$ molecule can be observed, allowing to conclude that the palladium precursor likely inserts stepwise into the P-P bond of $(PDip)_3$, dissociating firstly CAAC ligand and later pyridine.

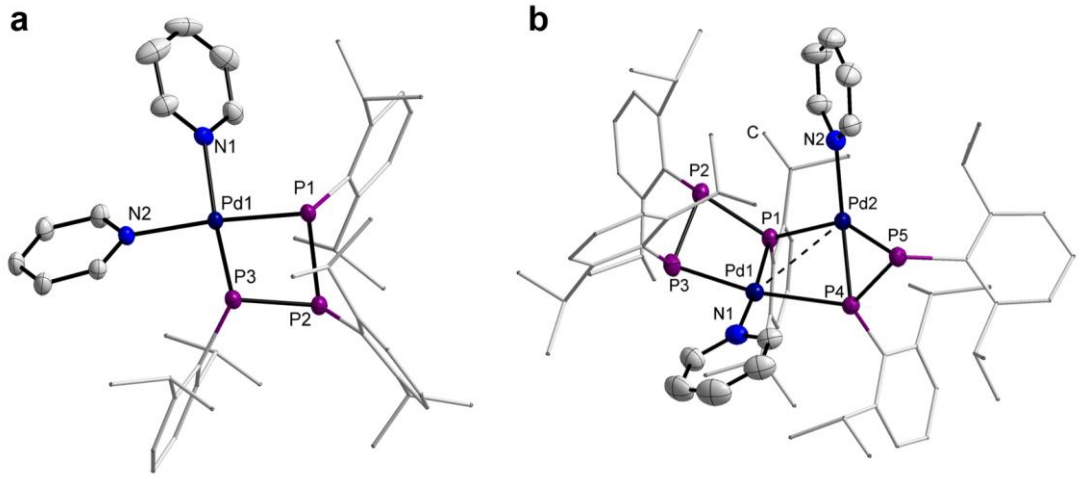

Figure 8.7: Molecular structures of a) **2** and b) **3** in the solid state. Color code: dark blue (Pd), purple (P), blue (N), grey (C).

Intrigued by the coordinative unsaturation of **1**, we tested if it was feasible to achieve further coordination to the cubic core. Exposing **1** to an atmosphere of ethylene in an *in situ* NMR experiment in C_6D_6, a shift of 4 ppm can be detected in ^{31}P NMR spectrum, affording a new singlet centered at 537 ppm; this suggests a weak coordination of ethylene to the pallada-core. A similar shift has been detected in ^{1}H NMR as well, although the number of coordinated ethylene molecules can not be determined since uncoordinated gas saturates their signal. The hypothesis of weak interaction is confirmed by the removal *in vacuum* of coordinated ethylene, which returns the starting cluster **1**.

After this experiment, we decided to test *ortho*-xylyl isocyanide (CN^{o}Xyl) as capping agent. The cubic cluster can be decorated at room temperature by one, two, or four ligands according to ^{31}P and ^{1}H NMR spectra, albeit only tetracoordinate [Pd_8(Pdip)$_6$ (CN^{o}Xyl)$_4$], called hereafter cluster **4**, has been isolated.

UV-Vis spectrum of **4** has been recorded in benzene, showing peaks at 297 nm, 431 nm and a broad shoulder around 340 nm, all red-shifted compared to **1**. Vapor diffusion of pentane into a saturated solution of **4** in benzene afforded single crystals suitable for SCXRD, presenting two molecules of benzene and one molecule of pentane co-crystallized with **4**. Interestingly, similarly to the compound reported in **Figure 8.1 c**, the Pd_8 cube of **4** is distorted in the solid-state, as reported in **Figure 8.8 a**. This cluster can be disassembled as a pair of two staggered Pd_4 tetrahedra, represented in **Figure 8.8 c** by fuchsia (Pd-Pd ≈4.20 Å) and blue (Pd-Pd ≈3.48 Å) Pd_4 tetrahedra respectively, in which the vertexes of the larger one are coordinated by the isocyanide ligands.

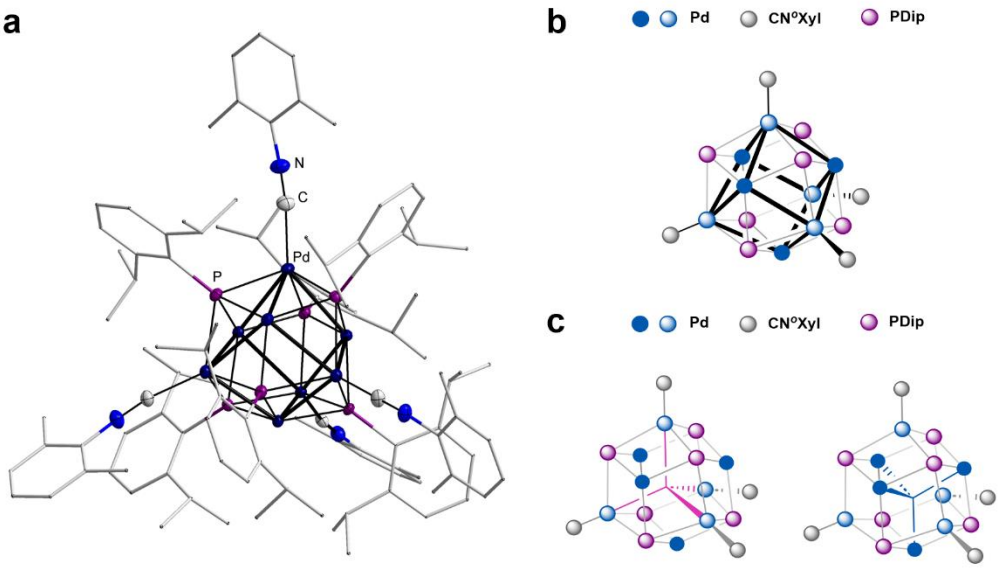

Figure 8.8: a) Molecular structure of **4** in the solid state. Color code: dark blue (Pd), purple (P), blue (N), grey (C). b) Illustration of the cluster **4**. c) Pd_4 tetrahedra in cluster **4** with Pd-Pd bonds, from left, of 4.20 Å (fuchsia) and 3.48 Å (blue).

In conclusion, upon treatment of palladium(0) precursors with the phosphinidene surrogate $(PDip)_3$, the cubic μ_4-hexaphosphinidene $[Pd_8(PDip)_6]$ cluster **1** can be isolated. This cluster has been characterized in detail by NMR, SCXRD, UV-Vis, HRMS and CV analyses. The formation of **2** and **3**, as well as cluster **1**, from (CAAC)Pd(py) complex provides insights to the cluster growth mechanism, likely led by insertion reaction of palladium precursor into the $(PDip)_3$ ring. The pallada-core has been proved to be coordinatively unsaturated, which allows the reversible coordination of ethylene. Isocyanide binding triggers structural rearrangement affording the pseudo-tetrahedral cluster **4**, with formula $[Pd_8(PDip)_6(CN^oXyl)_4]$. Albeit all reported Pd species appears as uncharged, in future XPS analysis on them will be performed to confirm the oxidation state of the palladium centers composing the cubic core.

8.3 BIBLIOGRAPHY

[1] B. Yin, Z. Luo, *Coord. Chem. Rev.* **2021**, *429*, 213643.
[2] S. Kenzler, A. Schnepf, *Chem. Sci.* **2021**, *12*, 3116–3129.
[3] H. Schnöckel, *Chem. Rev.* **2010**, *110*, 4125–4163.
[4] M. Schütz, C. Gemel, W. Klein, R. A. Fischer, T. F. Fässler, *Chem. Soc. Rev.* **2021**, *50*, 8496–8510.
[5] R. J. Wilson, N. Lichtenberger, B. Weinert, S. Dehnen, *Chem. Rev.* **2019**, *119*, 8506–8554.
[6] Y.-L. Li, H.-L. Wang, Z.-H. Zhu, F.-P. Liang, H.-H. Zou, *Coord. Chem. Rev.* **2023**, *493*, 215322.
[7] K. Tanifuji, S. Ohta, Y. Ohki, H. Seino, *Coord. Chem. Rev.* **2023**, *475*, 214838.
[8] D. A. Gálico, C. M. Santos Calado, M. Murugesu, *Chem. Sci.* **2023**, *14*, 5827–5841.
[9] J. Yano, V. Yachandra, *Chem. Rev.* **2014**, *114*, 4175–4205.
[10] C. Dong, Z. Gao, Y. Li, M. Peng, M. Wang, Y. Xu, C. Li, M. Xu, Y. Deng, X. Qin, F. Huang, X. Wei, Y.-G. Wang, H. Liu, W. Zhou, D. Ma, *Nat. Catal.* **2022**, *5*, 485–493.
[11] W. E. Kaden, T. Wu, W. A. Kunkel, S. L. Anderson, *Science* **2009**, *326*, 826–829.
[12] N. Jeddi, N. W. J. Scott, I. J. S. Fairlamb, *ACS Catal.* **2022**, *12*, 11615–11638.
[13] A. W. Cook, P. Hrobárik, P. L. Damon, G. Wu, T. W. Hayton, *Inorg. Chem.* **2020**, *59*, 1471–1480.
[14] T. N. Hooper, S. Lau, W. Chen, R. K. Brown, M. Garçon, K. Luong, N. S. Barrow, A. S. Tatton, G. A. Sackman, C. Richardson, A. J. P. White, R. I. Cooper, A. J. Edwards, I. J. Casely, M. R. Crimmin, *Chem. Sci.* **2019**, *10*, 8083–8093.
[15] T. Ishikawa, A. Kawamura, T. Sugawa, R. Moridaira, K. Yamamoto, T. Murahashi, *Angew. Chem. Int. Ed.* **2019**, *58*, 15318–15323.
[16] A. D. Burrows, J. C. Machell, D. M. P. Mingos, *J Chem Soc Dalton Trans* **1992**, 1991–1995.
[17] M. Molon, K. Dilchert, C. Gemel, R. W. Seidel, J. Schaumann, R. A. Fischer, *Inorg. Chem.* **2013**, *52*, 14275–14283.
[18] S. L. Benjamin, T. Krämer, W. Levason, M. E. Light, S. A. Macgregor, G. Reid, *J. Am. Chem. Soc.* **2016**, *138*, 6964–6967.
[19] N. Kojima, M. Kato, Y. Sunada, *Chem. Sci.* **2022**, *13*, 7610–7615.
[20] K. Nakamae, Y. Takemura, B. Kure, T. Nakajima, Y. Kitagawa, T. Tanase, *Angew. Chem.* **2015**, *127*, 1030–1035.
[21] E. G. Mednikov, N. K. Eremenko, V. A. Mikhailov, S. P. Gubin, Y. L. Slovokhotov, Y. T. Struchkov, *J. Chem. Soc. Chem. Commun.* **1981**, 989.
[22] M. Teramoto, K. Iwata, H. Yamaura, K. Kurashima, K. Miyazawa, Y. Kurashige, K. Yamamoto, T. Murahashi, *J. Am. Chem. Soc.* **2018**, *140*, 12682–12686.
[23] A. Hatano, T. Sugawa, R. Mimura, S. Kataoka, K. Yamamoto, T. Omoda, B. Zhu, Y. Tian, S. Sakaki, T. Murahashi, *J. Am. Chem. Soc.* **2023**, *145*, 15030–15035.
[24] D. Fenske, H. Fleischer, C. Persau, *Angew. Chem. Int. Ed. Engl.* **1989**, *28*, 1665–1667.
[25] L. D. Lower, L. F. Dahl, *J. Am. Chem. Soc.* **1976**, *98*, 5046–5047.
[26] D. Fenske, J. Hachgenei, F. Rogel, *Angew. Chem. Int. Ed. Engl.* **1984**, *23*, 982–983.
[27] D. Fenske, R. Basoglu, J. Hachgenei, F. Rogel, *Angew. Chem. Int. Ed. Engl.* **1984**, *23*, 160–162.
[28] D. Fenske, J. Queisser, H. Schottmüller, *Z. Für Anorg. Allg. Chem.* **1996**, *622*, 1731–1739.
[29] A. M. Geer, C. Tejel, in *Adv. Organomet. Chem.*, Elsevier, **2022**, pp. 243–330.
[30] V. J. Eilrich, E. Hey-Hawkins, *Coord. Chem. Rev.* **2021**, *437*, 213749.
[31] A. M. Geer, C. Tejel, in *Adv. Organomet. Chem.*, Elsevier, **2022**, pp. 243–330.
[32] E. A. Doud, C. J. Butler, D. W. Paley, X. Roy, *Chem. – Eur. J.* **2019**, *25*, 10840–10844.
[33] T. Wellnitz, C. Hering-Junghans, *Eur. J. Inorg. Chem.* **2021**, *2021*, 8–21.
[34] S. Nees, F. Fantuzzi, T. Wellnitz, M. Fischer, J. Siewert, J. T. Goettel, A. Hofmann, M. Härterich, H. Braunschweig, C. Hering-Junghans, *Angew. Chem. Int. Ed.* **2021**, *60*, 24318–24325.
[35] A. Schumann, F. Reiß, H. Jiao, J. Rabeah, J.-E. Siewert, I. Krummenacher, H. Braunschweig, C. Hering-Junghans, *Chem. Sci.* **2019**, *10*, 7859–7867.
[36] A. Schumann, F. Reiß, H. Jiao, J. Rabeah, J.-E. Siewert, I. Krummenacher, H. Braunschweig, C. Hering-Junghans, *Chem. Sci.* **2019**, *10*, 7859–7867.
[37] J. W. Arblaster, *Platin. Met. Rev.* **2012**, *56*, 181–189.
[38] F. Gam, J. Wei, S. Kahlal, J.-Y. Saillard, J.-F. Halet, in *50th Anniv. Electron Count. Paradig. Polyhedral Mol.* (Ed.: D.M.P. Mingos), Springer International Publishing, Cham, **2021**, pp. 69–102.
[39] J. Wei, R. Marchal, D. Astruc, S. Kahlal, J.-F. Halet, J.-Y. Saillard, *Nanoscale* **2022**, *14*, 3946–3957.
[40] W.-J. Yin, X. Gu, X.-G. Gong, *Solid State Commun.* **2008**, *147*, 323–326.
[41] A. Grünwald, B. Goswami, K. Breitwieser, B. Morgenstern, M. Gimferrer, F. W. Heinemann, D. M. Momper, C. W. M. Kay, D. Munz, *J. Am. Chem. Soc.* **2022**, *144*, 8897–8901.
[42] A. Grünwald, F. W. Heinemann, D. Munz, *Angew. Chem.* **2020**, *132*, 21274–21281.
[43] A. Grünwald, N. Orth, A. Scheurer, F. W. Heinemann, A. Pöthig, D. Munz, *Angew. Chem. Int. Ed.* **2018**, *57*, 16228–16232.
[44] J. Chu, D. Munz, R. Jazzar, M. Melaimi, G. Bertrand, *J. Am. Chem. Soc.* **2016**, *138*, 7884–7887.
[45] N. Marigo, B. Morgenstern, A. Biffis, D. Munz, *Organometallics* **2023**, *42*, 1567–1572.

9.0 CONCLUSIONS AND FUTURE PERSPECTIVES

In this PhD thesis we have performed an investigation on the direct reduction approach, aiming to synthesize novel AuNCs capped by NHCs. Following this purpose, we have synthesized a library of di-NHC- and (S)NHC-Au(I) complexes to understand which ligand proprieties were useful to stabilize gold clusters. Moreover, variations of reducing agents have been taken in account too.

Particularly interesting it is the synthesis of gold clusters capped by methyl anions, obtained when a [(di-NHC^a)Au_2Cl_2] complex, reported in **Figure 9.1**, is reduced by $NaBH_4$ in presence of DCM as solvent. We have been able to focus the synthesis towards a cluster with formula $[Au_{13}$(di-NHC$^a)_5(CH_3)_2]Cl_3$, in which coordinative Au-CH_3 bonds occur. The coordination of CH_3^-, which is unprecedented in cluster coordination chemistry, has been confirmed by high resolution mass spectrometry (HRMS) and NMR spectroscopy. We have demonstrated that imidazole-2-ylidene (NHC^a) units favor the reactivity of $[Au_{13}]^{5+}$ cluster towards the reduction of DCM promoted by $NaBH_4$, affording CH_3^- ligands bonded to the cluster core.

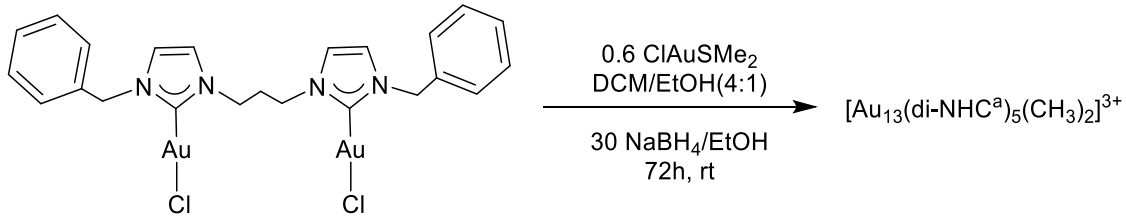

Figure 9.1: optimized synthesis of $[Au_{13}$(di-NHC$^a)_5(CH_3)_2]Cl_3$ cluster.

Despite this remarkable result, we have also proved that the direct reduction approach is not the most feasible method to get such AuNCs, since both variation of ligands and reducing agent did not generally afford AuNCs, limiting the use of such method.

Due to this, we have developed a new method to isolate AuNCs capped by PPh_3 and di-NHC ligands, exploiting the interaction of di-NHC gold(I) complexes, with general

formula [(di-NHC)Au_2Cl_2], with an [$Au_{11}(PPh_3)_8Cl_2$]Cl cluster. This reaction provides three new classes of AuNCs through a controllable reaction sequence. The synthesis involves an initial ligand metathesis reaction to produce [Au_{11}(di-NHC)$(PPh_3)_6Cl_2]^+$ (type 1 clusters), followed by a thermally induced rearrangement/metal complex addition with the formation of $[Au_{13}]^{5+}$ clusters presenting formula [Au_{13}(di-NHC)$_2(PPh_3)_4Cl_4]^+$ (type 2 clusters). Finally, an additional metathesis process yields [Au_{13}(di-NHC)$_3(PPh_3)_3Cl_3]^{2+}$ (type 3 clusters). The reaction scheme is reported in **Figure 9.2**. The electronic and steric properties of the employed di-NHC ligand affect the product distribution, leading to the isolation and full characterization of different clusters as the main product. Type 3 clusters have been also found to be strongly emissive in solution.

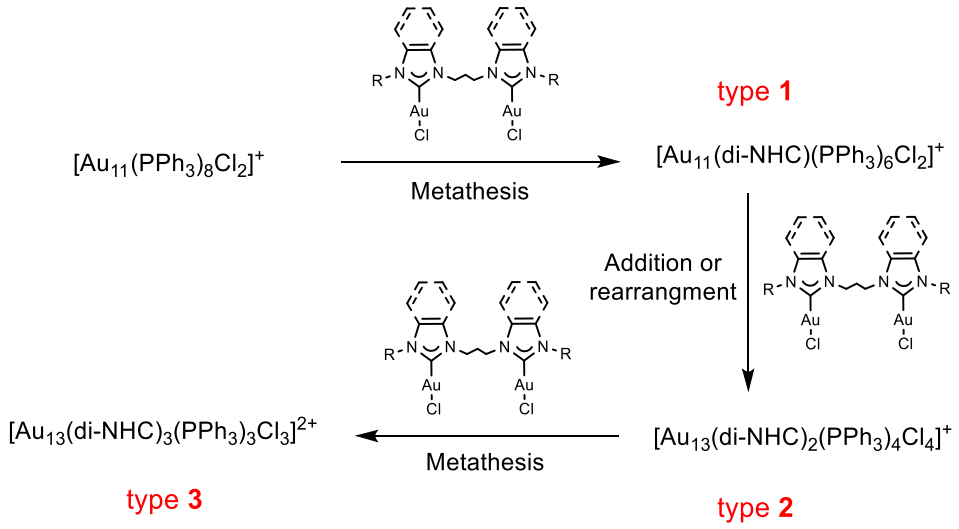

Figure 9.2: Steps involved in the stepwise process. From left, above, first metathesis affording type 1 cluster, followed by complex addition or thermal rearrangement affording type 2 cluster. Finally, the last step affords type 3 cluster, thanks to a further metathesis.

In future, this reactivity will be further exploited to get AuNCs stabilized by different di-NHCs ligands, testing the reactivity between [Au_{11}(di-NHC)$(PPh_3)_6Cl_2]^+$, derived from previous synthesis, and [(di-NHC')Au_2Cl_2] complexes. Indeed, we have already demonstrated that a cluster with formula [Au_{13}(di-NHC)$_2$(di-NHC')$_2(PPh_3)Cl_3]^{2+}$ can be obtained, expanding therefore the library of AuNCs synthesizable with our method. In

addition, we are planning to synthesize $[Au_{11}(PPh_3)_8Br_2]Br$, aiming to react it with [(S)NHC-Au-Br] complexes, obtaining therefore AuNCs capped by (S)NHCs, never reported so far.

After the synthesis of AuNCs using our stepwise approach, we have tested these clusters as anticancer pro-drugs, demonstrating that they exhibit strong anticancer efficiency. We interpret this results in terms of enhanced accumulation of the AuNCs in cancer cells, thanks to enhanced permeation and retention (EPR) effect, with subsequent slow degradation in biological environment leading to release of active species. The recorded high selectivity is promising since similar Au(I) complexes do not present the same behavior, attacking therefore both cancer and healthy cells. In the next future, we are planning to better understand the mechanism of action of our AuNCs, testing their corresponding di-NHC complexes and using the strong luminescence of type 3 cluster to understand where these AuNCs are located in the cellular system and to follow their degradation.

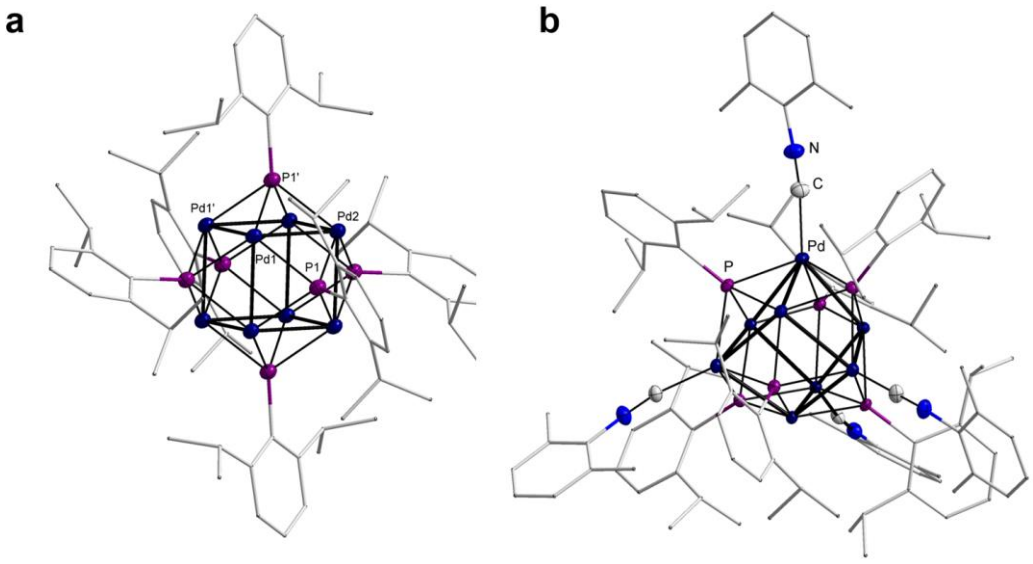

Figure 9.3: Molecular structure of a) $[Pd_8(PDip)_6]$ and b) $[Pd_8(PDip)_6(CN^oXyl)_4]$ in the solid state. Color code: dark blue (Pd), purple (P), blue (N), grey (C).

In collaboration with Prof. Munz and Prof. Kraus, we have tested one NHC ligand to stabilize gold nanowires, exploiting a ligand exchange reaction starting from oleyl ammine-stabilized AuNWs, aiming at enhancing the stability of such colloidal system. The used NHC present a long alkyl chain as wingtip group, a feature that should allow dispersion interactions between ligand and gold wires. We demonstrated that such stabilization can be obtained but affording a partial collapse of nanowires colloidal system, since the AuNWs partially aggregate after the anchoring of NHC ligands. In order to prevent this behavior, in future we are planning to use novel NHCs, presenting long chain in the backbone of the NHC scaffold, enhancing therefore the stabilization of AuNWs with formation of a larger organic protecting layer.

Finally, still in collaboration with Saarland University, we have synthesized and fully characterized an unsaturated and cubic palladium cluster capped by phosphinidene ligands, with formula $[Pd_8(PDip)_6]$. The unsaturation of such cluster has been demonstrated trough coordination of isocyanide ligands, affording $[Pd_8(PDip)_6(CN^oXyl)_4]$ as product. Both clusters are reported in **Figure 9.3**. We are currently running XPS analysis on palladium clusters to confirm the zero-valence nature of the pallada-cores.

10.0 EXPERIMENTAL SECTION

10.1 MATERIALS AND METHODS

10.1.1 MATERIALS

All analyses and operations were performed under ambient conditions unless otherwise specified. Hydrazine monohydrate, oleyl amine, triisopropylsilane, 1-dodecyl-3-methylimidazolium chloride, benzothiazole, benzimidazole, 1-benzyl imidazole, 1,3-dibromopropane, 1,3-dichloropropane, isopropyl bromide, benzyl chloride, benzyl bromide, potassium carbonate, lithium bromide, lithium chloride, (chloro)dimethylsulfide gold(I), (chloro)tetrahydrothiophene gold(I), tetrachloroauric(III) acid trihydrate, tris(dibenzylideneacetone)dipalladium(0), potassium bis(trimethylsilyl)amide, potassium hydride, sodium borohydride, deuterated sodium borohydride, metallic sodium, sodium chloride (dry), tetraethylammonium chloride monohydrate, ammonium hexafluorophosphate were purchased from Sigma-Aldrich and used as received. $[Au_{11}(PPh_3)_8Cl_2]Cl$[1], $[Au_9(PPh_3)_8](NO_3)_3$[2], benzyl iodide[3], 1-benzyl benzimidazole[4], 1-isopropyl benzimidazole[5], 1,3-di(1H-imidazol-yl)propane[6], 1,3-di(1-H-benzimidazol-yl)propane[7] together with imidazolium salts [**b**H_2]Br_2[8], [**d**H_2]Br_2[9], [**e**H_2]Br_2[10], [**f**H_2]Br_2[11], [**g**H_2]Br_2[11], [**h**H_2]Br_2[11], [**i**H_2]Br_2[11], [**I**H_2]$(PF_6)_2$[12], [**o**H]Br[13], [**p**H_2]$(BF_4)_2$[14], corresponding Au(I) complexes **b'**[8], **e'**[15], **f'**[11], **g'**[11], **h'**[11], **i'**[11], **I'**[12], **o**[16] and **p**[14] and complex $[Ag_2(di\text{-}NHC^b)_2](PF_6)_2$[17] were synthesized according to literature procedures. Hydrochloric acid (37%), hydrobromic acid (47.6%), acetone, acetonitrile (CH_3CN), dichloromethane (DCM), dichloroethane (DCE), diethyl ether (Et_2O), methanol (MeOH), isopropanol (*i*PrOH), ethanol (EtOH), *n*-hexane, cyclohexane, *n*-pentane, tetrahydrofuran (THF) and deuterated solvents were purchased from Sigma-Aldrich. Unless otherwise noted, all solvents were dry and of high purity grade and were used as received.

For the synthesis of Pd compounds **1**, **2**, **3**, **4** and the reductions of gold complexes using KH and Na/NaCl (5% w:w), all work was conducted under an atmosphere of dinitrogen, either using Schlenk-line techniques or an MBraun glovebox. Solvents were dried using a two-column solid-state purification system MBraun SPS 5/7 (MN Kieselgel 60, <0.08 mm), degassed *via* freeze-pump-thaw, and transferred to the glovebox without exposure to air. *Ortho*-difluorobenzene was dried by distillation from calcium hydride. Benzene, *n*-pentane and *n*-hexane were stored over a mirror of potassium. THF, *ortho*-difluorobenzene and diethyl ether were stored over activated 4 Å molecular sieves. Celite was dried by heating to 200 °C *in vacuo* for 48 h. NMR solvents (toluene-d_8, C_6D_6) were obtained dry and packaged under argon and stored over a mirror of potassium. Pyridine-d_5 was obtained dry and packaged under argon and stored over molecular sieves. $(PDip)_3$[18] and (^{im}CAAC)Pd(py)[19] were prepared according to the literature. All other reagents were obtained from commercial sources and used without further purification.

10.1.2 NMR SPECTROSCOPY

NMR spectra were recorded on a Bruker Avance 300 MHz (300.1 MHz for ^{1}H, 101 MHz for ^{13}C, 121.5 MHz for ^{31}P and 200 MHz for ^{19}F). The chemical shifts δ are calculated in ppm. The solvent residual signals of completely deuterated solvent molecules were used as internal reference for the ^{1}H NMR spectra and the respective carbon solvent signals for the ^{13}C NMR spectra. The multiplicities are reported as follows: singlet (s), doublet (d), triplet (t), quartet (q), quintet (qu), septuplet (st), multiplet (m), broad (br). The coupling constants (J) are reported in Hz.

For the NMR characterization of Pd compounds **1**, **2**, **3** and **4**, the ^{1}H, ^{31}P and ^{13}C NMR spectra were recorded on a Bruker Advance III HD 400 instrument operating at 400 MHz for ^{1}H, 162 MHz for ^{31}P and at 101 MHz for ^{13}C, respectively.

10.1.3 HIGH RESOLUTION MASS SPECTROMETRY

Molecular weight and elemental composition of synthesized compounds were analyzed by high-resolution mass spectrometry (HRMS) in flow injection mode (FIA – flow injection analysis). Ten microliters of each sample were injected into the FIA-HRMS system equipped with Agilent 1260 Infinity II LC System coupled to an Agilent 6545 LC/Q-TOF mass analyzer (Agilent Technologies, Palo Alto, CA, USA). The eluent was methanol at 0.5 ml/min flow rate. The MS conditions were: electrospray (ESI) ionization in positive mode, Gas Temperature 325°C, Drying Gas 5 l/min, Nebulizer 20 psi, Sheath Gas Temperature 275°C, Sheath Gas Flow 12 l/min, VCap 4000 V, Nozzle Voltage 2000 V, Fragmentor 180 V. Centroid and profile full scan mass spectra were recorded in the range 100–10000 m/z with a scan rate of 1 spectrum/s. MS/MS data were acquired in Targeted Mode with a scan rate of 1 spectrum/s, collision energy of 20 eV and Isolation Width of 4 Da. The Q-TOF calibration was daily performed with the manufacturer's solution in this mass range. The MS and MS/MS data were analyzed by the Mass Hunter Qualitative Analysis software (Agilent Technologies, Palo Alto, CA, USA).

HRMS-APPI spectrum of **1** were recorded on a Quadrupole Linear Ion Trap (QqLIT), AB Sciex API 5500 QTRAP.

10.1.4 UV-VIS SPECTROSCOPY

Absorption spectra of gold clusters were recorded dissolving them in dichloromethane, affording solutions with concentration of 10^{-4} M, and using a Perkin-Elmer λ950 or λ650 spectrophotometer. Absorption spectra of palladium clusters **1** and **4** were recorded dissolving them in benzene, affording solutions with concentration of 10^{-5} M, and using a Shimadzu UV-2600 spectrophotometer. Quartz cells with a path length of 1 cm was used in all analyses.

10.1.5 EMISSION SPECTROSCOPY

Corrected emission spectra were recorded with an Edinburgh photoluminescence spectrometer model FLS1000, with double monochromators, equipped with a 450 W Xe arc lamp as the excitation source. A photomultiplier tube R13456 with a spectral response from 185 to 980 nm was used as detector. For the emission spectra, the step and dwell time were set at 1 nm and 0.1 s, respectively, and the slit was kept at 0.1 nm and 3 nm for excitation and emission monochromators, respectively. Fluorescence Quantum yields (QY) were calculated by measuring the emission spectrum of samples dissolved in DCM in a $BaSO_4$ coated integration sphere, mounted in the FLS1000 instrument. A cuvette containing DCM solvent was used for the measurement of the reference spectrum. The excitation wavelength was fixed at 350 nm, 330 nm or 320 nm based on the sample analyzed. The emission spectra were recorded in the range 330-980 nm. The formula used for the calculation of FQY is:

$$FQY = \frac{\int I_{em,sample}}{\int I_{abs,solvent} - \int I_{abs,sample}}$$

where $\int I_{em,sample}$ is the integrated emission intensity of the sample, $\int I_{abs,sample}$ and $\int I_{abs,solvent}$ are the integrated absorption of the sample and DCM, respectively.

10.1.6 CYCLIC VOLTAMMETRY AND DIFFERENTIAL POTENTIAL VOLTAMMETRY ANALYSES

The electrochemical experiments on gold clusters were carried out in DCM (or CH_3CN) containing 0.1 M $TBAPF_6$, under an argon atmosphere, in a glass cell thermostated at 25 ± 1°C (unless otherwise specified). A 0.22 mm radius glassy carbon disk, prepared and activated as already described[20], was the working electrode, whereas a Pt wire was the counter electrode. An Ag wire was used as the quasi-reference electrode. At the end of each experiment, the potential of the latter

was calibrated against the ferricinium/ferrocene redox couple (in DCM/0.1 M TBAH, E^0 = 0.460 V against the KCl saturated calomel electrode, SCE). To minimize the ohmic drop between the working and the reference electrodes, careful feedback correction was applied. The experimental parameters were a peak amplitude of 50 mV, pulse width of 0.025 s, 4 mV increments per cycle, and pulse period of 0.05 s.

Cyclic voltammetric measurements of **1** were recorded with an EmStat^{3+} Blue potentiostat by PalmSens in a nitrogen filled glovebox, using a glassy carbon working electrode, platinum counter electrode and non-aqueous Ag/Ag^+ reference electrode as well as NBu_4PF_6 (0.2 m) as electrolyte. After the initial measurements, ferrocene was added as internal standard and the voltammograms were corrected by positioning the redox potential of ferrocene to 0 V. Compound **1** proved not soluble enough for CV in THF and is not compatible with DCM and CH_3CN. The CV was hence recorded in a saturated solution (*ca.* 10 mg of **1**) in *ortho*-difluorobenzene (4 ml), in which **1** proved at least moderately soluble.

10.1.7 MELTING POINT ANALYSIS

Melting points were determined in capillary tubes with an Electrothermal IA 9100 Melting Point Apparatus.

10.1.8 TRANSMISSION ELECTRON MICROSCOPY

Dry AuNWs and AuNPs samples were prepared by diluting AuNW and AuNP dispersions to concentrations of approximately 0.1 mg/ml and drop-casting 3 ml on a carbon-coated copper grid from Plano GmbH. All samples were characterized at an acceleration voltage of 200 kV in a JEM 2010 from JEOL GmbH.

10.1.9 BIOLOGICAL TESTS

$2 \cdot 10^3$ cells/well HCT116, MBA-MB-231, OVCAR3 and 10^4 cells/well MRC5 were seeded in 96-well plates. One day later, cells were treated using serial dilutions of drugs and viability were evaluated after 96 hours with CellTiter-Glo assay (Promega, Madison, WI, USA) with a BioTeck Synergy instrument. IC_{50} values were calculated from a dose-response curve. Averages and standard deviations were obtained from triplicates.

10.2 SYNTHESIS OF LIGAND PRECURSORS

*10.2.1 Synthesis of 1,1'-dibenzyl-3,3'-propylene-diimidazolium dibromide, [**a**H$_2$]Br$_2$*

[**a**H$_2$]Br$_2$ salt was synthesized according to a modified literature procedure.[21] A two-neck 50 ml balloon was capped with a bubble refrigerator connected with a vacuum line, filled with 1-benzyl imidazole (0.510 g, 3.22 mmol) and sealed with a silicone cap. The apparatus was disareated with three argon-vacuum cycles. 1,3-dibromopropane (140 µl, 1.38 mol) and CH_3CN (6 ml) were added. The mixture was heated under reflux in an oil bath for 48 hours. After this time, the balloon was placed in a water/ice bath for 15 minutes, after which it is possible to observe the formation of a white precipitate. The resulting solid was filtered and washed with 30 ml (3x10 ml) Et_2O. The resulting white solid was dried under vacuum to afford the product as a white powder. The ^{1}H NMR spectrum related to the product matches with the spectra reported in literature. The solid was used without further purification. Yield 450 mg (90%). ^{1}H NMR (300 MHz, DMSO-d_6): δ 9.41 (s, 2H), 7.83 (d, J = 4.65 Hz, 4H), 7.43 (m, 10H), 5.44 (s, 4H), 4.27 (t, J = 7.20 Hz, 4H), 2.42 (qu, J = 6.80 Hz, 2H).

*10.2.2 Synthesis of 1,1'-dibenzyl-3,3'-propylene-diimidazolium dichloride, [**a**H$_2$]Cl$_2$*

[**a**H$_2$]Cl$_2$ salt was synthesized according to a literature procedure.[21] A two-neck 50 ml balloon was capped with a bubble refrigerator connected with a vacuum line, filled with 1-benzyl imidazole (1.00 g, 6.32 mmol) and sealed with a silicone cap. The apparatus was disareated with three argon-vacuum cycles. 1,3-dichloropropane (300 µl, 3.15 mmol) and THF (13 ml) were added. The mixture was heated under reflux in an oil bath for 72 hours. After this time the solvent was evaporated under reduced pressure and 10 ml DCM were added. The resulting white precipitate was filtered and dried under vacuum to afford the product as a white powder. The ^{1}H NMR spectrum related to the product matches with spectra reported in literature. The solid was used

without further purification. Yield 405 mg (15%). ^{1}H NMR (300 MHz, $CDCl_3$): δ 10.49 (s, 2H), 8.20 (s, 2H), 7.40 (s, 10H), 6.99 (s, 2H), 5.41 (s, 4H), 4.71 (t, J = 6.09 Hz, 4H), 2.88 (qu, J = 7.22 Hz, 2H).

*10.2.3 Synthesis of 1,1'-dibenzyl-3,3'-propylene-dibenzimidazolium dichloride, [**b**H_2]Cl_2*

The following procedure for the preparation of [**b**H_2]Cl_2 salt was adapted from the literature.[22] A two-neck 20 ml balloon was filled with 1,3-di(1-H-benzimidazol-yl)propane (510 mg, 1.85 mmol) and sealed with a tap and a silicone cap. The apparatus was disareated with three argon-vacuum cycles. Benzyl chloride (450 µl, 3.91 mmol) and CH_3CN (3 ml) were added. The mixture was heated at 50 °C in an oil bath for 72 hours. After 24 h it was possible to notice the formation of a white precipitate. After 72 h this precipitate was filtered and washed with 20 ml (2 x 10 ml) Et_2O. The solid was dried under vacuum to afford the product as a white powder. The ^{1}H NMR spectrum related to the product matches with the spectra reported in the literature for corresponding dibromide salt. The solid was used without further purification. Yield 636 mg (65%). ^{1}H NMR (300 MHz, DMSO-d_6): δ 10.50 (s, 2H), 8.22 (d, J = 7.44 Hz, 2H), 7.97 (d, J = 8.10 Hz, 2H), 7.78-7.57 (m, 8H), 7.47-7.32 (m, 6H), 5.84 (s, 4H), 4.79 (t, J = 7.59 Hz, 4H), 2.70 (qu, J = 7.61 Hz, 2H).

*10.2.4 Synthesis of 1,1'-diisopropyl-3,3'-propylene-dibenzimidazolium dibromide, [**c**H_2]Br_2*

The following procedure for the preparation of [**c**H_2]Br_2 salt was adapted from the literature.[5] A two-neck 20 ml balloon capped with a bubble refrigerator was filled with 1-isopropyl benzimidazole (243 mg, 1.52 mmol). The apparatus was disareated with three argon-vacuum cycles. 1,3-dibromopropane (70 µl, 0.67 mmol) and CH_3CN (3 ml) were added. The mixture was heated at 90 °C in an oil bath for 72 hours. After 24 h it was possible to notice the presence of a white precipitate. After 72 h the white precipitate was filtered and washed with 3 x 10 ml toluene and 2 x 10 ml Et_2O. The

solid was dried under vacuum to afford the product as a white powder. The ^{1}H NMR spectrum related to the product matches with the spectra reported in the literature. The solid was used without further purification. Yield 201 mg (83%). ^{1}H NMR (300 MHz, $CDCl_3$): δ 11.06 (s, 2H), 8.78 (d, J = 8.13 Hz, 2H), 7.83-7.53 (m, 6H), 5.20 (t, J = 7.75 Hz, 4H), 4.89 (qu, J = 6.39 Hz, 2H), 3.08 (st, J = 7.70 Hz, 2H), 1.82 (d, J = 6.98 Hz, 12H).

*10.2.5 Synthesis of 1,1'-diisopropyl-3,3'-propylene-dibenzimidazolium di-hexafluorophosphate, [**c**H_2](PF_6)$_2$*

A one-neck 10 ml balloon was filled with [**c**H_2]Br_2 (400 mg, 0.77 mmol) and 1.5 ml MeOH and was stoppered with a silicone cap. An aqueous solution of NH_4PF_6 (428 mg, 2.32 mmol, in 1.5 ml H_2O) was prepared and added dropwise to the solution containing the imidazolium salt. The mixture was left under stirring for 2 hours. The resulting white precipitate was filtered and washed with 2 x 5 ml MeOH:H_2O (1:1 v:v) solution. The solid was dried under vacuum to afford the product as a white powder. Yield 441 mg (88%). ^{1}H NMR (300 MHz, CD_3CN): δ 9.19 (s, 2H), 7.98-7.91 (m, 4H), 7.76-7.73 (m, 4H), 5.00 (qu, J = 7.29 Hz, 2H), 4.61 (t, J = 67.49 Hz, 4H), 2.71 (st, J = 7.50 Hz, 2H), 1.71 (d, J = 6.66 Hz, 12H).

*10.2.6 Synthesis of 1-benzyl-benzothiazolium bromide, [**m**H]Br*

The following procedure for the preparation of [**m**H]Br salt was adapted from the literature.[23] A 100 ml pressure tube was filled with benzothiazole (5.81 g, 4.7 ml, 43 mmol) and benzyl bromide (7.35 g, 5.2 ml, 43 mmol) and stoppered with a Teflon cap. The mixture was heated at 90 °C in an oil bath for 48 hours. After 2 h it was possible to notice the presence of a white precipitate. After 48 h the mixture was cooled down and dissolved in MeOH (5 ml). The resulting solution was added dropwise to a solution of Et_2O (100 ml) under stirring, affording a white precipitate. The supernatant was decanted and the solid was dried under reduced pressure, affording a white powder.

The ^{1}H NMR spectrum related to the product matches with the spectra reported in the literature. The solid was used without further purification. Yield 12.75 g (96%) ^{1}H NMR (400 MHz, DMSO-d_6): δ 10.95 (s, 1H), 8.61 (d, J = 8.70 Hz, 1H), 8.35 (d, J = 8.70 Hz, 1H), 7.90-7.78 (m, 2H), 7.57-7.54 (m, 2H), 7.45-7.35 (m, 3H), 6.24 (s, 2H).

*10.2.7 Synthesis of 1-isopropyl-benzothiazolium bromide, [**n**H]Br*

The following procedure for the preparation of [**n**H]Br salt was adapted from the literature.[23] A 100 ml pressure tube was filled with benzothiazole (5.81 g, 4.7 ml, 43 mmol) and isopropyl bromide (10.6 g, 8.1 ml, 86 mmol) and stoppered with a Teflon cap. The mixture was heated at 110 °C in an oil bath for 72 hours. After 24 h it was possible to notice the presence of a red oil. After 72 h the mixture was cooled down and dissolved in MeOH (5 ml). The resulting solution was added dropwise to a solution of Et_2O (100 ml) under stirring, affording a red oil as precipitate. The supernatant was decanted and the oil was dissolved in *i*PrOH (4 ml) and placed at - 30°C for 24 h. After that time it is possible to notice the presence of crystalline yellowish powder. The supernatant was decanted and the remaining solid was dried under reduced pressure, affording a yellowish powder. The ^{1}H NMR spectrum related to the product matches with the spectra reported in the literature. The solid was used without further purification. Yield 580 mg (5%).^{1}H NMR (400 MHz, DMSO-d_6): δ 10.77 (s, 1H), 8.61 (d, J = 8.23 Hz, 1H), 8.51 (d, J = 8.23 Hz, 1H), 7.96 (t, J = 7.20, 1H), 7.88 (t, J = 7.20, 1H), 5.48 (st, J = 6.60 Hz, 1H), 1.71 (d, J = 6.96 Hz, 6H).

10.2.8 Synthesis of 1,3-bis(4,5-dicyanoimidazole)propane

The following procedure for the preparation of 1,3-bis(4,5-dicyanoimidazole)propane salt was adapted from the literature.[24] 4,5-dicyanoimidazole (2.54 g, 21.5 mmol) and potassium carbonate (3.17 g, 22.9 mmol) were added into a three-necks round bottom flask. The necks were closed with two silicon plugs and a condenser, and the latter capped with a vacuum tap. The apparatus was disareated with three argon-vacuum

cycles and then 50 ml of dry CH_3CN were added, followed by 1.16 ml (2.31 g, 1.4 mmol) of 1,3-dibromopropane. The reaction was heated to reflux (90°C) using an oil bath and kept under stirring for 24 h. The reaction apparatus was then cooled down and the reaction mixture was filtered. The filtrate was evaporated under vacuum and the resulting yellowish oil was redissolved in CH_3CN. The obtained solution was added dropwise under stirring to Et_2O (200 ml), giving an ivory solid. The ^1H NMR spectrum related to the product matches with the spectra reported in the literature Yield: 2.64 g (87%). ^1H NMR (300 MHz, acetone-d_6): 8.28 (s, 2H), 4.6 (t, J = 4.06 Hz, 4H), 2.75 (st, J = 7.40 Hz, 2H).

10.2.9 Attempts of functionalization of 1,3-bis(4,5-dicyanoimidazole)propane

Aiming at functionalizing 1,3-bis(4,5-dicyanoimidazole)propane (CN-Imz), several electrophilic molecules, such as benzyl chloride, benzyl bromide and benzyl iodide[3], were used, extensively varying the reaction conditions too. In these tests the reactions were performed in *neat* conditions, therefore using electrophiles as solvent. No one of these reactions provided satisfactory results, despite in some cases partial mono-substituted product was detected using ^1H NMR spectroscopy. Also using stronger electrophiles, such as benzyl trifluoromethanesulfonate (BnOTf) formed *in situ* from benzyl alcohol, trifluoromethanesulfonic acid, and 1,8-bis(dimethylamino)naphthalen in CH_2Cl_2, did not allow the isolation of desired di-imidazolium salt. The reaction conditions used in these tests are reported in **Table 10.1**.

Table 10.1: reaction conditions used in the attempts of functionalization of 1,3-bis(4,5-dicyanoimidazole)propane (CN-Imz) using different benzylic electrophiles. All reactions were performed in neat conditions. In (*) CH_2Cl_2 was used as solvent.

	CN-Imz (g)	Electrophiles (g)	Time (h)	Temperature (°C)
benzyl bromide	1.00	0.52	24	130
benzyl chloride	1.00	0.70	24	120
benzyl iodide	1.00	1.00	24	150
*BnOTf	0.14	1.80	96	-80; rt

10.2.10 Characterization of ligand precursors

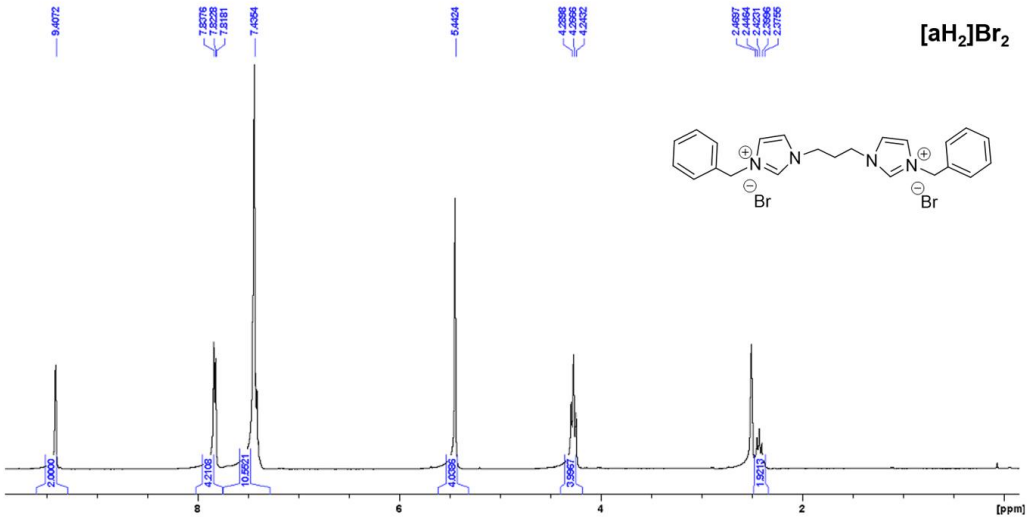

Figure 10.1: ^{1}H NMR spectrum of [**a**H_2]Br_2 in DMSO-d_6.

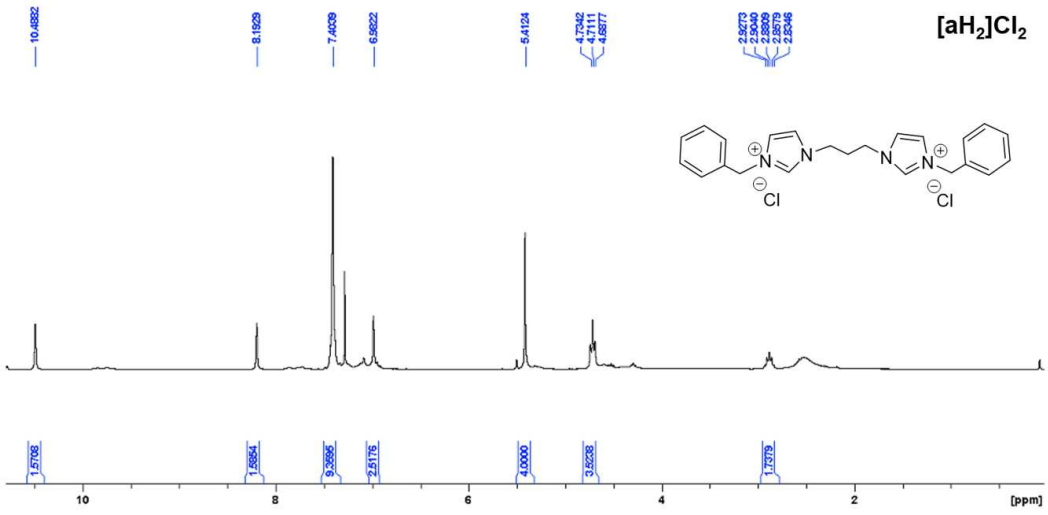

Figure 10.2: ^{1}H NMR spectrum of [**a**H_2]Cl_2 in $CDCl_3$.

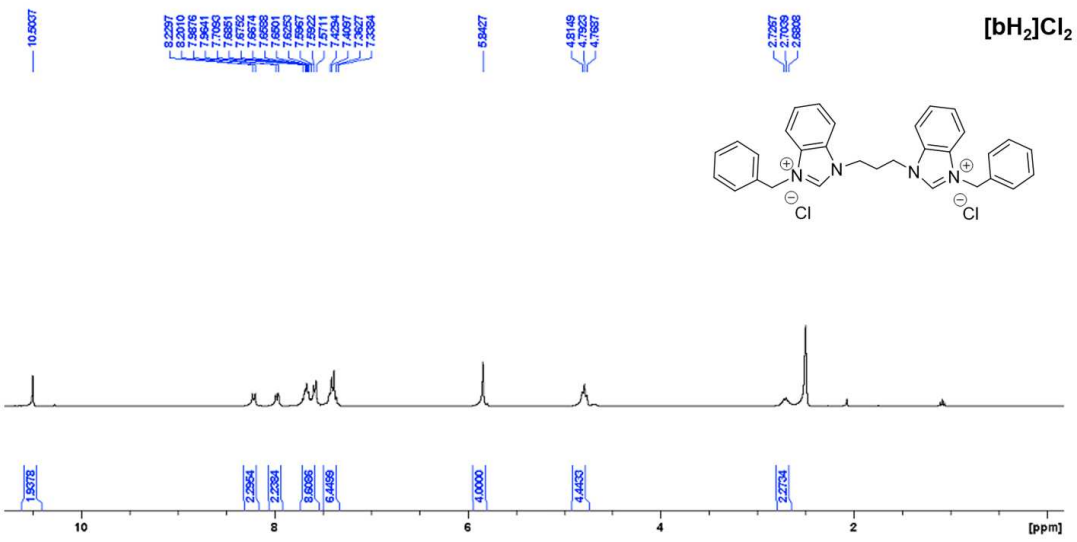

Figure 10.3: ^{1}H NMR spectrum of [**b**H_2]Cl_2 in DMSO-d_6.

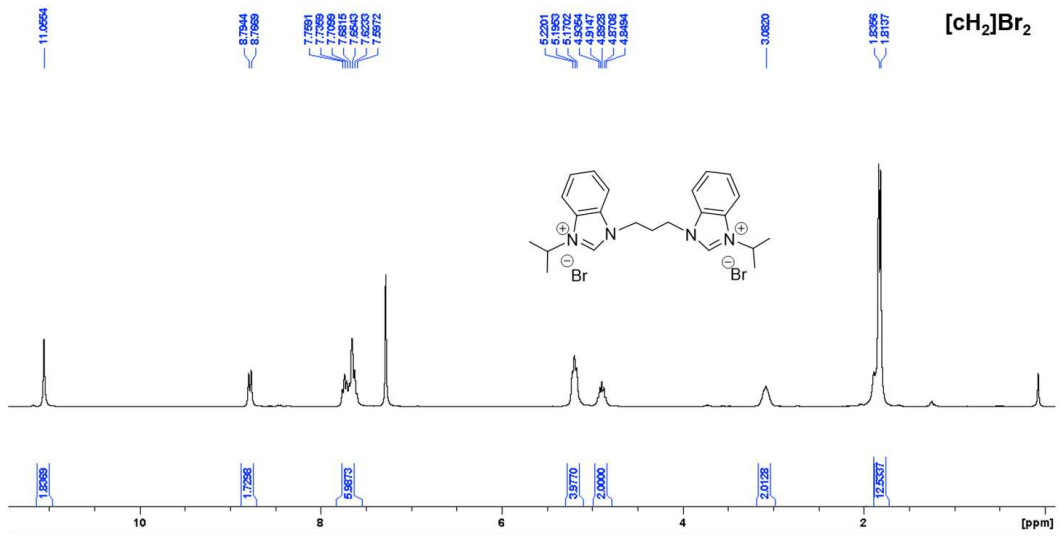

Figure 10.4: ^{1}H NMR spectra of [**c**H_2]Br_2 in $CDCl_3$.

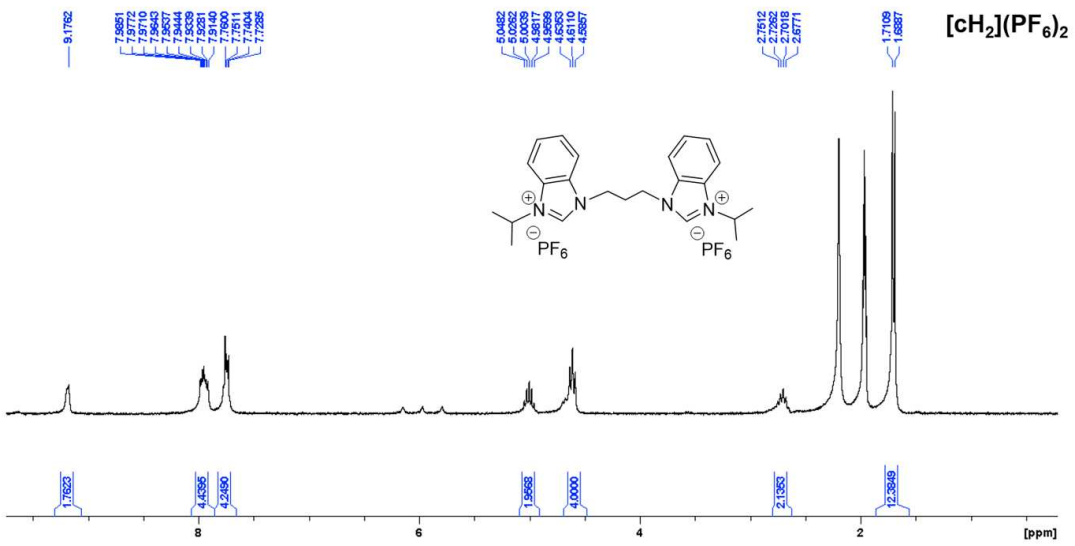

Figure 10.5: ^{1}H NMR spectra of [**c**H_2](PF_6)$_2$ in CD_3CN.

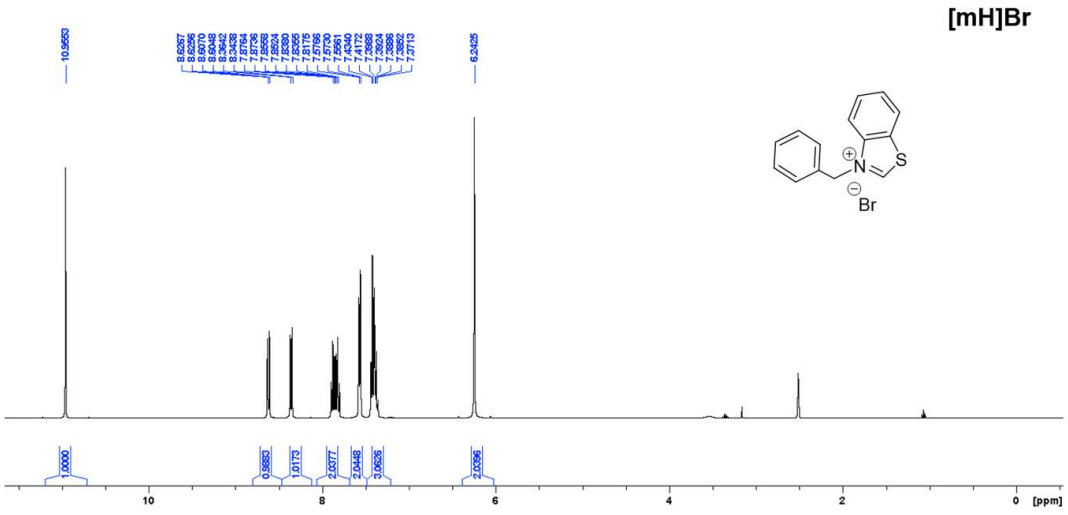

Figure 10.6: ^{1}H NMR spectra of [**m**H]Br in DMSO-d_6.

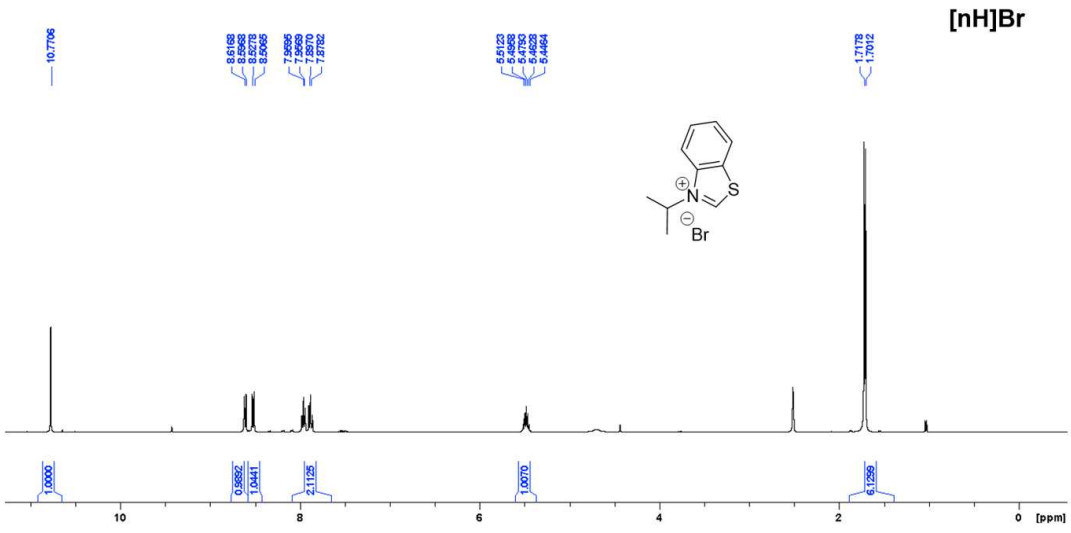

Figure 10.7: ^{1}H NMR spectra of [**n**H]Br in DMSO-d_6.

10.3 SYNTHESIS OF GOLD COMPLEXES

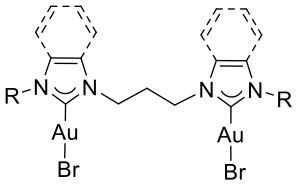

a' R: Bn, imidazole
b' R: Bn, benzimidazole
c' R: *i*Pr, benzimidazole
d' R: *i*Pr, imidazole
e' R: Me, imidazole

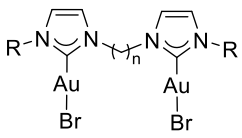

f' n:1; R: Dip
g' n:3; R: Dip
h' n:1; R: Mes
i' n:3; R: Mes

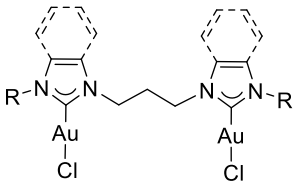

a R: Bn, imidazole
b R: Bn, benzimidazole
c R: *i*Pr, benzimidazole

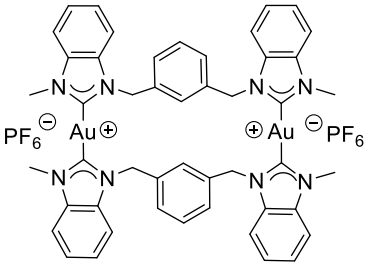

l'

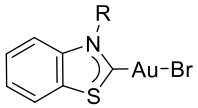

m R: Bn
n R: *i*Pr

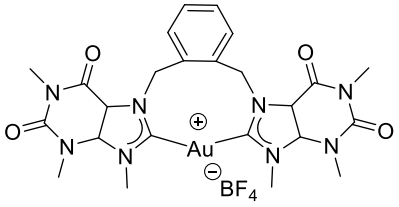

p

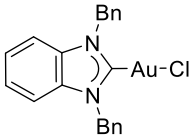

o

Figure 10.8: Au(I) complexes used in this work. Abbreviations: benzyl (Bn), isopropyl (*i*Pr), methyl (Me), 2,6-di-isopropyl-phenyl (Dip), 2,4,6-tri-methyl-phenyl (Mes).

*10.3.1 Synthesis of complex **a'***

A two-neck 25 ml balloon was filled with (chloro)dimethylsulfide gold(I) (213 mg, 0.72 mmol), [**a**H_2]Br_2 (176 mg, 0.34 mmol), K_2CO_3 (1.040 g, 7.52 mmol) and LiBr (163 mg, 1.88 mmol). The balloon was stoppered with a tap and a silicone cap. The apparatus was disareated with three argon-vacuum cycles and CH_3CN (14 ml) was added. The mixture was heated at 60 °C in an oil bath for 16 hours. The mixture was filtered and washed with 2 x 10 ml CH_3CN. The filtrate and washing solutions were combined and the solution was concentrated under vacuum to *ca.* 2 ml. The resulting solution was added dropwise to a solution of Et_2O under stirring, forming a white precipitate. The supernatant was decanted and the solid was dried under reduced pressure, affording a white powder. The ^{1}H NMR spectrum related to the product matches with the spectra reported in the literature.[25] Yield 222 mg (72%). ^{1}H NMR (300 MHz, $CDCl_3$): δ 7.38 (s, 10H), 7.06 (d, J = 1.89 Hz, 4H), 6.94 (d, J = 1.89 Hz, 4H), 5.47 (s, 4H), 4.28 (t, J = 6.65 Hz, 4H), 2.51 (qu, J = 6.68 Hz, 2H). Elemental analysis calc (%) for $C_{23}H_{24}N_4Br_2Au_2$: C 30.35, H 2.66, N 6.16; found: C 30.94, H 2.68, N 6.20.

*10.3.2 Synthesis of complex **a***

A two-neck 25 ml balloon was filled with (chloro)dimethylsulfide gold(I) (69 mg, 0.24 mmol), [**a**H_2]Cl_2 (50 mg, 0.12 mmol), K_2CO_3 (320 mg, 2.31 mmol), LiCl (50 mg, 1.18 mmol) and stoppered with a tap and a silicon cap. The apparatus was disareated with three argon-vacuum cycles and CH_3CN (3 ml) was added. The mixture was heated at 60 °C in an oil bath for 16 hours. The mixture was filtered and washed with 2 x 10 ml CH_3CN. The filtrate and washing solutions were combined and concentrated under vacuum to *ca.* 1 ml. 25 ml Et_2O were then added dropwise to the DCM solution to produce a white precipitate. The solid was filtered and dried under vacuum to afford the product as a white powder. The ^{1}H NMR spectrum related to the product matches with the spectra reported in the literature.[25] Yield 52.6 mg (44%). ^{1}H NMR (300 MHz,

$CDCl_3$): δ 7.37 (m, 10H), 7.07 (d, J = 1.80 Hz, 2H), 6.93 (d, J = 1.81 Hz, 2H), 5.44 (s, 4H), 4.28 (t, J = 6.50 Hz, 4H), 2.51 (qu, J = 6.93 Hz, 2H). Elemental analysis calc (%) for $C_{23}H_{24}N_4Cl_2Au_2$: C 33.64, H 2.95, N 6.82; found: C 33.30, H 3.12, N 6.68.

*10.3.3 Synthesis of complex **b***

A two-neck 25 ml balloon was filled with (chloro)dimethylsulfide gold(I) (72 mg, 0.24 mmol), [**b**H_2]Cl_2 (63 mg, 0.12 mmol), K_2CO_3 (320 mg, 2.31 mmol), LiCl (50 mg, 1.2 mmol) and stoppered with a tap and a silicon cap. The apparatus was disareated with three argon-vacuum cycles and CH_3CN (3 ml) was added. The mixture was heated at 60 °C in an oil bath for 16 hours. The mixture was filtered and washed with 2 x 10 ml CH_3CN. The complex was extracted from the filtered solid using 10 ml DCM. The resulting DCM solution was subsequently concentrated to *ca.* 1 ml under vacuum. 25 ml Et_2O were added dropwise to produce a white precipitate. The solid was dried under vacuum to afford the product as a white powder. The ^{1}H NMR spectrum related to the product matches with the spectra reported in the literature.[26] Yield 73.7 mg (69%). ^{1}H NMR (300 MHz, $CDCl_3$): δ 7.60-7.24 (m, 18H), 5.78 (s, 4H), 4.71 (t, J = 7.66 Hz, 4H), 2.82 (q, J = 7.67 Hz, 2H). Elemental analysis calc (%) for $C_{31}H_{28}N_4Cl_2Au_2$: C 40.41, H 3.06, N 6.08; found: C 40.21, H 3.50, N 5.89.

*10.3.4 Synthesis of complex **c'***

A two-neck 25 ml balloon was filled with (chloro)dimethylsulfide gold(I) (41 mg, 0.14 mmol), [**c**H_2]Br_2 (36 mg, 0.070 mmol), K_2CO_3 (261 mg, 1.89 mmol) and LiBr (42 mg, 0.48 mmol). The balloon was stoppered with a tap and a silicone cap. The apparatus was disareated with three argon-vacuum cycles and CH_3CN (5 ml) was added. The mixture was heated at 60 °C in an oil bath for 16 hours. The mixture was filtered and washed with 2 x 10 ml CH_3CN. The filtrate and washing solutions were combined and the solvent was evaporated under vacuum to obtain a green solid residue. The residue was dispersed in 5 ml DCM and the obtained solution was filtered through a

PTFE filter. The solvent was evaporated under reduced pressure and the solid residue was taken up in 1 ml DCM. The DCM solution was added dropwise to 25 ml of *n*-hexane to produce a white precipitate. The solid was filtered and dried under vacuum to afford the product as a white powder. Yield 48.4 mg (78%). ^{1}H NMR (300 MHz, $CDCl_3$): δ 7.75-7.60 (m, 4H), 7.57-7.40 (m, 4H), 5.42 (qu, J = 6.50 Hz, 2H), 4.68 (t, J = 6.96 Hz, 4H), 2.73 (st, J = 8.05 Hz, 2H), 1.74 (d, J = 6.72 Hz, 12H). ^{13}C NMR (101 MHz, DMSO-d_6): δ 179.77 ($C^{carbene}$), 134.33 ($CH^{benzimidazole}$), 132.90 ($CH^{benzimidazole}$), 125.94 ($CH^{benzimidazole}$), 125.75 ($CH^{benzimidazole}$), 114.71 ($CH^{benzimidazole}$), 113.76 ($CH^{benzimidazole}$), 54.24 ($\underline{CH_2}CH_2\underline{CH_2}$), 47.21 ($CH_2\underline{CH_2}CH_2$), 31.12 ($CH^{iPr}$), 23.13 ($CH_3^{iPr}$). Elemental analysis calc (%) for $C_{23}H_{28}N_4Br_2Au_2$: C 30.22, H 3.09, N 6.13; found: C 30.09, H 3.21, N 5.95.

10.3.5 Synthesis of complex ***c***

A two-neck 25 ml balloon was filled with (chloro)dimethylsulfide gold(I), (145 mg, 0.49 mmol), [**c**H_2]$(PF_6)_2$ (150 mg, 0.23 mmol), K_2CO_3 (696 mg, 5.04 mmol), $NEt_4Cl{\cdot}H_2O$ (91 mg, 0.50 mmol) and stoppered with a tap and a silicon cap. The apparatus was disareated with three argon-vacuum cycles and CH_3CN (8 ml) was added. The mixture was heated at 60 °C in an oil bath for 16 hours. The mixture was filtered and washed with 2 x 10 ml CH_3CN. The filtrate and washing solutions were combined and the solvent was evaporated under vacuum to obtain a green solid residue. 40 ml of MeOH were added and the resulting mixture was left under stirring for 10 minutes. The insoluble solid was filtered and dried under reduced pressure to afford the product as a brownish solid. The ^{1}H NMR spectrum related to the product matches with the spectra reported in **Paragraph 10.3.5** for corresponding dibromide complex **c'**. Yield 37.3 mg (20%).^{1}H NMR (300 MHz, $CDCl_3$): δ 7.66-7.57 (m, 4H), 7.55-7.37 (m, 4H), 5.44 (q, J = 6.57 Hz, 2H), 4.66 (t, J = 6.75 Hz, 4H), 2.71 (st, J = 7.94 Hz, 2H), 1.75 (d, J = 6.76 Hz, 12H). Elemental analysis calc (%) for $C_{23}H_{28}N_4Cl_2Au_2$: C 33.47, H 3.42, N 6.79; found: C 33.68, H 3.71, N 7.01.

*10.3.6 Synthesis of complex **m***

A two-neck 25 ml balloon was filled with (chloro)tetrahydrothiophene gold(I) (92 mg, 0.29 mmol), [**m**H]Br (80 mg, 0.26 mmol), K_2CO_3 (724 mg, 5.24 mmol) and LiBr (228 mg, 2.62 mmol). The balloon was stoppered with a tap and a silicone cap. The apparatus was disareated with three argon-vacuum cycles and CH_3CN (10 ml) was added. The mixture was heated at 60 °C in an oil bath for 2 hours. The mixture was filtered and washed with 2 x 10 ml CH_3CN. The filtrate and washing solutions were combined and the solvent was evaporated under vacuum to obtain a solid residue. The residue was dispersed in 2 ml DCM, loaded to a pad of silica and the product was eluted using DCM. The purified solution was collected and dried under vacuum, affording a white solid. Yield 40.2 mg (30%). Crystals suitable for single crystal X-ray diffractometric analysis were obtained through diffusion of Et_2O vapour into a DCM solution of the complex, after 3 days. ^{1}H NMR (400 MHz, CD_2Cl_2): δ 7.77 (d, J = 8.14 Hz, 1H), 7.63 (d, J = 8.14 Hz, 1H), 7.5 (m, 2H), 7.28 (br, 5H), 5.98 (s, 2H). ^{13}C NMR (101 MHz, CD_2Cl_2): δ 204.97 ($C^{carbene}$), 142.18 (C^{Ph}), 133.57 (C^{CN}), 133.52 (C^{CS}), 129.15 (CH^{Ph}), 128.88 (CH^{Ph}), 128.11 (CH^{Ph}), 126.96 ($CH^{benzothiazole}$), 126.53 ($CH^{benzothiazole}$), 122.91 ($CH^{benzothiazole}$), 115.88 ($CH^{benzothiazole}$), 59.33 (CH_2). ESI-MS calc $[M\text{-}Na]^+$ 523.93, found $[M\text{-}Na]^+$ 523.93. Elemental analysis calc (%) for $C_{14}H_{11}NSBrAu$: C 33.48, H 2.21, N 2.79; S 6.39 found: C 34.01, H 2.58, N 2.95, S 6.25.

*10.3.7 Synthesis of complex **n***

A two-neck 25 ml balloon was filled with (chloro)tetrahydrothiophene gold(I) (39 mg, 0.12 mmol), [**n**H]Br (30 mg, 0.12 mmol), K_2CO_3 (321 mg, 2.32 mmol) and LiBr (50.4 mg, 0.58 mmol). The balloon was stoppered with a tap and a silicone cap. The apparatus was disareated with three argon-vacuum cycles and CH_3CN (10 ml) was added. The mixture was heated at 60 °C in an oil bath for 6 hours. The mixture was filtered and washed with 2 x 10 ml CH_3CN. The filtrate and washing solutions were

combined and the solvent was evaporated under vacuum to obtain *ca.* 1 ml of a green solution. 110 ml of Et_2O were added and the resulting mixture was left under stirring for 10 minutes. The dispersion was filtered on pad of celite and the filtrate slowly dried under vacuum, affording the product as white powder. Yield 30.0 mg (57%). Crystals suitable for single crystal X-ray diffractometric analysis were obtained from a saturated solution in CH_3CN placed at -30°C for 3 days. ^1H NMR (400 MHz, DMSO-d_6): δ 8.36 (d, J = 8.51 Hz, 1H), 8.27 (d, J = 8.51 Hz, 1H), 7.79-7.77 (m, 2H), 5.78 (st, J = 7.74 Hz, 1H), 1.86 (d, J = 6.75 Hz, 6H). ^{13}C NMR (101 MHz, DMSO-d_6): δ 199.54 ($C^{carbene}$), 142.56 (C^{CN}), 133.16 (C^{CS}),128.62 ($CH^{benzothiazole}$), 127.20 ($CH^{benzothiazole}$), 124.01 ($CH^{benzothiazole}$), 116.91 ($CH^{benzothiazole}$), 49.08 ($CH^{i Pr}$), 22.92 ($CH_3{}^{i Pr}$). ESI-MS calc $[M-H]^+$ 453.95, found $[M-H]^+$ 453.95. Elemental analysis calc (%) for $C_{10}H_{11}NSBrAu$: C: 26.45; H: 2.44; N: 3.08; S: 7.06 found C: 26.38; H: 2.53; N: 3.06; S: 7.40.

10.3.8 Characterization of Au(I) complexes

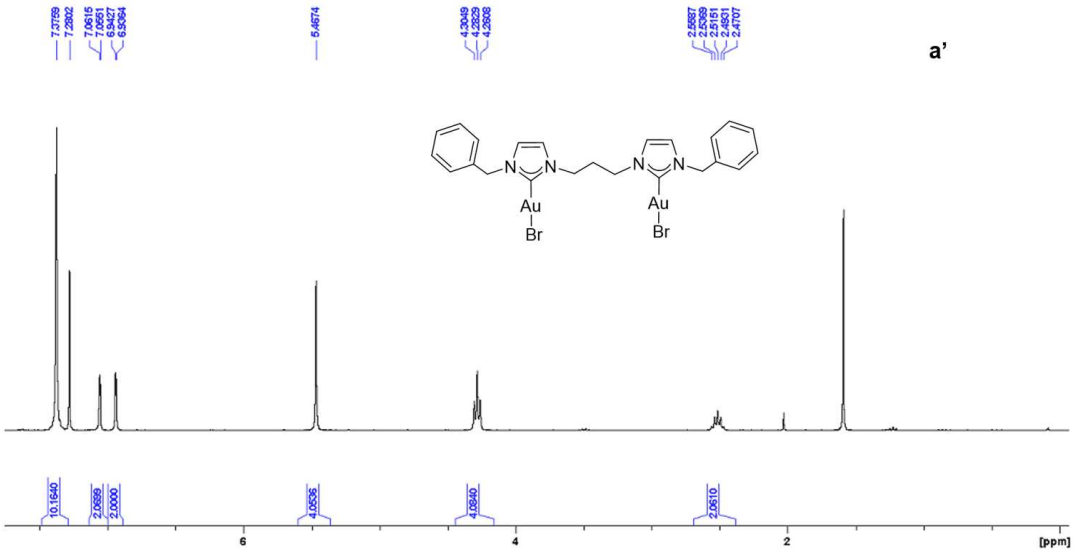

Figure 10.9: ^{1}H NMR spectrum of **a'** in $CDCl_3$.

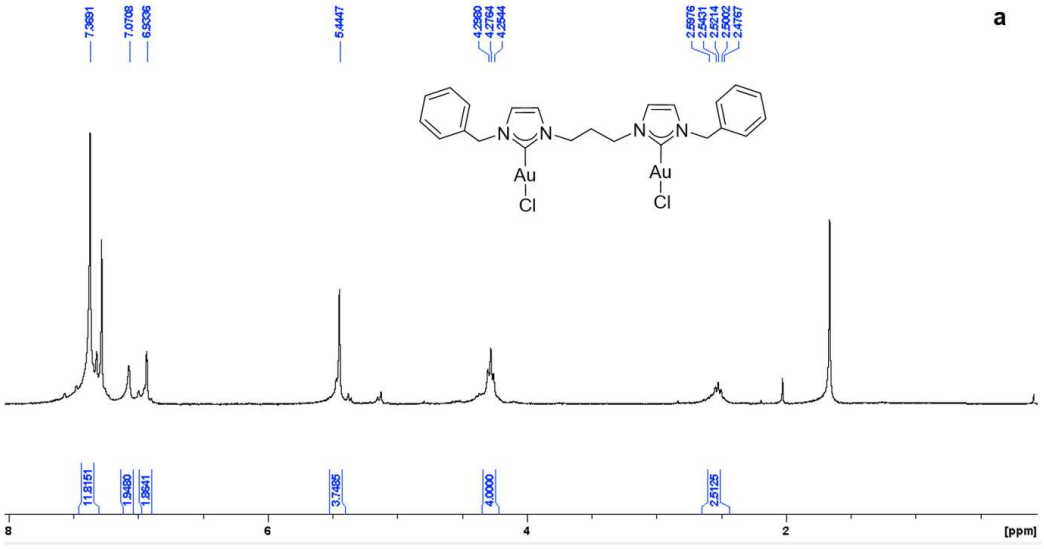

Figure 10.10: ^{1}H NMR spectrum of **a** in $CDCl_3$.

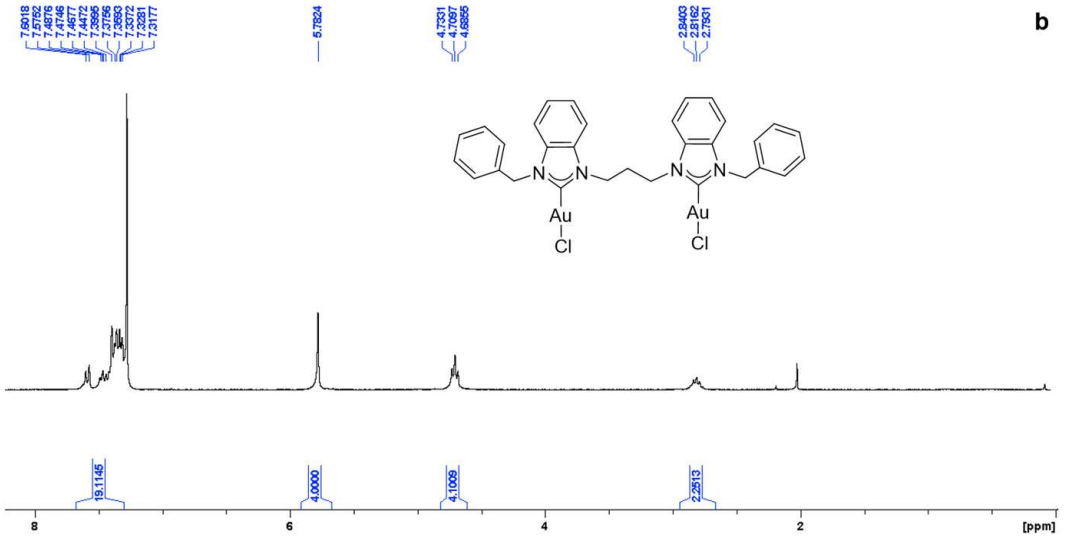

Figure 10.11: ^{1}H NMR spectrum of **b** in $CDCl_3$.

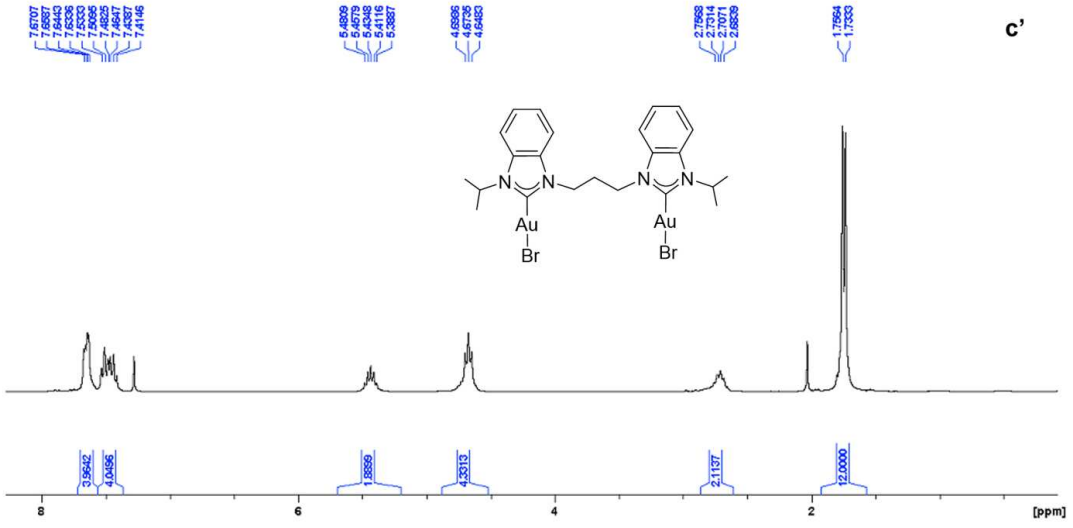

Figure 10.12: ^{1}H NMR spectra of **c'** in $CDCl_3$.

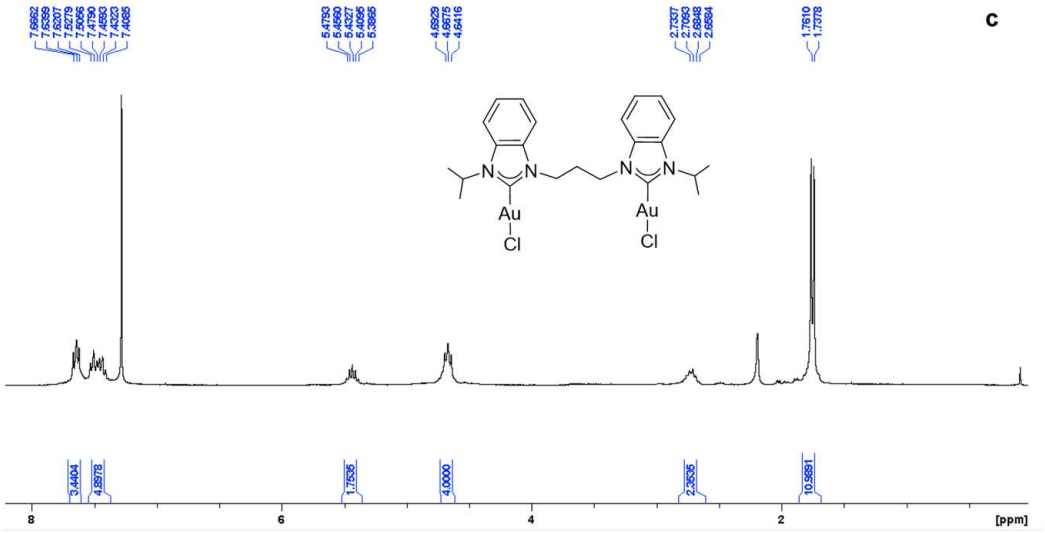

Figure 10.13: ^{1}H NMR spectra of **c** on $CDCl_3$.

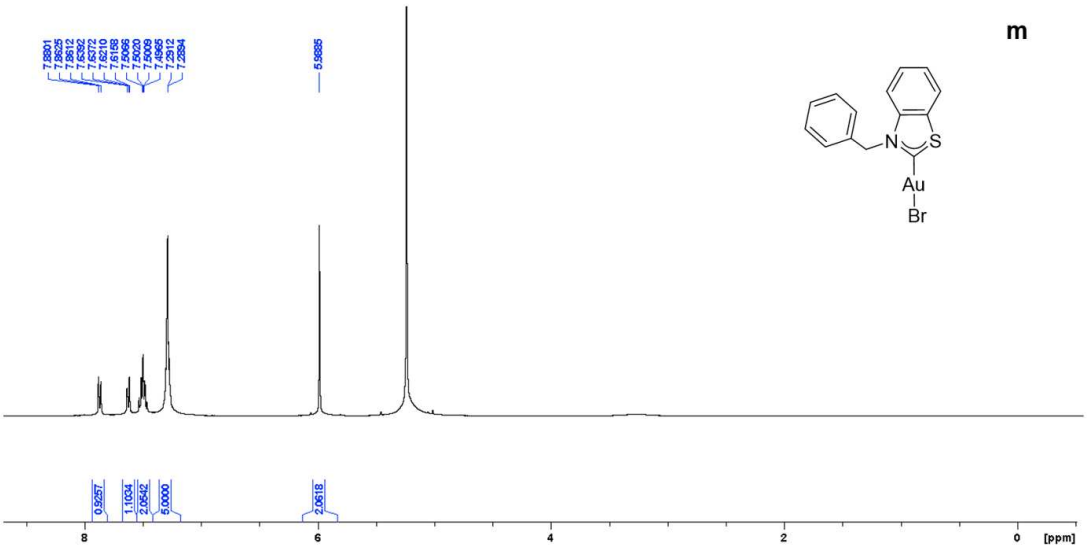

Figure 10.14: ^{1}H NMR spectra of **m** in CD_2Cl_2.

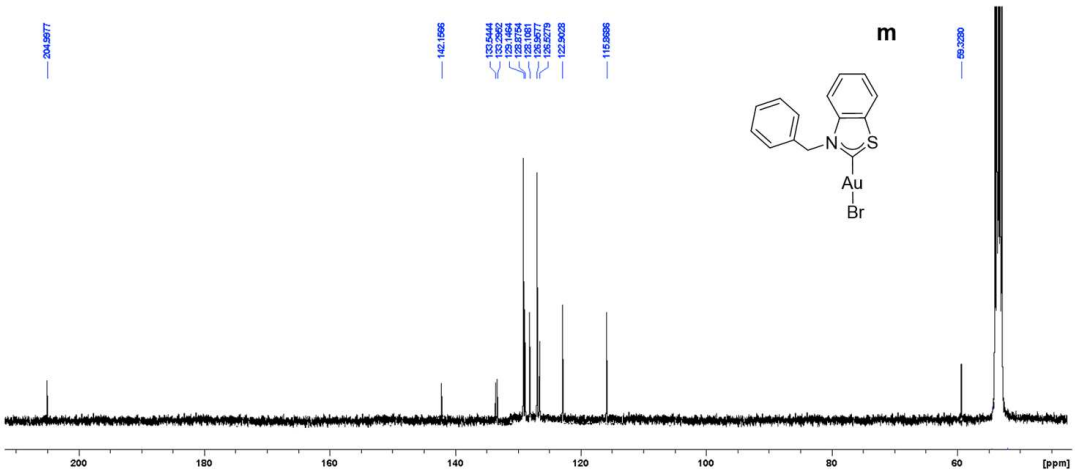

Figure 10.15: ^{13}C NMR spectra of **m** in CD_2Cl_2.

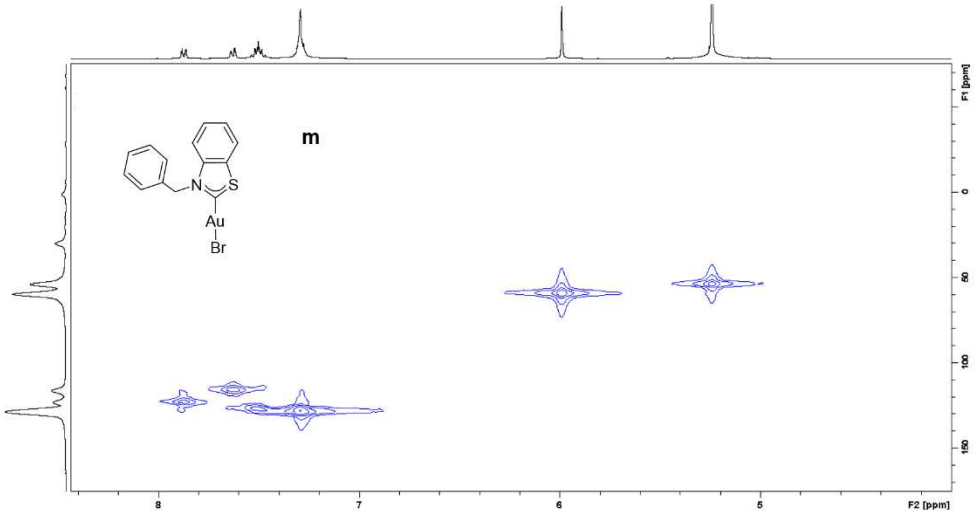

Figure 10.16: HMCQ (^1H,^{13}C) NMR spectra of **m** in CD_2Cl_2.

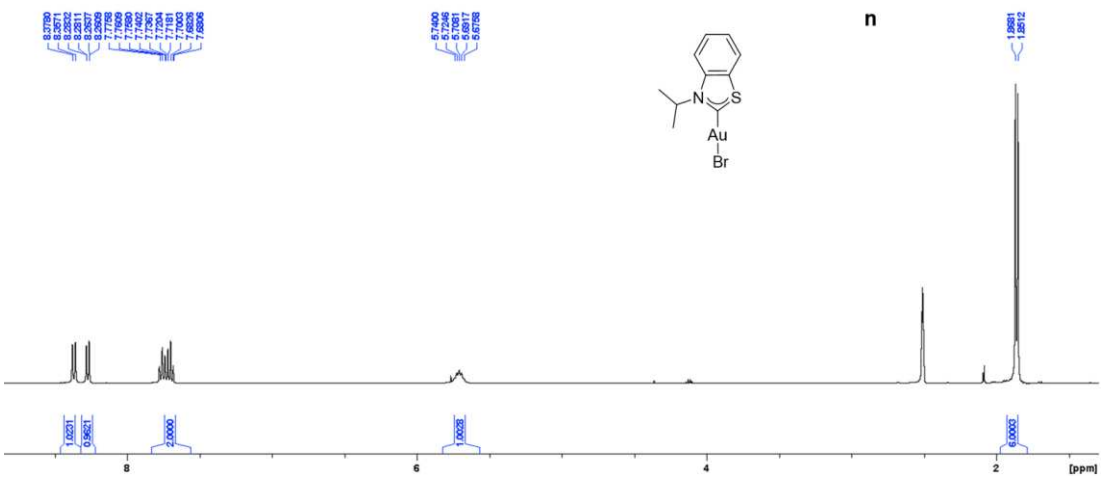

Figure 10.17: ^{1}H NMR spectra of **n** in DMSO-d_6.

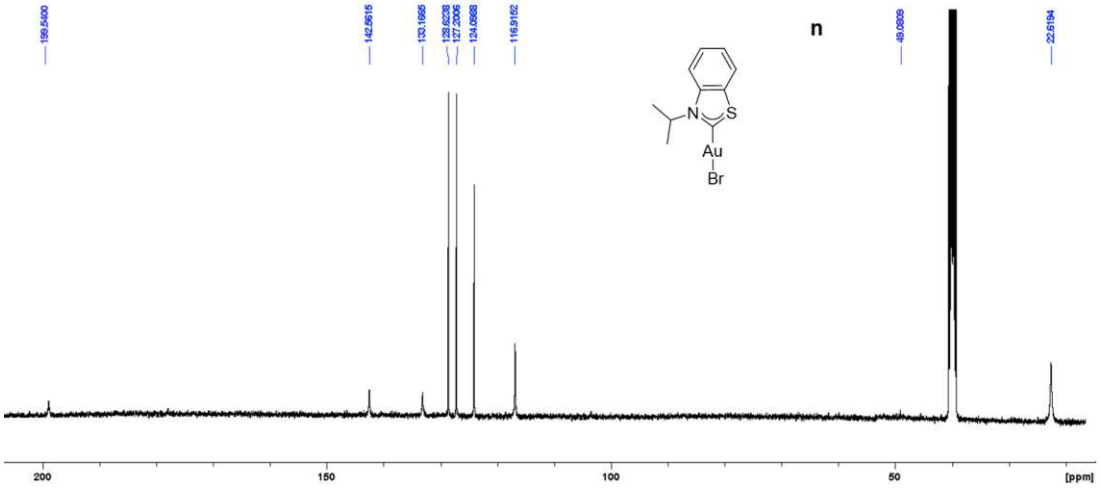

Figure 10.18: ^{13}C NMR spectra of **n** in DMSO-d_6.

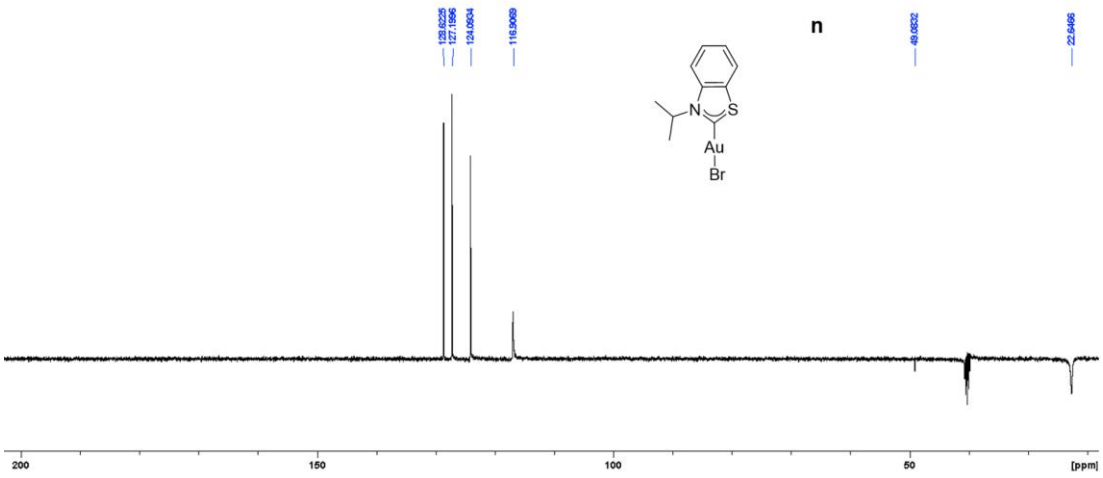

Figure 10.19: DEPT NMR spectra of **n** in DMSO-d_6.

*10.3.9 Single crystal X-ray diffractometry of **m** and **n** complexes*

The crystallographic data for compounds **m** and **n** were obtained by mounting well-formed single crystals on a glass fiber and transferring them in Fomblin YR-1800 perfluoro ether (Alfa Aesar) at ambient temperature. The samples **m** and **n** were cooled to 150(2) and 143(2) K during measurement, respectively. The data were collected on a Bruker D8 Venture diffractometer using monochromated MoKα and a Photon II detector. The structures were solved by intrinsic phasing (SHELXT)[27] and refined by full matrix least squares procedures (SHELXL)[27] with the Olex2[28] or ShelXle[29] platform, respectively. Semi-empirical absorption corrections (multiscan and additional spherical absorption correction) were applied to the diffraction data recorded using the SADABS application within the APEX4 platform.[30] All non-hydrogen atoms were refined anisotropically, hydrogen atoms were included in the refinement at calculated positions using a riding model. A summary on standard crystallographic parameters is subsequently provided in **Table10.2**.

Table 10.2: crystallographic data of **m** and **n** complexes.

name	**m**	**n**
Empirical formula	$C_{14}H_{11}NSBrAu$	$C_{10}H_{11}NSBrAu$
Formula weight	502.17	454.13
Temperature/K	152(2)	143(2)
Crystal system	orthorhombic	monoclinic
Space group	$P2_12_12_1$	$P2_1/n$
a/Å	4.6807(2)	8.5999(2)
b/Å	16.3340(6)	11.7998(4)
c/Å	17.2203(6)	12.1579(4)
α/°	90	90
β/°	90	110.5080(10)
γ/°	90	90
Volume/Å^3	1316.57(9)	1155.56(6)
Z	4	4
ρ_{calc}g/cm^3	2.533	2.610
μ/mm^{-1}	14.346	16.329
F(000)	928.0	832.0
Crystal size/mm^3	0.4 × 0.2 × 0.02	0.22 × 0.2 × 0.12
Radiation	MoKα (λ = 0.71073)	MoKα (λ = 0.71073)
2Θ range for data collection/°	3.436 to 61.436	4.972 to 65.23
Index ranges	-6 ≤ h ≤ 6, -23 ≤ k ≤ 23, -24 ≤ l ≤ 24	-13 ≤ h ≤ 13, -17 ≤ k ≤ 17, -18 ≤ l ≤ 18
Reflections collected	31967	64690
Independent reflections	4093 [R_{int} = 0.0361, R_{sigma} = 0.0195]	4212 [R_{int} = 0.0597, R_{sigma} = 0.0219]
Data/restraints/parameters	4093/0/164	4212/0/130
Goodness-of-fit on F^2	1.050	1.115
Final R indexes [I>=2σ (I)]	R_1 = 0.0222, wR_2 = 0.0644	R_1 = 0.0197, wR_2 = 0.0473
Final R indexes [all data]	R_1 = 0.0230, wR_2 = 0.0648	R_1 = 0.0211, wR_2 = 0.0478
Largest diff. peak/hole / e Å^{-3}	1.16/-2.37	2.03/-1.46
Flack parameter	0.484(13)	

$R1 = \sum|Fo - Fc|/\sum(Fo)$; $wR2 = [\sum[w(Fo^2 - Fc^2)^2]/\sum[w(Fo^2)^2]]^{1/2}$.

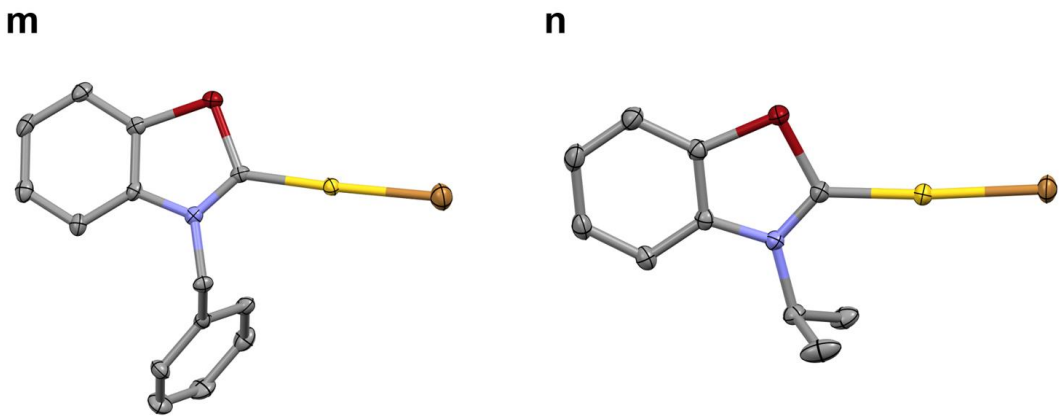

Figure 10.20: X-ray structures of **m** and **n** complexes. Ellipsoids are drawn at their 50 % probability level. Hydrogens are omitted for clarity. Color code: yellow (Au), brown (Br), purple (N), red (S), grey (C).

10.4 DIRECT REDUCTIONS OF GOLD(I) COMPLEXES WITH $NaBH_4$

All reactions were monitored using quadrupole-time-of-flight high resolution mass spectrometry (Q-TOF HRMS).

Gold complexes **a'** (0.005 mmol) was dissolved in 10 ml of DCM:MeOH (4:1 v:v) and subsequently $NaBH_4$ (0.05 mmol), pre-dissolved in 1 ml of EtOH, was added dropwise to complex solution under stirring. After 9 h at room temperature the solution was divided in two equal portions. In one, 100 eq. of HBr (48%) was added and the mixture was left under stirring at room temperature for 16 h. In the second, acid etching was not performed and the mixture was left under stirring at room temperature for other 16 h. After that 10 ml of water were added to the mixtures to remove the inorganic salts. The aqueous layer was decanted and the remained organic solution was dried with Na_2SO_4. The inorganic salt was filtered and the filtrates analyzed using Q-TOF HRMS.

This experiment was repeated also for **b'-l'**, **m**, **n** and **p** complexes.

In the experiments involving **m** and **n** complexes acid etching was not tested.

In the experiment involving **e** complex the reaction was performed exploiting CH_3CN as solvent.

Since only reduction of **a'**, **b'** and **c'** provided AuNCs, in the following we reported mass spectra related to these experiments only. These Q-TOF HRMS spectra highlighted signals (m/z) centered at:

- **a'**) $[Au_{13}(\text{di-NHC}^a)_5Br_2]^{3+}$ (1500.80), $[Au_{13}(\text{di-NHC}^a)_5Br(CH_3)]^{3+}$ (1479.17), $[Au_{13}(\text{di-NHC}^a)_5(CH_3)_2]^{3+}$ (1457.54).
- **b'**) $[Au_{11}(\text{di-NHC}^b)_4Br]^{2+}$ (2036.28), $[Au_{13}(\text{di-NHC}^b)_5Br_2]^{3+}$ (1667.88).
- **c')** $[Au_{13}(\text{di-NHC}^c)_5Br_2]^{3+}$ (1507.18).

Acid etching of the mixture provided Q-TOF HRMS spectra with signals (m/z) centered at:

- **a'**) $[Au_{13}(di\text{-}NHC^a)_5Br_2]^{3+}$ (1500.80), $[Au_{13}(di\text{-}NHC^a)_5Br(CH_3)]^{3+}$ (1479.17).
- **b'**) $[Au_{13}(di\text{-}NHC^b)_5Br_2]^{3+}$ (1667.88).
- **c')** $[Au_{13}(di\text{-}NHC^c)_5Br_2]^{3+}$ (1507.18).

These spectra are reported below in **Figures 10.22**, **10.23** and **10.24**, respectively.

In all Q-TOF HRMS spectra obtained from these reductions it is possible to detect $[Au_2(di\text{-}NHC)_2]^{2+}$ or $[Au(SNHC)_2]^+$ signals, complexes present as by-products of these reductions. An example of these is reported in **Figures 10.25**. The same complexes are observed also in ^1H NMR spectra of crude mixtures after the reductions. An example of these is reported in **Figure 10.26.**

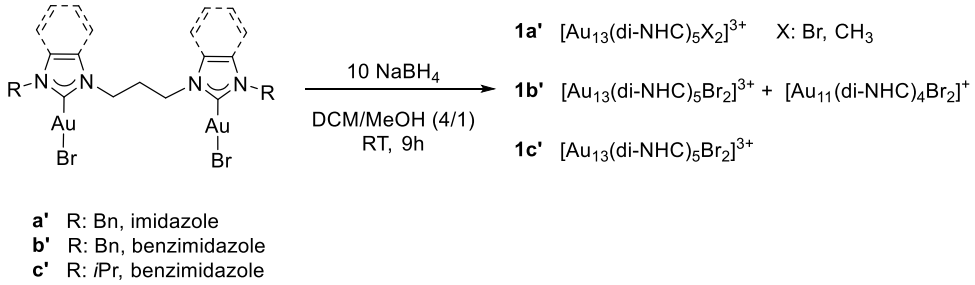

Figure 10.21: Reductions of **a'**, **b'** and **c'** complexes and corresponding obtained clusters.

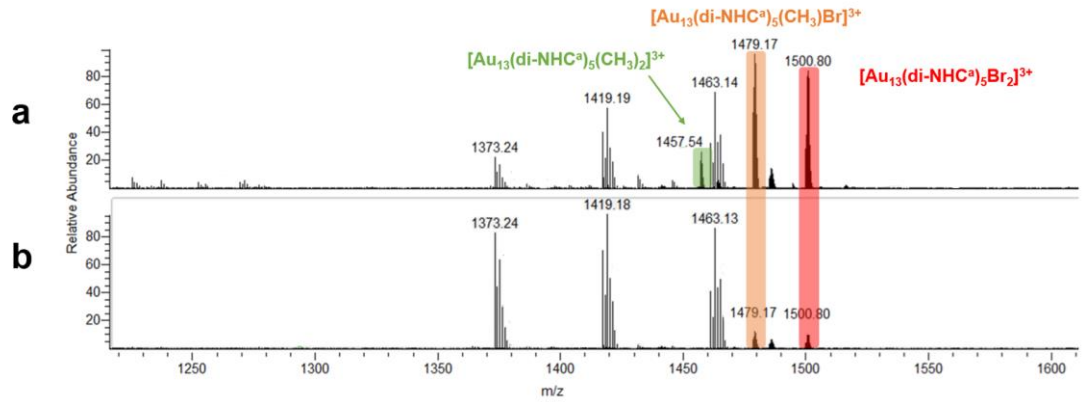

Figure 10.22: mass spectra after reduction of **a'** a) before and b) after acid etching. Color code: $[Au_{13}(di\text{-}NHC^a)_5Br_2]^{3+}$ (red), $[Au_{13}(di\text{-}NHC^a)_5Br(CH_3)]^{3+}$ (orange) and $[Au_{13}(di\text{-}NHC^a)_5(CH_3)_2]^{3+}$ (green).

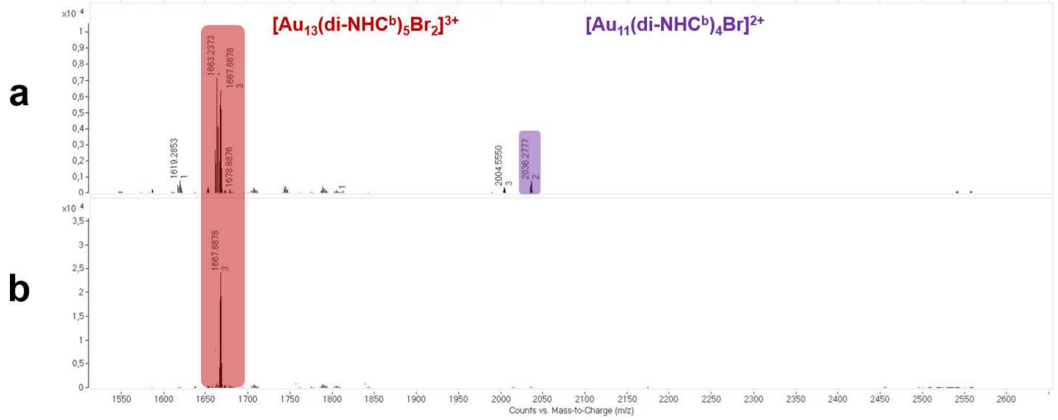

Figure 10.23: mass spectra after reduction of **b'** a) before and b) after acid etching. Color code: $[Au_{13}(di\text{-}NHC^{b})_5Br_2]^{3+}$ (red) and $[Au_{11}(di\text{-}NHC^{b})_4Br]^{2+}$ (purple).

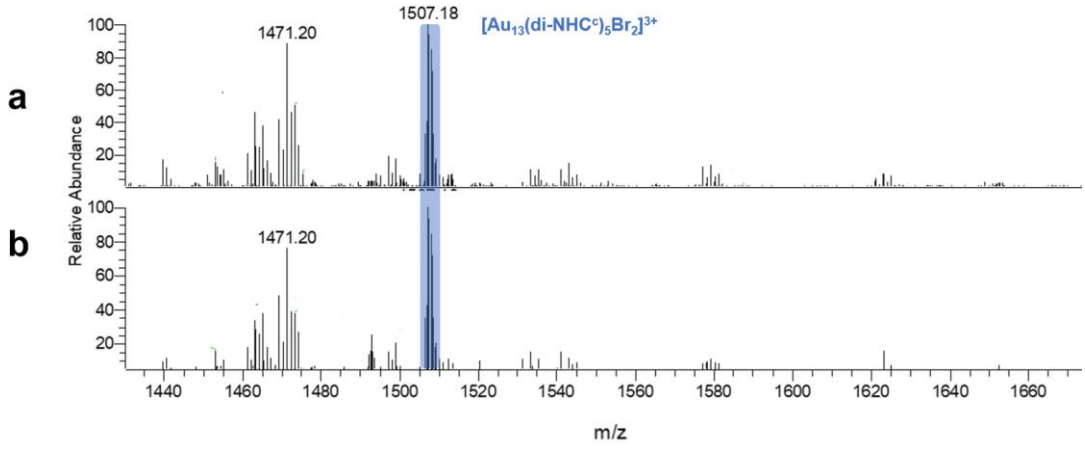

Figure 10.24: mass spectra after reduction of **c'** a) before and b) after acid etching. Color code: $[Au_{13}(di\text{-}NHC^{c})_5Br_2]^{3+}$ (blue).

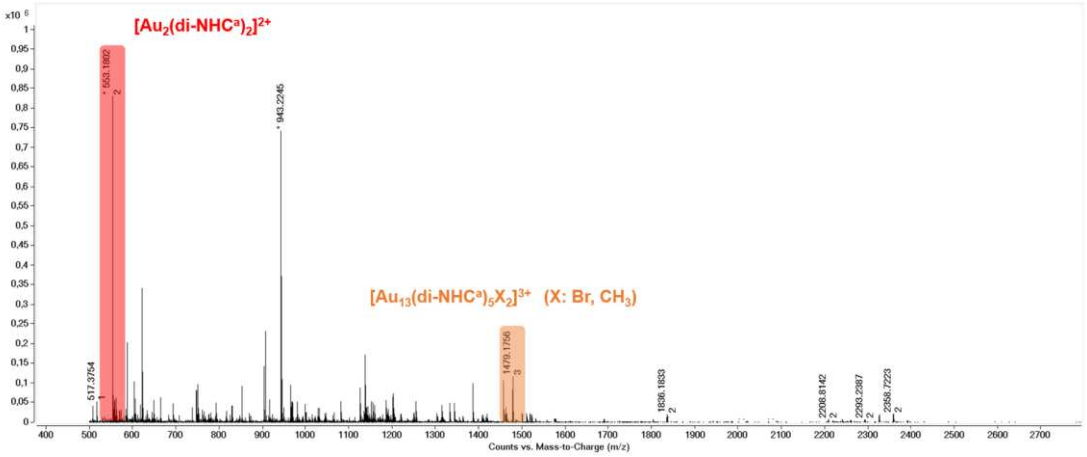

Figure 10.25: mass spectrum of the mixture derived from reduction of **a'** in which $[Au_2(di\text{-}NHC^a)_2]^{2+}$ is highlighted in red and $[Au_{13}(di\text{-}NHC^a)_5X_2]^{3+}$ (X : Br, CH_3) in orange.

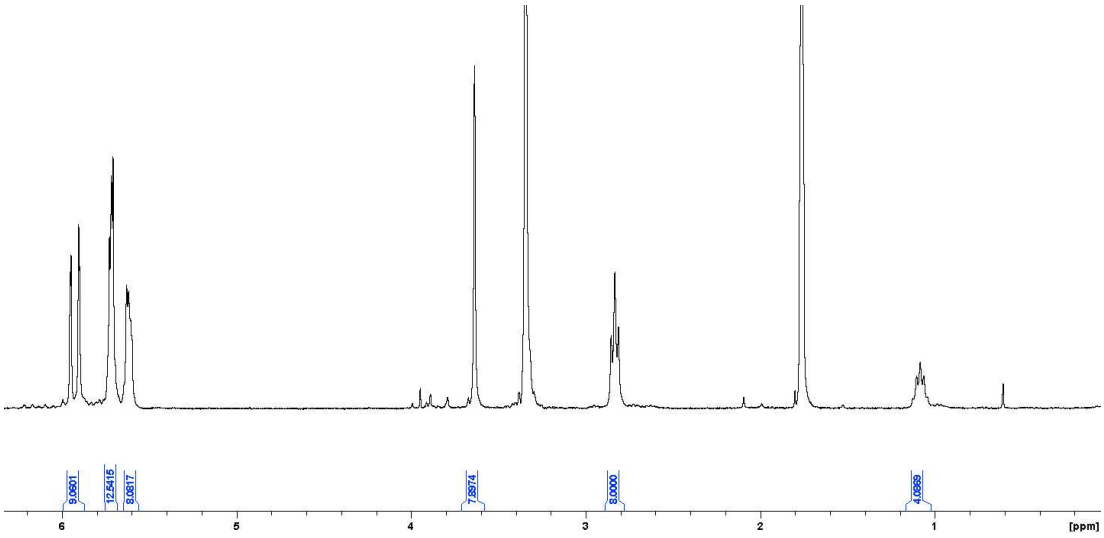

Figure 10.26: ^1H NMR of crude mixture derived from reduction of **a'** complex. The position of signals and their integrals match with $[Au_2(di\text{-}NHC^a)_2]^{2+}$ complex.

10.5 CH_3-CAPPED GOLD CLUSTERS

*10.5.1 First test with **a'**: synthesis of **[Br_2]**, **[$(CH_3)Br$]** and **[$(CH_3)_2$]** clusters*

A one-neck 25 ml of balloon was filled with **a'** (50.0 mg, 0.055 mmol) and 8 ml of a solution DCM:MeOH (4:1 v:v). A vial was filled with $NaBH_4$ (20.8 mg, 0.550 mmol) and 1.30 ml EtOH, stoppered with a Teflon cap and sonicated for 5 minutes. The obtained dispersion was added dropwise in **a'** solution, affording a variation of the solution color, from colorless to deep orange. The mixture was left under stirring for 24 h at room temperature. After that, the solution was filtered on a PTFE filter and the filter was washed with 3 ml of DCM. The filtrate and the washing solution were combined and 8 ml of distilled H_2O were added, to remove the inorganic salts. The supernatant aqueous solution was decanted and the DCM solution was dried with Na_2SO_4. The solid was filtered and the remaining red solution was dried under vacuum, affording a red solid. The solid was dispersed in 5 ml of DCM. The dispersion was filtered on a PTFE filter and the filter was subsequently washed with 3 ml of DCM. The filtrate and the washing solution were combined and concentrated under vacuum to *ca.* 3 ml. The concentrated solution was added dropwise to 20 ml of acetone, forming a fine solid dispersion in an orange solution. The dispersion was filtered on a PTFE filter and the filtrate was dried under reduced pressure, affording a red solid. The sample was dissolved in 3 ml of DCM:MeOH (3:1 v:v) and crystallized overnight upon condensation of Et_2O vapour at room temperature. The colorless supernatant was discharged and the remain red solid was dried under reduced pressure. The solid was dissolved in DCM and analyzed by Q-TOF HRMS (**Figure 10.27**), highlighting the presence of three clusters, with formulas $[Au_{13}(\text{di-NHC}^a)_5Br_2]^{3+}$ (1500.81 m/z), $[Au_{13}(\text{di-NHC}^a)_5(CH_3)Br]^{3+}$ (1479.18 m/z), $[Au_{13}(\text{di-NHC}^a)_5(CH_3)_2]^{3+}$ (1457.68 m/z), named respectively **[Br_2]**, **[$(CH_3)Br$]** and **[$(CH_3)_2$]**.

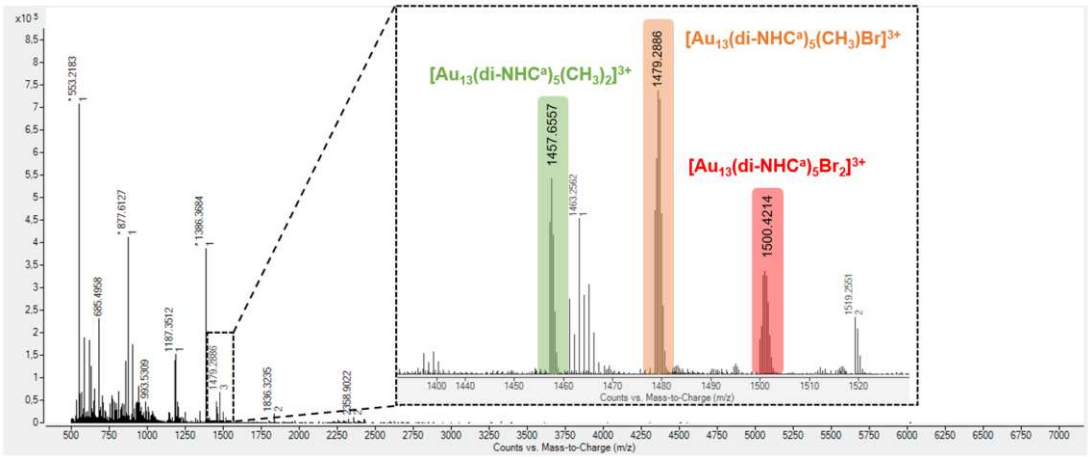

Figure 10.27: Q-TOF HRMS analysis related to the reduction of **a'** complex with 10 moles of $NaBH_4$ and 24 h as reaction time. The **[Br_2]** cluster is highlighted in red, **[($(CH_3)Br$]** in orange and **[($(CH_3)_2$]** in green.

*10.5.2 Second test with **a'**: synthesis and characterization of **[Br_2]***

A one-neck 25 ml of balloon was filled with **a'** (30.0 mg, 0.033 mmol), LiBr (28.7 mg, 0.33 mmol) and 5.30 ml of a solution DCM:MeOH (4:1 v:v). A vial was filled with $NaBH_4$ (12.5 mg, 0.331 mmol) and 1.30 ml of EtOH, stoppered with a Teflon cap and sonicated for 5 minutes. The obtained dispersion was added dropwise to **a'** solution, providing a change in the color of the solution, from colorless to deep orange. The mixture was left under stirring at room temperature for 24 h. After this time the solution was filtered on a PTFE filter and the filter was washed with 2 ml DCM. The filtrate and the washing solution were combined and 5 ml of distilled H_2O were added, to remove the inorganic salts. The supernatant solution was decanted and the DCM solution was dried with Na_2SO_4. The solid was filtered and the obtained red solution was dried under vacuum, affording a red solid. The solid was dispersed in 3 ml DCM and the dispersion was filtered on a PTFE filter. The filter was washed with 3 ml of DCM. The filtrate and the washing solution were combined and concentrated under vacuum to *ca.* 3 ml. The concentrated solution was added dropwise to 20 ml of acetone, forming a fine solid dispersion in an orange solution. The dispersion was filtered on a PTFE filter and the filtrate was dried under reduced pressure, affording a red solid. The solid

was dissolved in 1 ml DCM and the solution was placed in a pressure tube. LiBr (30.0 mg, 0.35 mmol) was added and the apparatus stoppered with a Teflon cap. The dispersion was heated at 30°C under stirring overnight. After this time the dispersion was filtered and the filtrate dried under reduced pressure, affording a red solid. The solid was dissolved in 1 ml of CH_3CN and purified by crystallization, upon condensation of Et_2O vapour at room temperature. After 24 h, the colorless supernatant was discharged and the remaining red solid was dried under reduced pressure, affording **[Br_2]** cluster as a red solid. Yield 2.2 mg (6.6%).

^{1}H NMR (300 MHz; CD_3CN): δ 7.21 (t, J = 7.29 Hz, 20H), 7.10 (t, J = 7.51 Hz, 20H), 7.06 (d, J = 1.83, 10H), 6.70 (d, J = 7.58 Hz, 20H), 6.42 (d, J = 16.00 Hz, 10H), 4.86 (m, 10H), 3.68 (m, 10H), 3.55 (d, J = 15.98 Hz, 10H), 2.06 (s, 10H).

Q-TOF HRMS: 1500.94 m/z $[Au_{13}(di\text{-}NHC^a)_5Br_2]^{3+}$, 2430.32 m/z $[Au_{13}(di\text{-}NHC^a)_5Br_2](AuBr_2)^{2+}$.

[Br_2] cluster is not stable in solution, affording starting **a'** complex after 10 days at -4°C in CD_3CN, as showed in **Figure 10.29**. Moreover, in repetitions of this synthesis, Q-TOF HRMS analysis highlighted the presence of both **[$Br(CH_3)$]** and **[Br_2]** clusters (**Figure 10.32**).

In order to transform the **[$Br(CH_3)$]** impurity into the **[Br_2]** cluster, the mixture was dissolved in 5 ml of DCM:MeOH (4:1 v:v) and 370 µl (3.30 mmol) HBr (48%) were added to it. The solution was left under stirring overnight. After that time 5 ml of distilled H_2O were added, to remove the inorganic acid and salts. The supernatant solution was decanted and the DCM solution was dried with Na_2SO_4. The solid was filtered and the obtained red solution was analyzed through Q-TOF HRMS, which reveals the presence of previously detected clusters (**Figure 10.33**).

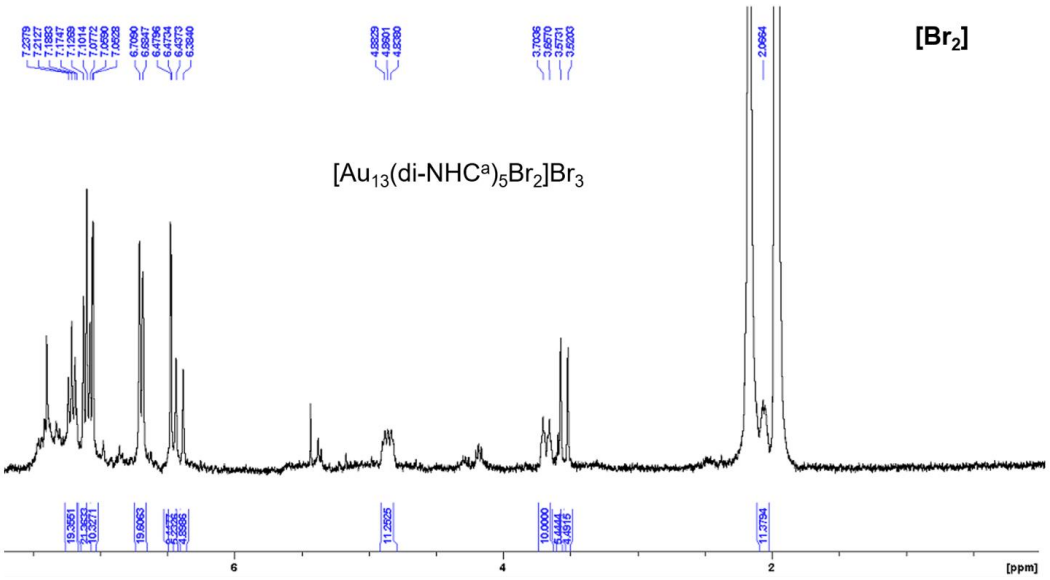

Figure 10.28: ^{1}H NMR spectrum of **[Br$_2$]** in CD_3CN.

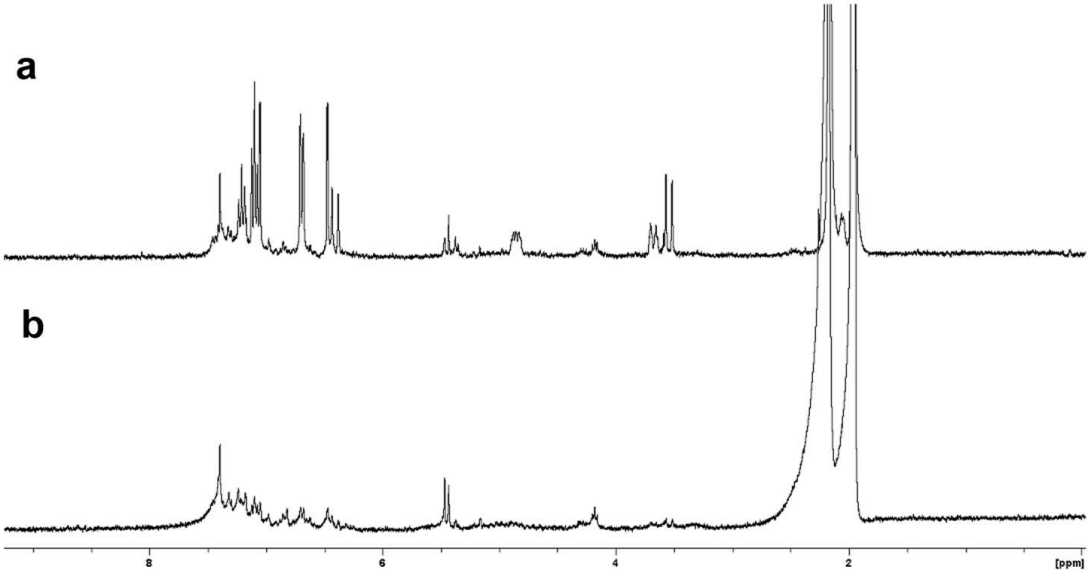

Figure 10.29: ^{1}H NMR spectrum of a) **[Br$_2$]** in CD_3CN and b) the spectra related to the same tube recorded after 10 days at -4°C.

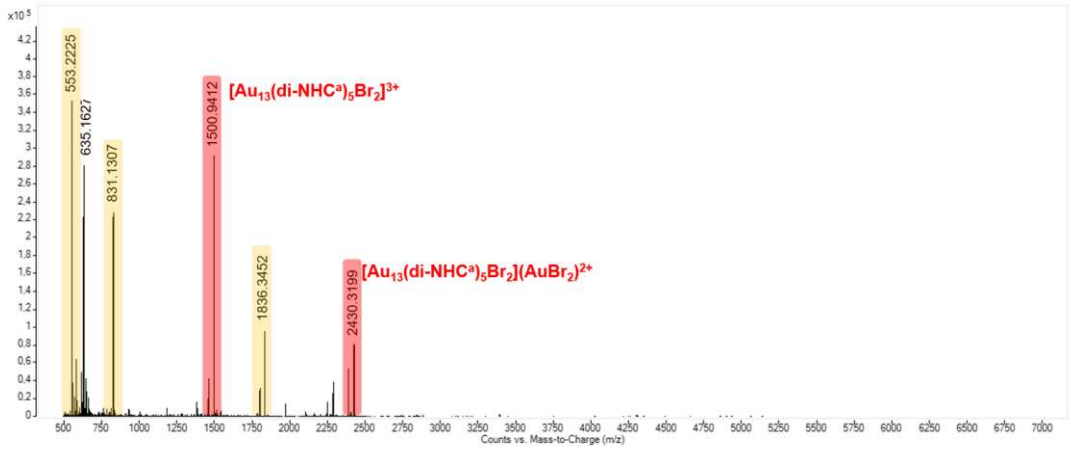

Figure 10.30: Q-TOF HRMS analysis related to **[Br_2]** cluster, highlighted in red, in DCM. The fragmentation peaks are highlighted in yellow. Likely also ion $[AuBr_2]^-$ derived from fragmentation of **[Br_2]** during the analysis.

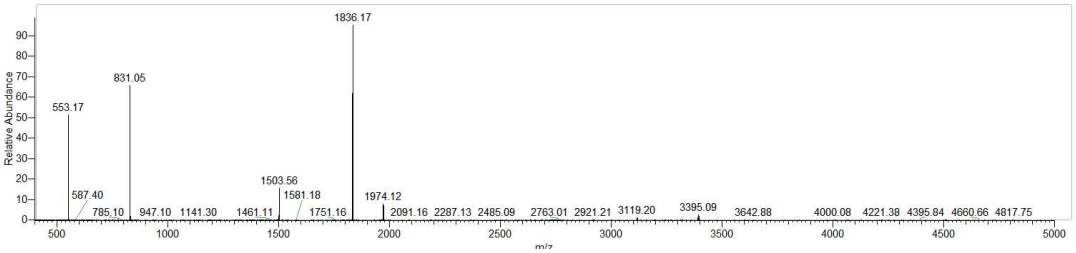

Figure 10.31: msms-Q-TOF HRMS analysis related to **[Br_2]** cluster.

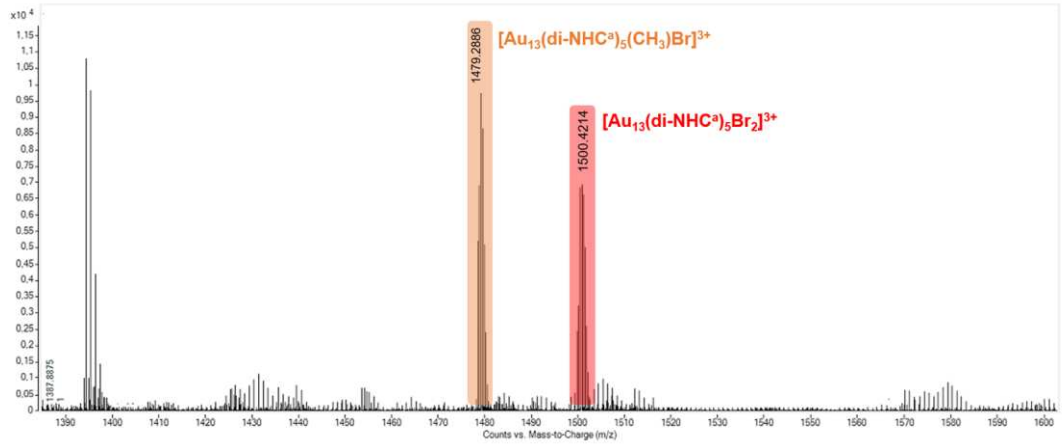

Figure 10.32: Q-TOF HRMS analysis related to one of the attempts to isolate **[Br_2]** cluster. The **[Br_2]** cluster is highlighted in red and **[(CH_3)Br]** in orange.

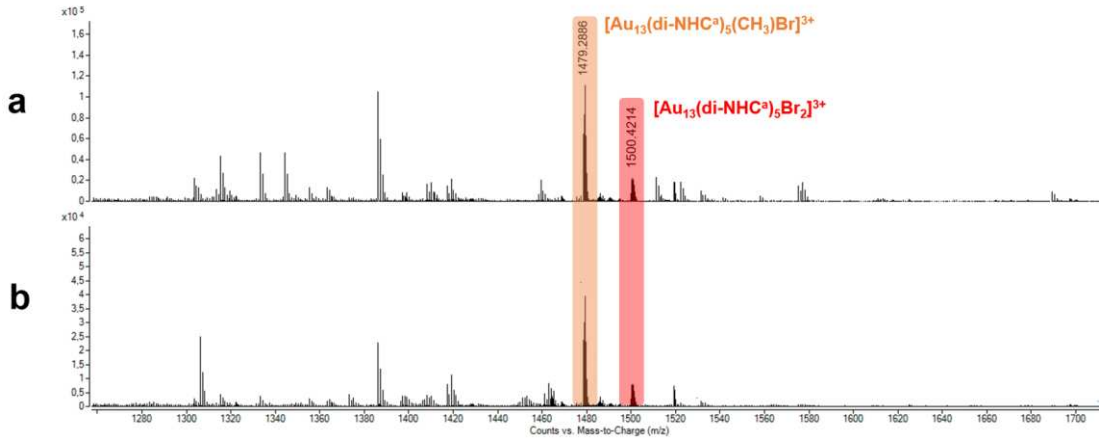

Figure 10.33: Q-TOF HRMS analysis related to two attempts to get **[Br_2]** cluster a) without and b) with hydrobromic acid addition. The **[Br_2]** cluster is highlighted in red and **[(CH_3)Br]** in orange.

10.5.3 Synthesis of [($(CH_3)_2$]

A one-neck 25 ml of balloon was filled with **a** (33 mg, 0.042 mmol) and (chloro)dimethylsulfide gold(I) (7.2 mg, 0.024 mmol). The solids were dissolved in 7 ml of a solution DCM:EtOH (4:1 v:v). A vial was filled with $NaBH_4$ (16 mg, 0.423 mmol) and 1 ml EtOH, stopped with a Teflon cap and sonicated for 5 minutes. The dispersion was added dropwise to the starting solution. The addition of $NaBH_4$ was repeated two more times, after 24 h and 48 h from the first addition respectively, for a total added quantity of $NaBH_4$ equal to 48 mg (1.27 mmol; 0.423 moles each 24 h), and a reaction time of 72 h. Subsequently, the solution was filtered on a PTFE filter and the filter was washed with 5 ml DCM. The filtrate and the washing solution were combined and 5 ml of distilled H_2O was added, to remove the inorganic salts. The supernatant solution was decanted and the DCM solution was dried with Na_2SO_4. The solid was filtered and the obtained red solution wad dried under vacuum, affording a red solid. The solid was dispersed in 5 ml DCM and the dispersion was filtered on PTFE filter, washing it with 5 ml DCM. The filtrate and the washing solution were combined and concentrated under vacuum to *ca*. 1 ml of solution. The concentrated solution was added dropwise in 60 ml of acetone under stirring, forming a fine solid dispersion in an orange solution.

The dispersion was filtered on a PTFE filter and the filtrate was dried under reduced pressure, affording a red solid. Sometimes, the synthesis affords also **[Cl(CH_3)]** cluster as by-product, that can be detected by ^{1}H NMR spectroscopy or Q-TOF HRMS. In these cases, the red solid is dissolved in 7 ml of a DCM:EtOH (4:1 v:v) solution and 33 mg (0.846 mmol) of $NaBH_4$ dispersed in 1 ml EtOH are added dropwise to the cluster solution. The mixture is left under stirring overnight in dark environment at room temperature. After this time the mixture is dried under reduced pressure and the resulting solid dispersed in 3 ml DCM. The dispersion is filtered and the filter is washed with 3 ml of DCM. The filtrate and the washing solution are combined and dried under reduced pressure.

Consecutive crystallizations were exploited to further enhance the purity of **[(CH_3)$_2$]**.

1° crystallization: the cluster was dispersed in 1.5 ml DCM. The solution was filtered and placed in a vial. 3 ml *n*-hexane was layered on the cluster solution. The vial was stoppered with a Teflon cap and placed at 5°C. After 24 h, the colorless supernatant was decanted and the remaining amorphous red solid was dried under reduced pressure.

2° crystallization: the solid cluster derived from the previous crystallization was dispersed in 1 ml DCM. The solution was filtered and placed in a vial. 3 ml Et_2O were layered on the DCM solution. The vial was stoppered with a Teflon cap and placed at 5°C. After 24 h, the colorless supernatant was decanted and the remaining amorphous red solid was dried under reduced pressure.

3° crystallization: the solid cluster derived from the previous crystallization was dispersed in 1 ml DCM. The solution was filtered and placed in a vial. 3 ml of *n*-pentane were layered on the DCM solution, the vial was stoppered with a Teflon cap and placed at 5°C. After 24 h, the colorless supernatant was decanted and the

remaining amorphous red solid was dried under reduced pressure, providing a pure sample of **[$(CH_3)_2$]** cluster. Yield 8.4 mg (22.50%).

^{1}H NMR (300 MHz, CD_3CN): δ 7.22 (t, J = 7.66 Hz, 10H), 7.09 (m, 30H), 6.66 (d, J = 7.39 Hz, 20H), 6.46 (d, J = 1.77 Hz, 10H), 6.38 (d, J = 15.40 Hz, 10H), 5.04 (m, 10H), 3.69 (dt, J = 13.70 Hz, 10H), 3.49 (d, J = 15.55 Hz, 10H), 2.07 (s, 10H), 0.29 (s, 6H).

^{1}H NMR (300 MHz, CD_2Cl_2): δ 7.23 (m, 20H), 7.11 (t, J = 7.30 Hz, 20H), 6.67 (d, J = 7.24 Hz, 20H), 6.46 (d, J = 15.30 Hz, 10H), 6.38 (d, J = 1.66 Hz, 10H), 5.11 (m, 10H), 3.81 (dt, J = 13.84 Hz, 10H), 3.47 (d, J = 15.15 Hz, 10H), 2.10 (s, 10H), 0.37 (s, 6H).

^{1}H NMR (300 MHz, CD_3OD): δ 7.24 (t, J = 7.45 Hz, 10H), 7.18 (d, J = 1.90 Hz, 10H), 7.12 (t, J = 7.38 Hz, 20H), 6.70 (d, J = 7.64 Hz, 20H), 6.56 (m, 15H), 6.52 (s, 5H), 5.19 (m, 10H), 3.71 (dt, J = 14.43 Hz, 10H), 3.47 (d, J = 15.60 Hz, 10H), 2.15 (s, 10H), 0.41 (s, 6H).

^{13}C NMR (101 MHz, CD_2Cl_2): δ 199.67 ($C^{carbene}$), 135.79 (C^{Bn}), 128.20 (CH^{Bn}), 127.12 (CH^{Bn}), 126.30 (CH^{Bn}), 120.32 ($CH^{imidazole}$), 120.18 ($CH^{imidazole}$), 52.61 (CH_2^{Bn}), 44.76 ($\underline{CH_2}CH_2\underline{CH_2}$), 34.15 ($CH_2\underline{CH_2}CH_2$), 26.10 ($CH_3$).

Q-TOF HRMS: 1457.54 m/z $[Au_{13}(di\text{-}NHC^a)_5(CH_3)_2]^{3+}$, 2203.80 m/z $[Au_{13}(di\text{-}NHC^a)_5(CH_3)_2]Cl^{2+}$.

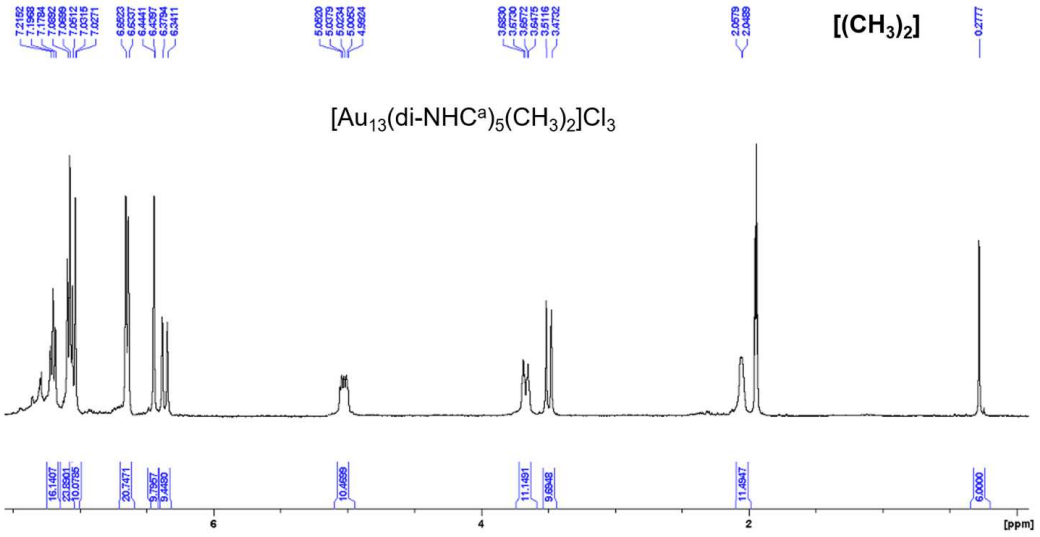

Figure 10.34: ^{1}H NMR spectrum of **[(CH₃)₂]** in CD_3CN.

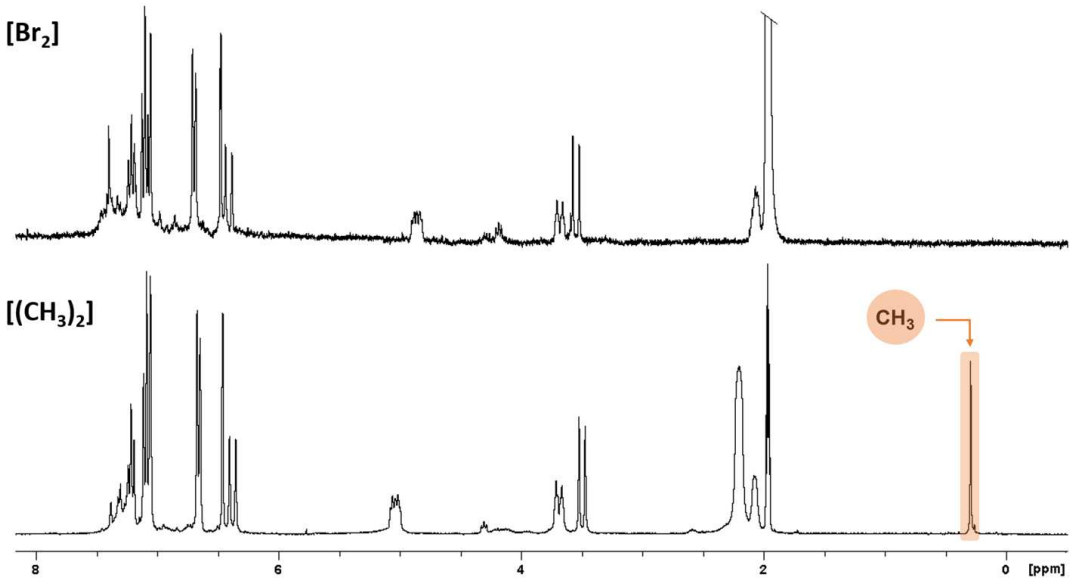

Figure 10.35: ^{1}H NMR spectra of **[Br₂]** (above) and **[(CH₃)₂]** (below) in CD_3CN.

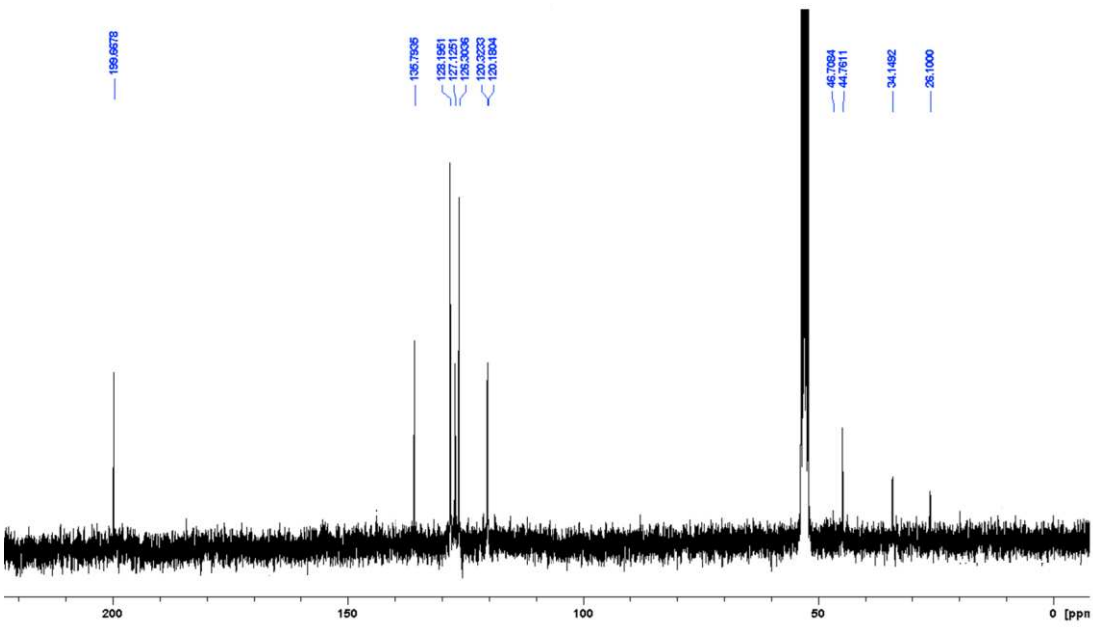

Figure 10.36: ^{13}C NMR spectrum of **[(CH₃)₂]** in CD_2Cl_2.

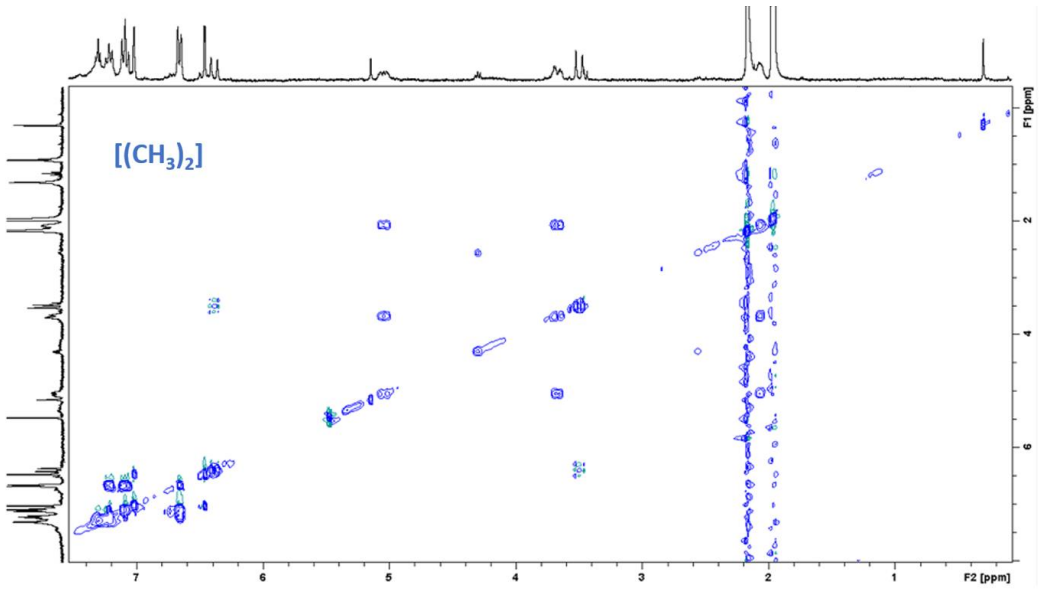

Figure 10.37: TOCSY NMR spectrum of **[(CH₃)₂]** in CD_3CN.

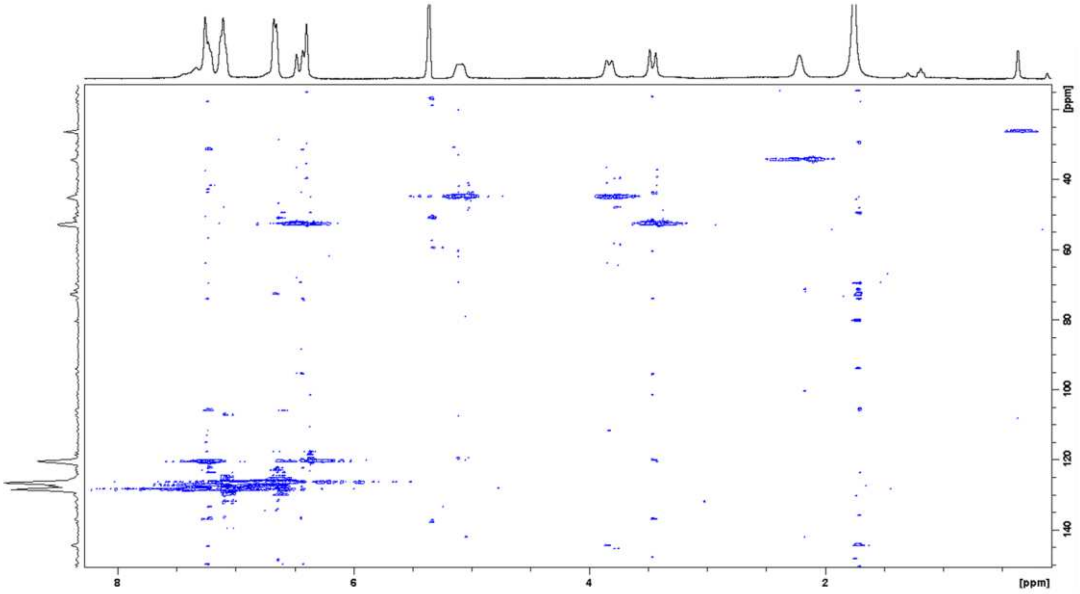

Figure 10.38: HMQC (^{1}H, ^{13}C) NMR spectrum of **[(CH$_3$)$_2$]** in CD_2Cl_2.

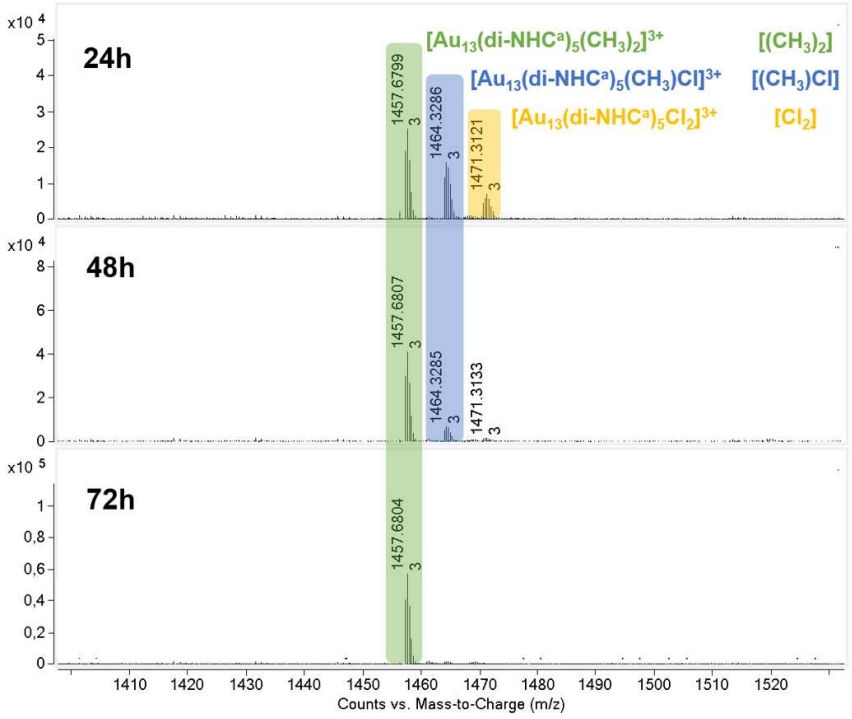

Figure 10.39: Q-TOF HRMS analysis related to withdrawals during the **[(CH$_3$)$_2$]** synthesis after 24 h, 48 h and 72 h of reaction time.

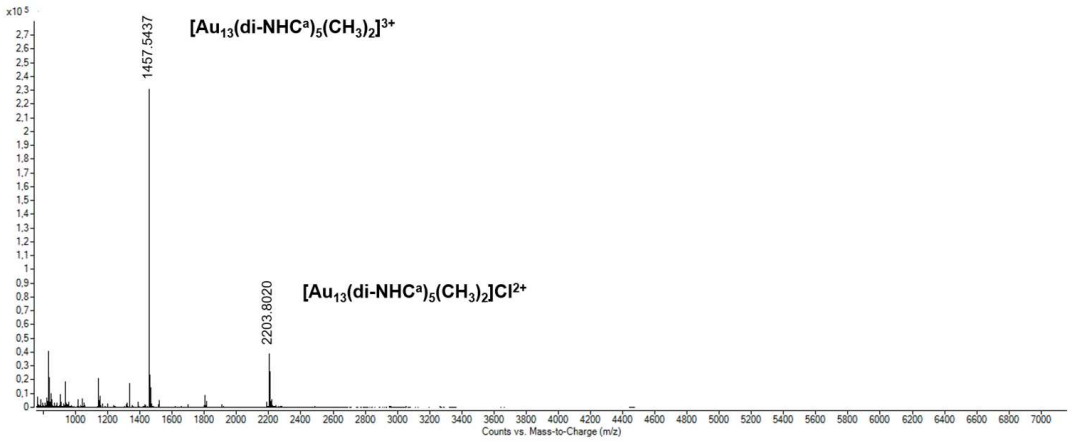

Figure 10.40: Q-TOF HRMS analysis related to **[$(CH_3)_2$]** cluster in DCM.

*10.5.4 Synthesis of **[(CH₃)₂](PF₆)₃** from **[(CH₃)₂]***

A one-neck 10 ml balloon was filled with **[(CH₃)₂]** (15.9 mg, $3.5 \cdot 10^{-3}$ mmol) and 2 ml CH_3CN. A vial was filled with KPF_6 (8 mg, $42.8 \cdot 10^{-3}$ mmol) and 1 ml EtOH and sonicated until a solution was obtained. The EtOH solution was added dropwise to the cluster solution. The mixture was left under stirring at room temperature for 2 h. Subsequently, the mixture was dried under reduced pressure, providing an orange solid, and 2 ml DCM were used to disperse the solid residue. The dispersion was filtered on PTFE filter and the filtrate was dried under reduced pressure, affording **[(CH₃)₂]-PF₆** as a red solid. Yield 16 mg (94%).

^{1}H NMR (300 MHz, CD_3CN): δ 7.22 (t, J = 7.67 Hz, 10H), 7.09 (t, J = 7.69 Hz, 20H), 7.02 (d, J = 2.19 Hz, 10H), 6.66 (d, J = 7.42 Hz, 10H), 6.46 (d, J = 1.84 Hz, 10H), 6.40 (d, J = 15.25 Hz, 10H), 5.04 (m, 10H), 3.67 (dt, J = 13.95 Hz, 10H), 3.49 (d, J = 15.93 Hz, 10H), 2.07 (s, 10H), 0.30 (s, 6H).

^{31}P NMR (121 MHz, CD_3CN): δ 144.62 (st, J = 707.07 Hz, 2P).

^{19}F NMR (200 MHz, CD_3CN): δ 73.27 (d, J = 709.00 Hz, 12F).

Q-TOF HRMS: 1457.66 m/z $[Au_{13}(di\text{-}NHC^a)_5(CH_3)_2]^{3+}$, $[Au_{13}(di\text{-}NHC^a)_5(CH_3)_2](PF_6)^{2+}$ 2258.98 m/z.

Quantum Yield: 6.28% (λ_{exc} =320 nm)

Decay time: 465.38 ns

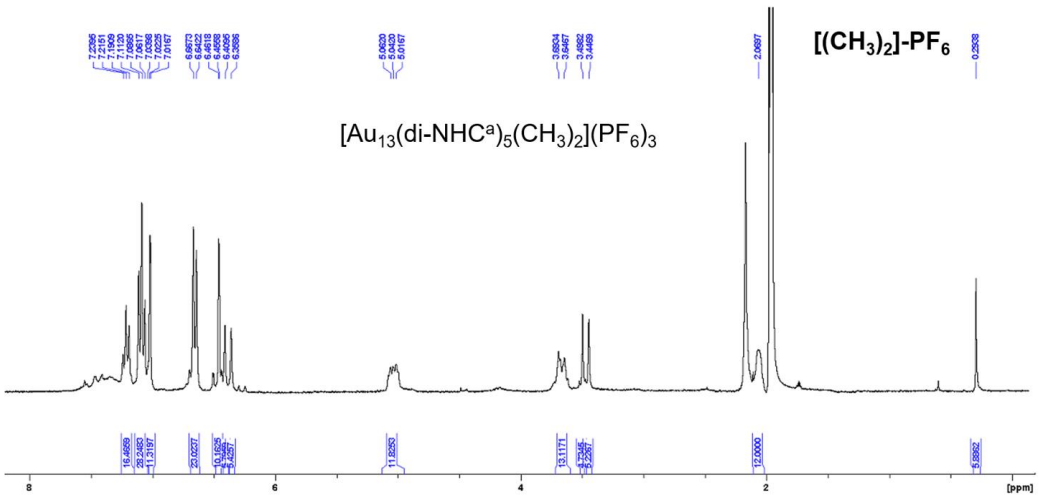

Figure 10.41: ^{1}H NMR spectra of **[(CH$_3$)$_2$]-PF$_6$** in CD_3CN.

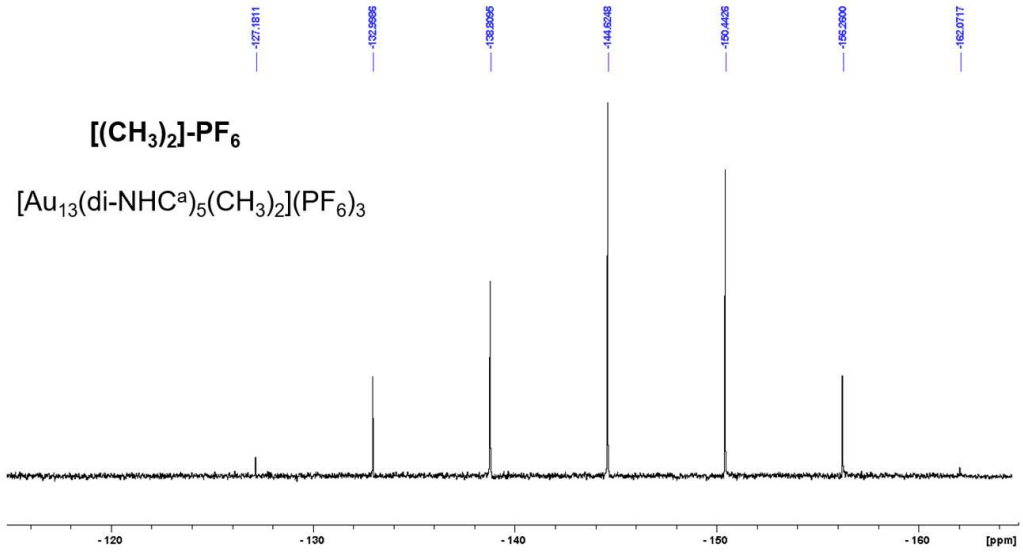

Figure 10.42: ^{31}P NMR spectrum of **[(CH$_3$)$_2$]-PF$_6$** in CD_3CN.

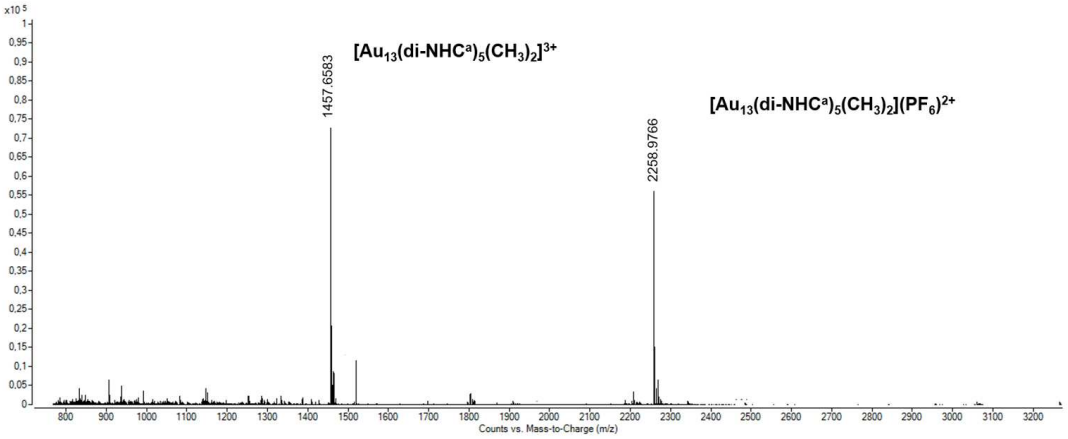

Figure 10.43: Q-TOF HRMS analysis related to **[$(CH_3)_2$]** cluster in DCM.

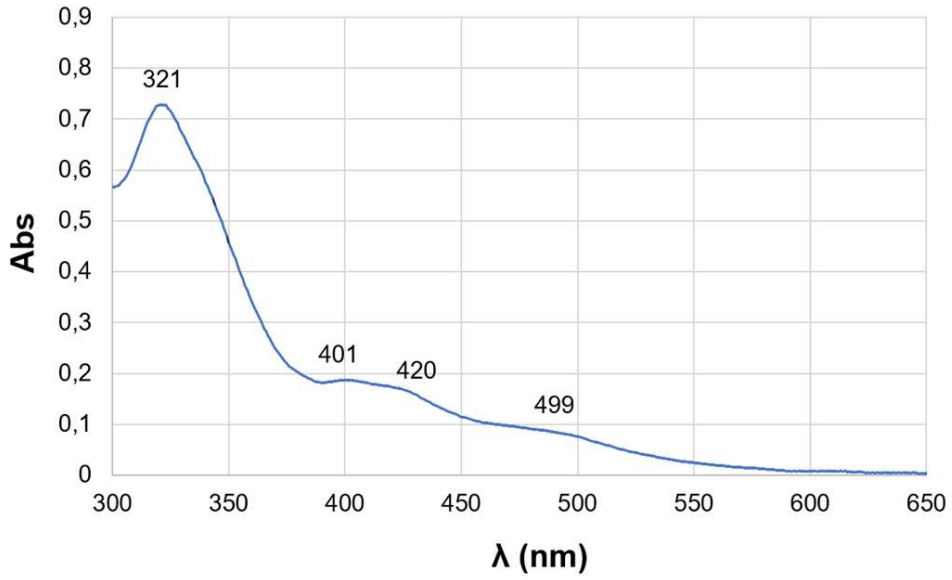

Figure 10.44: UV-Vis analysis related to **[(CH_3)]-PF_6** dissolved in DCM ($2 \cdot 10^{-4}$ M).

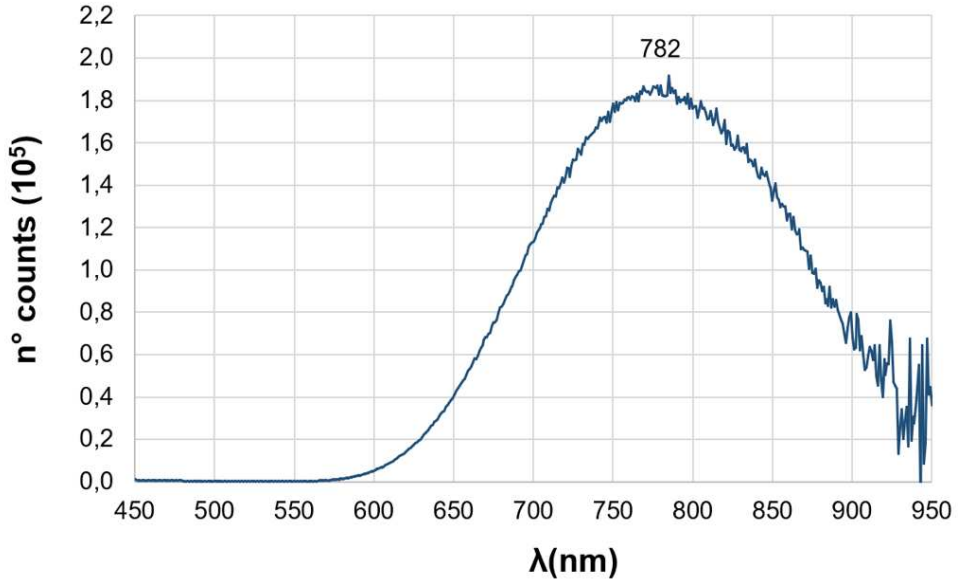

Figure 10.45: Emission spectra of **[(CH₃)]-PF₆** dissolved in DCM ($2 \cdot 10^{-4}$ M) obtained exciting the sample with a 320 nm monochromatic radiation.

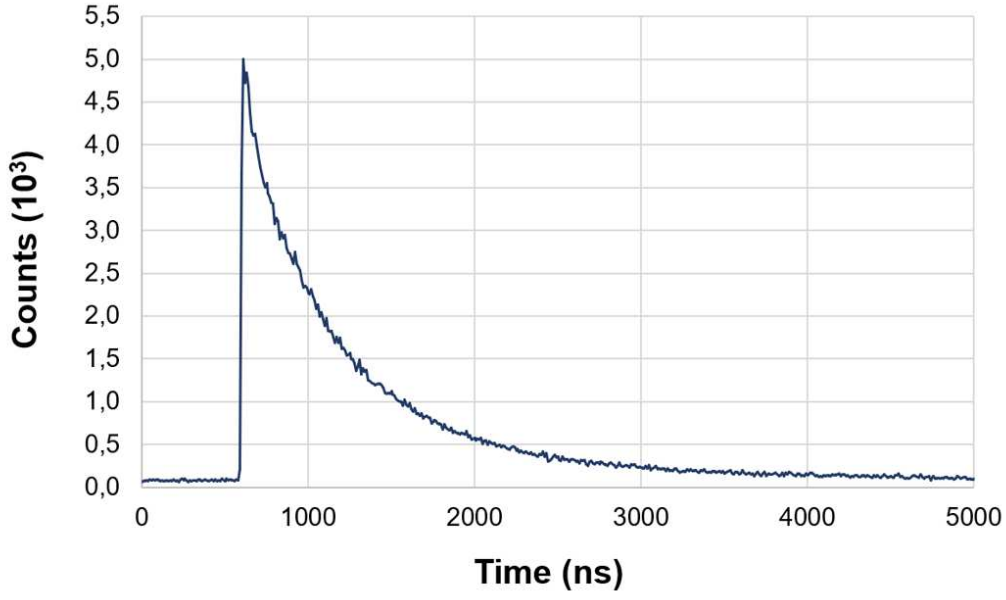

Figure 10.46: Luminescence lifetime decay spectrum of **[(CH₃)]-PF₆** dissolved in DCM.

*10.5.5 Reduction of **a** with $NaBD_4$*

This experiment is identical to that reported in **Paragraph 10.5.3** regarding the synthesis of **[$(CH_3)_2$]** but exploited $NaBD_4$ (51.5 mg, 1.26 mmol) as reducing agent. After work-up, both ^1H NMR and Q-TOF HRMS spectra were recorded. In the proton spectrum (**Figure 10.47**) the CH_3 signal, which is found at 0.29 ppm in the spectrum of **[$(CH_3)_2$]**, is still present despite the use of $NaBD_4$ as reducing agent, with an integral value of 5H. In the Q-TOF HRMS spectrum (**Figure 10.48**), a signal centered at 1458.19 m/z is present, matching with a cluster formula equal to $[Au_{13}(di\text{-}NHC^a)_5(CH_2D)_2]^{3+}$, presenting a calculated value of 1458.22 m/z.

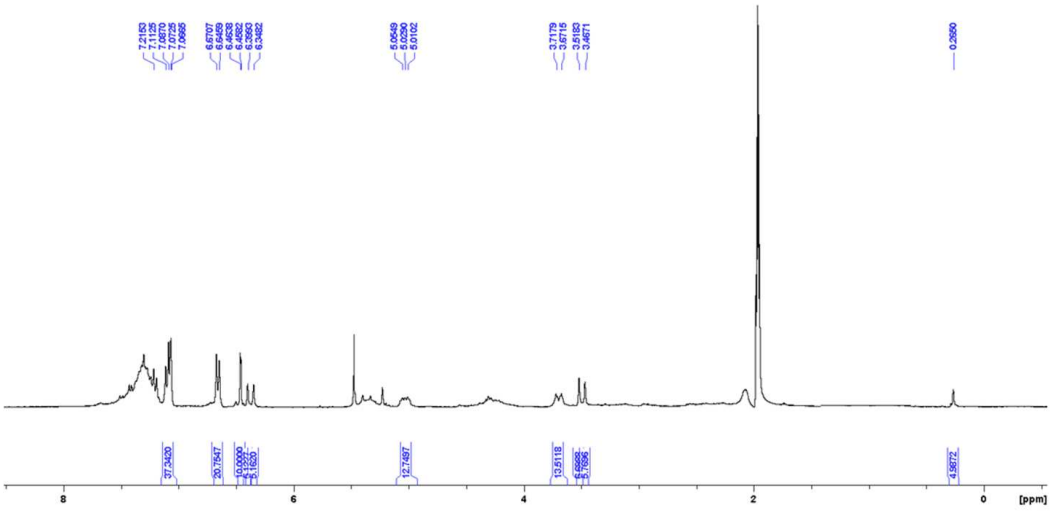

Figure 10.47: ^1H NMR spectrum in CD_3CN of the sample obtained from the reduction of **a** with $NaBD_4$.

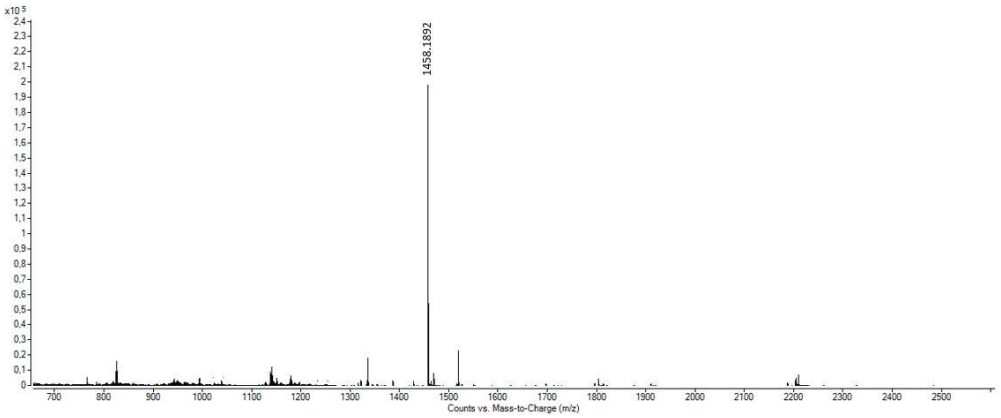

Figure 10.48: Q-TOF HRMS analysis related to the cluster obtained by reduction of **a** by $NaBD_4$.

*10.5.6 Reduction of **b***

This experiment is identical to that reported in **Paragraph 10.5.3** regarding the synthesis of **[$(CH_3)_2$]** but exploiting **b** (38.7 mg, 0.042 mmol) as starting complex. The reaction was followed by sample probes analyzed with Q-TOF HRMS, reported in **Figure 10.49**. After 72 h of reaction the Q-TOF HRMS highlighted the presence of clusters with formula $[Au_{11}(di\text{-}NHC^b)_5]^{3+}$ (1483.01 m/z), $[Au_{13}(di\text{-}NHC^b)_5(CH_3)_2]^{3+}$ (1624.34 m/z), $[Au_{13}(di\text{-}NHC^b)_5Cl(CH_3)]^{3+}$ (1631.33 m/z) and $[Au_{13}(di\text{-}NHC^b)_5Cl_2]^{3+}$ (1637.97 m/z).

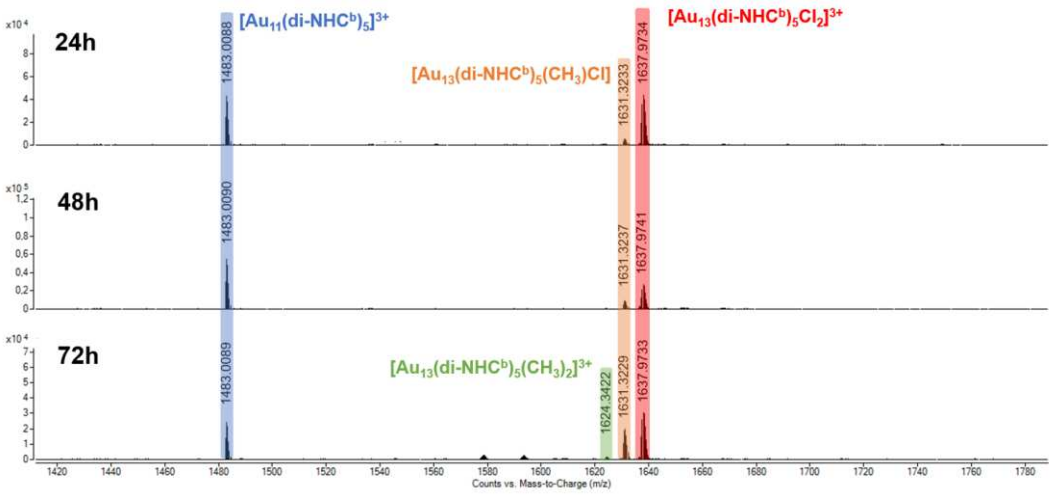

Figure 10.49: Q-TOF HRMS analysis related to withdrawals during the reduction of **b** complex. The clusters $[Au_{11}(di\text{-}NHC^b)_5]^{3+}$, $[Au_{13}(di\text{-}NHC^b)_5(CH_3)_2]^{3+}$, $[Au_{13}(di\text{-}NHC^b)_5Cl(CH_3)]^{3+}$ and $[Au_{13}(di\text{-}NHC^b)_5Cl_2]^{3+}$ are highlighted in blue, green, orange and red, respectively.

*10.5.7 Reduction of **a** using DCE as solvent*

This experiment is identical to that reported in **Paragraph 10.5.3** regarding the synthesis of **[$(CH_3)_2$]** but exploiting DCE:EtOH (4:1 v:v) as solvent. The reaction was followed by sample probes analyzed with Q-TOF HRMS, reported in **Figure 10.50**. After 1 h of reaction the Q-TOF HRMS highlighted the presence of cluster **[Cl_2]** with formula $[Au_{13}(di\text{-}NHC^a)Cl_2]^{3+}$ (1471.15 m/z). As expected, this cluster is not stable and despite further addition of $NaBH_4$ the Q-TOF HRMS analyses at 24 h, 48 h and 72 h do not show presence of signals related to AuNCs.

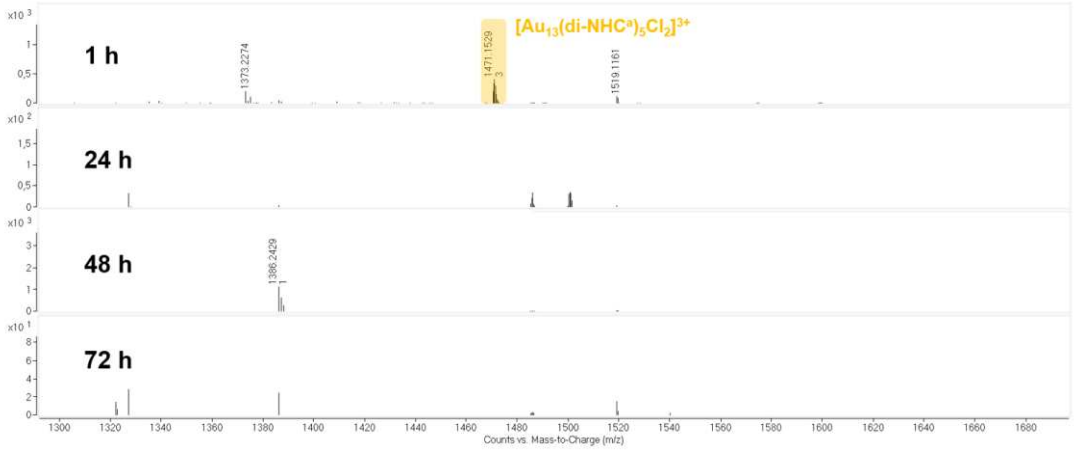

Figure 10.50: Q-TOF HRMS analysis related to withdrawals during the reduction of **a** complex using DCE: EtOH (4:1 v:v) as solvent. The cluster $[Au_{13}(di\text{-}NHC^a)_5Cl_2]^{3+}$ is highlighted in yellow.

*10.5.8 Evolution in solid state of **[(CH₃)₂]**: Synthesis of **[(CH₃)Cl]***

A solid sample of **[(CH₃)₂]** (4.2 mg, $9 \cdot 10^{-4}$ mmol) was left for 20 days at -16°C in dark environment. After this time, the sample was dispersed in DCM, affording a red solution and a black insoluble solid. The mixture was filtrated and dried under vacuum, affording a red solid. Yield 3 mg (95% considering the reaction reported below). Both ^{1}H NMR (**Figure 10.51**) and Q-TOF HRMS (**Figure 10.54**) spectra highlighted the total conversion of cluster **[(CH₃)₂]** to **[(CH₃)Cl]** and to the insoluble black solid by-product.

$4[Au_{13}(\text{di-NHC})_5(CH_3)_2]Cl_3 \rightarrow 3[Au_{13}(\text{di-NHC})_5(CH_3)Cl]Cl_3 + [Au_{13}(\text{di-NHC})_5(CH_3)_2](CH_3)_3$

We suppose that the cluster $[Au_{13}(\text{di-NHC})_5(CH_3)_2](CH_3)_3$ undergoes degradation, affording the insoluble black solid.

^{1}H NMR (400 MHz, CD_2Cl_2): δ 7.20 (m, 20H), 7.10 (t, J = 7.83 Hz, 20H), 6.72 (d, J = 7.29 Hz, 10H), 6.66 (d, J = 7.30 Hz, 20H), 6.47 (d, J = 15.79 Hz, 5H), 6.41 (d, J = 1.17 Hz, 5H), 6.32 (m, 10H), 5.01 (m, 5H), 4.87 (m, 5H), 3.88 (dt, J = 14.83 Hz, 10H), 3.63 (d, J = 16.00 Hz, 5H), 3.50 (d, J = 16.20 Hz, 5H), 3.47 (d, J = 16.20 Hz, 5H), 2.23 (s, 10H), 0.66 (s, 3H).

Q-TOF HRMS: 1464.19 m/z $[Au_{13}(\text{di-NHC})_5(CH_3)Cl]^{3+}$, 2214.27 m/z $[Au_{13}(\text{di-NHC})_5(CH_3)Cl]Cl^{2+}$.

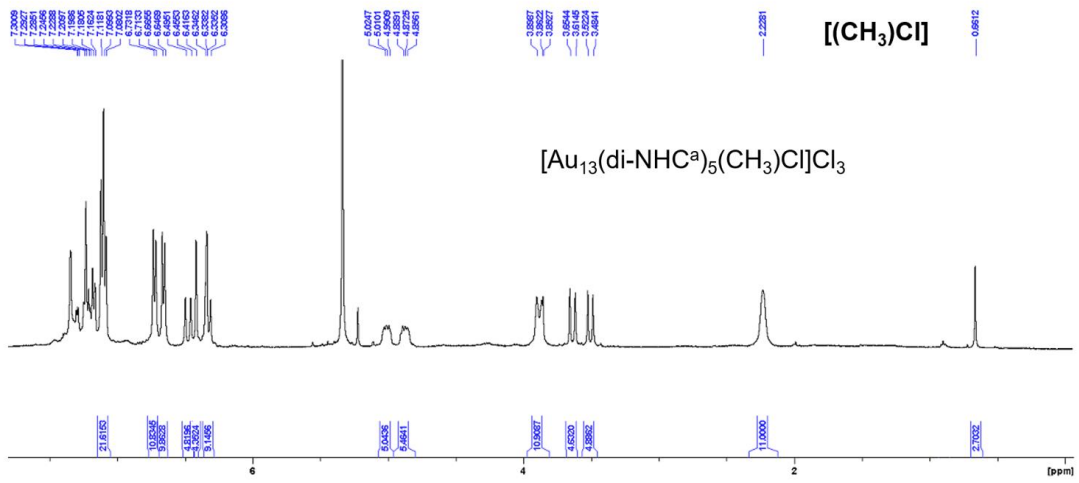

Figure 10.51: ^{1}H NMR spectrum of **[(CH$_3$)Cl]** in CD_2Cl_2.

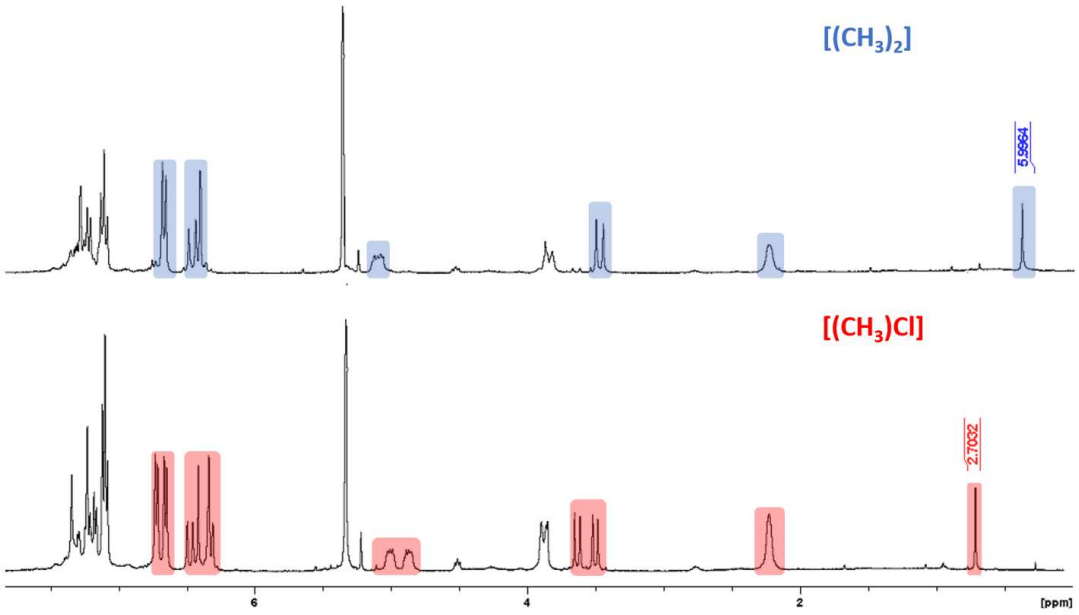

Figure 10.52: ^{1}H NMR spectra of **[(CH$_3$)$_2$]** (above) and **[(CH$_3$)Cl]** (below) in CD_2Cl_2.

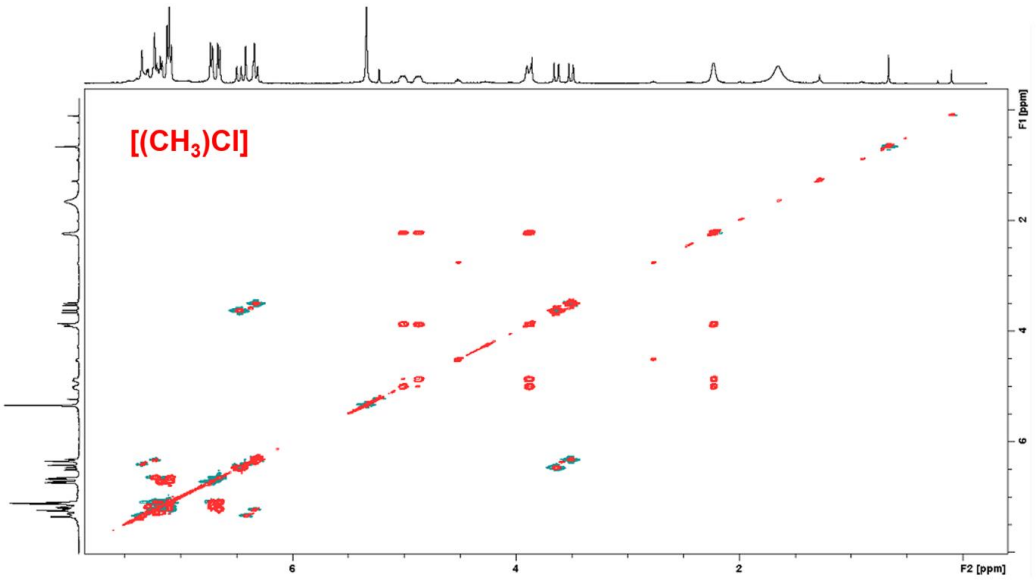

Figure 10.53: TOCSY NMR spectrum of **[(CH$_3$)Cl]** in CD_2Cl_2.

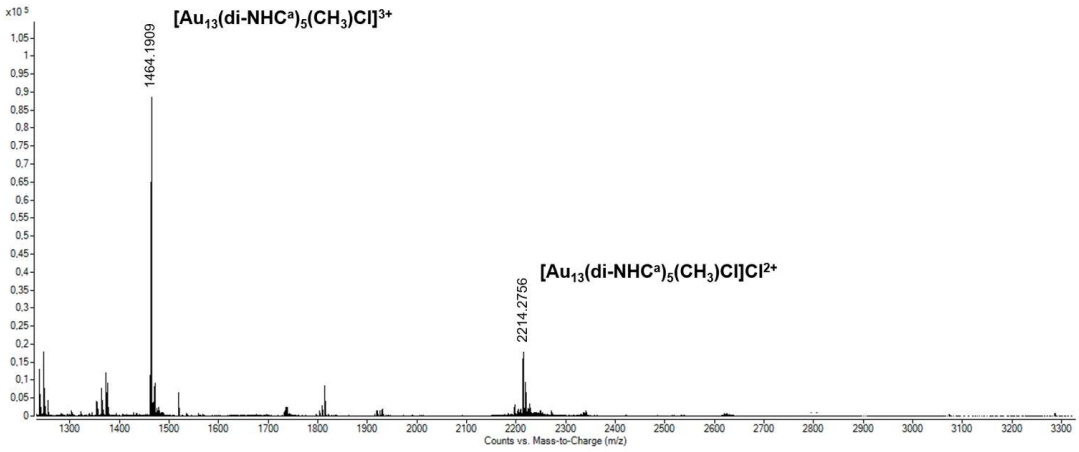

Figure 10.54: Q-TOF HRMS analysis related to **[(CH$_3$)Cl]** in DCM.

*10.5.9 Tests of conversion **[(CH₃)₂]→[(CH₃)Cl]** in deuterated solution*

A vial was filled with 16 mg ($3.5 \cdot 10^{-3}$ mmol) **[$(CH_3)_2$]** cluster and 3 ml DCM. The solution was split in four vials, 1 ml (4 mg cluster) per vial, and dried under reduced pressure. In the first vial 0.5 ml of CD_3OD were added, in the second 0.75 ml of CD_2Cl_2 and in the third 0.75 ml of CD_3CN. The last vial was discharged. The obtained solutions were loaded in three different NMR tubes and warmed at 40°C for eight days. The experiments were followed by ^1H NMR spectroscopy (**Figures 10.55, 10.56** and **10.57**). After eight days the **[$(CH_3)_2$]** cluster resulted stable since no variation can be detected in the proton spectra.

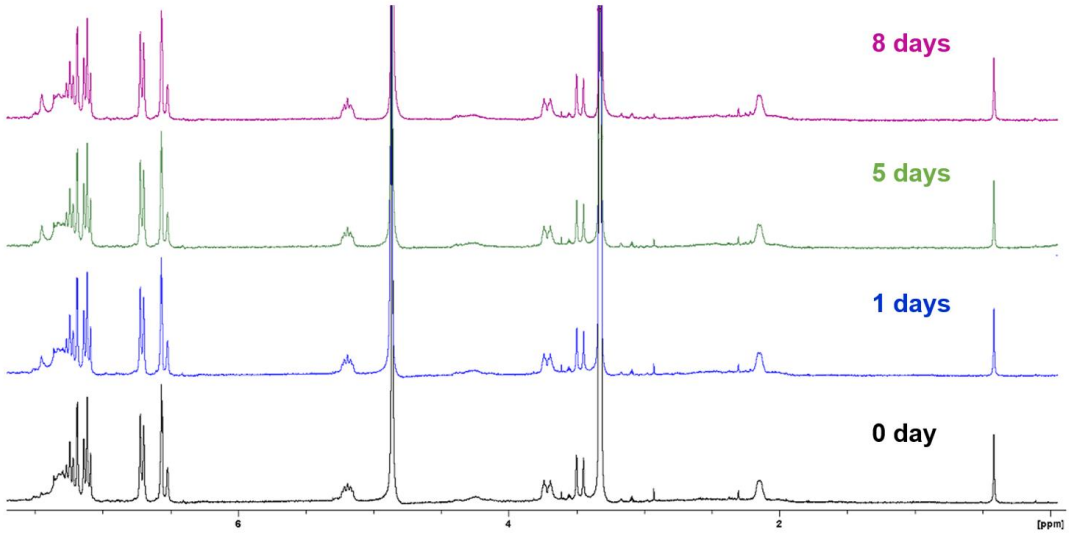

Figure 10.55: ^1H NMR spectra of **[$(CH_3)_2$]** in CD_3OD after 0 (black), 1 (blue), 5 (green) and 8 days (purple) under warming at 40°C.

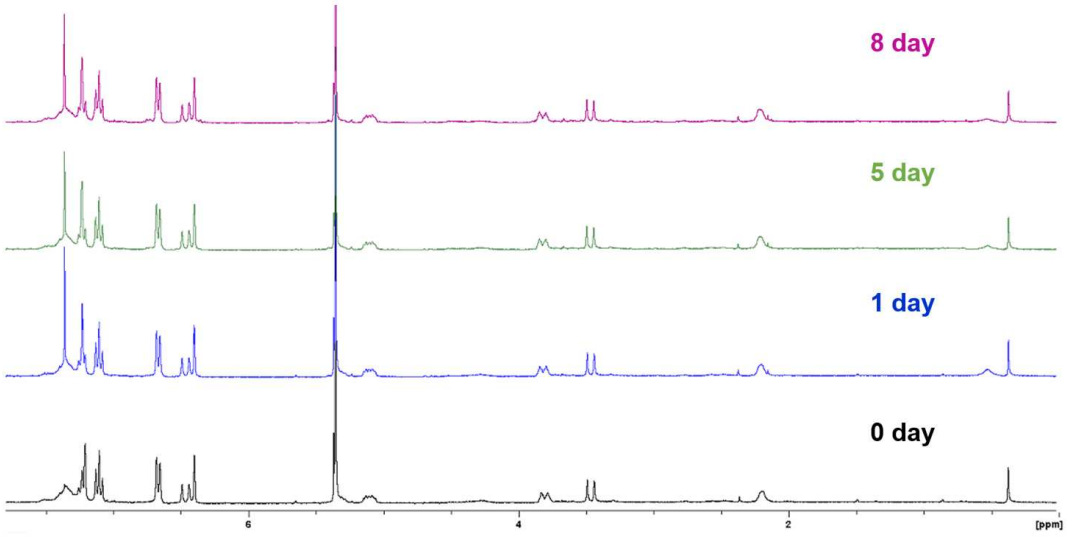

Figure 10.56: ^{1}H NMR spectra of **[$(CH_3)_2$]** in CD_2Cl_2 after 0 (black), 1 (blue), 5 (green) and 8 days (purple) under warming at 40°C.

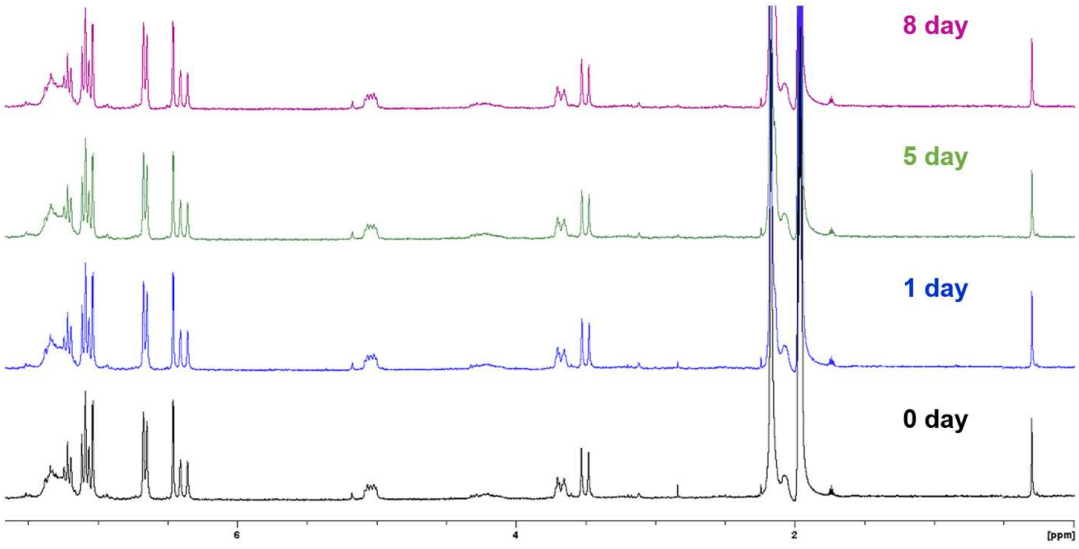

Figure 10.57: ^{1}H NMR spectra of **[$(CH_3)_2$]** in CD_3CN after 0 (black), 1 (blue), 5 (green) and 8 days (purple) under warming at 40°C.

*10.5.10 Q-TOF HRMS signals of clusters **[Br$_2$]**, **[Cl$_2$]**, **[(CH$_3$)Br]**, **[(CH$_3$)Cl]**, **[(CH$_3$)$_2$]***

Table 10.3 list of measured and calculated m/z peaks present in the Q-TOF HRMS analyses referred to AuNCs derived from reduction of **a** and **a'** complexes.

Cluster name	Measured (m/z)	Calculated (m/z)	Δm (ppm)	Formula
[(CH$_3$)$_2$]	1457.5437 2203.8020	1457.5500 2203.8096	4.3223 37.291	$[Au_{13}(C_{23}H_{24}N_4)_5(CH_3)_2]^{3+}$ $[Au_{13}(C_{23}H_{24}N_4)_5(CH_3)_2]Cl^{2+}$
[(CH$_3$)$_2$]-PF$_6$	1457.6583 2258.9766	1457.5500 2258.8074	74.297 74.901	$[Au_{13}(C_{23}H_{24}N_4)_5(CH_3)_2]^{3+}$ $[Au_{13}(C_{23}H_{24}N_4)_5(CH_3)_2](PF_6)^{2+}$
[(CH$_3$)Br]	1479.2886	1479.1692	80.714	$[Au_{13}(C_{23}H_{24}N_4)_5(CH_3)Br]^{3+}$
[(CH$_3$)Cl]	1464.1909 2214.2756	1464.1924 2214.2729	1.0245 1.2194	$[Au_{13}(C_{23}H_{24}N_4)_5(CH_3)Cl]^{3+}$ $[Au_{13}(C_{23}H_{24}N_4)_5(CH_3)Cl]Cl^{2+}$
[Br$_2$]	1500.9412 2430.3199	1500.8009 2430.3018	93.475 7.4476	$[Au_{13}(C_{23}H_{24}N_4)_5Br_2]^{3+}$ $[Au_{13}(C_{23}H_{24}N_4)_5Br_2](AuBr_2)^{2+}$
[Cl$_2$]	1471.1533	1471.1680	9.9922	$[Au_{13}(C_{23}H_{24}N_4)_5Cl_2]^{3+}$

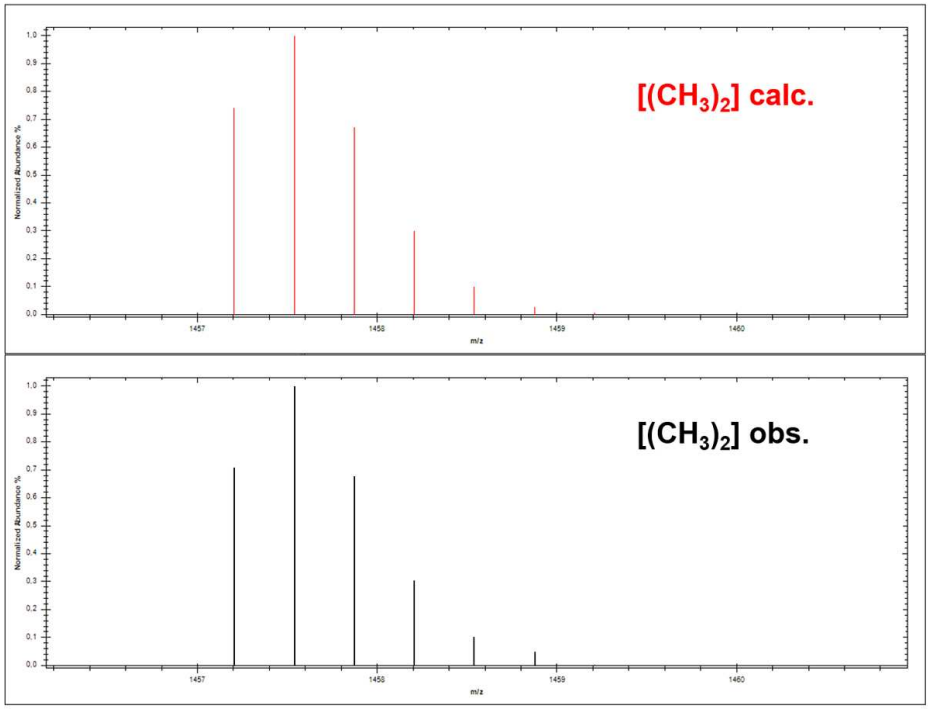

Figure 10.58: calculated (red) and observed (black) HRMS peaks refereed to **[(CH$_3$)$_2$]** cluster, presenting formula $[Au_{13}(C_{23}H_{24}N_4)_5(CH_3)_2]^{3+}$.

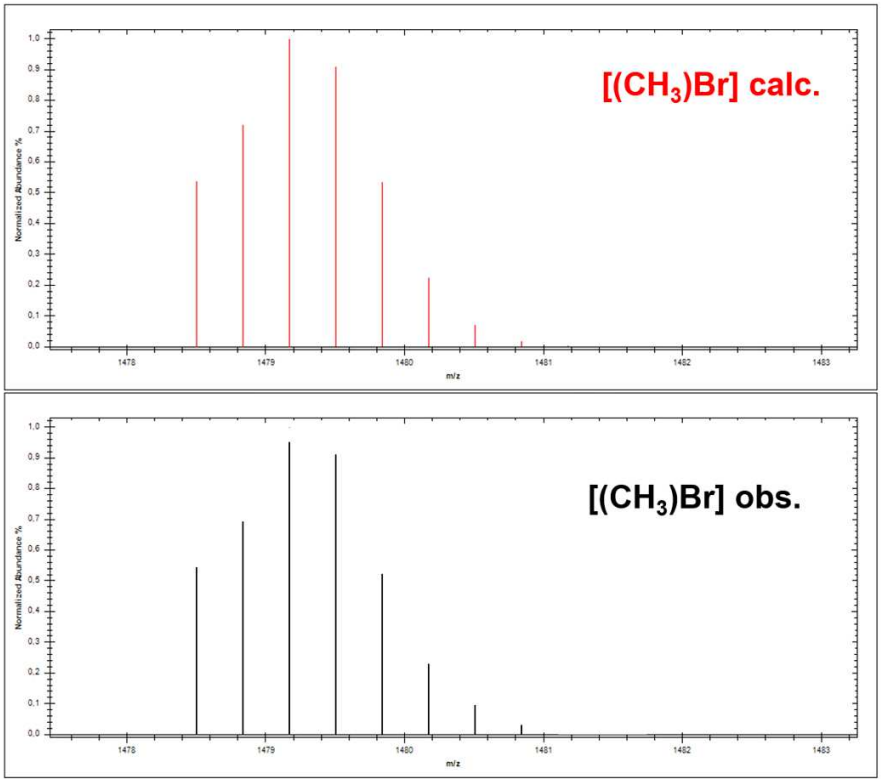

Figure 10.59: calculated (red) and observed (black) HRMS peaks refereed to **[(CH₃)Br]** cluster, presenting formula $[Au_{13}(C_{23}H_{24}N_4)_5(CH_3)Br]^{3+}$.

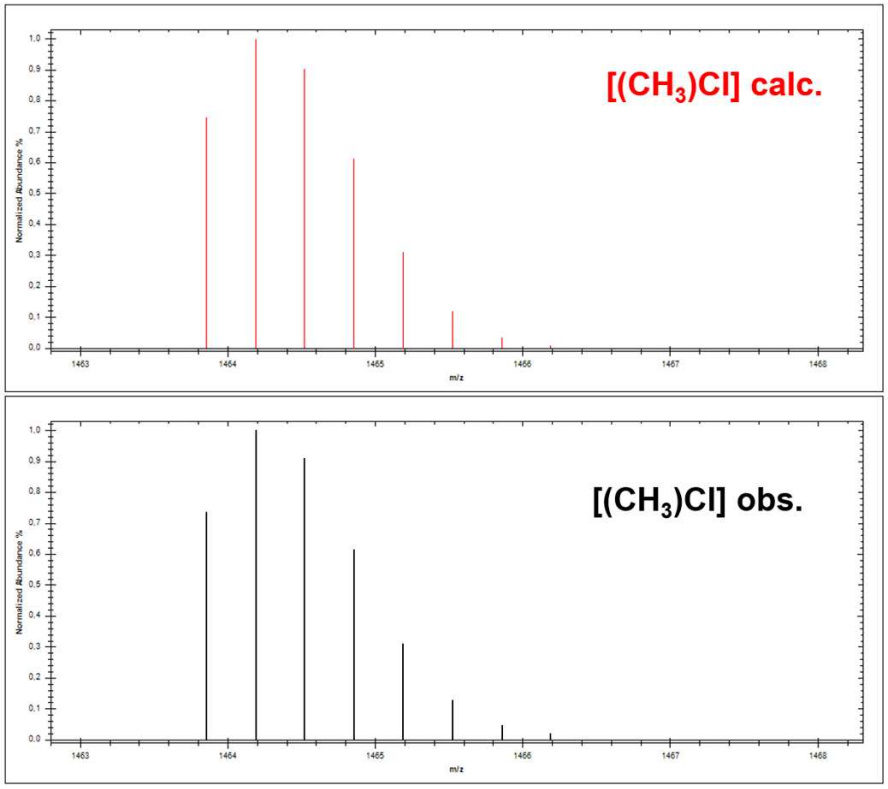

Figure 10.60: calculated (red) and observed (black) HRMS peaks refereed to **[(CH₃)Cl]** cluster, presenting formula $[Au_{13}(C_{23}H_{24}N_4)_5(CH_3)Cl]^{3+}$.

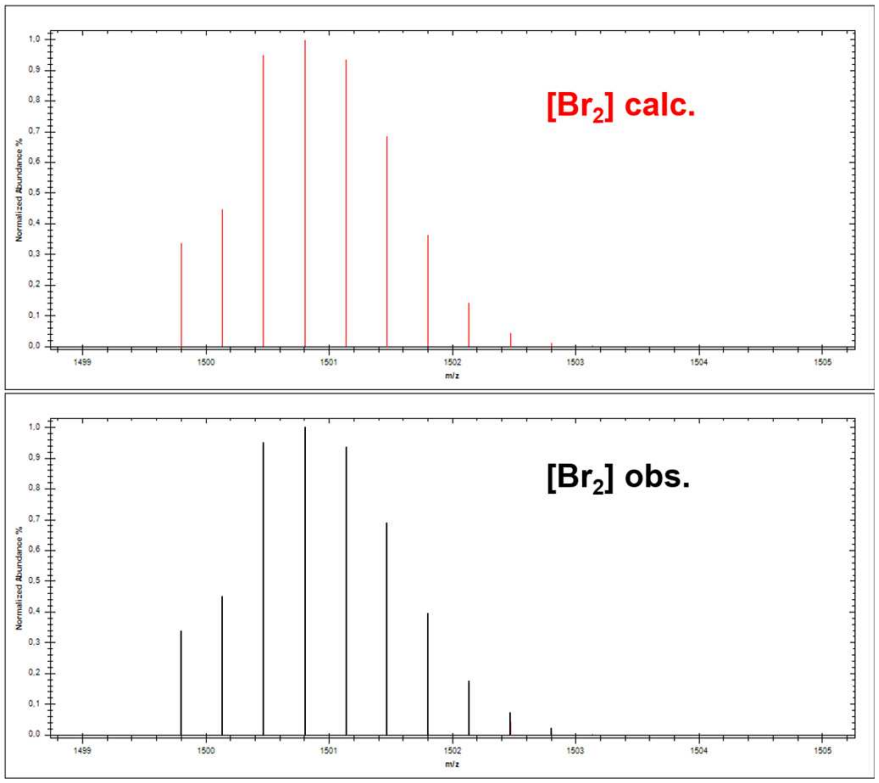

Figure 10.61: calculated (red) and observed (black) HRMS peaks refereed to **[Br_2]** cluster, presenting formula $[Au_{13}(C_{23}H_{24}N_4)_5Br_2]^{3+}$.

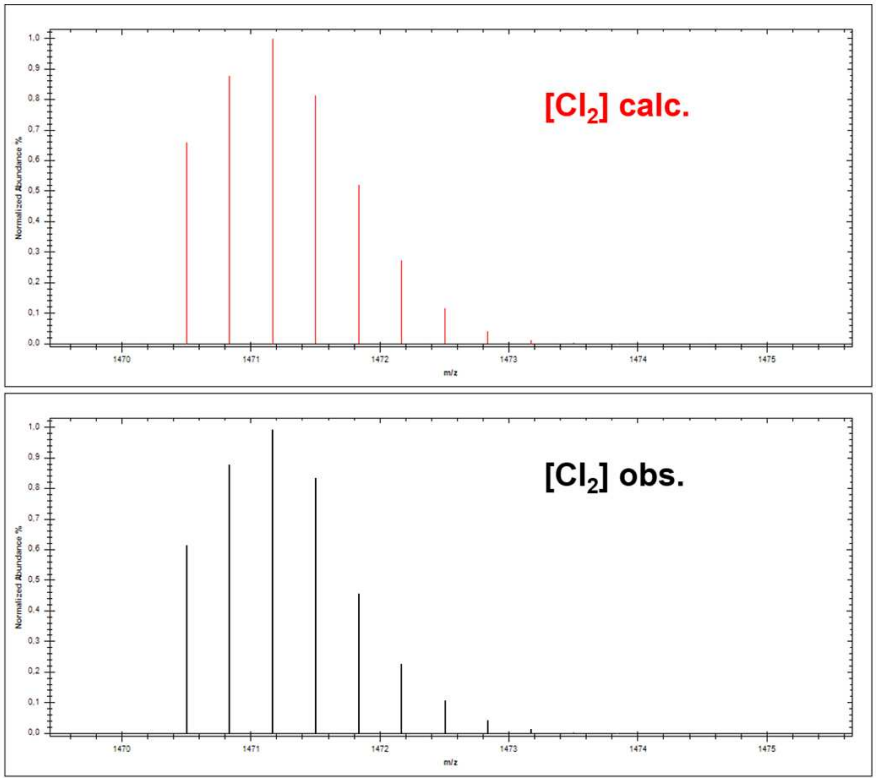

Figure 10.62: calculated (red) and observed (black) HRMS peaks refereed to **[Cl_2]** cluster, presenting formula $[Au_{13}(C_{23}H_{24}N_4)_5Cl_2]^{3+}$.

10.5.11 Single crystal X-ray diffractometry of ***[Cl$_2$]***

The crystallographic data for compound **[Cl$_2$]** was collected on a Bruker D8 Venture Photon II single-crystal diffractometer working with monochromatic Mo-Kα radiation and equipped with an area detector. The structure was solved and refined against F^2 with SHELXL-2014/7 with anisotropic thermal parameters for all non-hydrogen atoms.[31,32] Idealized geometries were assigned to the hydrogen atoms, excepted those of the water solvent molecules. Crystallographic data were deposited with the Cambridge Crystallographic Data Centre as supplementary publication. Copy of the data (CCDC Deposition Number 2264795) can be obtained free of charge on application to the CCDC, 12 Union Road, Cambridge CB2 1EZ, U.K. (fax, (+44) 1223 336033; e-mail, deposit@ccdc.cam.ac.uk). Crystal data and refinement parameters are reported in **Table 10.4**

Table 10.4: Crystal data and structure refinement of **[Cl$_2$]**.

Empirical formula	$C_{119}H_{142}N_{20}O_7Cl_{13}Au_{13}$
Formula weight	4985.93
Temperature/K	200(2)
Crystal system	triclinic
Space group	*P*-1
a/Å	16.3933(4)
b/Å	18.9537(6)
c/Å	23.4801(7)
α/°	80.862(2)
β/°	84.531(2)
γ/°	73.669(2)
Volume/Å^3	6902.5(4)
Z	2
ρ_{calc}g/cm^3	2.399
μ/mm^{-1}	14.064
F(000)	4600.0
Crystal size/mm^3	0.18 × 0.17 × 0.15
Radiation	MoKα (λ = 0.71073)
2Θ range for data collection/°	3.21 to 71.344
Index ranges	-25 ≤ *h* ≤ 25, -30 ≤ *k* ≤ 28, -36 ≤ *l* ≤ 37
Reflections collected	410101
Independent reflections	51057 [R_{int} = 0.0827, R_{sigma} = 0.0719]
Data/restraints/parameters	51057/0/1549
Goodness-of-fit on F^2	1.041
Final R indexes [I>=2σ (I)]	R1 = 0.0408, wR2 = 0.0914
Final R indexes [all data]	R1 = 0.0979, wR2 = 0.1098

R1 = ∑|Fo − Fc|/∑(Fo); wR2 = $[\sum[w(Fo^2 - Fc^2)^2]/\sum[w(Fo^2)^2]]^{1/2}$.

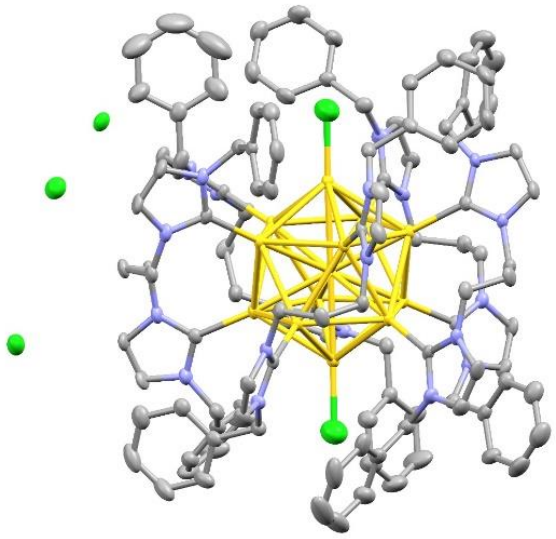

Figure 10.63: X-ray structure of **[Cl_2]**. Ellipsoids are drawn at their 30 % probability level. Hydrogens atoms, dichloromethane and water crystallization molecules are omitted for clarity. Color code: yellow (Au), green (Cl), purple (N), grey (C).

10.6 REDUCTION OF GOLD COMPLEXES WITH Na/NaCl (5% w/w)

These reactions were performed in glovebox. Gold complexes **b, c'**, **m** and **n** (0.05 mmol) were dispersed in 5 ml of THF. The mixtures were loaded in 20 ml pressure tubes and subsequently 0.5 mmol of Na/NaCl (5% w/w), based on sodium(0), were added in one portion. The mixtures were left under stirring for 24 h at room temperature. In all experiments a variation of color was detected after 1-3 h, affording black solids dispersed in red or green solutions. After 24 h under stirring the mixtures were filtered on celite and the filtrates dried under vacuum. The obtained solids were dissolved in MeOH and analyzed by Q-TOF HRMS.

No one of the tested complexes provided AuNCs detectable by Q-TOF HRMS. One of the recorded HRMS spectra is reported as example in **Figure 10.64**.

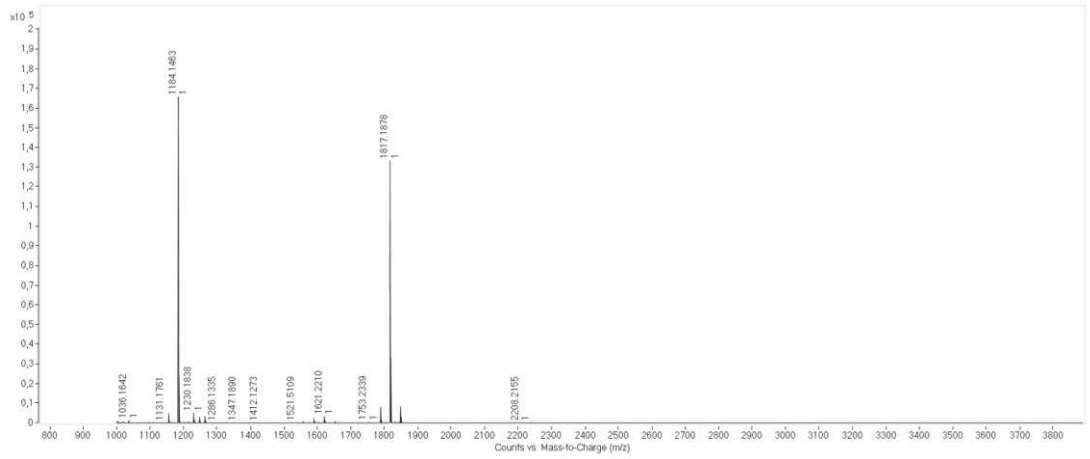

Figure 10.64: Q-TOF HRMS spectrum after reduction of **m** complex using Na/NaCl (5% w/w).

10.7 REDUCTION OF GOLD COMPLEXES WITH KH

These reactions were performed in glovebox. Gold complexes **b, c'**, **m** and **n** (0.05 mmol) were dispersed in 5 ml of THF. The mixtures were loaded in 20 ml pressure tubes and subsequently 0.5 mmol of KH were added in one portion. The dispersions were left under stirring for 24 h at room temperature. In all experiments a variation of color was detected after 1-3 h, affording red or purple mixtures. After 24 h the mixtures were filtered on celite and the filtrate collected in 20 ml vials. The vials were placed under air and MeOH (3 ml) was slowly added, to quench the excess of KH. The mixtures were left under stirring at room temperature for 15 minutes, affording dispersed solids in purple/reddish solutions. The mixtures were filtered on celite and the filtrates dried under vacuum, affording purple/reddish solids. These latter were dispersed in DCM (3 ml), filtered on celite and the filtrates dried under vacuum, affording again purple solids. 4 ml of MeOH were added to the solid residues, affording dispersed purple solids in reddish solutions. The mixtures were filtered on celite and the reddish filtrates (**MeOH fraction**) analyzed by Q-TOF HRMS. The solids remained on celite were recovered with DCM and the obtained solution (**DCM fraction)** analyzed by Q-TOF HRMS as well.

Only Q-TOF HRMS spectra of **MeOH fraction** derived from reduction of **b** complex showed one detectable AuNC signal at 1114.27 m/z (z: +2), despite it was not possible to determine its stoichiometric formula. In addition, classic $[Au_{13}(di\text{-}NHC^{b})_5Cl_2]^{3+}$ (1637.91 m/z) was detected in the same spectrum, confirming a low selectivity related to such reduction. The corresponding Q-TOF HRMS analysis is reported in **Figure 10.65**.

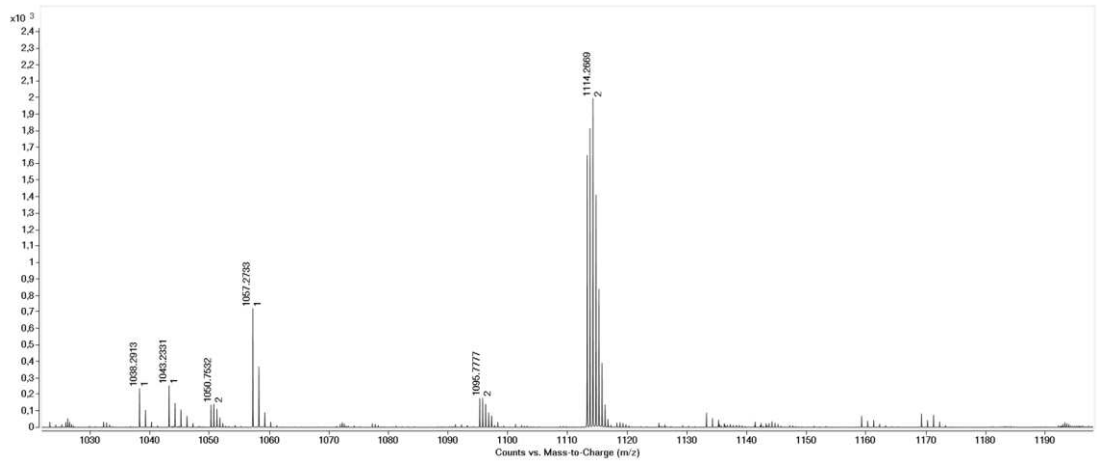

Figure 10.65: Q-TOF HRMS spectrum of fraction **MeOH** after reduction of **b** complex using KH.

In the experiment involving **n** complex it was possible to observe small AuNPs in TEM analysis related to the **DCM fraction**, reported in **Figure 10.66**. The UV-Vis analysis of this fraction (**Figure 10.67**) shows bands correlated to the presence of small AuNCs, in agreement with TEM analysis.

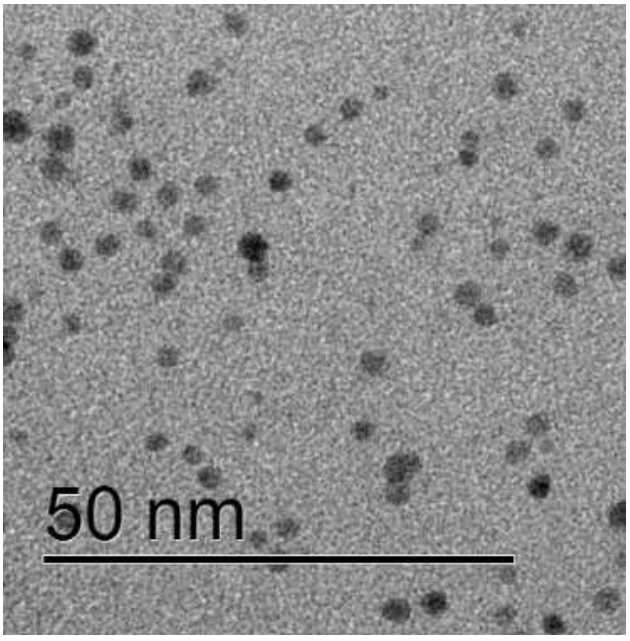

Figure 10.66: TEM imaging of small AuNPs derived from reduction of **n** complex with KH.

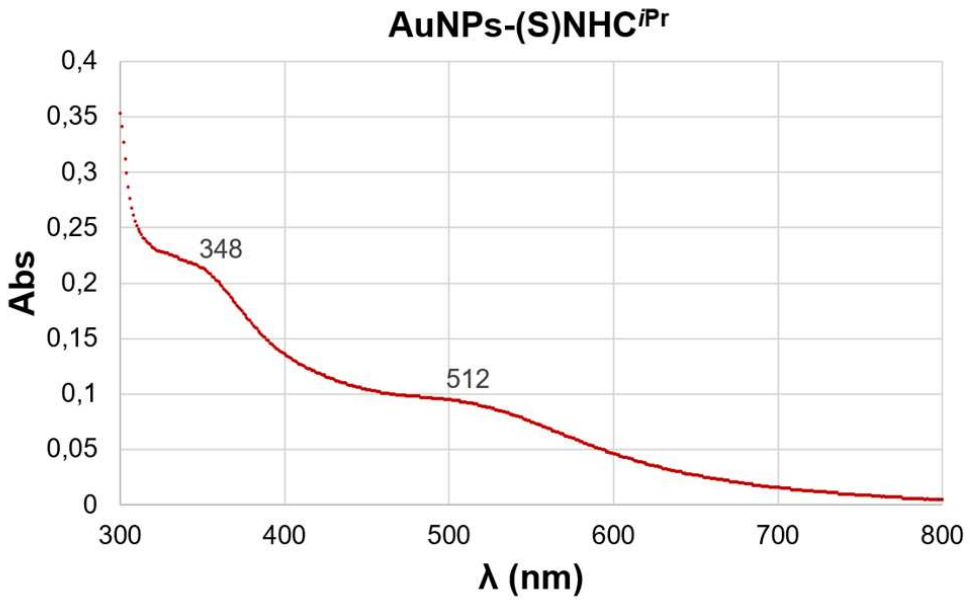

Figure 10.67: UV-Vis spectrum of small AuNPs derived from reduction of **n** complex with KH dissolved in DCM.

10.8 REDUCTION OF GOLD COMPLEXES BY HYDRAZINE MONOHYDRATE

10.8.1 Reduction of NHC Au(I) complexes

Au(I) complexes were loaded in 10 ml vials and dissolved in 1 ml of DCM:MeOH (4:1 v:v). Hydrazine monohydrate (10 equivalents) diluted in 4 ml of DCM was slowly added to complex solutions, kept under stirring. After few minutes from the addition the solutions assumed a blue-gray color, affording a black precipitate. To activate the hydrazine, 100 equivalents of KOH, pre-dissolved into 1 ml MeOH, were added into the solutions. After this addition, a yellow-orange color started slowly appearing. The reactions were left under stirring for 96 h at room temperature, and 100 µL withdrawals were performed at 3 h, 24 h, 48 h and 72 h. The reagents used in these experiments are reported in **Table 10.5**.

Each withdrawal and the reaction products were subjected to the following work-up: the solutions were evaporated to dryness, then DCM was added (0,5 ml for the withdrawals, 7 ml for the whole batch), affording dispersions of inorganic salts. The dispersions were sonicated and the solutions were filtered using a syringe PTFE filter. The filtrate was dried under vacuum, yielding an orange solid.

The corresponding Q-TOF HRMS spectra related to withdrawals of these experiments are reported in **Figure 10.68**, **10.69**, **10.70**, **10.71** and **10.72**.

Table 10.5: reagents used in the reduction of gold complexes with hydrazine.

	Complex (g)	Hydrazine (µl)	KOH (g)
a'	0.0188	11	0.1310
b'	0.0200	10	0.1234
c'	0.0409	25	0.3340
o	0.0198	19	0.2372

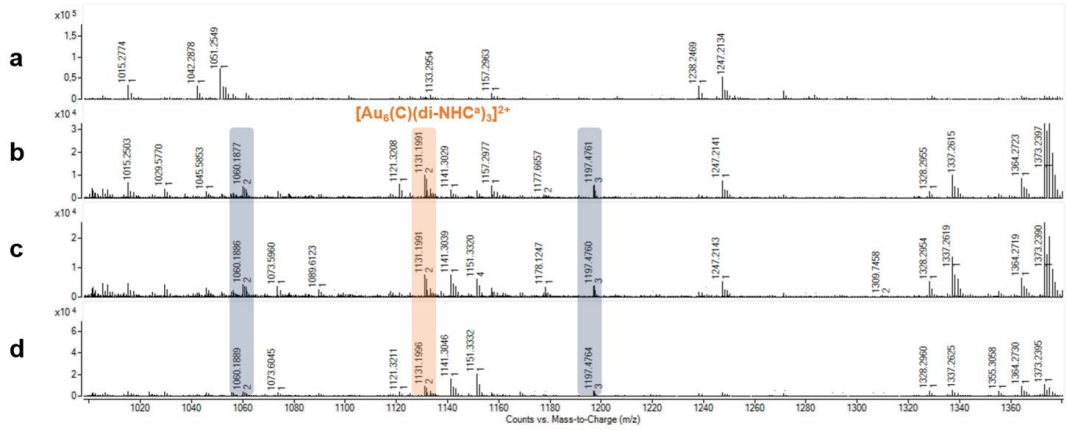

Figure 10.68: Q-TOF HRMS analysis related to withdrawals during the reduction of **a'** complex at a) 3 h, b) 24 h, c) 48 h and d) 72 h. The cluster $[Au_6(C)(di\text{-}NHC^a)_3]^{2+}$ is highlighted in orange. The unknown clusters are highlighted in grey.

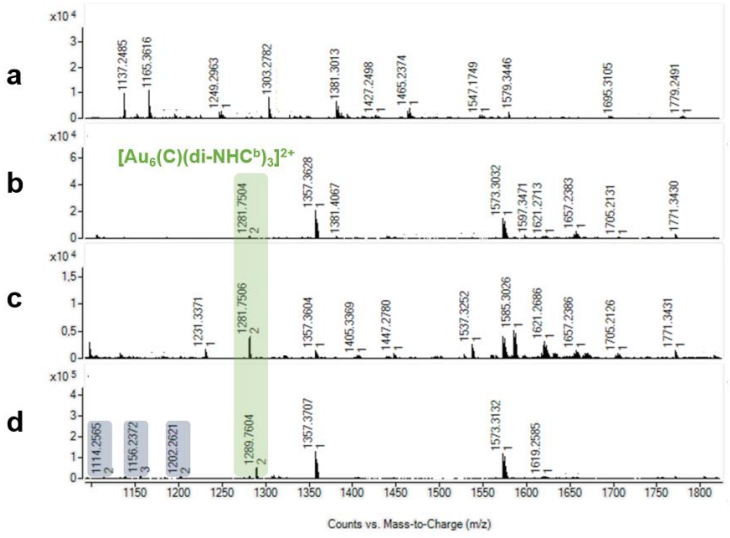

Figure 10.69: Q-TOF HRMS analysis related to withdrawals during the reduction of **b'** complex at a) 3 h, b) 24 h, c) 48 h and d) 72 h. The cluster $[Au_6(C)(di\text{-}NHC^b)_3]^{2+}$ is highlighted in green. The unknown clusters are highlighted in grey.

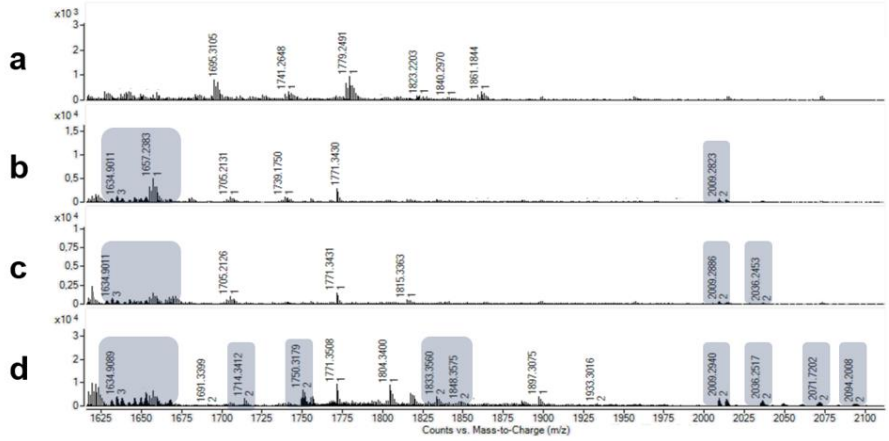

Figure 10.70: zoomed Q-TOF HRMS analysis related to withdrawals during the reduction of **b'** complex at a) 3 h, b) 24 h, c) 48 h and d) 72 h. The unknown clusters are highlighted in grey.

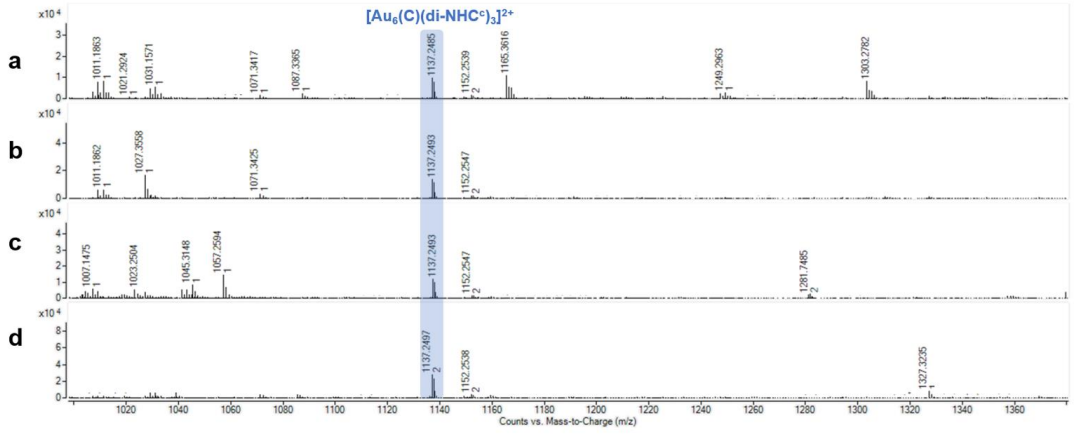

Figure 10.71: Q-TOF HRMS analysis related to withdrawals during the reduction of **c'** complex at a) 3 h, b) 24 h, c) 48 h and d) 72 h. The cluster $[Au_6(C)(di\text{-}NHC^c)_3]^{2+}$ is highlighted in blue.

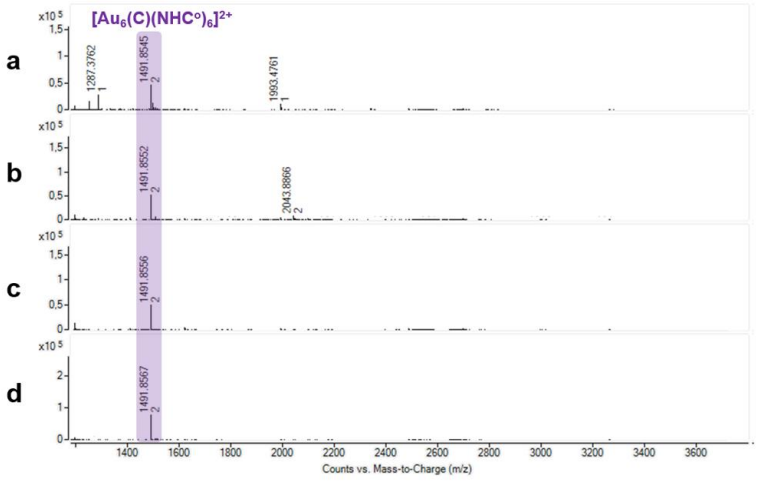

Figure 10.72: Q-TOF HRMS analysis related to withdrawals during the reduction of **o** complex at a) 3 h, b) 24 h, c) 48 h and d) 72 h. The cluster $[Au_6(C)(NHC^o)_6]^{2+}$ is highlighted in purple.

10.8.2 Attempts of purification of $[Au_6(C)(di\text{-}NHC^b)_3]^{2+}$ and $[Au_6(C)(di\text{-}NHC^c)_3]^{2+}$ clusters

In case of **b'** and **c'** complexes reduction a chromatographic separation on silica column was attempted, using DCM:MeOH (9:1) as eluent.

With the experiment involving **b'** the separation did not work properly, affording fractions containing different AuNCs.

With the experiment involving **c'** the separation was satisfactory, affording a fraction (Rf: 0.15) in which the main peak is $[Au_6(di\text{-}NHC^c)_3]^{2+}$, with a value of 1337.23 m/z, as reported in **Figure 10.73**, yielding 2 mg of red solid (6%). However, repeating the separation on further syntheses, the isolation of desired ionic cluster was not satisfactory, making this purification difficult to perform. Moreover, the values of integrals in the ^1H NMR spectrum (**Figure 10.75**) of this fraction does not match with the stoichiometric formula detected by Q-TOF HRMS. The UV-Vis and emission spectra are reported in **Figure 10.76** and **10.77**, respectively. The voltammogram of $[Au_6(di\text{-}NHC^c)_3]^{2+}$ is reported in **Figure 10.78**.

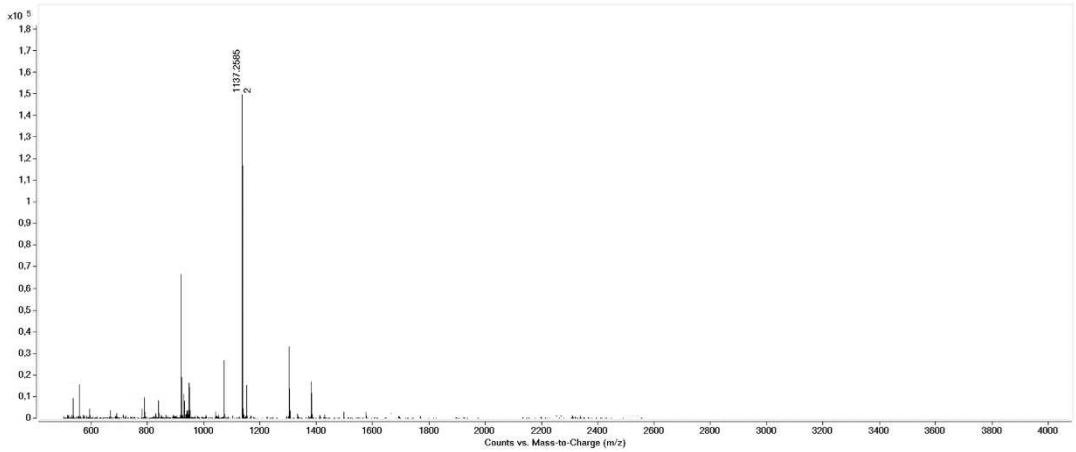

Figure 10.73: Q-TOF HRMS analysis related to purified fraction of $[Au_6(C)(di\text{-}NHC^c)_3]^{2+}$ derived from chromatographic separation.

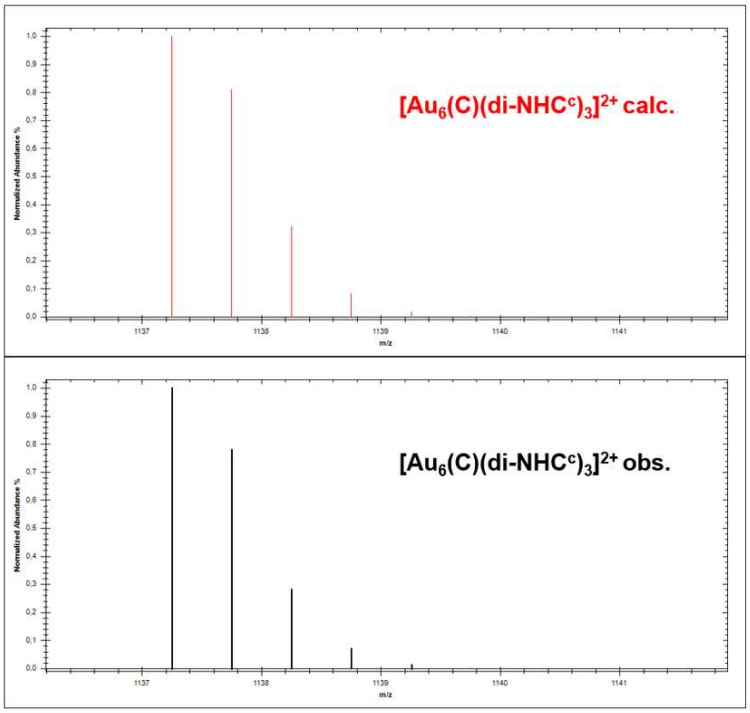

Figure 10.74:calculated (red) and observed (black) HRMS spectra of $[Au_6(C)(di\text{-}NHC^c)_3]^{2+}$, presenting formula $[Au_6(C)(C_{23}H_{28}N_4)_3]^{2+}$.

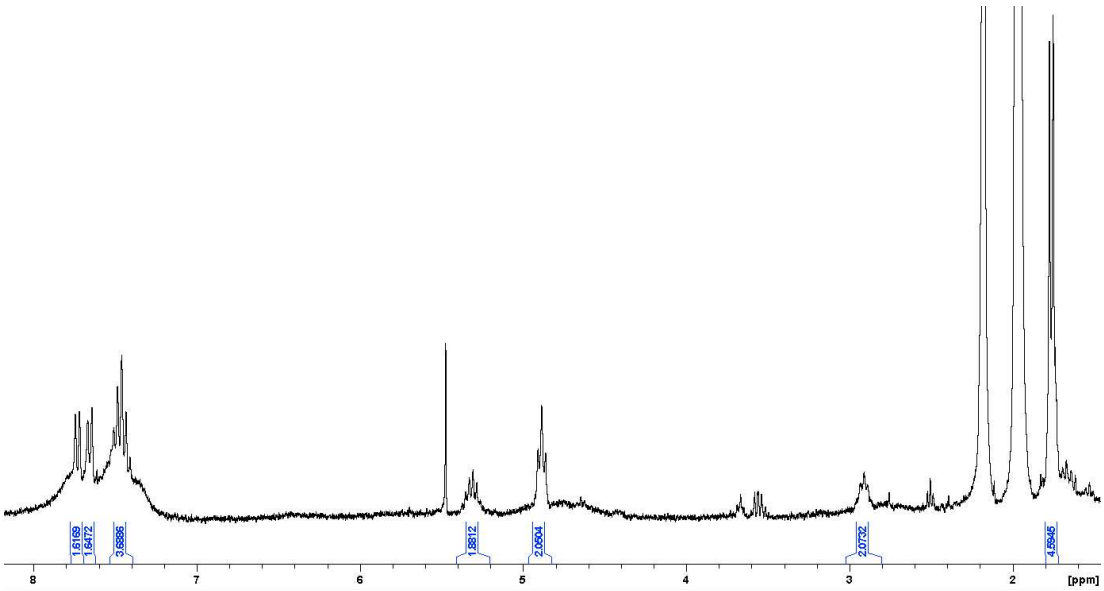

Figure 10.75: ^{1}H NMR spectrum related to purified fraction of $[Au_6(C)(di\text{-}NHC^c)_3]^{2+}$ derived from chromatographic separation.

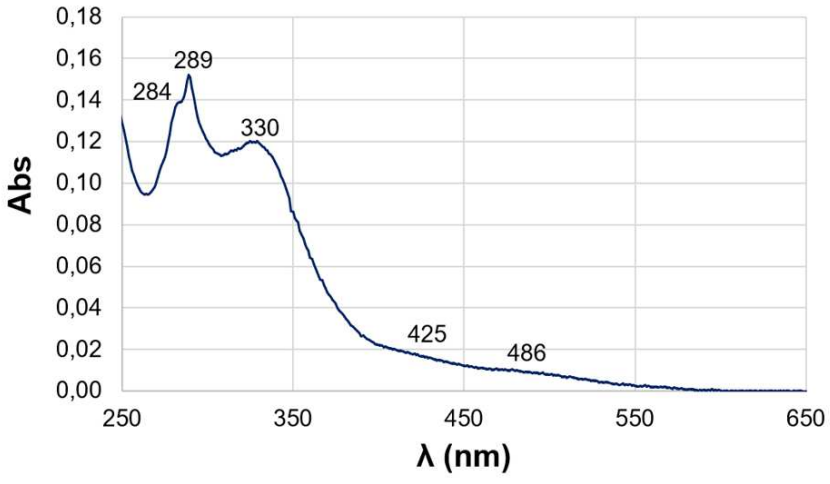

Figure 10.76: UV-Vis spectrum related to purified fraction of $[Au_6(C)(di\text{-}NHC^c)_3]^{2+}$, derived from chromatographic separation, dissolved in DCM.

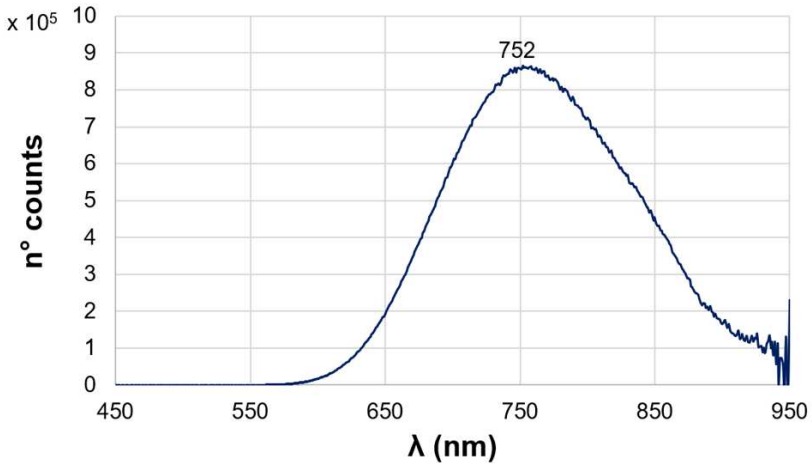

Figure 10.77: Emission spectrum related to purified fraction of $[Au_6(C)(di\text{-}NHC^c)_3]^{2+}$, derived from chromatographic separation, dissolved in DCM. QY: 1.64%.

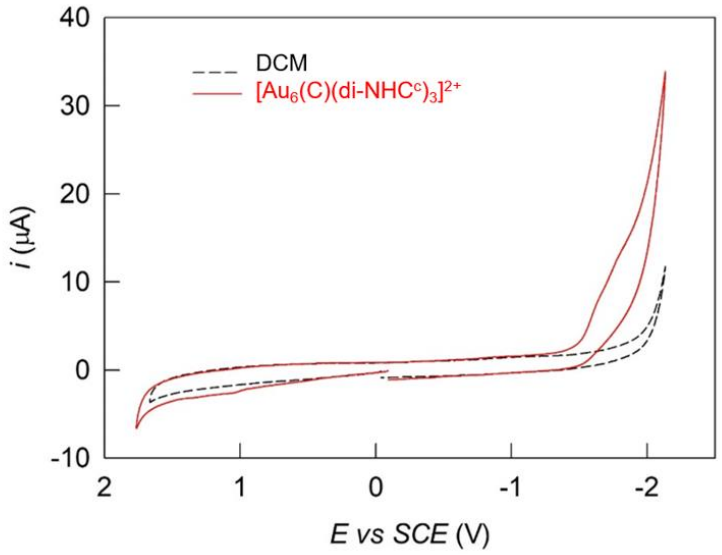

Figure 10.78: CV analysis related to purified fraction of $[Au_6(C)(di\text{-}NHC^c)_3]^{2+}$, derived from chromatographic separation, dissolved in DCM.

*10.8.3 Attempt of acid etching of the experiment involving **b'** complexes*

The crude product derived from **b'** reduction was dissolved in 6 ml of DCM:MeOH (4:1 v:v). 0.5 ml of concentrated HBr (48%) were mixed with 0.70 ml of distilled water. 0.5 ml of the resulting acid solution were added to the cluster solution (around 100 equivalents of HBr with respect to the starting complex). The color shifted overnight from orange to bright red. The dispersion was extracted with water three times (20 ml) and the organic phase was dried using sodium sulfate. The mixture was filtered and the resulting clear red filtrate was dried under vacuum, yielding a red solid. A sample of the solid was dissolved in DCM and analyzed via Q-TOF HRMS. This spectrum is reported in **Figure 10.79**, in which it is possible to detect $[Au_{13}(di\text{-}NHC^b)_5Br_2](X)^{2+}$ (X: Br, $AuCl_2$, $AuBr_2$) and $[Au_{11}(di\text{-}NHC^b)_4Br]^{2+}$ clusters.

$[Au_6(C)(di\text{-}NHC^b)_3]^{2+}$ is not present in this spectrum, confirming that acid etching degrades it.

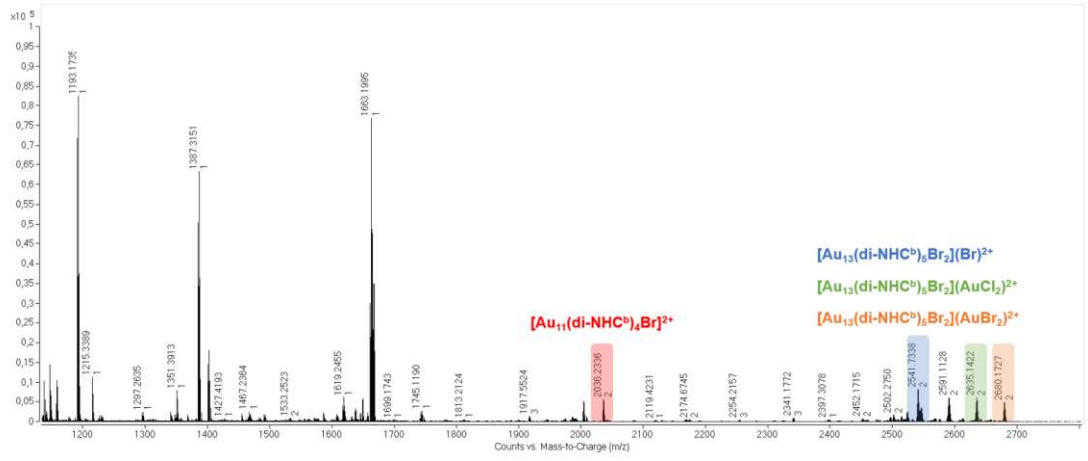

Figure 10.79:Q-TOF HRMS analysis recorded after acid etching on crude mixture derived from reduction of **b'** complexes. $[Au_{11}(di\text{-}NHC^b)_4Br]^{2+}$ and $[Au_{13}(di\text{-}NHC^b)_5Br_2](X)^{2+}$ (X: Br, $AuCl_2$, $AuBr_2$) clusters are respectively highlighted in red, blue, green and orange.

10.9 THE STEPWISE APPROACH

All reactions were performed in air using DCM as solvent. All reactions were monitored using Q-TOF HRMS.

10.9.1 Experiment with 1 equivalent of gold(I) complex

$[Au_{11}(PPh_3)_8Cl_2]Cl$ (5.8 mg, $1.3 \cdot 10^{-3}$ mmol) and **c'** (1.2 mg; $1.3 \cdot 10^{-3}$ mmol) were weighed in two different vials. The solids were each dissolved in 0.25 ml of DCM to afford a total volume of solution equal to 0.5 ml. The obtained solutions were mixed and stirred at room temperature for 31 days. After 21 days, Q-TOF HRMS highlighted the presence of the **1c** cluster. After 31 days the mixture was placed in a 40°C oil bath and left under stirring for 16 h. After the overnight warming, Q-TOF HRMS highlighted the presence of the **2c** cluster. The mixture was further stirred at room temperature for another 15 days, after which it was possible to observe degradation of the solution with formation of a black precipitate.

10.9.2 Experiments with 2 equivalents of gold(I) complex

*10.9.2.1 Experiment with complex a: **2a** cluster synthesis*

$[Au_{11}(PPh_3)_8Cl_2]Cl$ (4.0 mg, $0.92 \cdot 10^{-3}$ mmol) and **a** (1.5 mg, $1.8 \cdot 10^{-3}$ mmol) were weighed in two different vials. The solids were each dissolved in 0.75 ml DCM, to afford a total volume of solution equal to 1.50 ml. The obtained solutions were mixed and left under stirring at 40°C for 16 hours. Subsequently, the mixture was stirred at room temperature for 21 days. After this time Q-TOF HRMS highlighted the presence of clusters **2a** and **3a**. The solvent was evaporated under reduced pressure and 0.75 ml DCM were added. The sample underwent crystallization upon condensation of Et_2O vapour at -4°C: after one night, a pale orange solution and a deep red solid on the vial bottom were present. The solution was discharged and the red solid was dispersed in 1.40 ml of DCE. The solution was filtered on a PTFE filter and placed

under Et_2O vapour at room temperature for one day, causing again the separation of a deep red solid. The solution was removed and the red solid residue was dissolved in 0.3 ml DCM. The solution was loaded on a chromatographic silica column and eluted using DCM:MeOH (9:1 v:v) as eluent (Rf_{2a}: 0.68). Orange fractions were collected and solvent evaporation afforded cluster **2a** as a red solid. Yield 0.9 mg (22%).

^{31}P NMR (121 MHz, CD_2Cl_2): δ 57.11 (q, J = 5.04 Hz, 1P), δ 53.52 (q, J = 5.03 Hz, 1P), δ 51.09 (q, J = 5.05 Hz, 1P), δ 50.79 (q, J = 5.04 Hz, 1P).

Q-TOF HRMS (m/z): 4463.33 ($[Au_{13}(di\text{-}NHC^a)_2(PPh_3)_4Cl_4]^+$), 2243.16 m/z ($[Au_{13}(di\text{-}NHC^a)_2(PPh_3)_4Cl_4](Na)^{2+}$), 721.15 ($[Au(PPh_3)_2]^+$; fragmentation peak).

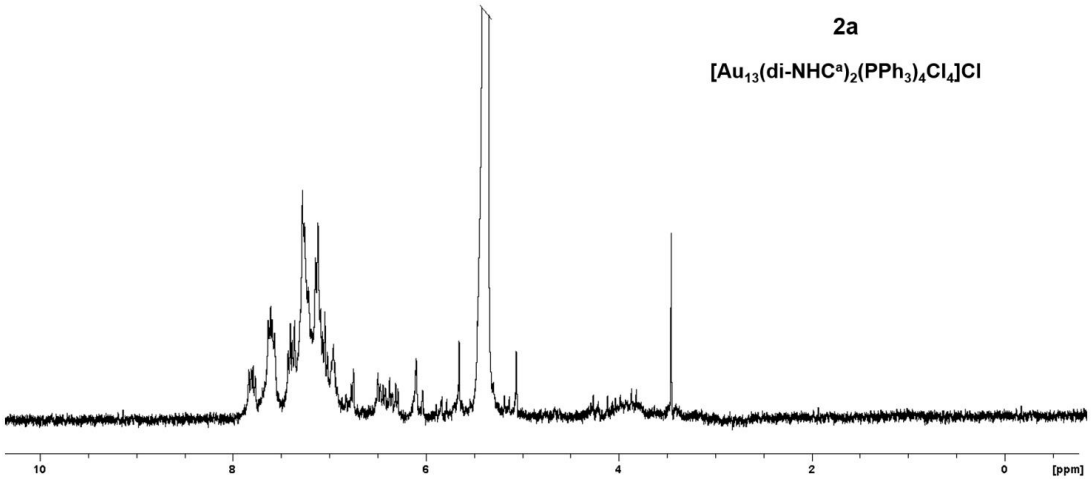

Figure 10.80: ^1H NMR spectrum of **2a** in CD_2Cl_2.

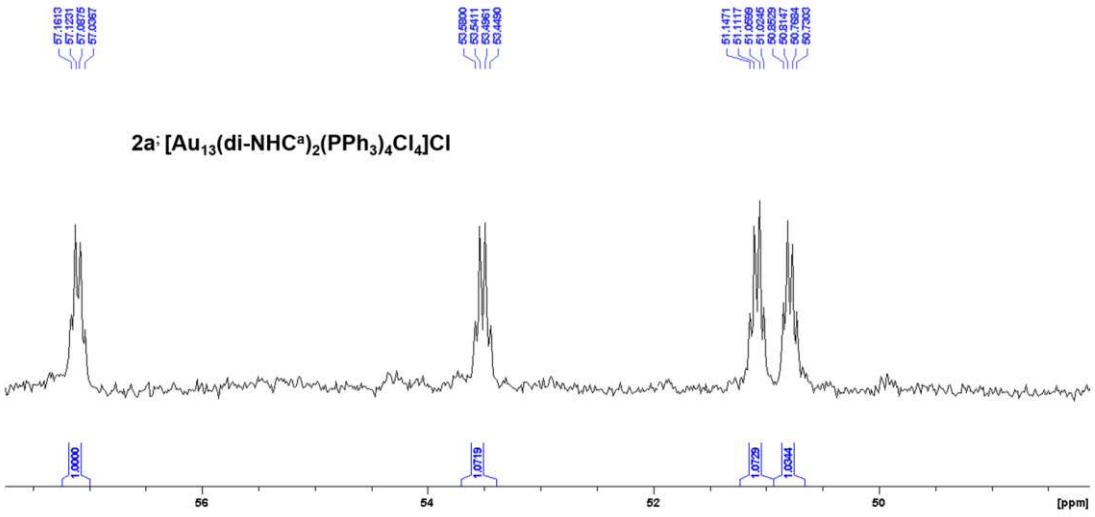

Figure 10.81: ^{31}P NMR spectrum of **2a** in CD_2Cl_2.

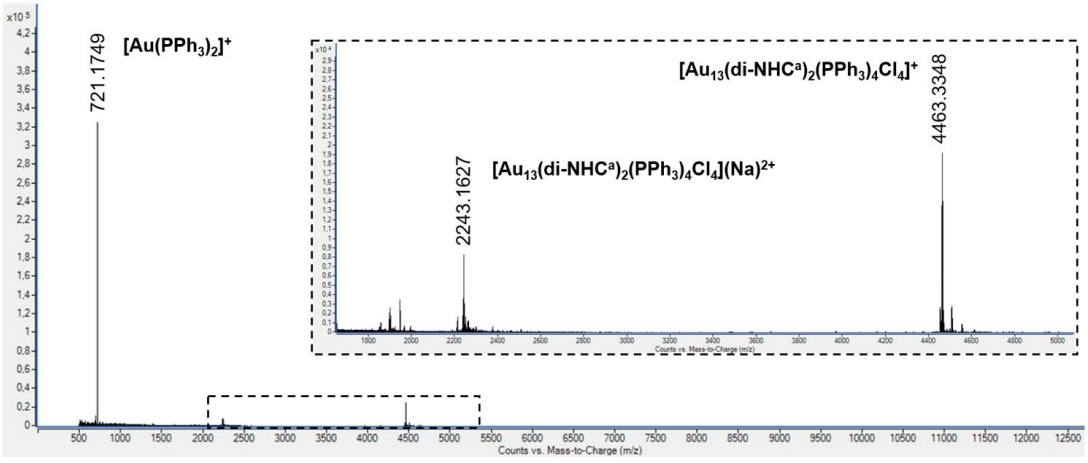

Figure 10.82: Q-TOF HRMS spectrum of **2a** in DCM.

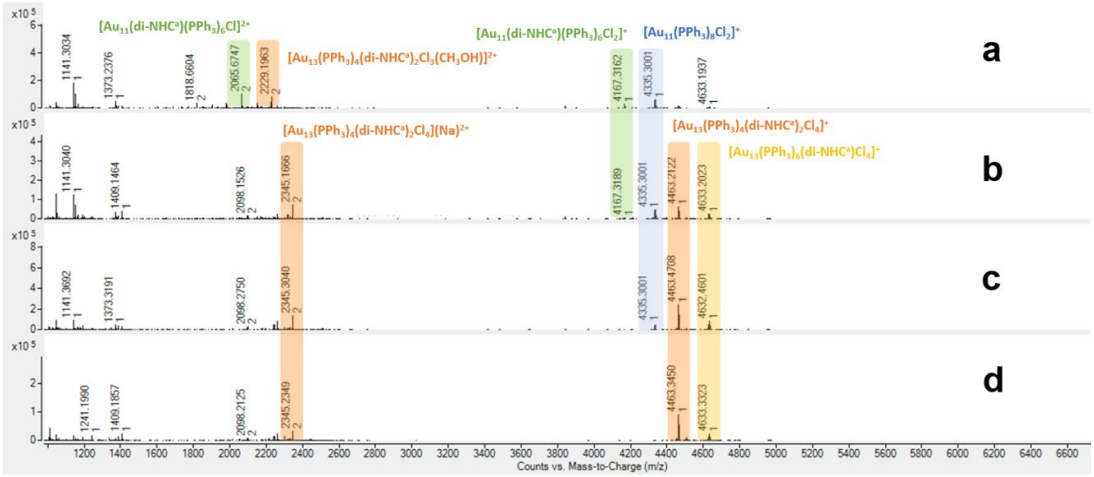

Figure 10.83: Q-TOF analyses of the reaction of $[Au_{11}(PPh_3)_8Cl_2]Cl$ with 2 equivalents of complex **a**. From above, a) after overnight warming, b) after 7 days, c) 14 days and d) 21 days at room temperature.

*10.9.2.3 First experiment with complex b: **3b** cluster synthesis*

$[Au_{11}(PPh_3)_8Cl_2]Cl$ (4.0 mg, $0.92 \cdot 10^{-3}$ mmol) and **b** (1.7 mg, $1.9 \cdot 10^{-3}$ mmol) were weighed in two different vials. The solids were each dissolved in 0.75 ml DCM, to afford a total volume of solution equal to 1.50 ml. The obtained solutions were mixed and left under stirring at 40°C for 16 h. Subsequently, the mixture was stirred at room temperature for 17 days. After this time, Q-TOF HRMS highlighted the presence of **2b** and **3b** clusters. The solvent was evaporated and 0.75 ml DCM were added. The sample underwent a crystallization upon condensation of Et_2O vapour at room temperature. After one day, a pale orange solution and deep red solid on the vial bottom were present. The solution was removed with a Pasteur pipette and the red solid was dried under reduced pressure. The solid was dispersed in 1.00 ml DCE. The obtained mixture was filtered on a PTFE filter and placed under Et_2O vapour at room temperature for one day, causing again the separation of a deep red solid. The solution was removed and the red solid was dissolved in 0.3 ml CD_2Cl_2. Both ^{31}P-NMR (**Figure 10.87**) and Q-TOF HRMS (**Figure 10.88**) highlighted the presence of clusters **2b** and **3b**. The mixture was loaded on a chromatographic silica column and eluted using DCM:MeOH (9:1 v:v) as eluent (Rf_{3b}: 0.30). Orange fractions were

collected and solvent evaporation afforded cluster **3b** as a red solid. Yield 1.7 mg (40%).

^{31}P NMR (121 MHz, CD_2Cl_2): δ 60.83 (s, 3P).

Q-TOF HRMS (m/z): 2411.73 ($[Au_{13}(di\text{-}NHC^b)_3(PPh_3)_3Cl_3]^{2+}$), 721.15 ($[Au(PPh_3)_2]^+$; fragmentation peak).

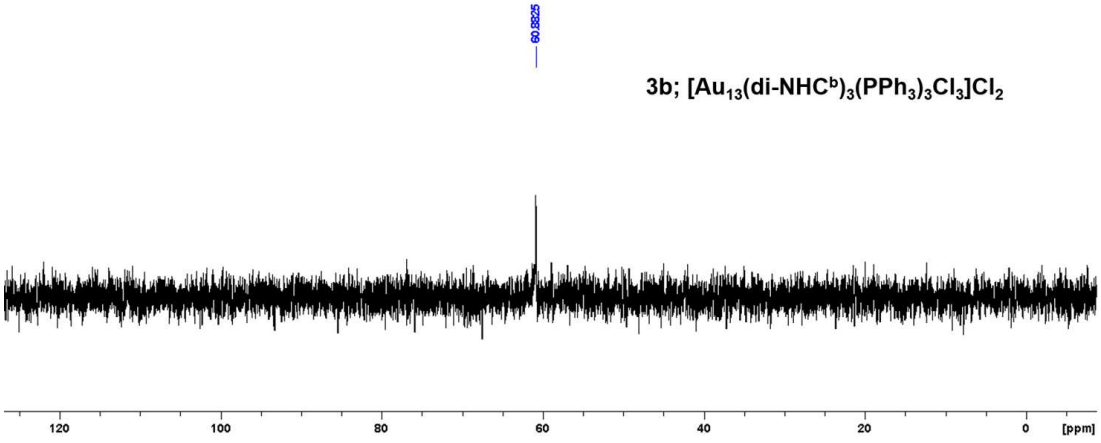

Figure 10.84: ^{31}P NMR spectrum of **3b** in CD_2Cl_2.

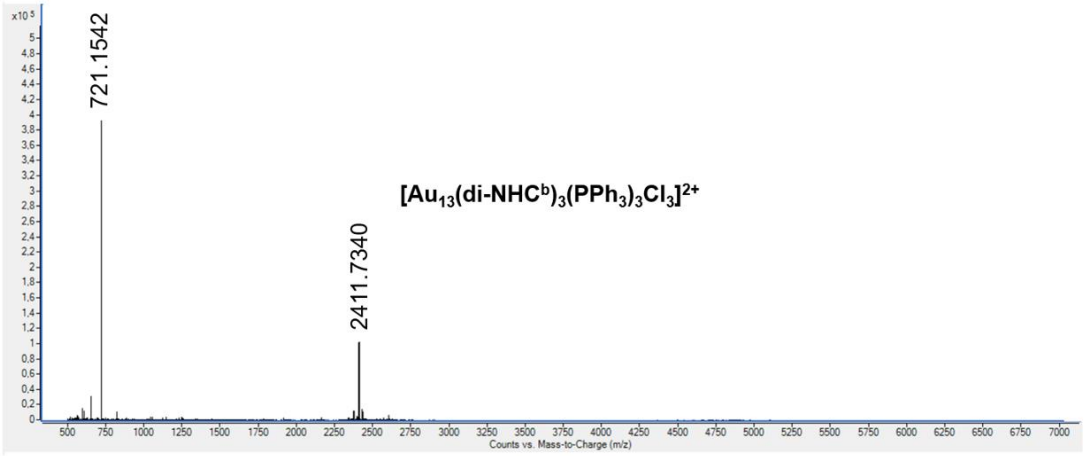

Figure 10.85: Q-TOF HRMS spectrum of **3b** in DCM.

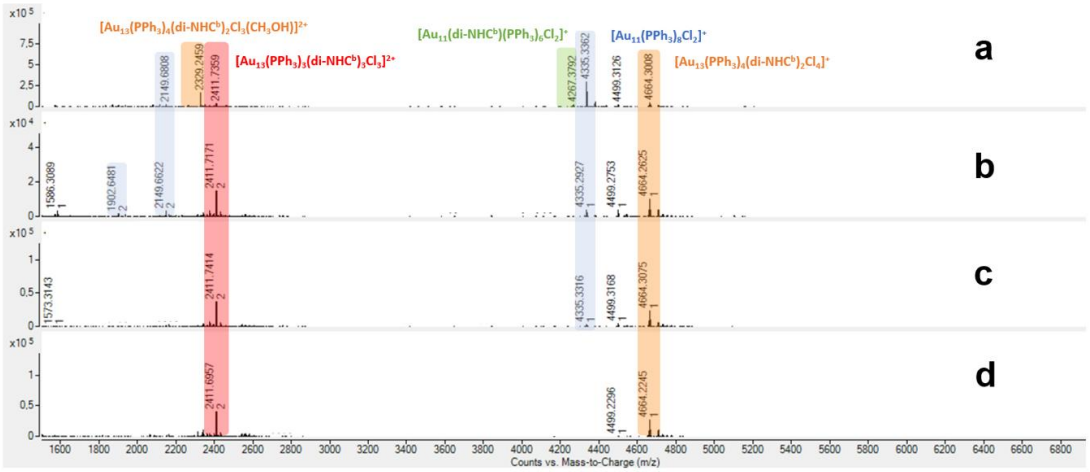

Figure 10.86: Q-TOF analyses of the reaction of $[Au_{11}(PPh_3)_8Cl_2]Cl$ with 2 equivalents of complex **b**. From above, a) after overnight warming, b) after 10 days, c) 15 days and d) 17 days at room temperature.

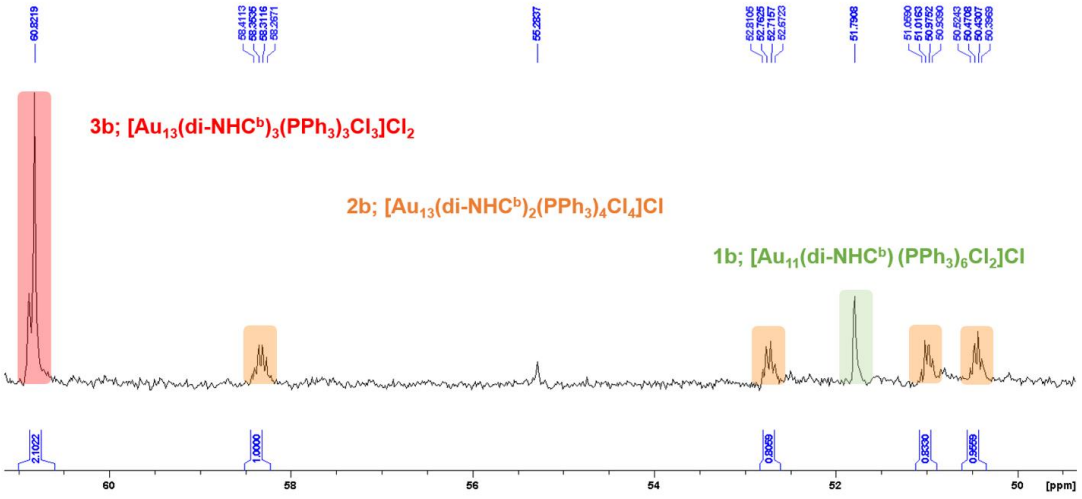

Figure 10.87: ^{31}P NMR spectra of reaction mixture dissolved in CD_2Cl_2 containing **2b** (orange), **3b** (red) and **1b** (green) before purification provided by chromatographic column.

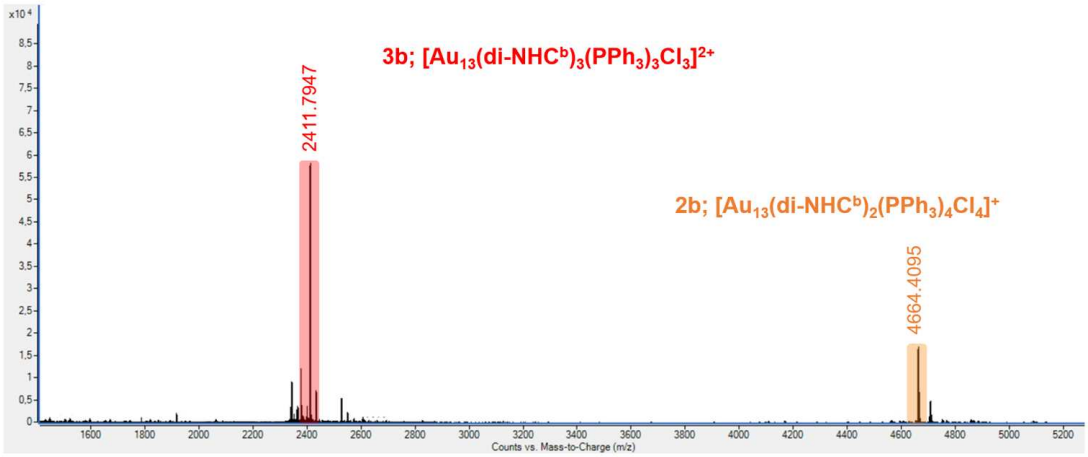

Figure 10.88: Q-TOF HRMS analysis of reaction mixture containing **2b** and **3b** before purification provided by chromatographic column.

*10.9.2.4 Second experiment with complex b: **1b** cluster synthesis*

$[Au_{11}(PPh_3)_8Cl_2]Cl$ (19.6 mg, $4.5 \cdot 10^{-3}$ mmol) and **b** (9.0 mg, $9.0 \cdot 10^{-3}$ mmol) were weighed in two different vials. The solids were each dissolved in 4 ml DCM, to afford a total volume of solution equal to 8 ml. The obtained solutions were mixed and left under stirring at 40°C for 72 h. The obtained mixture was filtered on a PTFE filter, loaded on a chromatographic silica column and eluted, using DCM:MeOH (9:1 v:v) as eluent (Rf_{3b}: 0.40). Orange fractions were collected and solvent evaporation afforded cluster **1b** as a red solid. Yield 2.3 mg (12%).

^{31}P NMR (121 MHz, CD_2Cl_2): δ 52.31 (s, 6P).

Q-TOF HRMS (m/z): 4267.70 ($[Au_{11}(di\text{-}NHC^b)(PPh3)_6Cl_2]^+$), 2067.68 ($[Au_{11}(di\text{-}NHC^b)(PPh_3)_6Cl]^{2+}$).

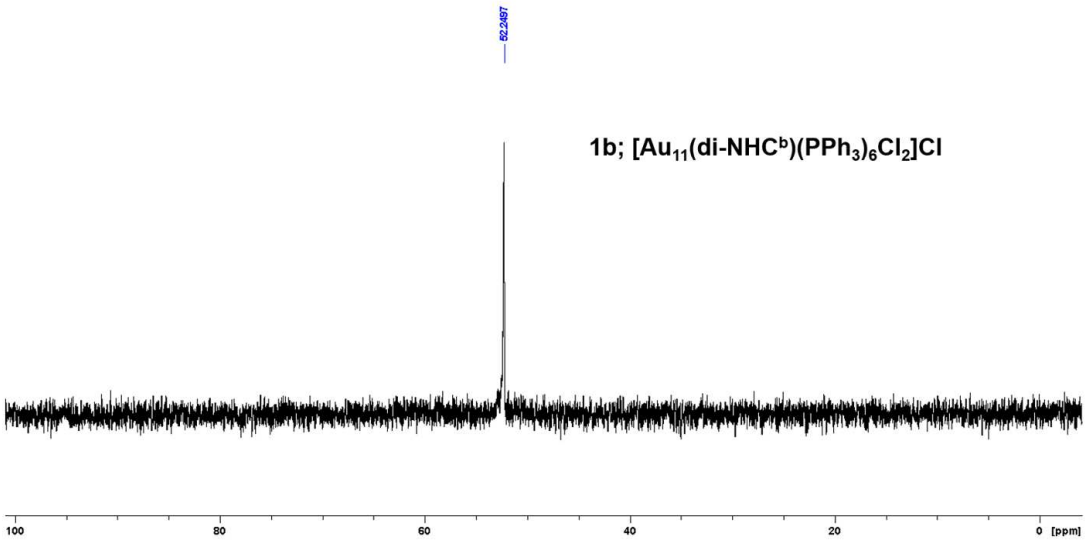

Figure 10.89: ^{31}P NMR spectrum of **1b** in CD_2Cl_2.

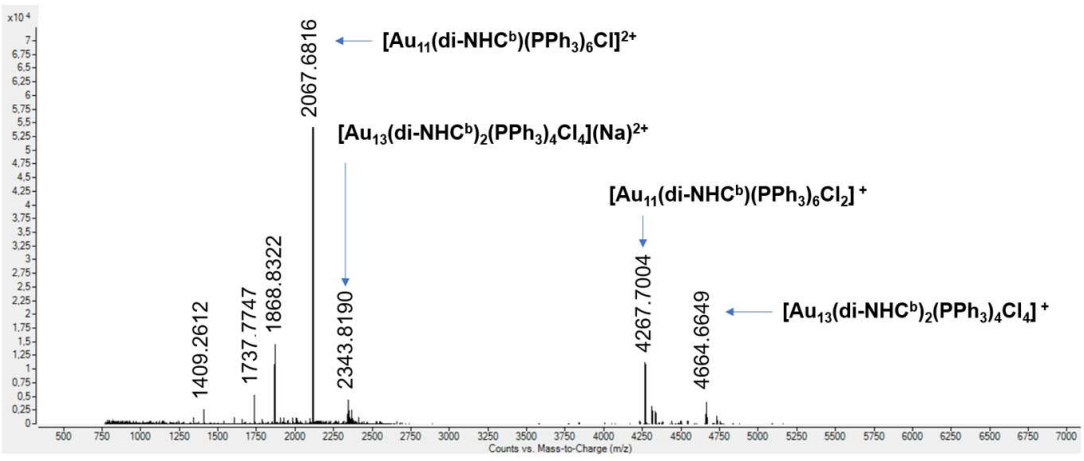

Figure 10.90: Q-TOF HRMS spectrum of **1b** in DCM.

10.9.2.5 First experiment with complex c

$[Au_{11}(PPh_3)_8Cl_2]Cl$ (4.0 mg, $0.92 \cdot 10^{-3}$ mmol) and **c** (1.5 mg; $1.8 \cdot 10^{-3}$ mmol) were weighed in two different vials. The solids were each dissolved in 0.75 ml DCM, to afford a total volume of solution equal to 1.50 ml. The obtained solutions were mixed and placed under stirring at 40°C for 16 h. Subsequently, the mixture was stirred at room temperature for 40 days. After 32 days, Q-TOF HRMS (**Figure 10.91**) highlighted the presence of cluster **1c**, together with smaller amounts of clusters **2c** and **3c**. After 45 days it was possible to observe degradation of the solution with formation of a black precipitate.

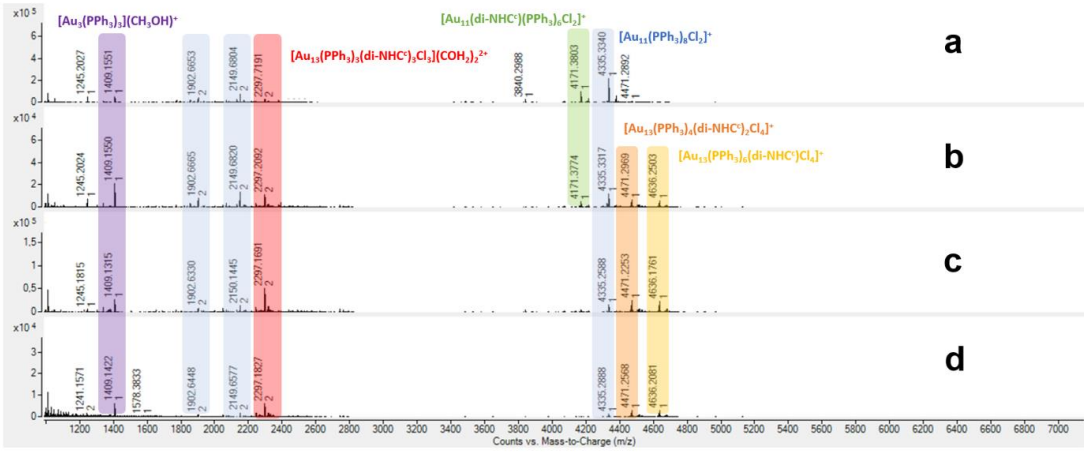

Figure 10.91: Q-TOF analyses of the reaction of $[Au_{11}(PPh_3)_8Cl_2]Cl$ with 2 equivalents of complex **c**. From above, a) after overnight warming, b) after 15 days, c) 30 days and d) 45 days at room temperature.

*10.9.2.6 Second experiment with complex c: **1c** cluster synthesis*

$[Au_{11}(PPh_3)_8Cl_2]Cl$ (16.2 mg; $4.05 \cdot 10^{-3}$ mmol) and **c** (6.1 mg; $7.40 \cdot 10^{-3}$ mmol) were weighed in two different vials. The solids were each dissolved in 3.25 ml DCM, to afford a total volume of solution equal to 6.50 ml. The obtained solutions were mixed and placed under stirring at 40°C for 3 days. The solution was subsequently filtered on a PTFE filter and the solvent was evaporated at reduced pressure; 1 ml DCM was then added to the red residue. The sample underwent an overnight crystallization upon condensation of Et_2O vapour at room temperature. The orange solution derived from crystallization was collected, concentrated and loaded on a chromatographic silica column, using DCM:MeOH (9:1 v:v) as eluent. All orange fractions were collected and solvent evaporation afforded cluster **1c** as a red solid. In this case, a trace of cluster $[Au_{11}(PPh_3)_8Cl_2]Cl$ was detected in the final sample; exploiting ^{31}P NMR spectrum integrals, it is possible to estimate the purity of cluster **1c** to be around 99%. Yield 3.7 mg (22%).

^{1}H-NMR (400 MHz, CD_2Cl_2): δ 7.48-7.29 (m, 57H), 7.03-6.94 (m, 17H), 6.89-6.79 (m, 24H), 6.20 (br, 2H), 4.10 (br, 4H), 3.00 (br, 2H), 0.92 (d, J = 6.15 Hz, 12H).

^{31}P NMR (121 MHz, CD_2Cl_2): δ 52.71 (br, 5P), 51.37 (br, 1P).

Q-TOF HRMS (m/z): 4171.34 ($[Au_{11}(di\text{-}NHC^c)(PPh3)_6Cl_2]^+$) , 721.15 ($[Au(PPh_3)_2]^+$; fragmentation peak).

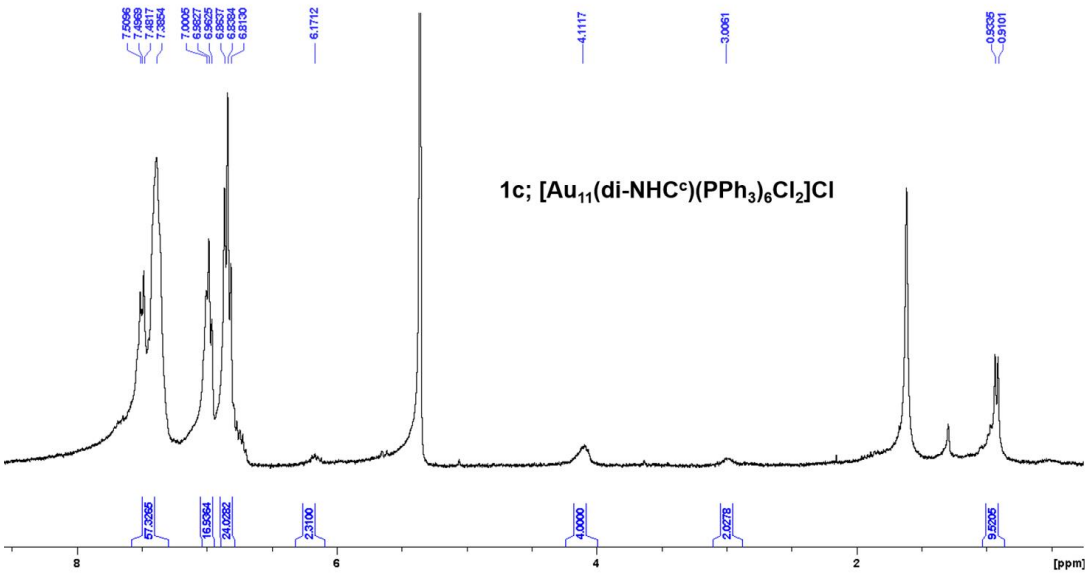

Figure 10.92: ^{1}H NMR spectrum of **1c** in CD_2Cl_2.

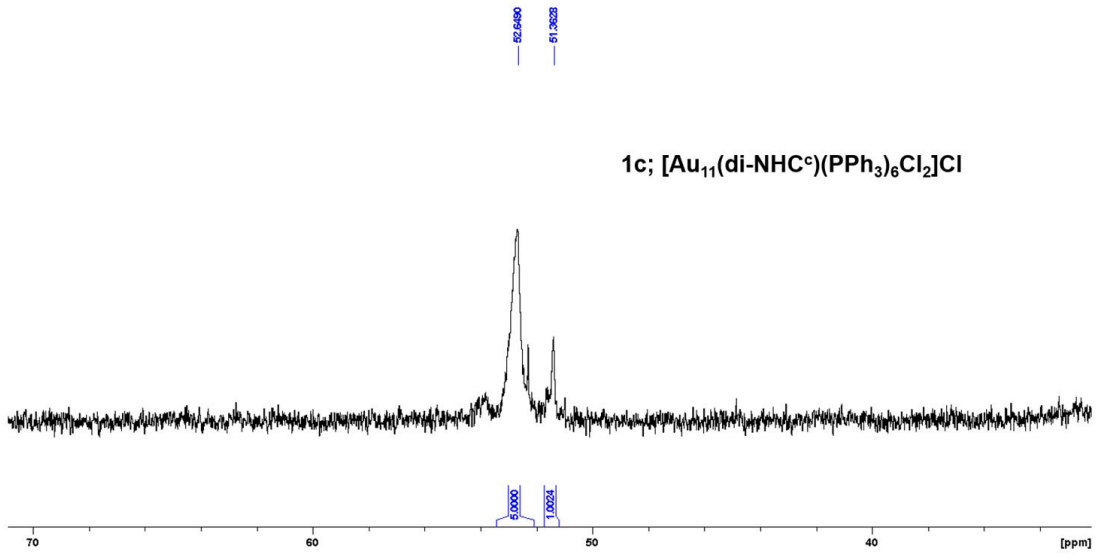

Figure 10.93: ^{31}P NMR spectrum of **1c** in CD_2Cl_2.

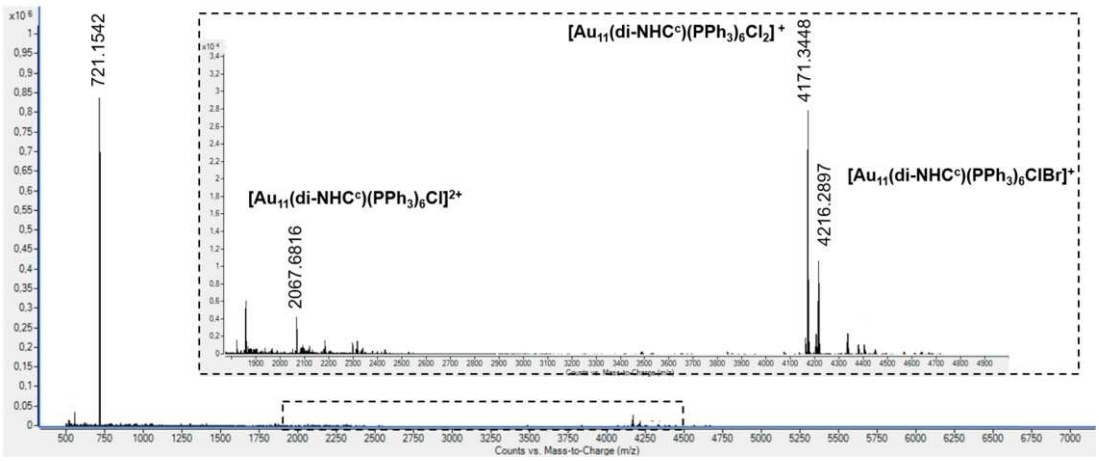

Figure 10.94: Q-TOF HRMS spectrum of **1c** in DCM.

10.9.3 Experiments with 3 equivalents of gold(I) complex

10.9.3.1 Experiment with complex a

$[Au_{11}(PPh_3)_8Cl_2]Cl$ (3.8 mg; $0.87 \cdot 10^{-3}$ mmol) and **a** (2.1 mg; $2.6 \cdot 10^{-3}$ mmol) were weighed in two different vials. The solids were each dissolved in 0.75 ml DCM, to afford a total volume of solution equal to 1.50 ml. The obtained solutions were mixed and placed under stirring at 40°C for 24 h. After this time a white precipitate was noticed in solution and filtered. Q-TOF HRMS of the orange solution (**Figure 10.95**) highlighted the presence of clusters **2a** and **3a** in traces only, together with $[Au_2(di\text{-}NHC^a)_2]^{2+}$, detected at 553.17 m/z.

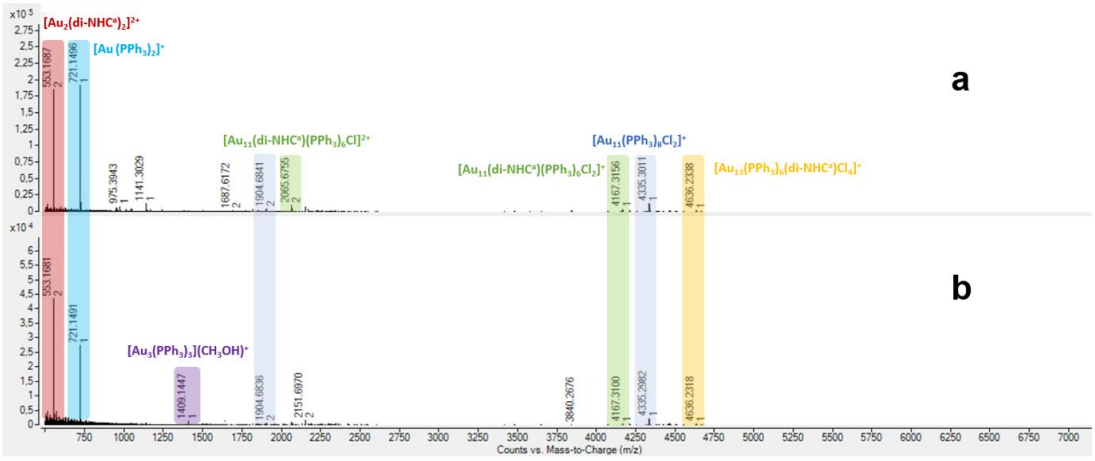

Figure 10.95: Q-TOF analyses of the reaction of $[Au_{11}(PPh_3)_8Cl_2]Cl$ with 3 equivalents of complex **a**, from above, a) after 21 h and b) 48 h under stirring at 40°C.

*10.9.3.2 Experiment with complex b: **2b'** and **3b** cluster synthesis*

$[Au_{11}(PPh_3)_8Cl_2]Cl$ (20.2 mg; $4.60 \cdot 10^{-3}$ mmol) and **b** (12.8 mg; $13.9 \cdot 10^{-3}$ mmol) were weighed in two different vials. The solids were each dissolved in 4.00 ml DCM, to afford a total volume of solution equal to 8.00 ml. The obtained solutions were mixed and placed under stirring at 40°C for 3 days. After this time, Q-TOF HRMS highlighted the presence of clusters **2b'** and **3b**. The reaction mixture was directly loaded on a chromatographic silica column and eluted using DCM:MeOH (9:1 v:v). The first orange fraction (Rf_{2b}: 0.60) was collected and set aside. The second orange fraction (Rf_{3b}: 0.30) was collected and the solvent was evaporated under reduced pressure to afford **3b** as a red solid. Yield 5.0 mg (22%). The first orange fraction was evaporated to dryness to obtain a red solid, which was redissolved in 0.50 ml DCM. This solution was again loaded on a chromatographic silica column and eluted using the same eluent as before. The first orange fraction (Rf_{2b}: 0.60) was collected and solvent evaporation under reduced pressure afforded cluster **2b'** as a red solid. Yield 2.3 mg (11%).

2b': ^{31}P NMR (121 MHz, CD_2Cl_2): δ 27.45 (s, 4P). Q-TOF HRMS (m/z): 4664.31 ($[Au_{13}(di\text{-}NHC^b)_2(PPh_3)_4Cl_4]^+$), 2343.65 m/z ($[Au_{13}(di\text{-}NHC^b)_2(PPh_3)_4Cl_4](Na)^{2+}$), 721.15 ($[Au(PPh_3)_2]^+$; fragmentation peak).

3b: ^{31}P NMR (121 MHz, CD_2Cl_2): δ 60.83 (s, 3P). Q-TOF HRMS (m/z): 2411.74 ($[Au_{13}(di\text{-}NHC^b)_3(PPh_3)_3Cl_3]^{2+}$), 721.15 ($[Au(PPh_3)_2]^+$; fragmentation peak).

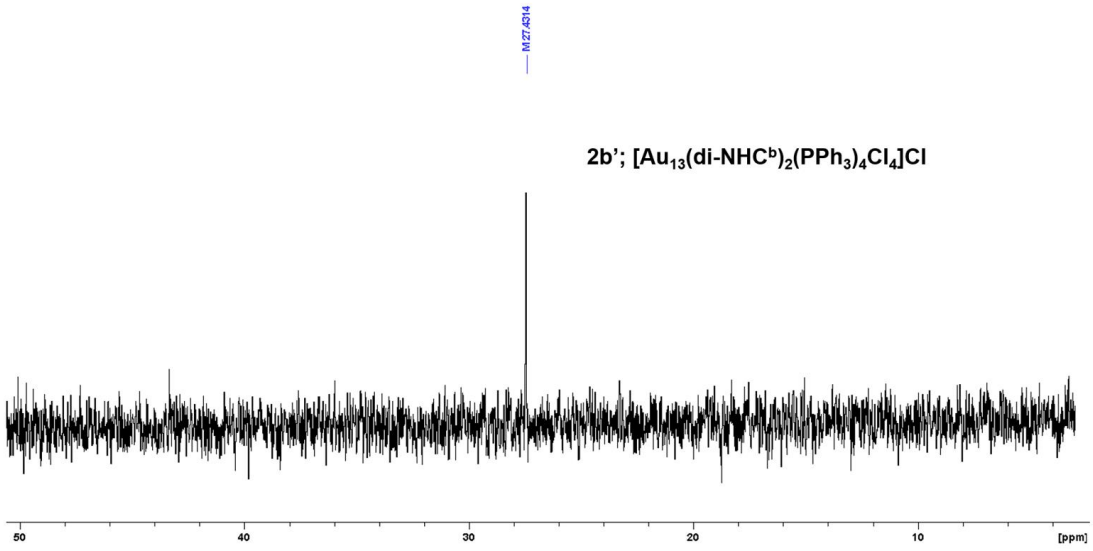

Figure 10.96: ^{31}P NMR spectrum of **2b'** in CD_2Cl_2.

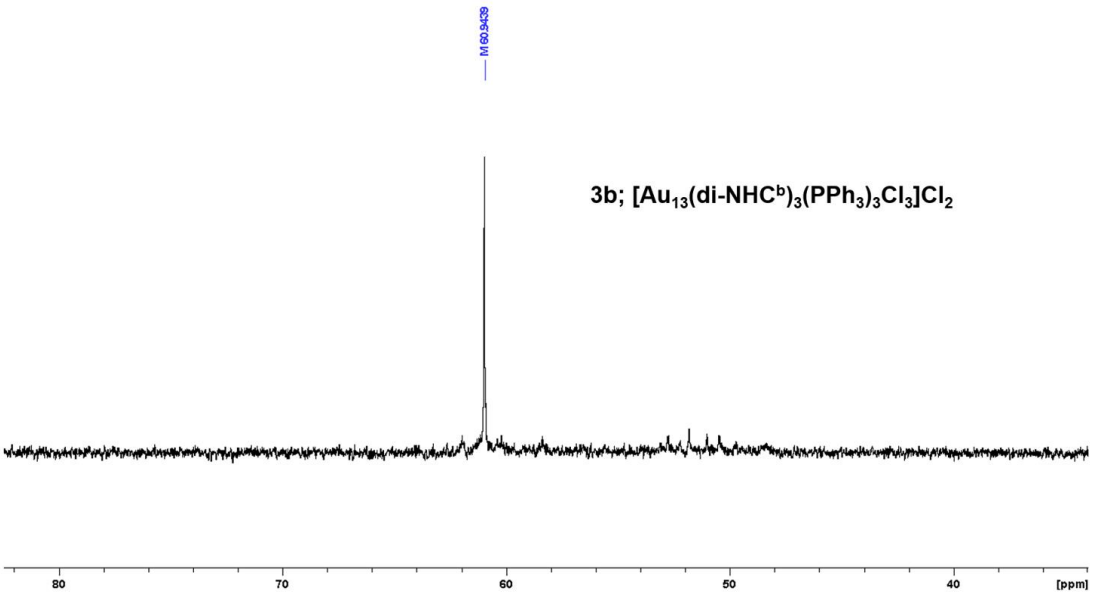

Figure 10.97: ^{31}P NMR spectrum of **3b** in CD_2Cl_2.

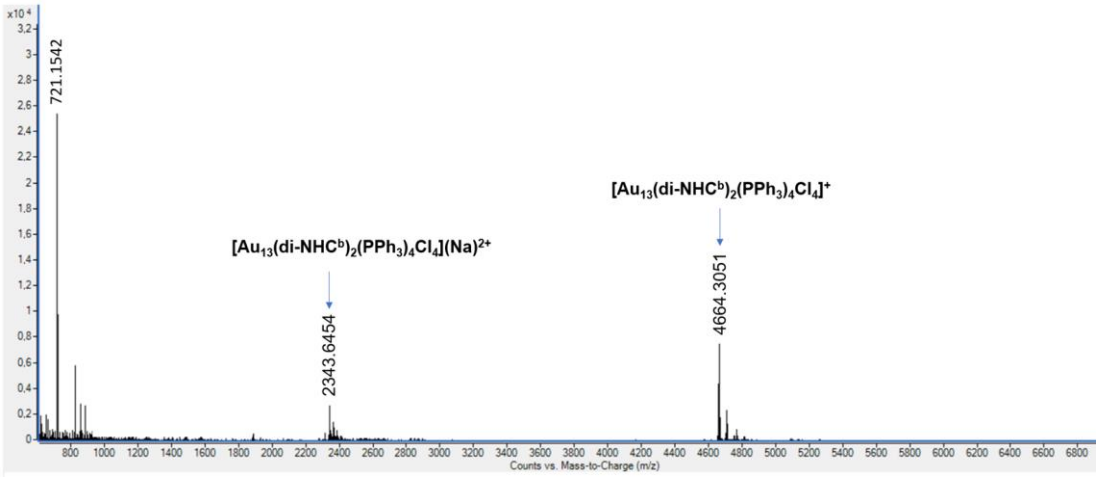

Figure 10.98: Q-TOF HRMS analysis of **2b'** in DCM.

*10.9.3.3 Second experiment with complex b: **3b** cluster synthesis*

$[Au_{11}(PPh_3)_8Cl_2]Cl$ (19.8 mg; $4.51 \cdot 10^{-3}$ mmol) and **b** (12.6 mg; $13.68 \cdot 10^{-3}$ mmol) were weighed in two different vials. The solids were each dissolved in 4.00 ml DCM, to afford a total volume of solution equal to 8.00 ml. The obtained solutions were mixed and placed under stirring at 40°C for 5 days. After this time Q-TOF HRMS (**Figure 10.99**) highlighted the presence of cluster **3b**. The reaction mixture was directly loaded on a chromatographic silica column and eluted using DCM:MeOH (9:1 v:v) as eluent. The orange fraction was collected and solvent was evaporated under reduced pressure to afford **3b** as a red solid. Yield 7.1 mg (32%).

^{31}P NMR (121 MHz, CD_2Cl_2): δ 60.83 (s, 3P).

Q-TOF HRMS (m/z): 2411.74 ($[Au_{13}(di\text{-}NHC^b)_3(PPh_3)_3Cl_3]^{2+}$).

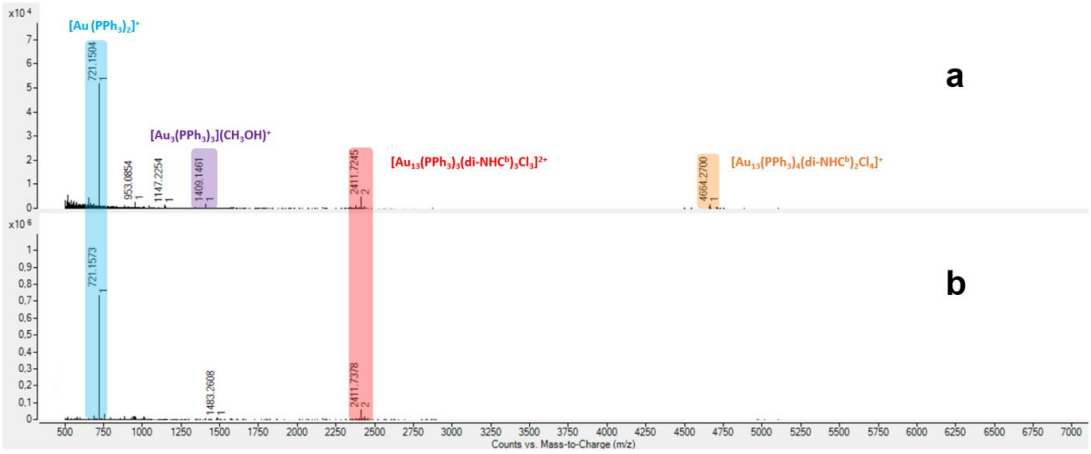

Figure 10.99: Q-TOF analyses of the reaction of $[Au_{11}(PPh_3)_8Cl_2]Cl$ with 3 equivalents of complex **b**. From above, a) after 3 days and b) 5 days under stirring at 40°C.

10.9.4 Experiments with 4 equivalents of gold(I) complex

*10.9.4.1 Second experiment with complex a: **2a** and **3a** cluster synthesis*

$[Au_{11}(PPh_3)_8Cl_2]Cl$ (8.0 mg, $1.84 \cdot 10^{-3}$ mmol) and **a** (3.0 mg, $3.6 \cdot 10^{-3}$ mmol) were weighed in two different vials. The solids were each dissolved in 1.50 ml DCM, to afford a total volume of solution equal to 3.00 ml. The obtained solutions were mixed and left under stirring at 40°C for 16 hours. Subsequently, the mixture was stirred at room temperature for 21 days. After this time Q-TOF HRMS mass spectrometry highlighted the presence of clusters $[Au_{11}(PPh_3)_8Cl_2]Cl$, **2a** and **3a**. Additional 3 mg of **a** complex were added and the reaction was stirred at room temperature for additional 30 days. After this time Q-TOF HRMS mass spectrometry highlighted the presence of clusters **2a** and **3a**. The solvent was evaporated under reduced pressure and 1.50 ml DCM were added. The sample underwent a crystallization upon condensation of Et_2O vapour at -4°C: after one night, a pale orange solution and a deep red solid on the vial bottom were present. The solution was discharged and the red solid was dispersed in 3 ml of DCE. The solution was filtered on a PTFE filter and placed under Et_2O vapour at room temperature for one day, causing again the separation of a deep red solid. The solution was removed and the red solid residue was dissolved in 1.0 ml DCM. The solution was loaded on a chromatographic silica column and eluted using DCM:MeOH (9:1 v:v) as eluent. The first orange fraction (Rf_{2a}: 0.68) was collected and solvent evaporation afforded **2a** cluster. Yield 3.0 mg (36%). The second orange fraction (Rf_{3a}: 0.22) was collected and solvent evaporation afforded cluster **3a** as a red solid. Yield 0.8 mg (10%).

2a: ^{31}P NMR (121 MHz, CD_2Cl_2): δ 57.11 (q, J = 5.04 Hz, 1P), δ 53.52 (q, J = 5.03 Hz, 1P), δ 51.09 (q, J = 5.05 Hz, 1P), δ 50.79 (q, J = 5.04 Hz, 1P). Q-TOF HRMS (m/z): 4463.33 ($[Au_{13}(di\text{-}NHC^a)_2(PPh_3)_4Cl_4]^+$), 2243.16 ($[Au_{13}(di\text{-}NHC^a)_2(PPh_3)_4Cl_4](Na)^{2+}$).

3a: ^{31}P NMR (121 MHz, CD_2Cl_2): δ 60.02 (s). Q-TOF HRMS (m/z): 2261.18 ([Au_{13}(di-NHC^a)$_3$(PPh_3)$_3Cl_3$]$^{2+}$).

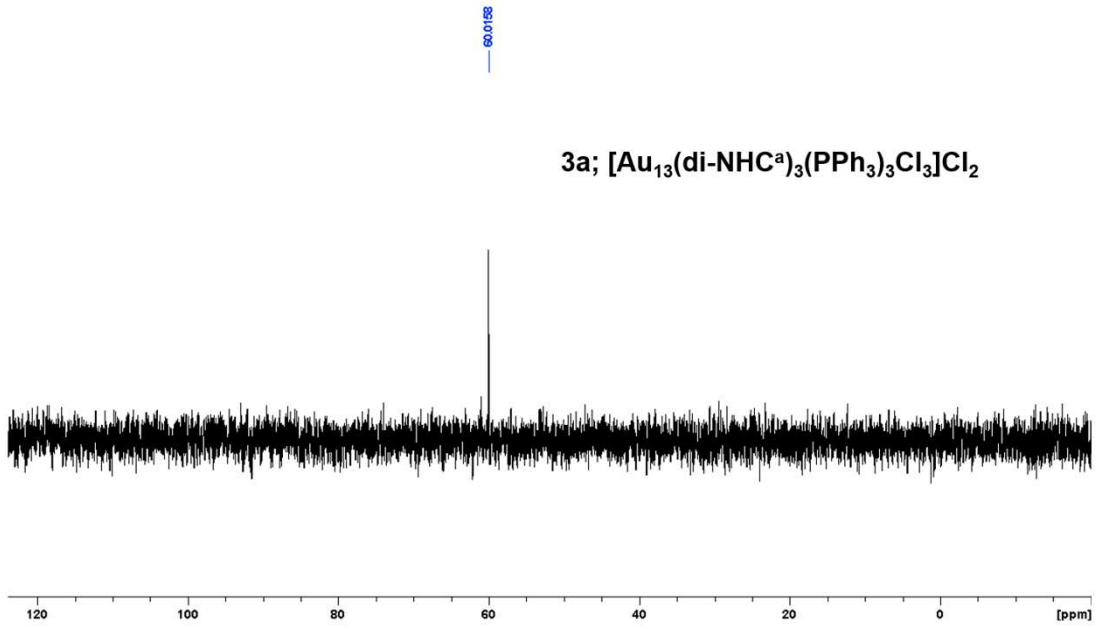

Figure 10.100: ^{31}P NMR spectrum of **3a** in CD_2Cl_2.

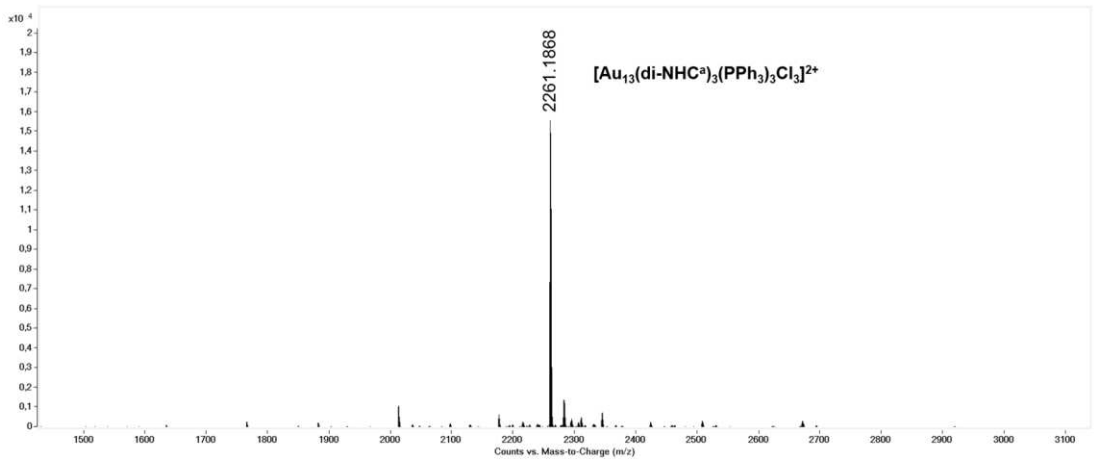

Figure 10.101: Q-TOF HRMS analysis of **3a** in DCM.

10.9.5 Q-TOF HRMS signals of clusters synthetized through stepwise approach

Table 10.6: list of measured and calculated m/z peaks present in Q-TOF HRMS analyses referred to AuNCs obtained with stepwise approach.

Cluster name	measured (m/z)	calculated (m/z)	Δm(ppm)	formula
2a	4461.2188	4461.2048	3.1381	$[Au_{13}(C_{23}H_{24}N_4)_2(PC_{18}H_{15})_4Cl_4]^+$
	4505.2070	4505.1543	11.698	$[Au_{13}(C_{23}H_{24}N_4)_2(PC_{18}H_{15})_4BrCl_3]^+$
	2242.1688	2242.0970	32.023	$[Au_{13}(C_{23}H_{24}N_4)_2(PC_{18}H_{15})_4Cl_4](Na)^{2+}$
3a	2261.1868	2261.1730	6.103	$[Au_{13}(C_{23}H_{24}N_4)_3(PC_{18}H_{15})_3Cl_3]^{2+}$
1b	4265.6941	4265.3474	81.276	$[Au_{11}(C_{31}H_{28}N_4)(PC_{18}H_{15})_6Cl_2]^+$
	2115.3641	2115.1890	82.775	$[Au_{11}(C_{31}H_{28}N_4)(PC_{18}H_{15})_6Cl]^{2+}$
2b	2342.1240	2342.1283	1.8359	$[Au_{13}(C_{31}H_{28}N_4)_2(PC_{18}H_{15})_4Cl_4](Na)^{2+}$
	4705.1975	4705.2169	4.1230	$[Au_{13}(C_{31}H_{28}N_4)_2(PC_{18}H_{15})_4BrCl_3]^+$
3b	2410.4472	2410.2191	94.639	$[Au_{13}(C_{31}H_{28}N_4)_3(PC_{18}H_{15})_3Cl_3]^{2+}$
1c	4169.7432	4169.3474	94.921	$[Au_{11}(C_{23}H_{28}N_4)(PC_{18}H_{15})_6Cl_2]^+$
	4213.7001	4213.2979	95.451	$[Au_{11}(C_{23}H_{28}N_4)(PC_{18}H_{15})_6ClBr]^+$
	2067.3894	2067.1890	96.934	$[Au_{11}(C_{23}H_{28}N_4)(PC_{18}H_{15})_6Cl]^{2+}$

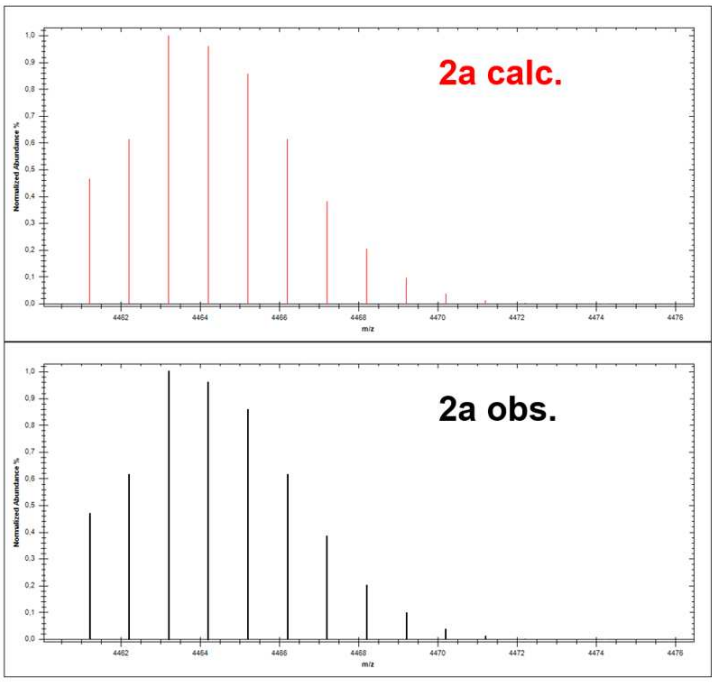

Figure 10.102: calculated (red) and observed (black) HRMS peaks refereed to **2a** cluster, presenting formula $[Au_{13}(C_{23}H_{24}N_4)_2(PC_{18}H_{15})_4Cl_4]^+$.

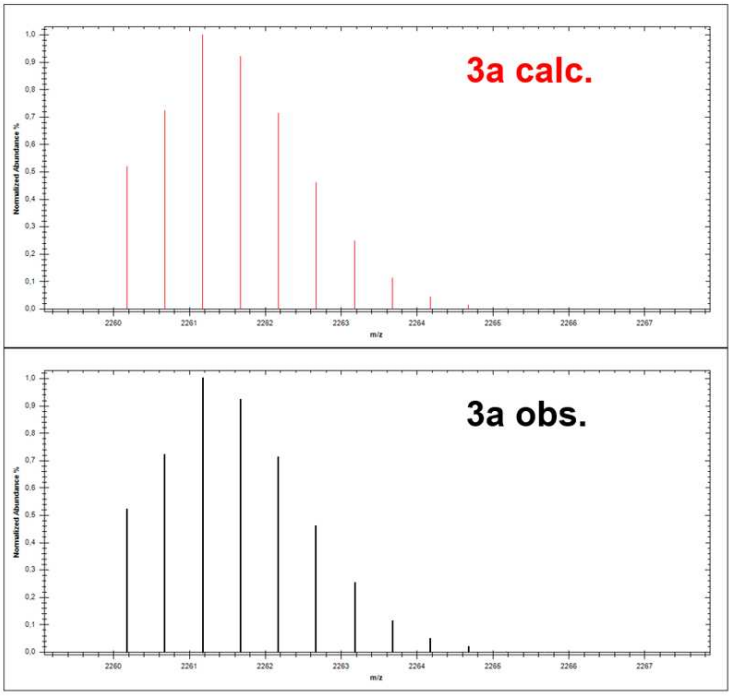

Figure 10.103: calculated (red) and observed (black) HRMS peaks refereed to **3a** clusters, presenting formula $[Au_{13}(C_{23}H_{24}N_4)_3(PC_{18}H_{15})_3Cl_3]^{2+}$.

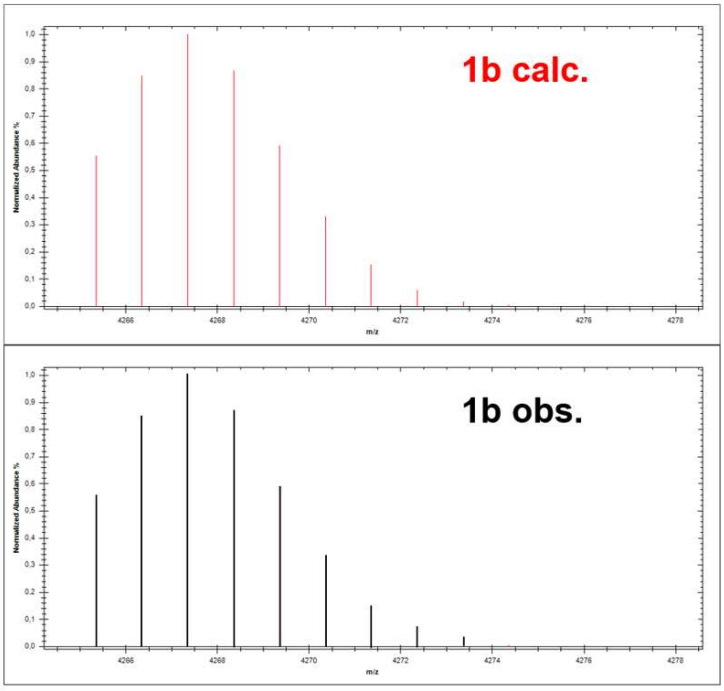

Figure 10.104: calculated (red) and observed (black) HRMS peaks refereed to **1b** clusters, presenting formula $[Au_{11}(C_{31}H_{28}N_4)(PC_{18}H_{15})_6Cl_2]^+$.

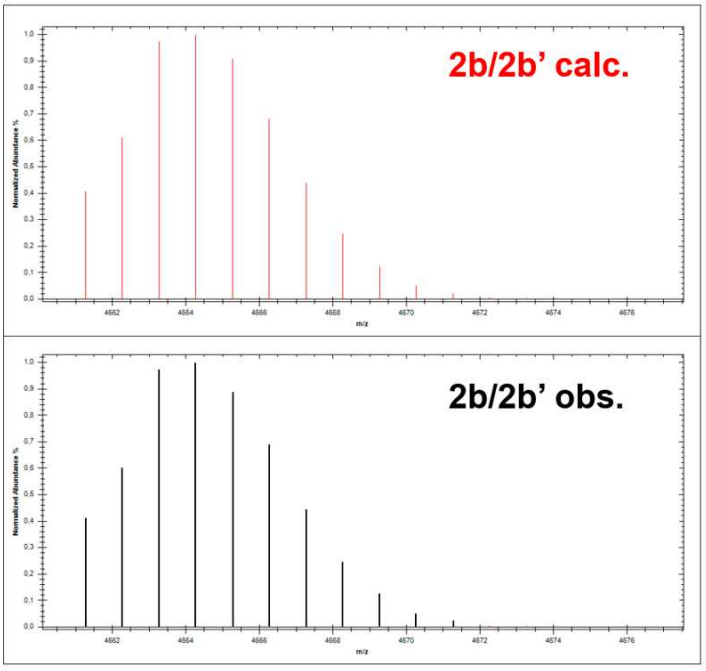

Figure 10.105: calculated (red) and observed (black) HRMS peaks refereed to **2b/2b'** clusters, presenting formula $[Au_{13}(C_{31}H_{28}N_4)_2(PC_{18}H_{15})_4Cl_4]^+$.

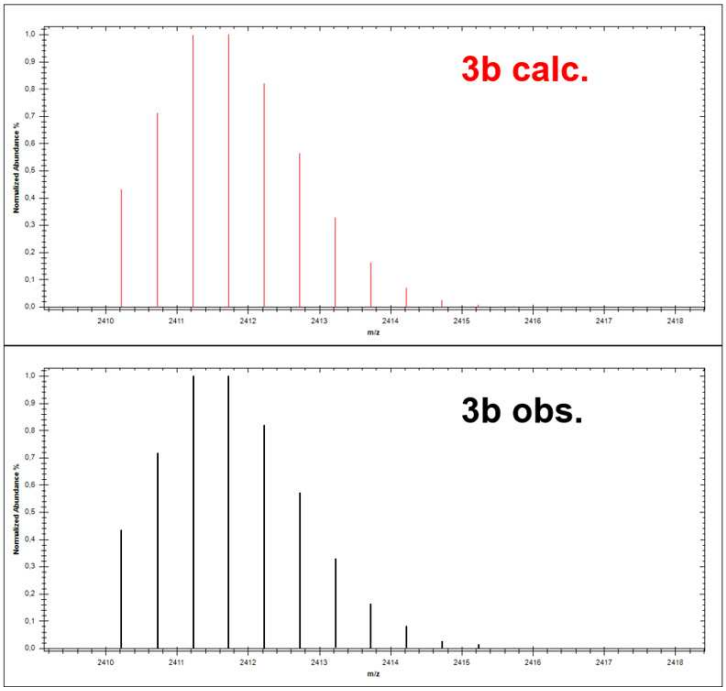

Figure 10.106: calculated (red) and observed (black) HRMS peaks refereed to **3b** cluster, presenting formula $[Au_{13}(C_{31}H_{28}N_4)_3(PC_{18}H_{15})_3Cl_3]^{2+}$.

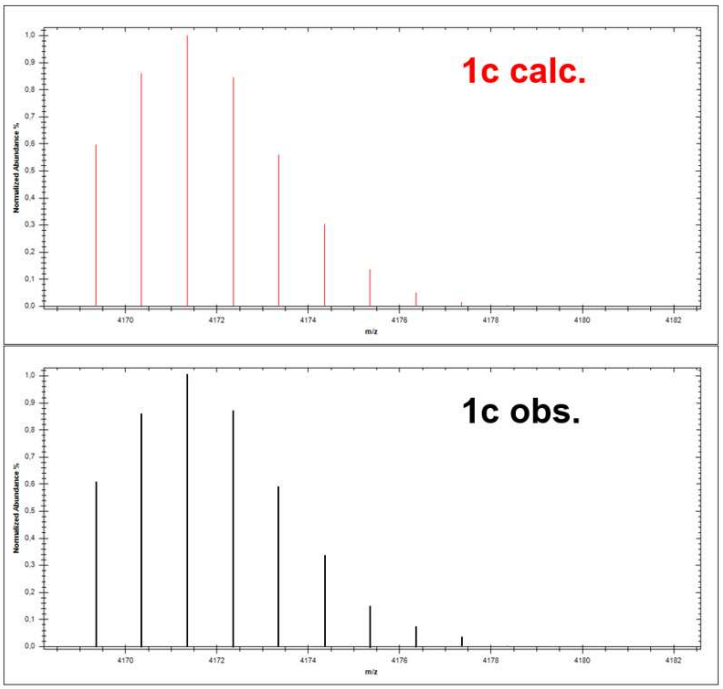

Figure 10.107: calculated (red) and observed (black) HRMS peaks refereed to **1c** clusters, presenting formula $[Au_{11}(C_{23}H_{28}N_4)(PC_{18}H_{15})_6Cl_2]^{+}$.

10.9.6 UV-Vis spectra of cluster obtained from stepwise synthesis

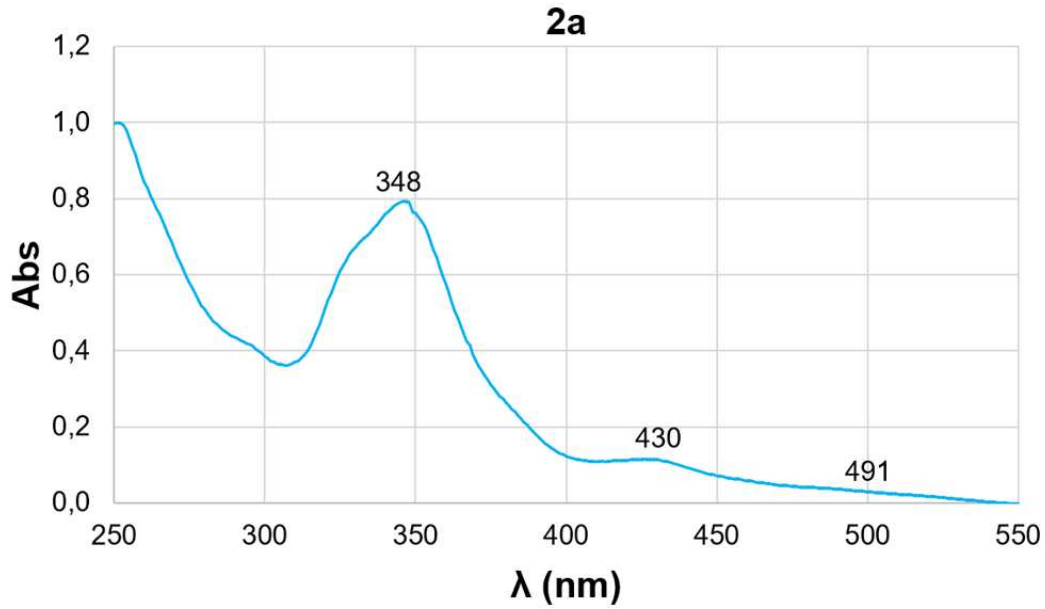

Figure 10.108: normalized UV-Vis spectrum of **2a** cluster ($2 \cdot 10^{-4}$ M) in DCM.

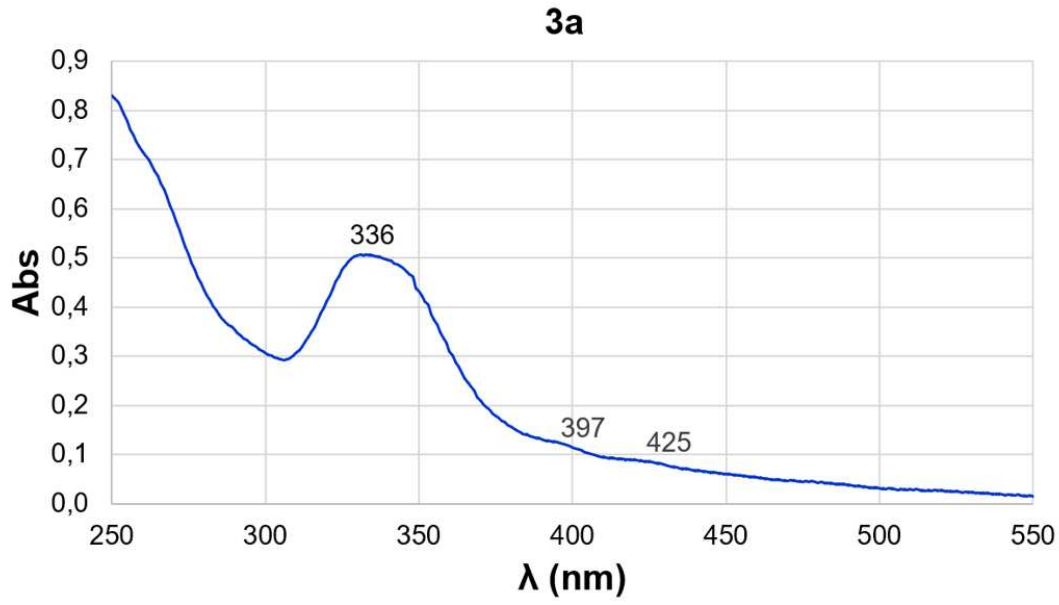

Figure 10.109: normalized UV-Vis spectrum of **3a** cluster ($2 \cdot 10^{-4}$ M) in DCM.

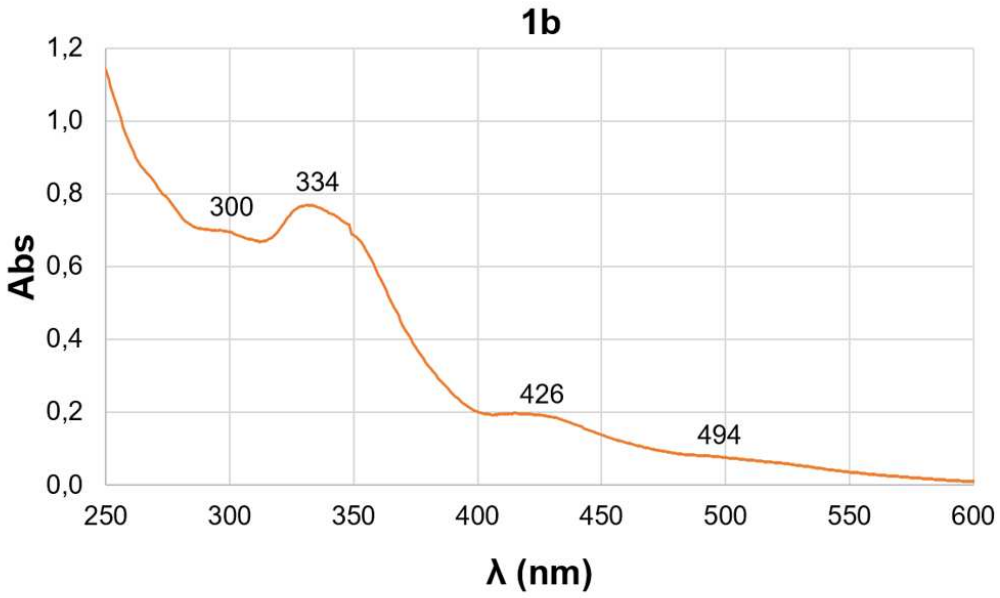

Figure 10.110: normalized UV-Vis spectrum of **1b** cluster ($2 \cdot 10^{-4}$ M) in DCM.

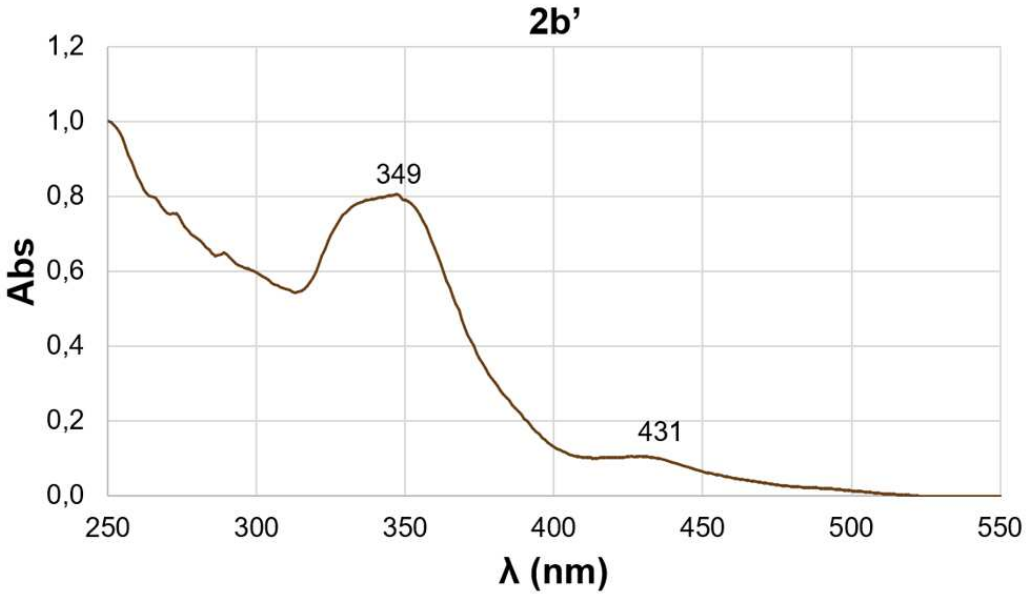

Figure 10.111: normalized UV-Vis spectrum of **2b'** cluster ($2 \cdot 10^{-4}$ M) in DCM.

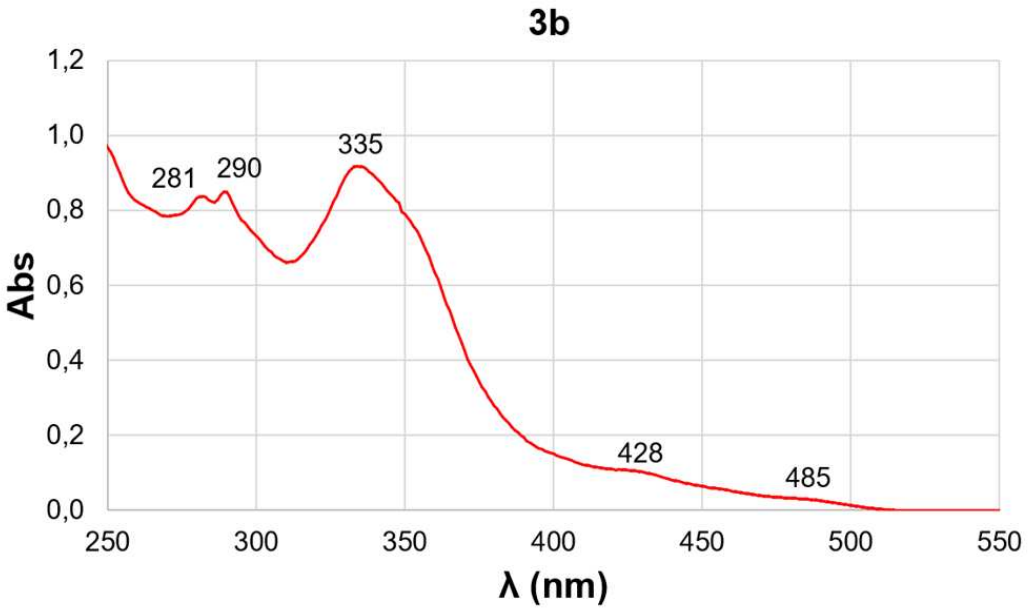

Figure 10.112: normalized UV-Vis spectrum of **3b** cluster ($2 \cdot 10^{-4}$ M) in DCM.

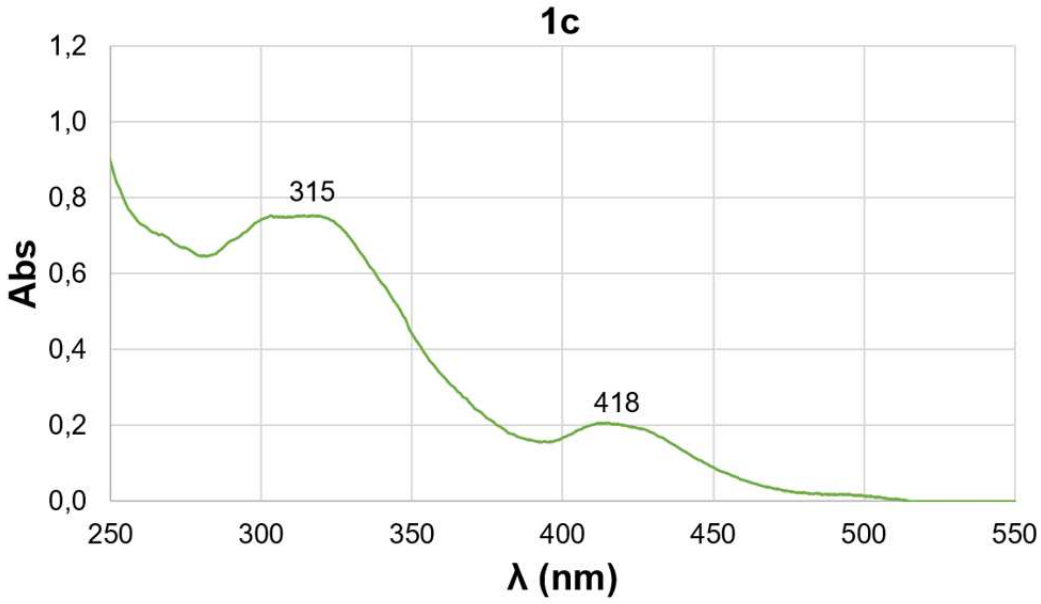

Figure 10.113: normalized UV-Vis spectrum of **1c** cluster ($2 \cdot 10^{-4}$ M) in DCM.

10.9.7 Emission spectra of clusters obtained from stepwise synthesis

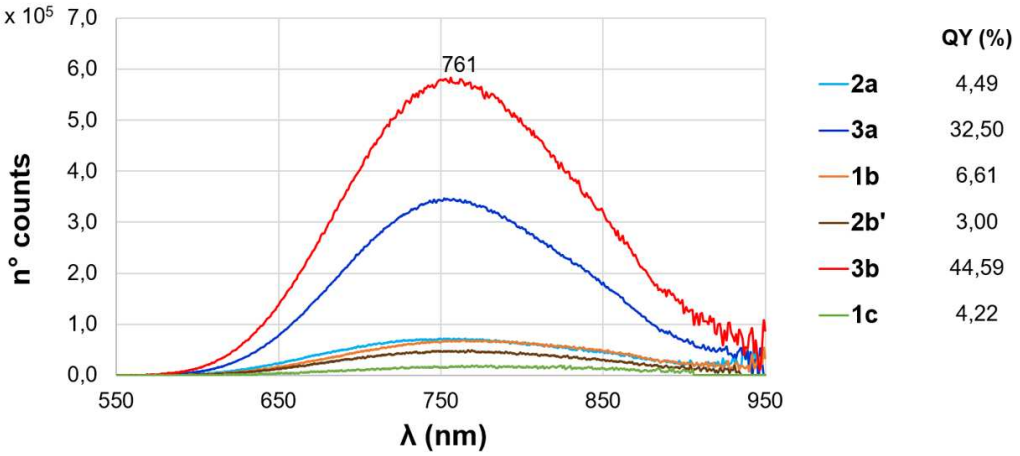

Figure 10.114: overlapped emission spectra of **2a, 3a, 1b, 2b', 3b** and **1c** clusters in DCM, concentration: $2 \cdot 10^{-4}$ M, (room temperature). For **2a**, **2b**', **3b** and **1c** λ_{exc}: 350 nm. For **1b** and **3a** λ_{exc}: 330 nm. All reported spectra are normalized for the absorbance values found at 350 nm or 330 nm presented in the UV-vis spectra. The corresponding quantum yield (QY) values are reported too.

Table 10. 7: lifetime decays of **2a**, **3a**, **1b**, **2b'**, **3b** and **1c** clusters. All values indicate a fluorescence emission.

Cluster	τ_1(ns)	τ_2(ns)
2a	215	776
3a	964	4447
1b	117	808
2b'	207	669
3b	4352	-
1c	175	1007

*10.9.8 Single crystal X-ray diffractometry of **3b***

The crystallographic data for compound **3b** were obtained by mounting a well-formed single crystal on a glass fiber and transferring it to a Bruker D8 Venture Photon II Bruker diffractometer. The APEX 3 program package was used to obtain the unit cell and the geometrical parameters and for the data collection. The raw frame data were processed using SAINT and SADABS[30] to obtain the data file of the reflections. The structure was solved using SHELXT[31] (Intrinsic Phasing method in the APEX 3

program). The refinement of the structure (based on F2 by full-matrix least-squares techniques) was carried out using the SHELXTL-2014/7 program[32] in the WinGX suite v.2014.1. Detailed of the crystallographic data are reported in **Table 10.8**. Crystallographic data have been deposited with the Cambridge Crystallographic Data Centre as supplementary publication CCDC 2170527. Copies of the data can be obtained free of charge on application to the CCDC, 12 Union Road, Cambridge CB2 1EZ, U.K. (fax, (+44) 1223 336033; e-mail, deposit@ccdc. cam.ac.uk).

Table 10.8: crystallographic data for **3b**

Formula	$[C_{147}H_{129}Au_{13}Cl_3N_{12}P_3]$ 7,5(CH_2Cl_2) Cl OH
Molecular weight	5512.84
Crystal system	Trigonal
Space group	R -3
a/Å	24.2867(3)
b/Å	24.2867(3)
c/Å	55.3721(10)
α/°	90.00
β/°	90.00
γ/°	120.00
Volume, Å^3	28285.1(9)
T (K)	200(2)
Z	3
D_{calc}/g cm^{-3}	1.942
F(000)	15354
□(Mo-Kα)/mm^{-1}	10.41
Reflections collected	268625
Unique reflections	12884
Observed reflections [I>2□(*I*)]	11265 [R_{int} = 0.0653]
R [$I > 2\sigma(I)$]	R_1 = 0.0334
	wR_2 = 0.1000
R [all data]	R_1 = 0.0404
	wR_2 = 0.1083

$R_1 = \Sigma|Fo - Fc|/\Sigma|Fo|$; $wR_2 = [\Sigma[w(Fo^2 - Fc^2)^2]/\Sigma[w(Fo^2)^2]]^{1/2}$

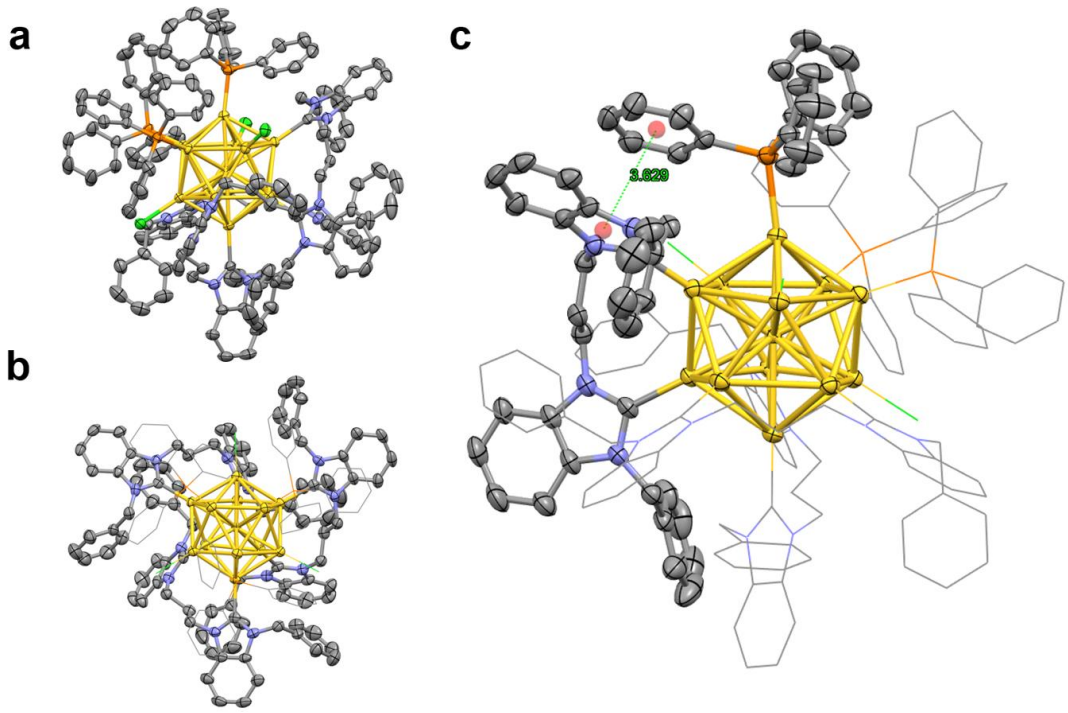

Figure 10.115: X-ray structure of **3b**; ellipsoids are drawn at their 50 % probability level. a) Full view of the cluster structure, b) full view after removal of the PPh_3 phenyl groups, c) π-π interaction among NHCs and PPh_3 ligands. For clarity, hydrogens are omitted in all figures. Color code: yellow (Au), green (Cl), orange (P), purple (N), grey (C).

10.9.9 CV and DPV analysis on AuNCs capped by di-NHCs, PPh_3 and Cl ligands

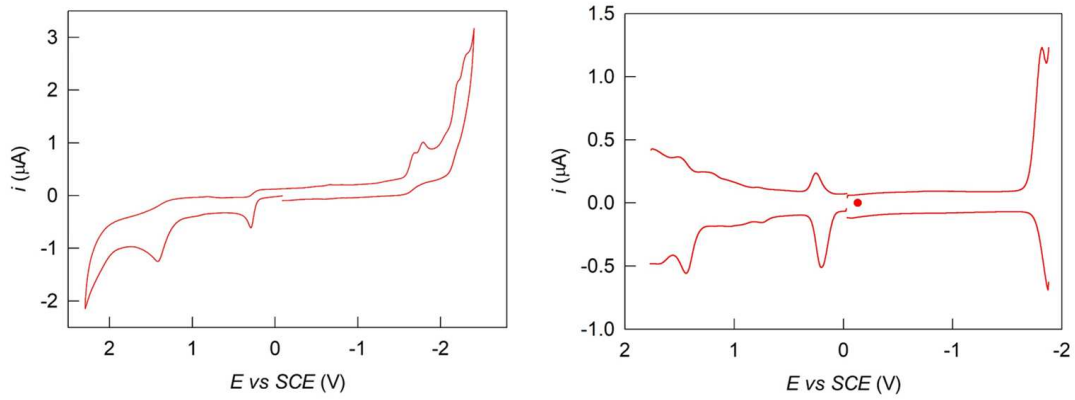

Figure 10.116: CV analysis recorded in CH_3CN (left) and DPV analysis recorded in DCM (right) of $[Au_{11}(PPh_3)_8Cl_2]Cl$ cluster.

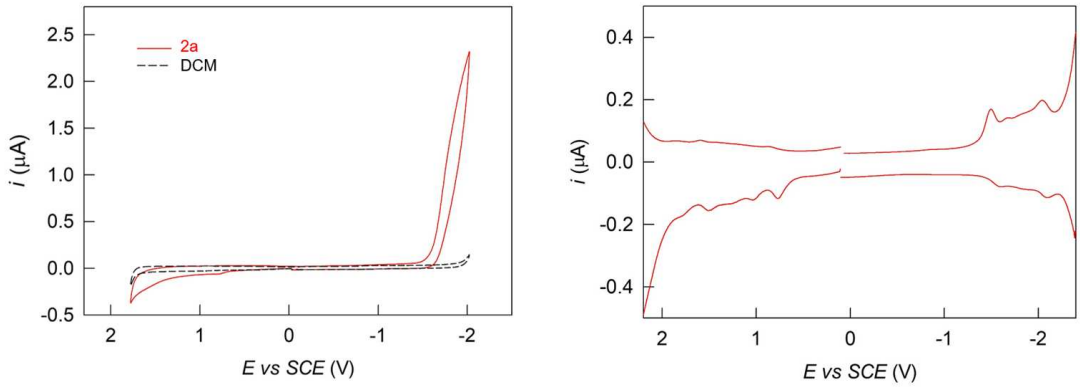

Figure 10.117: CV analysis recorded in DCM (left) and DPV analysis recorded in CH_3CN (right) of **2a** cluster.

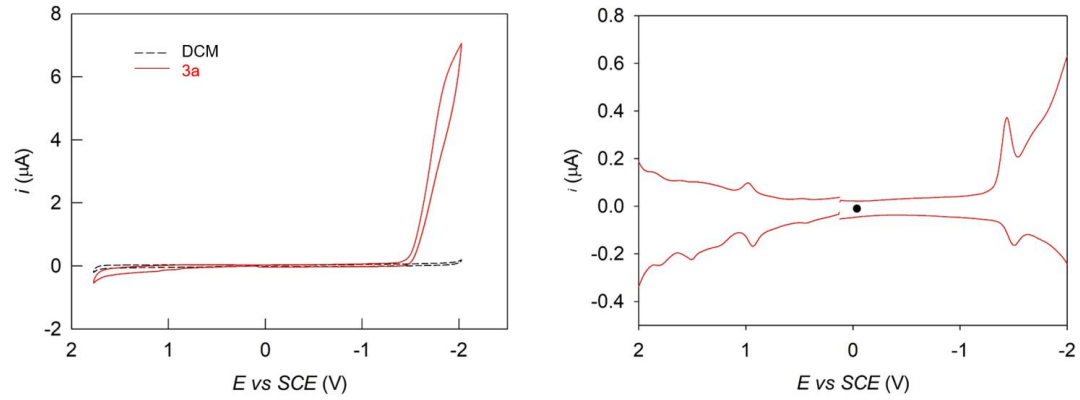

Figure 10.118: CV analysis recorded in DCM (left) and DPV analysis recorded in CH_3CN (right) of **3a** cluster.

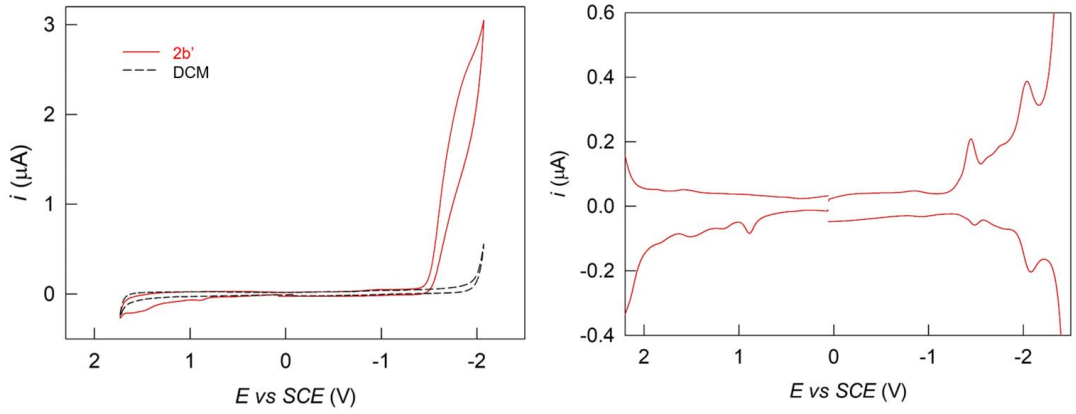

Figure 10.119: CV analysis recorded in DCM (left) and DPV analysis recorded in CH_3CN (right) of **2b'** cluster.

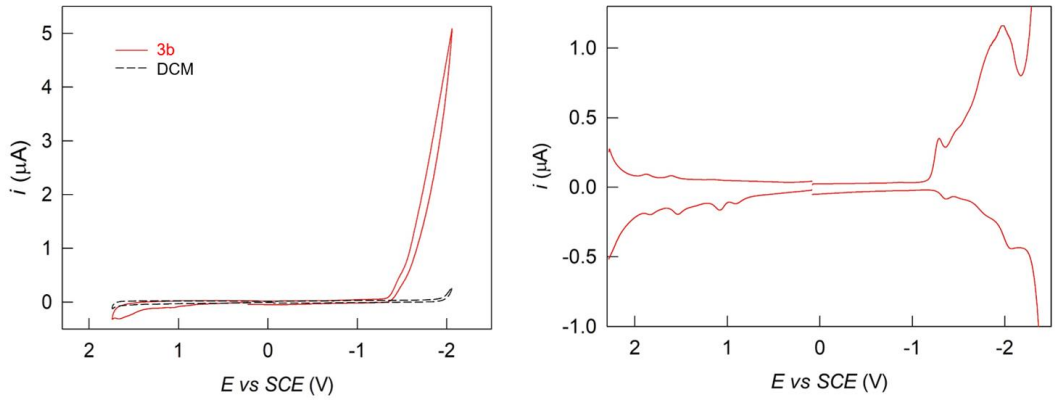

Figure 10.120: CV analysis recorded in DCM (left) and DPV analysis recorded in CH_3CN (right) of **3b** cluster.

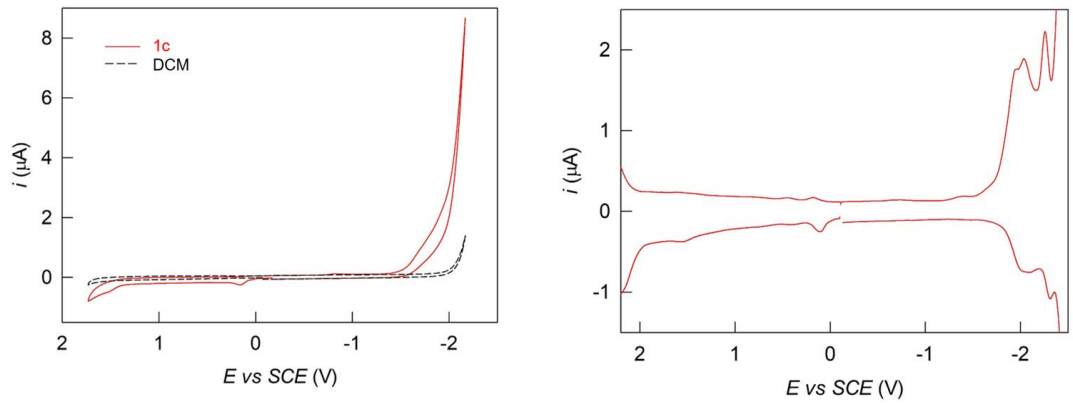

Figure 10.121: CV analysis recorded in DCM (left) and DPV analysis recorded in CH_3CN (right) of **1c** cluster.

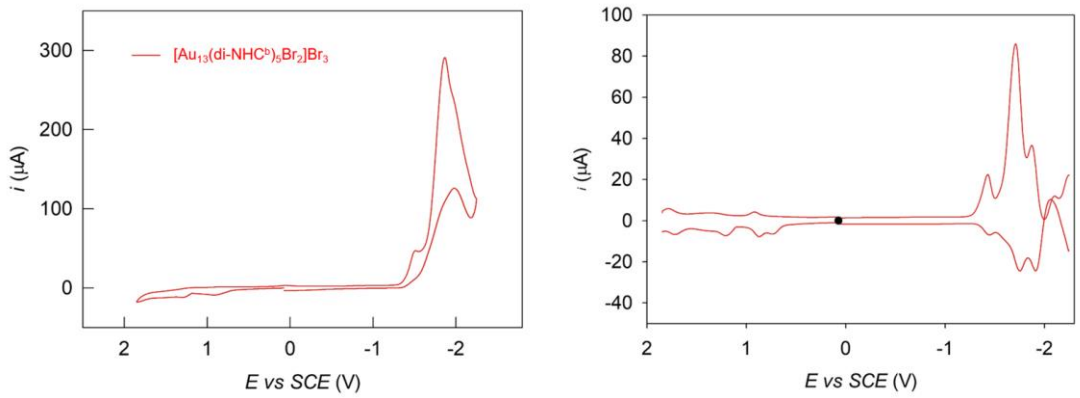

Figure 10.122: CV analysis recorded in CH_3CN (left) and DPV analysis recorded in CH_3CN (right) of $[Au_{13}(di\text{-}NHC^b)_5Br_2]Br_3$ cluster.

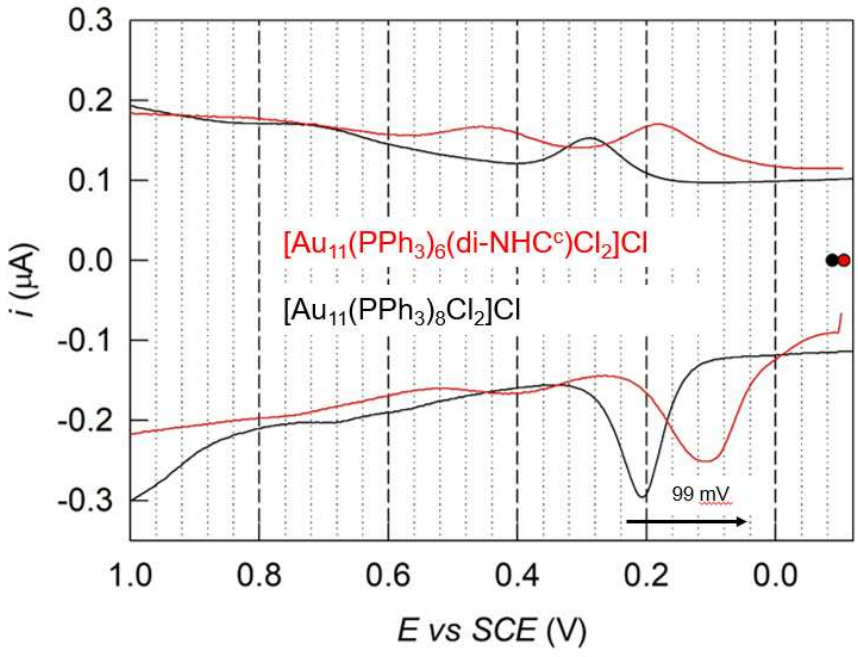

Figure 10.123: detail of DP voltammogram of **1c** (red) and $[Au_{11}(PPh_3)_8Cl_2]Cl$ (black) clusters dissolved in CH_3CN. The arrow highlights the shift of the first oxidation peak.

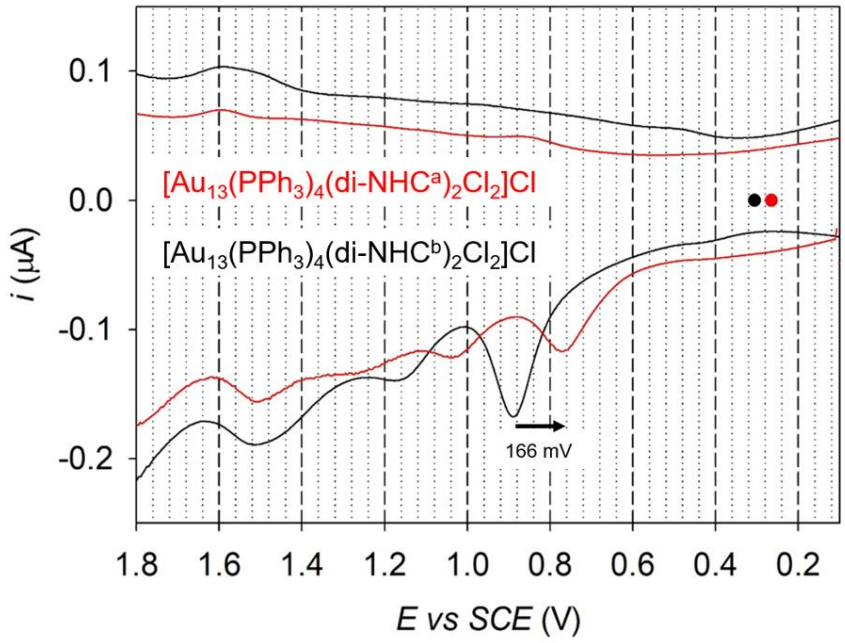

Figure 10.124: details of DP voltammograms of **2a** (red) and **2b'** (black) clusters dissolved in CH_3CN. The arrow highlights the shift of the first oxidation peak.

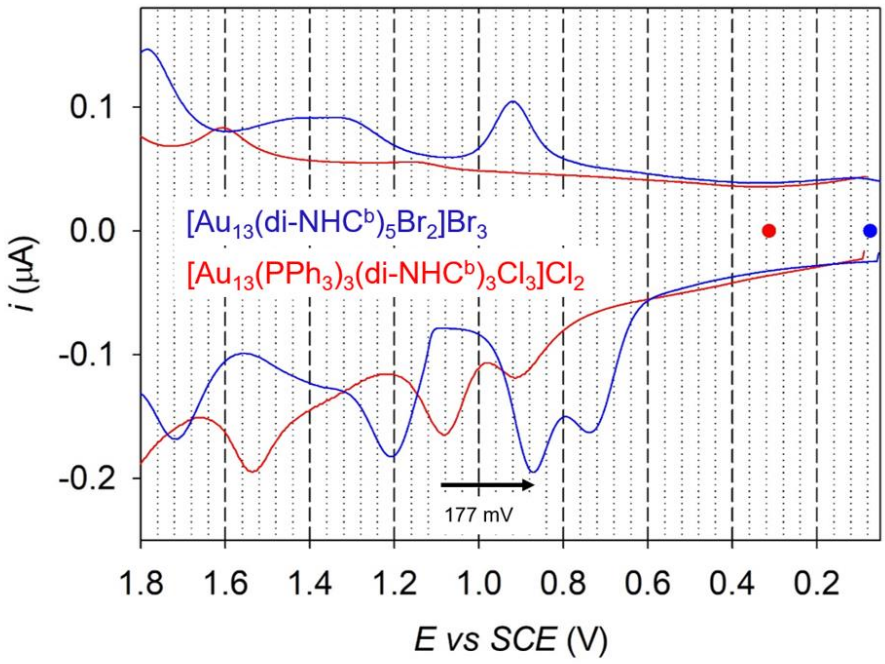

Figure 10125: detail of DP voltammograms of $[Au_{13}(di\text{-}NHC^b)_5Br_2]Br_3$ (blue) and **3b** (red) clusters dissolved in CH_3CN. The arrow highlights the shift of the first oxidation peak.

*10.9.10 Reactivity of **1b** cluster*

Cluster **1b** (1.7 mg, $0.36 \cdot 10^{-3}$ mmol), with formula $[Au_{11}(di\text{-}NHC^b)(PPh_3)_6Cl_2]Cl$, and **b** (0.4 mg, $0.36 \cdot 10^{-3}$ mmol) were weighed in two different vials. The solids were each dissolved in 1.50 ml DCM, to afford a total volume of solution equal to 3.00 ml. The obtained solutions were mixed and left under stirring at 40°C for 72 hours. Q-TOF HRMS mass spectrometry was used to monitor the evolution of reaction, as reported in **Figure 10.126**.

A control experiment was conducted at the same time, identical to that reported above but using exclusively **1b** cluster, without **b** complex. Q-TOF HRMS mass spectrometry was used to monitor this reaction too, as reported in **Figure 10.127**.

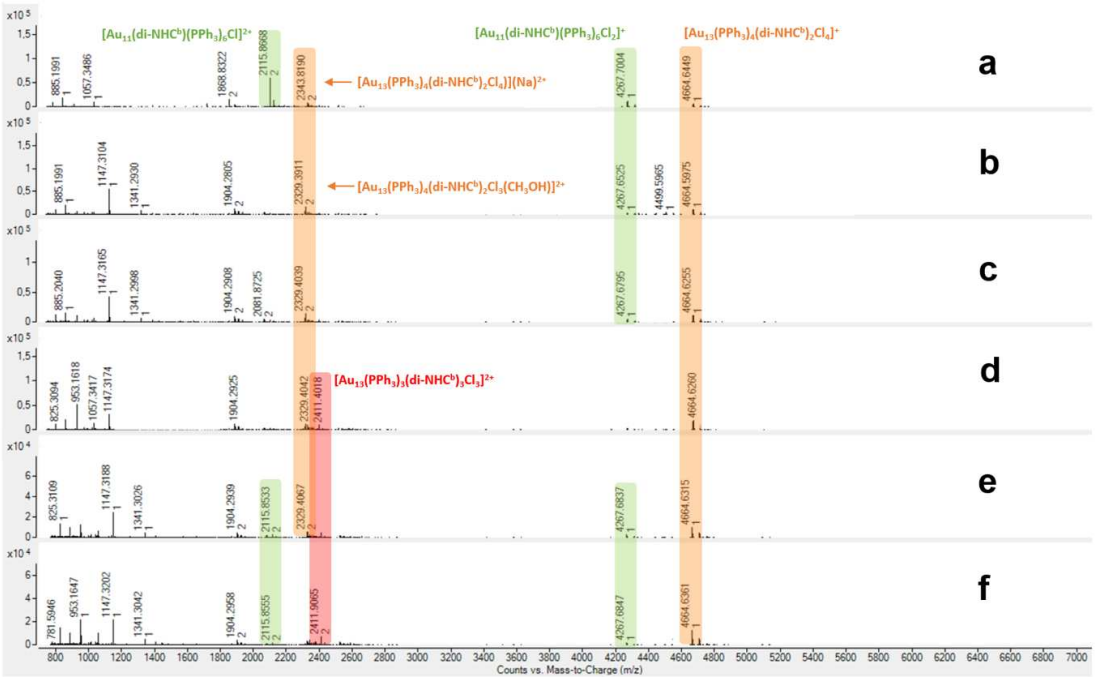

Figure 10.126: Q-TOF HRMS analyses of the reaction of **1b** with 1 equivalents of complex **b**, from above, after a) 0 h, b) 2 h, c) 17 h, d) 38 h, c) 50 h and f) 72 h under stirring at 40°C.

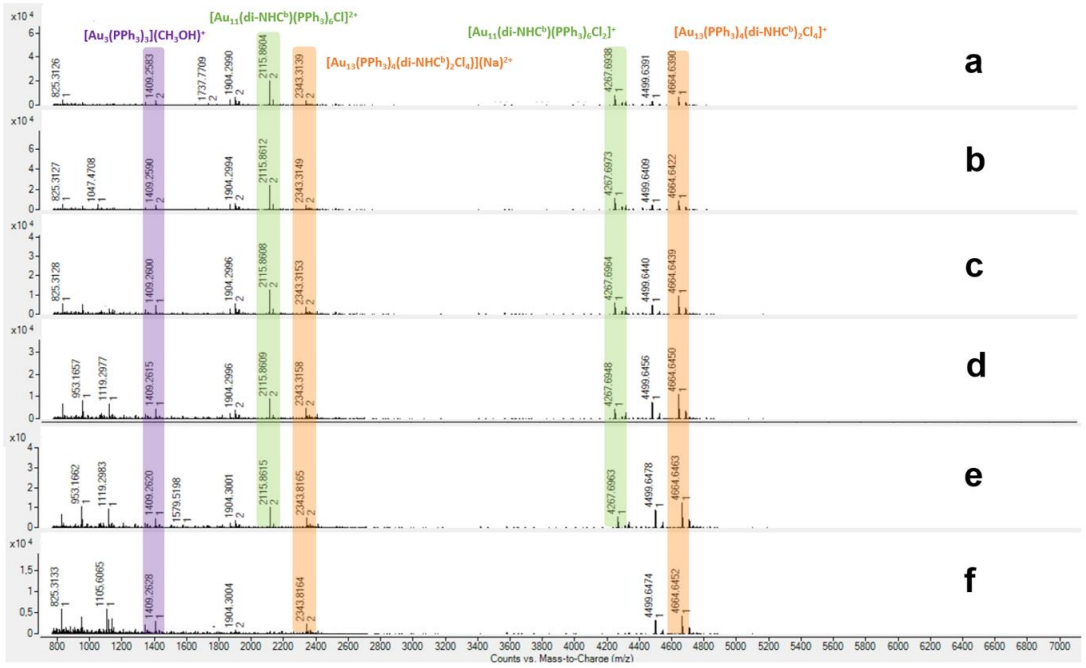

Figure 10.127: Q-TOF analyses of **1b** solution in DCM, from above, after a) 0 h, b) 2 h, c) 17 h, d) 38 h, e) 50 h and f) 72 h under stirring at 40°C.

*10.9.11 Reactivity of **1c** cluster with **b** complex*

Cluster **1c** (2.5 mg, $0.60 \cdot 10^{-3}$ mmol), with formula $[Au_{11}(di\text{-}NHC^c)(PPh_3)_6Cl_2]Cl$, and **b** (1.1 mg, $1.2 \cdot 10^{-3}$ mmol) were weighed in two different vials. The solids were each dissolved in 1.50 ml DCM, to afford a total volume of solution equal to 3.00 ml. The obtained solutions were mixed and left under stirring at 40°C for 72 hours. Q-TOF HRMS was used to monitor the evolution of the reaction, as reported in **Figure 10.128**. The analysis at room temperature (**Figure 10.128 a**) highlighted the presence of **1c** and a novel cluster, with formula $[Au_{13}(di\text{-}NHC^c)_2(di\text{-}NHC^b)_2(PPh_3)Cl_3]^{2+}$, with a signal at 2281.42 m/z. Warming did not further focus the reaction mixture.

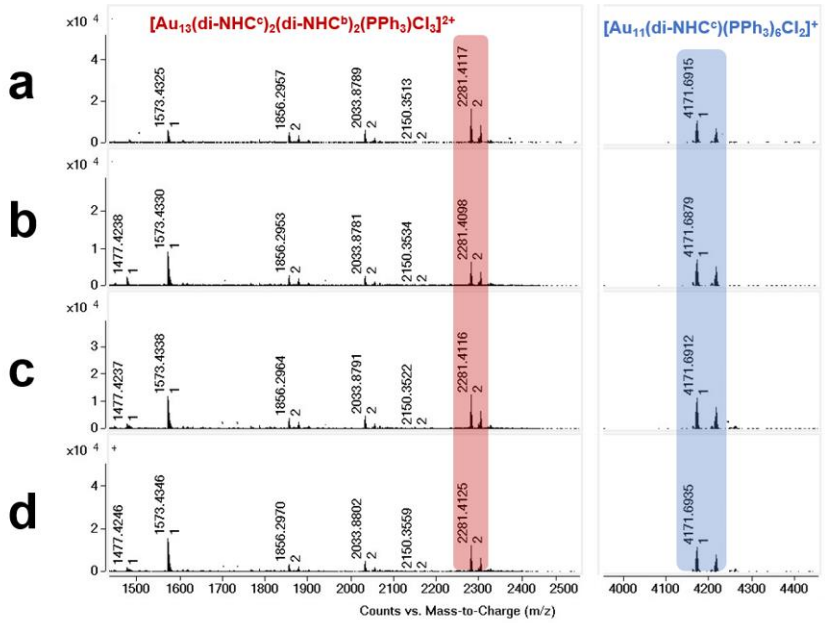

Figure 10.128: analysis of the reaction of **1c** with 2 equivalents of complex **b**, from above, after a) 0 h, b) 24 h, c) 48 h and d) 72 h under stirring at 40°C. The highlighted peaks match with $[Au_{13}(di\text{-}NHC^c)_2(di\text{-}NHC^b)_2(PPh_3)Cl_3]^{2+}$ (red) and $[Au_{11}(di\text{-}NHC^c)(PPh_3)_6Cl_2]^{+}$ (blue) stoichiometry, respectively.

10.9.12 Synthesis of Ag-doped clusters with stepwise synthesis

Cluster $[Au_{11}(PPh_3)_8Cl_2]Cl$ (4.0 mg, $0.90 \cdot 10^{-3}$ mmol) and $[Ag_2(di\text{-}NHC^b)_2](PF_6)_2$ (1.3 mg, $0.90 \cdot 10^{-3}$ mmol) were weighed in two different vials. The solids were dissolved in 1.50 ml of DCM, affording a total volume of solution equal to 3.00 ml. The obtained solutions were mixed and left under stirring at 40°C for 72 hours. Q-TOF HRMS was used to monitor the evolution of reaction, as reported in **Figure 10.129**. The mass spectrometry highlighted several clusters during the reaction. Among them it was possible to interpretate only the peaks of one cluster, with formula $[Au_9Ag_2(PPh_3)_8Cl_2]^+$ (2061.12 m/z).

The same experiment was repeated using 3 eq. (4.0 mg, $2.70 \cdot 10^{-3}$ mmol) and 10 eq. (13.0 mg, $9.00 \cdot 10^{-3}$ mmol) of $[Ag_2(di\text{-}NHC^b)_2](PF_6)_2$. Also here, mass spectrometry highlighted several clusters during the reaction, with general formula $[Au_{13-n}Ag_n(di\text{-}NHC)_3(PPh_3)_3Cl_3]^{2+}$, in which n is equal to 5, 6 or 7, using 3 equivalents of starting Ag complex. Using instead 10 equivalents of the same complex n increases, reaching values of 7, 8 and 9. The corresponding spectra are reported in **Figure 10.130** and **Figure 10.131**.

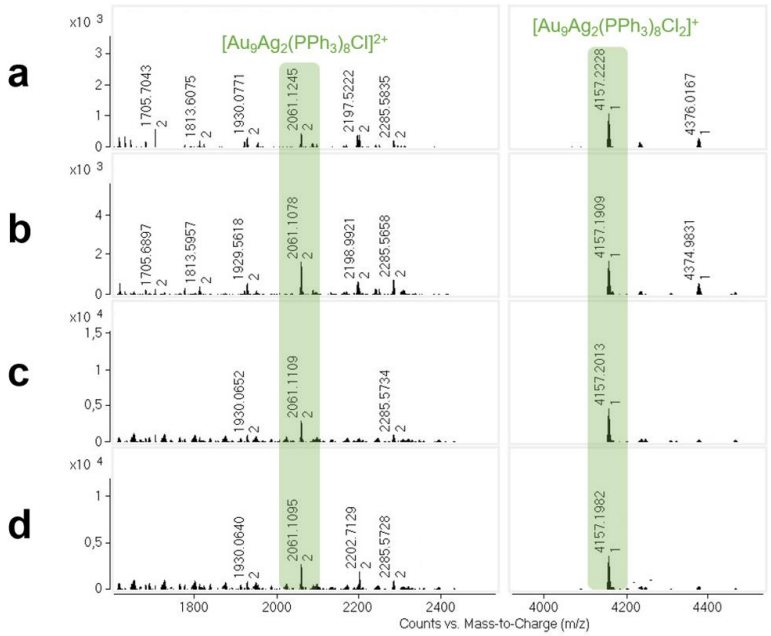

Figure 10.129: reaction with $[Au_{11}]$:$[Ag_2(\text{di-NHC}^b)_2(PF_6)_2]$ molar ratio equal to 1:1, monitored at a) 2 h, b) 24 h, c) 48 h and d) 72 h. The highlighted peaks match with $[Au_9Ag_2(PPh_3)_8Cl_2]^+$ stoichiometry.

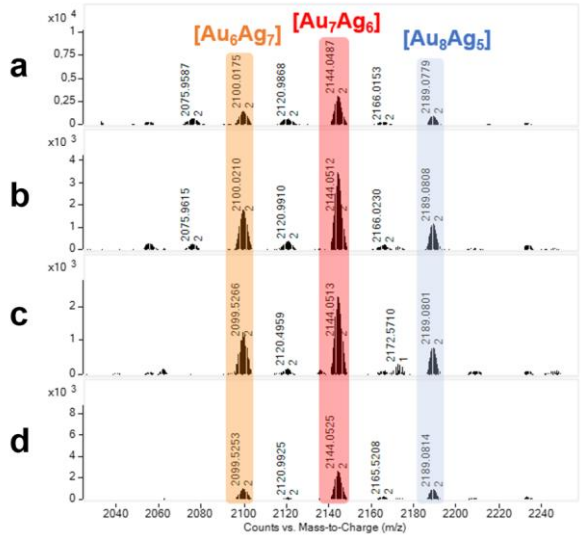

Figure 10.130: reaction with $[Au_{11}]$:$[Ag_2(\text{di-NHC}^b)_2(PF_6)_2]$ molar ratio equal to 1:3, monitored at a) 2 h, b) 24 h, c) 48 h and d) 72 h. The highlighted peaks match with clusters presenting formula $[Au_8Ag_5(\text{di-NHC}^b)_3(PPh_3)_3Cl_3]^{2+}$ (blue), $[Au_7Ag_6(\text{di-NHC}^b)_3(PPh_3)_3Cl_3]^{2+}$ (red) and $[Au_6Ag_7(\text{di-NHC}^b)_3(PPh_3)_3Cl_3]^{2+}$ (orange).

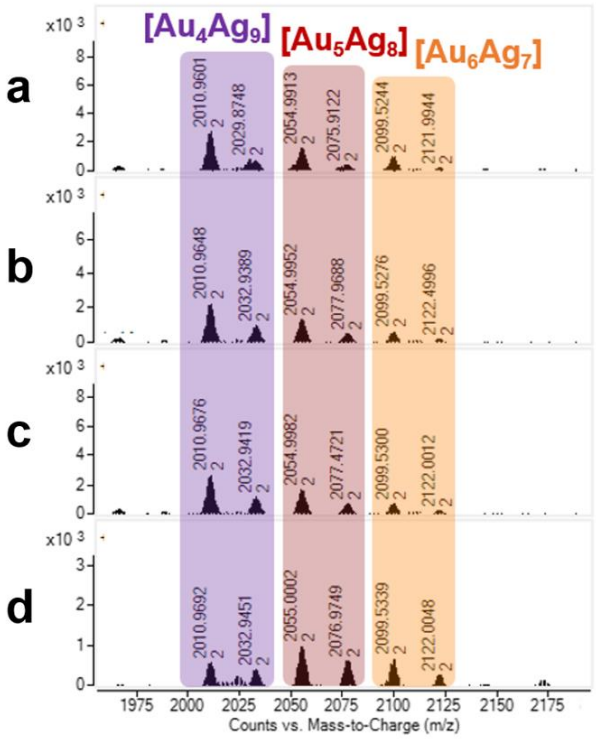

Figure 10.131 reaction with $[Au_{11}]$:$[Ag_2(\text{di-NHC}^b)_2(PF_6)_2]$ molar ratio equal to 1:10, monitored at a) 2 h, b) 24 h, c) 48 h and d) 72 h. The highlighted peaks match with clusters presenting formula, $[Au_6Ag_7(\text{di-NHC}^b)_3(PPh_3)_3Cl_2X]^{2+}$ (orange), $[Au_5Ag_8(\text{di-NHC}^b)_3(PPh_3)_3Cl_2X]^{2+}$ (brown) and $[Au_4Ag_9(\text{di-NHC}^b)_3(PPh_3)_3Cl_2X]^{2+}$ (purple). X: Cl or Br. The bromide anions derive from impurities present during the analysis.

*10.9.13 Reactivity of $[Au_9(PPh_3)_8](NO_3)_3$ with **c'** and **b** complexes*

The mass spectrum of $[Au_9(PPh_3)_8](NO_3)_3$, reported in **Figure 10.132**, presents several fragmentation peaks. These fragments complicate the interpretation of experiments involving this cluster, reported below.

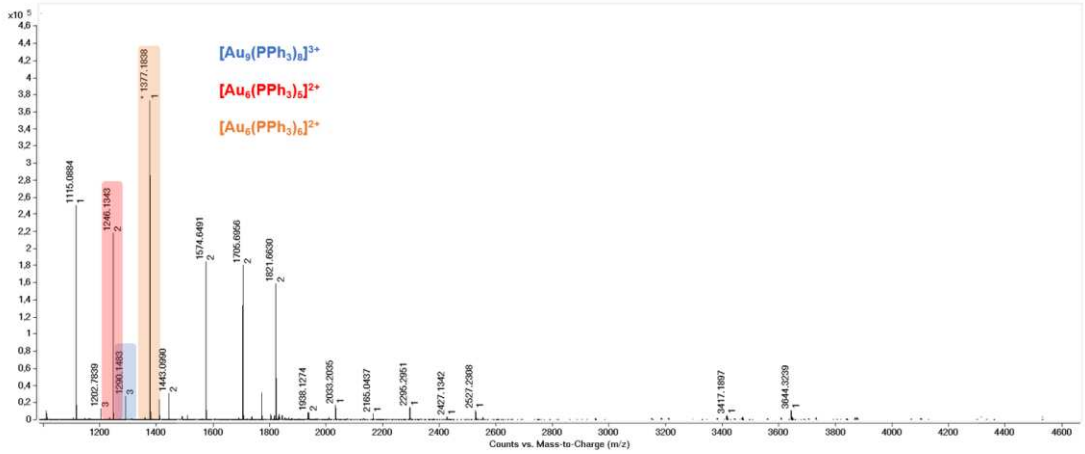

Figure 10.132: Q-TOF HRMS analysis of $[Au_9(PPh_3)_8](NO_3)_3$ cluster. The molecular peak is highlighted in blue. Fragmentation peaks $[Au_6(PPh_3)_5]^{2+}$ and $[Au_6(PPh_3)_6]^{2+}$ are highlighted in red and orange, respectively. Signals centered at 1574.65, 1705.70 and 1821.66 m/z were not assigned.

Cluster $[Au_9(PPh_3)_8](NO_3)_3$ (25.0 mg, $6.16 \cdot 10^{-3}$ mmol) and **c'** (5.8 mg, $6.34 \cdot 10^{-3}$ mmol) were weighed in two different vials. The solids were dissolved in 4.00 ml of DCM, affording a total volume of solution equal to 8.00 ml. The obtained solutions were mixed and left under stirring at 40°C for 72 hours. Q-TOF HRMS was used to monitor the evolution of reaction, as reported in **Figure 10.133**. Mass spectrometry highlighted several clusters during the reaction. Given the low selectivity of this reaction and the complicated mass spectrum, we discharged this sample.

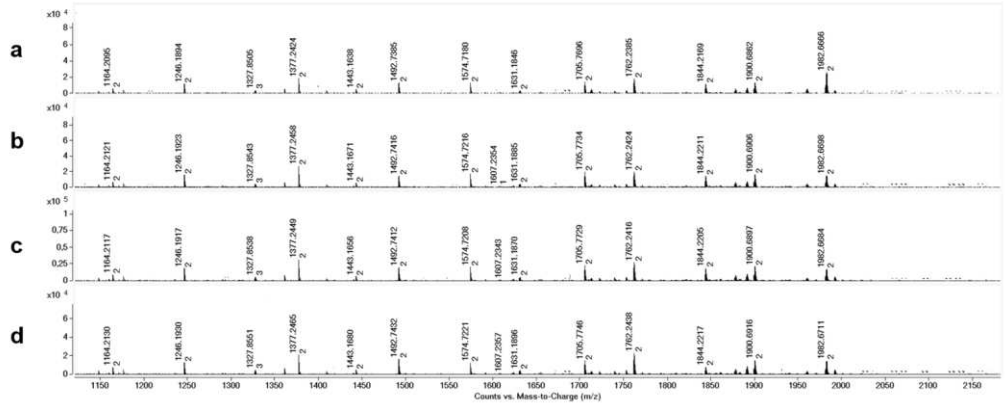

Figure 10.133: reaction with [Au_9]:[c'] molar ratio equal to 1:1, monitored at a) 3 h, b) 24 h, c) 48 h and d) 72 h.

Cluster $[Au_9(PPh_3)_8](NO_3)_3$ (25 mg, $6.16 \cdot 10^{-3}$ mmol) and **b** (5.4 mg, $6.29 \cdot 10^{-3}$ mmol) were weighed in two different vials. The solids were dissolved in 4.00 ml of DCM, affording a total volume of solution equal to 8.00 ml. The obtained solutions were mixed and left under stirring at 40°C for 72 hours. Q-TOF HRMS mass spectrometry was used to monitor the evolution of reaction, as reported in **Figure 10.134**. Mass spectrometry highlighted several clusters during the reaction. Given the low selectivity of this reaction and the complicated mass spectrum, we discharged this sample.

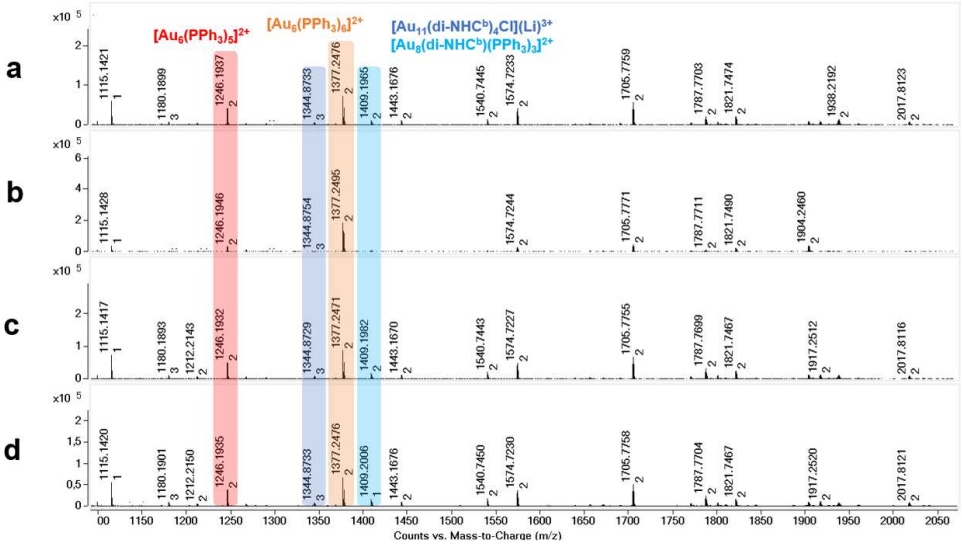

Figure 10.134: reaction with [Au_9]:[b] molar ratio equal to 1:1, monitored at a) 3 h, b) 24 h, c) 48 h and d) 72 h. Only the peaks highlighted in blue and light blue represent clusters presenting di-NHC^b ligands. The peaks highlighted in orange and red are fragmentation peaks of starting $[Au_9(PPh_3)_8]^{3+}$ cluster.

10.10 ANTICANCER ACTIVITY OF AuNCs

10.10.1 Stability of AuNCs in aqueous environment

2b', **3b** and **1c** clusters are dissolved in DMSO:H_2O (1:30 v:v) affording solution with concentration of $0.8 \cdot 10^{-3}$, $0.9 \cdot 10^{-3}$ and $1.2 \cdot 10^{-3}$ mM, respectively. UV-Vis spectroscopy was used to monitor the clusters degradation during time at room temperature after 4, 7, 8 and 9 days from preparation of solutions. For **1c** a spectrum after 3 days was also recorded. The corresponding spectra are reported in **Figure 10.135**, **10.136** and **10.137**.

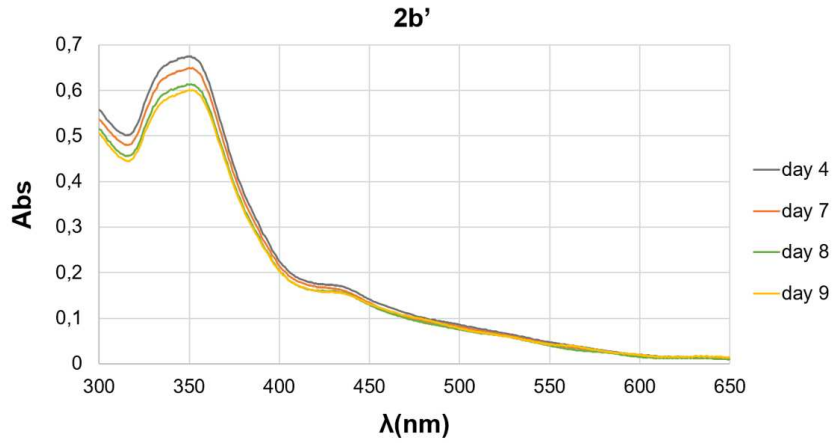

Figure 10.135: monitoring of UV-Vis spectrum of **2b'** recorded in H_2O/DMSO (1:30 v:v) solution.

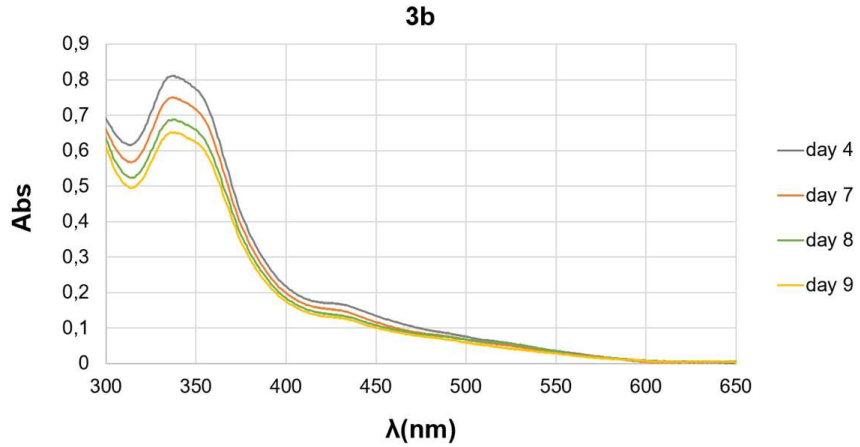

Figure 10.136: monitoring of UV-Vis spectrum of **3b** recorded in H_2O/DMSO (1:30 v:v) solution.

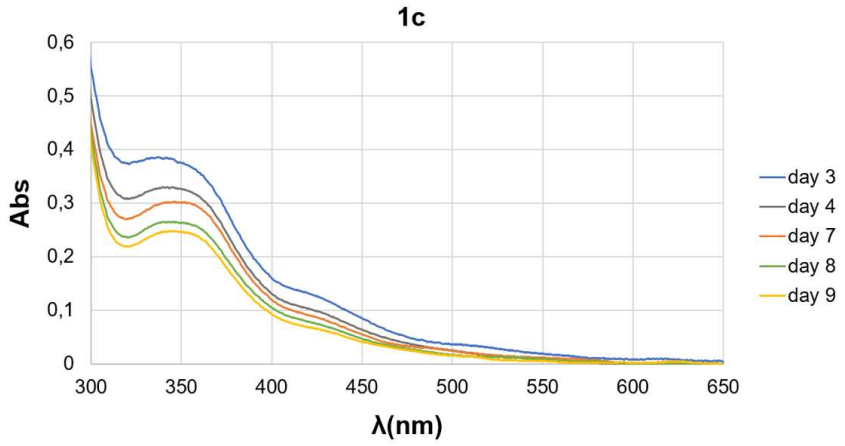

Figure 10.137: monitoring of UV-Vis spectrum of **1c** recorded in H_2O/DMSO (1:30 v:v) solution.

10.10.2 Anticancer activity of AuNCs

Table 10.9: IC_{50} (μM) related to different AuNCs tested in different cancer cellular lines and one healthy cellular line. The name of di-NHCs correspond to **a**: 1,1′-dibenzyl-3,3′-propylenediimidazol-2,2′-diylidene; **b**: 1,1′-dibenzyl-3,3′-propylenedibenzimidazol-2,2′-diylidene; **c**: 1,1′-diisopropyl-3,3′-propylenedibenzimidazol-2,2′-diylidene.

CELL LINES	DRUG	IC_{50} (μM)
HCT	$[Au_{11}(PPh_3)_8Cl_2]Cl$	0,01386
	$[Au_{13}(di\text{-}NHC^a)_2(PPh_3)_4Cl_4]Cl$	0,06755
	$[Au_{11}(di\text{-}NHC^b)(PPh_3)_6Cl_2]Cl$	0,05211
	$[Au_{13}(di\text{-}NHC^b)_2(PPh_3)_4Cl_4]Cl$	0,1026
	$[Au_{13}(di\text{-}NHC^b)_3(PPh_3)_3Cl_3]Cl_2$	0,1023
	$[Au_{11}(di\text{-}NHC^c)(PPh_3)_6Cl_2]Cl$	0,1453
	$Pt(NH_3)_2Cl_2$	1,372
MDA	$[Au_{11}(PPh_3)_8Cl_2]Cl$	1,751
	$[Au_{13}(di\text{-}NHC^a)_2(PPh_3)_4Cl_4]Cl$	0,1585
	$[Au_{11}(di\text{-}NHC^b)(PPh_3)_6Cl_2]Cl$	1,915
	$[Au_{13}(di\text{-}NHC^b)_2(PPh_3)_4Cl_4]Cl$	26,46
	$[Au_{13}(di\text{-}NHC^b)_3(PPh_3)_3Cl_3]Cl_2$	3,533
	$[Au_{11}(di\text{-}NHC^c)(PPh_3)_6Cl_2]Cl$	2,715
	$Pt(NH_3)_2Cl_2$	20,44
OVCAR3	$[Au_{11}(PPh_3)_8Cl_2]Cl$	2,185
	$[Au_{13}(di\text{-}NHC^a)_2(PPh_3)_4Cl_4]Cl$	10,65
	$[Au_{11}(di\text{-}NHC^b)(PPh_3)_6Cl_2]Cl$	3,365
	$[Au_{13}(di\text{-}NHC^b)_2(PPh_3)_4Cl_4]Cl$	~ 12153
	$[Au_{13}(di\text{-}NHC^b)_3(PPh_3)_3Cl_3]Cl_2$	14,85
	$[Au_{11}(di\text{-}NHC^c)(PPh_3)_6Cl_2]Cl$	3,045
	$Pt(NH_3)_2Cl_2$	3,165
MRC5	$[Au_{11}(PPh_3)_8Cl_2]Cl$	~ 169486
	$[Au_{13}(di\text{-}NHC^a)_2(PPh_3)_4Cl_4]Cl$	~ 184480
	$[Au_{11}(di\text{-}NHC^b)(PPh_3)_6Cl_2]Cl$	~ 162165
	$[Au_{13}(di\text{-}NHC^b)_2(PPh_3)_4Cl_4]Cl$	~ 115022
	$[Au_{13}(di\text{-}NHC^b)_3(PPh_3)_3Cl_3]Cl_2$	~ 237304
	$[Au_{11}(di\text{-}NHC^c)(PPh_3)_6Cl_2]Cl$	~ 214301
	$Pt(NH_3)_2Cl_2$	119,9

10.11 EXPERIMENTS ON GOLD NANOWIRES

10.11.1 Synthesis of 1-dodecyl-3-methylimidazolium tetrafluoroborate

The imidazolium salt 1-dodecyl-3-methylimidazolium chloride (500 mg, 1.74 mmol) was dissolved in 7 ml H_2O. 4 ml of saturated aqueous solution of $NaBF_4$ were added dropwise to the starting solution, affording a sticky precipitate. The solid was filtered and washed with 10+10 ml of H_2O. The solid was dispersed in 10 ml benzene and the suspension filtered on celite. The filtrate was concentrated under vacuum to obtain a volume of solution equal to 1 ml. This latter solution was added dropwise to a stirred solution of *n*-pentane, affording a white solid. The solid was dried under vacuum at 130°C overnight. Yield: 529 mg (90%). ^{1}H NMR (400 MHz, DMSO-d_6): δ 9.09 (s, 1H), 7.76 (br, 1H), 7.69 (br, 1H), 4.14 (t, J = 7.37 Hz, 2H), 3.83 (s, 3H), 1.76 (q, J = 7.65 Hz, 2H), 1.24 (br, 18H), 0.88-0.82 (m, 3H).

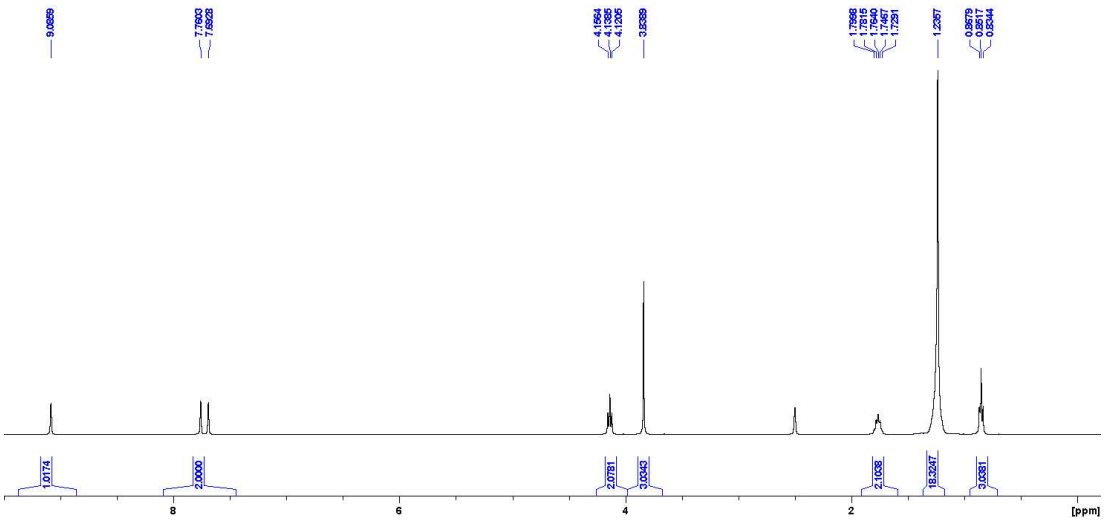

Figure 10.138: ^{1}H NMR spectrum of 1-dodecyl-3-methylimidazolium tetrafluoroborate in DMSO-d_6.

10.11.2 Synthesis of 1-dodecyl-3-methylimidazol-2-ylidene

This experiment was conducted in glovebox. 1-dodecyl-3-methylimidazolium tetrafluoroborate (27.0 mg, 0.08 mmol) and KHMDS (17.0 mg, 0.08 mmol) were dissolved in 1 ml of benzene into two different vials. The two solutions were combined and left under stirring for 30 minutes at room temperature, affording a white dispersion in a yellowish solution. After that time, the mixture was filtered on celite and dried under vacuum, affording a yellowish sticky solid. Yield: 18 mg (90%). ^{1}H NMR (400 MHz, C_6D_6): δ 6.45 (s, 1H), 6.35 (s, 1H), 3.88 (t, J = 7.37 Hz, 2H), 3.41 (s, 3H), 2.03 (Br, 2H), 1.36-1.15 (br, 18H), 0.95-0.89 (m, 3H). ^{13}C NMR (101 MHz, C_6D_6): δ = 201.13 ($C^{carbene}$), 120.72 ($CH^{imidazole}$), 119.02 ($CH^{imidazole}$), 51.37 (NHC-CH_2), 38.26 (NHC-CH_3), 32.37 (CH_2), 32.17 (CH_2), 30.12 (CH_2), 30.04 (CH_2), 29.98 (CH_2), 29.88 (CH_2), 27.00 (CH_2), 23.17 (CH_2), 14.43 (CH_3^{chain}).

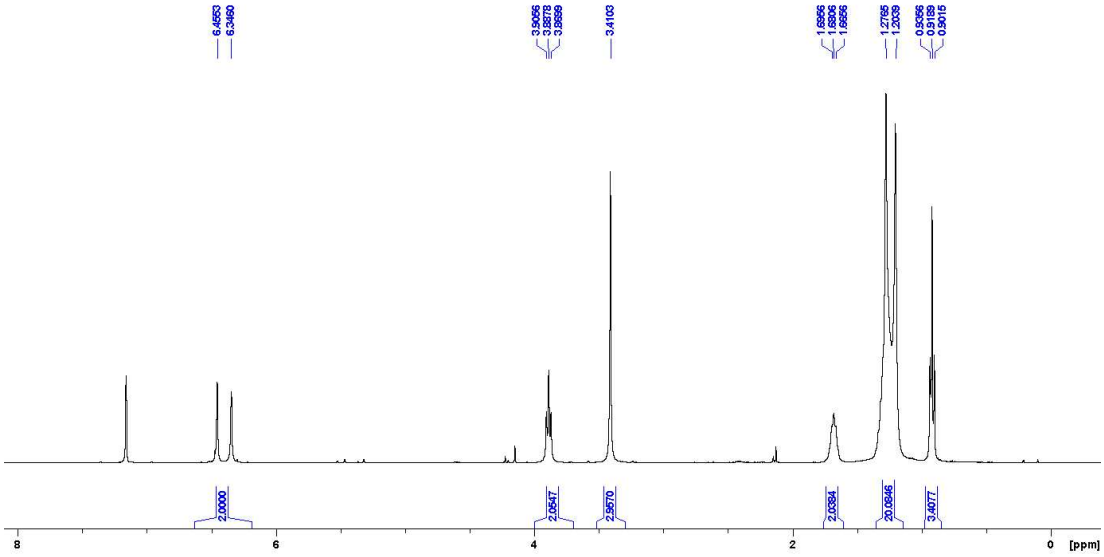

Figure 10.139: ^{1}H NMR spectrum of 1-dodecyl-3-methylimidazol-2-ylidene in C_6D_6.

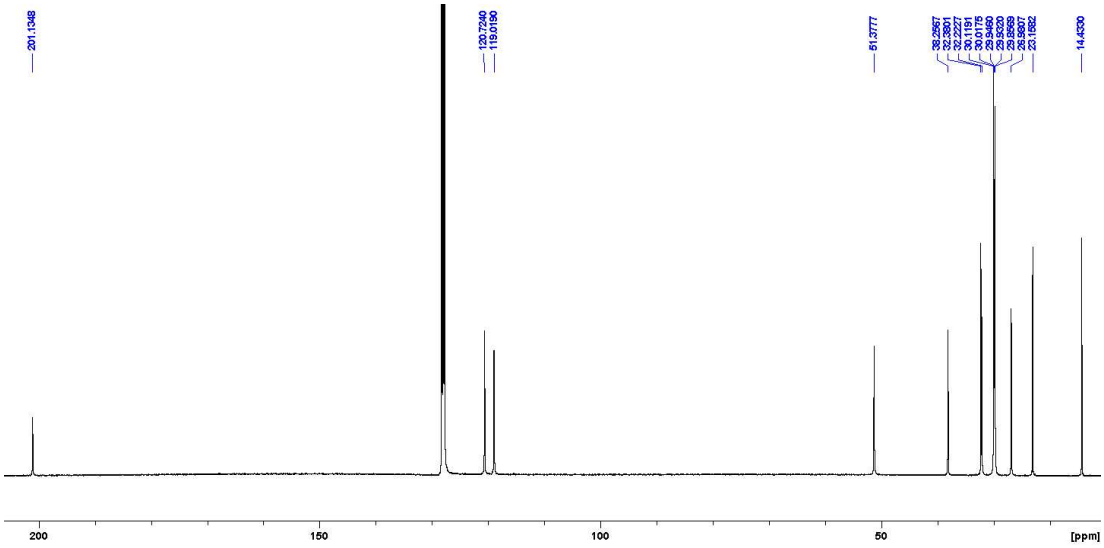

Figure 10.140: ^{13}C NMR spectrum of 1-dodecyl-3-methylimidazol-2-ylidene in C_6D_6.

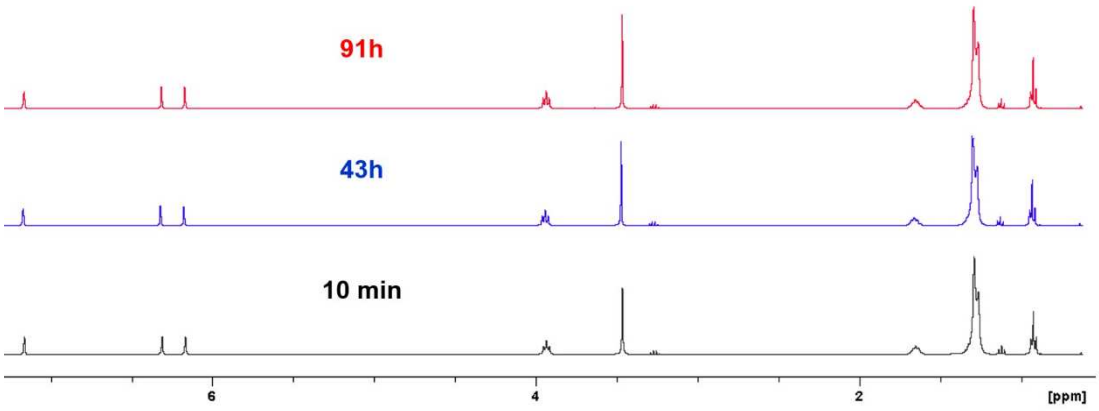

Figure 10.141: ^{1}H NMR spectra of 1-dodecyl-3-methylimidazol-2-ylidene after 10 minutes (black), 43 h (blue) and 91 h (red) in C_6D_6.

10.11.3 Ligand exchange on AuNWs

1-dodecyl-3-methylimidazolium tetrafluoroborate (34.0 mg, 0.10 mmol) and KHMDS (21.0 mg, 0.10 mmol) were dissolved in 1 ml benzene into two different vials. The two solutions were combined and left under stirring for 30 minutes at room temperature, affording a white dispersion in a yellowish solution. After that time, the mixture was filtered on celite and dried under vacuum, affording a yellowish sticky solid. The solid was dissolved in cyclohexane and the obtained solution loaded in a Schlenk tube. The solution was transferred by cannula into a dispersion of oleyl amine protected AuNWs in cyclohexane, with a concentration of 0.01 mmol/ml and volume 1 ml ([Au]:[NHC] of 1:10), affording a purple precipitate. The supernatant was decanted, dried under vacuum and analyzed by ^{1}H NMR, which confirms the presence of free oleyl ammine (**Figure 10.142**). The precipitate was washed with EtOH, dried under vacuum and partially redispersed in THF. Such dispersion was analyzed by TEM and UV-Vis analysis, both reported in **Figure 10.143**, in comparison with starting AuNWs. The sample of wires obtained after the precipitation is not enough soluble to perform an ^{1}H NMR analysis on them, therefore it was not possible to confirm the presence of NHC ligands anchored on gold wires.

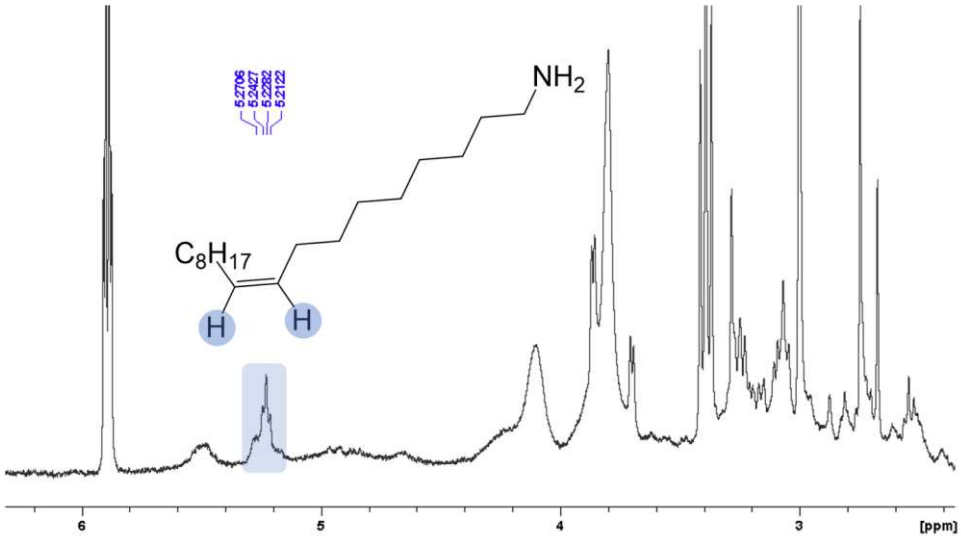

Figure 10.142: ^{1}H NMR spectrum (THF-d_8) of supernatant after the precipitation of AuNWs. The characteristic signal of oleyl amine, related to its unsaturated chain, is highlighted in blue.

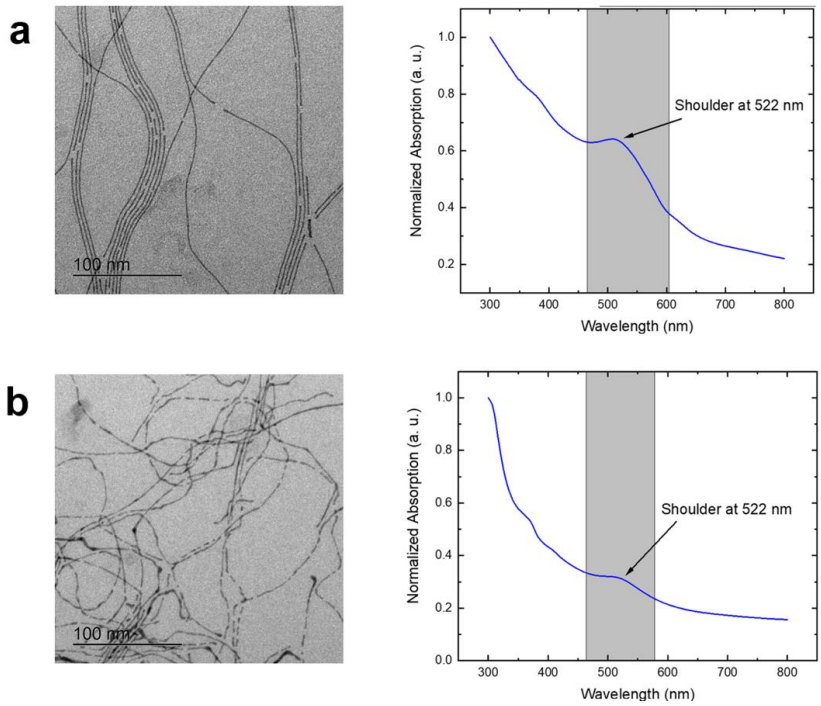

Figure 10.143: TEM and UV-Vis analyses of a) oleyl amine-capped AuNCs and b) AuNWs precipitate after the addition of free NHC ligand.

10.11.4 Complex addition on AuNWs

A 0.02 mM solution of complex **m** in $CHCl_3$ was added dropwise to a dispersion of oleyl amine protected AuNWs in the same solvent, with a concentration of 0.01 mmol/ml and volume of 1 ml ([Au]:[m] of 1:2). The addition did not afford any detectable variation of color of solution, and it was not possible to observe formation of precipitate after the addition. The dispersion was dried under vacuum and redispersed in THF. This dispersion was analyzed by TEM and UV-Vis analysis, both reported in **Figure 10.144 a**. These analyses highlighted the degradation of AuNWs after the addition of **m** complex, evidenced by the presence of AuNPs in the TEM analysis and plasmonic band in the corresponding UV-Vis spectrum. The same experiment was performed also using **n** complex, still affording degradation of starting wires, as proved by UV-Vis and TEM analyses reported in **Figure 10.144 b**.

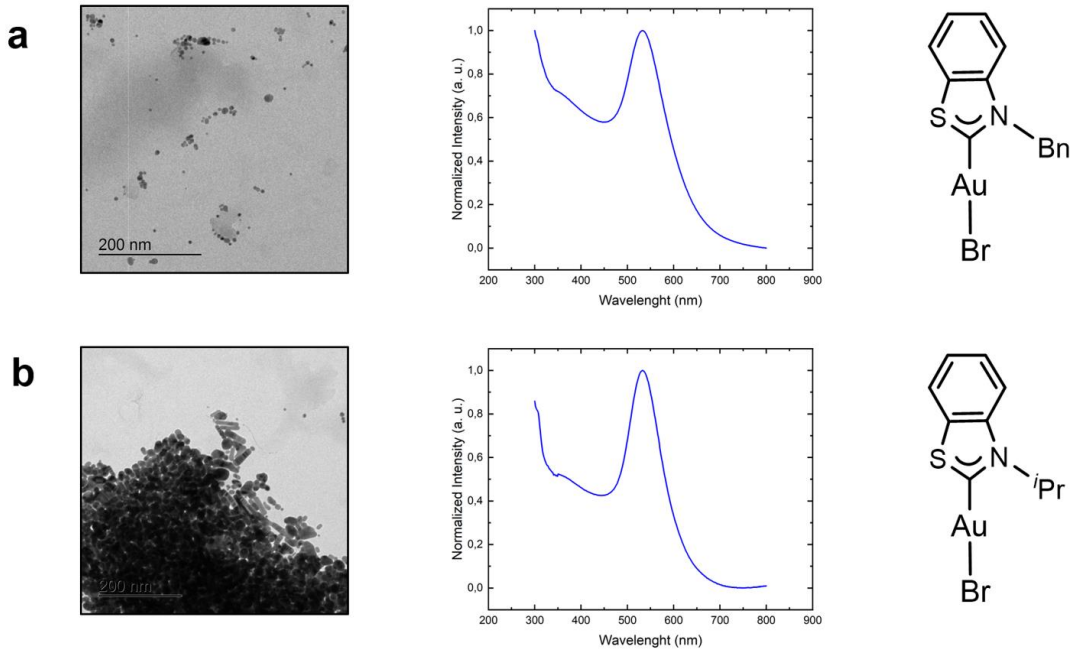

Figure 10.144: TEM and UV-Vis analyses of experiment performed with a) **m** and b) **n** complexes addition to oleyl amine-stabilized AuNWs.

10.12 PHOSPHINIDENE STABILIZED Pd_8 CLUSTER

*10.12.1 Synthesis of **1** [$Pd_8(PDip)_6$] and intermediates*

10.12.1.1 Synthesis from $Pd_2(dba)_3$

In a nitrogen-filled glovebox, three batches of $Pd_2(dba)_3$ (70 mg, 0.076 mmol) and 1,2,3-tris[2,6-bis(isopropyl)phenyl]triphosphirane (22 mg, 0.038 mmol) were mixed in three Schlenk flasks and each dissolved in benzene (2 ml). The dark mixtures were stirred outside the glovebox at 90 °C for 24 h and then concentrated *in vacuo* to *ca.* 0.4 ml. A quantitative (D1 = 30 s) ^{31}P spectroscopic analysis at this stage indicated a mixture of two compounds with a phosphorus ratio of 3:1, thus suggesting a crude yield of >75% considering that some of the product already precipitated from the solution. The crude product was quantitatively precipitated by addition of 20 ml *n*-hexane to each batch. The suspensions were filtered over celite, depositing the precipitates on top. Each batch was washed with 2×10 ml of *n*-hexane. The remaining dark solids, which are poorly soluble in benzene, were each extracted with 20 ml of C_6H_6, affording dark solutions. The insoluble solids deposited on celite were each dispersed in 40 ml of C_6H_6 and stirred for 5 min. The dark-orange suspensions were filtered, and the filtrates were combined with the previous C_6H_6 fractions. The three batches were then combined and concentrated to *ca.* 5 ml *in vacuo*. Within 16 h, dark red-to-black crystals, suitable for single crystal X-ray diffraction, formed. The crystalline material was collected and dried *in vacuo* to afford the dark-reddish-brown product in a yield of 21% (21 mg, 0.012 mmol).

^1H NMR (400 MHz, C_6D_6): δ 1.20 (d, J = 6.72 Hz, 72H), 5.11 (st, J = 6.61 Hz, 12H), 7.12 (d, J = 7.65 Hz, 12H), 7.26 (t, J = 7.70 Hz, 6H). Once precipitated, cluster **1** is only moderately soluble in C_6D_6. Hence, it was heated to 80 °C to over-saturate the solution prior to acquisition.

^{31}P NMR (162 MHz, C_6D_6): δ 533.37 (s). Once precipitated, cluster **1** is only moderately soluble in C_6D_6. Hence, it was heated to 80 °C to over-saturate the solution prior to acquisition.

^{13}C NMR (101 MHz, C_6D_6): δ 146.71 (CH^o), 131.61 (CH^p), 123.27 (CH^m), 32.71 (CH^{iPr}), 24.49 (CH_3^{iPr}). Once precipitated, cluster **1** is only moderately soluble in C_6D_6. Hence, it was heated to 80 °C prior to over-saturate the solution to acquisition; CP could not be detected due to the low concentration.

Melting point: 291 °C (decomposition).

APPI-MS, $[Pd_8(PC_{12}H_{17})_6]^+$: Calculated 2003.87 m/z, observed 2004.02 m/z. No signal was obtained in ESI mode.

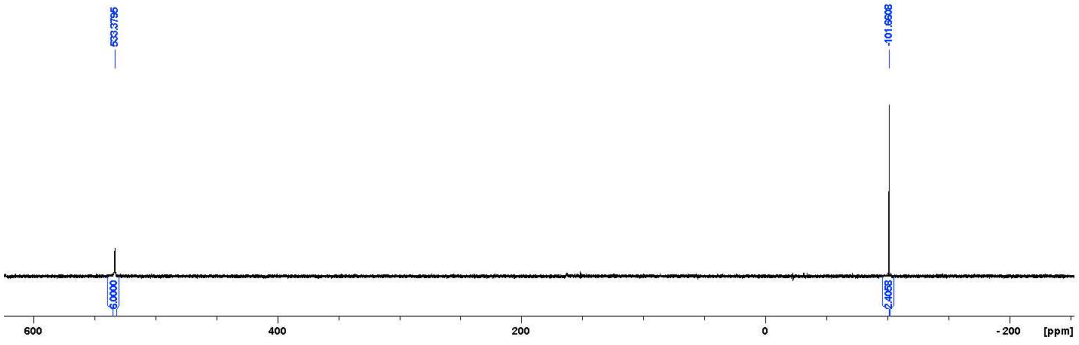

Figure 10.145: ^{31}P NMR (162 MHz, D1 = 30 sec., C_6D_6) spectrum of the crude mixture after heating to 90 °C for 24 h and cooling to room temperature.

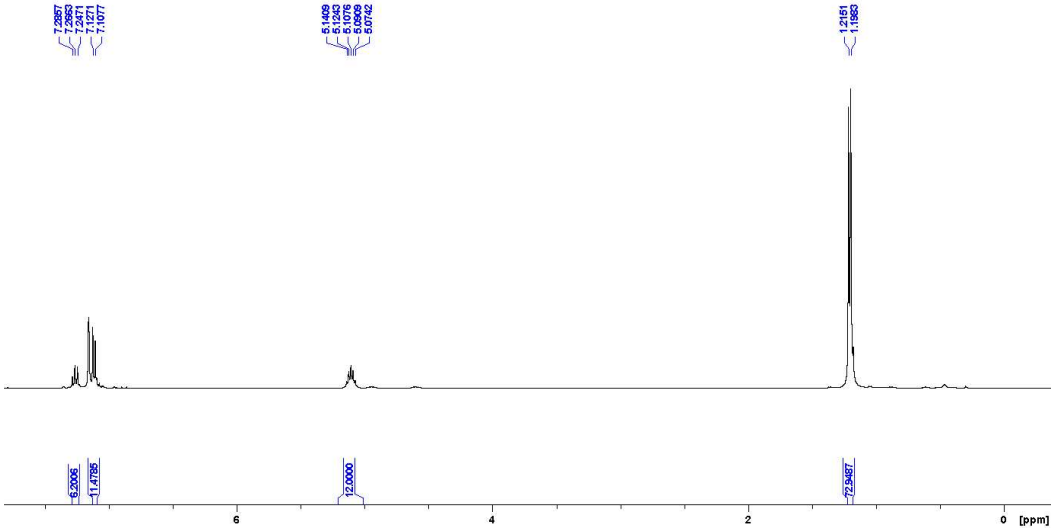

Figure 10.146: ^{1}H NMR spectrum of **1** in C_6D_6.

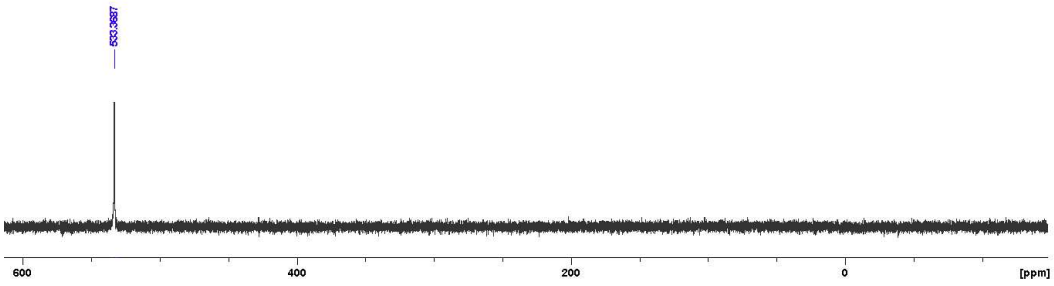

Figure 10.147: ^{31}P NMR spectrum of **1** in C_6D_6.

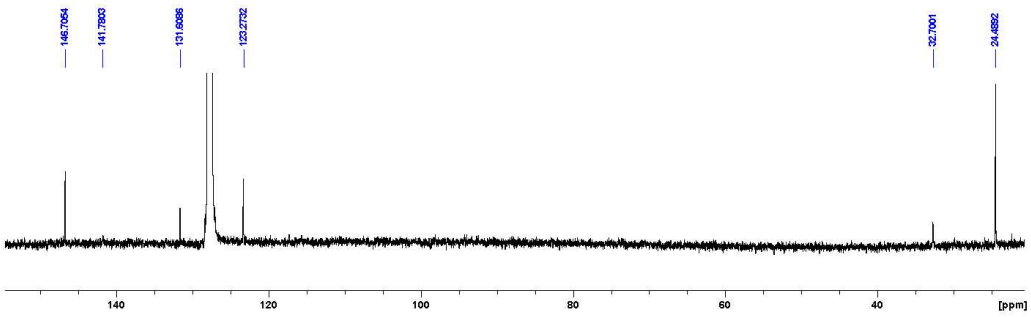

Figure 10.148: ^{13}C NMR spectrum of **1** in C_6D_6.

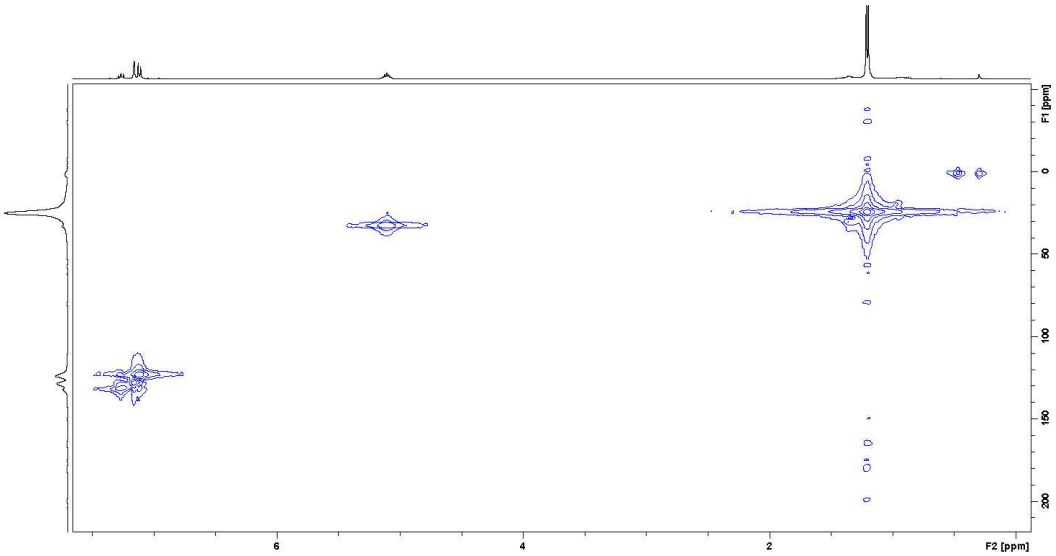

Figure 10.149: HMQC(^{1}H,^{13}C) NMR spectrum of **1** in C_6D_6.

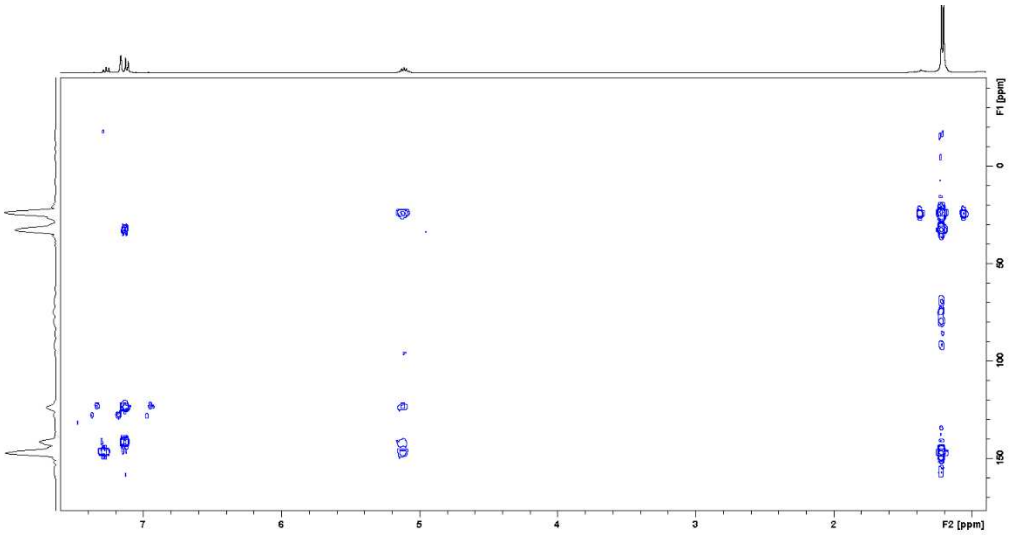

Figure 10.150: HMBC(^{1}H,^{13}C) NMR spectrum of **1** in C_6D_6.

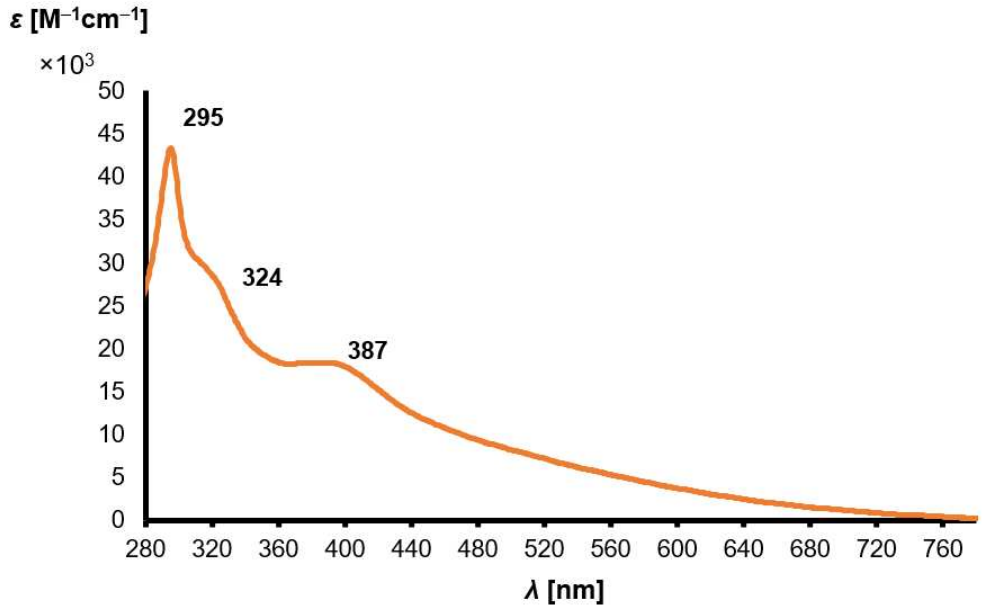

Figure 10.151: UV-Vis electronic absorption spectrum of **1** dissolved in C_6H_6, concentration 1.7×10^{-5} M.

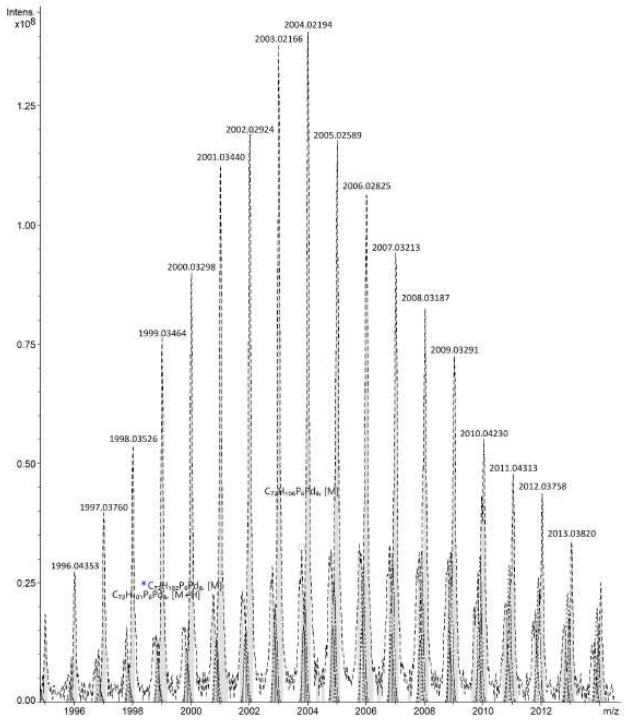

Figure 10.152: Mass spectrum of **1** dissolved in THF, APPI ionization source.

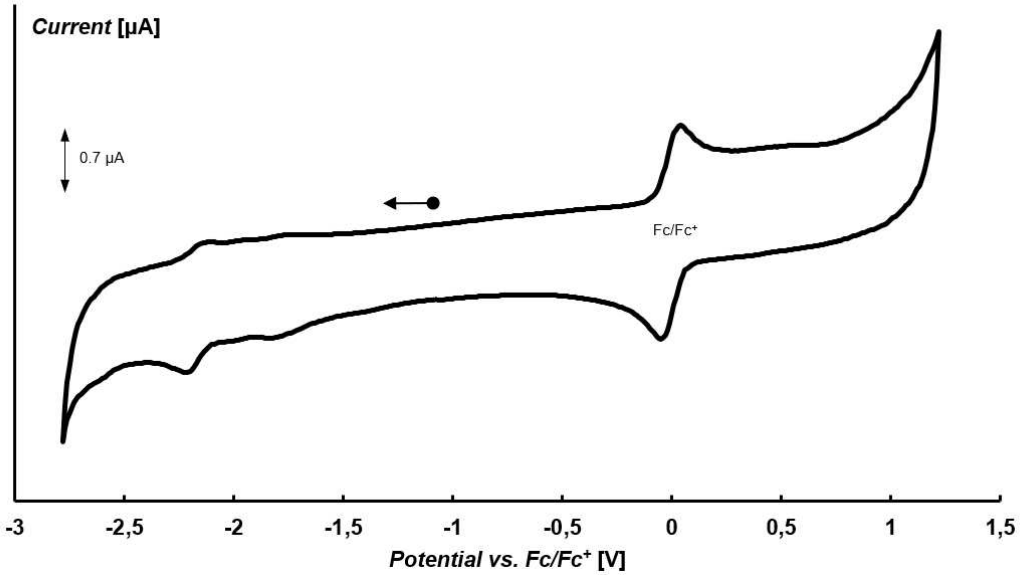

Figure 10.153: Cyclic voltammogram for **1**, measured at 100 mV s^{-1} in 0.2 M NBu_4PF_6 *ortho*-difluorobenzene solution, in the presence of the internal ferrocene standard.

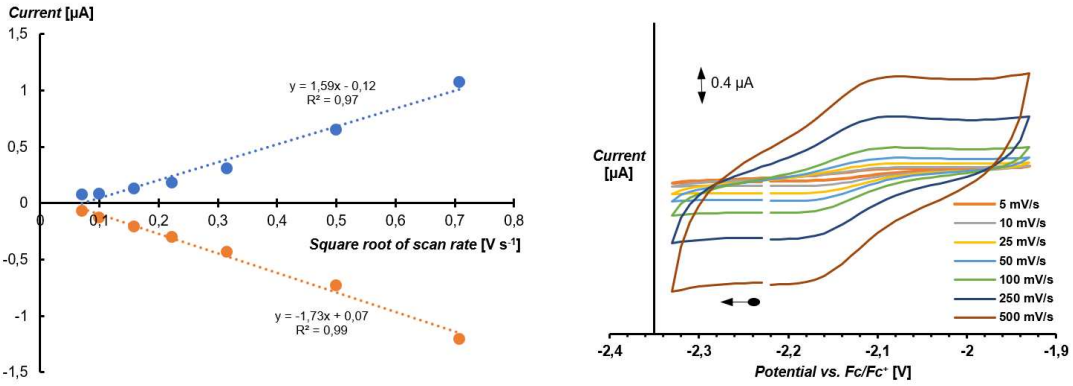

Figure 10.154: The Randles-Ševčík plot (left) suggests that the redox-event at 2.13 V (right; second scan of two is shown) is reversible.

10.12.1.2 Synthesis from (^{im}CAAC)Pd(py)

In a nitrogen-filled glovebox, (^{im}CAAC)Pd(py) (30 mg, 0.043 mmol) and 1,2,3-tris[2,6-bis(isopropyl)phenyl]triphosphorane (8 mg, 0.014 mmol) were dissolved in C_6D_6 and combined in a J-Young tube at room temperature. The dark mixture was analyzed *via* ^{1}H NMR, ^{31}P NMR and ^{31}P{^{1}H} NMR immediately, showing the formation of new species (**Figure 10.155**, #, 314.21; §, −1.14 (d, 220.8 Hz); −3.31 (d, 217.7 Hz)). After 13 h at room temperature these species partially converted to further intermediates (%, 111.88 (dd, 182.4 Hz, 28.8 Hz); 56.34 (d, 182.0 Hz); 53.02 (d, 181.7 Hz)). The intermediates are tentatively assigned to a four-membered PdP_3 oxidative addition product, follow-up multinuclear species, including **1** (*, 533.41 (s)). Aiming at increasing the conversion of intermediates into **1**, the reaction mixture was heated to 60 °C for 2 h and again analyzed *via* NMR, followed by additional 1 h at 90 °C, followed by another NMR spectroscopic analysis. These analyses reveal the presence of title compound **1** and by-products centered at −38.07 (s) and −101.68 (s), called &. Note that the product at −101.68 ppm, in the non-^{1}H-decoupled ^{31}P spectrum shows a doublet (J = 231.6 Hz), indicating the formation of a P–H bond. Upon cooling, a dark solid precipitated. Workup was performed as indicated in **Paragraph 10.12.1.1**.

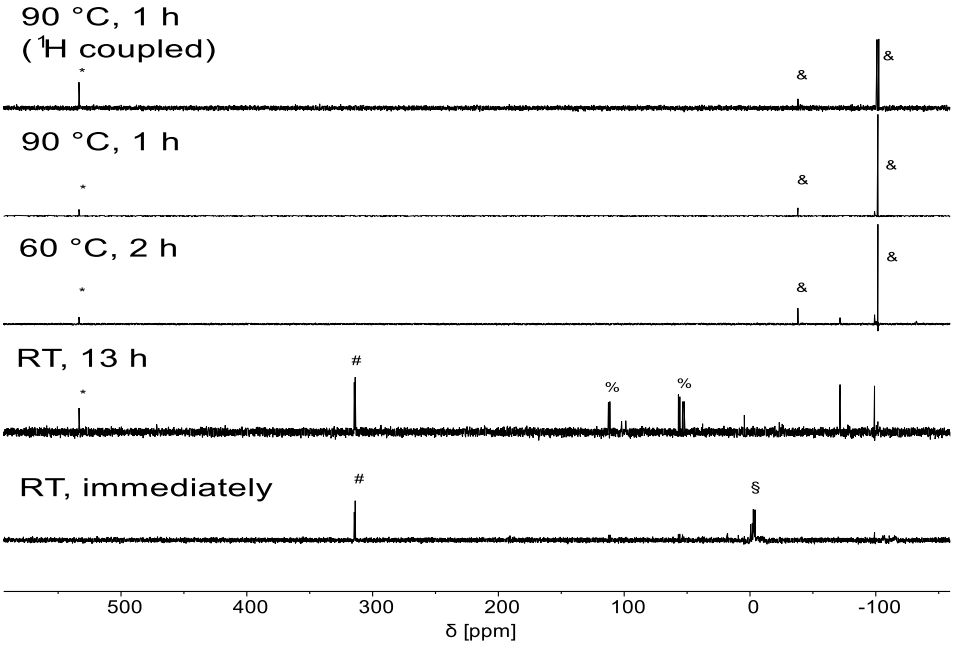

Figure 10.155: ^{31}P NMR for the reaction of (^{im}CAAC)Pd(py) with (PDip)$_3$ in C_6D_6.

*10.12.1.3 Crystallization of Intermediates **2** and **3***

[Pd(py)$_2$(PDip)$_3$] (**2**)

In a nitrogen-filled glovebox, (^{Im}CAAC)Pd(py) (30 mg, 0.043 mmol) and 1,2,3-tris[2,6-bis(isopropyl)phenyl]triphosphorane (24 mg, 0.042 mmol) were dissolved in melting pyridine-d$_5$ and kept at room temperature overnight. During this time, the complex crystallized from the solution as dark-orange platelets.

[Pd$_2$(py)$_2$(PDip)$_2$(PDip)$_3$] (**3**)

In a nitrogen-filled glovebox, (^{Im}CAAC)Pd(py) (30 mg, 0.043 mmol) and 1,2,3-tris[2,6-bis(isopropyl)phenyl]triphosphorane (8 mg, 0.014 mmol) were dissolved in melting toluene-d$_8$ and kept at room temperature overnight. From the dark reaction mixture, deep dark-red crystals were obtained through vapor diffusion of *n*-pentane into the toluene solution at −35 °C.

Both pyridine complexes are insoluble in a wide range of solvents, thus preventing further analysis.

*10.12.2 Synthesis of **4** $Pd_8(PDip)_6(CN^oXyl)_4$*

In a nitrogen-filled glovebox, **1** (6 mg, 0.003 mmol) was dissolved in 1 ml of C_6D_6. A stock solution of 2,6-dimethylphenylisocyanide (9 mg dissolved in 1 ml of C_6D_6) was prepared and 210 µl (2.36 mg, 0.018 mmol) were added. ^{31}P and ^{1}H NMR spectra were recorded, indicating the clean and quantitative formation of the desired product. The addition of 10 ml of *n*-hexanes quantitatively precipitated the dark-brown product. The suspension was filtered over celite, which was washed with 10 ml of *n*-hexane. The product was then recovered by rinsing with 2 ml of C_6H_6. Volatiles were removed *in vacuo* to afford a dark-brown solid. Single crystals suitable for X-ray diffractometry were obtained by vapor diffusion of *n*-pentane into a solution in C_6H_6. Yield: 6 mg (80%).

^{1}H NMR (400 MHz, C_6D_6): δ 1.46 (d, J = 6.12 Hz, 72H), 1.63 (s, 24H), 5.17 (q, J = 6.44 Hz, 12H), 6.59 (d, J = 7.50 Hz, 8H), 6.71 (t, J = 7.81 Hz, 4H), 7.18 (d, J = 8.20 Hz, 12H), 7.29 (t, J = 7.80 Hz, 6H).

^{31}P NMR (162 MHz, C_6D_6): δ 519.35 (s) ppm.

^{13}C NMR (100 MHz, C_6D_6): *δ* 150.30 (C≡N), 134.98 (CN-C), 130.09 (Dip-CH^p), 128.77 (Dip-C^o), 128 (Ph-$CH^{m/p}$, superimposed with C_6D_6 signal, HMQC), 127.23 (Ph-C^o), 123.00 (Dip-CH^m), 30.95 (CH^{iPr}), 25.97 (Ph-CH_3), 18.17 ($CH_3{}^{iPr}$). CP could not be detected due to the low solubility.

Melting point: 280 °C (decomposition).

APPI-MS: Despite various attempts, only the starting material **1** was detected with appropriate intensity. CN^oXyl ligands are likely removed during the ionization process. ESI-mode proved likewise unproductive.

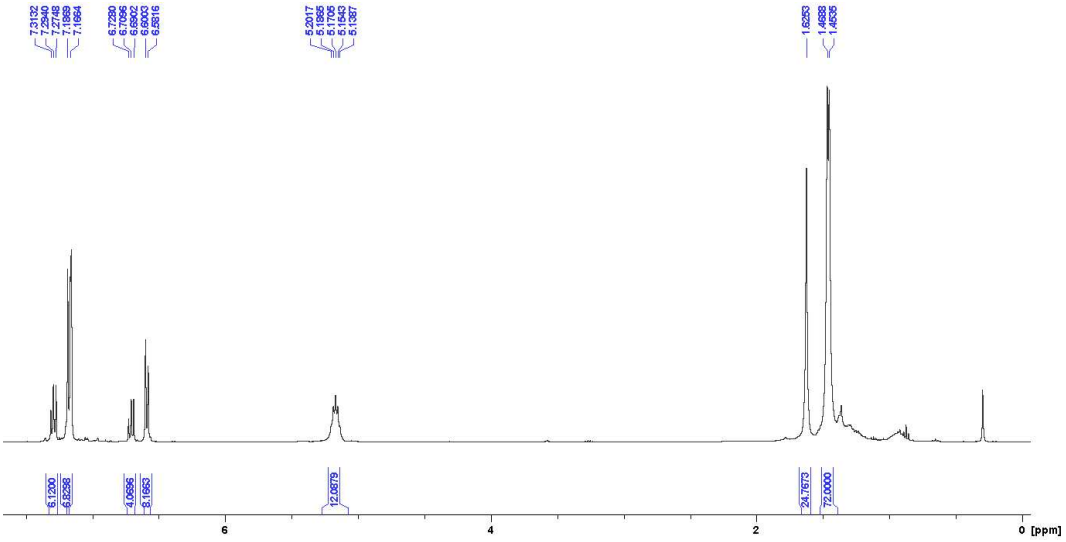

Figure 10.156: ^{1}H NMR spectrum of **4** in C_6D_6.

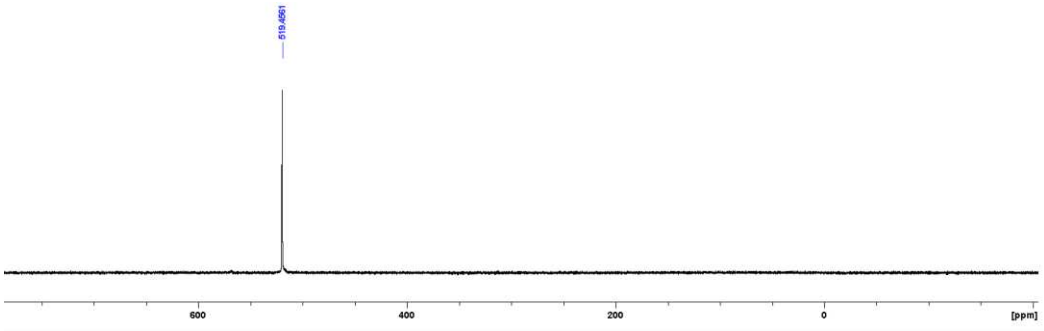

Figure 10.157: ^{31}P NMR spectrum of **4** in C_6D_6.

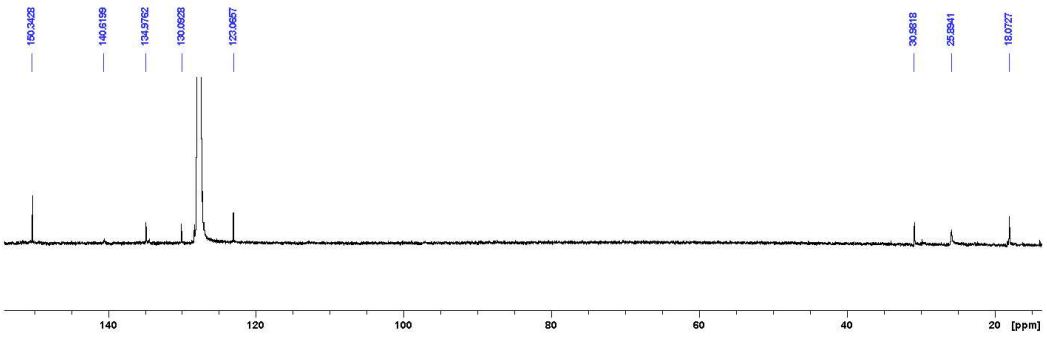

Figure 10.158: ^{13}C NMR spectrum of **4** in C_6D_6.

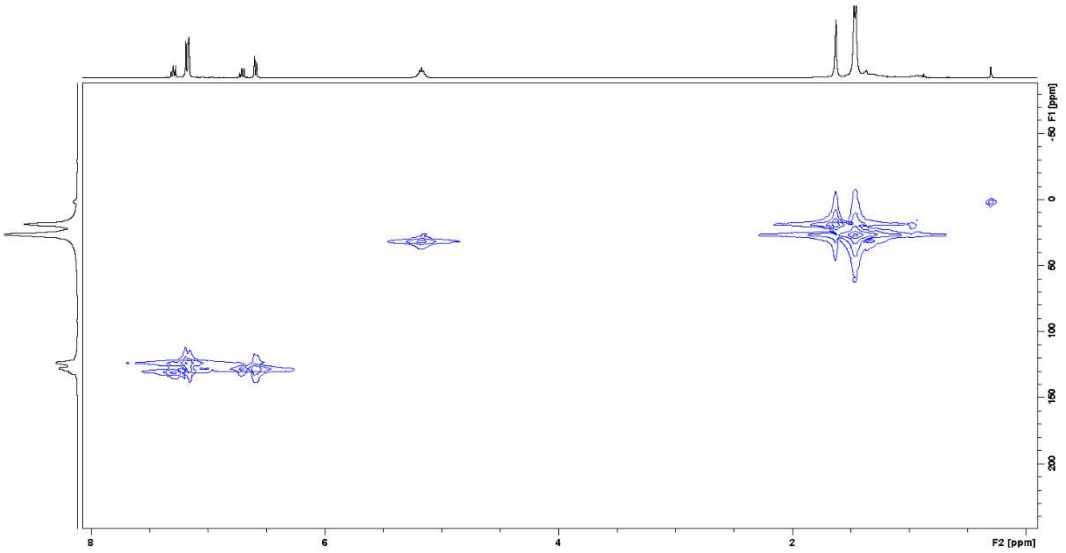

Figure 10.159: HMQC (^{1}H,^{13}C) NMR spectrum of **4** in C_6D_6.

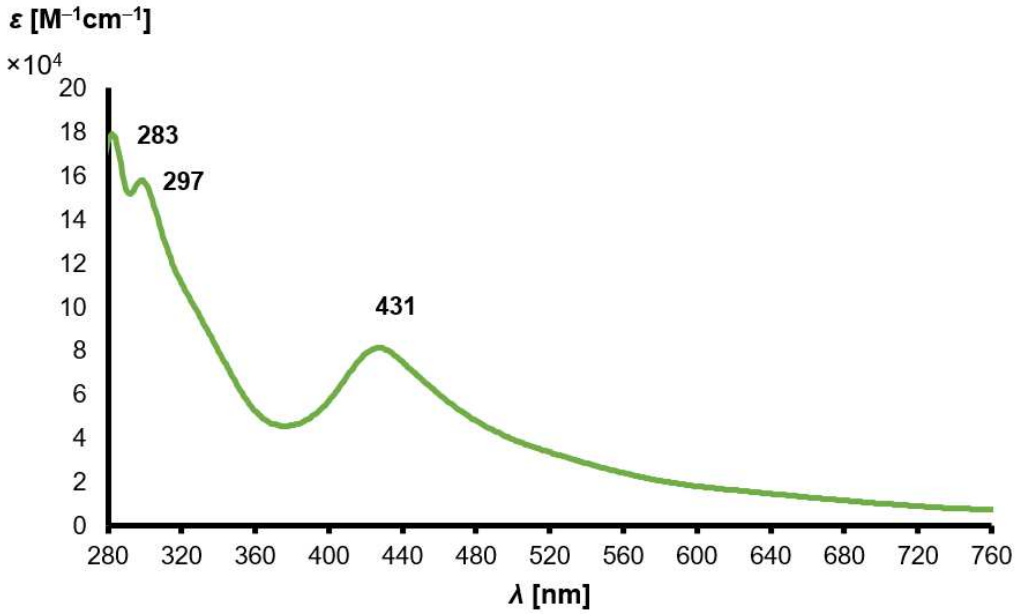

Figure 10.160: UV-Vis spectrum of **4** dissolved in C_6H_6, concentration 0.6 $\times 10^{-5}$ M.

10.12.3 Titration of 1 with 2,3-dimethylphenylisocyanide

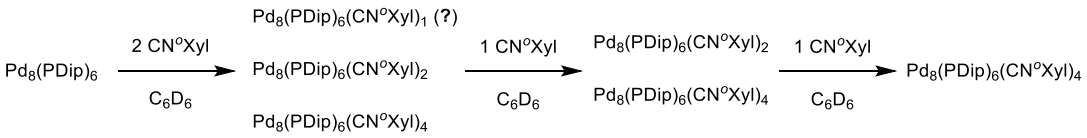

Figure 10.161:schematic representation of titration of **1** with 2,3-dimethylphenylisocyanide

In a nitrogen-filled glovebox, **1** (6 mg, 0.003 mmol, 1 eq.) was dissolved in 1 ml of C_6D_6. A stock solution of 2,6-dimethylphenylisocyanide (9 mg dissolved in 1 ml of C_6D_6) was prepared and aliquots of 70 µl (0.39 mg, 0.001 mmol, 2 eq.), 105 µl (overall 3 eq.), 140 µl (overall 4 eq.) and 210 µl (overall 6 eq.) were added to the cluster solution consecutively. For each addition step, ^{31}P and ^{1}H NMR spectra were recorded. The number of coordinated isocyanides in the clusters were determined using the integration values in the ^{1}H spectra. Upon the addition of 2 equivalents, a mixture of three compounds was obtained, which we tentatively assign to mono-, di- and tetra-isocyanide clusters. Addition of another equivalent leaves two clusters, which relate to $Pd_8(PDip)_6(CN^oXyl)_2$ and $Pd_8(PDip)_6(CN^oXyl)_4$. Upon the addition of overall 4 equivalents, only $Pd_8(PDip)_6(CN^oXyl)_4$ remains in solution. Adding more equivalents of isocyanide did not lead to further higher-coordinated species.

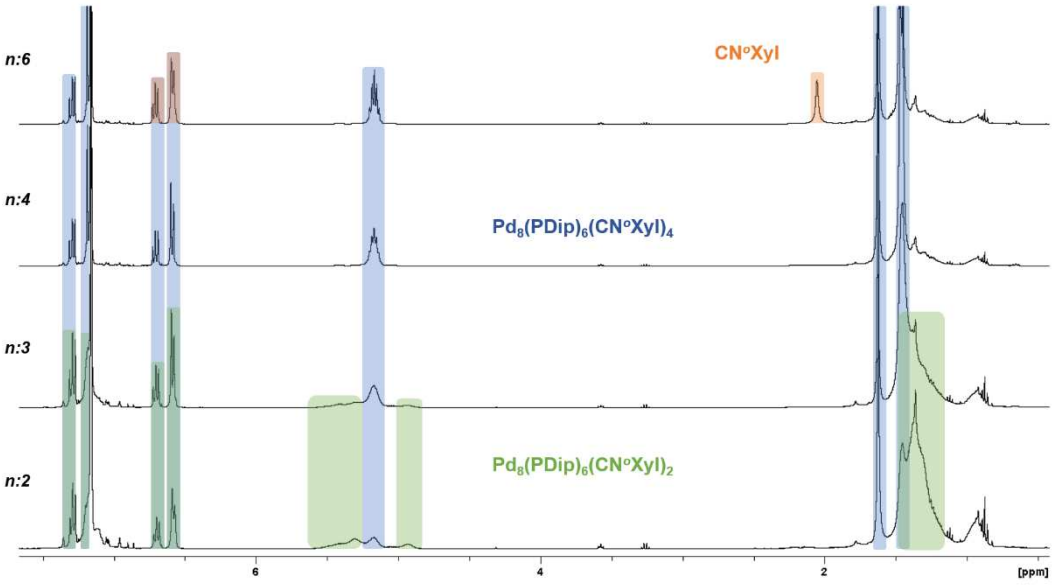

Figure 10.162: ^{1}H NMR spectra of **1** titrated with n-equivalents of 2,6-dimethylphenylisocyanide (CNºXyl) in C_6D_6. $Pd_8(PDip)_6(CN^oXyl)_2$, $Pd_8(PDip)_6(CN^oXyl)_4$ (**4**) and uncoordinated CNºXyl are highlighted in green, blue and orange color, respectively.

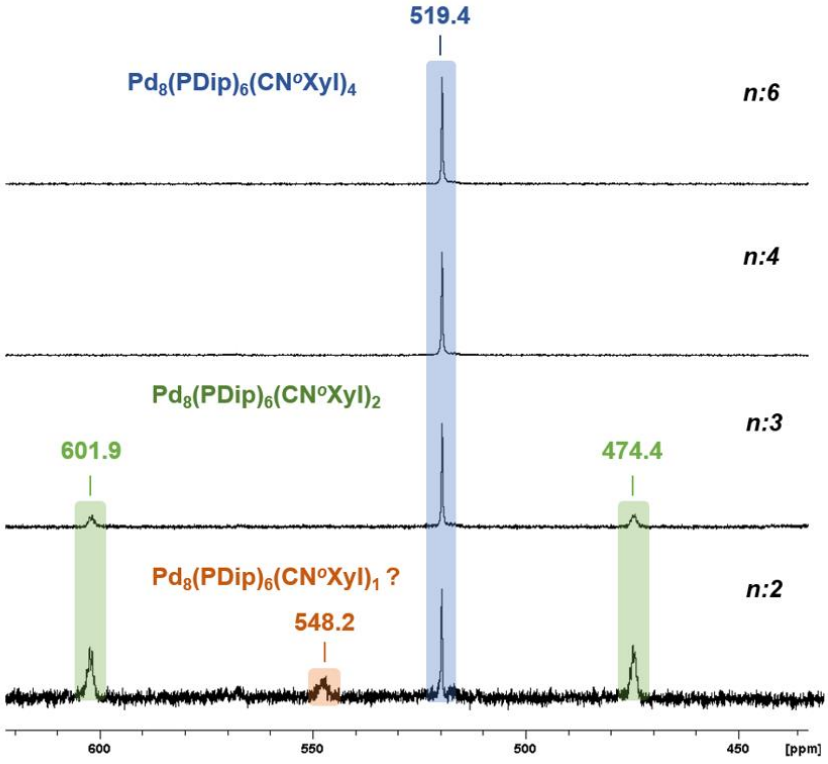

Figure 10.163: ^{31}P NMR spectra of **1** titrated with n-equivalents of 2,6-dimethylphenylisocynade (CNºXyl) in C_6D_6. $Pd_8(PDip)_6(CN^oXyl)_1$, $Pd_8(PDip)_6(CN^oXyl)_2$ and $Pd_8(PDip)_6(CN^oXyl)_4$ (**4**) are highlighted in orange, green and blue color, respectively.

*10.12.4 C_2H_4 Coordination with **1***

In a nitrogen-filled glovebox, **1** (3 mg, 0.002 mmol) was dissolved in 0.5 ml of C_6D_6 and loaded in an NMR tube equipped with a J-Young valve. Using a Schlenk line, the solution was saturated with ethylene gas and analyzed by NMR spectroscopy. In the ^{31}P spectrum, a shift of 4 ppm in respect to the starting material **1** was detected. In the ^{1}H spectrum, a slight shift of 0.02 ppm was observed for the CH signals of the *i*Pr groups and 0.01 ppm for CH^{m} of Dip ring. Upon removal of volatiles in *vacuo* and redissolution in C_6D_6, the clean regeneration of **1** was observed.

^{1}H NMR (400 MHz, C_6D_6): δ 1.21 (d, J = 6.82 Hz, 72H), 5.09 (st, J = 6.61 Hz, 12H), 5.25 (s, excess of C_2H_4), 7.12 (d, J = 7.65 Hz, 12H), 7.27 (t, J = 7.70 Hz, 6H). Cluster **1** is only moderately soluble in C_6D_6. Hence, it was heated to 80 °C to over-saturate the solution prior to acquisition.

^{31}P NMR (162 MHz, C_6D_6): δ 537.5 (s). Cluster **1** is only moderately soluble in C_6D_6. Hence, it was heated to 80 °C to over-saturate the solution prior to acquisition.

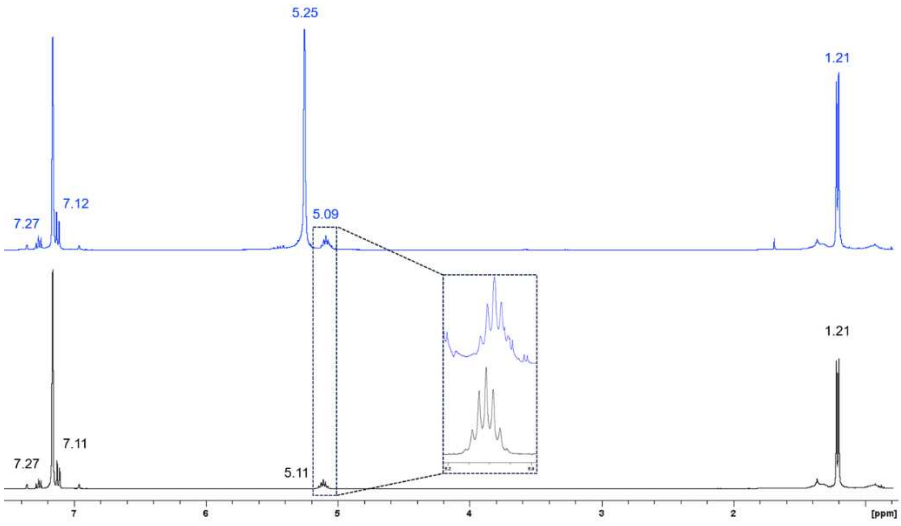

Figure 10.164: ^{1}H NMR spectrum of $Pd_8(PDip)_6(C_2H_4)_n$.(blue) in comparison with of $Pd_8(PDip)_6$ spectrum (black) in C_6D_6. The values of chemical shifts are reported in the spectra. The shift of CH^{iPr} of Dip groups is highlighted in the black square.

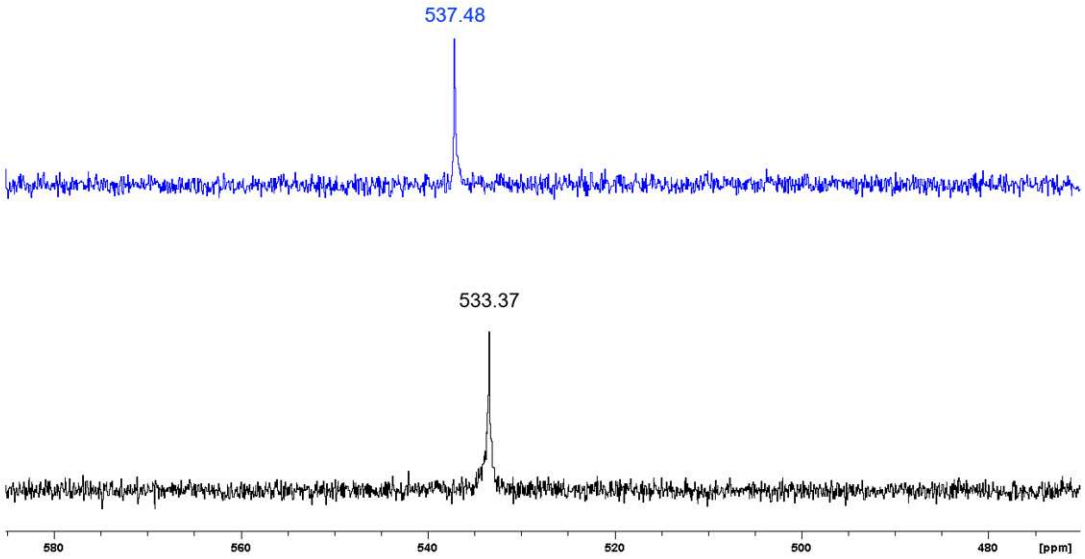

Figure 10.165: ^{31}P NMR spectrum of $Pd_8(PDip)_6(C_2H_4)_n$ (blue) in comparison with $Pd_8(PDip)_6$ spectrum (black) in C_6D_6. The values of chemical shifts are reported in the spectra.

*10.12.5 X-ray structures of **1**, **2**, **3** and **4***

The crystallographic data for Pd compounds **1**, **2**, **3**, and **4** were obtained by mounting well-formed single crystals on a glass fiber and transferring them in Fomblin YR-1800 perfluoro ether (Alfa Aesar) at ambient temperature. The samples were cooled to 150(2) K (except compound **4**: 143(2)K) during measurement. The data were collected on a Bruker D8 Venture diffractometer using monochromated MoKα (λ = 0.71073 Å; compound **4**) or CuK_α radiation (λ = 1.54178 Å; compounds **1**–**3**), respectively, and a Photon II detector. The structures were solved by intrinsic phasing (SHELXT)[27] and refined by full matrix least squares procedures (SHELXL)[27] with the Olex2[28] or ShelXle[29] platform, respectively. Semi-empirical absorption corrections (multiscan and additional spherical absorption correction) were applied to the diffraction data recorded using the SADABS application within the APEX4 platform.[30] All non-hydrogen atoms were refined anisotropically, hydrogen atoms were included in the refinement at calculated positions using a riding model. All special refinement details (if required) for disordered or twinned structures as well as molecular structure representations are summarized below. A summary on standard crystallographic parameters as well as the CSD entry numbers within the Cambridge Crystallographic Data Centre (CCDC) are subsequently provided in **Table 10.10**.

Special Refinement Details:

*Compound **3**, disorder*: One of the Dip groups was found to be disordered, and a disorder model was described for tilting of the whole fragment containing C33, C32, C31, C71, C72 and C73. Two respective split positions have been refined according to the free variable 2 (FVAR2), which refined into occupancies of 0.57 and 0.43. To fix the refinement, soft DELU and ISOR restraints were embedded to the refinement reaching more reasonable displacement.

*Compound **4**, disorder*: One of the dimethylphenyl substituents is split over two positions according to the free variable 4 (FVAR4) (0.53:0.47). Two benzene solvent molecules share their position with two *n*-pentane solvent molecules. Their occupancy factors refined to 0.42:0.58 and 0.48:0.52, according to FVAR 2 and 3 respectively. For the refinement of the disorder restraints (RIGU, SADI, FLAT, SIMU, DFIX) were applied for the solvent molecules. *Twinning:* The structure was refined as a non-merohedral two-component twin. The twin matrix was found to be (1.000 -0.606 -0.124, 0.000 -1.000 0, -0.007 0.000 -1.000) from the DOMAIN routine of APEX4. The structure was solved using the hklf4 file and then refined to convergence using the hklf5 routine of SHELXL. The BASF value refined to 0.3964(5).

Molecular Structure Representations**: 1, 2, 3** and **4** molecular structure representations in this section as well as the main text have been prepared with the Diamond software package, mixed representation of ellipsoid plots as well as wires/sticks was chosen for clarity.

Table 10.10: Crystallographic details for **1**-**4**.

Compound	1	2	3	4
Empirical formula	$C_{72}H_{102}P_6Pd_8$	$C_{46}H_{61}N_2P_3Pd$	$C_{70}H_{95}N_2P_5Pd$	$C_{118.91}H_{156.55}N_4P_6Pd_8$
Formula weight	2004.55	841.27	1332.12	2678.94
Temperature/K	150(2)	150(2)	150(2)	143(2)
Crystal system	trigonal	monoclinic	monoclinic	triclinic
Space group	*R*–3	$P2_1/c$	$P2_1/c$	*P*–1
a/Å	24.4510(8)	10.9572(2)	16.3306(3)	15.5015(6)
b/Å	24.4510(8)	16.0580(3)	14.3551(3)	16.3071(6)
c/Å	10.4546(6)	24.8673(5)	33.8651(6)	24.4515(8)
α/°	90	90	90	84.533(2)
β/°	90	102.3760(10)	90.4070(10)	82.6620(10)
γ/°	120	90	90	70.8390(10)
Volume/Å^3	5412.9(5)	4273.74(14)	7938.7(3)	5781.3(4)
Z	3	4	4	2
ρ_{calc}g/cm^3	1.845	1.307	1.115	1.539
μ/mm^{-1}	17.260	4.807	4.862	2712.0
F(000)	2976.0	1768.0	2784.0	2712.0
Crystal size/mm^3	0.21 × 0.08 × 0.05	0.24 × 0.22 × 0.05	0.26 × 0.24 × 0.19	0.260 × 0.200 × 0.100
Radiation	CuKα (λ = 1.54178)	CuKα (λ = 1.54178)	CuKα (λ = 1.54178)	MoKα (λ = 0.71073)
2Θ range for data collection/°	7.23 to 133.21	6.598 to 133.36	5.218 to 133.298	3.794 to 56.646
Index ranges	-28 ≤ h ≤ 29, -29 ≤ k ≤ 29, -12 ≤ l ≤ 12	-12 ≤ h ≤ 13, -19 ≤ k ≤ 19, -29 ≤ l ≤ 29	-19 ≤ h ≤ 19, -17 ≤ k ≤ 17, -40 ≤ l ≤ 40	-20 ≤ h ≤ 20, -21 ≤ k ≤ 21, 0 ≤ l ≤ 32
Reflections collected	20219	35130	106743	28765
Independent reflections	2140 [R_{int} = 0.0873, R_{sigma} = 0.0374]	7440 [R_{int} = 0.0790, R_{sigma} = 0.0499]	14020 [R_{int} = 0.0550, R_{sigma} = 0.0277]	28765 [R_{int} = *, R_{sigma} = 0.0413]
Data/restraints/parameters	2140/0/134	7440/0/481	14020/43/762	28765/884/1434
Goodness-of-fit on F^2	1.088	1.042	1.044	1.194
Final R indexes [I>=2σ (I)]	R_1 = 0.0399, wR_2 = 0.0882	R_1 = 0.0413, wR_2 = 0.0822	R_1 = 0.0278, wR_2 = 0.0659	R_1 = 0.0441, wR_2 = 0.0917
Final R indexes [all data]	R_1 = 0.0555, wR_2 = 0.0979	R_1 = 0.0635, wR_2 = 0.0925	R_1 = 0.0342, wR_2 = 0.0684	R_1 = 0.0664, wR_2 = 0.1040
Largest diff. peak/hole / e Å^{-3}	3.70/-0.90	0.69/-0.76	1.17/-0.86	1.50/-0.86
Absolute structure parameter	-	-	-	-
CCDC #	2287222	2287223	2287224	2287552

* refined as a two-component twin.

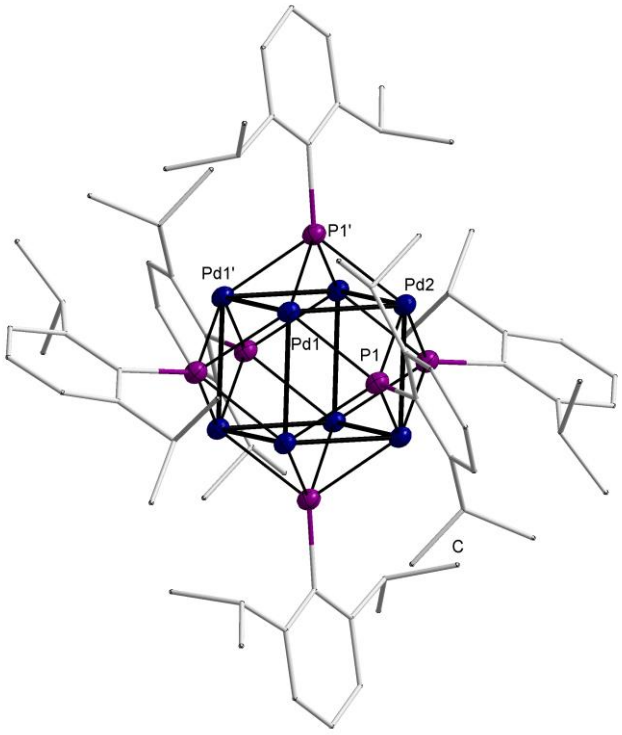

Figure 10.166: Molecular structure representations of **1**. Ellipsoids are drawn at their 50 % probability level. Hydrogens are omitted for clarity. Color code: dark blue (Pd), purple (P), grey (C).

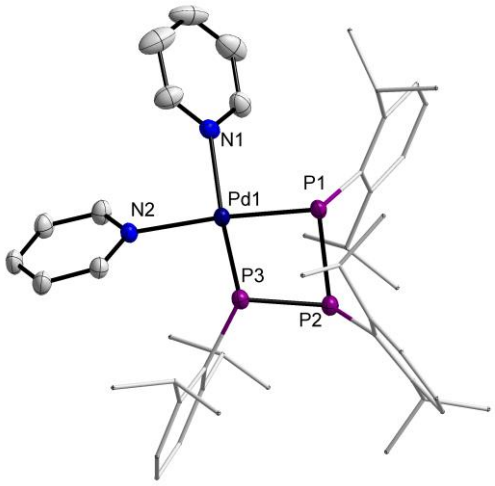

Figure 10.167: Molecular structure representations of **2**. Ellipsoids are drawn at their 50 % probability level. Hydrogens are omitted for clarity. Color code: dark blue (Pd), purple (P), blue (N), grey (C).

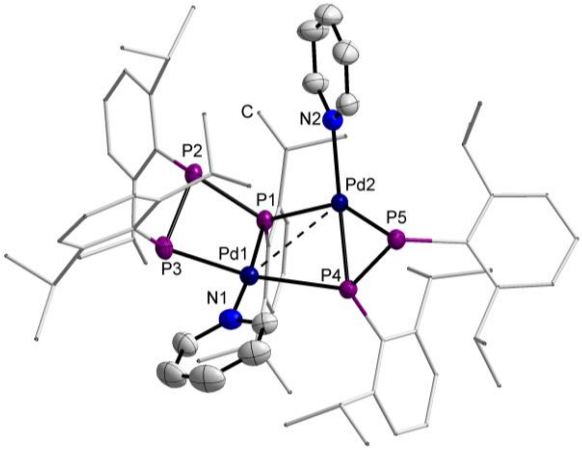

Figure 10.168: Molecular structure representations of **3**. Ellipsoids are drawn at their 50 % probability level. Hydrogens are omitted for clarity. Color code: dark blue (Pd), purple (P), blue (N), grey (C).

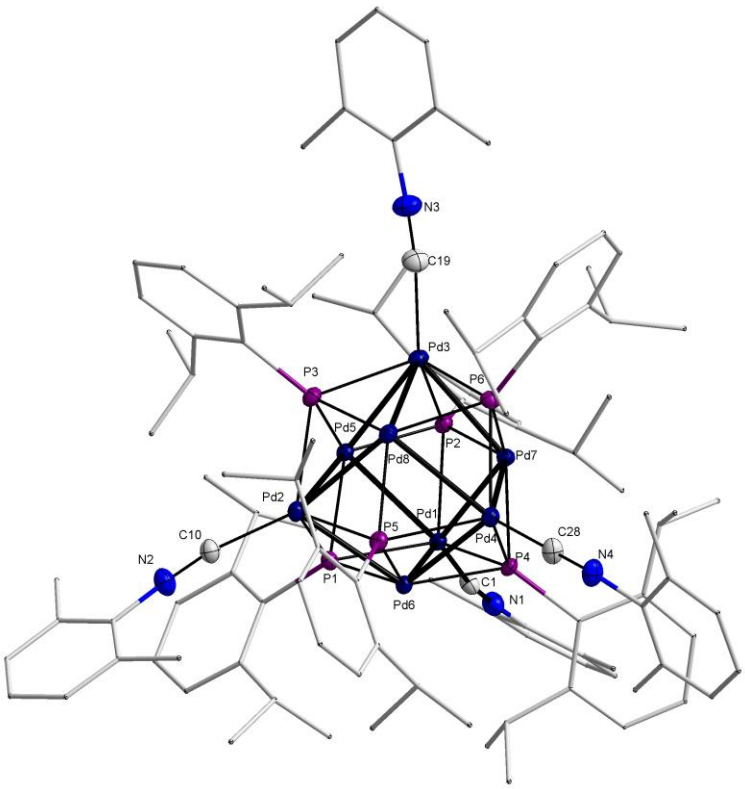

Figure 10.169: Molecular structure representations of **4**. Ellipsoids are drawn at their 50 % probability level. Hydrogens are omitted for clarity. Color code: dark blue (Pd), purple (P), blue (N), grey (C).

10.13 BIBLIOGRAPHY

[1] M. R. Narouz, K. M. Osten, P. J. Unsworth, R. W. Y. Man, K. Salorinne, S. Takano, R. Tomihara, S. Kaappa, S. Malola, C.-T. Dinh, J. D. Padmos, K. Ayoo, P. J. Garrett, M. Nambo, J. H. Horton, E. H. Sargent, H. Häkkinen, T. Tsukuda, C. M. Crudden, *Nat. Chem.* **2019**, *11*, 419–425.
[2] F. Cariati, L. Naldini, *J. Chem. Soc. Dalton Trans.* **1972**, 2286.
[3] C.-H. Lee, S.-M. Lee, B.-H. Min, D.-S. Kim, C.-H. Jun, *Org. Lett.* **2018**, *20*, 2468–2471.
[4] L. Kathuria, N. U. Din Reshi, A. G. Samuelson, *Chem. – Eur. J.* **2020**, *26*, 7622–7630.
[5] W. Mansour, M. Fettouhi, B. El Ali, *Appl. Organomet. Chem.* **2020**, *34*, DOI 10.1002/aoc.5636.
[6] R. McKie, J. A. Murphy, S. R. Park, M. D. Spicer, S. Zhou, *Angew. Chem.* **2007**, *119*, 6645–6648.
[7] S. Ma, P. Toy, *Molecules* **2016**, *21*, 1100.
[8] H. Shen, S. Xiang, Z. Xu, C. Liu, X. Li, C. Sun, S. Lin, B. K. Teo, N. Zheng, *Nano Res.* **2020**, *13*, 1908–1911.
[9] D. Canella, S. J. Hock, O. Hiltner, E. Herdtweck, W. A. Herrmann, F. E. Kühn, *Dalton Trans* **2012**, *41*, 2110–2121.
[10] F. M. Nachtigall, Y. E. Corilo, C. C. Cassol, G. Ebeling, N. H. Morgon, J. Dupont, M. N. Eberlin, *Angew. Chem.* **2008**, *120*, 157–160.
[11] M. Baron, E. Battistel, C. Tubaro, A. Biffis, L. Armelao, M. Rancan, C. Graiff, *Organometallics* **2018**, *37*, 4213–4223.
[12] M. Monticelli, C. Tubaro, M. Baron, M. Basato, P. Sgarbossa, C. Graiff, G. Accorsi, T. P. Pell, D. J. D. Wilson, P. J. Barnard, *Dalton Trans.* **2016**, *45*, 9540–9552.
[13] N. Touj, A. S. Al-Ayed, M. Sauthier, L. Mansour, A. H. Harrath, J. Al-Tamimi, I. Özdemir, S. Yaşar, N. Hamdi, *RSC Adv.* **2018**, *8*, 40000–40015.
[14] V. Stoppa, T. Scattolin, M. Bevilacqua, M. Baron, C. Graiff, L. Orian, A. Biffis, I. Menegazzo, M. Roverso, S. Bogialli, F. Visentin, C. Tubaro, *New J. Chem.* **2021**, *45*, 961–971.
[15] E. Marcheggiani, C. Tubaro, A. Biffis, C. Graiff, M. Baron, *Catalysts* **2019**, *10*, 1.
[16] A. I. Sullivan, J. F. DeJesus, S. Malola, S. Takano, T. Tsukuda, H. Häkkinen, C. M. Crudden, *Chem. Mater.* **2023**, *35*, 2790–2796.
[17] Y. L. Loh, U. F. M. Haziz, R. A. Haque, A. A. Amirul, O. N. Aidda, Mohd. R. Razali, *J. Coord. Chem.* **2019**, *72*, 894–907.
[18] T. Wellnitz, C. Hering-Junghans, *Eur. J. Inorg. Chem.* **2021**, *2021*, 8–21.
[19] J. Chu, D. Munz, R. Jazzar, M. Melaimi, G. Bertrand, *J. Am. Chem. Soc.* **2016**, *138*, 7884–7887.
[20] A. Belèn Meneses, S. Antonello, M. C. Arévalo, F. Maran, *Electroanalysis* **2006**, *18*, 363–370.
[21] T.-H. Hsiao, T.-L. Wu, S. Chatterjee, C.-Y. Chiu, H. M. Lee, L. Bettucci, C. Bianchini, W. Oberhauser, *J. Organomet. Chem.* **2009**, *694*, 4014–4024.
[22] A. A. Penney, V. V. Sizov, E. V. Grachova, D. V. Krupenya, V. V. Gurzhiy, G. L. Starova, S. P. Tunik, *Inorg. Chem.* **2016**, *55*, 4720–4732.
[23] N. Ding, J. Zhang, T. S. A. Hor, *Dalton Trans.* **2009**, 1853.
[24] P. Pinter, A. Biffis, C. Tubaro, M. Tenne, M. Kaliner, T. Strassner, *Dalton Trans.* **2015**, *44*, 9391–9399.
[25] J. Gil-Rubio, V. Cámara, D. Bautista, J. Vicente, *Organometallics* **2012**, *31*, 5414–5426.
[26] A. A. Penney, G. L. Starova, E. V. Grachova, V. V. Sizov, M. A. Kinzhalov, S. P. Tunik, *Inorg. Chem.* **2017**, *56*, 14771–14787.
[27] G. M. Sheldrick, *Acta Crystallogr. Sect. Found. Adv.* **2015**, *71*, 3–8.
[28] O. V. Dolomanov, L. J. Bourhis, R. J. Gildea, J. A. K. Howard, H. Puschmann, *J. Appl. Crystallogr.* **2009**, *42*, 339–341.
[29] C. B. Hübschle, G. M. Sheldrick, B. Dittrich, *J. Appl. Crystallogr.* **2011**, *44*, 1281–1284.
[30] L. Krause, R. Herbst-Irmer, G. M. Sheldrick, D. Stalke, *J. Appl. Crystallogr.* **2015**, *48*, 3–10.
[31] G. M. Sheldrick, *Acta Crystallogr. Sect. C Struct. Chem.* **2015**, *71*, 3–8.
[32] L. J. Farrugia, *J. Appl. Crystallogr.* **2012**, *45*, 849–854.